MINISTÉRIO DA SAÚDE

FUNDAÇÃO OSWALDO CRUZ

INSTITUTO OSWALDO CRUZ

UNIVERSITEIT ANTWERPEN

Joint PhD in Doctoral Program in Parasite Biology of Instituto Oswaldo Cruz
(PGBP/IOC/Fiocruz) and in Biomedical Sciences of Universiteit Antwerpen

EVALUATION OF PHENOTYPIC PROFILE, PHARMACOLOGICAL ASPECTS AND MODE-OF-ACTION OF NOVEL ANTIPARASITIC AGENTS FOR NEGLECTED DISEASES

CAMILA CARDOSO SANTOS

Rio de Janeiro

Antwerp

December 2021

INSTITUTO OSWALDO CRUZ

Programa de Pós-Graduação em Biologia Parasitária

Post-Graduate Program in Parasite Biology

UNIVERSITY OF ANTWERP

Post-Graduate Program in Biomedical Sciences

Faculty of Pharmaceutical, Biomedical and Veterinary Sciences

Camila Cardoso Santos

EVALUATION OF PHENOTYPIC PROFILE, PHARMACOLOGICAL ASPECTS AND MODE-OF-ACTION OF NOVEL ANTIPARASITIC AGENTS FOR NEGLECTED DISEASES

> Thesis presented to the Oswaldo Cruz Institute and University of Antwerp as one of the requirements to obtain the title of Doctor in Parasite Biology (Fiocruz) and in Biomedical Sciences (UAntwerp)

Advisors: Prof. Dr. Maria de Nazaré Correia Soeiro

Prof. Dr. Guy Caljon

Prof. Dr. Louis Maes

RIO DE JANEIRO

ANTWERP

December 2021

Cardoso Santos, Camila.

Evaluation of phenotypic profile, pharmacological aspects and mode-of-action of novel antiparasitic agents for neglected diseases / Camila Cardoso Santos. - Rio de Janeiro, 2021.
295 f.; il.

Tese (Doutorado) – Instituto Oswaldo Cruz, Pós-Graduação em Biologia Parasitária, 2021.

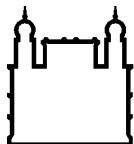Orientadora: Maria de Nazaré Correia Soeiro.
Orientador: Guy Caljon.
Orientador: Louis Maes.

Bibliografia: f. 152-187

1. Drug Discovery. 2. Neglected Tropical diseases. 3. Trypanosomatid parasites. 4. Preclinical Research. 5. Drug mode-of-action. I. Título.

Ministério da Saúde

FIOCRUZ
Fundação Oswaldo Cruz

Universiteit
Antwerpen

INSTITUTO OSWALDO CRUZ

Programa de Pós-Graduação em Biologia Parasitária

Post-Graduate Program in Parasite Biology

UNIVERSITY OF ANTWERP

Post-Graduate Program in Biomedical Sciences

Faculty of Pharmaceutical, Biomedical and Veterinary Sciences

AUTHOR: CAMILA CARDOSO SANTOS

EVALUATION OF PHENOTYPIC PROFILE, PHARMACOLOGICAL ASPECTS AND MODE-OF-ACTION OF NOVEL ANTIPARASITIC AGENTS FOR NEGLECTED DISEASES

ADVISORS: Prof. Dr. Maria de Nazaré Correia Soeiro

Prof. Dr. Guy Caljon

Prof. Dr. Louis Maes

Approved in: 13/12/2021

Board members:

Prof. Dr. Rubens Lima do Monte Neto (Instituto René Rachou-Fiocruz Minas):
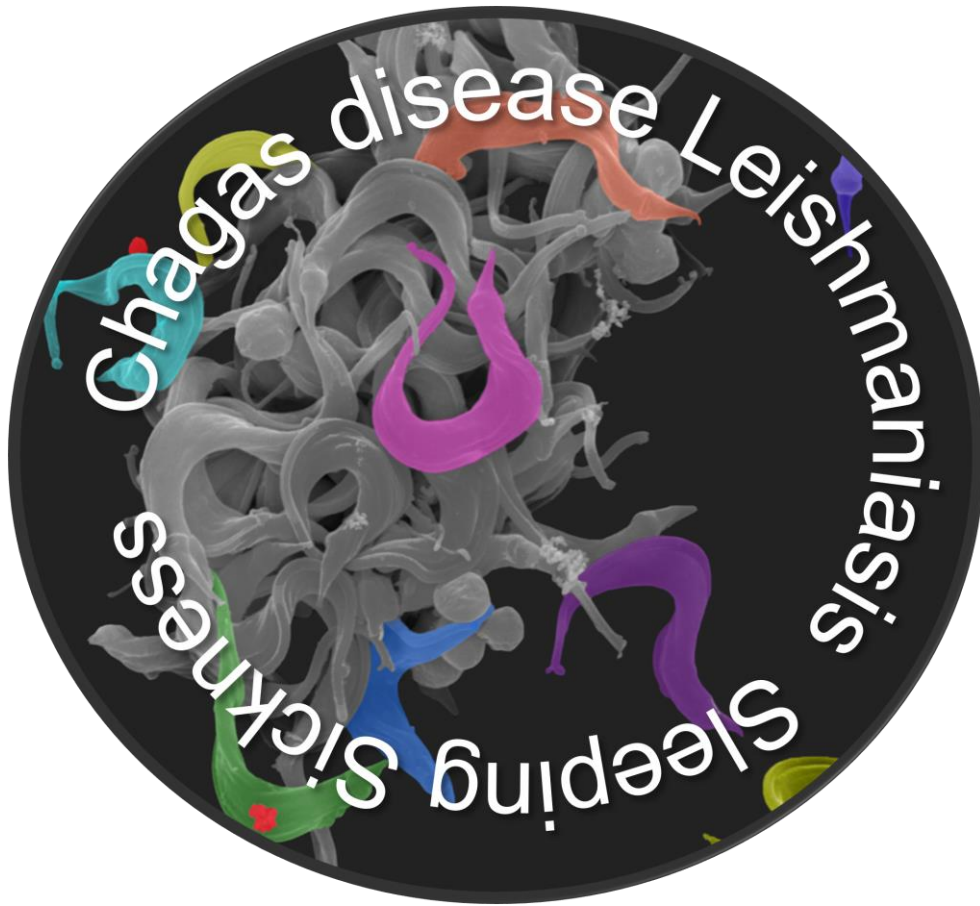*chairman*

Prof. Dr. Van Ostade Xaveer (Universitait Antwerpen)

Prof. Dr. Wim Vanden Berghe (Universitait Antwerpen)

Prof. Dr. Otacílio Moreira   (Instituto Oswaldo Cruz-Fiocruz)

Prof. Dr. Louis Maes (Universitait Antwerpen)

Rio de Janeiro, December 13th, 2021

Chagas disease Leishmaniasis Sleeping Sickness

I dedicate my work to all those who suffer from parasitic diseases arisen from the convenient blindness of society.

D E C L A R A Ç Ã O

Declaramos que a defesa pública da tese de doutorado acadêmico em Biologia Parasitária, área de concentração: Genética e Bioquímica, de Camila Cardoso Santos, realizou-se no décimo terceiro dia do mês de dezembro de dois mil vinte e um, às quatorze horas, de forma síncrona remota.

Título da tese de doutorado acadêmico: **"Evaluation of phenotypic profile, pharmacological aspects and mechanism-of-action of novel antiparasitic agents for neglected diseases"**
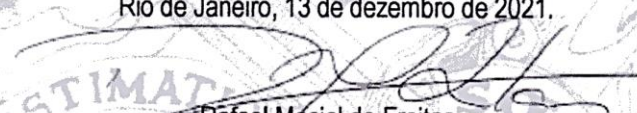
Orientação: Drª. Maria de Nazaré Correia Soeiro
Revisão: Dr. Rubens Lima do Monte Neto
Banca Examinadora: Dr. Rubens Lima do Monte Neto – IRR/FIOCRUZ (Presidente)
    Dr. Xaveer Van Ostade – UNIVERSITY OF ANTWERP/BÉLGICA (Membro titular)
    Dr. Wim Vanden Berghe – UNIVERSITY OF ANTWERP/BÉLGICA (Membro titular)
    Dr. Otacilio da Cruz Moreira - IOC/FIOCRUZ (Suplente)
    Dr. Louis Maes - UNIVERSITY OF ANTWERP/BÉLGICA (Suplente)

Informamos ainda que a referida aluna deve cumprir exigências previstas em regimento da Pós-graduação em Biologia Parasitária para a obtenção de seu título.

Rio de Janeiro, 13 de dezembro de 2021.

Rafael Maciel de Freitas
Matrícula SIAPE 1603050
Coordenador do Programa de Pós-Graduação em Biologia Parasitária
Instituto Oswaldo Cruz/Fiocruz

Documento registrado sob nº DCE-4351/21 no livro nº III, folha 65v em 13/12/2021.

Av. Brasil, 4365 Manguinhos Rio de Janeiro RJ Brasil **CEP:** 21040-360
Contatos: (21) 2562-1201 / 2562-1299 **E-mail:** atendimentoseac@ioc.fiocruz.br **Site:** www.fiocruz.br/iocensino

7

AGRADECIMENTOS

Eu gostaria de agradecer a todos que participaram da construção da pessoa que sou e aos que fizeram essa pessoa alçar voos no doutorado.

A começar pelo suporte e amor da **família** e **amigos.** Em especial aos meus **avós** (*in memoriam*) pela infinita fonte de amor e cuidados. Às minhas tias **Silvana, Simone e Sônia**, mulheres exemplares que me tratam com tanto carinho e consideração de filha. Aos meus queridos **tios Renato** e **Fabio**, meus amores que se orgulham tanto de mim. Ao meu querido padrasto **Ronny** (*in memoriam*), que me ensinou algumas tantas formas de resolver dever de casa. Ao meu **pai Afonso**, ao me acalmar nas angústias. E principalmente à minha **mãe Luciana**, minha heroína e principal referência de resiliência. Obrigada mãe, por carinhosamente me vestir para escola enquanto eu dormia. Por me ensinar dever de casa, após um dia inteiro de trabalho e faculdade noturna. Por sempre lutar e me proporcionar o melhor da vida. Eu te amo! E às minhas amigas do coração, guardiãs e fontes de luz distribuídas neste mundo **Ana, Júlia** e **Thais**. Nossa amizade e conexão espiritual são incríveis. Obrigada pela existência e apoio.

À minha orientadora de mestrado e de doutorado, **doutora Nazaré Soeiro**. Pesquisadora brilhante e mulher forte e justa, sempre me apoiou a crescer na carreira científica, incluindo a seleção do doutorado em cotutela. Foram 7 anos de muito aprendizado e respeito que carregarei para vida toda. Eu espero que, como pesquisadora, consiga honrar seu tempo dedicado.

O doutorado não é uma escolha fácil e pode ser ainda mais estressante em outra cidade, mas com a equipe LBC/Fiocruz é menos difícil. Eu gostaria de agradecer a esta rede maravilhosa de seres humanos, técnicos e pesquisadores de excelência, em especial: à **Raíza, Ludmila, Denise, Cristiane, Aline, Ana Lia, Mari, Gabi, Marcos, Roberson** e **Patrícia** pela paciência, cooperação, risos e apoio nos momentos difíceis. Sem vocês não seria possível.

Obrigada aos meus orientadores da Antuérpia, os **doutores Louis Maes** e **Guy Caljon**, por também intermediarem o duplo doutorado e através deste, proporcionarem novos desafios, vivências e áreas de conhecimento em minha trajetória cientifica. Agradeço o suporte científico e administrativo do time LMPH, incluindo **Dorien, Pim, Rik, Mandy**, **An** and **Natascha**. Agradeço o acolhimento caloroso e novas amizades na

8

Antuérpia que me deram forças para seguir, incluindo **Juliana, Tatiana, Laura, Agnese, Abraham, Gonca**, **Yury** and **Angela**. Nossos momentos de gargalhadas, cervejas, comida e doces foram valiosíssimos e espero reencontrá-los futuramente. Existem pessoas especiais que aparecem em nossas vidas e **Juliana** é uma delas. Como eu sou grata ao universo de tê-la conhecido na Antuérpia, pelo suporte emocional e acolhimento que me deu, pela amiga que é. Se eu sou uma "bola de demolição", você é uma escultora dos mais delicados detalhes. É muito amor e admiração envolvidos.

As experiências fora da caixa não pararam por aí. Para completar meus objetivos do doutorado, tive a colaboração importantíssima da doutora **Ana Paula Lima** do instituto de biofísica da UFRJ. Obrigada por abrir seu espaço no LBBM, por me explicar inúmeras vezes o que estávamos fazendo com CRISPR, pelos ensinamentos e trabalho desenvolvido. Obrigada por todo suporte oferecido por **Letícia, Tati, Dani, Nat** e **Felipe**. E um agradecimento mais que especial ao meu presente do LBBM chamado **Amy Goundry**. A pessoa mais correta, legal, doadora, sensível, amiga e talentosa que ganhei no meu último round de doutorado no Rio. Compartilhamos muitos momentos de alegria, correria, de suporte em experimentos e de vida. Que bom que você existe!

O meu "eu-científico" precisa de sua metade artística, dançante e musical. Concomitante ao doutorado, tive a oportunidade de fazer aulas de tango com o talentoso professor e belo ser humano **Paulo Araújo**, no espaço Vira Lapa. Neste cantinho fiz amigos formidáveis, dentre eles **Annie, Wagner, Deise, Diego** e **Flavinha**. E por fim agradeço à **Escola de Música Villa Lobos** por tornar acessível o aprendizado de teoria e prática musical; um sonho desde a infância que virou realidade. Dentre as pessoas que lá conheci, agradeço principalmente ao meu professor de prática de piano **Gilson**: pelo afeto e respeito às limitações com que ensina, pelo estímulo a aprender a tocar independente do nível que comecei e da falta de tempo para me dedicar. Ambos os mestres são amigos para vida!

Finalmente, meu agradecimento mais que especial vai para meu companheiro de vida **Gabriel**, que sempre esteve ao meu lado nos momentos de percalço e incondicionalmente me apoiou na carreira científica, independente da distância geográfica. Que tolerou meus inúmeros atrasos devido a um experimento imprevisto, me faz acreditar todos os dias que eu sou capaz e de me ajudar a ser minha melhor versão. Sou deveras abençoada por te ter como marido e pela linda família que me presenteou.

ACKNOWLEDGEMENTS

Antwerp, giving me guts to go on. Our moments of laughs, beers, boardgames and sharing food were invaluable, and I hope to see you again. While in Antwerp, **Juliana** was my anchor. I am so grateful to the universe for had having her as my BF in Antwerp, for the emotional support given and sincere welcome, for the amazing friend she still is. If I'm a wrecking ball, she is a sculptor of the finest details. It's a lot of love and admiration involved.

The out-of-the-box experiences didn't stop there. To complete my doctoral research, I had the very important collaboration of **Dr. Ana Paula Lima** from the Institute of Biophysics at UFRJ. I thank her for opening her space at LBBM, for explaining to me countless times what we were doing with CRISPR, for the teaching and work done. I am glad for all the help provided by **Letícia, Tati, Dani, Naty** and **Felipe**. Plus, I received the best gift from LBBM called **Amy Goundry**. The most correct, nice, unselfish, sensitive, supportive and talented person I met in my last year of PhD in Rio. We shared many moments of joy, rush, experimental assistance, and life support. Thanks for your existence.

My scientific self needs its dancing and musical artistic half. Concurrent with the doctorate, I had the opportunity to take tango classes and learn from the most talented teacher and best human being named **Paulo Araújo**, at Espaço Vira Lapa. In this beloved space I made formidable friends, among them my best fellows and dance partners **Annie, Wagner, Deise, Diego** and **Flavinha**. And finally, I would like to thank the **Villa Lobos Music School** for making the learning of musical theory and practice accessible and an old dream to became true. Among the people I met, I am especially grateful for my piano practice teacher **Gilson**: who treated me with affection, respecting my limitations and encouraging me to learn how to play piano regardless the lack of previous experience and time. Both are my friends for life.

Finally, my major gratitude belongs to my life partner **Gabriel**, who hold my hand whenever necessary and unconditionally supported my scientific career apart from geographical distance. Thank you for tolerating my numerous delays due to unpredictable experiments, to be patient, comprehensive and to make me be the best version of myself. I am truly blessed to have you as my husband and for the beautiful family you gave me.

ABSTRACT

"Evaluation of phenotypic profile, pharmacological aspects and mode-of-action of novel antiparasitic agents for neglected diseases"
Camila Cardoso Santos - PhD Thesis in Parasite Biology and Biomedical Sciences

This PhD research is aligned to the current and urgent need for alternative treatment options for neglected tropical diseases (NTDs). NTDs lack effective vaccines and satisfactory therapies despite high incidence and death rates in poor communities in underdeveloped tropical and subtropical areas, mainly in Africa, Latin America and Asia. Thus, new, better, safer, and affordable treatments are urgently needed. Different *in silico, in vitro* and *in vivo* approaches were employed to search for novel drug candidates for Chagas disease, sleeping sickness and cutaneous leishmaniasis (CL) caused by the trypanosomatid parasites *Trypanosoma cruzi*, *Trypanosoma brucei* spp. and *Leishmania amazonensis*, respectively. Firstly, compounds were assessed *in vitro* and *in vivo* in *L. amazonensis* CL experimental models. These included: (i) compounds derived from shape-based virtual screening of an oxazolo[4,5-b]pyridine derivative (GNF5343); (ii) compounds belonging to a series of natural product-inspired phenyl sulfonyl acetamides, acetates, and pentacyclic triterpenoids; (iii) nitroaromatic agents derived from 4-nitrophenylacetyl and 4-nitro-1H-imidazolyl scaffolds. Three out of 55 compounds were found active and selective *in vitro* (IC_{50} <10 μM, selectivity index (SI) ≥50) against intracellular *L. amazonensis* in infected macrophages: one sulfonyl (Cp**30**) and two nitro-derivative (Cp**6** and **7**) compounds. However, when *L. amazonensis* infected animals were treated for 14 days by oral gavage at 10 mg/kg twice a day (bid), neither the size of the animal lesions nor the parasite load evaluated by qPCR were reduced. In sequence, 7-substituted nucleoside analogues were (iv) screened *in vitro* and *in vivo* against a panel of trypanosomatid parasites (*T. cruzi* DTUs and *T. brucei* spp) besides (v) evaluating *in vitro* metabolic stability (in presence of CYP_{450} superfamily and uridine glucuronosyl transferase enzymes). Also, the modes-of-action (MoA) of some nucleoside analogues was explored at the molecular level (RNAi and CRISPR/Cas9 methods for *T. brucei* and *T. cruzi,* respectively). Our main findings demonstrated that two 7-substituted nucleoside analogues (FH11706 and FH10714) were highly active against *T. cruzi* (IC_{50} 0.20-0.05 μM - SI >300), selective and metabolically stable, hence justifying their future analysis *in vivo*. Regarding FH8512, the use of a mouse model of acute *T. cruzi* infection under an extended period of treatment (up to 60 consecutive days) at 25 and 2.5 mg/kg bid resulted in parasitemia suppression and animal survival. However, this long-term therapy did not prevent parasite relapse as evidenced by PCR. MoA studies with a *T. brucei* genome-wide RNA interference (RNAi) library revealed adenosine kinase (ADKIN), rac-serine kinase (RSKIN) and an NADPH-binding oxidoreductase as putative targets for the studied nucleoside analogues. Next, the corresponding gene orthologues were chosen as starting point to infer the MoA in the *T. cruzi* Dm28 strain using a CRISPR/Cas9 gene editing approach. The inability for double knockout retrieval and the reduced fitness of the heterozygous RSKIN +/- clones suggest that the tested targets in *T. cruzi* are essential genes. Additional in-depth studies are underway to further characterize the generated heterozygous parasite clones.

RESUMO

"Avaliação do perfil fenotípico, aspectos farmacológicos e modo-de-ação de novos agentes antiparasitários para doenças negligenciadas"

Camila Cardoso Santos - Tese de Doutorado em Biologia Parasitária e Ciências Biomédicas

A proposta de doutorado em cotutela está alinhada à necessidade atual e urgente de alternativas de tratamento para doenças tropicais negligenciadas (DTNs). As DTNs carecem de vacinas eficazes e tratamentos satisfatórios, apesar de sua alta incidência e taxas de mortalidade em comunidades pobres em áreas tropicais e subtropicais subdesenvolvidas, principalmente na África, América Latina e Ásia. Assim, tratamentos novos, mais eficazes, seguros e acessíveis são urgentemente necessários. Diferentes abordagens *in silico, in vitro* e *in vivo* foram empregadas na busca de novos candidatos a fármacos para doença de Chagas, doença do sono e leishmaniose cutânea (LC) causadas pelos tripanossomatídeos *Trypanosoma cruzi, Trypanosoma brucei* ssp e *Leishmania amazonensis*, respectivamente. Primeiramente, os compostos foram avaliados *in vitro* e *in vivo* em modelos experimentais de LC causado por *L. amazonensis*, incluindo: (i) derivados de triagem virtual baseada em ligante (derivado de oxazolo [4,5-b] piridina (GNF5343)); (ii) pertencentes a uma série de fenilsulfonilacetamidas, acetatos e triterpenóides pentacíclicos inspirados em produtos naturais; (iii) agentes nitroaromáticos derivados de moldes de 4-nitrofenilacetil e 4-nitro-1H-imidazolil. Três dos 55 compostos foram ativos e seletivos *in vitro* (IC_{50} <10 µM, índice de seletividade ≥ 50) contra formas intracelulares de *L. amazonensis* presentes em macrófagos infectados: um sulfonil (Cp**30**) e dois nitro-derivados (Cp**6** e **7**). No entanto, quando animais infectados com *L. amazonensis* foram tratados por 14 dias por gavagem oral com 10 mg / kg duas vezes ao dia (bid), não houve redução do tamanho das lesões dos animais nem da carga parasitária avaliada por qPCR. Em sequência, os análogos de nucleosídeos (7-deazapurinas) foram (iv) triados *in vitro* e *in vivo* contra um painel de parasitas tripanossomatídeos (diferentes DTUs de *T. cruzi* e *T. brucei* spp), além de (v) avaliar a estabilidade metabólica *in vitro* (na presença de enzimas da superfamília CYP450 e uridina glucuronosil transferase). Além disso, o modo-de-ação (MoA) de alguns análogos de nucleosídeos foi explorado em nível molecular (métodos RNAi e CRISPR/Cas9 para *T. brucei* e *T. cruzi*, respectivamente). Dentre os principais achados, Dois análogos de nucleosídeos (FH11706 e FH10714) foram muito ativos sobre *T. cruzi* (IC_{50} 0.20-0.05 μM), seletivos e metabolicamente estáveis *in vitro*, exibindo elevados índices de seletividade (IS> 300), justificando sua futura análise *in vivo*. Em relação à FH8512, o uso de um modelo murino de infecção aguda por *T. cruzi* sob um período prolongado de tratamento (até 60 dias de administração consecutivos) com 25 e 2.5 mg / kg bid, resultou na supressão da parasitemia e sobrevivência dos animais. No entanto, a terapia a longo prazo não evitou a reincidência do parasita evidenciada por qPCR. Estudos de MoA com uma biblioteca de interferência de RNA do genoma de *T. brucei* (RNAi) revelaram adenosina quinase (ADKIN), rac-serina quinase (RSKIN) e uma NADPH-oxidorredutase como alvos putativos dos análogos de nucleosídeos estudados. Em seguida, os genes ortólogos correspondentes foram escolhidos como ponto de partida para inferir o MoA na cepa Dm28 de *T. cruzi* usando uma abordagem de edição de gene CRISPR / Cas9. A inaptidão para a recuperação de duplo nocaute e fitness reduzido dos clones heterozigotos RSKIN +/- sugerem que os alvos testados em *T. cruzi* sejam genes essenciais. Estudos adicionais em maior grau de detalhamento estão em andamento para melhor caracterizar os clones de parasitas heterozigotos gerados.

ABSTRACT

"Evaluatie van de fenotypische en farmacologische eigenschappen en actiemechanismen van nieuwe geneesmiddelen tegen verwaarloosde parasitaire ziekten"

Camila Cardoso Santos - Doctoraatsthesis in Parasitologie en Biomedische Wetenschappen

Dit doctoraatsonderzoek (PhD) komt tegemoet aan de dringende nood voor alternatieve behandelingsopties voor verwaarloose tropische ziekten (NTDs). Voor NTDs bestaan nog geen effectieve vaccins en de huidige behandelingen zijn onvoldoende bevredigend, ondanks de hoge incidentie en mortaliteit binnen achtergestelde gemeenschappen in onderontwikkelde tropische en subtropische gebieden, voornamelijk Afrika, Latijs Amerika en Azië. Betere, meer veilige en betaalbare behandelingen zijn bijgevolg nodig. In dit onderzoek werden *in silico, in vitro* en *in vivo* benaderingen gebruikt in de zoektocht naar nieuwe kandidaat geneesmiddelen voor de behandeling van Chagas disease, slaapziekte en cutane leishmaniasis (CL), respectievelijk veroorzaakt door *Trypanosoma cruzi*, *Trypanosoma brucei* ssp and *Leishmania amazonensis*. In een <u>eerste</u> groep experimenten werden stoffen geëvalueerd in *in vitro* en *in vivo* *L. amazonensis* CL modellen. Dit omvatte (i) stoffen afgeleid uit op 'vorm-gebaseerde' virtuele screening van een oxazolo[4,5-b]pyridine afgeleide (GNF5343); (ii) stoffen uit een natuurproduct serie van fenyl sulfonyl acetamides, acetaten en pentacyclische triterpenoïden, en (iii) nitroaromatische stoffen afgeleid van 4-nitrophenylacetyl en 4-nitro-1H-imidazolyl scaffolds. In een <u>tweede</u> groep van experimenten werden 7-gesubstitueerde nucleoside analogen (iv) gescreend *in vitro* en *in vivo* op een panel van trypanosoom parasieten (*T. cruzi* DTUs en *T. brucei* spp), aangevuld met (v) *in vitro* metabole stabiliteit (in aanwezigheid van CYP_{450} superfamily en uridine glucuronosyl transferase enzymes). Het moleculair werkingsmechanisme van enkele nucleoside analogen werd eveneens verkend via RNAi en CRISPR/Cas9, respectievelijk voor *T. brucei* en *T. cruzi*. Uit het <u>eerste</u> set van experimenten bleek dat 3 stoffen uit een groep van 55 selectieve *in vitro* activiteit vertoonden (IC_{50} <10 µM, selectiviteitsindex (SI) ≥50) op intracellulair *L. amazonensis* geïnfecteerde macrofagen: één sulfonyl (Cp**30**) and twee nitro-afgeleiden (Cp**6** and **7**). Na 14 dagen behandeling van *L. amazonensis* geïnfecteerde muizen via orale gavage aan 10 mg/kg 2x per dag (bid) was er evenwel geen reductie van de lesie grootte noch van het aantal parasieten (via qPCR). De belangrijkste bevindingen uit de <u>tweede</u> serie experimenten toonden aan dat twee 7-gesubstitueerde nucleoside analogen (FH11706 and FH10714) hoog aktief tegen *T. cruzi* (IC_{50} 0.20-0.05 µM - SI >300), niet-toxisch en metabool stabiel waren, wat een verdere *in vivo* evaluatie kon verantwoorden. In een muismodel voor acute *T. cruzi* infectie en verlengde behandeling (tot 60 opeenvolgende dagen met uitzondering van de weekends aan 25 en 2.5 mg/kg bid) gaf teststof FH8512 een onderdrukking van de parasitemie en een verlengde overleving. Helaas kon deze langetermijn behandeling een heropflakkering van de parasiet (volgens PCR) niet verhinderen. Studies naar het werkingsmechanisme van de nucleoside analogen via een *T. brucei* genoom-wijde RNA interferentie (RNAi) bibliotheek gaf adenosine kinase (ADKIN), rac-serine kinase (RSKIN) en een NADPH-bindend oxidoreductase aan als mogelijke targets. Vervolgens werden de overeenkomstige orthologen gekozen as startpunt voor het werkingsmechanisme in *T. cruzi* (Dm28 stam) via CRISPR/Cas9 gene editing. De onmogelijkheid om een dubbele knock-out te selecteren in combinatie met een verminderde 'fitness' van de heterozygote RSKIN +/- clones suggereren dat de geteste targets essentiële genen voor *T. cruzi* zijn. Aanvullende studies zijn lopende om de gegenereerde heterozygote parasieten clonen in detail te karakteriseren.

INDEX

INDEX OF FIGURES

microscopy (TEM); and adapted from the quoted references. Legend: Nucleus (N), Kinetoplast (K), Mitochondrion (M), Golgi complex (G); Cytostome (C); Flagellar pocket (FP), Flagellum (F) and lipid inclusion (l).

20

(22) (b) Enzyme activity involved in T. cruzi purine salvage. Known reactions are represented by solid lines and hypothetical reactions by dashed lines. Enzyme activities: 1- Phosphoribosyltransferase; 2- nucleoside kinase; 3- nucleoside hydrolase; 4- nucleoside phosphorylase; 5- adenine aminohydrolase; 6- adenosine aminohydrolase. Abbreviations: A (adenine); Hx (hypoxanthine); G (guanine); ADO (adenosine); INO (inosine); GNO (guanosine); AMP, IMP, GMP (adenosine, inosine and guanosine monophosphate). Adapted from: Gutteridge & Davies, 1981 (23).

gel with PCR products from extracted DNA of transfected clones for TCDM_01513 knockout (b) 29, 34, 35 36 & 37 selected with blasticidin, (c): 4, 9, 11 & 15 selected with puromycin, and control strain Dm28T7Cas9 (c), using the following set of primers: *5´INTG* plus *3´ INTG* (possible drug-repair cassette integration)*; UP-FW* plus *DR-KO* (drug-repair cassette integration)*; 5´INTG plus DR-KO or 3´INTG plus UP-FW* (drug-repair cassette integration on the right locus)*; and ORF-FW* plus *ORF-REV* (GOI ORF presence). Kb, kilobase; bp, base pair; EL, endogenous locus; *BSD*, blasticidin gene; PAC, puromycin gene; 1kb, 1kb DNA ladder.

LIST OF TABLES

LIST OF ACRONYMS AND ABBREVIATIONS

A

ABC	ATP-binding cassette
ACD	acute chagas disease
ADKIN	adenosine kinase protein
ADKIN	adenosine kinase coding gene
ADMET	absorption, distribution, metabolism, excretion and toxicity
AE	adverse effects
AmB	amphotericin B deoxycholate
AMP	adenosine monophosphate
AGO	argonaute protein
ATP	adenosine triphosphate
AQP1	aquaglyceroporin 1
AQP2	*aquaglyceroporin 2 coding gene*
ARM	antimony resistance markers

B

bid	twice a day
bsd	blasticidin
BSD	blasticidin resistance gene
BT	bloodstream trypomastigotes
Bz	benznidazole

C

CanL	canine leishmaniasis
Cas9	CRISPR associated protein 9
CC	cardiac cells
CD	chagas disease
CEUA	Committee of Ethics for the Use of Animals
CYP450	cytocrome P450
CL	cutaneous leishmaniasis
CNS	central nervous system
CNV	copy number variations
Cp**1**	GNF5343-based shape hit

Cp**2**	GNF5343 analogue
Cp**6**	nitroaromatic 4-nitrophenylacetyl derived compound
Cp**7**	nitroaromatic 4-nitro-1*H*-imidazolyl derived compound
Cp**30**	adamantyl-based phenyl sulfonyl acetamide
Cpd**1**	FH8512 nucleoside analogue
CPRG	chlorophenolred ß-D-galactopyranoside
CRK3	cyclin-dependent protein kinase coding gene
crRNA	CRISPR RNA
CRISPR	clustered regularly interspaced short palindromic repeats

D

DALYs	disability-adjusted life years
DAPI	4′,6-diamidino-2-phenylindole
DD	drug discovery
DIC	differential interference contrast
diCre	dimerised Cre recombinase
Dm28T7-SpCas9	*T. cruzi* Dm28 engineered expressing T7 RNAP and SpCas9
DMPK	drug metabolism and pharmacokinetic
DMSO	dimethyl sulfoxide
DNDi	drugs for neglected disease initiative
DPI	days post-infection
DR	drug resistance
DR-KO	downstream-reverse KO primer that anneals to drug-repair cassette homologous region
DSB	double strand break
dsRNA	double-stranded RNAs
DTUs	discrete type units
DW-FW	downstream forward primer that anneals to
DW-TAG	downstream reverse tag primer that anneals to drug-repair cassette homologous region

E

4EIP	4E interacting protein
4EIP	4E interacting protein coding gene
EndG	Endonuclease G

ESI	electrospray ionization

F

FBS	fetal bovine serum
FDA	food and drug administration
FF	free amastigote forms
FICI	fractional inhibitory concentration index
FLA	FLA1-binding protein
FP	flagellar pocket

G

GFP	green fluorescent protein
GRESAG 4	receptor-type adenylate cyclase coding gene
gDNA	genomic DNA
g-HAT	HAT caused by *Trypanosoma brucei gambiense*
GMP	guanosine monophosphate
GOI	gene of interest

H

HAT	human african trypanosomiasis
HR	homology repair
HSP	retrotransposon hot spot protein 5

I

IA	intracellular amastigote forms
IAC	internal amplification control
IC$_{50}$	50% inhibitory concentrations
IC$_{90}$	90% inhibitory concentrations
ICTB	Institute of Science and Biomodels Technology
IDM	innovative and intensified disease management
iFCS	inactivated foetal calf serum
IHC	infected host cells
II	infection index
INTG primers	UTR regions flanking GOI annealing primers
ISG	invariant surface glycoprotein

K

k   kinetoplast

Kb   Kilobases

kDNA   kinetoplast deoxyribonucleic acid

KO   knockout

L

LAFEPE   Laboratory of the State of Pernambuco

LF   lymphatic filariasis

LIT   liver infusion tryptose

LMT   Leishmania Miltefosine transporter

LPG   lipophosphoglycans

L929   mouse fibroblast

M

MASP   mucin-associated surface proteins

MCL   mucocutaneous leishmaniasis

MDG   millennium development goals

MDR1   multidrug resistance protein 1

MIL   miltefosine

MMOA   molecular mechanism of action

MoA   mode-of-action

MRC   Human lung fibroblast, SV40 transformed

MRM   multiple reaction monitoring

mRNA   messenger ribonucleic acid

MRPA   multidrug resistance-associated protein A

MS²   mass spectrometry

MT   metacyclic trypomastigotes

MT™   milteforan™

N

NAD   nicotinamide adenine dinucleotide

NADP   nicotinamide adenine dinucleotide phosphate

NADPH   reduced nicotinamide adenine dinucleotide phosphate

NEB10	high efficiency competent *E. coli*
NECT	nifurtimox-eflornithine combination therapy
Nif	nifurtimox
NTDs	neglected tropical diseases
NTR1	nitroreductase 1
NW	New World
NYSM	New York single marker

O

ODC	ornithine decarboxylase
ORF	open reading frame
ORF-FW	start codon of the ORF annealing forward primer
ORF-REV	internal region in the ORF annealing reverse primer
OW	Old World
OXRED	pyridine nucleotide disulfide oxidoreductase / NAD(P) binding Rossmann-like domain containing protein coding gene

P

Pac	puromycin
PAC	puromycin resistance gene
PAM	protospacer adjacent motif
PBS	phosphate buffered saline
PCT	preventive chemotherapy and transmission control
PEN-STR	penicillin-streptomycin
PIC	parasites per infected cells
PO	oral administration
PoC	proof-of-concept
pPOT	PCR only tagging plasmid
Pt	pentamidine
PTGS	posttranscriptional gene silencing
PMM	peritoneal macrophages
PRP1	pentamidine resistance protein 1

Q

| qd | once a day |
| qPCR | quantitative polymerase chain reaction |

R

R&D	research and development
RE	reservosomes
RISK	RISC
r-HAT	HAT caused by *Trypanosoma brucei rhodesiense*
RNAi	RNA interference
RNP	ribonucleoprotein
RNHO	hydronitroxyl
RPMI-1640	Roswell Park Memorial Institute 1640
RT	room temperature

S

SaCas9	*Staphylococcus aureus* Cas9
SpCas9	*Streptococcus pyogenes* Cas9
Sb(III)	trivalent antimonial
Sb(V)	pentavalent antimonial
sgRNA	single-guide RNA
sgRNA primers	primers sharing homology to regions flanking GOI and Cas9-backbone
SI	selective index
siRNA	small interfering RNAs
SSG	sodium stibogluconate
SSG&PM	sodium-stibogluconate-paromomycin
STH	soil-transmitted helminth

T

T_a	annealing temperature
T7 RNAP	T7 RNA polymerase
TbAAT6	*T. brucei* amino acid transporter 6
TbAQP2/TbAQP3	*T. brucei aquaglyceroporin 2 and 3 coding gene*
TbAT1	*T. brucei* P2 aminopurine transporter *coding gene*
TbDCL	*T. brucei* dicer-like enzyme

TCDM_01513	*T. cruzi* Dm28c adenosine kinase gene ID
TCDM_01526	*T. cruzi* Dm28c rac serine-threonine gene ID
TCDM_04666	*T. cruzi* Dm28c adrenodoxin reductase gene ID
TCP	target candidate profile
TcNTR	*T. cruzi* nitroreductase
TcOYE	*T. cruzi* old yellow enzyme
tdTomato	constitutively fluorescent orange fluorescent protein
T_m	melting temperature
TPP	target product profile
tracrRNA	trans-activating CRISPR RNA
TriTryps	*T. brucei, T. cruzi and L. major*
TS	trans-sialidase

U

UBE1	ubiquitin activating enzyme coding gene
UDPGA	uridine diphosphate glucuronic acid
UP-FW	upstream forward primer anneals to drug-repair cassette homologous region
UGT	uridine glucuronosyl transferase
UPLC	Ultra Performance Liquid Chromatography
UTR	untranslated region

V

VL	visceral leishmaniasis
VSG	variable surface glycoprotein

W

WHO	world health organization

Part 1

Chapter 1- General Introduction

Chapter 2- Research Proposal: Objectives and Outline

1. GENERAL INTRODUCTION

1.1 The background of Neglected Tropical Diseases

Neglected Tropical Diseases (NTDs) comprise a group of communicable diseases caused by viruses, fungi or parasites, mostly affecting poor people living worldwide. According to the World Health Organization (WHO), NTDs affect more than one billion people, lead to high death rates besides creating profound social stigmas (27).

The 2000 Millenium Summit was a hallmark in the fight against NTDs, after the adoption of the Millenium Development Goals (MDGs). The MDGs aimed to accelerate the global progress in more sustainable actions. At that time, it mainly focused on control measurements for HIV, malaria and tuberculosis, leaving behind many other tropical diseases with great global impact (28). Now, WHO categorizes 20 NTDs, focusing on control policies such as (i) Preventive Chemotherapy and Transmission Control (PCT) and (ii) Innovative and Intensified Disease Management (IDM) (29,30).

The PCT include the three major soil-transmitted helminth (STH) diseases (ascariasis, trichuriasis and hookworm diseases), schistosomiasis, lymphatic filariasis (LF), onchocerciasis, trachoma, leprosy and dracunculiasis. As a result, a dramatic reduction in global prevalence of LF, onchocerciasis, and trachoma is already observed in many countries (31), whereas soil-transmitted helminth infections or schistosomiasis still represent serious challenges (28).

Buruli ulcer, yaws and kinetoplastid diseases [American Trypanosomiasis or Chagas disease (CD), human African trypanosomiasis (HAT) or Sleeping Sickness, Cutaneous (CL) and Visceral (VL) leishmaniasis] are grouped as IDM due to challenges related to early diagnosis, treatment and follow-up (32).

In fact, fast and global actions are needed to reach earlier diagnosis and therapies besides sustainable vector control measurements. Safer and more effective drugs and vaccines are needed aiming to achieve control of these poverty-related diseases.

1.2 Chagas disease, Cutaneous Leishmaniasis, and Sleeping sickness

1.2.1 Clinical and epidemiological features

In 1909, Chagas disease (CD) was described in a small village in Minas Gerais (Lassance city) by Dr. Carlos Justiniano Ribeiro Chagas, physician and researcher of the Instituto Soroterápico de Manguinhos, now called Oswaldo Cruz Institute. Besides reporting the new disease, Carlos Chagas also described the protozoan etiological agent, *Trypanosoma cruzi*, the invertebrate vectors, Hemiptera of the Triatominae sub-family, commonly known as "kissing bugs" (33). In addition to vectorial transmission, other routes are known including blood transfusion and organ transplantation, oral transmission, mother-to-child transmission, laboratory accidents, among others (34). In Brazil, oral transmission represents the main route of new acute cases of CD with outbreaks mostly found in the Amazon region, associated with consumption of contaminated water and drinks such as sugarcane, *açaí*, palm heart and guava juice (35).

CD is characterized by a short (up to eight weeks), asymptomatic/ oligosymptomatic acute phase with detectable parasitemia in direct blood examination. At this initial phase, some infected individuals may display early pathognomonic signs (Romaña sign and chagoma (Figures 1.1a-b)), fever, adenopathy, oedema, hepatosplenomegaly, myocarditis, and meningoencephalitis in those severe cases (children under 2 years-old and immunocompromised people) (36,37). Due to an effective host immune response, parasitism is controlled but not eliminated and infected people enter a second stage of the disease, the chronic asymptomatic phase. Due to not fully known mechanisms, after years or decades, 30-40% of the cases may evolve to the digestive forms leading to megaesophagus (Fig 1.1c) and megacolon (Fig 1.1d), cardiac forms (Fig 1.1e) and to a lesser extent, neurological disorders (36). In cases with immunosuppression, relapses occur leading to high parasitemia, myocarditis and severe meningoencephalitis (37).
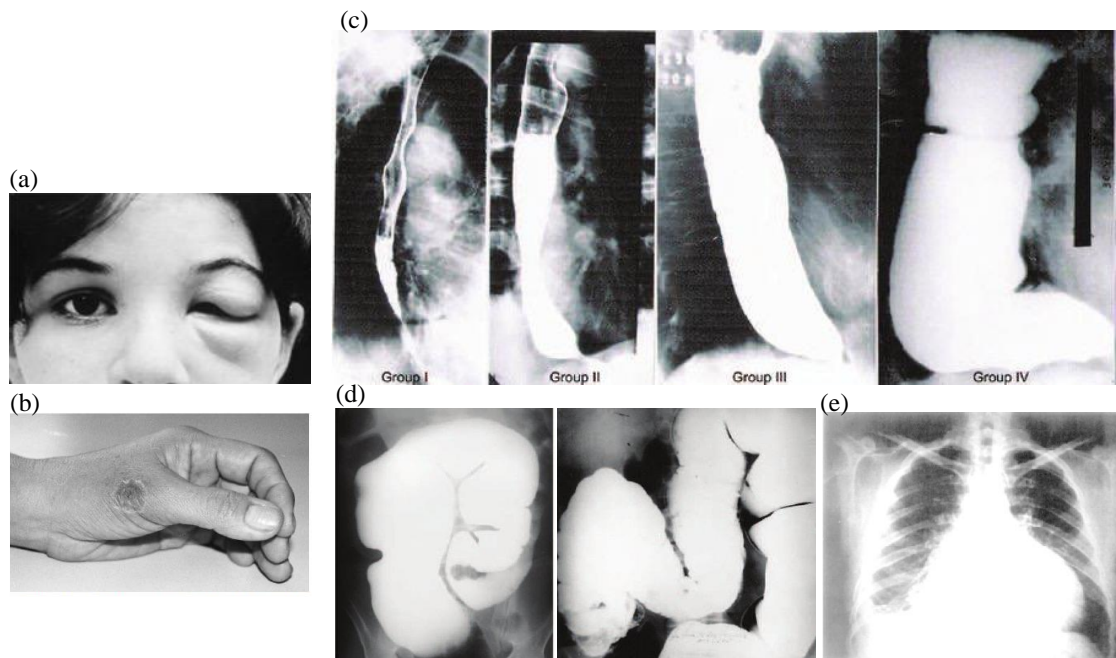
Figure 1.1 Chagas disease (CD) clinical manifestations in acute (a,b) and chronic (c,d,e) phases. In Acute Chagas disease (ACD), (a) a swelling of the child's eyelid called Romaña sign and (b) a chagoma at the dermal site of the kissing bug bite. The disease may evolve to chronic complications such as (c) chagasic megaesophagus, classified in four groups according to the disease stage and (d) chagasic megacolon, with rectum and sigmoid dilatation (*left figure*) and less frequent megacolon dilatation (right figure) and (e) heart disease, with a hypertrophy of the heart. Figure credits, adapted and retrieved from: (**a**) https://www.cdc.gov/parasites/chagas/gen_info/vectors/index.html#list (**b**) Kinoshita-Yanaga *et al* 2009 (1), (**c**) Rezende *et al.* 1960 (2) (**d**) Rassi *et al* 2010 (3) (**e**) Coura *et al* 2013 (4).

It is estimated that more than 6 million people are infected with *T. cruzi* mainly in endemic areas of 21 Latin American countries (38). Less than 1% has access to diagnosis and treatment (39). CD is responsible for approximately 10,000 deaths annually, killing more people than any other parasitic disease in Latin America (40). A total loss of 550,000 years of life (DALYs) is attributed to this illness resulting from premature death and/or disability (41,42), causing a great economic and social impact. Bolivia has the highest prevalence, with an estimated 607,186 cases (43,44).

Classically associated with poverty in rural areas, CD now also represents a public health problem in other non-endemic countries (e.g. North America and Europe) due to populational migration of infected people to these areas (45,46). The Center for Disease Control and Prevention estimates that there are more than 300,000 people infected with *T. cruzi* in the United States (47).

In 1885, *Leishmania* parasites in cutaneous lesions were observed by the Scottish doctor David Douglas Cunningham (48). This etiological agent was officially reported

in 1903 by the Scottish pathologist William Leishman, who described ovoid bodies in smears taken post-mortem from the spleen of a soldier (49). At the same time, the Irish doctor Charles Donovan (50) described similar bodies in splenic samples taken during life and at autopsy from a native Indian (51). The gender and observed species were coined by Ross as *Leishmania donovani* (52). In 1911, the Brazilian doctor Gaspar Vianna identified *Leishmania braziliensis* as a new species retrieved from ulcers of many cases observed in Bauru city, and introduced the antimony tartar emetic as an unprecedented treatment for Leishmaniasis (51).

Leishmaniasis comprises a broad spectrum of clinical manifestations caused by over 20 different *Leishmania* spp and is transmitted by female sand flies, mainly *Phlebotomus* (Old world) and *Lutzomyia* (New World) (53). This complex of diseases is widespread in 98 countries with 350 million people living at risk in Asia, East Africa, South America and the Mediterranean region (54). The most relevant clinical manifestations are cutaneous (CL), mucocutaneous (MCL) and visceral (VL) leishmaniasis (Figure 1.2): CL is characterized by the presence of ulcerated lesions on the skin (Fig 1.2a); MCL leads to irreparable partial or full destruction of the mucosa of the nose, mouth (Fig 1.2b) or throat, whereas VL affects organs such as liver, spleen (Fig 1.2c) and bone-marrow, being lethal in a short period of 6 months if not treated (55). About 1 million new cases of CL and 400,000 cases of VL occur annually, leading to more than 20,000 deaths (56). About 90% of cases of MCL occur in Bolivia, Brazil, Ethiopia and Peru (57,58). VL and MCL are the most severe and disabling form of the disease respectively; CL is the commonest and most disregarded form in terms of R&D investments (59,60).
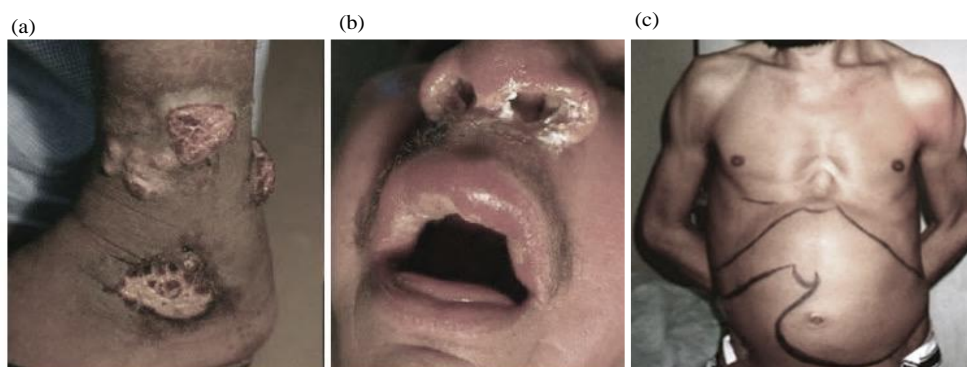
Figure 1.2 Clinical manifestations of Leishmaniasis. (a) Cutaneous Leishmaniasis: papules, nodules and infiltrated, ulcerated plaques with a granulomatous core in the left lower limb (b) Mucocutaneous Leishmaniasis: superficial ulceration of the labial and nasal mucosa and (c) Visceral Leishmaniasis:

hepatosplenomegaly. Adapted figures **a** and **b** retrieved from Murback, Nathalia Dias Negrão *et al.* 2011 (5). Figure C *credits:* Costa, JML, CPq GM-Fiocruz, Brazil.

CL cases are mostly caused by *L. major* and *L. tropica* in Asia and Africa, commonly leading to self-limiting ulcers. In the Americas, the disease is caused by several species, including *L. braziliensis, L. mexicana, L. guyanensis, L. naiffi,* and *L. amazonensis* (61). The clinical presentations range from self-healing localized skin lesions to disfiguring mucocutaneous ulcerations (59,62). Annually, about 1.2 million new CL cases are reported, and a significant number of patients develop severely disfiguring permanent scars, which results in social stigma and loss of economic productivity (56,63).

Sleeping sickness or human African trypanosomiasis (HAT) was the first reported kinetoplastid-caused illness and is intrinsically related to slave trade. The first case was described in 1734, by the English naval surgeon John Aktins (64). The association of tsetse flies and animal trypanosomiasis (nagana) was first reported by the Scottish missionary David Living in 1852, but only 40-50 years later the etiological agents of cattle-nagana (1895) and HAT were identified (1902), as well as the vectorial transmission by the tsetse flies confirmed by David Bruce (1903) (64). The human causative agent (*Trypanosoma brucei gambiense*) was named by the English physician Joseph Everett in 1902 and the species related to sleeping sickness reported by the Italian physician and pathologist Aldo Castellani, in the same year, through the detection of trypanosomes in the cerebrospinal fluid of sleeping sickness patients (64). In 1909, the German military surgeon Friedrich Karl Kleine showed the cyclical transmission of *T. brucei* in the vector (65) and one year later, the parasitologists John William Watson Stephens and Harold Benjamin Fantham described a new HAT agent, *T. b. rhodesiense* (66).

HAT is endemic in 36 African countries (67), transmitted by tsetse flies and caused by two sub-species: *T. b. gambiense* (West and Central Africa) which accounts for 97% of the total burden leading to chronic disease (g-HAT) and *T. b. rhodesiense* (East Africa) (r-HAT) (68).

Both forms of HAT progress from skin (inoculation chancre, with *in situ* trypanosome multiplication) as shown in Figure 1.3, up to the dissemination into the bloodstream and lymph (haemolymphatic, stage-1) (69). The infection gradually progresses with parasite invasion of the central nervous system (CNS) by crossing the blood-brain barrier (meningoencephalitic, stage-2), leading to sleeping disruption, severe

neuropsychiatric disorders, convulsions, and coma (69,70). When left untreated, the mortality rate of HAT is close to 100% (67,71).
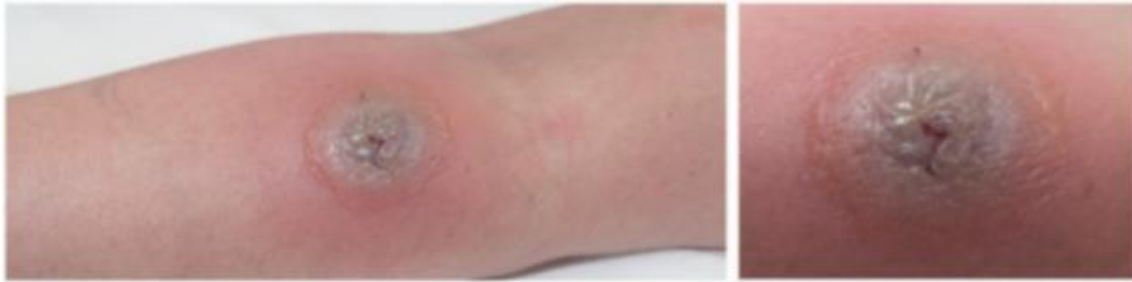
Figure 1.3 Inoculation chancre after blood meal of infected tse-tse fly, the Sleeping Sickness vector. The picture shows a well-demarcated, indurated, red nodule central bulla on the left forearm. Figure retrieved from Vingerhoets *et al* 2011, a published study case of East African trypanosomiasis in a 26-year-old traveler returning from Tanzania (6).

HAT incidence rate is difficult to determine; 300,000 new cases per year were registered in 1998 and sharply dropped to 992 cases in 2019 (72). This advance in disease elimination was a consequence of public-private efforts coordinated by WHO for epidemiological surveillance, novel diagnostic methods and population assessment for new and improved treatments free-of-charge (73–76). Still, r-HAT is extremely difficult to eliminate since cattle are the main animal reservoirs of the human parasites (77), differently from g-HAT (human reservoir) (72).

Nagana is a fatal African trypanosomiasis in cattle, mainly caused by *T. b. brucei*, together with *T. vivax* and *T. congolense*, widely distributed throughout the tsetse fly habitat (78). The infected animals, especially indigenous breeds, lose condition and become increasingly anaemic and lethargic at chronic stage (79). Nagana is a major obstacle to the economic development of affected rural areas (80), leading to an agriculture economic loss around US$ 1.0 to 1.2 billion in cattle production (81).

1.2.2 Kinetoplastid: a peculiar group

The kinetoplastid name is derived from a unique structure firstly identified by Hertha Meyer in 1958 and called kinetoplast (K) (Figure 1.4 b2, d2, e), containing a network of circular DNA (called kDNA) observed in the matrix of a large, singular and ramified mitochondria, always located close to the flagellar basal body Fig 1.4a) (9,82). The kDNA is composed by about thousand minicircles that encode guide RNAs

responsible for maxicircle transcript editing and few dozen maxicircles encoding ribosomal RNA and subunits of the respiratory complex (9,83).

The kinetoplastids are peculiar eukaryotes that diverged early (84) and present unique features of gene expression (85). They inherited from prokaryotes the polycistronic transcription of a large number of their genes (86,87). RNA polymerase I mediates the transcription of protein-coding genes (88) whereas in other eucaryotes RNA pol II is responsible for messenger RNAs (mRNA) transcription (89). Kinetoplastids also lack individual gene transcription control, which is compensated at post-transcriptional level by mRNA processing, translation and degradation (87). Also, distinct from other eukaryotic mRNA processing, trypanosomatids generate mature capped mRNAs by trans-splicing (85,90) and RNA transcribed from mitochondrial genes is subjected to deep editing (85,91).

In 2005, drafts of the sequenced genomes of *T. brucei, T. cruzi and L. major* (TriTryps) were released and contributed to better understanding of different biological features of these parasites (92). More than 50% of the genome consists of repeated sequences, such as retrotransposons and genes related to large families of surface molecules, including trans-sialidases, mucins, gp63s, and mucin-associated surface proteins (MASP) that are molecules involved in parasite:host cell interaction, infection establishment and evasion of the host immune response (92–95).

Trypanosomatid life cycles include at least two of the following major forms: trypomastigote, epimastigote, promastigote and amastigote (Figure 1.4a). In trypomastigotes, the K is located posterior to the nucleus and flagellum is attached to the cell body over most of its length (Fig 1.4a-b) (7). In epimastigote, promastigote and amastigote forms the K is located anterior to the nucleus (Fig 1.4a) (7) and the flagellum emerges at various positions according to the parasite form, which can be near the kinetoplast with the proximal part attached to the cell body (epimastigote, Fig 1.4b *1-2*) (10); close to the anterior end of the cell and mostly free from the elongated body (promastigote) and entirely located in the flagellar pocket (10) (amastigote, Fig 1.4a,e).

Regarding characteristic trypanosomatid structures, there are specialized organelles called glycosomes where glycolytic processes occur that normally take place in the cytosol of other eukaryotes. Also, another typic characteristic is the presence of vacuolar structures named acidocalcisomes containing electron-dense deposits (Fig 1.4e) and involved in ion storage required for pH homeostasis and osmoregulation (96).

The secretory pathway is formed by the endoplasmic reticulum, Golgi complex (Fig 1.4 b3) and a system of vesicles that migrate toward the flagellar pocket (FP) where they fuse and discharge their contents into the FP (Fig 1.4 c2) (9,97). The endocytosis occurs through the FP but in epimastigotes, the main uptake processes arise in the cytostome, an opening that emerges from the plasma membrane (Fig 1.4 c3) and followed by a deeper invagination, called the 'cytopharynx'. The internalized molecules are then shuttled to subsequently early and late endosomes and lysosomes (called reservosomes (RE) in epimastigotes) (Fig 1.4 c4), for metabolization (98).
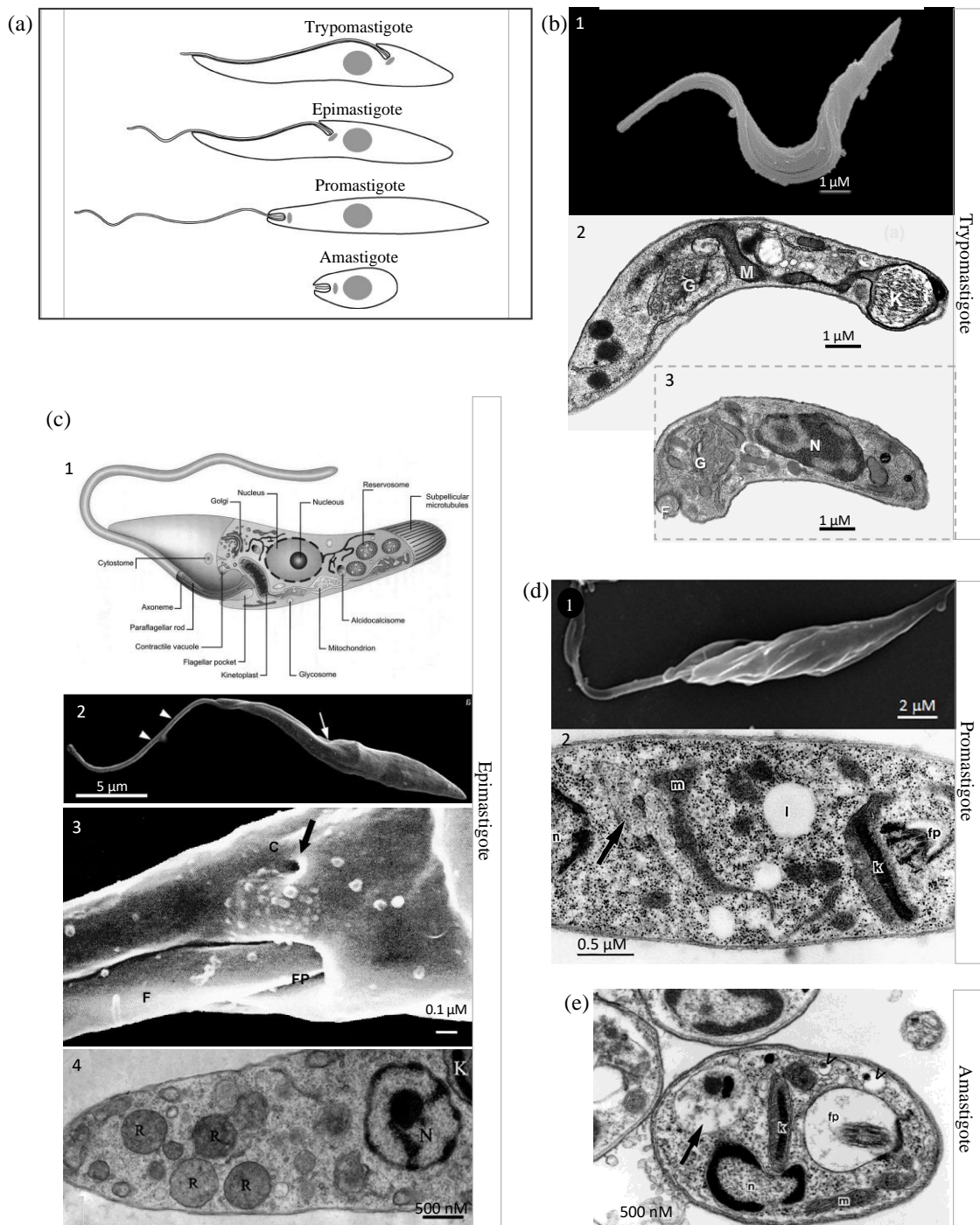
Figure 1.4 *Major kinetoplastid forms and structures* **(a)** Cartoon of main kinetoplastid cell forms with defined nucleus (gray circle), kinetoplast (gray ellipse), and flagellum emergence points from the basal body (Hayes *et al* 2014 (7)). The kinetoplasts are disk-shape in **(b2)** trypomastigotes and bar-shape in **(c1 & 4)** epimastigotes**, (d2)** promastigotes and **(e)** amastigotes. Electron micrographs of **(b)** *T. cruzi* BT trypomastigotes, with *1* flagellum attached to the cell body along most of its length and *2,3* typical organelles present in trypanosomatids, such as Golgi complex, nucleus, and mitochondria. Credits: Camila Cardoso Santos (Santos *et al.* 2018 (8)) **(c)** *T. cruzi* epimastigotes, *1* with core structures and organelles represented in the diagram (de Souza, 2008 (9)), *2* the flagellum (arrowheads), emerges from the flagellar pocket (arrow) and detach from the parasite body (Miranda Rocha *et al* 2010 (10)), *3* Cytostome (VataruNakamura *et al.* 2005, (11)) and *4* Reservosomes localized in the posterior part of epimastigotes (Zuma *et al* 2021 (12); adapted from de Souza, 2009 (13)); **(d)** promastigotes of *Leishmania sp* exhibiting *1* elongated body and emerging flagellum (Marinho *et al* 2014, (14)) and internal structures *2* besides its **(e)** round-shape amastigote counterparts, where acidocalcisomes are pointed with **(<)** (Alberio *et al* 2004, (15)). Figures **b1, c2** and **d1** were obtained by scanning electron microscopy (SEM), and **b2-3**, **c3-4**, **d2** and **e,** by transmission electron microscopy (TEM); and adapted from the quoted references. Legend: Nucleus (N), Kinetoplast (K), Mitochondrion (M), Reservosome (R), Golgi complex (G); Cytostome (C); Flagellar pocket (FP), Flagellum (F) and lipid inclusion (l).

1.2.3   The life cycle of trypanosomatids

Trypanosomatids have a heteroxenic life cycle and different parasite forms as discussed before. The insect and vertebrate stages of *L. major, T. cruzi* and *T. brucei* are portrayed in figure 1.5 and the vectors involved in transmission of leishmaniasis, American and African trypanosomiasis are shown in figure 1.6.

As shown in the outer cycle of figure 1.5, metacyclic *Leishmania sp.* promastigotes are introduced intradermally into the vertebrate host during the blood feeding of an infected female phlebotomine (Figure 1.6a). Neutrophils are firstly recruited to the bite site, engulfing the parasites, and providing a temporary shelter. Infected neutrophils and free parasites are then taken up by other professional phagocytic cells, like macrophages and dendritic cells. Briefly, after initial attachment, *Leishmania* promastigotes initiate caveolae-dependent phagocytosis in host macrophages (99). Parasite lipophosphoglycans (LPG) are inserted into the phagosome, transitionally preventing the lysosome/endosomes fusion and acquisition of cathepsin D and vesicular proton-ATPases into the newly formed *Leishmania*-containing vacuoles, avoiding intracellular phagosome acidification and microbicidal activity. This provides sufficient time for promastigotes to differentiate into amastigotes (94,100). Although *Leishmania* infects a variety of host cell types, macrophages, neutrophils and dendritic cells are the

most important hosts that regulate the outcome of infection. Due to their longer life span as compared to the other phagocytes, macrophages are the most prominent host cell for parasite proliferation (101). The amastigotes multiply within the phagolysosomes and after a number of cell cycles are released into the extracellular milieu following host cell rupture. Release amastigotes next invade new phagocytes. Different host cell receptors have been implicated in *Leishmania* recognition, including receptors for mannose-fucose ligands, complement and fibronectin (102,103). The phosphatidylserine exposure on the *Leishmania* surface allows silent entry in phagocytic cells avoiding host cell activation (104). Interestingly, there are many parasite genetic and host immunological parameters that play a role in the clinical outcome, determining whether conditions are self-healing or advance to disseminated cutaneous or visceral leishmaniasis (55,105). The transmission cycle is completed when infected phagocytes or extracellular parasites are taken up by feeding sand flies, hosting a complex development in the sand flies gut (106), with differentiation into infective, metacyclic promastigotes in the thoracic midgut and cardia of the proventriculus (107).

The *Trypanosoma cruzi* life cycle is shown in the mid circle of figure 1.5. During vectorial transmission, after blood meal, the infected triatomine vector or "kissing" bug (Figure 1.6b) release metacyclic trypomastigotes (MT) in feces and urine near the site of the bite wound. The parasites gain access through small wounds caused by scratching or through intact mucosal membranes and infected nucleated host cells (108). Due to consumption of contaminated beverages, MTs can invade stomach epithelial cells. Many different ligands and receptor signaling systems are reported in the *T. cruzi*-host cell interaction (109–112). One of them involves the parasite trans-sialidase (TS). During parasite adhesion, surface sialic acid residues of host cells (or even from the plasma) are transferred to various parasite surface mucins by *T. cruzi* TS. The parasite sialylation allows its binding to host receptors, escape from the parasitophorous vacuole (PV) into the host cell cytosol and evasion from host immune responses (113,114). During the steps of parasite adhesion and invasion, many different cell signaling responses are triggered, involving either lysosomal recruitment at the invasion site or invagination/projection of the host plasma membrane followed by the localization of the parasite in a PV that fuses with endosomes and lysosomes (115). After the escape from the PV, trypomastigotes fully differentiate into proliferative amastigotes and, after several replication cycles, back to trypomastigotes that are the main parasite form released after host cell rupture. Parasites then spread into different tissues and organs through the blood and lymphatic systems, being able to infect new host cells (115). The life cycle is completed when

trypomastigotes or amastigotes are ingested by the vector, wherein they differentiate back into replicative epimastigotes in the midgut and migrate to accomplish final MT differentiation in the hindgut (116).

Finally, *T. brucei* life cycle is portrayed in the inner cycle of figure 1.5. During a blood meal on the mammalian host, an infected tsetse fly (genus *Glossina*) (Figure 1.6c) injects metacyclic trypomastigotes into skin (65,117). In the vertebrate host, metacyclic forms differentiate into the long slender multiplicative trypomastigotes that give rise to parasitemia peaks. These forms can be carried to other tissues, including the CNS, and undergo morphological and biochemical differentiation to non-replicating bloodstream trypomastigote (BT) stumpy forms which is triggered by quorum sensing (78). The tsetse fly becomes infected with stumpy forms during its blood meal on an infected mammalian host (118). In the fly's midgut, the parasite transforms into proliferative procyclic trypomastigotes, migrate to the ectoperitrophic space and finally differentiate into epimastigotes that attach to the salivary gland epithelium (119). An asymmetric division next gives rise to metacyclic trypomastigotes that are free-living in the saliva and synthesize variable surface glycoproteins (VSG) to again become infective for the vertebrate host (120). Recent findings showed that proliferating slender stages are also able to complete the complex life cycle in the fly as successfully as the stumpy stage, and require only a single parasite for productive infection (121,122). Protection of BT against the complement cascade and host immune response machinery is mediated by the VSG coat (93). These glycoproteins, anchored by glycosyl phosphatidyl inositol groups, are encoded by over 1000 different genes and can be transcribed from 20 expression sites of which only one is active at a time (123).
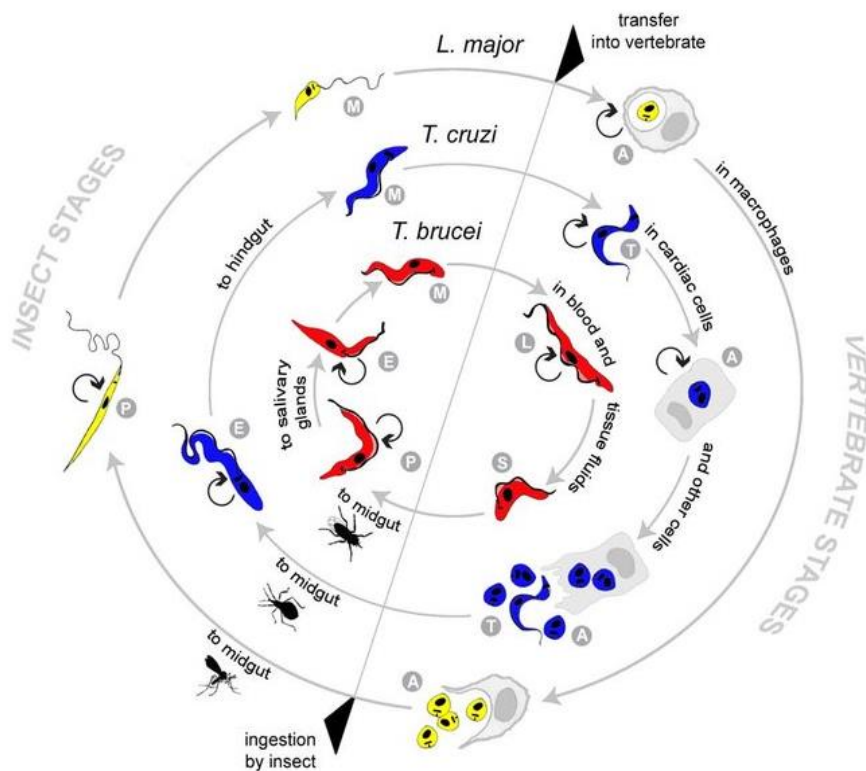
Figure 1.5 Tritryps life cycle with insect and vertebrate parasite stages in extra and intracellular environment: (A) Amastigote; (P) Promastigote; (M) Metacyclic; (E) Epimastigote; (T) Bloodstream trypomastigote; (L) Long, slender and (S) Short, stumpy trypomastigotes. Retrieved from El-Sayed *et al.* 2005, Supplementary Figure 1 (16).
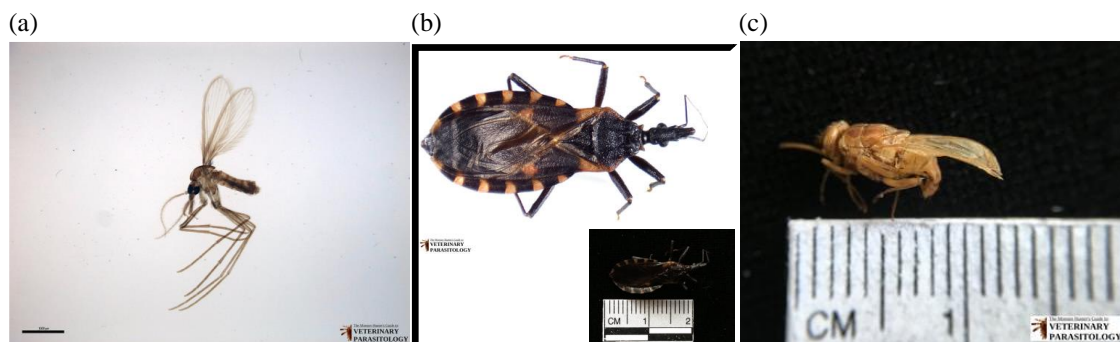
Figure 1.6 Leishmaniasis, American and African trypanosomiasis vectors. (a) *Lutzomyia longipalpis* female sand fly, 12.5× magnification, 1,000 μm scale bar (b) *Triatoma sp*. (kissing bug), 2 cm scale bar (c) *Glossina sp* (tsetse fly), 2 cm scale bar. All images were retrieved from https://www.veterinaryparasitology.com on the 27/09/2021; credits © Lance Wheeler, 2018; Photographer: Lance Wheeler; Owner of Specimen: Texas A&M College of Veterinary Medicine, Department of Veterinary Pathobiology.

1.2.4 Current available treatments and drawbacks

46

There is an urgent need to identify new therapeutic alternatives to treat the above-described NTDs since the available medicines exhibit at least one of the following drawbacks: high toxicity, low efficacy, high cost, long treatment, painful administration and inadequacy for prophylaxis (71,124–127). In addition, these parasites display high genetic diversity with multiple species (for HAT (128) and *Leishmania* (56,62,63,129)) and strains (belonging to the different VII *T. cruzi* discrete type units (DTUs)(130,131), resulting in resistance and/or treatment failure. The international scientific community is making efforts to explore new treatment options but only few are under trial or recently released, such as the combined therapy using fexinidazole and nifurtimox (Nif) and the combo Nif-eflornithine for stage-2 HAT, sodium-stibogluconate and paromomycin for VL and benznidazole pediatric formulation for CD. However, those efforts do not fully comply with the current demand for a novel (ideally) orally available drug that could be administered for short periods of time, with safer and more efficacious profile than the current therapies (132).

Pentavalent antimonials (sodium stibogluconate (SSG) and meglumine antimoniate) are the first-line treatment for CL and in refractory cases alternative agents include the anti-cancer drug miltefosine (MIL) (17), the antifungal amphotericin B deoxycholate (AmB) and pentamidine isethionate (Pt) (133,134). However, all induce severe adverse effects (62,135). The most frequently reported for pentavalent antimonials and pentamidine are musculoskeletal pain, gastrointestinal disturbances, headache and fatigue; cardio and hepatotoxicity (136). Mild side effects such as nausea, vomit, decrease in appetite were registered for the potential teratogenic drug MIL (137).

The safer liposomal formulation of AmB is highly costly and still under evaluation for effectiveness against CL (133). The treatment of choice depends on the clinical CL manifestation (local or diffuse), recurrent cases and parasite species (63,138). For instance, intradermal administration of pentavalent antimonials is the first choice to treat lesions of Old (OW) and New World (NW) CL, the last caused by *L. naiffi*, *L. chagasi*, and *L. mexicana spp.* (61). A systemic approach with MIL or antimonial/pentamidine/ AmB is preferred in more severe cases of multiple lesions or mucosal involvement, mostly related to *L. major* (OW) or *L. panamensis*, *L. amazonensis*, and *L. guyanensis* species (NW) (139,140).

Pentavalent antimonials were used to treat leishmaniasis the first time on and remain the standard antileishmanial treatment around the world for all forms of leishmaniasis (141). Early findings suggested that pentavalent antimonial mode-of-action

(MoA) is related to the inhibition of *Leishmania sp.* type I DNA topoisomerase (142) and to the enhancement of antigen presentation through T cell stimulation (143). In fact, pentavalent antimonial is a prodrug that contains Sb(V) that is reduced into active trivalent antimonial (Sb(III)) by the amastigotes and/or macrophages (138). Sb(III) mechanism of action is involved to parasite redox potential unbalance by inducing the export of both trypanothione and glutathione thiols– components of the parasite antioxidant machinery (144) and inhibiting the trypanothione reductase enzyme (145), which leads to parasite death by oxidative stress (145). Leishmaniasis treatment failure with pentavalent antimony is widely reported in different regions, reaching 65% in Bihar and 24% in Nepal (143).

Therefore, its use has been discontinued in India since 2005 (146). Drug resistance (DR) seems to be due to multiple factors (134,146). The membrane carrier aquaglyceroporin 1 (AQP1) modulates antimonial uptake (147) (Figure 1.7) and its downregulation or gene deletion is related to a resistant profile (17). Overexpression of the antimony resistance markers (ARM) 56 and 58 is correlated to decreased drug uptake (148). DR is also associated with Sb efflux or sequestration by transporters belonging to ATP-binding cassette (ABC) family, including the "multidrug resistance-associated protein A" (MRPA) (17), together with increased production of intracellular thiols to bind to Sb(III) (149,150). Sb(V) efflux and parasitic persistence are likewise triggered by parasite glycans, that contribute to the upregulation of host cell anti-inflammatory mediators such as the cytokine IL-10, provoking overexpression of multidrug resistance protein 1 (MDR1) (151).
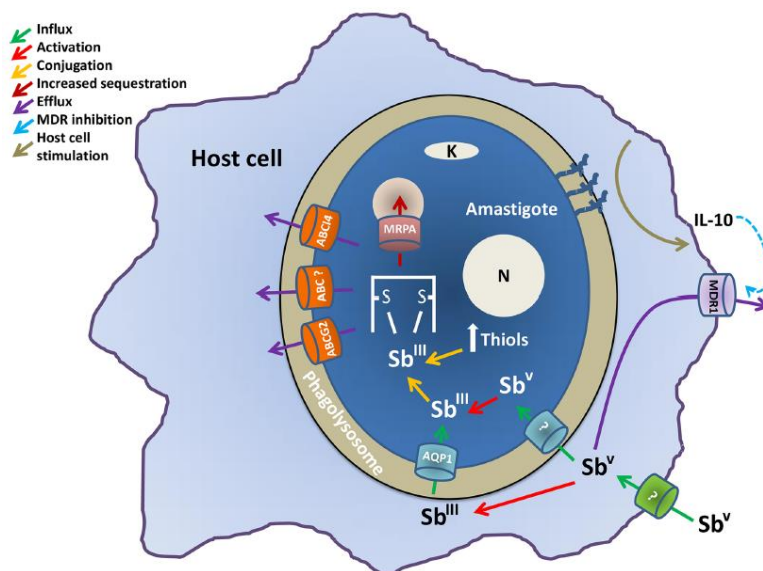
Figure 1.7 Molecular mechanisms of antimonial DR in *Leishmania*. The figure illustrates an amastigote inside a macrophage phagolysosome, the influx and activation of antimony in the parasite, and the intracellular mechanisms conveying a resistant phenotype. ABC, ATP-binding cassette; MRPA, multidrug resistance-associated protein A; AQP, aquaporin; DR, drug resistance; IL-10, interleukin 10; MDR1, multidrug resistance protein 1. Figure and legend retrieved from Ponte-Sucre *et al.* 2017 (17).

Up to now, the only oral and less toxic drug approved by FDA to treat leishmaniasis is MIL; which is still unavailable in many poor countries (60). Since 2002, MIL replaced SSG as a first choice for VL treatment with a cure rate close to 94% (152); but decreasing it 4% one decade later (153). MIL uptake (described in literature for *L. donovani*) is related to the P-type ATPase known as Leishmania Miltefosine transporter (LMT)/Ros3 machinery involved in phospholipid translocation (154). Its MoA has been attributed to host immunomodulation and to different parasite targets such as fatty acid and sterol metabolisms, cytochrome C oxidase inhibition and induction of apoptosis-like death in *L. donovani* (155,156). MIL mechanisms of DR are mainly linked to drug uptake decrease by LMT and/or Ros3 mutation (157), efflux increase mediated by the overexpression of the ABC transporter P-glycoprotein (154), besides changes in the levels of parasite ergosterol, fatty acids length and saturation (158).

Systemic pentamidine is the treatment of choice for *L. guyanensis* lesions in Suriname and Guyana, and second choice for antimonial resistant cases; yet its efficacy is low, around 50–60% in Manaus, Brazil (159). Its antileishmanial MoA is possibly related to polyamine biosynthesis, minor groove kDNA binding and effects on the mitochondrial membrane potential (160). Mechanisms of drug resistance are likely related to PRP1 ABC transporter upregulation (161) and drug extrusion from the mitochondrion (162).

Amphotericin B deoxycholate is a potent leishmanicidal drug, with its use limited by serious side effects including high nephrotoxicity (163). It is still an alternative therapy in refractory CL in regions where the cost of liposomal amphotericin is prohibitive (164). AmB can interfere in membrane permeability of both parasites and macrophages due to sterol sequestration (165,166). DR has been attributed to the upregulation of stress proteins and glycolytic enzymes that play a role in intracellular survival and vesicular trafficking of the parasites (167).

Last clinical trials for CL were mostly based on drug repurposing and/or combination but unfortunately the overall findings were not very successful to demonstrate an improvement of therapeutic efficacy, such as the combination of

pentavalent antimonial with imiquimod (168) and the topical use of 3% AmB (169). A phase-II clinical trial regarding a shorter course of oral MIL administrated in combination with thermotherapy, conducted in Peru and Colombia, ended in 2019 but the outcomes were not published yet (170). Topical paromomycin was shown to be a viable alternative treatment for CL caused by New World species, but still leading to less than 80% of cure rate (171). A few new small molecules are currently in preclinical and clinical development against *Leishmania*. One example is the first-in-class kinetoplastid-selective proteasome inhibitor LXE408. LXE408 was discovered by Novartis with financial support from the Welcome Trust. LXE408 is efficacious in the murine model of CL, and it is under clinical evaluation for treatment of VL (172).

For over 50 years, the nitroderivatives nifurtimox (Nif) (5-nitrofurane, Bayer 2502; Bayer, Germany) and benznidazole (Bz) (2-nitroimidazole; Pharmaceutical Laboratory of the State of Pernambuco [LAFEPE], Brazil, ELEA/Mundo Sano, Argentina) have been the medication used for the treatment of CD (173,174). Since 2011, pediatric formulation of Bz (and more recently of Nif evaluated by CHICO clinical trial (175)) was implemented, reducing the risks of incorrect administration of the drug to children affected by CD (176). Among their limitations to treat CD, both drugs have low efficacy in the late chronic stage, restricting the therapeutic benefit for millions of chronic infected individuals (177,178). Also, they require long-term administration and elicit several side effects such as anorexia, psychic depressions, convulsions (179,180), cutaneous and neurological changes (polyneuritis) (3,181), leading to low patient adherence or discontinuation of treatment. They are contraindicated in pregnant women and in people suffering from liver or kidney failure or neurological disorders (174,182,183). As shown in figure 1.8, the pro-drug bioactivation process is triggered by the mitochondrion NADH-dependent type-I nitroreductase (TcNTR) (124), generating reactive metabolites such as the radicals RNO^{2-} and hydronitroxyl (RNHO) for Nif and Bz respectively, inducing a toxic environment to the parasite. Reactions of RNO^{2-} with oxygen can generate superoxide anion O^{2-} after redox cycles. RNHO, on the other hand, comes from a nitro-reductive process followed by the formation of corresponding amino derivatives during biotransformation (174,184).
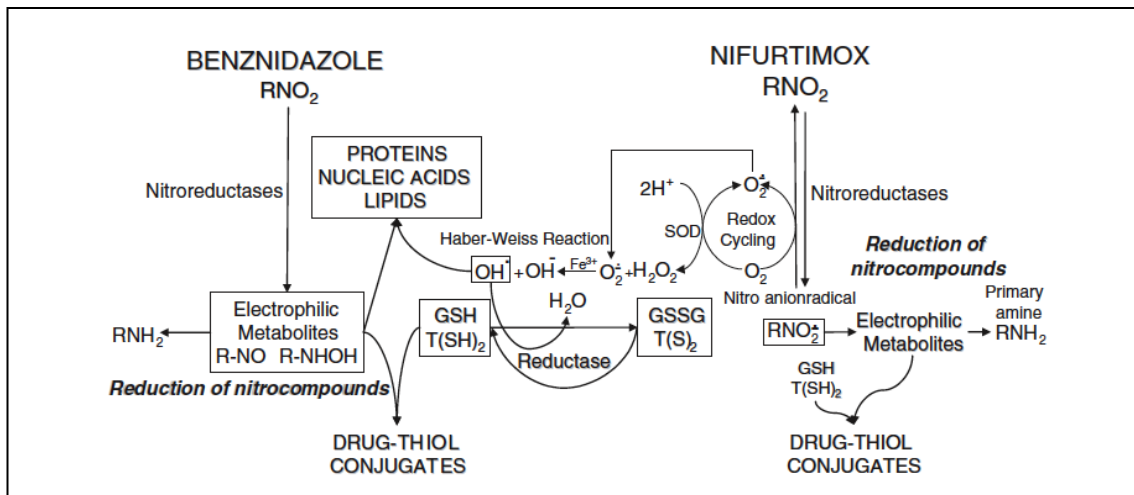
Figure 1.8 Benznidazole and nifurtimox metabolism in *T. cruzi*. The nitro group of both antichagasic drugs is reduced to free radicals or electrophilic metabolites by *T. cruzi* cytochrome P450-related nitroreductases. The nifurtimox-derived free radicals may undergo redox cycling with oxygen, and it is produced H_2O_2 by the further action of superoxide dismutase (SOD). The produced oxygen derived free radicals and electrophilic metabolites bind to intracellular macromolecules damaging them. In the parasite, trypanothione ($T(SH)_2$) and glutathione (GSH) neutralize the Nif and Bz derived metabolites (by conjugation) producing drug-thiol conjugates that will be further metabolized in the mammal host. Free radicals are neutralized by oxidation of reduced GSH or $T(SH)_2$. Glutathione and trypanothione reductases reduce the oxidized GSSG and $T(S)_2$. Retrieved from Maya *et al.* 2007 (18).

Both Bz and Nif efficiency varies for the parasite DTUs isolated from different hosts and geographic areas (185–187) and the occurrence of naturally resistant strains is well established (188,189). Resistance has been related to distinct aspects including differences in expression of: NTR1 (188); superoxide dismutase enzymes, as they remove excess of O_2 generated by oxidative stress (190); host "old yellow enzyme" (TcOYE protein), which generates toxic radicals against the parasite (191) and interferes in host-parasite interaction (192); unidirectional membrane transporters such as AQP1, AQP9 and ABC-like transporters (193,194), among others including DNA repair enzymes (195). Those mechanisms are part of a complex system in which distinct mechanisms act together to generate the resistance phenotype (188). Perspectives for clinical trials with new drug entities to treat CD rely on short-course regimens of fexinidazole for adults [Phase-II Proof-of-Concept (PoC) study], the first oral drug recently approved for *g*-HAT (in 2018), and of oxaborole (DNDI-6148), a lead candidate for VL and CL, still to be evaluated in human Phase-I studies (196).

Pentamidine (1940) and suramin (1920) are ancient drugs used for decades to treat first stage of *g*-HAT and *r*-HAT respectively, despite their undesirable side effects

including hepatotoxicity, nephrotoxicity, blindness and allergic reactions (78,197). They are not effective against the second CNS stage, since they cannot cross the blood–brain barrier. The arsenic derivative melarsoprol (discovered in 1949) was used to treat second stage of both *g*- and *r*-HAT, until being discontinued for *g*-HAT due to high death rate of patients (5%), mainly caused by reactive encephalopathy (198). Other side effects may include fever, headache, joint pain, gastrointestinal disturbances, renal damage, and hypertension (78). Eflornithine was launched as a less toxic alternative for 2nd stage g-HAT as a monotherapy (1990), or combined with nifurtimox (NECT) in 2009 (199). Even though NECT contributed to a reduction in treatment duration and number of infusions, the regimen is complex besides cumbersome to apply, requiring specialized hospital administration and trained staff (73).

As above briefly mentioned, the recent big mark for g-HAT therapy is fexinidazole. It is administrated orally for 10 days as recommended by the European Medicines Agency for both stages of *g*-HAT. Since 2019, fexinidazole was included in the WHO Essential medicines list and WHO guidelines for therapy of HAT (73,200). Acoziborole is a lead identified from Anacor chemical library and is under clinical trial for second stage *g*-HAT as a single oral dose (201). Fexinidazole is also in clinical trial for *r*-HAT, but so far the toxic melarsoprol remains the only drug for second-stage *r*-HAT (73).

Most aspects related to the mechanism-of-action of the anti-*T. brucei* drugs remain unknown. As described for *Leishmania*, pentamidine acts in *T. brucei* by mitochondrion destabilization, kDNA damage and glycosomal enzyme inhibition similar to melarsoprol (128). This also affects trypanosome redox metabolism (phosphogluconate dehydrogenase and trypanothione reductase inhibition) and mitosis (126,202). Eflornithine irreversibly inhibits ornithine decarboxylase (ODC), an enzyme responsible for the synthesis of polyamines (203), affecting parasite division and proliferation (128).

In NECT therapy, nifurtimox induces oxidative attack (as reported for *T. cruzi*) upon weakened trypanosomes treated with eflornithine (128). In *T. brucei*, fexinidazole derived metabolites sulfoxide and sulfone are generated by the *bacterial-like* nitroreductases and are capable of damaging DNA and proteins (204,205).

Drug uptake transporters, as portraited in figure 1.9, are frequently involved in the mechanisms of drug resistance in *T. brucei*. Both pentamidine and melarsoprol enter by two transporters: P2 aminopurine transporter encoded by *TbAT1* (*AT1P2*) and *aquaglyceroporin 2* (*AQP 2*) (Fig 1.9) (19). The influence of aquaglyceroporin

transporters on cross-resistance to pentamidine and melarsoprol was inferred by *in vitro* RNAi loss-of-function studies (206). Later, rearrangements of the *TbAQP2/TbAQP3* locus accompanied by *TbAQP2* gene loss were reported in *T. b. gambiense* conferring a higher resistance to both drugs (207). Due to the high molecular weight and negative charge of suramin, its uptake is mediated by endocytosis, and the invariant surface glycoprotein (ISG75) is its major surface receptor (19). It was recently demonstrated that the variant surface glycoprotein (VSG^Sur) expression has a major impact on suramin uptake, and that its expression in *T. brucei* was synergistic to ISG75 downregulation leading to drug resistance (208). Finally, loss of the amino acid transporter (TbAAT6) (Fig 9) responsible for eflornithine uptake, has been attributed to drug resistance but needs further confirmation (19).
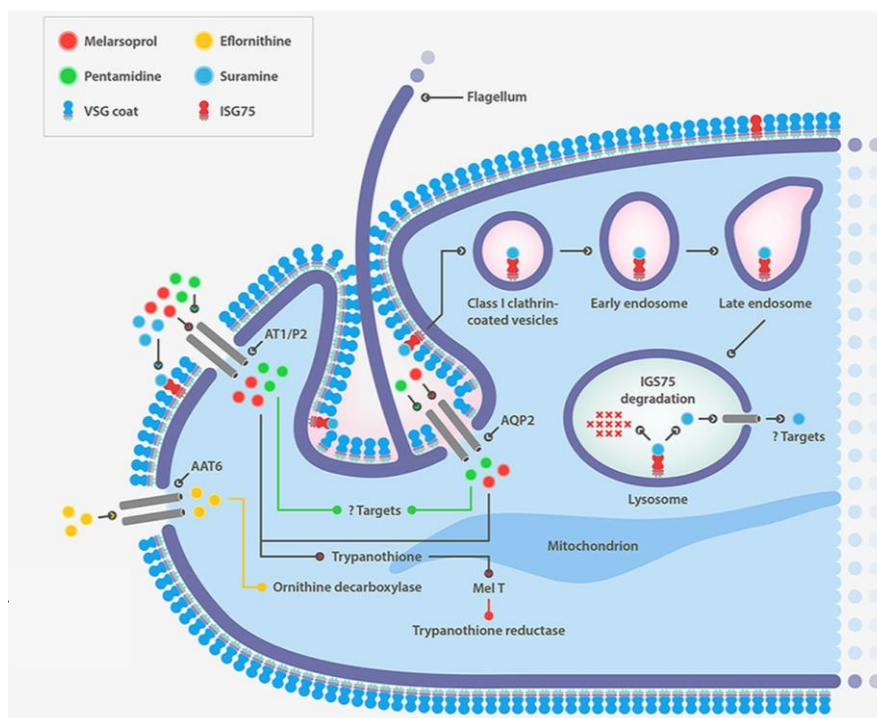
Figure 1.9 Drug transporters in *T. brucei*. AQP2 promotes the uptake of suramin, melarsoprol, and pentamidine, the last two drugs also taken by AT1/P2. ISG75 is the major surface receptor for suramin uptake mediated by endocytosis and AAT6, responsible for eflornithine uptake. *Legend* AQP2: aquaglyceroporin 2 transporter, P2: aminopurine transporter, AAT6: amino acid transporter, ISG75: invariant surface glycoprotein 75. (Adapted from Garcia-Salcedo *et al.* 2020 (19).

2   RESEARCH PROPOSAL: OBJECTIVES AND OUTLINE

2.3   Main Objective

Our aim was to investigate the antiparasitic effect of 7-nitroderivative scaffold-driven compounds, 32 GNF5343-*based shape* hits, a series of 21 natural product-inspired phenyl sulfonyl acetamides and acetates, and 2 pentacyclic triterpenoids in experimental models of CL. Another 16 optimized C7-substituted nucleoside analogues (named FH8512, FH10678, FH11708, FH11709, FH11710, FH11711, FH11712, FH10714, FH10715, FH11702, FH11703, FH11704, FH11705, FH11706, FH11707 and JB588) were envisaged to be evaluated in CD/HAT disease models, to provide a strong PoC for the most promising candidates with metabolic stability assessment, different drug therapy regimens to obtain sterile cure and MoA studies to inspire further molecule optimization.

2.4   Specific Objectives

1. To evaluate the leishmanicidal activity and selectivity of novel compounds against *L. amazonensis* (strain *LTB0016*) *in vitro* upon:

> 1.1 Free amastigotes (*ex vivo*) collected from mouse lesions.
>
> 1.2 Intracellular forms using primary cultures of peritoneal macrophages as mammalian host cells.

2. To analyze the most promising drug candidates in a BALB/c mouse CL model infected with *L. amazonensis*, applying a 14-day oral treatment schedule (reference-drug treatment period for lesion regression).

3. To evaluate the activity effect and selectivity of nucleoside analogues against Nagana/HAT and CD causative agents in *in vitro* assay systems using clinically relevant forms such as:

> 3.1 Trypomastigotes of *T. b. brucei* and *T. b. rhodesiense*.
>
> 3.2 Intracellular amastigote forms *(*Tulahuen strain in L929 cells) and bloodstream trypomastigotes (Y train) of *T. cruzi*.

4. In depth exploration through different *in vitro* approaches (combined therapy, washout assays, and pre-treatment of bloodstream trypomastigotes) of the phenotypic effects of a promising anti-*T. cruzi* nucleoside analogue (FH8512).

5. To assess the *in vitro* metabolic stability of the promising nucleoside analogues using mouse and human microsomal fractions in the presence of Phase-I and Phase-II-metabolic enzymes.

6. To explore efficacy of a promising anti-*T. cruzi* nucleoside analogue (FH8512) in a mouse model of acute Chagas disease.

7. To analyze the MoA in *T. brucei* of the most active nucleoside analogues.

8. To evaluate/validate putative targets in *T. cruzi* by gene editing of candidate genes (identified in *T. brucei*).

2.5 Outline

The content developed in the thesis will be next split into four Chapters, each divided into six sections: State-of-the-art, Research Objective, Material & Methods, Results, Discussion and Conclusion. Chapter 3: "*Phenotypic Assay upon Cutaneous Leishmaniasis*" covers specific objectives 1 and 2, related to *in vitro* and *in vivo* efficacy of the tested compounds in CL experimental models respectively. Chapter 4: "*Phenotypic analysis of Nucleoside analogs for Chagas disease and Sleeping sickness*" includes specific objectives 3, 4 and 5, related to phenotypic screening against a panel of trypanosomatids, followed by metabolic stability assessment of the most promising candidates, and finally detailed phenotypic evaluation of FH8512 (Cpd**1**) including: Bz combination *in vitro* and *in vivo*, sterile cure evaluation by washout experiments, impact on trypomastigote fitness by pre-treatment prior to infection and prolonged periods of treatment *in vivo*. In Chapter 5: "*Unravelling the mode-of-action of antitrypanosomal nucleoside analogs using RNA interference*" the MoA of selected nucleoside analogues FH8512, FH11706, FH10714 and JB588 – active against both *T. brucei* and *T. cruzi* species – were first evaluated upon a genome-wide *T. brucei* RNAi library (specific objective 7) and then, in Chapter 6: "*Attempts to experimentally validate identified drug targets by gene editing in T. cruzi*", by target knockout in a *T. cruzi* strain constitutively expressing the CRISPR/Cas9 machinery, as described in specific objective 8.

Part 2

Chapter 3: Search for new drug candidates for Cutaneous Leishmaniasis

Chapter 4: Phenotypic analysis of nucleoside analogs against experimental CD and HAT

Chapter 5: Nucleoside analogues: mode-of-action in *T. brucei*

Chapter 6: Attempts to experimentally validate identified drug targets by gene editing in *T. cruzi*

3 Search for new drug candidates for Cutaneous Leishmaniasis

The chapter was based on the following (3) published manuscripts

(20) **Cardoso Santos C**, Batista MM, Ullah AI, Reddy TRK, Soeiro MdNC. Drug screening using shape-based virtual screening and *in vitro* experimental models of cutaneous Leishmaniasis. Parasitology. 2021; 148. 98–104. https://doi.org/10.1017/S0031182020001900

(21) **Cardoso Santos C**, Zhang H. Batista MM, de Oliveira GM, Demarque KC, da Silva-Gomes NL, Moreira OC, Ogungbe IV, Soeiro MdNC. *In vitro* and *in vivo* evaluation of an adamantyl based phenyl sulfonyl acetamide against cutaneous leishmaniasis models of *Leishmania amazonensis*. Antimicrob Agents Chemother. 2020; 64:e01188-20. https://doi.org/10.1128/AAC.01188-20

(62) **Cardoso Santos C**; Zhang H; Batista MM; de Oliveira GM; Demarque KC; da Silva-Gomes NL; Moreira OC Ogungbe IV and Soeiro MdNC. Phenotypic investigation of 4 nitrophenylacetyl- and 4-nitro-1H-imidazoyl-based compounds as antileishmanial agents. Parasitology. Accepted Dec 2021, published Feb 2022; 3:1-6. doi: 10.1017/S0031182021002079.

3.1 State-of-the-art

As detailed in the Introduction chapter, CL is one of the most mistreated illnesses among the NTDs. The large variation of drug susceptibility among the diverse parasite species makes the drug discovery (DD) process even more difficult (61,209). First-line CL treatment includes the pentavalent antimonials sodium stibogluconate and meglumine antimoniate, which present several drawbacks in terms of efficacy, safety (cardiotoxicity and hepatotoxicity), and protracted periods of drug administration (135). Alternative systemic agents such as Pt and AmB are also limited by severe adverse effects (61). Thus, there is an urgent need for safer, more selective, and easily accessible therapies for CL.

3.1.1 Drug discovery approaches

Preclinical approaches used to identify potential drug candidates are mainly based on molecular target-based (hypothesis-driven) and phenotypic (empirical) screenings, relying on phenotypic analysis in whole cell systems and animal models (210). The latter is important for identification of first-in-class molecules in the early drug discovery phase, followed by increased efforts to address specific hypotheses regarding target identification and molecular mechanism of action (MMOA), so that the drug target of the best-in-class molecules is known (210,211).

Natural products provide new inspiring scaffolds and starting points for new drug candidates (212) and renewed sources for compound optimization (211). Due to the complexity and scarcity of highly active and selective agents, follow-up studies are usually difficult and rarely pursued in DD for NTDs, making updated techniques of computer-aided drug design complementary to the exploration of natural libraries and product synthesis optimization (21,213,214).

Computer-aided drug design represents a promising strategy to identify active compounds and has been successfully employed in the discovery of new anti-fungal and anti-bacterial agents (211). As a starting point, it is based on the principle that diverse structures sharing similar shape and electrostatic potential surface or topology will have high probability to bind to the same pocket and consequently share a similar activity to the query compound (215). The main advantages of this approach are that it only needs a

single active compound as the starting point and that a target crystal structure is not a requirement.

3.1.2 Leishmania amazonensis as a model for CL drug screening

The entire process of drug discovery is extremely costly and takes at least one decade of pre-clinical and clinical studies: 1 out of 10.000 drug candidates succeeds in this long flowchart and finally reaches the market successfully (216). In this context, more reliable and reproducible experimental models (*in vitro* and *in vivo*) are needed to obtain a better correlation between pre-clinical and clinical outcomes of novel antiparasitic drugs (217,218). Presently, our analysis was performed on *L. amazonensis* using two consecutive approaches: evaluating the activity against *ex vivo* amastigotes collected from mouse lesions and on intracellular forms using primary cultures of mouse peritoneal macrophages as mammalian host cells for these obligate intracellular parasites (219). The infection of peritoneal macrophages is a well-standardized *in vitro* experimental model for CL closely related to *in vivo* conditions (125,220,221). Also, *L. amazonensis* was chosen since, although in Asia and Africa continents CL is mainly caused by *L. major* and *L. tropica*, it is a major cause of the disease in the Americas (58,61).

3.1.3 The molecules assessed in this study

Ligand-based shape screenings. Due to the limited information on drug targets in *L. amazonensis*, ligand-based shape screening was one of the chosen approaches for hit identification. It was carried out using compound GNF5343, an oxazolo[4,5-b]pyridine derivative (Figure 3.1) very active against the kinetoplastid parasites (*T. cruzi* 50% inhibitory concentrations (IC$_{50}$) equal to 75±0.8 nM, *T. brucei* (IC$_{50}$ = 150±7.5 nM) and *L. donovani* (IC$_{50}$ = 7.3±0.6 nM), possibly acting on a conserved target across these species (222,223). A set of 60,000 chemically diverse compounds from the Asinex database (http://www.asinex.com/) were screened *in silico*, ranked based on the phase similarity score and then 32 were evaluated *in vitro* in *L. amazonensis* CL models, including the active analog (Cp**1**) of the query compound (GNF5343) and the hit Cp**2**. These compounds were visually inspected to assess their structural diversity and synthetic accessibility (20).

Natural product-inspired synthetic products. A series of 21 natural product-inspired phenyl sulfonyl acetamides and acetates, as well as two pentacyclic triterpenoids

(Fig 3.1) previously reported to be highly active against kinetoplastids including *T. brucei* (214,224) were evaluated in *L. amazonensis in vitro* models.

     Nitroaromatic compounds based on a natural product-derived motif. Some of the compounds in development for CL include nitroaromatic compounds such as DNDI-8219, DNDI-VL2098, and DNDI-0690, a class historically used to treat several protozoan parasitic diseases (129). Thus, 7 nitroaromatic compounds (62) (Fig 3.1b) derived from two easily synthesizable scaffolds (4-nitrophenylacetyl and 4-nitro-1*H*-imidazolyl) were evaluated *in vitro* whereas Cp**6** and **7** were also tested in *in vivo* CL experimental models.
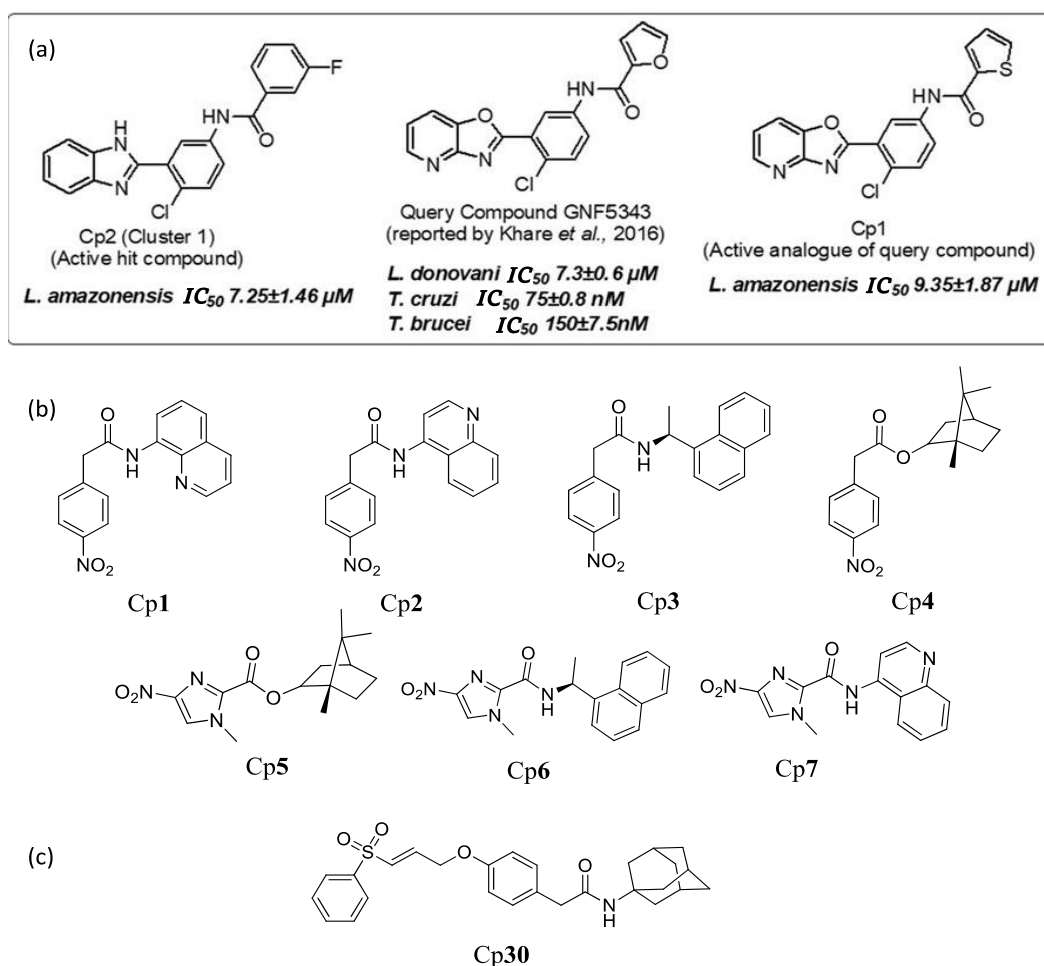
Figure 3.1 Molecular structures of the tested compounds and background. (a) shape-based virtual screening compounds (active analog (Cp1) of the query compound (GNF5343) and the hit Cp2, plus their associated activity data (b) a series of nitroaromatic and (c) a sulfonyl natural product-inspired compounds named:

Cp**1**: (2-(4-nitrophenyl)-N-(quinolin-8-yl)acetamide;

Cp**2** : 2-(4-nitrophenyl)-N-(quinolin-4-yl)acetamide;

Cp**3** : (S)-N-(1-(naphthalen-1-yl)ethyl)-2-(4-nitrophenyl)acetamide;

Cp**4** : (1S,4S)-1,7,7-Trimethylbicyclo[2.2.1]heptan-2-yl 2-(4-nitrophenyl)acetate;

Cp**5** : (1S,4S)-1,7,7-Trimethylbicyclo[2.2.1]heptan-2-yl 1-methyl-4-nitro-1H-imidazole-2-carboxylate;

Cp**6** : (*S*)-1-methyl-*N*-(1-(naphthalen-1-yl)ethyl)-4-nitro-1*H*-imidazole-2-carboxamide ;

61

Cp**7** ; 1-methyl-4-nitro-N-(quinolin-4-yl)-1H-imidazole-2-carboxamide ;

Cp**30** : *N*-(adamantan-1-yl)-2-(4-((€-3(phenylsulfonyl)allyl)oxy)phenyl)acetamide. Adapted from Santos *et al.* 2020 (20,21) and 2022 (62)

3.2   Research Objective

Our aim was to explore the *in vitro* antileishmanial effect of (i) 7 nitro-derivative scaffold-driven compounds (62), (ii) 32 GNF5343-*based shape* hits (20) and (iii) a series of 21 natural product-inspired phenyl sulfonyl acetamides and acetates, as well as 2 pentacyclic triterpenoids (21) against *L. amazonensis* amastigotes (strain *LTB0016*) purified from paw lesions (*ex vivo* amastigotes) or present in infected peritoneal macrophages. The most selective compounds (2 nitro and 1 sulfonyl derivatives) progressed to evaluation in *L. amazonensis*-infected BALB/c mice.

3.3   Material and Methods

3.3.1   *Compound solutions/dilutions*

Dimethyl sulfoxide (DMSO, Merk) stock solutions (30 mM) of the compounds (Fig 3.1) and Miltefosine ≥98% (Sigma-Aldrich) were diluted, just before the *in vitro* experiments, into RPMI-1640 medium (pH 7.2 to 7.4) without phenol red (Sigma-Aldrich R7509) but supplemented with 1% L-alanyl-L-glutamine (GLUTAMAX I, Gibco^{TM}). 1% penicillin-streptomycin (5,000 U/mL PEN-STR, Gibco™) and 10% heat-inactivated sterile-filtered fetal bovine serum (FBS, Cultilab, Brazil). The concentration of DMSO was less than 0.6% for all *in vitro* experiments to prevent non-specific toxicity to host cells (225). For *in vivo* assays, two nitro-derivatives (Cps **6** and **7)** and one sulfonyl derivative, Cp**30**, were daily diluted using a solution composed of 5% Gum Arabic from acacia tree (Sigma-Aldrich), 6% DMSO and 3% Tween™80 Surfact-Amps™ Detergent Solution (Thermo Scientific™). The reference drug, Milteforan™ (Mt^{TM}), was dissolved in sterile deionized water.

3.3.2   *Parasite strain and mammalian host cell culture*

L. amazonensis (strain *LTB0016*) was used throughout the study. Amastigotes were purified from male BALB/c mice. Briefly, the foot paws were inoculated subcutaneously with 20 µL containing 10^6 amastigotes and the skin lesions were aseptically removed 30 days post-infection (dpi). The intralesional parasites were mechanically dispersed by pipetting and used for the assays (226). The compounds were tested on (i) *ex vivo* amastigote forms (FF); (ii) intracellular amastigote forms (IA) in peritoneal macrophages (PMM); and (iii) BALB/c mouse models infected with amastigotes as described (20). PMM were obtained from Swiss male mice (18-20 g) inoculated with 3% Brewer Thioglycollate Medium (Merck) diluted in water and autoclaved. After 4 days of stimulation, the cells were recovered from the animals' peritoneum with RPMI 1640. The cells were subsequently seeded in 24- ($3x10^5$ cells/well) and 96-well plates ($5x10^4$ cells/well) for antileishmanial activity analysis and cytotoxicity assays, respectively. Cell cultures were maintained at 37°C in 5% CO_2 atmosphere in RPMI 1640 medium (pH 7.2 to 7.4) without phenol red, but supplemented with 1% L-glutamine, 1% (PEN-STR), 10% FBS. Assays using FF were maintained at 32ºC using RPMI culture medium containing 5% FBS.

3.3.3 *Cytotoxicity and in vitro leishmanicidal analysis*

At least two assays were performed in biological duplicate. The results were expressed as % reduction in parasite burden and the IC_{50} and IC_{90} were calculated by non-linear regression analysis using GraphPad Prism v.9.1.2.

The toxicity of the compounds on host cells was evaluated 24 h after seeding PMM into culture plates. The compounds (0-500 µM) were added into the wells and incubated for 48 h as above described. Cellular viability was evaluated using the AlamarBlue assay (20, 227) (Invitrogen) according to the manufacturer's recommendations. The effect of the compounds (0-20 µM, 48 h of incubation) on FFs was evaluated using 10^6 parasites per well (0.2 mL) and parasite viability assessed with AlamarBlue tests as reported (21,228). Briefly, 50 µL resazurin per well was added and after 6 h of incubation, the parasite growth assessed fluorimetrically (λ_{ex} 550 nm, λ_{em} 590 nm). Phenotypic screenings against IAs were performed by infecting $3x10^5$ PMMs with $9x10^5$ amastigotes, multiplicity of infection (MOI) 3. After 48 h of drug treatment, cultures were rinsed with saline, fixed 5 min with Bouin (229) and stained for 15 min with Giemsa solution (Sigma-Aldrich, 32884) (226,230). Samples were subsequently evaluated by light microscopy and microphotographs made using the Zeiss AxioObserver MI microscope (Oberkochen, Germany). The percentage of infected host cells, the

number of parasites per infected cell, and the corresponding infection index were obtained. Only parasites with well-defined nuclei and kinetoplasts were counted as surviving since irregular structures could mean parasites undergoing death (231).

3.3.4   *In vivo efficacy analysis*

Male BALB/c mice (18-20 g) obtained from the animal facilities of ICTB (Institute of Science and Biomodels Technology/Fiocruz/RJ/Brazil) were housed 5 per cage, kept in a room at 20 to 24˚C under a 12 h light dark cycle, and provided with sterile water and chow *ad libitum.* Animals were acclimatized 7 days before being subcutaneously inoculated with 5×10^5 amastigotes on the left foot paw (21, 62, 227). The treatment started 15 dpi, corresponding to the lesion onset (size diameter of 3-4 mm) (62, 129), assuring animal welfare during the period of treatment, while avoiding lesion ulceration (endpoint). The sulfonyl Cp**30** (21) and the nitro derivatives Cps **6** and **7** (62) were given for 14 days by oral gavage (100 µL) at 10 mg/kg twice a day (bid). Mt^{TM} was administered at a standardized dose (40 mg/kg) once a day (qd). The lesions were measured regularly in 3 dimensions (height, width, and depth), and animals were euthanized at 31 dpi. Skin lesions, aseptically removed and placed in a microtube filled with RNA *later*, were used for molecular analysis of parasite load by qPCR and light microscopy inspections of *imprints* (232). For qPCR, standard curves were constructed using DNA samples extracted from mouse skin fragments spiked with 10^6 amastigotes of *L. amazonensis* and parasite load expressed as equivalents of parasite DNA/mg tissue (eq par/mg tissue) (232). All procedures were carried out in accordance with the guidelines established by the FIOCRUZ Committee of Ethics for the Use of Animals (CEUA L038/2017).

Statistical analysis was conducted in GraphPad Prism v.9.1.2 by ANOVA: (i) one-way Fisher's LSD test or (ii) two-way unpaired T-test with Welch's correction, significance $p < 0.05$ (95% confidence interval).

3.3.5   *In vivo combination assays*

Cp**30** at 10 mg/kg of body weight was also assayed in co-administration with Mt^{TM} suboptimal dosage of 4 mg/kg qd. Mt^{TM} was also administered once at a 4 mg/kg qd as control for the combination.

3.4 Results

3.4.1 *In vitro susceptibility essays*

Initially, the compounds were screened using a colorimetric phenotypic assay on *L. amazonensis* FF using a fixed concentration of 5 µM for phenyl sulfone derivatives (including Cp **30)** or 10 µM for GNF5343-based shape hits (including Cps **1** and **2**) and the scaffold driven nitroaromatic compounds (Cps **6** and **7**). Cp **30** and Cps **1, 2, 6** and **7** led to ≥ 44 % reduction in the number of viable FF after 48 h of treatment. Next, these five compounds were further analysed in concentration-response assays using FF. The IC_{50} values ranged from 10 to 15 µM, being all less potent than the reference drugs pentamidine (Pt) (0.71 ± 0.05 µM) and Mt (4.37±0.11) (Table 1). Host cell viability showed that the natural-inspired compounds (**30**, **6** and **7**) did not exhibit any toxicity up to the highest tested concentration, leading to IC_{50} values (PMM) >500 µM, while Cps **1** and **2** IC_{50PM} were between 62 and 66 µM, being less toxic than Pt (15.88±0.59 µM).

The compounds were further evaluated against IF in PMM by light microscopy. Our data showed that all compounds were active against IF and more potent than Mt IC_{50}=13.3 ± 3.03 µM, exhibiting IC_{50} values lower than 10 µM (Table 1). Cps **1** and **2** displayed low selectivity indexes (<10) against free and intracellular forms.

Cps **6**, **7** and **30** safe profiles assured considerable SIs (ranging >38 and >125), especially against intracellular forms (>54 up to >125). These favorable results prompted us to conduct preliminary *in vivo* PoC studies using **Cp 30, 6** and **7**.

Table 3.1 Phenotypic studies of the tested compounds against free (FF, *ex vivo)* and intracellular (IF) forms of *L. amazonensis* and their corresponding toxicity profile upon peritoneal macrophages (PMM).

Compound	IC_{50} (µM) PMM	IC_{50} (µM) FF	IC_{50} (µM) IF[*]	SI FF	SI IF
1	62.75±0.27	13.03±2.69	9.35±1.87	5	7
2	65.39±0.61	14.09±2.25	7.25±1.46	5	9
6	>500	10.78±0.80	4.57±0.08	>46	>109
7	>500	13.12±1.70	9.19±0.68	>38	>54
30	>500	12.07±1.78	4.00±1.79	>41	>125
Pentamidine	15.88±0.59	0.71±0.05	1.94±0.5	22	8
Miltefosine	169.69±5.07	4.37±0.11	13.30±3.03	>39	>13

L. amazonensis (LTB0016 strain) purified from animal lesions. IF: intracellular forms in PMM; IC$_{50}$ is reported as mean and SD values; SI: Selective index. *Statistical analysis was performed with GraphPad prism v.9.1.2. by Ordinary ANOVA test.

Low IC$_{90}$ values (90% inhibitory concentration) were obtained for Cp**30** (7.16 µM) (21) and Cp**6** (9.14 µM) (62), with 10 µM leading to 100 and 92% of decreases in PMM infection, respectively (Fig 3.2b-c). Compound **7** was less active (IC$_{90}$ = 17.20 µM) (62) similarly to Cp **1** and **2** (17.25 and 18.54 µM, respectively) (20), reaching burden reductions only at 20 µM (Fig 3.2a-c).
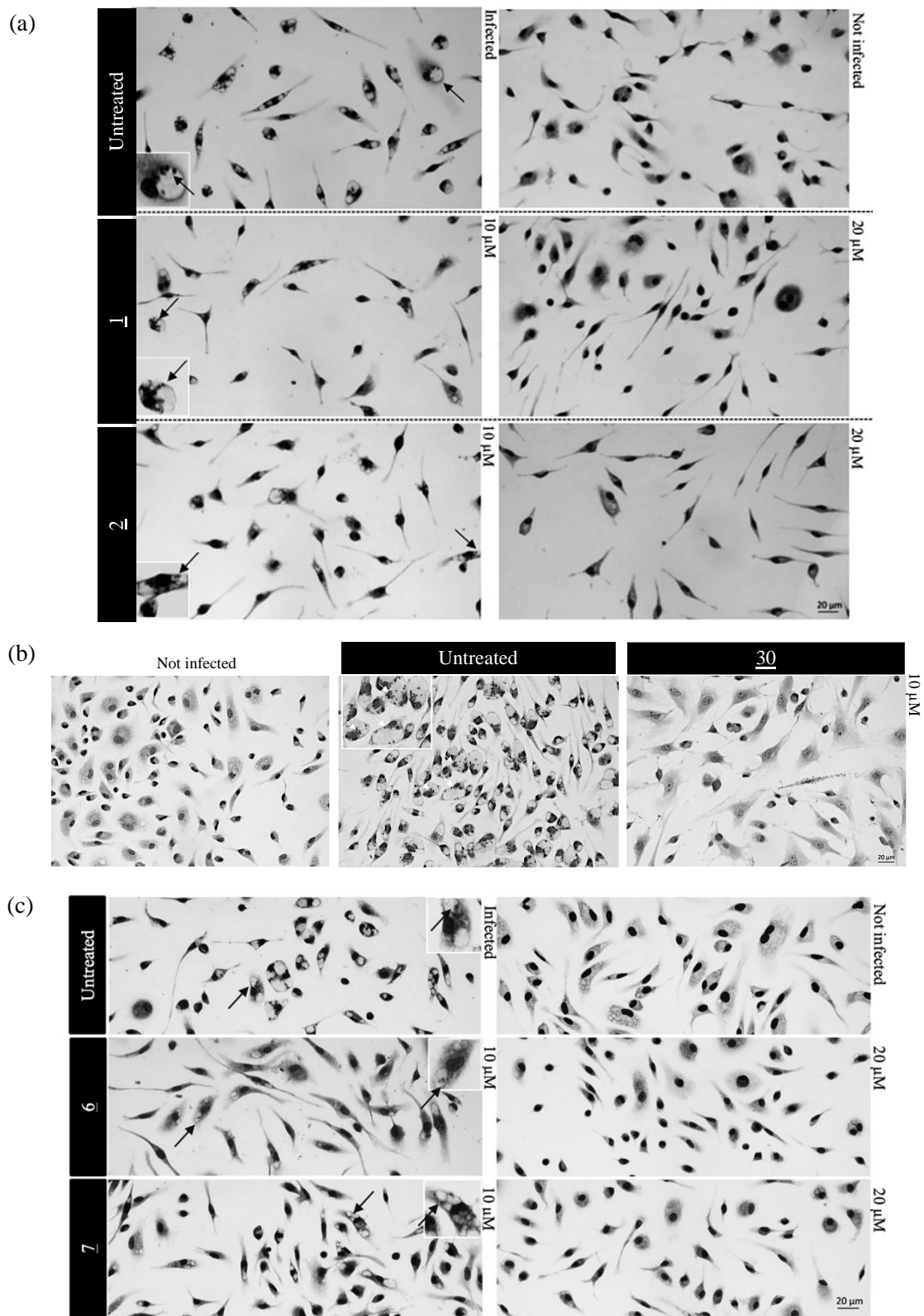
Figure 3.2 Light microscopy images of Giemsa-stained uninfected and infected PMM with intracellular amastigotes of *L. amazonensis* untreated or treated with 10 or 20 µM of the tested compounds (a) **1, 2,** (b) **30,** (c) **6** and **7**. Arrows: intracellular parasites. Scale bar=20µM. Adapted from Santos *et al.* 2020 (20,21) and 2022 (62).

3.4.2 *In vivo activity*

Efficacy was checked *in vivo* in *L. amazonensis*-infected BALB/c mice and the results are displayed in figures 3.3 (Cp **30)** and 3.4 (Cps **6** and **7**).

The *in vivo* infection led to a gradual increase in skin lesion size of mice treated with the drug vehicle alone, reaching 438.8 ± 42.1 mm^3, at the endpoint (Fig 3.3a). Cp **30** given alone (10 mg/kg, bid, 14 days) led to a marginal increase (19%) in lesion sizes, with a mean value of 550.7 ± 23.15 mm^3 ($p = 0.0328$). When **30** was co-administered with a suboptimal dose of Mt^{TM} (10 mg/kg of Cp **30** plus 4 mg/kg of Mt^{TM}, qd, 14 days), ($p = 0.0934$) the lesions decreased by 20%.

Mt^{TM} alone at optimal dose (40 mg/kg, qd, 14 days) led to about 72% significant reduction in the size of the lesions ($p < 0.0001$), thereby, reverting the clinical condition (Fig 3.3a-b).

The molecular readout (qPCR) showed treatment with Cp**30** alone (160496 ± 45419 eq par/mg tissue) ($p = 0.0018$) or in co-administration with Mt^{TM} (170706 ± 28584 eq par/mg tissue) ($p = 0.0010$) led to an increase in parasite load (6 to 7-fold) as compared to vehicle treated group (27753 ± 9539 eq par/mg tissue) at the 31 dpi (Fig 3.3c).

As expected, Mt^{TM}, given at 40 mg/kg, suppressed (0.256 ± 0.1022 eq par/mg tissue, 99.99%) ($p = 0.00196$) parasite load in infected mice (9).

The analysis of lesion imprints on Giemsa-stained slides using light microscopy (Fig 3.3d-e) showed that vehicle treated mice (Fig 3.3d) have numerous intracellular parasites (arrow) in macrophages besides inflammatory diffuse infiltrates. Cp**30** lesions (Fig 3.3e) also revealed similar pattern, besides exhibiting high parasitemia.
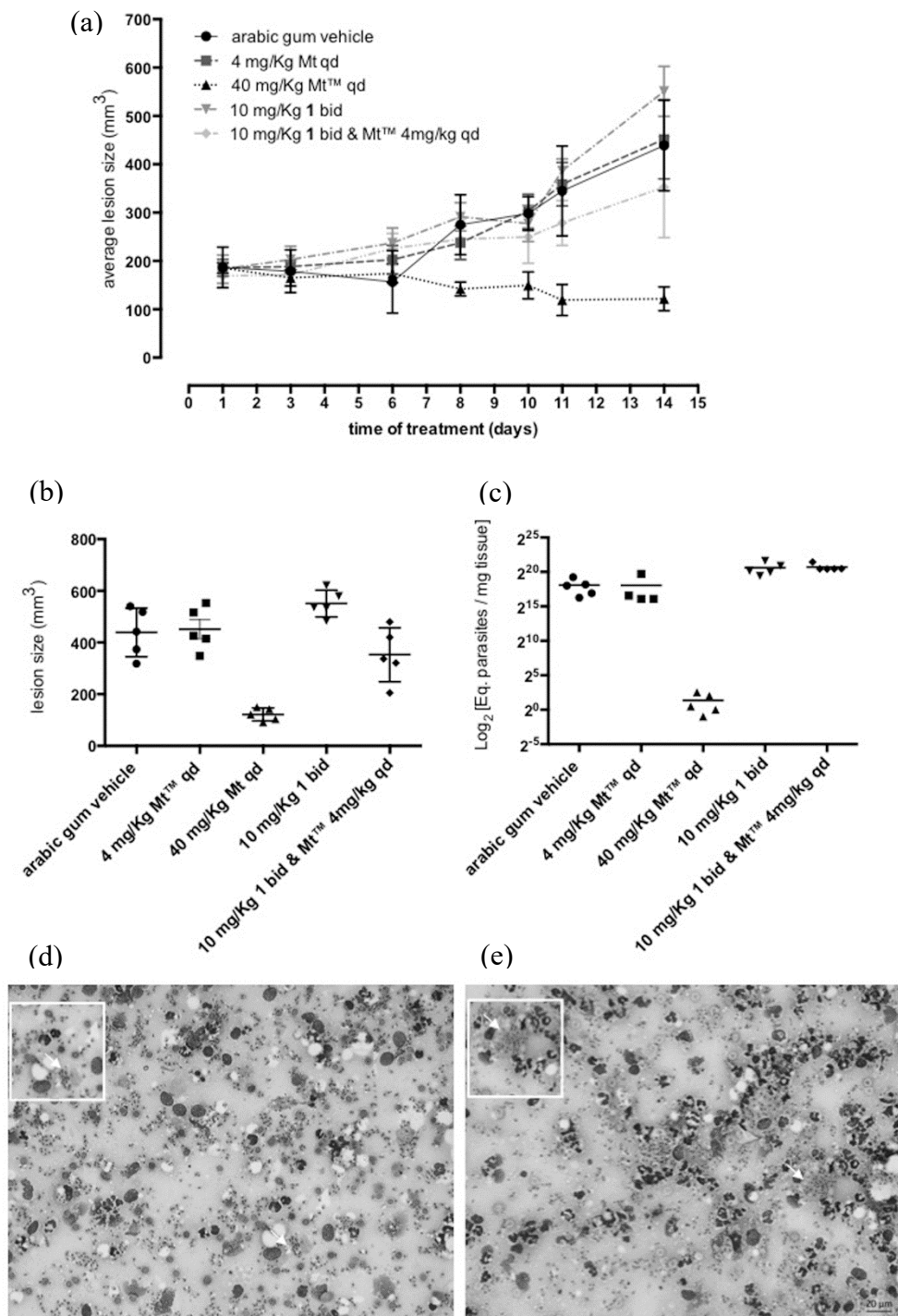
Figure 3.3 Activity of **30** in the *L. amazonensis*-BALB/c model of CL. The graphics show (a) average lesion size during treatment, (b) lesion size average and (c) parasite load by qPCR at 31 dpi, according to each experimental group. Light microscopy of lesion imprints of infected mice treated with (d) vehicle and (e) Cp **30** at 10 mg/kg, po, bid. Arrow: Intracellular parasites. (21). Adapted from Santos *et al.* 2020 (21).

For **6** and **7**, we observed a gradual increase in skin lesion size of mice treated with the vehicle alone, reaching 438.8 ± 42.05 mm^3 at the endpoint (Figure 3.4a) (62). Mice treated with compound **6** displayed similar lesions size (443.7 ± 47.76 mm^3, $p = 0.4798$) while a slight increase was observed using **7** (550.9 ± 30.23 mm^3, $p = 0.2398$), as compared to the vehicle-treated group. Mt^{TM} achieved a 72% decrease in the size of skin lesions and significantly improved the clinical condition ($p < 0.0001$ (Fig 3.4 a-b).

At 31 dpi, qPCR readout expressed as DNA equivalents per milligram of tissue showed a 5 to 10-fold increase in the parasite load of mice treated with **6** ($276,526 \pm 40,519$ eq. par/mg tissue, $p = 0.0208$) and **7** ($153,765 \pm 54,932$ eq. par/mg tissue, $p = 0.0829$) as compared to vehicle-treated group ($27,753 \pm 9,539$ eq par/mg tissue) (Fig 3.4c). Mt^{TM} completely suppressed (99.99%) parasite load (0.256 ± 0.1022 eq par/mg tissue, $p = 0.0437$) (11). The qPCR showed that all studied compounds lacked *in vivo* efficacy, corroborating the qualitative light microscopy analysis of lesions *imprints* (Fig 3.4c). The findings clearly showed that both **6** and **7** treated animal groups have high parasitemia coupled with the presence of lymphomononuclear diffuse infiltrates and many parasites inside mononuclear host cells (Fig 3.4c).
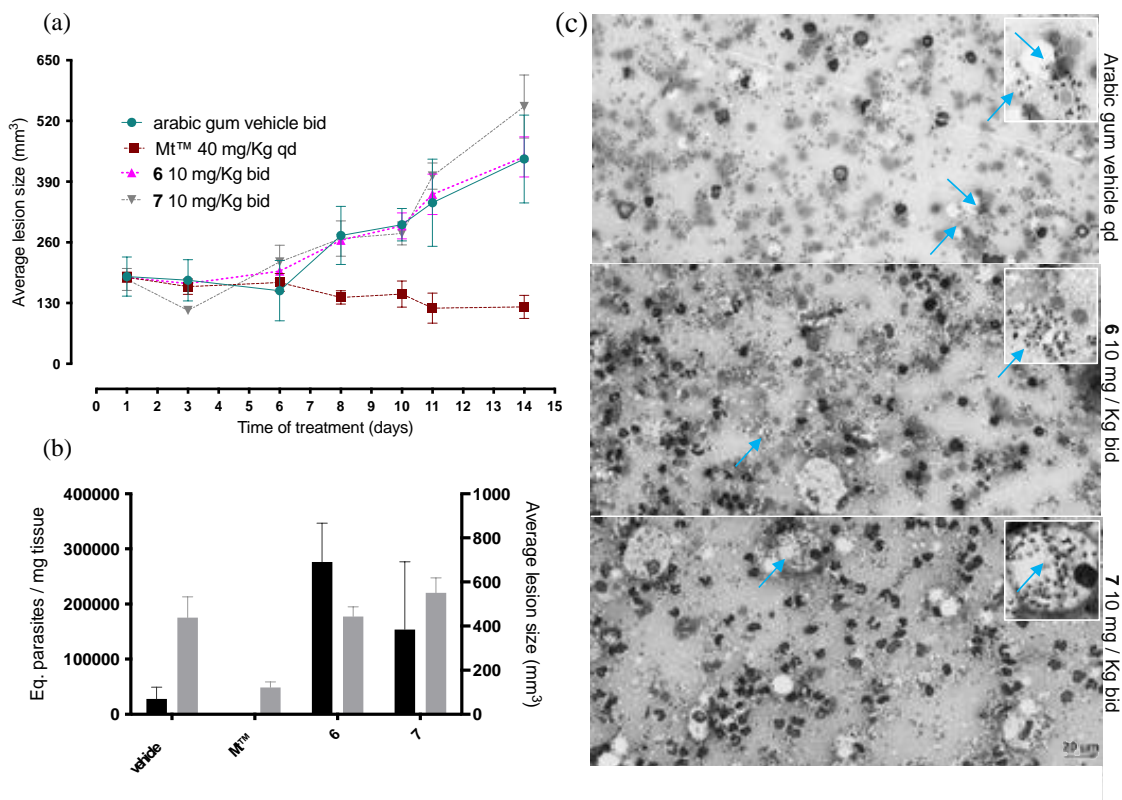
Figure 3.4 The effect of **6** and **7** in experimental CL mouse models using BALB/c mice infected with *L. amazonensis*. The graphics show: average lesion size during treatment (a), the correlation between parasite load by qPCR (black bars), and average lesion size measurements (grey bars) at 31 dpi (b), according to

70

each experimental group. Light microscopy of lesions imprints of infected mice treated with vehicle and after administration of compounds 6 and 7 at 10 mg/kg bid po (c). Arrow: intracellular parasites. Adapted from Santos *et al.* 2022 (62).

For qPCR, standard curves (Fig 3.5a) were constructed using DNA samples extracted from mouse skin fragments spiked with 10^6 amastigotes of *L. amazonensis.* Parasite load expressed as equivalents of parasite DNA/mg tissue (eq par/mg tissue) showed a 93.2 % efficiency for the target 18S rDNA in *Leishmania*, with linearity coefficient of 0.98 (Fig 3.5b). For the mouse reference gene (GAPDH), an efficiency of 91.4 % was observed, with a linearity coefficient of 0.99 (Fig 3.5b), confirming a robust parasite detection and quantification.
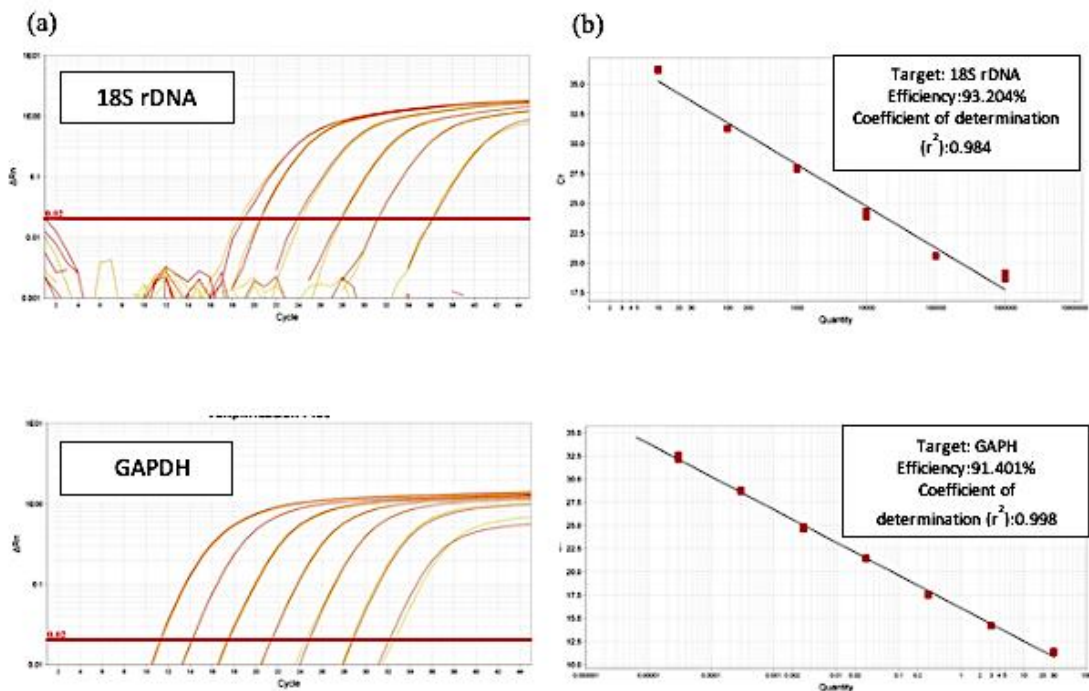
Figure 3.5 Real time quantitative PCR assays for parasite load quantitation in skin lesions of BALB/c mice infected with *L. amazonensis*. The panel shows representative amplification plots with the fluorescent signal magnitude for *Leishmania* 18S rDNA and BALB/c GAPDH targets (a) Amplification plots for *Leishmania* 18S rDNA (top panel) and BALB/c GAPDH (bottom panel) targets indicate the dynamic range of the qPCR, (b) Standard curves for *Leishmania* 18S rDNA (top panel) and BALB/c GAPDH (bottom panel) targets indicate the linearity of the qPCR assays, as well as the efficiency and coefficient of determination (r^2). qPCR assays were performed using TaqMan assays. Adapted from Santos *et al.* 2020 (21) and 2022 (62), Supplementary material.

3.5 Discussion

L. amazonensis is one of the most common *Leishmania* species in Brazil, known to cause a wide spectrum of disease manifestations, including very severe and diffuse cutaneous leishmaniasis (233).

Presently, our analysis besides evaluating the effect against *ex vivo* amastigotes, also included primary cultures of peritoneal macrophages infected with *L. amazonensis* since professional phagocytes are the main host cells for those obligate intracellular parasites (219). This *in vitro* standardized experimental model for CL drug screening is claimed to closely reproduce *in vivo* conditions (220) therefore contributing to novel drug candidate screenings for this neglected illness (221,234). Another interesting point to be addressed is the use of protocols that enable the identification of antiparasitic drugs that induce rapid parasite lysis (235). This is an especially desired characteristic as most CL patients live in very poor areas with difficult access to public health services (236) and therefore frequently display advanced pathologies, demanding a *fast killing* drug (237). Aiming to fulfill this demand, we established a period of 48 h of drug exposure while testing the parasites and mammalian host cells, which is a shorter period of incubation as compared to others reported in the current literature for *in vitro* CL models (129).

Natural products have been widely explored in anti-infective drug discovery (212). Many anti-infective agents currently used in clinical settings are based on natural products such as the antimalarials quinine and artemisinin and the anthelmintic avermectins (212,238,239). A series of natural product-inspired phenyl sulfonyl acetamides and acetates, as well as two pentacyclic triterpenoids previously investigated against the causative agent of sleeping sickness *T. brucei* (214, 224), were evaluated against *L. amazonensis*. Cp **6**, **7** and **30** presented relatively low IC_{90} against IF (≤17.2 µM), which is a desirable feature to avoid parasitic relapses and drug resistance (240, 241).

Moreover, the Giemsa readout by light microscopy clearly demonstrated that Cps **6, 7** and **30** have a cidal rather than static effect on the parasites. Especially Cp**30** has a fast action and clears the infection from infected host cells at 10 µM. The *in vitro* data demonstrated that the two 4-nitro-1*H*-imidazolyl compounds (**6** and **7**) have acceptable selectivity indices (at least 50 for *L. amazonensis* IF). The sum of these phenotypic findings encouraged us to move compounds **6, 7** and **30** to LC mouse models.

The compounds were administered in BALB/c mouse CL models for 14 days at a relatively low dose, starting therapy at the onset of lesion formation (21,62). The results showed that the *in vitro* potency of the hits compounds **6,7** and **30** did not translate to *in vivo* efficacy. The measurements of the mouse lesions (using a paquimeter) and the molecular analysis of animal parasitism (qPCR) demonstrated a lack of *in vivo* activity of these three compounds, even in combination with subefficacious of Milteforan^{MT}, while Mt at optimal dosage suppressed both parameters, as reported (129). The lack of *in vivo* efficacy of the tested compounds could be, at least in part, due to low bioavailability and/or high metabolic clearance. In fact, the poor *in vivo* results for Cp**30** are potentially related to lipophilicity. Its relatively high lipophilicity (cLogP of 4.3) (21) actually impaired its use at a higher dose such as the one used for the reference drug Mt (40 mg/kg). Drugs in clinical use for leishmaniasis generally have high aqueous solubility.

Thus, ongoing optimization work on analogues of compound **30** is required to improve aqueous solubility and reduce obvious metabolic liabilities aiming to contribute to the drug discovery and development pipeline of leishmaniasis. Also, as nitro-drugs are activated by *Leishmania* nitroreductases (NTR2) (242), it is possible that **6** and **7** may be activated in a similar way and may be used as templates for nitroimidazole-based antileishmanial DD programs focusing on analogs that have the appropriate TPP for new CL drugs (243).

The present study also explored the leishmanicidal effect of Cp**1** (an analogue of GNF5343) and Cp**2** (a benzimidazole analogue) identified using shape-based virtual screening approach. Both Cp**1** and Cp**2** achieved quite relevant potency against amastigotes, especially those lodged inside macrophages, reaching IC$_{50}$ values below 10 µM, an important threshold characteristic preconized for an anti-*Leishmania* hit (218, 244). Remarkably, clearance on *L. amazonensis* infection was found at 20 µM in the infected PMM, a relevant feature to mitigate the possible occurrence of parasite drug resistance and relapses after ceasing drug administration (245). The Cp**1** and Cp**2** were less toxic than the reference drug (pentamidine) still in use for leishmaniasis, but their selectivity indexes (< 10) discouraged progression towards *in vivo* proof of concept, even with low IC$_{90}$ values (17.25 ± 0.21 µM and 18.54 ± 0.96 µM) against IFs. However, their chemical optimization for a wider therapeutic window and promotion of potency is largely desirable to continue further studies using these compounds. Currently, structural modifications of Cp**2** are being made to improve potency, selectivity, and pharmacological profile, favoring reinvigorated *in vitro* screening and *in vivo* evaluation,

aiming to contribute to the discovery of new chemical entities for CL. These analogues will also be tested against other kinetoplastid parasites to assess their activity.

3.6   Conclusion

Our present phenotypic study demonstrated that the presence of host cell in *in vitro* trial is important step to be considered to evaluate the compound activation against pathologically relevant intracellular forms, attributing better $IC_{50}s$ in comparison to the assay performed directly against the "free" amastigote and therefore, important as primary model to screen CL candidates.

Based on the results presented, *in vivo* bioavailability studies are important to stablish pharmacokinetic parameters and useful to set up dosage regiments prior to efficacy evaluation.

Although not reaching the anticipated *in vivo* outcomes, our present phenotypic study brings novel knowledge in the field of drug discovery for CL aiming to deliver new therapies for patients suffering from this disregarded neglected tropical disease.

4 Phenotypic analysis of nucleoside analogues against experimental CD and HAT

Chapter 4

4.1 State-of-the-art

4.1.1 *Purine salvage as drug target in trypanosomatids*

As already discussed in Chapter 1, there is an urgent need to find safer and effective treatments for diseases caused by trypanosomatids such as Chagas disease (38), Sleeping Sickness (72) and Nagana, the latter a livestock disease responsible for important economic losses in rural areas of Africa (80).

The purine biosynthesis pathway represents a promising drug target in different auxotrophic pathogens (245, 246). In fact, several agents that disrupt purine metabolism are in clinical use for different diseases including allopurinol, an inhibitor of the purine degradation enzyme xanthine oxidase, used to treat canine leishmaniasis (247); azathioprine, which after conversion into the purine analogue 6-mercaptopurine presents anticancer and immunosuppressant effects (248), and the purine analogue acyclovir, used to treat herpes as well as other viral infections (249).

As trypanosomatids cannot synthetize purine *de novo* and rely on host salvage of intermediates (250), this pathway and exploitation of nucleoside transporters represent interesting avenues to pursue in DD (251). Purine uptake seems to be an ancient trypanosomatid mechanism as predicted in cell evolution studies using trypanosomatids carrying endosymbionts (Figure 4.1a). Symbiont enzymes such as apyrase and adenosine deaminase would metabolize the purine intermediates after active and/or passive transport (22). Interestingly, nucleotidases required for hydrolysis and deamination of extracellular nucleotides were absent in symbiont-bearing trypanosomatids species (Fig 4.1) (22), but detected in other trypanosomatids like *Leishmania spp.* (without symbionts) (252), playing a role in purine salvage pathway and establishment of infection (253,254). *Trypanosoma cruzi*, similarly to the symbiotic counterparts, converts purines into nucleotides via a pool of intracellular enzymes, such as adenine and hypoxanthine-guanine phosphoribosyltransferase, adenylate kinase, AMP deaminase, inosine monophosphate dehydrogenase and GMP synthetase, besides hydrolases and kinases (Fig 4.1b) (23), among other molecules (255), that deserve further exploitation.
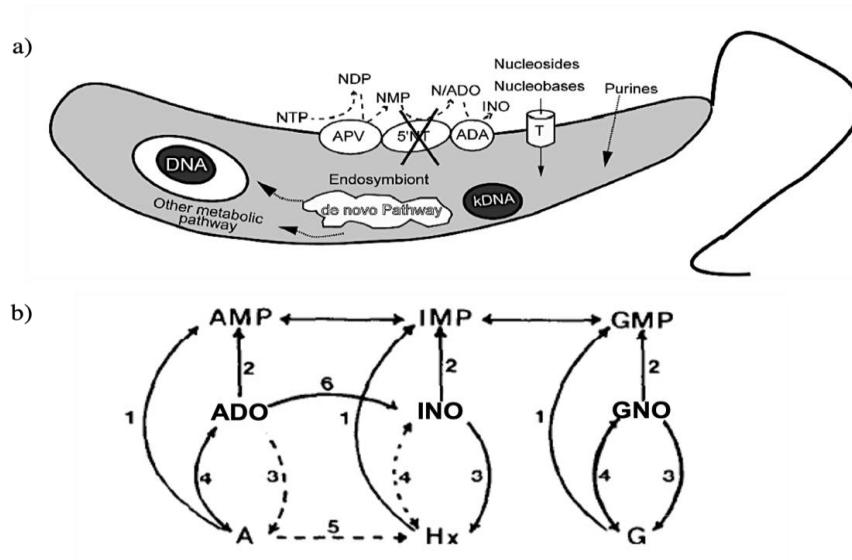
Figure 4.1 (a) *Purine salvage pathway model in the endosymbiont-bearing trypanosomatids Angomonas deanei and Strigomonas culicis.* The endosymbiont enzymes APV and ADA could be responsible for the generation of extracellular nucleosides, nucleobases, and purines, that could be acquired by the parasite through membrane transporters (T) or diffusion and incorporated into the parasite genome after processing. Abbreviations: APV (Apyrase); ADA (adenosine deaminase); NTP (nucleoside triphosphate), NDP (nucleoside diphosphate), NMP (nucleoside monophosphate), N (nucleobase), ADO (adenosine), INO (inosine). Retrieved from Machado Motta *et al* 2013 (22) (b) *Enzyme activity involved in T. cruzi purine salvage.* Known reactions are represented by solid lines and hypothetical reactions by dashed lines. Enzyme activities: 1- Phosphoribosyltransferase; 2- nucleoside kinase; 3- nucleoside hydrolase; 4- nucleoside phosphorylase; 5- adenine aminohydrolase; 6- adenosine aminohydrolase. Abbreviations: A (adenine); Hx (hypoxanthine); G (guanine); ADO (adenosine); INO (inosine); GNO (guanosine); AMP, IMP, GMP (adenosine, inosine and guanosine monophosphate). Adapted from: Gutteridge & Davies, 1981 (23).

The literature reports some agents that interfere in purine metabolism and hold anti-trypanosomatid activity including allopurinol. This compound displays modest effect *in vitro* and *in vivo* in experimental models of *T. cruzi* infection (180,256,257) and was ineffective during the acute and chronic phase of CD (258,259). Allopurinol is a current option to treat human CL (260,261) and canine leishmaniasis (CanL) (262). The proposed mechanism of action in trypanosomatids (263) is depicted in figure 4.2, and consists of different steps of allopurinol metabolization up to the incorporation of an adenosine triphosphate (ATP) analogue into the parasite RNA (24).
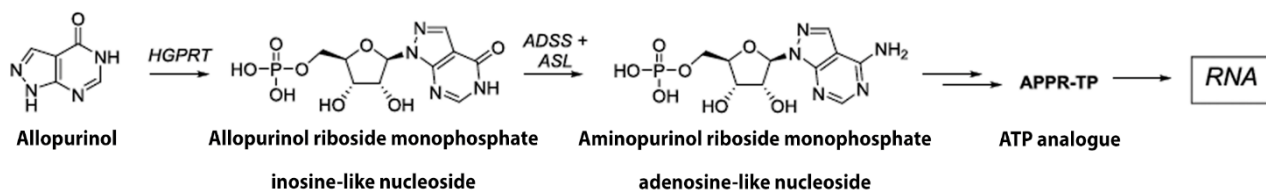
Figure 4.2 Allopurinol metabolism in *Leishmania* spp and *T. cruzi*. HGPRT: hypoxanthine guanine phosphoribosyltransferase; ADSS: adenylosuccinate synthetase; ASL: adenylosuccinate lyase; APPR-TP: example of an ATP analogue. Adapted from Bouton *et al.* 2021 (Figure 1C) (24).

Tubercidin is a natural antibiotic with a wide spectrum of biological activity (264), and together with other analogues such as Formycin A, B and cordycepin, also displays activities against *T. cruzi* and *T. brucei* spp. (265–267), which encouraged the synthesis of new purine analogues by different medicinal chemistry groups including the one headed by Prof. Serge Van Calenbergh (Chemistry department at University of Gent). They synthetized a series of C7 substituted analogues and demonstrated that some have high potency against *T. brucei* (268). One of them, a 3'-deoxytubercidin (named 9 in (269)) that emerged from a series of 3'-deoxy-7-deazaadenosine nucleosides, cleared the parasitemia in mouse models of acute and CNS-stage of human African trypanosomiasis (HAT). The P2 aminopurine transporter and adenosine kinase are involved in its uptake and activation, respectively (269). A structure-activity relationship analysis demonstrated that C7 modifications increase affinity for the P1 nucleoside transporter in *T. brucei*, while generally retaining high affinity for P2 (270). Thus, a wide range of compound optimization was applied (Figure 4.3) to search for novel antiparasitic lead compounds. The compounds were phenotypically screened *in vitro* against a broad panel of trypanosomatid species, at both LMPH and LBC laboratories. Some promising published data related to *T. cruzi* are summarized in Table 4.1.
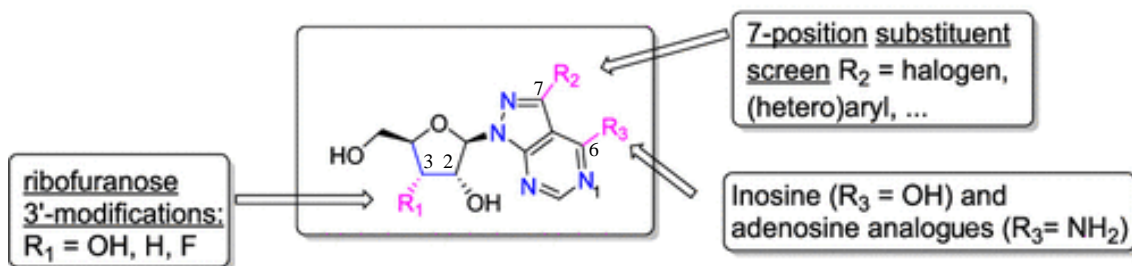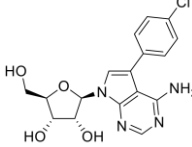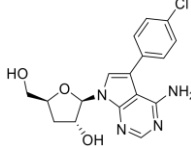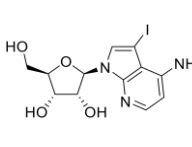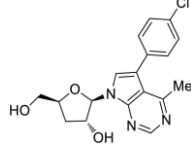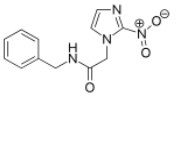
Figure 4.3 Structural modifications explored for 7-deazapurine nucleoside analogues. Adapted from Bouton *et al.* 2021 (Figure 1D) (24).

The metabolically stable purine nucleosides named TH1012 (Fig 4.3: R1=OH, R2= chlorophenyl), FH8512 (Fig 4.3: R1=H, R2= chlorophenyl), and FH5319 (Fig 4.3: R1= OH, R2= I) – all with the amino group (NH_2) at C6 position (R3) – exhibited a highly potent activity against intracellular forms of *T. cruzi* (Y and Tulahuen strains) in primary culture of cardiac cells (CC) and mouse fibroblast (L929) cultures respectively. Most of them exhibited activity at nanomolar and submicromolar range (IC_{50} range of 0.47-0.029 µM). Both iodine (I) or chlorophenyl at C7 position conferred desirable activity regardless 3´ hydroxy group (OH) removal from the ribofuranose (sugar) part. TH1012, FH8512 and FH5319 also presented outstanding *in vitro* and *in vivo* safety profiles, with high selectivity index (SI >57), suppressing parasitemia and conferring 100% survival of mice after a treatment regimen of 5 days at 25 mg/kg bid. In CL2204 compound, the C6 amino group replacement by methyl group (Me) decreased *in vitro* activity and selectivity (≥5 and 8-fold) upon intracellular forms of Y and Tulahuen strains. CL2204 was ineffective in *in vivo* experimental models. However, in all treated groups, parasitemia relapse was observed after cyclophosphamide immunosuppression. This could be due to, at least in part, the lack of potency against BT forms (Table 3.1) and/or short period of treatment (only 5 days).

Table 4.1 Published data compilation from *in vitro* and *in vivo* drug phenotypic screening of the most promising nucleoside analogs against different experimental models of Chagas disease.

		TH1012	FH8512	FH5319	Cl2204	Bz
in vitro — Y strain (BT)	$IC_{50\ BT\ trypo}$ [a],*	>20	>20	>70	>81	11.5 ± 1.1
	$IC_{50\ IA}$ [b],*	0.029 ± 0.0	0.029 ± 0.0	0.089±0.0	0.77±0.0	0.354 ± 0.2
	SI_{IA}	9400	9700	>4400	625	>1100
in vitro — Tulahuen strain (intracellular)	$IC_{50\ IA}$ [c],*	0.47 ± 0.25	0.047 ± 0.006	0.040 ± 0.013	2.58 ± 0.67	2.28 ± 0.22
	SI_{IA}	57	410	>1600	>25	ND
in vivo [d] — Swiss mice + Y strain 25 mg/Kg, PO bid	Survival rate	100%	100%	100%	80%	100%
	Parasitemia reduction	99.8%	94.6%	99.8%	92%	>99%
	Relapse after immune-suppression?	Yes	Yes	Yes	Yes	Yes
	References	(265)	(265)	(266)	(271)	(265,266,271)

[a]Bloodstream trypomastigote forms (BT trypo) purified by heart punction of infected mice followed by 24 h drug exposition. *Half Inhibitory Drug Concentration (IC_{50}) are displayed in µM. [b]Cardiac or [c]MRC-5 cells were used as host cells for intracellular amastigotes (IA) assays, using [b]48 or [c]168 h of drug exposure. The IC_{50}s against host cells (not shown) allowed the estimation of the selectivity index (SI) = (IC_{50} host cells) / (IC_{50} *T. cruzi*). [d]Male swiss mice applied in *in vivo* evaluation.

4.1.2 *In vitro metabolic stability assessment prior to animal testing*

High potency is desirable but not at the expense of poor physicochemical properties or drug metabolism and pharmacokinetic (DMPK) characteristics, including absorption, distribution, metabolism, excretion and toxicity (ADMET). These aspects are typically part of drug discovery (218) and improvement for *in vivo* efficacy studies (272). ADMET profile characterization prior to *in vivo* efficacy evaluation supports validation of initial 'hits' and contribute to a stronger PoC in defining 'lead' potential (273).

In that sense, metabolic stability assessment is an important and reasonable approach in the early phase of drug discovery, evaluating compound susceptibility to biotransformation by microsomal enzymes. The results are usually reported as intrinsic clearance and used for secondary pharmacokinetic parameter calculation such as bioavailability and half-life (274).

An easy-to-use and relatively inexpensive screening system for metabolic stability was incorporated into the present studies using commercially available microsomal liver S9 fractions from different species together with phase I and II metabolic enzymes (275).

4.2   Research Objective

Encouraged by the previous promising trypanocidal performance in pre-clinical studies (Table 4.1) (265,266,271), our aim was to further investigate the antiparasitic effect of novel nucleoside derivatives in experimental models of CD and/or HAT disease. To reach this goal, the antiparasitic effect of a new series of optimized 7-deazapurine nucleosides with C7 substituents (named FH10678, FH11708, FH11709, FH11710, FH11711, FH11712, FH10714, FH10715, FH11702, FH11703, FH11704, FH11705, FH11706, FH11707 and JB588) was evaluated *in vitro* through phenotypic studies and their metabolic stability analysed using mouse and human microsomal fractions in the presence of Phase I and Phase II-metabolic enzymes. Also, the efficacy of FH8512 (4-amino-5-(4-chlorophenyl)-N7-(3′-deoxy-β-D-ribofuranosyl)-pyrrolo[2,3-d]pyrimidine, Cpd**1)** was further assessed in an experimental mouse model of acute Chagas disease, adopting a dose titration, extended treatment, and co-administration with a subtherapeutic dose of the reference drug Bz. Finally, *in vitro* washout assays were performed to determine the cidal activity profile of Cpd**1** against *T. cruzi*, besides exploring the effect of pre-treatment protocols on the fitness of bloodstream trypomastigotes (241).

4.3   Material and Methods

4.3.1   *Compound solutions/dilutions*

Compound stock solutions were prepared at 20 mM in 100% dimethyl sulfoxide (DMSO) for *in vitro* screening assays. The compounds were serially diluted in DMSO followed by a second dilution in sterile deionized water to assure a final in-test DMSO

concentration of <1%. Assays are performed in sterile 96-well microtiter plates, in triplicates. Benznidazole (Bz) (LAFEPE, Brazil) was used as reference drug (38).

4.3.2 Parasite strains and mammalian cell cultures

T. cruzi Tulahuen CL2 (DTU VI) expressing *E. coli* β- galactosidase (276), *T. b. brucei* Squib 427 (277) and T. *b. rhodesiense* STIB-900 (278) were used as reference strains for drug screening. *T. brucei* strains were maintained in Hirumi (HMI-9) medium supplemented with 10% inactivated fetal calf serum (iFCS); *T. cruzi* on MRC-5$_{SV2}$ (human lung fibroblast) cells in MEM medium supplemented with 1% L-glutamine and 5% iFCS. MRC-5$_{SV2}$ cells were cultured in MEM + Earl's salts-medium, supplemented with L-glutamine, $NaHCO_3$ and 5% iFCS. All cultures and assays were conducted at 37°C under an atmosphere of 5% CO_2.

Y strain BT forms (DTU II) were obtained by cardiac puncture of infected Swiss Webster mice on the peak of parasitemia (279). Trypomastigote forms of Tulahuen expressing *E. coli* β- galactosidase were purified from the supernatant of previously infected L929 cell cultures (10 host cell : 1 parasite ratio) (225). Purified parasites were added to RPMI 1640 medium supplemented with 5% FBS to perform assays at 37ºC in 5% CO_2.

Primary cultures of mouse embryonic cardiac cells (CC) were obtained from Swiss mice (280). Briefly, hearts of 18-day-old mice were removed under aseptic conditions, the atria trimmed away and ventricles minced into small fragments that were washed and dissociated until cardiomyocytes were obtained, as described (280,281). CC cultures were maintained in Dulbecco's modified Eagle medium (DMEM; without phenol red; Sigma-Aldrich) supplemented with 2% chicken embryo extract, 5% fetal bovine serum (FBS), 10% horse serum, 1 mM L-glutamine and 2.5 mM $CaCl_2$ at 37°C (282). L929 cell lines were cultivated (4.000 cells/well) in 96-well microplates at 37°C in RPMI 1640 medium (Sigma-Aldrich) (pH 7.2 to 7.4) without phenol red supplemented with 10% FBS and 2 mM L-glutamine (225).

4.3.3 Susceptibility assays

At least two assays were performed in biological duplicate. The results were expressed as % reduction in parasite burden compared to untreated control and IC$_{50}$ were

calculated by non-linear regression analysis. Statistical analysis ($p \leq 0.05$) was performed using GraphPad Prism Version 9.1.0.

At LMPH, *T. cruzi* assays were performed in sterile 96-well microtiter plates, each well containing 10 μl of the compound dilutions together with 190 μL of MRC-5$_{SV2}$ cell/parasite inoculum (4×10^3 cells/well + 4×10^4 parasites/well). Parasite growth was compared to untreated-infected controls and non-infected controls after 7 days incubation at 37°C and 5% CO_2. Parasite burden was assessed after adding the substrate CPRG (chlorophenolred ß-D-galactopyranoside): 50 μl/well of a stock solution containing 15.2 mg CPRG + 250 μl Nonidet in 100 ml phosphate buffered saline (PBS). The change in colour was measured spectrophotometrically after 4 h incubation at 37°C. The test compound was classified as inactive when the IC$_{50}$ >20 μM, moderate active 20μM $\geq$ IC$_{50}$ > 5 μM and highly active if IC$_{50}$ $\leq$ 5μM in absence of cytotoxicity. *T. brucei* assays were performed in sterile 96-well microtiter plates, each well containing 10 μl of the compound's dilutions together with 190 μl of the parasite suspension (1.5×10^4 *T. brucei*/well). After 72 h incubation, 50 μL resazurin per well was added and parasite growth assessed fluorimetrically (λex 550 nm, λem 590 nm) after 6 h (*T. rhodesiense*) or 24 h (*T. brucei*) at 37°C. The test compound was classified as moderately active when the 5 μM $\geq$ IC$_{50}$ >1 μM and highly active if IC$_{50}$ $\leq$ 1μM in absence of cytotoxicity. Benznidazole and suramin were included as reference drugs for CD and HAT, respectively (268).

MRC-5$_{SV2}$. Cytotoxicity assays were performed in sterile 96-well plates, each well containing 10 μl of the compound dilutions together with 190 μl of MRC-5 inoculum (1.5×10^5 cells/ml). Cell growth was compared to untreated-control wells (100% cell growth) and medium-control wells (0% cell growth). After 72 h of incubation, 50 μL resazurin per well was added to determine cell viability. After 4 h at 37°C, fluorescence was measured (265).

At LBC, the analysis of intracellular forms of *T. cruzi* was performed in sterile 96- and 24-well microtiter plates, using a 10:1 parasite host cell ratio.

Pre-treated Y strain BT forms. Bloodstream trypomastigotes were incubated for 24 h with Cpd**1** and Bz at their corresponding IC$_{50}$ (23 ± 4 and 11.5 ± 1.1 μM, respectively) (265). Parasites were washed to remove free compound, and the number of live and motile parasites were determined by light microscopy using a Neubauer chamber to adjust the parasite:host cell ratio. After 24 h of interaction, the infected CC were rinsed to remove non-internalized parasites, fixed with Bouin or submitted to additional

incubation up to 72h (283). After fixation and staining with Giemsa, light microscopic analysis was performed to determine the number of infected host cells (IHC), parasites per infected cells (NPC) and infection index (II - percentage of infected cells multiplied by the average number of intracellular parasites per infected host cell). Only characteristic parasite nuclei and kinetoplasts were counted as viable parasites since irregular structures could mean parasites undergoing cell death.

Wash-out assays After 24 h of plating, CC were infected for 24 h at 37°C with BT (Y strain). The cultures were rinsed to remove free parasites and treated for 168 h at 37°C with the compounds at the non-toxic concentration of 5 μM in culture medium that was replaced every 48 h. After 168 h of drug exposure, the cultures were rinsed using PBS and drug-free culture medium was added for another 168 h. The number of parasites released into the medium was quantified using light microscopy and Neubauer chambers (266).

Drug combination assays. The interactions of Bz + Cpd**1** *in vitro* was assessed by colorimetric readout using L929 cells that were infected for 2 h with trypomastigote forms (Tulahuen-β-gal strain), followed by rinsing the cultures to remove non-internalized parasites and further incubation for 24 h before drug administration using a fixed-ratio method (230,284). Predetermined IC_{50} values were used to determine the top concentrations of each drug ensuring that the IC_{50} fell at the midpoint of a seven-point 2-fold dilution series. The fixed ratios of 5:0, 4:1, 3:2, 2:3, 1:4 and 0:5 were used (284,285). At least 2 independent experiments in triplicate were performed. The Fractional Inhibitory Concentration index (FICI) at the IC_{50} of each drug was calculated as the ratio of the IC_{50} of combination and the IC_{50} of the drug alone. The sum of FICI of each compound (ΣFICI) was obtained (285). The mean ΣFICI (xΣFICI) was calculated as the average of ΣFICI. Isobolograms were built by plotting the FICI values. The ΣFICI was used to classify the nature of interaction as recommended by Odds (284): synergy for xΣFICI ≤ 0.5, no interaction for xΣFICI 0.5 – 4 and antagonism for xΣFICI > 4.

4.3.4   *In vitro metabolism*

At LMPH, *in vitro* metabolic stability was studied through the CYP450 superfamily (Phase-I metabolism) by fortification with reduced nicotinamide adenine dinucleotide phosphate (NADPH) and through uridine glucuronosyl transferase (UGT) enzymes (Phase-II metabolism) by fortification with uridine diphosphate glucuronic acid

(UDPGA). For the CYP450 and other NADPH-dependent enzymes, compounds were incubated at 5 μM together with 0.5 mg/mL liver microsomes (S9) fraction of mice and human in PBS in a reaction started by the addition of 1 mM NADPH and stopped at 0, 15, 30 and 60 minutes. At these time points, 20 μl were withdrawn from the reaction mixture and 80 μl cold acetonitrile (ACN) added to inactivate the enzymes and precipitate the protein. The mixture vortexed for 30 sec and centrifuged at 4°C for 5 min at 15,000 rpm. The supernatant was stored at -20°C until analysis. For the UGT enzymes, compounds were incubated at 5 μM together with 0.5 mg/mL liver microsomes in a reaction started by the addition of 2 mM UDPGA cofactor. The corresponding loss of parent compound was determined using ultraperformance liquid chromatography (UPLC) (Waters AquityTM) coupled with tandem quadrupole mass spectrometry (MS²) (Waters XevoTM), equipped with an electrospray ionization (ESI) interface, and operated in multiple reaction monitoring (MRM) mode. A compound is considered satisfactorily metabolically stable if >50% of parent compound is still present after 30 minutes incubation (265).

4.3.5   *In vivo activity*

At LBC, male Swiss Webster mice (18−20 g, 4−5 weeks of age) obtained from the animal facilities of the Institute of Science and Biomodels Technology (ICTB) Fiocruz were housed at a maximum of 6 per cage, kept in a specific-pathogen-free room at 20 to 24°C under 12 h light and 12 h dark cycle, and provided sterilized water and chow *ad libitum*. The animals were acclimated for 7 days before starting the experiments. Infection was performed by intraperitoneal (ip) injection of 10^4 bloodstream trypomastigotes (Y strain). Age-matched non-infected mice were maintained under identical conditions. The animals were divided into the following groups (n ≥5): untreated (infected but treated only with citrate buffer vehicle) and treated (infected and treated with the compounds). *T. cruzi* (Y strain)-infected mice were treated by oral gavage for 60 consecutive days (except for weekends) starting at dpi, which corresponds to the parasitemia onset, using 0.25-25 mg/kg (bid) of Cpd**1** or 100 mg/kg/day Bz. Co-administration for 11 days at suboptimal doses of Cpd**1** (2.5 mg/kg/day) + Bz (10 mg/kg/day) was also performed. Bz at 100 mg/kg/day as optimal dose was run in parallel. Cpd**1** was diluted in 10% (v/v) EtOH, 0.1 M aqueous citrate buffer (pH 3.02, 1.8 mg/ml and then dosed according to body weight of the animals and drug dose). The drug formulations were freshly prepared before each administration. Only mice with positive

parasitemia were used in the infected groups. Parasitemia was individually checked by direct microscopic counting of parasites in 5 µL blood, and mice were examined daily for mortality until 261 dpi when blood was collected from surviving animals for qPCR analysis. Animal survival is expressed as the percent survival rate at the endpoint. For blood qPCR analysis, 500 µL of blood was diluted in a 1:2 volume of guanidine solution and heated for 60 s in boiling water, followed by DNA purification using High Pure PCR Template Preparation Kit (Roche Applied Science) and quantitative Realtime multiplex PCR assays. TaqMan probes were used for quantification of both *T. cruzi* satellite nuclear DNA and internal amplification control (IAC) (Figure 6) (286). Standard curves were constructed for absolute quantification through the serial dilution of total DNA, ranging from 10^5 parasite equivalents to 1 parasite equivalent per mL of blood, obtained with a negative blood sample in guanidine-EDTA. Parasite load was then expressed as equivalent of parasite DNA per mL of blood (287). All animal studies were carried out in strict accordance with the guidelines established by the FIOCRUZ Committee of Ethics for the Use of Animals (CEUA L038-2017).

4.4 Results

4.4.1 Susceptibility assay
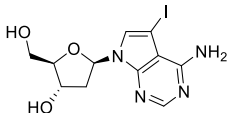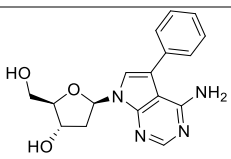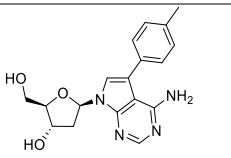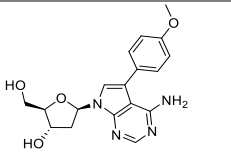
The susceptibility assays were performed on the relevant forms of the trypanosomatid agents of CD, Nagana and sleeping sickness. The outcomes are summarized in table 4.2. The compounds (Cpd) were indicated by their two last digits.
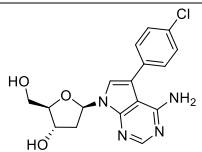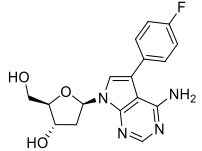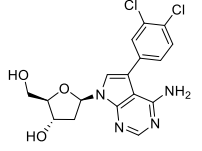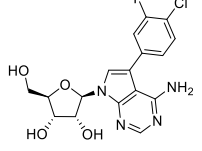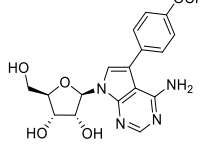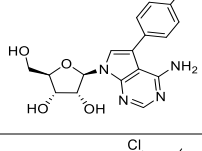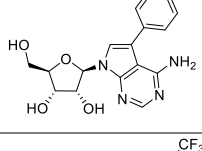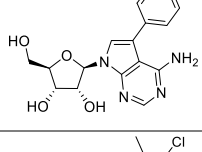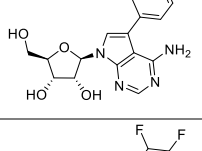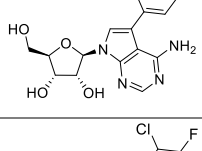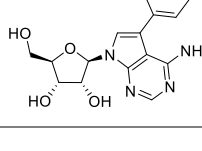
Except from two Cpd (**78** and **10**), 14 out of 16 compounds were highly active ($IC_{50} < 5$ µM) against intracellular forms of *T. cruzi* when evaluated in Tulahuen / MRC-5 model upon 7 days of drug exposure; with 8 Cpds showing sub-micromolar activity and being more potent than the reference drug, Bz. Based on toxicity values measured against MRC-5 for safety assessment, these 14 Cpds were at least 15 times more active against *T. cruzi*. The unmodified ribofuranose analogues **14** and **06**, with 3-fluoro-4-chlolophenyl or 3,4-difluorophenyl substituent groups in C7 position respectively, were the most potent derivatives against Tulahuen, being at least 300 times more active against the parasite. Cpd**05** and the hit 2´-deoxy-ribofuranose analogue **11**, were also highly selective, presenting SIs =137 and 66, respectively, the later showing the highest unspecific cytotoxicity (IC_{50}=11.39 µM towards MRC-5). The analogue JB588 displayed
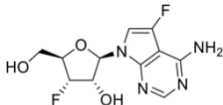
considerable activity against the three trypanosomatid species and IFs of *L. infantum* in peritoneal macrophages (IC$_{50}$= *2* µM) when parallelly assayed but was highly toxic when tested in a golden Syrian hamster VL model, therefore not assayed *in vivo* for CD or HAT.

The compounds share similar activity against *T. b. brucei* and *T. b. rhodesiense* parasites, but none of them exhibited half inhibitory concentrations in nanomolar range as the reference compound suramin (0.015 and 0.025 µM, respectively). Among the five Cpds that displayed moderate activity (between 1 and 5 µM), only Cpd**78** showed values lower than 1 µM in a single biological assay (IC$_{50}$ = 0.08 µM), resulting in a SI of 51. Still, the toxicity against MRC-5 cells (72 h of incubation) was considerably excessive (IC$_{50}$ = 4 µM). The anti- *T. cruzi* Cpd**14** (IC$_{50}$ = 0.05 ± 0.00 µM) also exhibited moderate activity (<2 µM) against *T. brucei*; a similar biological behaviour to Cpd**1** (IC$_{50}$ = 0.047 µM against *T. cruzi*) (265), with a potency against *T. brucei* of about 2 µM (data not shown).

Table 4.2 Nucleoside analogues inhibitory activity (IC$_{50}$) in µM assayed in different cell models *in vitro*, against human lung fibroblast cell lines (MRC-5), *T. cruzi* Tulahuen intracellular forms, *T. b. brucei* and *T. b. rhodesiense* trypomastigote forms, and safety profile determined by Selectivity Index (SI) = (IC$_{50}$ MRC-5 cells)/ (IC$_{50}$ parasite).

		MRC-5 IC$_{50}$	*T. cruzi Tulahuen* IC$_{50}$	SI	*T. b. brucei* IC$_{50}$	SI	*T. b. rhodesiense* IC$_{50}$	SI
FH10678		4	8*	< 1	0.47	8	0.08*	51
FH11708		53.2	3.59*	15	0.28 ± 0.34	< 2	16.93*	3
FH11709		15.29 ± 8.79	0.69 ± 0.07	22	9.79 ± 2.34	< 2	9.56 ± 3.75	2
FH11710		23.63 ± 8.02	9.43 ± 1.33	< 3	29.78 ± 1.33	< 1	27.46 ± 4.61	1

ID	Structure							
FH11711		11.39 ± 1.85	0.17 ± 0.01	66	2.25 ± 0.12	5	3.65 ± 2.4	3
FH11712		>64	1.26 ± 0.11	49	8.01 ± 0.19	< 8	11.66 ± 4.89	5
FH11713		6.71 ± 0.52	0.18 ± 0.01	38	2.00 ± 0.06	3	1.62 ± 0.26	4
FH10714		20.74 ± 1.54	0.05 ± 0.00	400	1.81 ± 0.03	11	1.55 ± 0.39	13
FH10715		46.26 ± 8.4	2.63 ± 0.41	18	28.34 ± 2.29	2	20.95 ± 3.9	2
FH11702		21.77	1.25*	17	38.24	1	19.15*	1
FH11703		7.74	0.18*	43	7.70	1	3.08*	3
FH11704		56.37 ± 0.92	2.63 ± 0.41	21	24.24 ± 3.18	2	23.32 ± 2.72	2
FH11705		24.39 ± 4.64	0.18 ± 0.09	137	7.45 ± 0.31	3	5.26 ± 1.77	5
FH11706		>64	0.20 ± 0.02	>300	7.78 ± 0.04	> 8	7.13 ± 2.19	> 8
FH11707		30.62 ± 7.39	0.65 ± 0.69	47	7.30 ± 0.99	4	5.89 ± 0.28	5

88

JB588		5.97±0.21	0.20 ± 0.02	29.85	0.48 ± 0.05[a]	12	0.06 ± 0.08	99
	Bz	N.D.	2.68± 0.23	N.D.				
	Suramin	N.D.			0.025 ± 0.007	N.D.	0.015±0.007	N.D.

*Results from one single assay from the platform. N.D. (Not determined).

[a] Preliminary data

4.4.2 Metabolic stability

The promising active and selective compounds JB588, FH11706 and FH10714 were metabolic stable up to 60 minutes of exposure to mouse and human liver microsomal fractions with CYP-NADPH (Phase-I) or UGT (Phase-II) enzymes, with at least 94% of parent compound available (Table 4.3).

Table 4.3 Assessment of *in vitro* Phase-I and Phase-II metabolic stability of FH11706, FH10714 and JB588 in mouse and pooled human S9 microsomal fractions[a].

Microsomes	Phase I or II	Time[b]	Remaining (%)						
			FH11706		FH10714		JB588		
			Mean	SD	Mean	SD	Mean	SD	
Mouse	CYP-NADPH	0	100	0	100	0	100	0	
		15	99	5.1	99	2.5	88.5	2.5	
		30	92	4.4	92	2.5	93.5	2.5	
		60	94	4.9	99.5	7.5	99.5	7.5	
	UGT enzymes	0	100	0	100	0	100	0	
		15	99	8.0	99	1	99	1	
		30	101	5.4	102	8	102	8	
		60	99	1.9	104	2	104	2	
Human	CYP-NADPH	0	100	0	100	0	100	0	
		15	97	9	101	1.4	97.5	2.5	
		30	97	4	112	13.1	98	0	
		60	97	7.5	101	9.0	102	1	
	UGT enzymes	0	100	0	100	0	100	0	
		15	105	5.7	96	2.5	100	1	
		30	103	10.6	101	4.2	102.5	3.5	
		60	106	11.4	105	1.5	99.5	1.5	

[a]Percentages of parent compound remaining at various time points of incubation[b] (0, 15, 30, and 60 min). Mean values were calculated from two replicates of two independent experiments. Proper functioning of the *in vitro* assay was confirmed with the reference drugs diclofenac, which is susceptible to phase-I and phase-II metabolism, and fluconazole, which is metabolically stable through phase-I (data not shown).

4.4.3 Pre-treatment of bloodstream trypomastigotes

We checked the anti-*T. cruzi* properties of Cpd**1** using *in vitro* protocols of pre-treatment of bloodstream trypomastigotes before their interaction with mammalian host cells. Although not presenting considerable potency against the non-multiplicative BT forms, Cpd**1** induced marked morphological alterations (round-shaped phenotype) suggestive of impaired fitness. When treated parasites were used to infect CC, although no major effect could be found after 24 h post infection (hpi), a high and statistically significant (p <0.025) drop in all parameters (% IHC, PIC and II rates) was observed for Cpd**1** pre-treated trypomastigotes after 48 and 72 h of CC infection. With Bz pre-treated parasites, PIC values gave a statistically relevant decrease (p = 0.0135) only at 48 hpi, while after 72 h all parameters were reduced (p ≤ 0.0093) (Fig 4.4a-d). Cpd**1** and Bz interfere with parasite fitness, impairing the parasite's ability to successfully establish and sustain infection *in vitro*, affecting the proliferative capacity as clearly shown at 72 hpi with earlier and greater reduction rates triggered by Cpd**1** leading to >90% decrease in the infection indexes (Fig 4.4c).
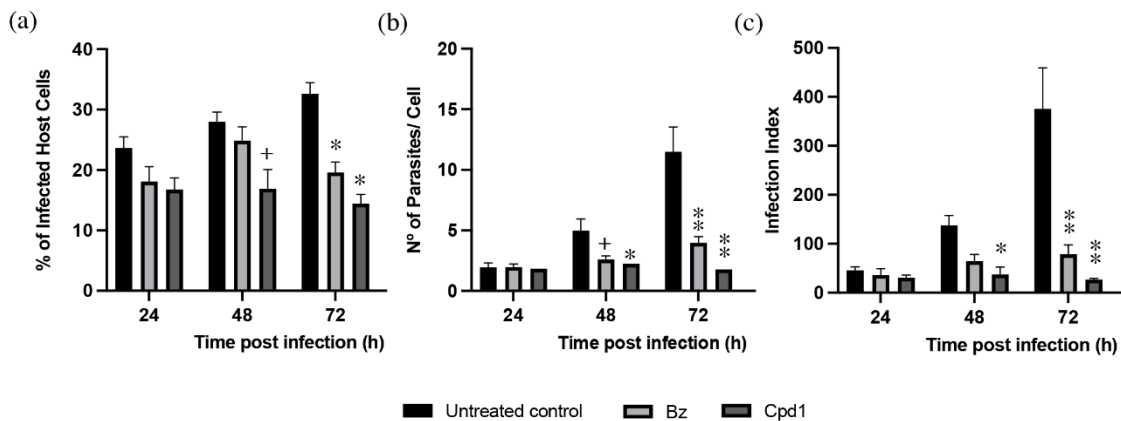
Figure 4.4 Pre-treatment assays of *T. cruzi* (Y strain) with Cpd**1** or Bz before parasite - host cell interaction. Bloodstream trypomastigotes (BT) were treated or not (untreated control) for 24 h with the compounds (corresponding IC_{50}), rinsed and used to infect cardiac cell cultures (moi 10:1) in drug-free medium. Percentage of infected host cells (a), number of parasites/cell (b) and infection index (c) presented in the graphs are the mean and standard deviation for each time-point. Statistical analysis was performed by 2-way multiple comparison ANOVA with Tukey's test (p < 0.05, 95% confidence interval) with + (p < 0.05), * (p < 0.01) and ** (p < 0.001) symbols displayed on the graphs. Infected Host Cells (IHC); Parasite per Infected Cell (PIC); Infection Index (II). Retrieved from Santos *et al*. 2021 (245).

Drug combination

Aiming to tackle simultaneously two different parasite targets, drug combination assays were performed using L929 cell cultures infected with trypomastigote forms of the

β-gal Tulahuen strain, with a fixed-ratio method assessed by colorimetric readout ((8,284). The result of xΣFICI equal to 0.72 obtained from Cpd**1** and Bz combination confers the status of a merely additive effect (Figure 4.5). The most promising results were obtained with the drug ratio of 1:4 (Cpd1:Bz) leading to the lowest IC_{50} and ΣFICI = 0.27 revealing a synergistic profile (Fig 4.5a). The isobolograms (Figure 4.5b) show the drug interaction profile with almost all ratios below the graphic threshold, except for 4:1 Cpd1:Bz ratio (ΣFICI=1.11).

A proof-of-concept *in vivo* co-administration study was conducted with Cpd**1** and Bz in male Swiss mice infected with Y strain (5 animals per group). The chosen drug ratio was near to that which gave the best results *in vitro* (synergy profile reached at 1:4 of Cpd1:Bz ratio). Cpd1, Bz and their combination gave similar declines in parasite load, reaching ≥94% at peak on 8 dpi (Fig 4.5c). Cpd**1** (2.5 mg/kg) given alone resulted in 60% of animal survival. However, mice treated with Bz + Cpd**1** showed increased death rates (80% mortality) and enhanced toxicity, exhibiting urination impairment, prostatic and hunched postures with weight loss. All surviving mice in the different groups showed parasite relapse after interrupting drug administration. Based on the still promising results of Cpd**1** in monotherapy at 2.5 mg/kg producing >97% reduction in blood parasitemia, follow-up experiments were conducted adopting a dose-titration analysis with reduced Cpd**1** doses and introducing long-term drug administration (60 days) aiming to check if sterile cure could be achieved.

A

Drug ratio	IC$_{50}$ (μM) Mean±SD		FICI		ΣFICI	xΣFICI
	Cpd1	**Bz**	**Cpd1**	**Bz**		
5:0	0.246±0.097					
4:1	0.101±0.064	1.396±0.097	0.41	0.70	1.11	
3:2	0.082±0.059	1.059±0.064	0.33	0.53	0.86	
2:3	0.056±0.045	0.695±0.059	0.23	0.35	0.57	0.72
1:4	0.028±0.024	0.319±0.045	0.11	0.16	0.27	
0:5		2.006±1.024				

Figure 4.5 *In vitro* (a, b) and *in vivo* (c) analysis of Cpd**1** and Benznidazole (Bz) combination. Isobolograms (b) of fractional inhibitory concentration index (FICI) values (a) were calculated based on the *in vitro* activity (IC$_{50}$) against intracellular forms of *T. cruzi* after 168 h of drug exposure. (c) *In vivo* evaluation of Cpd**1** in *T. cruzi* mouse model of acute infection displaying parasitemia levels of animal groups. Male Swiss mice were infected (ip) with 10^4 bloodstream trypomastigotes (Y-strain) and drug administration (11 days) started at 5 dpi. Bz alone was given at 100 mg/kg (qd, orally) as reference drug given at optimal dose. Co-administration of Bz (10 mg/kg, qd, orally) and Cpd**1** (2.5 mg/kg, bid) is depicted (c). Control group received only vehicle (citrate buffer, bid). Adapted from Santos *et al.* 2021 (245).

4.4.4 In vivo dose-titration and long-term drug administration

To check for parasite sterilization *in vivo*, an extended and dose-response protocol of drug administration (Cpd**1** at 0.25-25 mg/kg for 60 days, excluding weekends) was used in a mouse model of experimental acute *T. cruzi*-infection. Cpd**1** induced a dose-dependent decrease in both parasitemia levels and mortality rates (Figure 4.6a-b). At 25 and 2.5 mg/kg, a sharp drop (>98%) in blood parasite load was reached similarly to Bz at 100 mg/kg (Fig 4.6a). Cpd**1** at 0.25 mg/kg resulted in >50% of parasitemia decline although not being able to prevent animal mortality (Fig 4.6a-b).
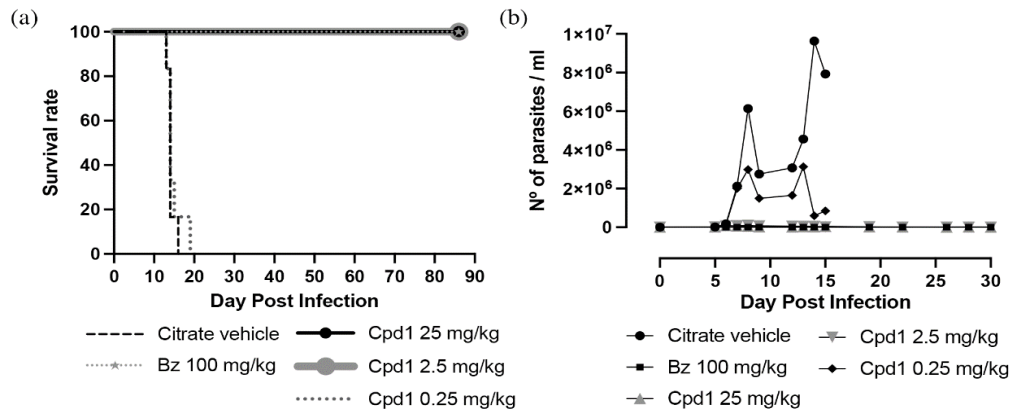
Figure 4.6 *In vivo* evaluation of Cpd**1** in mouse model of *T. cruzi* acute infection. (a) Survival rates (b) and parasitemia levels of animal groups. Male Swiss mice were infected (ip) with 10^4 bloodstream trypomastigotes (Y-strain). Cpd1 administration (0.25-25 mg/kg, bid, orally) was initiated at 5 dpi and given for 60 days. Bz was included as a reference drug (100 mg/kg, qd, orally). The control group received only vehicle (citrate buffer, bid). Retrieved from Santos *et al*. 2021 (245).

Blood analysis by qPCR of the surviving animals showed that the standard curves ranged from 10^5 to 1 parasite equivalent per mL of blood. Parasite load referred as equivalent of parasite DNA per mL of blood sample (eq par/mL) showed 76% efficiency for the satellite nuclear DNA target with a linearity coefficient of 0.996 (Figure 4.7), confirming the accuracy of parasite detection and quantification.
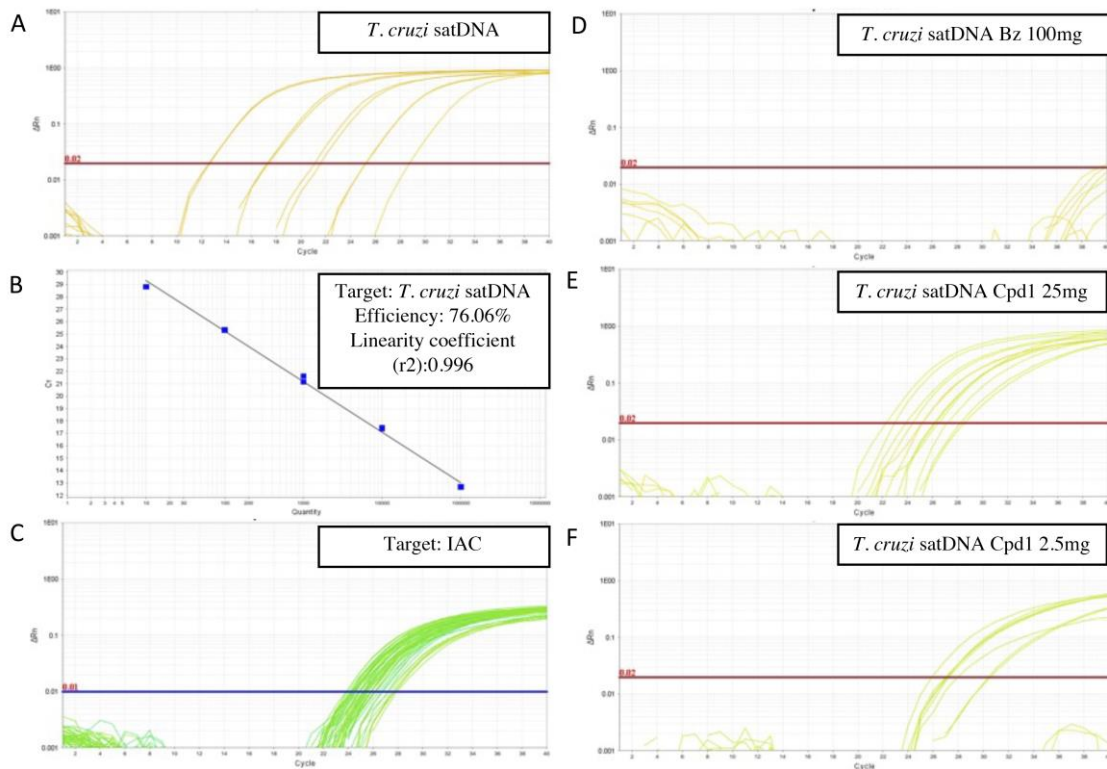
Figure 4.7 Performance of qPCR assays for parasite load quantitation from blood of Swiss mice infected with *T. cruzi* (Y strain) and treated or not with Cpd**1** and Bz. The amplification plots exhibit standard curves with the fluorescent signal magnitude for *T. cruzi* satellite nuclear DNA (*T. cruzi* satDNA) (a) and Internal Amplification Controls (IAC) (b) indicating dynamic extension; in (c) PCR efficiency and linearity coefficient of the reaction. In (d, e and f) *T. cruzi* satDNA amplification plots from Bz 100mg, Cpd**1** at 25 and 2.5 mg mice blood samples, respectively. The qPCR assays were performed using TaqMan probes. Adapted from Santos *et al.* 2021, Supplementary material (245).

When infected mice were treated with Bz, 3 out of 5 animals presented negative blood qPCR (60% of cure) while other mice showed very low amplification (0.0247 eq par/mL) (Figure 4.8). Doses of 25 and 2.5 mg/kg of Cpd1 also decreased the blood parasite load but to a lesser extent than Bz, with one animal from the 25 mg/kg group displaying negative qPCR (17% cure) (Fig 4.8). Statistical analysis indicated no significant differences between the groups (ANOVA p >0.31).
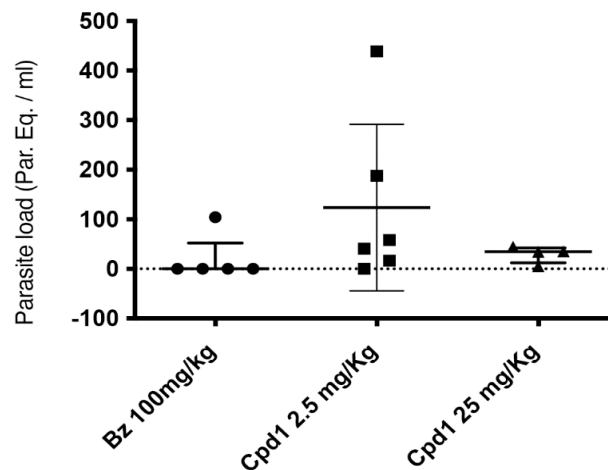
Figure 4.8 Blood qPCR analysis of surviving Swiss male mice infected with *T. cruzi* (Y strain) and orally treated with Cpd**1** (25 and 2.5mg/kg, bid,) and Bz (100mg/kg, qd). Parasite load is referred as number of parasite equivalents per mL. Each symbol on the scatter dot plots represents an individual value. Bars represent the median values and whiskers represent the interquartile range. Statistical analysis was performed by one-way multiple comparison ANOVA with Tukey's test between the experimental groups (p <0.05, 95% confidence interval), all displaying no significant (ns) difference: $0.31 < p < 0.43$. Retrieved from Santos *et al*. 2021 (245).

4.4.5 *Wash-out assays*

As low parasitology cure was observed even under long-term drug administration in the *in vivo* model of *T. cruzi* acute infection, washout assays were conducted to assess *in vitro* drug sterilization. For this purpose, the number of released parasites into the

supernatant of infected CC cultures was quantified by light microscopy at different time-points (Figure 4.9a).

Both Bz and Cpd**1**-treated cultures sustained a marked and significant (p ≤0.001) reduction in the number of released parasites compared to the untreated samples which showed a continuous discharge of trypomastigotes into the culture medium peaking at 144 h with >200 par/mL (Figure 4.9a-b). Before drug withdrawal, Cpd**1** fully suppressed parasitism (light microscopy observation) while Bz resulted in a minor parasite release (≈8 par/mL) at 144 hpi (Fig 4.9a). After drug removal at 168 h, Bz and Cpd**1** were able to sustain the absence of parasites into the culture supernatant for 24 h, while untreated cultures exhibited >75 parasites per mL. However, trypomastigotes re-emerged from the 4th day of drug removal (at 264 h) in Bz- as well as Cpd**1**-treated cultures. Bz and Cpd**1** incubation resulted in comparable parasitism (6 and 10 par/mL, respectively) that was at least 19-fold lower than the untreated group (180 par/mL). At the last time point (312 h or 6th day post drug withdrawal), the number of released parasites reached 15 (Cpd**1**) and 13 (Bz) par/mL, being about 15-fold lower than the untreated control (>210 par/mL). Wash-out assays demonstrated a similar capacity of Cpd**1** and Bz to temporarily arrest parasite growth, ensuing a reduced number of released parasites into the supernatant of infected CC cultures. Cpd**1** could not provide definite *in vitro* sterile cure (Fig 4.9) even upon using long-term drug administration (Figures 4.6).
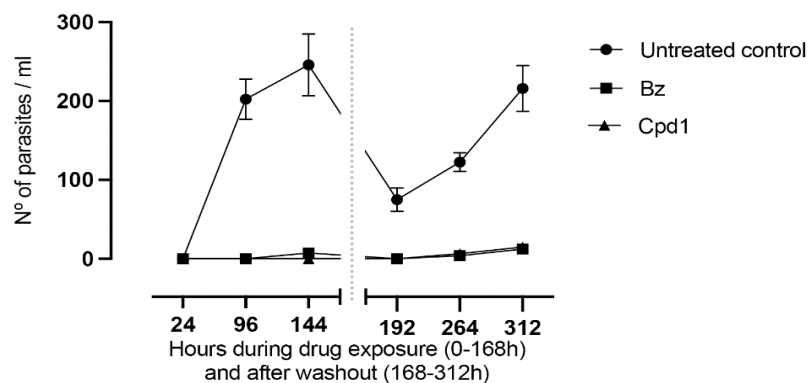
Figure 4.9 Wash-out experiments of *T. cruzi*-infected cardiac cell cultures. Panel A: Number of culture-released trypomastigotes as a function of incubation time. Infected cultures (Y strain) were incubated for 168 h with Cpd**1** or Bz and then another 168 h with drug-free medium before assay readout. Data represents mean ± SD of two independent experiments. The grey line indicates the time point at which compound exposure is halted by changing to drug-free medium. Statistically significant values between control and treated groups were calculated by Welsh multiple nonparametric t-test (p <0.05, 95% confidence interval) and p values ranging $0.000009 \leq p <0.002$. Retrieved from Santos *et al*. 2021 (245).

4.5 Discussion

Former studies of our group reassessed the natural antibiotic tubercidin and a series of 7-substituted analogues aiming to identify novel hits against *T. brucei*, the agent of HAT (269). Besides being very active against *T. brucei*, some phenyl-substituted analogues also presented high *in vitro* potency against *T. cruzi*, which motivated us to further explore nucleoside derivatives.

The new series of nucleoside analogues analysed in the present thesis showed a higher number of promising analogues upon *T. cruzi* in comparison to *T. brucei spp.* (although the later displayed some compounds with moderate activity), and that merits further analysis in preclinical *in vitro* and *in vivo* models. In fact, most of the studied nucleoside derivatives are not active against the non-replicative BT of *T. cruzi* (Y strain), even with recently assayed concentrations up to 81 µM. Conversely, outstanding activity against intracellular forms (representative DTUs and strains such as Y, Colombiana and Tulahuen, corresponding to DTUs II, I and VI) was observed.

Some of the previously studied 3′-deoxy-d-ribofuranose derivatives, such as the Cpd**1**, showed an acceptable safety and efficacy profile in mouse models of *T. cruzi* infection (265). Cpd**1** also presented desirable drug-like properties, such as good oral bioavailability and *in vitro* metabolic stability, which are essential characteristics to meet the TPP and allow potential clinical translation. The current criteria for 'hit' and 'lead' candidate selection for CD comprises definition of compound profile activity (preferably trypanocidal) (241), efficacy against different *T. cruzi* discrete type units (DTUs) and parasite forms relevant for human infection (288,289), host-parasite interaction exploitation (132), capacity to sustain sterile cure *in vitro* (241) and parasitemia suppression and survival rates with sterile cure *in vivo* (290). Most of these criteria were approached for Cpd**1,** which proved highly potent against intracellular forms of different parasite strains and DTUs, displayed very high selectivity indices (>410 up to 9,700) and was metabolically stable in the presence of mouse, human, rat and dog S9 microsomal fractions (265). When administered for 5 consecutive days (at 25 mg/kg, bid), no sterile cure could be achieved despite its high capacity to fully suppress parasitemia and provide 100% survival in mouse models of *T. cruzi* infection (265). As also observed with other purine nucleoside analogues (24,266,271), Cpd**1** was inactive against bloodstream

trypomastigotes despite its outstanding intracellular activity upon o infection of different mammalian host cells including primary cardiac cell cultures ($IC_{50} = 0.029 \pm 0.006\ \mu M$) and L929 cell lines ($IC_{50} = 0.25 \pm 0.17\ \mu M$) (265). At that time, the lack of *in vivo* sterilization by Cpd**1** was attributed at least in part to its inefficacy towards BT and/or to the short treatment period that was adopted as proof-of-concept *in vivo*.

Then, further studies were performed to check those hypotheses as underlying basis for *in vivo* therapeutic failure. Our findings demonstrated that although Cpd**1** is not potent to induce a rapid lysis of trypomastigotes, it induces important morphological alterations (round-shaped phenotype) suggestive of impaired fitness. To check if these treated and surviving parasites were able to invade host cells and differentiate into intracellular amastigotes, a pre-treatment assay on BT before infection was performed, revealing impairment of the parasite's ability to develop a successful infection in cardiac cell cultures. The pre-incubation of BT with Cpd**1** followed by rinsing and quantification of the live and motile forms to normalize the parasite:host cell ratio resulted in a substantial drop of both the percentage of parasitized cells and the number of parasites per infected host cell, ensuing reduced infection indices (>90%) as compared to infection with untreated parasites.

When evaluated in a mouse model of acute *T. cruzi* infection under extended drug administration (60 days, except weekends), Cpd**1** controlled parasitemia but was unable to induce full sterile cure as confirmed by qPCR analysis. *In vitro* wash-out assays corroborated these findings as Cpd**1** was unable to accomplish sterilization even though the number of released trypomastigotes was >90% lower than in untreated controls. As proposed in immunocompromised CD patients, it is probable that trypomastigotes can flourish from "dormant forms" located in different organs, including the gastrointestinal tract (291,292). Our present assays argue in favor of dormant forms since even not able to lyse trypomastigotes, Cpd**1** impairs their ability to establish a successful *in vitro* infection. Despite outstanding efficacy against intracellular forms (Fig 4.10), Cpd**1** is not able to induce *in vitro* sterilization possibly due to its inefficacy against parasites with a low metabolism, such as the persister and bloodstream forms.

Drug combinations have largely been encouraged to find more efficient, shorter and safer therapies for different diseases, thereby also mitigating drug resistance. This approach represents an important strategy for novel therapeutic alternatives for NTDs (293). For more than one decade, combinations of nifurtimox-eflornithine (NECT) (76) and sodium-stibogluconate-paromomycin (SSG&PM) (294) have been successfully used

for respectively HAT and cutaneous leishmaniasis, but no combination therapy is yet available for CD. Along those lines (295), Bz was combined with Cpd**1**. Our data indicated an additive interaction profile when Bz + Cpd**1** was used *in vitro*. *In vivo* co-administration using sub-optimal doses of both agents did not improve the outcomes of each compound used separately. Conversely, an unexpected toxic profile (urination impairment) was noted that could be related to the exacerbation of renal injuries induced by *T. cruzi* infection (296).

Our drug research complies with current criteria for DD programs of NTDs caused by kinetoplastids, seeking robust proof-of-concept in preclinical trials to infer the ability of novel compounds to eliminate residual parasite nests and avoid relapses. We also recently reported the synthesis and evaluation against *T. cruzi* and *L. infantum* of a library of 7-substituted and ribofuranose-modified pyrazolo[3,4-d]pyrimidine nucleosides with 3′- and 7-modifications comprising both inosine-like (allopurinol riboside) and adenosine-like (aminopurinol riboside) analogues (24). It remains attractive to evaluate nucleoside prodrugs to check for improved permeability and/or improved *in vivo* efficacy as novel drug candidates for NTDs like CD and HAT.

4.6   Conclusion

Cpd**1** and Bz interfere with parasite fitness, impairing the parasite's ability to successfully establish and sustain infection *in vitro*, Wash-out assays demonstrated a similar capacity of Cpd**1** and Bz to temporarily arrest parasite growth, ensuing a reduced number of released parasites into the supernatant of infected CC cultures. The excellent profile of Cpd**1** on intracellular amastigote forms and on trypomastigote fitness were not enough to achieve *in vitro* nor *in vivo* sterilization possibly due to the presence of dormant forms of *T. cruzi*. Parasite recrudescence was observed even after Cpd**1** long term administration, corroborating the hypothesis of therapeutic failure due to subpopulations of dormant forms and/or genetic factors in persister parasites involved in natural drug resistance. Still, nucleoside analogues proven to be a promising source of potent and selective candidates for CD *in vitro* that deserve further characterization.
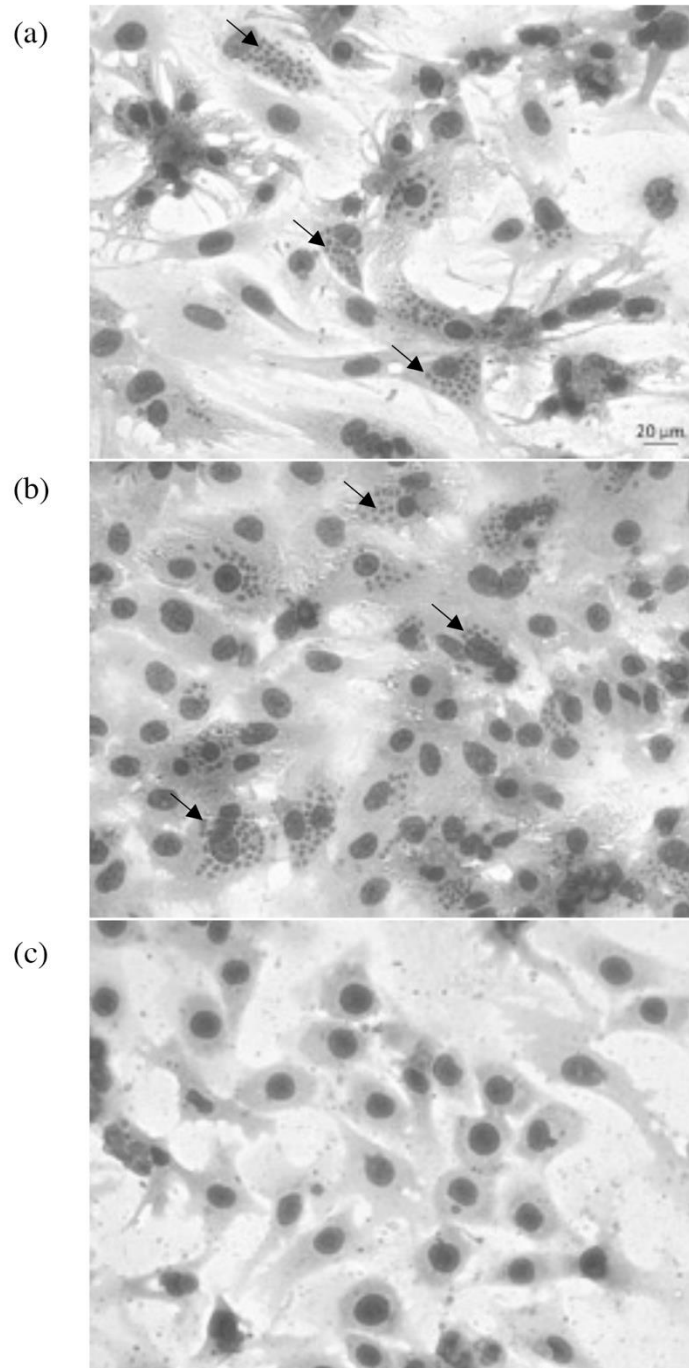
Figure 4.10 Light microscopy of cardiac cell cultures infected with *T. cruzi* (Y strain). (a) Untreated and treated with 1 µM (b) Bz and (c) Cpd**1**. Arrow: intracellular amastigotes. Retrieved from Santos *et al.* 2021 (245).

5   Nucleoside analogues: mode-of-action in *T. brucei*

[1] Laboratory of Microbiology, Parasitology and Hygiene (LMPH), University of Antwerp, 2610 Wilrijk, Belgium.

[2] Laboratório de Biologia Celular (LBC), Instituto Oswaldo Cruz (IOC/Fiocruz), Rio de Janeiro 21040-900, Brazil.

[3] Laboratory for Medicinal Chemistry, Campus Heymans, Ghent University, 9000 Gent, Belgium.

[4] Current affiliation: Janssen Pharmaceutica N.V., Turnhoutseweg 30, 2340 Beerse, Belgium

* Correspondence: guy.caljon@uantwerpen.be

5.1 State-of-the-art

Some nucleoside analogues proved to be highly active against CD and HAT agents *in vitro* and *in vivo* and deserve further exploration regarding their MoA to identify and validate their cellular targets and enable compound optimization. For that purpose, RNA interference (RNAi) technology represents a powerful tool for a genome-wide screening (297,298) and the current study makes used of the advantage that *T. brucei* expresses this regulation machinery.

5.1.1 RNAi background and discovery in T. brucei

Small interfering RNAs (siRNAs) participate in posttranscriptional gene silencing (PTGS) that regulates eukaryotic gene expression during development and in response to stresses including viral infections (299). The RNAi engineering has been used in several applications, including discovery of druggable targets (297), pesticides (300) and therapy, such as ONPATTRO (Patisiran), the first RNAi drug approved by FDA in 2018 (298). In 1998, double-stranded RNAs (dsRNA) were first identified as relevant agents for PTGS in *Caenorhabditis elegans*, a fact referred to as RNA interference (RNAi) (301). Gene silencing has been observed in several organisms (302,303), non-coding RNAs disclosed as regulators of gene expression and the whole machinery gradually revealed (304). In summary, short double-stranded RNA fragments originating from nuclear mRNAs or exogenous dsRNA are cleaved by the endoribonuclease Dicer into 20-25 base pairs long fragments called microRNA and small interfering RNA, respectively. These RNA fragments are assembled to Argonaute (AGO) proteins, forming the RNA-induced silencing complex (RISC) (299). The RNAi antisense strand is used to guide sequence-specific silencing of complementary target mRNAs, suppressing pre- or post-initiation translation by catalytic activity (305).

Being a potential tool for gene regulation, the RNAi mechanism has been extensively researched also in trypanosomatids. In 1998, RNAi was demonstrated in *T. brucei* (306) as a mechanism to maintain the integrity of the parasite genome by destroying viral transcripts derived from transposons (307). In *T. brucei,* the argonaute (TbAGO1) slicer is predominantly localized in the cytoplasm but also detected in nuclei while TbCL1 and TbCL2 (307,308) are found in the cytoplasm and nuclei respectively, as shown in figure 5.1.

T. brucei-RNAi constructed libraries allowed the simultaneous identification of a large number of genes related to essentiality, parasite fitness, parasite:host interaction, drug action and resistance (93,269,309). Genome-wide loss-of-function studies were first evaluated in procyclic forms (present in insect vector) (310–312) and later extended to BT forms when stably transformed parasites were obtained (313,314). With BT RNAi libraries (314), important aspects related to parasite:host interaction could be addressed, besides drug resistance development and mechanisms of antigenic variation (123), therefore applied in the current study.
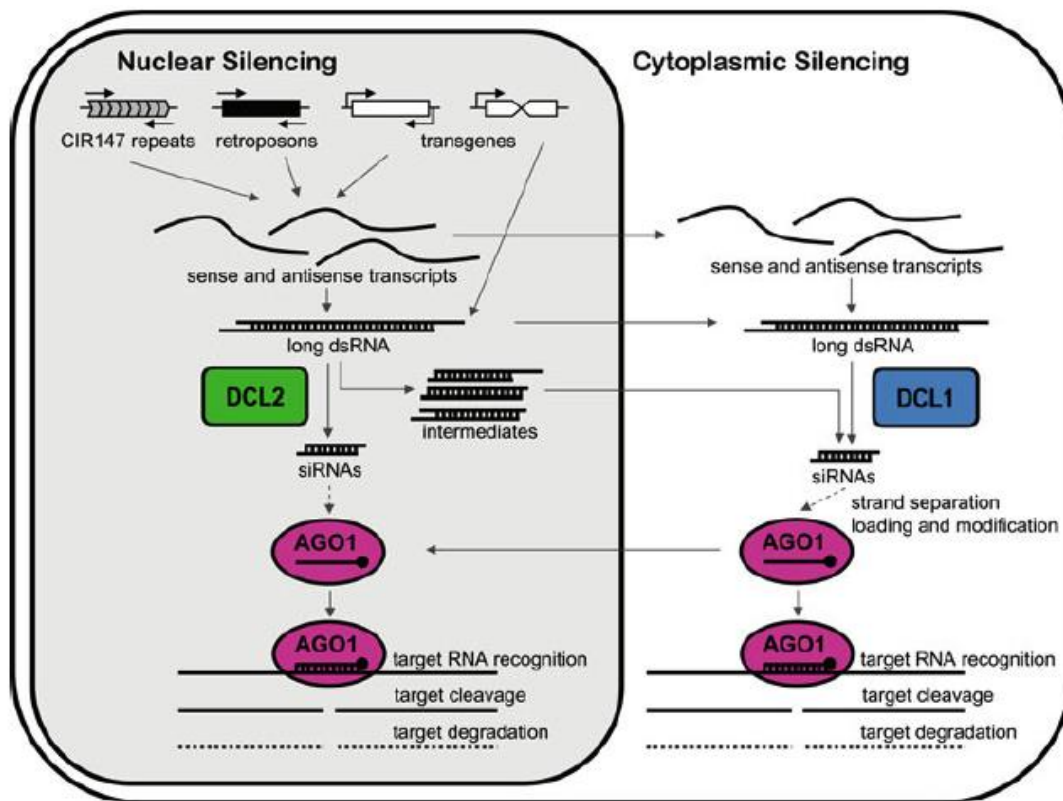
Figure 5.1 RNAi machinery in *T. brucei*. The TbDCL2 and DCL1 enzymes process long dsRNAs derived from sense and antisense transcripts from retroposons and repeats into siRNA duplexes in the nucleus and the cytoplasm, respectively. AGO1 is programmed with single-stranded "guide" siRNA following siRNA strand separation, loading, and modification, to form RISC. AGO1 finds transcripts complementary to the bound siRNA in both compartments of the cell, and base pairing between the siRNA and the target leads to RNA cleavage and degradation. TbDCL: *T. brucei* Dicer-like enzyme; dsRNA: RNA duplex; AGO 1: Argonaute; RISC: NA-induced silencing complex. Figure retrieved from Ullu *et al.* 2011 (25) (Fig 8.1).

5.2   Research objective

The present main objective was to gain insights into the MoA of 4 novel antitrypanosomal nucleoside analogues (FH8512, FH11706, FH10714 and JB588) selected by *in vitro* screening against a panel of trypanosomatids. A genome-wide bloodstream *T. brucei* RNAi library (provided by Prof. Isabel Roditi, University of Bern, Switzerland) (314) was used for the analysis of gene involvement in the MoA of these 4 compounds.

5.3   Material and Methods

5.3.1   Stock solutions

Compounds FH8512, FH11706, FH10714 and JB588 were prepared as described in Chapter 4, part 1.

5.3.2   Parasite strains and cell culture.

The bloodstream forms of the following recombinant *T. b. brucei* strains were used to MoA evaluation (*T. brucei*-MoA) (a) *T. b. brucei MITat 1.2* (New York single marker (NYSM) line): the strain used to generate the RNAi library, (b) ADKIN: RNAi clone, knock down for adenosine kinase (c) 4EIP: RNAi clone, knock down for 4E interacting protein, (d) BS221 (TbAT1KO background strain), (e) TbAT1KO (P2 transporter knockout), (f) Endonuclease G (EndG), (g) FLA1-binding protein (FLA) and (h) retrotransposon hot spot protein 5 (HSP). The parasites were diluted (1:5) in 5 mL of HMI-9 culture medium supplemented with 10% inactivated Fetal Calf Serum (iFCS) and cultured for 5 consecutive days. For RNAi expression, 1 µg/mL tetracycline was daily added to the medium.

5.3.3   Susceptibility assays

Assays were performed in sterile 96-well microtiter plates, each well containing 10 µL of FH8512, FH11706, FH10714 and JB588 4-fold dilutions (64 – 16 – 4 – 1 – 0.25 – 0.0625 – 0.015625 – 0.0039 – 0.000975 and 0.00024 µM) together with 190 µl of the parasite suspension with 4×10^3 parasites per ml. After 72 h incubation, 50 µL resazurin

per well was added and parasite growth assessed fluorometrically (λ_{ex} 550 nm, λ_{em} 590 nm), after 24 h at 37°C (315).

5.3.4   Screening of the RNAi library

Trypanosoma b. brucei BT forms (3×10^6) of the RNAi library (transfected to carry RNAi inserts) were diluted (1:10) in 30 mL of HMI-9 culture medium supplemented with 10% iFCS plus 1 µg/mL tetracycline and incubated for 3 days to induce the RNAi phenotype. Ten mL of the culture was maintained without tetracycline induction to serve as a negative control. After 62 h of induction, different concentrations of the test compounds FH8512 (4.29, 4.78, 5.65 µM), FH10714 (6.56, 7.00, 7.67, 15.34, 30.68, 46.02 µM) and JB588 (0.39, 0.46, 0.59, 1.18, 2.36, 3.54 µM) were added to 10 mL of individual cultures containing 1×10^5 parasites/mL. The drug concentrations were based on their $IC_{98/99}$ values as previously determined in resazurin-based susceptibility assays. The parasites were daily monitored by light microscopy.

Under drug pressure, as soon as the non-induced RNAi cultures collapsed and the induced cultures grew normally, they were diluted 1:10 in fresh medium containing tetracycline and the respective drug at $IC_{98/99}$. After 2-3 passages, the parasites were harvested for analysis and identification of the RNAi inserts. Only cultures exposed to FH10714 at 30.68 and 46.02 µM collapsed; in this case the parasites exposed to 15.34 µM were recovered in medium without drug pressure as soon as they restarted to grow, and their DNA purified to identify the RNAi inserts.

5.3.5   RNAi insert identification

The genomic DNA (gDNA) of the drug-exposed parasites was isolated from 20 mL of a stationary phase culture using the QIAamp DNA mini kit (QIAGEN). The DNA concentration was determined using a nanodrop and diluted to 20 ng/µL gDNA in PCR water. The RNAi inserts were amplified using p2T7_seq (5'-CCGCTCTAGAACTAGTGGA-3') as forward and p2T7hygPJ4 (5'-GGAAAGCTAGCTTGCATGCCTG-3') as reverse primer (PCR program: 1 cycle for 1' at 98°C, 25 cycles for 10" at 98°C, 30" at 58°C, 1' at 72°C and 1 cycle for 10' at 72°C).

PCR products were resolved on a 1% agarose gel (100 V for 120') to see the number and size of the amplified inserts. PCR products were purified using the ExoSAP-IT™ PCR Product Cleanup kit (ThermoFisher Scientific). A nested PCR was performed (PCR program: 1 cycle for 3' at 94°C, 30 cycles for 1' at 94°C, 1' at 50°C, 2'30" at 72°C

and 1 cycle for 10' at 72°C) and PCR products analysed on a 1% agarose gel (100V for 120'). Interesting inserts, meaning they were present in the tetracycline positive clones but absent in the tetracycline negative clones, were extracted from the gel using the GenEluteTM Gel Extraction Kit (Sigma-Aldrich).

Finally, the PCR products were ligated in the PCR Topo 2.1 vector system (ThermoFisher Scientific), transformed into high-efficiency competent *E. coli* cells (NEB10) and plated onto LB agars with ampicillin. Five colonies per target were selected to perform a colony PCR (PCR program: 1 cycle for 3' at 98°C, 30 cycles for 1' at 98°C, 1' at 50°C, 1'30" at 72°C and 1 cycle for 10' at 72°C) and subsequently analysed on a 1% agarose gel (100V for 120'). Positive clones were selected and sent for sequencing. The RNAi insert was sequenced from both sides with primers p2T7_seq and p2T7linker_rev (5'-AGGGCCAGTGAGGCCTCTAGAG-3'). Sequences were blasted against *T. brucei* transcripts on the TriTrypDB and homology detection using comparison of hidden Markov Models (https://toolkit.tuebingen.mpg.de/hhpred).

5.3.6 *Validation of the RNAi phenotype*

To validate the RNAi effect of the different RNAi inserts, the insert was back cloned into a p2T7Bern vector for transformation into *NYSM* cells. First, a PCR was performed on the PCR 2.1 vector containing the RNAi inserts with the P2T7_seq forward primer containing the *Nde*I restriction site (GGAATTC**CATATG**-CCGCTCTAGAACTAGTGGA) and the P2T7linker_rev reverse primer containing the *Xho*I restriction site (*CCG***CTCGAG**-AGGGCCAGTGAGGCCTCTAGAG). PCR products were analysed on a 1.2% agarose gel and correct lanes extracted from the gel using the GenElute^{TM} Gel Extraction Kit (Sigma-Aldrich). The purified PCR product and the p2T7Bern vector were digested overnight at 37°C with *Nde*I and *Xho*I restriction enzymes. The digested DNA was ligated using a T4 ligase for 2 h at room temperature. Finally, the ligated product was transformed into high-efficiency competent *E. coli* cells (NEB10) by electroporation and plated onto LB agars with ampicillin. A colony PCR was performed to identify the colonies containing the vector which were then sent for sequencing. Next, 10 µg of the P2T7Bern DNA containing the RNAi inserts was digested with *Not*I restriction enzyme to obtain linear DNA and purified using the QIAquick PCR purification kit (QIAGEN). 4×10^{7} *NYSM* cells were transferred to a 2 mm gap cuvette together with 10 µg linear plasmid DNA. The cells were subjected to two consecutive pulses of 1.2 kV with 186 Ω resistance and 50 µF capacitance. After transformation, the cells were transferred to HMI-9 medium containing 10% iFCS. After 18-22 h, 2.5 µg/mL

of hygromycin B was added to the cells. After 6 days, the hygromycin B pressure was increased to 5 µg/mL. After sufficient cell growth, the culture was cloned to obtain monoclonal cell populations. Monoclonal cell populations were subjected to a resazurin-based susceptibility assay to determine the 50% inhibitory concentration as described previously.

5.4 Results

5.4.1 Susceptibility of NYSM

Apart from FH11706, all compounds reached high potency, with $IC_{50} < 1.5$ µM and were assessed in *T. brucei* RNAi library for MoA. JB588 was the most active against *T. brucei* NYSM, with potency at nanomolar range (Figure 5.2).

$IC_{50NYSM}=1.41 \pm 0.09$ $IC_{50NYSM}= 6.41 \pm 0.52$ $IC_{50NYSM}= 1.50 \pm 0.15$ $IC_{50NYSM}= 0.08 \pm 0.01$
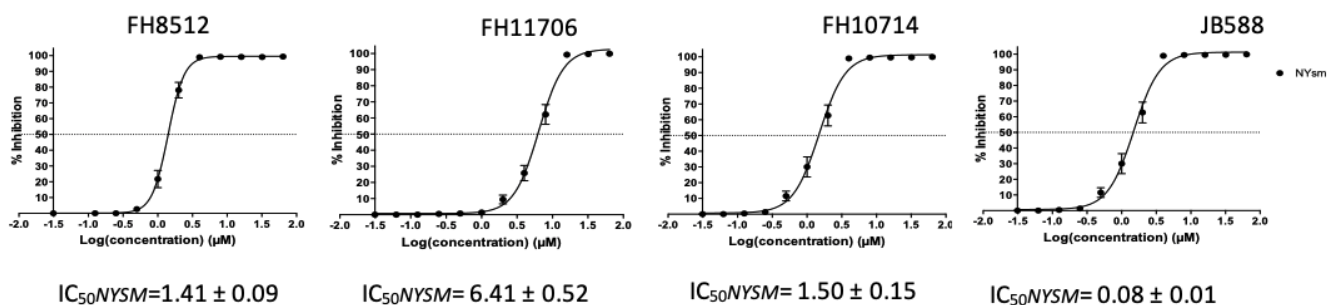
Figure 5.2 Concentration-response curves of FH8512, FH11706, FH10714, JB588 on *T. brucei NYSM* parasites. IC_{50} values expressed in µM.

5.4.2 Genome-wide T. brucei RNAi library

Trypanosoma brucei brucei bloodstream forms of the RNAi library (NYSM line) were exposed to the concentrations corresponding to the $IC_{98/99}$ values of JB588, FH8512 and FH10714 for the selection of the resistant pool (exposed or not to tetracycline) and then for gDNA amplification. The results of the gDNA amplification are shown on figures 5.3 a and c and their respective PCR shown in figures 5.3 b and d. Positive clones were selected, sent for sequencing and results are detailed in Table 5.1.
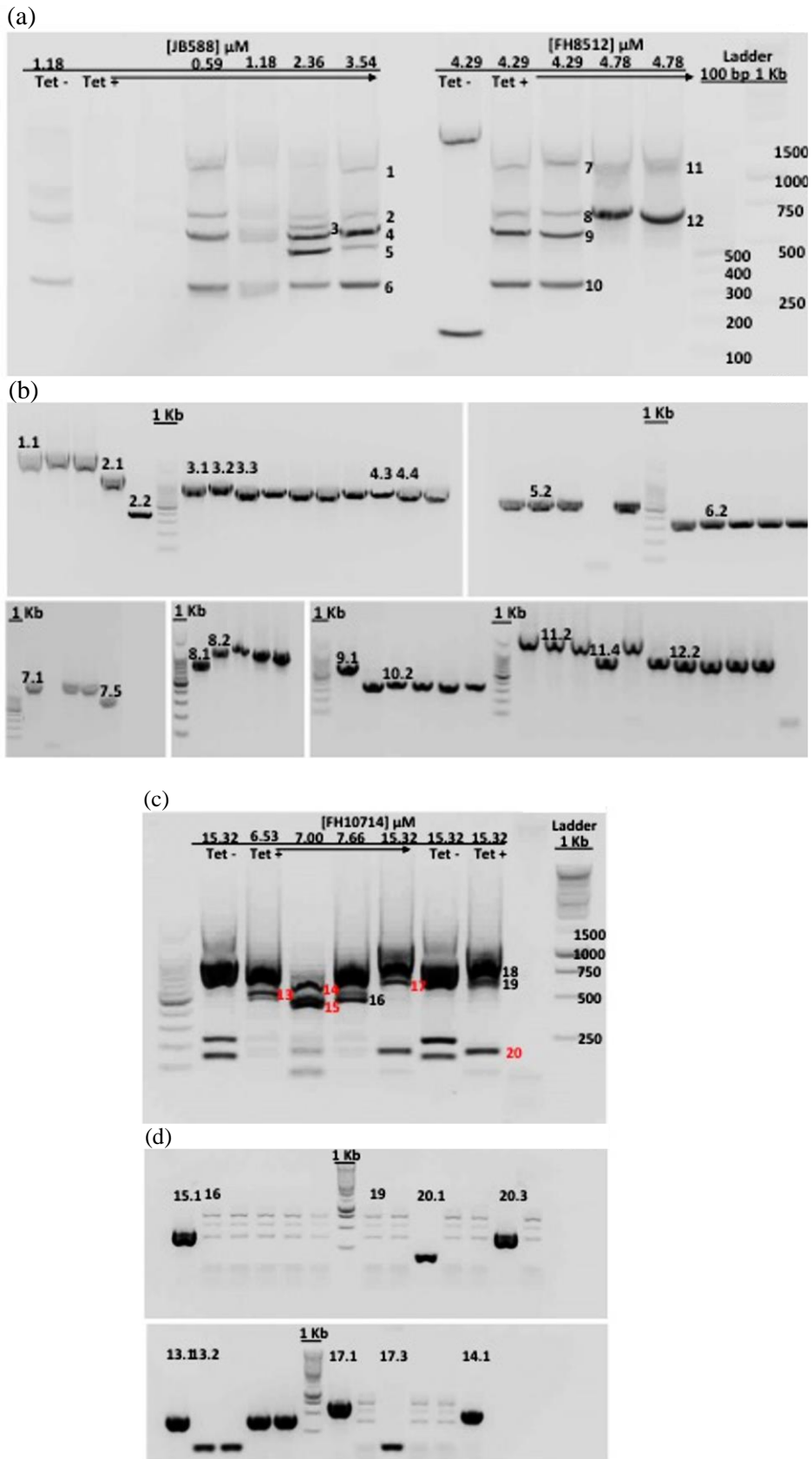
Figure 5.3 RNAi inserts identification. The RNAi inserts were amplified using p2T7_seq as forward and p2T7hygPJ4 regarding JB588 & FH8512 (a) and FH10714 (c) selections. When available, at least 5 colonies per target were selected to perform a colony PCR with primers p2T7_seq and p2T7linker_rev regarding JB588 & FH8512 (b) and FH10714 (d), after ligation of the PCR products in the PCR 2.1 vector

system (ThermoFisher Scientific), transformation of the high-efficiency competent *E. coli* cells (NEB10) and plating in LB agars with ampicillin. The red numbers (c) refer to the targets that were amplified in the colony PCR (D). All the targets in (a) were amplified in the colony PCR (b). The PCR products were analysed on a 1% agarose gel.

Table 5.1 RNAi insert identification after sequencing. Sequences were blasted against *T. brucei* transcripts on the TriTrypDB and homology detection using comparison of hidden Markov Models (https://toolkit.tuebingen.mpg.de/hhpred).

	Band nr	Gene	Gene product
JB588	1.1	Tb927.8.4040	endonuclease G, putative
		Tb927.8.4050	FLA1-binding protein
	2.1	Tb927.6.170	receptor-type adenylate cyclase GRESAG 4, putative
		Tb927.2.980	retrotransposon hot spot protein 5 (RHS 5), degenerate
	2.2,6.2	Tb427_000612500:pseudogene	Trypanosome variant surface glycoprotein (A-type), putative
		Tb427_000612500:pseudogene	Trypanosome variant surface glycoprotein (A-type), putative
	3.1,4.3,4.4,5.2	Tb927.6.2300	adenosine kinase, putative
		Tb927.6.2300	adenosine kinase, putative
	3.2,3.3	Tb427tmp.244.0480	variant surface glycoprotein (VSG), degenerate
		Tb427tmp.244.0480	variant surface glycoprotein (VSG), degenerate
FH8512	7.1	Tb927.8.4040	endonuclease G, putative
		Tb927.8.4050	FLA1-binding protein
	7.5,8.2	Tb927.6.170	receptor-type adenylate cyclase GRESAG 4, putative
		Tb927.2.980	retrotransposon hot spot protein 5 (RHS 5), degenerate
	8.1,9.1	Tb927.6.2300	adenosine kinase, putative
		Tb927.6.2300	adenosine kinase, putative
	10.2	Tb11.v5.0841	Trypanosome variant surface glycoprotein (A-type), putative
		Tb427_000612500:pseudogene	Trypanosome variant surface glycoprotein (A-type), putative
	11.2	Tb927.5.3430	ubiquitin-activating enzyme e1, putative
		Tb427.05.3430	ubiquitin-activating enzyme e1, putative
	11.4,12.2	Tb427.06.2250	protein kinase, putative
		Tb927.6.2250	rac serine-threonine kinase, putative

		Tb11.v5.0841	prostaglandin F synthase
FH10714	13.1,15.1,20.4	Tb427_100026500.1	pyridine nucleotide-disulphide oxidoreductase/NAD(P)-binding Rossmann-like domain containing protein, putative
	13.2,17.3,20.1	Tb11.v5.0841	prostaglandin F synthase
		Tb11.v5.0597	trypanothione reductase
	14.1	Tb927.2.720	retrotransposon hot spot protein 5 (RHS5), degenerate
		Tb927.2.720	retrotransposon hot spot protein 5 (RHS5), degenerate
	17.1	Tb927.6.2250	rac serine-threonine kinase, putative
		Tb927.6.2250	rac serine-threonine kinase, putative

Among the identified gene products in Table 5.1, adenosine kinase (ADKIN), rac serine threonine kinase (RSKIN), Endonuclease G (EndG), FLA1-binding protein (FLA), retrotransposon hot spot protein 5 (HSP) and variant surface glycoprotein A appear under the pressure of two different compounds.

.

5.4.3 Susceptibility of T. brucei – MoA strains

Among the identified targets, the *T. brucei brucei* RNAi clones for the following knockdown targets: ADKIN, EndG, FLA and HSP were already available in the lab and their susceptibility was next evaluated upon JB588, FH8512, FH10714 and FH11706 (Figure 5.4). In parallel, the 4E interacting protein (4EIP) knockdown and P2 transporter knockout (BS221/TbAT1KO) strains were also included in the nucleoside analogs MoA assessment.
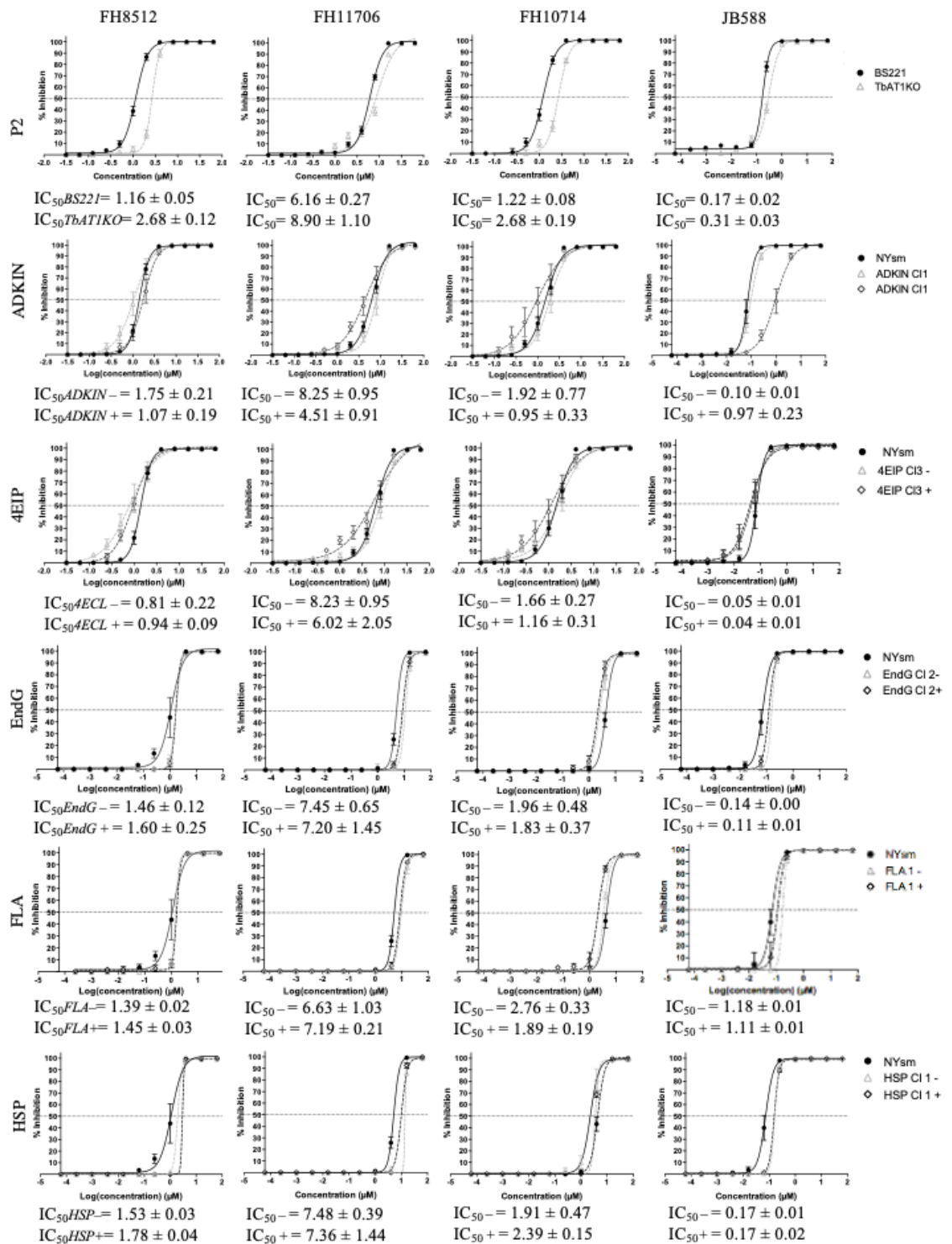
Figure 5.4 Concentration-response curves of FH8512, FH11706, FH10714, JB588 on *T. brucei*–MoA strains specified in the legend. IC$_{50}$ values are expressed in µM. +=tetracycline-induced clones, -= non-induced clones.

After concentration-response analysis of the test compounds against the *T. brucei*–MoA strains and IC$_{50}$ determination as detailed in figure 5.4, it was observed that parasites with a deficient adenosine kinase expression showed a significant decrease in

JB588 susceptibility comparable to the non-induced negative control. IC_{50} of this compound was almost 10-fold higher against the induced ADKIN strain.

Also, slight shifts in the curves were observed for P2 knockout (TbAT1KO) strains exposed to the candidates in comparison to the background BS221, except for JB588. Still, it is unlikely that P2 transporter plays some role in drug uptake, since IC_{50} shifts do not exceed a factor 3 (figure 5.5).

Finally, the other targets also do not seem to play a significant role in the MoA of the four tested molecules, as observed by the compiled IC_{50} values of knockdown strains and their backgrounds displayed in figure 5.5.
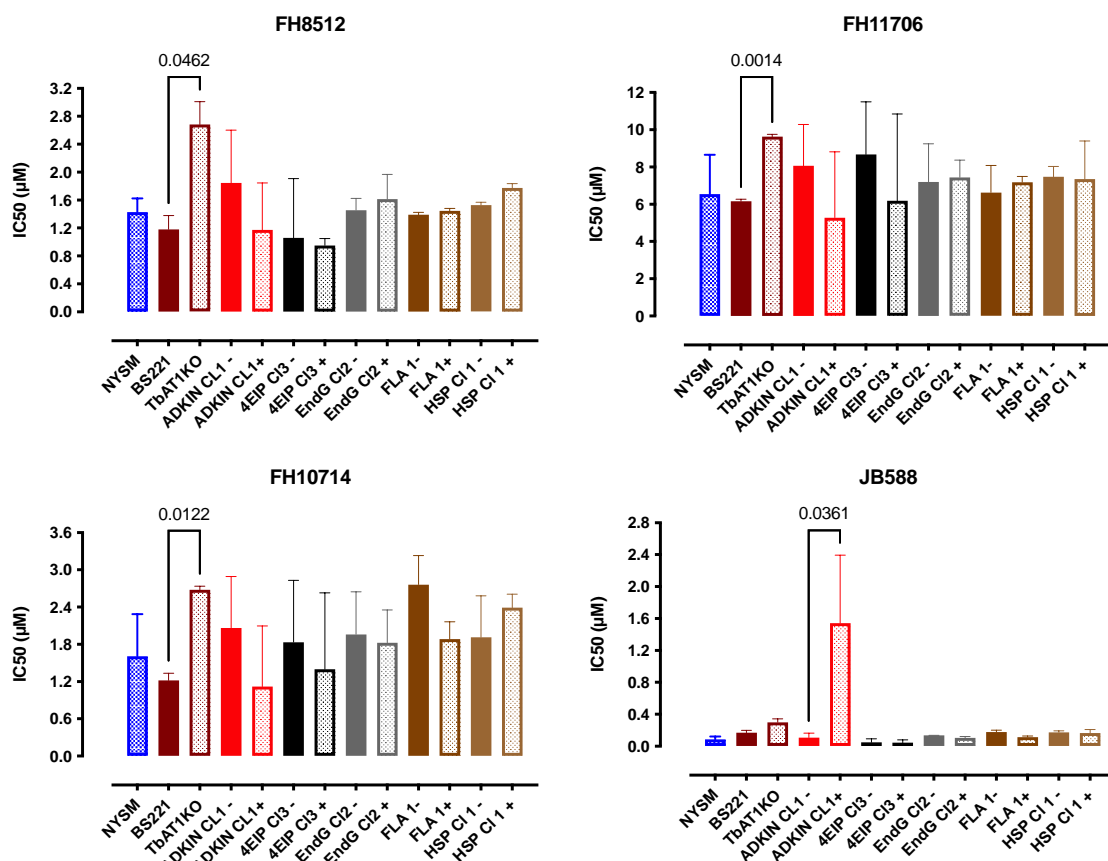
Figure 5.5 T-test statistical analysis performed by GraphPad prism v9.2.0 on independent IC_{50} values of FH8512, FH11706, FH10714, JB588 tested on *T. brucei* engineered strains. No significant difference (ns) when $p > 0.05$. (+) tetracycline-induced clones; (-) non-induced clones.

5.4.4 Susceptibility of T. brucei RNAi constructs evaluation

RNAi constructs were made for the following genes: (i) *ubiquitin activating enzyme* (*UBE1*); (ii) *receptor-type adenylate cyclase (GRESAG 4)* and (iii) *pyridine nucleotide disulfide oxidoreductase / NAD(P) binding Rossmann-like domain containing*

protein (*OXRED*). For each of the 3 genes, two independent RNAi clones were subjected to an IC_{50} determination: No major effects were apparent; some limited effects of increased sensitivity may be seen with the UBE1 clone 1 (Figure 5.6, dark red bar) which deserves further exploration.
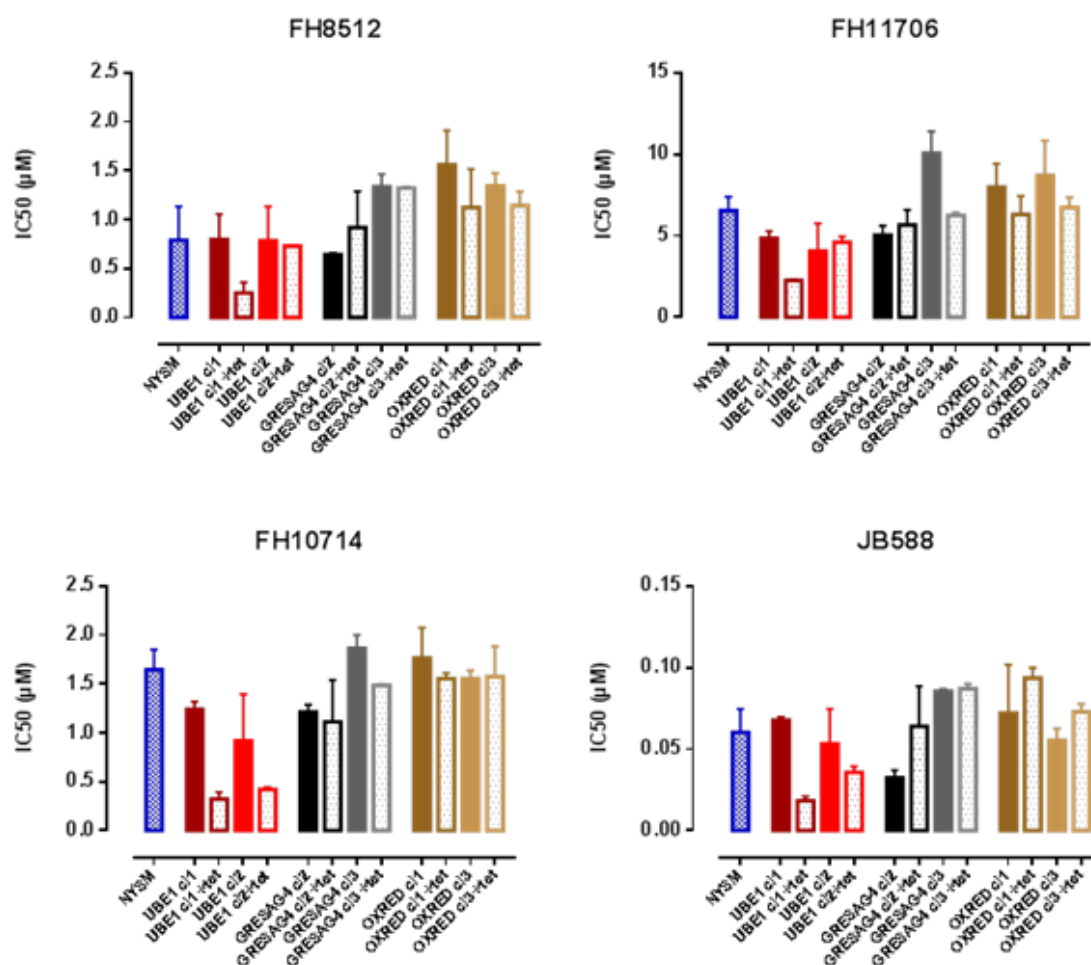
Figure 5.6 Drug susceptibility of RNAi clones targeting UBE1, GRESAG4 and OXRED to FH8512, FH11706, FH10714 and JB588. (+) tetracycline-induced clones, (-) non-induced clones.

5.5   Discussion

Besides the promising *in vitro* and *in vivo* activity reported for some nucleoside analogues, the presence of numerous purine transporters at the level of the blood-brain barrier (316) increases the chance of finding a new effective compound to treat the late chronic stages of HAT disease, including the r-HAT for which arsenic treatments are still in use (132).

Besides cross-resistance evaluation for mechanisms involving the P2 transporter, eight out of eleven gene products revealed by a genome-wide *T. brucei* RNAi loss-of-

function study were evaluated for mode-of-action of nucleoside analogues and, apart from ADKIN, none triggered substantial parasite resistance by target downregulation.

The adenosine transporter P2 is encoded by TbAT1 which also mediates melarsoprol and pentamidine uptake and therefore related to parasite drug cross-resistance (317–319).

In the nucleoside biosynthesis pathway and purine salvage, ADKIN phosphorylates adenosine to generate adenosine nucleotides (80,320), and therefore is considered an important target for this class of compounds (80,320,321). In fact, it was shown that *T. brucei* ADKIN RNAi clones have a reduced sensitivity to a 7-deaza adenosine analogue (TH1008) (315), among other analogs derived from tubercidin and cordycepin scaffolds (269), although not essential for parasite growth and infectivity in mice (315). The JB588 MOA also seems to be related to ADKIN, since in RNAi clones, drug resistance increased almost 10-fold as compared to the wildtype strain. Alternative processing pathways and/or source of purines (80,322) could explain the independence from ADKIN of the other compounds. RNAi clones for RSKIN is under construction to target validation, since there is evidence of this putative target to be involved in two distinct nucleoside analogs MoA.

In sequence, FLA-binding protein performs a structural function through attachment of the flagellum to the trypanosomal plasma membrane. This protein is more abundant in procyclic than bloodstream forms of *T. brucei* (323) utilized in the current study, potentially explaining the difference with another study where this target was confirmed for the same class of compounds (315).

HSP5 protein belongs to a large family of HSPs involved in chromatin modeling (324), transcription elongation and mRNA export in *T. brucei* (325). Still, its downregulation could not confirm involvement in the MoA of the evaluated drugs.

Also, similar results were observed for 4E interacting protein (4EIP), which controls gene expression by mRNA-CAP dissociation after binding to the cap-binding protein 4E1 and suppressing translation (326). Recently, Mabille and colleagues reported that the TH1008 MoA can be partially attributed to 4EIP independently of 4E1 and that a rapid clearance of parasite burden was reached in mice upon infection with the *T. brucei* 4EIPKO strain (315). This identified 4EIP as a promising novel drug target for HAT therapy. Yet, the studied compounds need to undergo a structure-activity relationship analysis (270,327) to have a better insight in the biological activity divergencies between the different chemical structures.

UBE1 is responsible for the parasite protein stability and cellular processes like cell cycle (328) by ATP-Mg2+ assembly and ubiquitin C-terminal acyl adenylation. Recent studies unveiled that components of the ubiquitination and proteasome machinery are potential drug targets in trypanosomatids. The identification of UBE1 as target enzyme (329) was supported by selective and parasite-specific UBE1 inhibitors (330). In the current study, the absence of *T. brucei* UBE1 slightly, but not significantly, increased parasite susceptibility to nucleoside analogs.

Receptor-type adenylate cyclase 4 (GRESAG) belongs to a large family of transmembrane receptors, related to parasite pathogenesis in *T. brucei*, by host immune response inhibition (331), cytokinesis and social motility (332). It is a polymorphic family, and gene plasticity may be linked to the observed lack of an RNAi effect *in vitro* (333).

EndG is a mitochondrial *T. brucei* endonuclease that triggers parasite apoptosis by nuclear DNA damage after migration (334) and is induced by the human serum apolipoprotein (315). Concentration-response assays signalized the lack of EndG participation in the Moa of the evaluated compounds.

Finally, the pyridine nucleotide disulfide oxidoreductase/NAD(P) binding Rossmann-like domain containing protein (OXRED), although a promising target due to the potential influence on purine/pyrimidine biosynthesis, could not be confirmed to be involved in the MoA of the studied nucleoside analogues. Compensation by other members of oxidoreductase family (335,336) sharing similar functions to OXRED could potentially be responsible for the absence of an RNAi phenotype.

5.6   Conclusion

RNAi studies suggest the involvement of ADKIN in the MoA of the nucleoside analogue JB588 against *T. bruc*ei since an approximate 10-fold increase in IC_{50} values was recorded in the knockout strain as compared to the control parasite line. The transport of the presently studied nucleoside analogues was not associated to P2, an important finding for future candidates in DD.

6 Attempts to experimentally validate identified drug targets by gene editing in *T. cruzi*

[1] Laboratory of Microbiology, Parasitology and Hygiene (LMPH), University of Antwerp, 2610 Wilrijk, Belgium.

[2] Laboratório de Biologia Celular (LBC), Instituto Oswaldo Cruz (IOC/Fiocruz), Rio de Janeiro 21040-900, Brazil.

[3] Instituto de Biofísica Carlos Chagas Filho, Centro de Ciências da Saúde, Universidade Federal do Rio de Janeiro, Rio de Janeiro, RJ 21941-902, Brazil.

6.1 State-of-the-art

6.1.1 *Trypanosoma cruzi challenges for gene editing*

Trypanosoma cruzi is an intriguing parasite. Like other heteroxenic organisms, this kinetoplastid developed several strategies to ensure adaptation to changing environments, including gene and chromosomal copy number variations (CNV) (337), with different levels of genomic plasticity in distinct strains (338,339). Gene transcription is polycistronic (87) and regulation occurs mainly at post-transcriptional level (340–342).

T. cruzi is also highly polymorphic, exhibiting intracellular and extracellular forms with a complex genomic architecture, important for successful parasite evolution (95,343), but turning gene manipulation much more challenging in comparison to *T. brucei* and *Leishmania sp.* Moreover, *T. cruzi* has no RNAi machinery*,* which is an powerful tool for unbiased genome-wide and target-specific studies in parasites (343). Classical methods of gene knockout in *T. cruzi* are time-consuming and laborious, besides exhibiting a low-efficiency rate.

The CRISPR/Cas9 technology, also known as "genetic scissors," revolutionized DNA editing protocols in terms of simplicity and precision, contributing to new cancer therapies and strategies for inherited diseases (344–346). This methodology has improved efficiency in *T. cruzi* genome edition, single or family gene disruption, protein localization and *in vivo* follow-up studies (26,347–350).

6.1.2 *The background for CRISPR/Cas9 technology until application in T. cruzi*

The term *clustered regularly interspaced short palindromic repeats* (CRISPR) was coined by the Jansen group in 2002 (351), but the history of CRISPR discovery started with a publication in 1993, when Mojica and collaborators characterized sequences in the *Archaea Haloferax mediterranei* with repeated motifs located in non-coding regions that seemed to be more susceptible to cleavage (352). Regularly spaced repeats were further detected in other organisms (353,354) and in bacteriophages (355,356), hypothesizing a role of those repeats in bacterial immune responses. Then, the gaps in the CRISPR machinery were filled by different groups. Bolotin *et al.*, in 2005, demonstrated an unusual CRISPR locus on *Streptococcus thermophilus*, just sequenced at that time, and new Cas sequences carrying nuclease motifs in the vicinity of the CRISPR structure (357). He also identified in the *extrachromosomal donor*, elements at

a conserved distance relative to the spacer-matching region. This sequence is now called protospacer adjacent motif (PAM), important for target recognition.

Important discoveries included the identification of guide RNAs, termed CRISPR RNAs (crRNAs), transcribed from spacer sequences (358) to target DNA (359): the first insight of a powerful tool to be used in other organisms. Then, the target DNA was demonstrated to be cleaved by the Cas9 enzyme, precisely upstream of the PAM region (357,360,361). Emmanuele Charpentier`s group (2011) found out the last piece of the puzzle in *Streptococcus pyogenes*: a trans-activating CRISPR RNA (tracrRNA) which forms duplex with crRNA, guiding Cas9 to its targets (362). A Cas9-mediated cleavage system was further biochemically characterized by Virginijus Siksnys group (2012), including the finding that a crRNA of 20 nt in size was enough for efficient cleavage, and the possibility of Cas9 reprograming to target a site of choice (363). The CRISPR/Cas9 system, so far entirely described *in vitro* (360), was also optimized by Charpentier and Jennifer Doudna (2012) for application in experimental biology in living cells, by fusing both *cr* and *tracr* RNAs to produce a single synthetic RNA guide (364).

The first eucaryotic genome edition by CRISPR/Cas9 machinery systems was harnessed by Feng Zhang (2013), adapting both *S. thermophilus* and *S. pyogenes* systems to human gene edition. In 2014, Peng *et al* published the first work describing the adaptation of the CRISPR/Cas9 system for *T. cruzi* genetic modification (349), in which the parasite was edited to constitutively express SpCas9 (348). The group also showed that induced double strand break (DSB) repair in *T. cruzi* is considerably enhanced by the presence of DNA fragments with homology sequences flanking the cleavage site leading to homologous recombination (HR) instead of reliance in microhomology-mediated end-joining (MMEJ) DNA repair (349). It is called donor DNA and can be provided either as a plasmid, a PCR product, or a single-stranded oligonucleotide (348).

The first endogenous gene tagging in *T. cruzi* was performed in 2016 by Lander *et al.*, for inositol 1,4,5-trisphosphate receptor localization. Parasites were transfected with a single plasmid (episome) harboring the Cas9 and sgRNA constitutively expressed and a donor DNA, encoding any resistance marker with a tag (365).

Another efficient, rapid and selection-free method of gene editing is by delivery to the parasite of synthetized ribonucleoprotein (RNP) complexes composed of recombinant Cas9 from *Staphylococcus aureus* (SaCas9) and *in vitro*-transcribed sgRNAs (366). It was also demonstrated that highly efficient rates of disruption of GP72

were achieved either by transfecting parasites stably expressing SpCas9 with transcribed sgRNA or wild type parasites with recombinant saCas9 associated with sgRNA RNP.

Gene-knockout and tagging systems are also based on transfecting parasites engineered to constitutively express SpCas9, with PCR-generated DNA templates for sgRNA and donor DNA (26). The system was optimized for transcription of PCR products in kinetoplastids by T7 RNA polymerase, besides an online resource (LeishGEdit.net) for automated primer design (26). The advances in rapid generation of null mutants and fluorescently tagged parasites provided rapid assessment of *in vivo* phenotypes in *T. cruzi*, including individual parasite visualization within CD chronically infected murine tissues (350).

6.2   Research Objective

Previous molecular studies (RNAi) in *T. brucei* gave us insights in putative targets of nucleoside derivatives that could be validated in *T. cruzi* using the CRISPR/Cas9 technology. Some of the nucleoside derivatives were highly active against both *T. cruzi* and *T. brucei*, increasing the chances of similar modes-of-action in both species. Plus, those classes of enzymes perform essential functions such as phosphorylation of substrates in the purine metabolic pathways and protection against oxidative stress, supporting their role as potential targets in DD.

In the current work, *T. cruzi* Dm28 stably expressing *Streptococcus pyogenes* Cas9 (SpCas9) and T7 RNA polymerase (T7 RNAP) was used in attempts to generate knockouts and gene tagging for adenosine kinase (TCDM_01513), rac serine-threonine kinase (TCDM_01526), and adrenodoxin reductase (TCDM_04666). The methodology was based on the transfection of the engineered SpCas9 - *T. cruzi* strain with DNA templates (amplified by PCR and purified) for (i) single guide RNAs (sgRNAs), with homologous sequences able to recognize both SpCas9 complex and gene of interest (GOI) DSB cleavage site (ii) donor DNAs: possessing homologous sequences to the locus of interest for GOI knockout or tagging, providing conditions for DSB repair by HR. pPOT plasmid (350,367) was used as a scaffold to generate for drug-selectable repair cassettes containing different drug resistance markers, or repair cassettes for gene tagging to generate a fusion protein with the green fluorescent protein mNeonGreen. Primers were generated using the LeishGEdit platform (26), and the *T. cruzi* Dm28c PACBIO genome 2014. The rationale for the method is displayed in Figure 6.1.
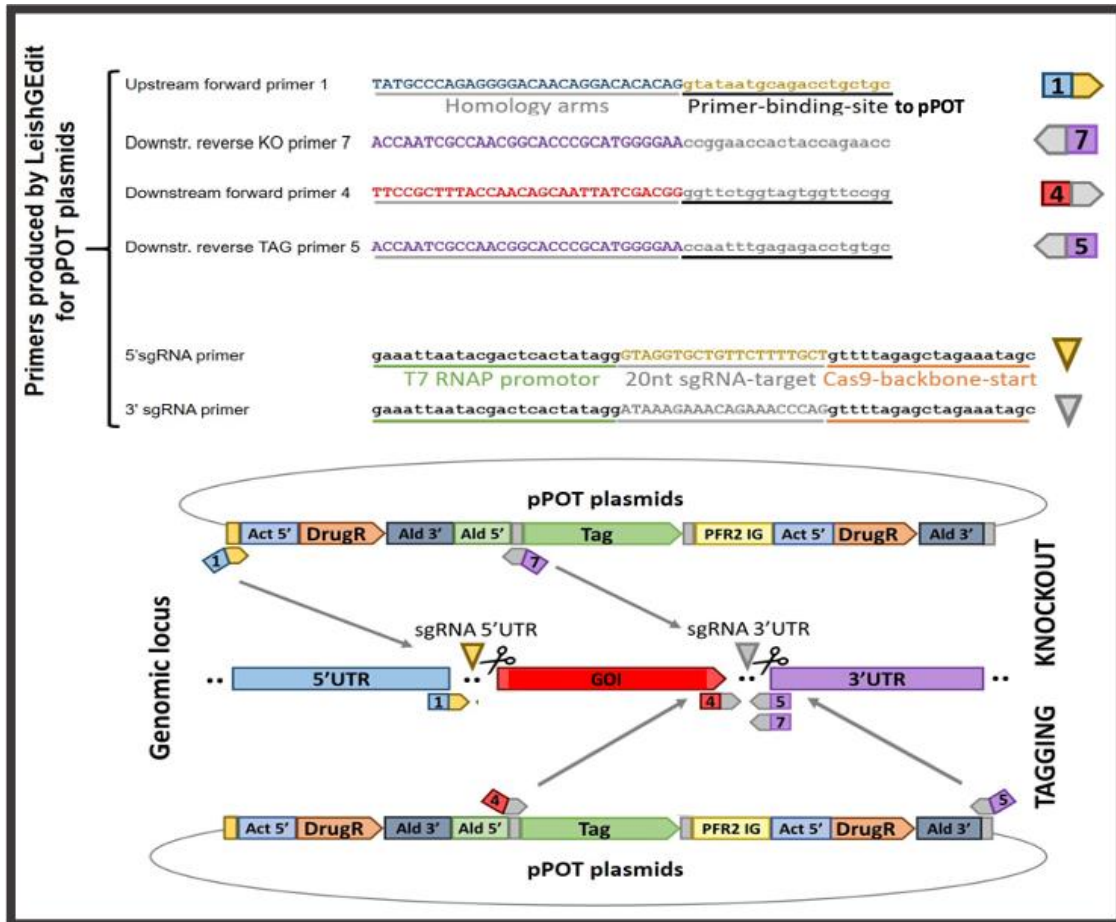
Figure 6.1 The rationale for ADKIN, RSKIN and ADRED knockout in *T. cruzi* Dm28 constitutively expressing T7 RNA Polymerase and SpCas9, and primer design by LeishEdit platform for pPOT plasmids, carrying information for drug-repair cassettes or gene *tagging*. The templates for sgRNA (i) and drug-repair cassette (ii) are generated by PCR using: (i) 3´ and 5´sgRNA primers (yellow and grey triangles) comprised of T7 RNA polymerase promotor, 20nt overlap sequences for targeting the locus for DSB and SpCas9 backbone recognition and (ii) *upstream forward* and *downstream reverse KO* primers (**1** and **7**, respectively) comprised of *primer binding sites* compatible to pPOT plasmids and 30nt homology arms for HR. For gene tagging at C-terminal part of the protein, templates for sgRNA are generated by *3´ sgRNA* primer (grey triangle) and donor DNA by *downstream forward* and *downstream reverse TAG primers* (**4** and **5**, respectively). Figure adapted from http://www.leishgedit.net/Home.html (26).

6.3   Material and Methods

6.3.1   *Parasite strains and culture*

Trypanosoma cruzi Dm28 (DTU I) wild strain and the engineered expressing *Streptococcus pyogenes* Cas9 (SpCas9) cleavage system and T7 RNA polymerase (T7 RNAP) were used in this work. (26,350). The epimastigote (epi) forms were cultured in liver infusion tryptose (LIT) medium, supplemented with 10 % of qualified, South American FBS Gibco™ (cat Nº 12657029), pH 7.2, prepared with: NaCl, 4 g.L^{-1}; KCl,

0.4 g.L^{-1}; Glucose, 2 g L^{-1}; Na$_2$HPO$_4$, 8 g.L^{-1}; tryptose, 5 g L^{-1}; liver infusion, 3 g. L^{-1}, 1 mg hemin diluted in 100 µL of 0.5 M NaOH and 10 mg of folic acid in 100µL of 1 M NaOH solution. The transfected parasites for the target genes were routinely maintained on their selective agent puromycin (*pac*) 50 µg ml-L and/or blasticidin (*bsd*), 25 µg mL^{-1}. The epi cultures were incubated at 27ºC.

6.3.2 Automated primer design

The primer sequences for genes tagging and/or knockout were retrieved by the online tool LeishGEdit, a resource for CRISPR/Cas9 kinetoplastid genome editing (26), and sequences listed in Table 6.1 from 5´- to 3´-end. The single-guide RNA (sgRNA) primers were characterized by coding sequences for T7 RNA promoter followed by a region complementary to the target and the SpCas9 scaffold. The other primers were composed of homology arms to the target gene (upper case letters) and sequences homologous to the pPOT vector (350,367) (low case letters); a backbone plasmid containing *BSD* or *PAC* resistance genes flanked by the UTRs of *T. cruzi* histone.

Table 6.1 List of single guide RNAs ("sgRNA") and "Upstream and Downstream" primers produced by LeishGEdit primer-design (http://www.leishgedit.net/Home.html), designed for the generation of sgRNA templates and pPOT plasmid-derived drug-repair cassettes by PCR. The upper-case letters represent sequence homology to the locus of interest in the parasite genome.

Primers	TCDM_015213	TCDM_01526	TCDM_04666
5´ sgRNA	gaaattaatacgactcactataggA AACAAAACAAAAAAA ACCCgttttagagctagaaatagc	gaaattaatacgactcactataggA ACAACAAAAAGCAGG CAACgttttagagctagaaatagc	gaaattaatacgactcactataggG CTTTTTTTATTAGTGGT TTgttttagagctagaaatagc
3´ sgRNA	gaaattaatacgactcactataggT TTTTTTTTTTTGACCAG AGgttttagagctagaaatagc	gaaattaatacgactcactataggT ATTTATTTGTATTTGTT TTgttttagagctagaaatagc	gaaattaatacgactcactataggC AGAAAAGAAGAAGTA ACGCgttttagagctagaaatagc
Upstream forward	ACAACTTATTTAAAAT TCTAGAAAAACAAAgta taatgcagacctgctgc	GTAACAACAGCAGCA CCAGAAAAAATAAAAg tataatgcagacctgctgc	ACGCCTGCATGAGCGT TTACAATAGTTGTAgtat aatgcagacctgctgc
Downstream reverse KO	AAGTGCCCTCCGCGTG TGCCTGCAGGTCCGccg gaaccactaccagaacc	ATCACCACTGTACCAC AAAAACAAGAACCAcc ggaaccactaccagaacc	AAACACAAAAGACAC AAGAAAAAGGAAAAG ccggaaccactaccagaacc
Downstream forward	CCCGAGAAGCCAATTC TTTCCCCCTGGGAAggtt ctggtagtggttccgg	TTTTCCTTTGATGGAC AAATGGGTCCTGCTggtt ctggtagtggttccgg	CAGCGTGTGTGTCTAC GAATATGTTACCTTggtt ctggtagtggttccgg

Downstream reverse TAG	AAGTGCCCTCCGCGTG TGCCTGCAGGTCCGcca atttgagagacctgtgc	ATCACCACTGTACCAC AAAAACAAGAACCAcc aatttgagagacctgtgc	AAACACAAAAGACAC AAGAAAAAGGAAAAG ccaatttgagagacctgtgc

6.3.3 PCR amplicons for gene knockout

Four different PCR reactions were performed for each target gene to amplify DNA template for: (i) 3´ and (ii) 5´ sgRNAs, (iii) *BSD*-containing donor DNA and (iv) *PAC*-containing donor DNA with two repair cassettes and antibiotic resistance genes. For sgRNA templates, 0.2 mM dNTPs, 2 µM of sgRNA scaffold G00 primer (5´AAAAGCACCGACTCGGTGCCACTTTTT CAAGTTGATAACGGACTAGCTTATTTTAACTTGCTATTTCTAGCTCTAAAAC-3´) and a 3 or 5´ sgRNA primer and 1 unit of Q5® High-Fidelity DNA Polymerase (NEB) were mixed in 1× Q5 reaction buffer (diluted with pyrogenic water), total volume of 20 µL. The PCR steps were: 1 cycle for 7 min at 98 ºC, 40 cycles for 30 sec at 98 ºC, 30 s at 60 ºC, 2 min at 72 ºC and a final elongation cycle of 10 min at 72 ºC.

For amplification of drug-repair cassettes, 15 ng of circular *BSD* or *PAC* pPOT plasmid, 0.2 mM dNTPs, 2 µM each of gene-specific UP-FW and DR-KO primers, 1 unit of Q5® High-Fidelity DNA Polymerase (NEB) were mixed in 1× Q5 reaction buffer (diluted with pyrogen-free water), total volume of 50 µL. The PCR steps were: 1 cycle for 5 min at 95ºC, 30 cycles for 30 sec at 95ºC, 30 s at 55ºC, 1 min at 72ºC and one final cycle for 10 min at 72ºC.

One microliter of each reaction was run with 1× loading dye (6 µL final volume) on 0.8% agarose gel to check for the presence of the expected products, beside 1kb DNA ladder G5711 (Promega). Subsequently, all PCR products were pooled together and purified using QIA® PCR Purification Kit and stored at -20ºC.

6.3.4 Nucleofection

Dm28T7-SpCas9 epimastigotes were seeded at 2×10^6 parasites/ml four days before electroporation. At mid-log phase, 3×10^7 parasites were washed in Hanks` Balanced Salt Solution (BSS), pH 7.4, prepared with glucose, 1.1 g L^{-1}; MgSO$_4$, 0.154 g L^{-1}; CaCl$_2$, 0.012 g L^{-1}; NaCl, 8 g L^{-1}; KCl, 0.4 g L^{-1}; Na$_2$HPO$_4$, 0.39 g L^{-1}; KH$_2$PO$_4$, 0.15 g L^{-1} and 2.5 mL of phenol red solution 0.1%. The pellet was then centrifuged at 3000 rpm for 10 min in Sorvall™ ST 16 Centrifuge. The supernatant was gently removed.

The cells were resuspended in 100 mL of Nucleofection solution (82 µM of Nucleofector solution and 18 µL of supplement 1 solution from the Human T Cell Nucleofector™ Kit), and mixed with 20 µL of purified DNA, and the mix was carefully pipetted into the bottom of the 0.2 cm electroporation cuvette. The Nucleofector®II (Lonza) device was set for the program U033 and parasites were submitted to nucleofection with one pulse. The transfected pool was transferred to 3 mL (gene tagging) or 5 mL (gene knockout) of LIT medium supplemented with 10% SFB and incubated at 27 °C, for 48 h.

6.3.5   Selection of transgenic parasites

After 48 h of parasite transfection, three independent selections using blasticidin 25 µg mL^{-1}, puromycin 100 µg mL^{-1}, or both antibiotics, were performed by diluting 1.5 mL of the transfected population into 3.5 mL of fresh medium (final culture volume of 5 mL with the respective antibiotic). The culture medium was replaced by fresh medium with blasticidin and/or puromycin within 10 days, and puromycin concentration in the cultures was decreased to 50 µg mL^{-1}, until parasite growth recovery. Drug resistant parasite populations were further cultured for 2-3 weeks (with weekly passages in fresh medium). Log-phase parasites cultures (1×10^7/mL) were diluted to 3×10^5 epimastigotes in 200 µL of LIT medium supplemented with 10% SFB, and plated in petri dishes containing solid LIT-agarose medium (8 mL of LIT 2×, 4 mL of SFB and 10 mL of sterile agarose 2% (368)), and grown at 27ºC for 3-5 weeks. A maximum of 24 colonies by condition were hand-picked and seeded in 500 µL of LIT medium 20% SFB, in 48 well culture plates, without antibiotics and grown at 27ºC for 7-10 days. Each clone (5×10^6 parasites) was subsequently inoculated in 1 mL of LIT medium 10% SFB with the respective antibiotics and cultivated at 27ºC for 1 week. The cultures were passed twice before genomic DNA (gDNA) extraction was performed using the High Pure PCR Template Preparation Kit (Roche).

Aliquots (1×10^7 epi) of the drug-resistant populations, selected at different stages, were frozen at -70ºC, in 100 µL of DMSO in 900 µL of BFS, per cryogenic tube.

In the second attempt to generate null mutants, blasticidin-resistant heterozygous clones were transfected with DNA templates for 5` guide RNA, 3` guide RNA and the repair cassette containing the PAC drug resistance marker and the transfected populations were selected as described above, using either puromycin alone, or both blasticidin and puromycin.

6.3.6 Diagnostic PCRs

Diagnostic pairs of primers composed of 21 to 23 bases, were designed to check parasite drug-resistant clones for the presence of the GOI or the integration of the drug-selectable editing cassettes at the locus of the GOI. All sequences are depicted in the 5´ to 3´ orientation, in Table 6.2 The Open Reading Frame (ORF) *upstream forward* (ORF-UF) *primer* homologous region begins at the start codon of the target gene and the *ORF downstream reverse* (ORF-DW) primer, is directed to an internal region of the ORF, in the appropriate reverse complement orientation. The 5´ and 3´ *integration primers* target the untranslated regions (UTRs) flanking the target gene.

Table 6.2 List of "Diagnostic primers" designed to check parasite clones for the presence of the gene of interest (GOI) Open Read Frame (ORF) or the integration of the drug-selectable editing cassettes, after transfection.

Diagnostic Primers	**TCDM_015213**	**TCDM_01526**	**TCDM_04666**
ORF upstream forward	ATGTCTCACCCCGC AAAGCTC	ATGTCCGTTGAATA CTCGGGC	ATGTTTTTTCATGCGA CACGGCG
ORF downstream reverse	CGCCATCCTTCTCC GCAGAATTC	GGGCTGTTCCCTAT TTTCCGG	CGGCCGTGTACTGCTC AAGAAGC
5´ upstream integration	CGCAGAAATCCAC GTAACAAC	CTGCGAAAACGGC GGGTCCAG	GCAGGTGGCACAAGC GATCAC
3´ downstream integration	AGCCACCACGCGG CCCTTTTTC	CACCGCAGATCAGT AGGCTCG	GGCCTTAAAACTTTAA TTCTTC

For diagnostic PCRs, the proportion of 0.2 mM dNTPs, 2 µM each of Upstream and Downstream primers, 0.25 µL of GoTaq® DNA Polymerase 5 U/µL (Promega) were mixed in $1 \times$ GoTaq® Green Reaction Buffer (diluted 5 times with pyrogen-free water), total volume of 50 µL. The PCR steps were: 1 cycle for 2 min at 95 ºC, 30 cycles for 30 sec at 95 ºC (denaturation), 30 s at 42-55 ºC (annealing), 1 min/kb at 72 ºC (extension) and one final cycle for 10 min at 72 ºC. The annealing temperature (T_a) was equal to the lowest melting temperature (T_m) from the set of primers minus 5 Celsius degrees.

6.3.7 Growth curve

The growth curve was performed in triplicate, in 15 mL test tubes, starting with a population of 1×10^6 parasites per mL. The culture was daily quantified by light microscopy by using a Neubauer chamber, for ten consecutive days.

6.3.8 Gene tagging

For tagging the protein encoded by the GOI at the C-terminus to generate a fusion protein with the green fluorescent protein (GFP) mNeonGreen, two PCR reactions were performed. The first, to produce the template for 3′ sgRNA, as previously described; the second to generate the donor DNA sequence containing a homologous part of the target gene and the mNeonGreen coding sequence, also using the pPOT *BSD* or *PAC* vectors. The reagents and PCR conditions are the same as detailed for drug-repair cassette amplification, except from the downstream forward (DW-FW) and downstream reverse tag (DW-TAG) pairs of primers. PCR products were evaluated by 0.8% agarose gel electrophoresis, followed by PCR purification to be applied in nucleofection.

6.3.9 Microscope analysis of tagged parasites

First, cleaned round coverslips were treated with poly-L-lysine solution and placed into a petri dish coated with Parafilm M film and humid filter paper on the top. After, 1×10^7 parasites at log phase were washed twice in a 15 mL tube with 8 mL of PBS pH 7.2 and pelleted at 3000 rpm for 10 min. The pellet was gently resuspended in 1 mL of methanol-free paraformaldehyde diluted to 4% in PBS 1× (Thermo Scientific™ 16% original solution), for 30 minutes at RT, for parasite fixation. The fixed pool was diluted to 10^5 with PBS, 50 µL was spread over the coverslip surface and incubated for 30 min at RT for parasite adhesion. The remaining liquid was gently removed, from the coverslip surface and a drop of ProLong™ Diamond Antifade Mountant with DAPI was added to the fixed-attached parasites. The excess of antifade mounting solution was gently removed and the coverslip placed into a clean dry slide and sealed with nail polish. After the slides dried for 120 minutes at room temperature (RT), the samples were analysed in a Zeiss confocal microscope, reading two colors simultaneously; blue from the nuclei acid stained with DAPI (BP λ_{ex} 359/24nm, λ_{em} 445/50nm) and green, from the translated target and mNeonGreen fused protein, GFP (BP λ_{ex} 470/20nm, λ_{em} 525/50nm).

6.4   Results

6.4.1   Primer design of Genes of Interest

The *T. brucei* targets, selected from *T. brucei* genome-wide RNAi library under nucleoside analogs exposure, were checked for the presence of orthologues in *T. cruzi* Dm28c 2014 strain using the TritrypDB online resource (369): the syntenic orthologues

in *T. cruzi* are listed in Table 6.3: Adenosine Kinase (ADKIN), Rac serine-threonine kinase (RSKIN) and Adrenodoxin Reductase (ADRED).

Table 6.3 *T. cruzi* Dm28 strain (gene ID) orthologous genes for the *T. brucei* potential candidates for drug-targets identified in the wide-screen, retrieved from https://tritrypdb.org/tritrypdb/app .

T. brucei Gene ID	*T. cruzi* Gene ID	*T. cruzi* Gene product
Tb927.6.2300	TCDM_01513	Adenosine kinase
Tb927.6.2250	TCDM_01526	Rac serine-threonine kinase
Tb427_100026500	TCDM_04666	Adrenodoxin reductase

Then, we used the LeishGEdit program (26) for automated design of CRISPR primers, 5' and 3' sgRNAs, upstream forward (UP-FW) and downstream reverse KO (DW-KO), listed in Table 6.1, to generate (by PCR) DNA templates for: (i) 3' guide RNA (ii) 5' guide RNA (sgRNAs), (iii) BSD-containing and (iv) PAC-containing repair cassettes, the last two using pPOTc plasmids (Figure 1).

The sgRNAs primers include the sequence for the T7-RNA polymerase promoter, a 20 nt homology sequence (capital letters) to the target gene encompassing the PAM site (NGG) (preferably located at the UTR), and a complementary region to the G000 primer (Table 6.1). The G000 encodes the SpCas9-backbone site for nuclease binding and assembly of the ribonuclease complex. The DNA for the guide RNA templates were generated by PCR using the respective guide primer and the G000 primer, as described in methods. The resulting ribonuclear complex should perform DSB just before the PAM sites (NGG), at the 5` and 3` of the GOI locus (Figure 6.1, Table 6.1). The drug-repair cassette primers included "homology arms" flanking the GOI (Figure 6.1, Table 6.1), providing conditions for DSB repair by HR.

6.4.2 Generation of T. cruzi transgenic lines

Epimastigote forms of the Dm28 *T. cruzi* strain were modified to constitutively express the T7 RNA polymerase and the SpCas9 enzyme (Dm28T7Cas9) and used in an attempt to generate single or double knockouts for ADKIN, RSKIN and ADRED. Parasites were transfected with four PCR-generated DNA templates to allow: (i) the synthesis of sgRNAs by T7 RNA polymerase, providing information of the target sequence for the DSB by SpCas9 and (ii) to repair the DSB by the repair cassettes with selectable marker. The two sgRNAs directed to the 5` end and 3` end of the GOI, should result in the excision of the GOI by SpCas9, therefore, removing the endogenous locus.

The two repair cassettes containing the drug-resistance genes *BSD* or *PAC*, should allow DSB repair by homologous recombination and provide the flexibility to select transfected populations simultaneously with different drug combinations, offering the possibility to achieve double knock-out after a single transfection. Two days after transfection, the cultures were submitted to different selective environments, being first exposed to high concentrations of each antibiotic alone (Blasticidin 25 μg ml^{-1}, Puromycin 100 μg ml^{-1}) or both in combination. The next steps of selection involved reduction in the concentration of puromycin concentration. The drug-resistant populations of parasites transfected for the KO of Adenosine Kinase (ADKIN), Rac-serine threonine kinase (RSKIN) or Adrenodoxin reductase (ADRED), were recovered for the three independent selections (bsd, pur or bsd+pur) and plated for cloning and subsequent scrutiny of mutants. After extraction of genomic DNA, the clones were checked for gene knockout using diagnostic primers described in table 3, or with upstream forward and downstream reverse KO primers, on Table 6.1.

For gene knockout validation, the forward and reverse primers listed below were used in 4 different PCR reactions, followed by 0.8% agarose gel scrutiny (Figures 2, 3 and 4b and c). The endogenous and recombined locus were differentiated by the sizes of the PCR fragments:

- 5´ and 3´ INTG primers: anneal at the UTR regions flanking GOI. It allows the detection of DNA fragments corresponding to the endogenous locus, one or two integrated repair cassette(s), inferring the profile of single, double-gene knockout or lack of gene deletion.

-UP-FW and DR-KO primers: the 3` end of the primers share homology to the pPOT plasmid and were used to generate the repair cassettes used in the transfection, allowing a more precise evaluation for the presence of the drug-repair cassette.

-5´ INTG and DR-KO or 3´ INTG and UP-FW primers: pairs of primers that bind to parasite DNA UTR region flanking the GOI (5´ or 3´ INTG), and the homologous region to the drug-repair cassette (DR-KO or UP-FW*)*, allowing the verification of repair cassette integration in the locus of interest.

-ORF-FW and ORF-REV primers: bind to the start codon of the ORF of GOI and internal region in the ORF, allowing the verification of target gene presence by amplifying a piece of the endogenous locus.

The results for each GOI are displayed below.

6.4.3 Adenosine Kinase

The results for the attempt of ADKIN KO by selection with blasticidin and/or puromycin are displayed in Figure 6.2. Parasite clones (cl) checked with 3´ plus 5´ *INTG* primers were screened for the presence of DNA fragments matching the expected sizes for the *BSD repair cassette* 1.368 kilobases (kb); the *PAC* repair cassette 1.568 kb, or the endogenous locus (EL), equal to 1.288 kb (Fig 6.2a). In this first set, the PCRs of blasticidin-resistant clones (Fig 6.2b) show a strong band in all clones as well as in control parental strain (c), indicating presence of the EL. However, given the small difference in size for the expected fragments for BSD-donor DNA (1.368 kb) and EL (1.288 kb), making it difficult to distinguish them in 0.8% agarose gels, this could be the result of heterozygous clones bearing a single *BSD*-cassette (Fig 6.2b). The presence of a *BSD* cassette was confirmed by the *UP-FW* plus *DR-KO* PCR (Fig 6.2b), showing an amplified DNA fragment close to 1.2 kb (Fig 6.2a) in all clones, except from clone 36, and from the parental control (c). The integration of the *BSD* cassette in the corresponding ADKIN locus was confirmed for all clones (29, 34 ,35 and 37), exhibiting a fragment of the expected size of 1.296 kb (Fig 3b, *5´INTG* plus *DR-KO*). The presence of the ADKIN ORF was observed, by the amplified DNA fragments of 319 bp (Fig 6.2a), seen for the last set of primers (ORF-*FW* plus *REV)*. These results are indicative of heterozygous clones for ADKIN with the single *BSD* cassette integration.

On the other hand, clones derived from puromycin selection didn't exhibit the desired profile of a successful gene knockout. Both EL (Fig 6.2a, 1.288 Kb) and ADKIN ORF (Fig 6.2a, 319 bp) fragments are present in all clones (Fig 6.2c), together with discrepant results for drug-repair cassette integration diagnosis with *UP-FW* plus *DR-KO* primers (Fig 6.2c). We did not observe amplification of DNA fragments with the expected size for the PAC-cassette either in the *UP-FW* plus *DR-KO* combination nor in the *3´INTG - UP-FW* combination, suggesting no integration of the PAC- cassette in those parasite clones. Unexpected large size fragments (>2.000 kb) were observed for all analysed clones and fragments corresponding to *BSD* DNA donor (between 1.000 and 1.500 Kb) for clones 9, 11 and 15. Also, a band around 500 bp was detected in all clones, when checked for integration of drug-repair cassette in the expected locus (Fig 6.2c, *3´INTG* plus *UP-FW*), being smaller than an expected integrated PAC-donor DNA (Fig 6.2a, 1.481Kb) or *BSD-* donor DNA incorporation (Fig 6.2a, 1.296 Kb). Those fragments can be the result of unspecific binding of the primers, thus resulting in faint bands in the abovementioned samples.

At least 20 clones derived from ADKIN KO population selected with both antibiotics were checked for double knockout, and all epimastigote clones displayed the ORF fragment in 0.8% agaroses gel (data not shown).

(a)
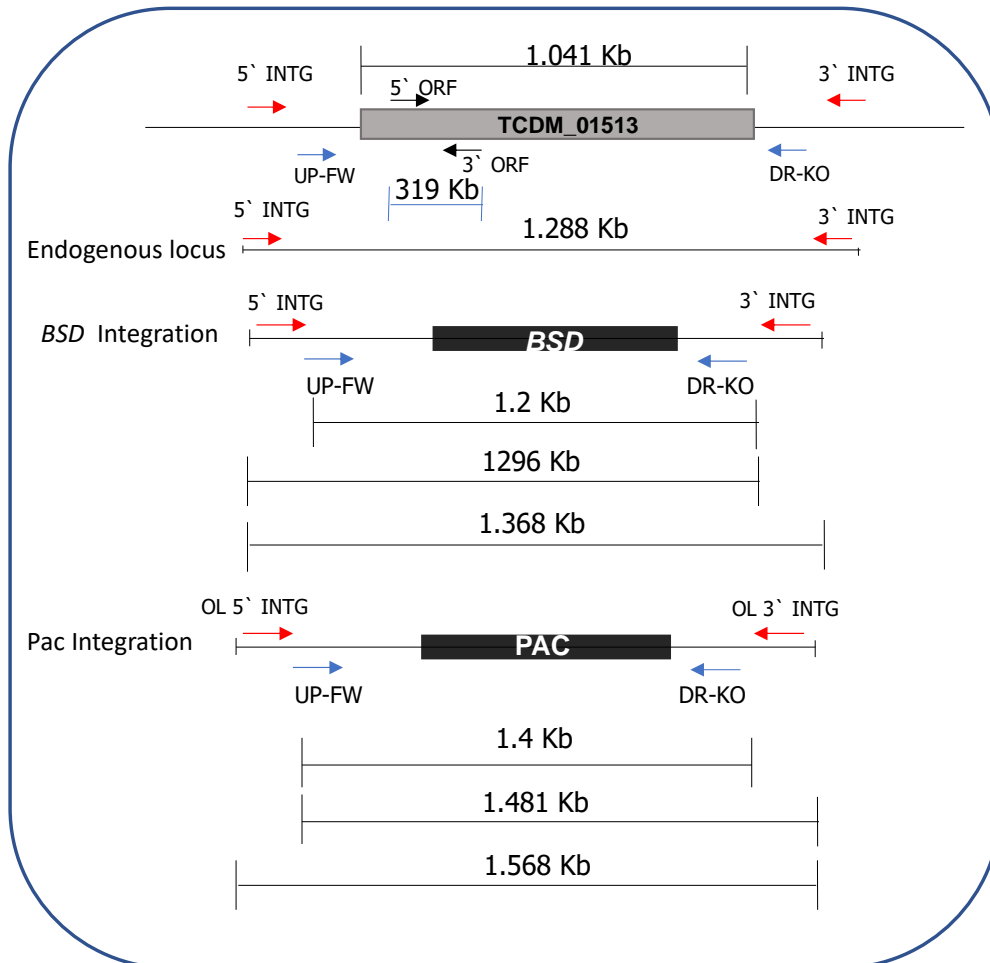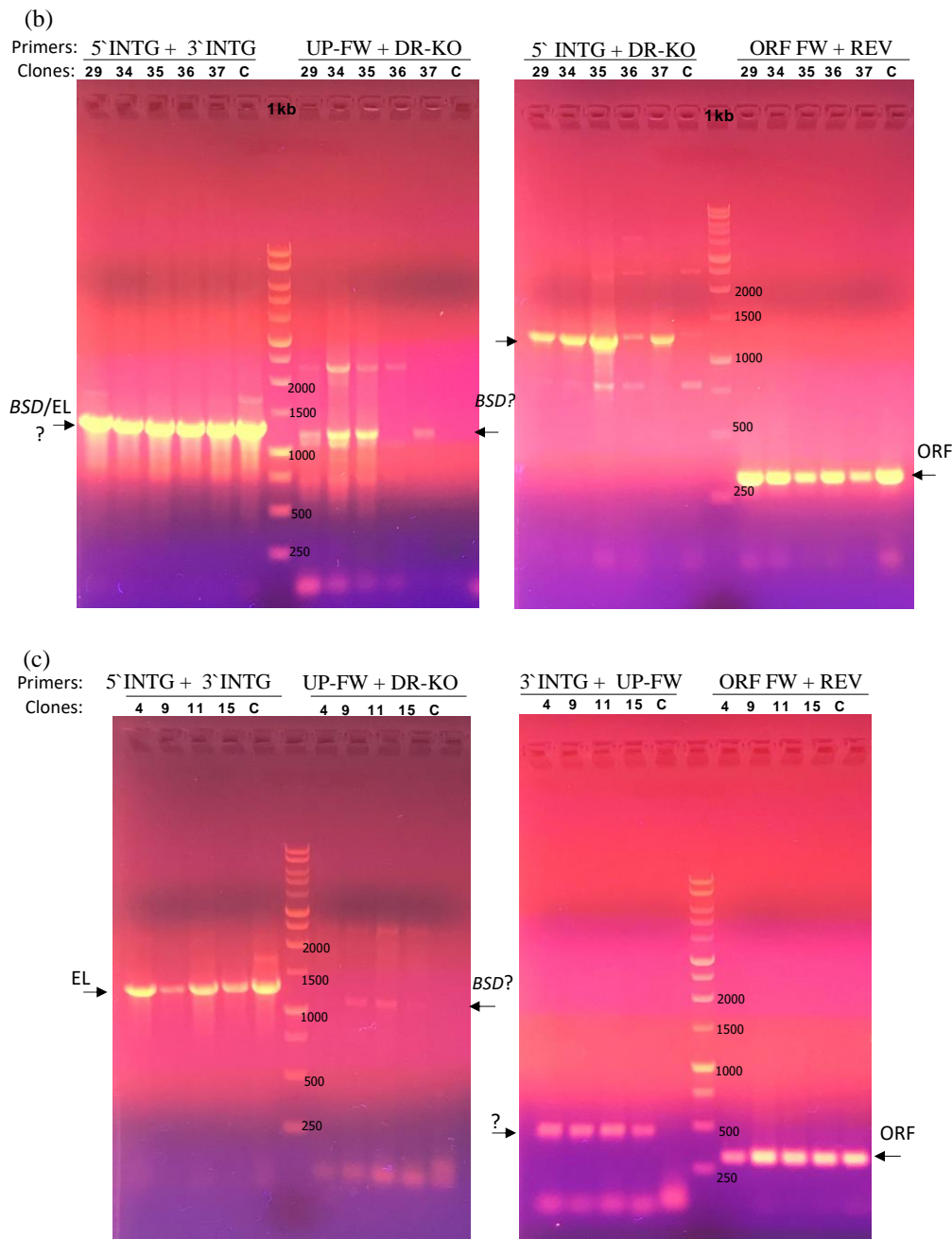
Figure 6.2 *Adenosine kinase (TCDM_01513) knockout*. (a) Schematic illustration of expected DNA fragment sizes after 4 "diagnostic PCRs" performed with different pairs of primers for the detection of drug cassette integration and endogenous locus. 0.8% agarose gel with PCR products from extracted DNA of transfected clones for TCDM_01513 knockout (b) 29, 34, 35 36 & 37 selected with blasticidin, (c): 4, 9, 11 & 15 selected with puromycin, and control strain Dm28T7Cas9 (c), using the following set of primers: *5´INTG* plus *3´ INTG* (possible drug-repair cassette integration)*; UP-FW* plus *DR-KO* (drug-repair cassette integration)*; 5´INTG plus DR-KO or 3´INTG plus UP-FW* (drug-repair cassette integration on the right locus)*; and ORF-FW* plus *ORF-REV* (GOI ORF presence). Kb, kilobase; bp, base pair; EL, endogenous locus; *BSD*, blasticidin gene; PAC, puromycin gene; 1kb, 1kb DNA ladder.

130

6.4.4 Rac-serine kinase

After drug selection of transfected parasite populations (Dm28T7Cas9) for RSKIN KO, only populations selected with one antibiotic (blasticidin or puromycin) were recovered. The previous results for ADKIN single KO with *BSD* selection encouraged us to first analyse 5 clones obtained from blasticidin selection (1, 11, 12, 13 and 14). The results are outlined in figure 6.3. The PCR products matched the expected DNA fragment sizes as described in fig 6.3a. Fragments around 1.334 Kb (*5´INTG* plus *3´ INTG*) and 1.2 Kb (*UP-FW* plus *DR-KO*) are indicative of the *BSD* cassette, while the endogenous locus (EL) is shown by the 1.64 Kb fragment. The approximate 1.288 Kb amplicons (*5´INTG plus DR-KO*) reveal the insertion of the *BSD*-cassette in the RSKIN locus. The presence of EL (≈1646 Kb) and fragment of RSKIN ORF (≈318 bp) (Fig 6.3b) complete the heterozygous profile for RSKIN regarding the studied clones.
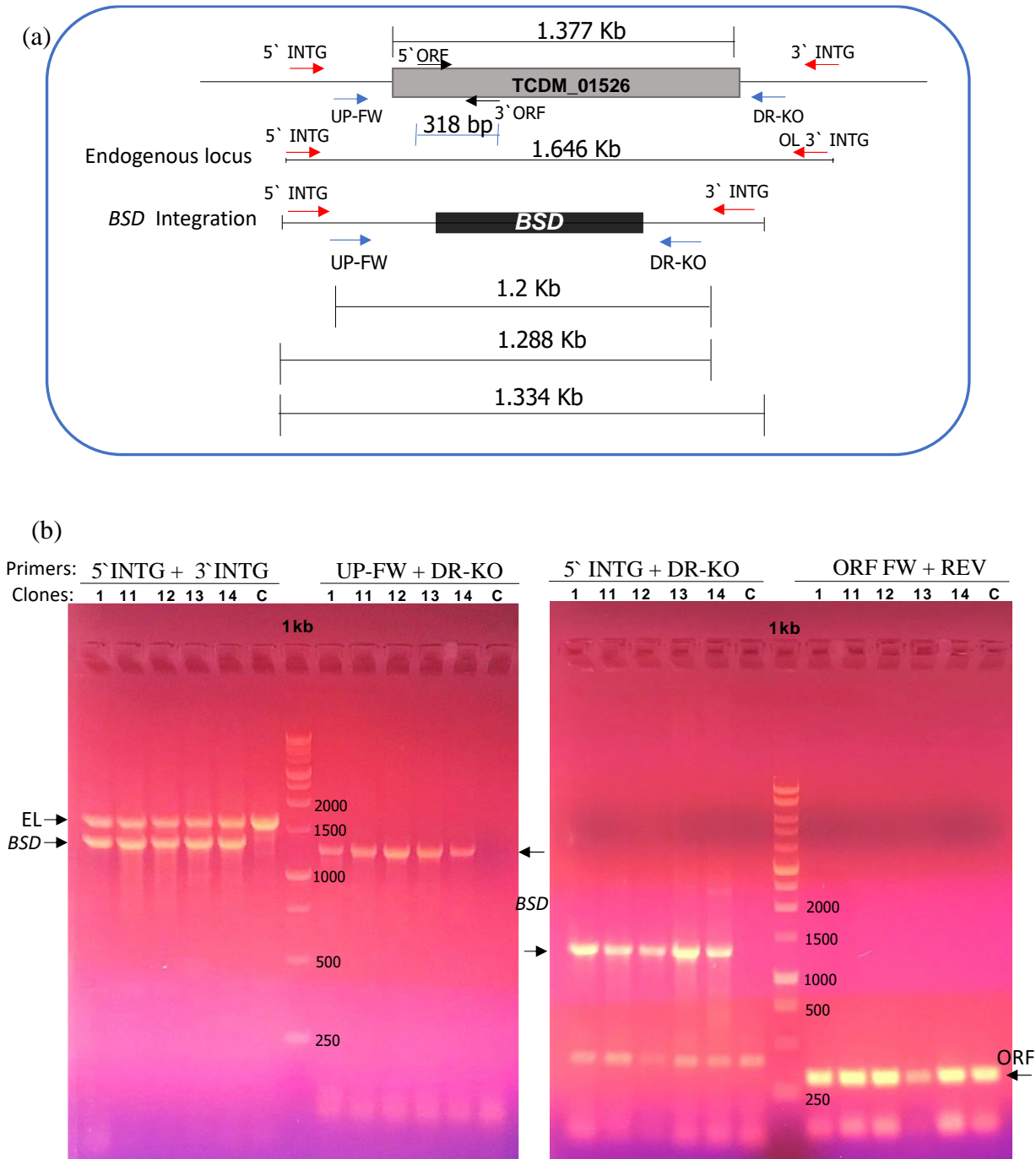
Figure 6.3 *Rac-serine kinase (TCDM_01526) knockout*. **(a)** Schematic illustration of expected DNA fragment sizes after 4 "diagnostic PCRs" performed with different pairs of primers for the detection of drug cassette integration and endogenous locus. **(b)** 0.8% agarose gel with PCR products from extracted DNA of transfected clones **1, 11, 12, 13 & 14** for TCDM_01526 knockout selected with blasticidin and control strain Dm28T7Cas9 **(c)**, using the following set of primers: *5´INTG* plus *3´ INTG* (possible *BSD-* cassette integration)*; UP-FW* plus *DR-KO* (*BSD-* cassette integration)*; 5´INTG plus DR-KO* (*BSD-* cassette integration on the right locus)*; and ORF-FW* plus *ORF-REV* (gene of interest ORF). Kb, kilobase; bp, base pair; EL, endogenous locus; *BSD*, blasticidin gene; 1kb, 1Kb DNA ladder.

6.4.5 Adrenodoxin reductase

The transfected population for ADRED deletion and selected with blasticidin was the only that was successfully recovered under antibiotic pressure. After plating, 5 retrieved clones (2, 3, 10, 11 and 12) were first analysed for ADRED knockout. Like ADKIN+/- clones, all replicates exhibited expected fragment sizes (Figure 6.4a) corresponding to ADRED+/- mutants (Figure 5b). Those PCR products are displayed in figure 6.4b and correspond to both EL of 2.136 kb and 1.2 kb *BSD*-cassette bands (*5´INTG* plus *3´ INTG*, Fig 6.4b); the last confirmed to be integrated in the ADRED locus by the 1.277 kb amplified product (*3´INTG plus UP-FW*, Fig 5b). The ORF is present in all clones.
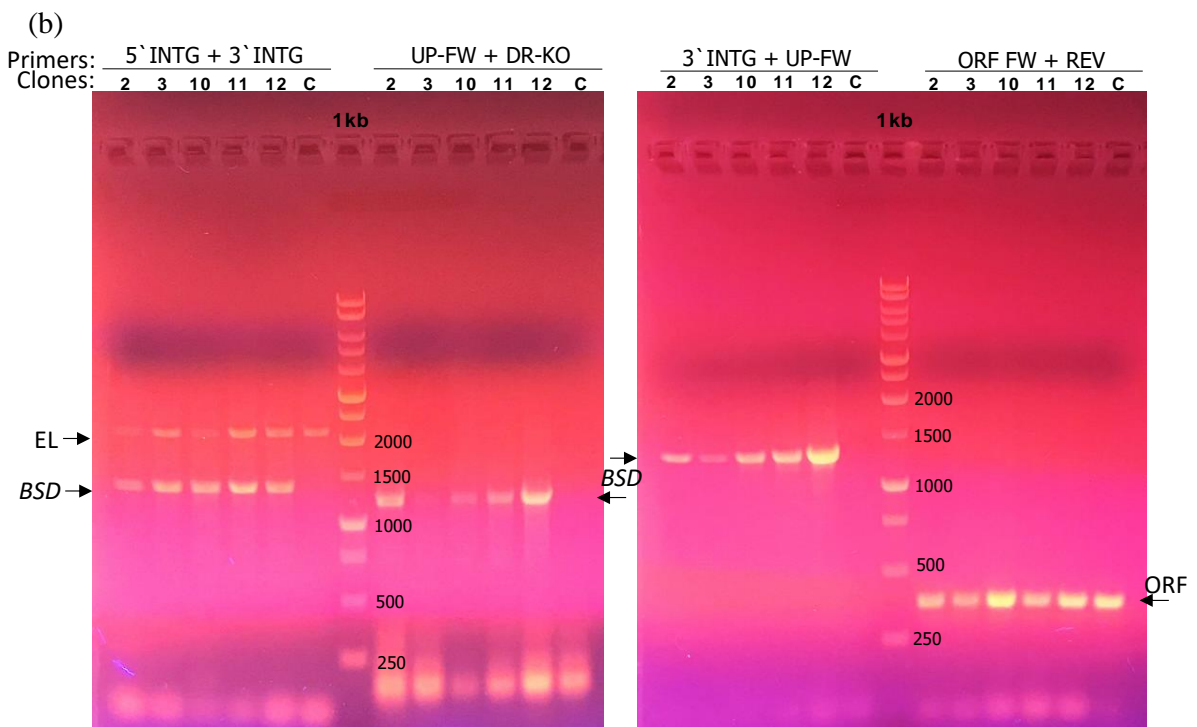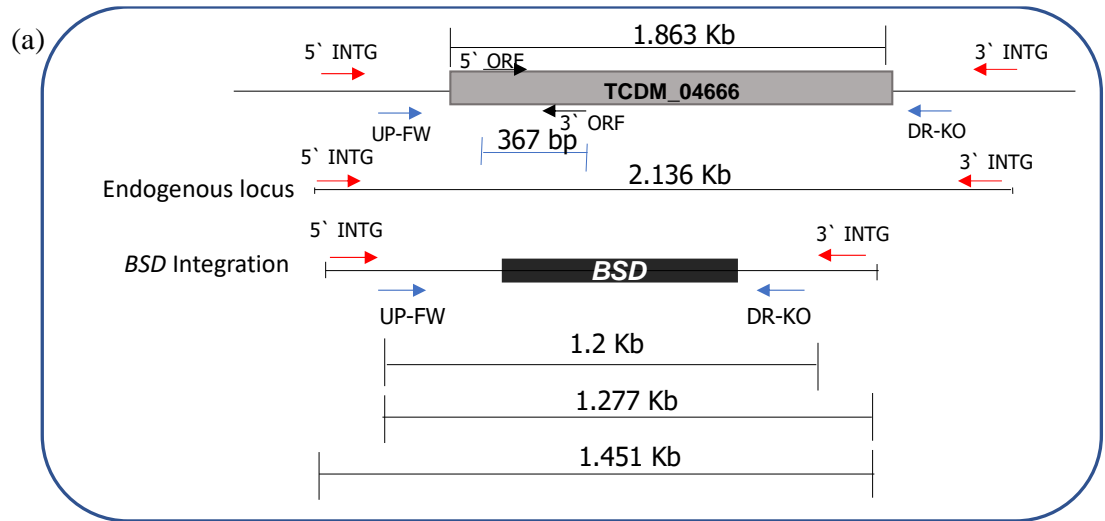
Figure 6.4 *Adrenodoxin reductase (TCDM_04666) knockout*. **(a)** Schematic illustration of expected DNA fragment sizes after 4 "diagnostic PCRs" performed with different pairs of primers for the detection of drug cassette integration and endogenous locus. **(b)** 0.8% agarose gel with PCR products from extracted DNA of transfected clones **2, 3, 10, 11 & 12** for TCDM_01526 knockout selected with blasticidin and control strain Dm28T7Cas9 **(c)**, using the following set of primers: *5´INTG* plus *3´ INTG* (possible *BSD*-cassette integration)*; UP-FW* plus *DR-KO* (*BSD*-cassette integration)*; 5´INTG plus DR-KO* (*BSD*-cassette integration on the right locus)*;* and *ORF-FW* plus *ORF-REV* (gene of interest ORF). kb, kilobase; bp, base pair; EL, endogenous locus; *BSD*, blasticidin gene; 1kb, 1kb DNA ladder.

6.4.6   New attempt to generate null mutants

As an attempt to generate null mutants, the following presumed heterozygous clones 01513B.29 (ADKIN), 01526B.2 (RSKIN), 0.4666B2 (ADRED) received a second round of transfection, this time with templates for sgRNAs and the *PAC*-repair cassette and exposed to both blasticidin and puromycin antibiotics to eliminate any heterozygous cells harbouring a copy of the target gene. The recombinant population for ADKIN did not survive.

On the other hand, 16 clones from populations resistant to both drugs, targeted to RSKIN and ADRED were retrieved from solid LIT medium plate. Only 2 clones, still positive for ORF, grew under antibiotic pressure on the former target. For ADRED, only 2 out of 15 clones were analysed for the presence of the ORF and confirmed in 0.8% agarose gel.

6.4.7   Growth curve

Since we were unable to generate null mutant lines for the GOI tested, we verified if the supposed heterozygote lines displayed any differences in growth. Then, growth curves were analysed in duplicate for 10 consecutive days, starting with 1×10^6 epimastigote cells per mL. The outcomes for parental lines (wild type) and SpCas9 expressing parasites together with heterozygous clones **2** and **3** for ADRED or **1, 11** and **12** for RSKIN are displayed in figure 6.5 a and b, respectively. The statistical analysis performed by unpaired *t*-test showed no statistical difference ($p > 0.05$) between wild-type and the T7spCas9 Dm28 modified cell line ($p = 0.4295$), providing evidence for the stability of the engineered cell line. Also, there was no significant difference between the

2 ADRED ($p = 0.9963$) or 3 RSKIN ($p = 0.3878$) +/- clones, calculated by t- and one-way ordinary ANOVA tests respectively. As observed in fig 6.5a, a slower parasite multiplication of RSKIN +/- clones in comparison to T7spCas9 Dm28 cells until third day (p *values* between 0.0001 and 0.009); and that after this time, both curves reach similar growth profile. Regarding ADRED +/- clones (Fig 6.5b), parasite growth peak (at 8th day) is 16% lower than the parental strain (p between 0.003 and 0.009), inferring a possible loss of fitness with a single loss of the respective gene.
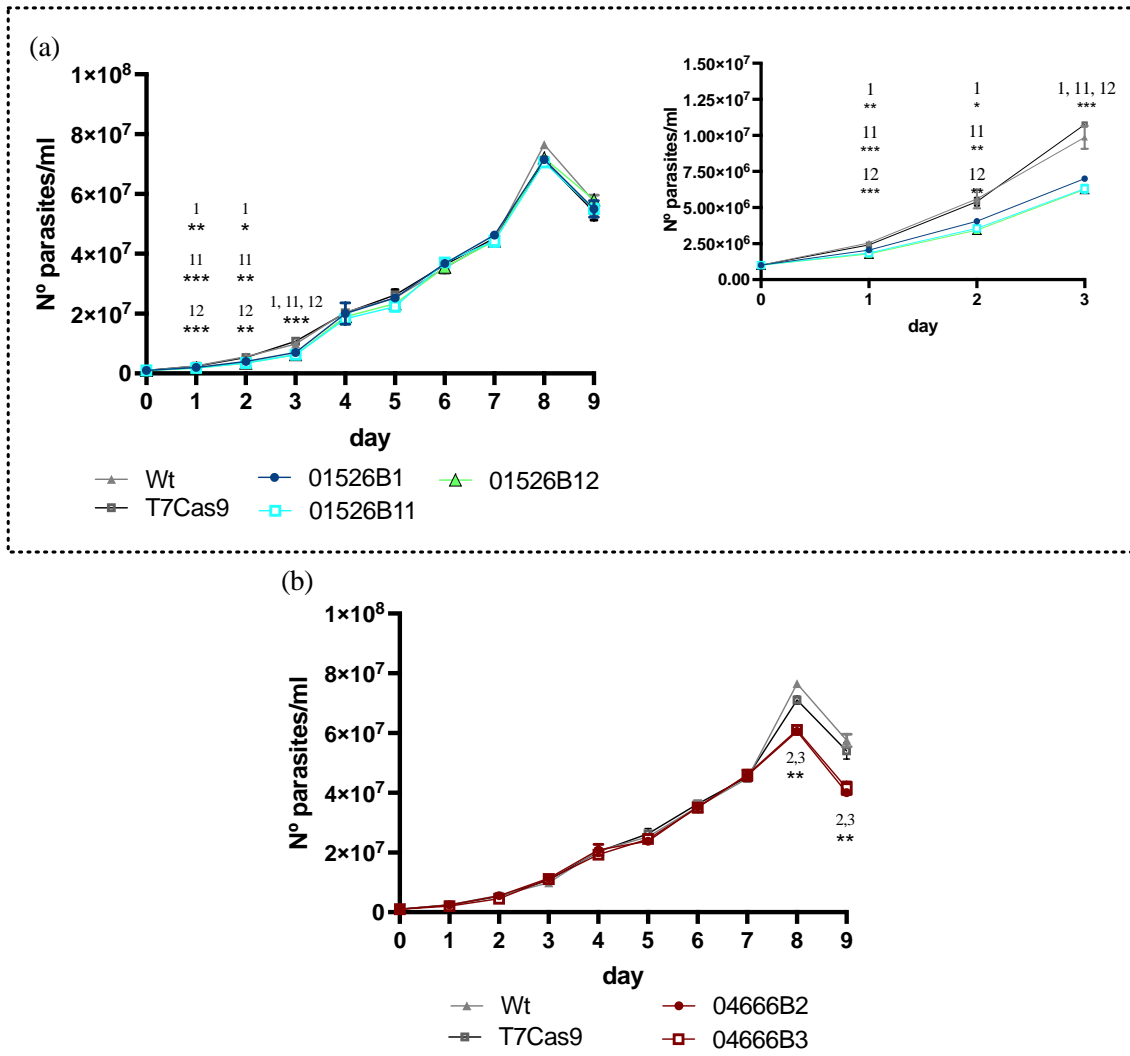
Figure 6.5 *The role of GOI single knockout on parasite growth*. *In vitro* growth of Dm28 epimastigote forms daily quantified for 10 days: Wild type (WT), parental T7SpCas9 Dm28 line, and 3 heterozygote mutant clones for: **(a)** Rac-Serine kinase (01526B): 1, 11 and 12 and **(b)** Adrenodoxin reductase (014666B): 2 and 3, described in the previous section. T7SpCas9 One-way ANOVA test CI 95% ($p < 0.05$) was performed between each clone and T7SpCas9; values by GraphPad prism v9.1.1.2 and results displayed on the graphs: * $p < 0.0332$, ** $p < 0.0021$, ***$p < 0.0002$. WT, Wild type; T7SpCas9, parenteral cell line SpCas9; T7SpCas9 expressing heterozygote clones 01526B 1,11 or 12 for ADRED and 04666B2 or B3, for ADRED.

6.4.8 Tagging

The attempt to determine the subcellular gene localization of the GOIs was performed by tagging the C-terminus of the proteins with the mNeonGreen green florescent protein. To that end, the TcDm28T7Cas9 strain was transfected with templates for the 3` sgRNA and the "Tag-repair cassette", amplified from the pPOTc plasmid (350,367). The results are displayed in Figure 6.6.
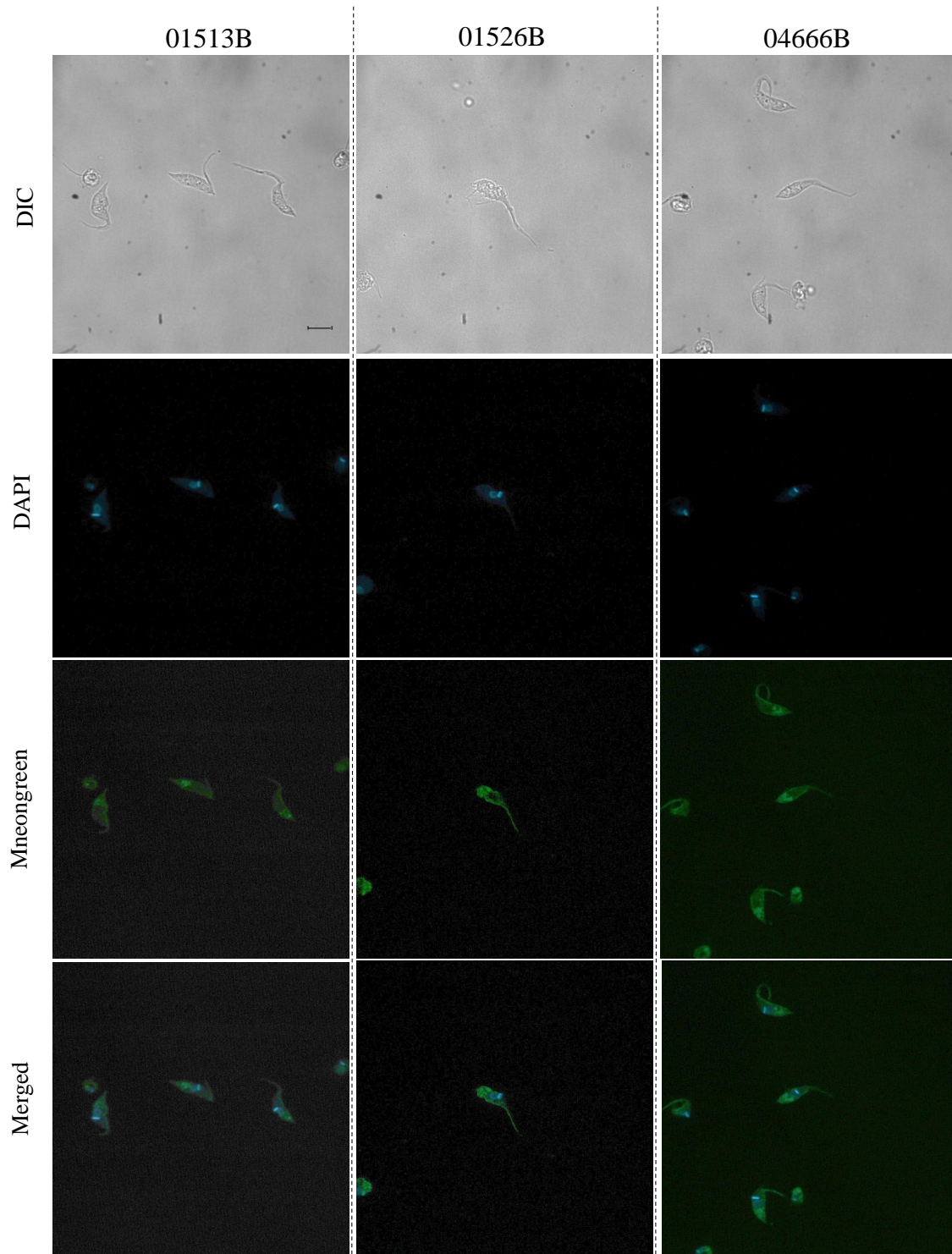
Figure 6.6 *Tagging* ADKIN, RSKIN and ADRED in *T. cruzi* epimastigote forms. Localization in the Dm28T7Cas9 strain of GOI C-terminally tagged with mNeonGreen - *green colour*, after transfection with 3´sgRNA template and Donor DNA (PCR:*BSD* pPOT plasmid, DW-FW, and REV- TAG *primers*) and nuclear staining with DAPI (4′,6-diamidino-2-phenylindole) - *blue colour, as indicated*. DIC: Differential Interference Contrast. Scale bar: 5 µM.

The fluorescent parasites (ADKIN, RSKIN and ADRED) gave an intracellular green straining with a cytoplasmatic localization at the posterior side of the parasite of the target enzymes. The merged image of ADRED tagged parasites, composed by the differential interferential contrast, DAPI (nuclei and kDNA staining) and mNeonGreen reveal a strong labeling at posterior end of the epimastigote body possibly related to reservosomes, which merits further investigation in co-localization studies using fluorescent endocytic ligands to confirm the enzyme presence in these acidic compartments. For RSKIN and ADRED-tagged parasites, besides the posterior end of epimastigotes, the flagellum is also intensively stained.

6.5   Discussion

As well documented, trypanosomatids are purine auxotrophs, relying on the salvage of precursors from the host to fulfill their demands (370). This makes precursor molecules, transporters and enzymes related to purine processing interesting drug targets (371). There is a set of purine enzymes essential to the purine salvage pathway (24) including kinases, essential for the phosphorylation and activation of purine precursors (372), and NADP(+) reductases, important to the sterol biosynthetic pathway and protection against oxidative stress (373,374). Indeed, many trypanosomatid kinases were described after the kinetoplastid genome sequencing and are considered as potential drug targets (80,92,321,372,375).

The current work attempted to evaluate the impact of genes knockout coding for two kinases (ADKIN and RSKIN) and one NADP(+) reductase (ADRED), considered to be crucial for parasite survival, and their KO effect in *T. cruzi* fitness. An optimize CRISPR/Cas9 DNA editing tool was used for gene KO, in an effort to enhance the chances to obtain at least successful single knockouts for essential genes (348). By growth curves analysis, epimastigote Dm28 engineered to constitutively express the CRSIPR/Cas9 machinery maintained its fitness in comparison to the wild strain proving to be viable to target gene deletion.

ADKIN proved to be a key player in nucleotide metabolism for *Leishmania* species and *T. brucei* subspecies (250,321), and adenosine, their main purine source (321,376). Apart from the presence of ADKIN in *T. cruzi*, demonstrated in 1982 by Kidder (377), not much was further described for ADKIN in this species. Also, little is known about purine/pyrimidine transport and their metabolic pathways in *T. cruzi*, apart from a recent trial to use *T. brucei* as a surrogate system to study *T. cruzi* nucleoside transporters (251).

Looking for its function prediction in TriTrypDB, as performed for the other targets, this kinase is putatively involved in adenine and adenosine salvage and purine metabolism. The attempts to generate an ADKIN KO line in Dm28T7Cas9 epimastigote forms were very challenging.

The approach for generating a double KO was ineffective, with the evidence of one of the wildtype ORF remaining present in all clones analysed, regardless the strategy of single or double transfection. The results for single knockout were very intriguing as well. By PCR, the clones retrieved after blasticidin selection exhibited the expected fragments for the *BSD* cassette repair when checked for the correct integration in the ADKIN locus, differently from the clones obtained from puromycin selection. Indeed, the higher pressure with puromycin upon the parasite the more puzzling the observed outcomes were, probably due to yet unknown mechanisms of parasite evasion and/or intrinsic resistance to drug pressure unrelated to gene editing and selectable cassette integration. In fact, DNA repair is essential for *T. cruzi* survival and infection and may be involved in drug resistance (378). Its components/machinery have been gradually demonstrated in literature for single and double strand break repair, or base excision repair under different circumstances, such as specific live stage environment, oxidative stress or drug pressure (379,380). They are also important to confer drug resistance against benznidazole (195) and played a role in epimastigote adaptation/selection upon blasticidin and/or puromycin exposure.

Regarding Rac serine threonine kinase (RSKIN), the knowledge concerning function and importance in kinetoplastids is scarce. The predicted function of the coded protein is displayed in TriTrypDB as non-specific Rac serine threonine or cAMP-dependent protein tRNA splicing endonuclease or PretRNA lyase (intron-removing; cyclic-2',3'-phosphate-forming). So far, this is the first work that explores this kinase knockout in *T. cruzi* and shows a loss of fitness of RSKIN heterozygous epimastigote forms (to be confirmed) at the level of early log phase parasite growth. RSKIN may

therefore represent a candidate target for drug therapy against Chagas disease, deserving further exploitation.

Adrenodoxin reductase (ADRED) is a flavoenzyme NADP(+) reductase, involved in substrate hydroxylation of the mitochondrial P450 cytochrome system (381) and sterol biosynthesis (382,383). Protein function prediction in TriTrypDB, computationally inferred ADRED to play an important role as NAD(+) or NADP(+) acceptor, which includes Ferredoxin or Adrenodoxin - NADP(+) reductase. So far, it was demonstrated that NADPH–cytochrome P450 reductase family in *Trypanosoma cruzi* is involved in the ergosterol biosynthesis pathway (373) and other essential functions such as oxidative stress defense, parasite growth and viability (384). Indeed, almost all enzymes from the redox pathway, such as trypanothione reductase, proved to be essential for trypanosomiasis considering the hostile intracellular environment and to be potential drug targets as a consequence (374). This also applies to ADRED gene essentiality, which is supported by the failure to recover parasites in an attempt to obtain a homozygous KO mutant by selection of the double transfected population for the selectable resistance markers on single or double antibiotics.

To sum up, further analysis will be performed to confirm the heterozygous profile of the clones scrutinized by diagnostic PCR by evaluating the effect at the protein expression level. Also, clones will be validated as viable tools to study the target in question in susceptibility analysis for nucleoside analogs. Last, gene essentiality needs to be further analysed by suitable techniques appliable for *T. cruzi* such as plasmid shuffle, in which an episome expressing the GOI is first transfected into the cell line, allowing it to survive the subsequent deletion of the chromosomal alleles (385). Subsequently, the drug selection pressure for the episome is removed and plasmid retention is followed-up as indicator for gene essentiality (385).

Another technique broadly practiced in *Leishmania* is the dimerized Cre recombinase (diCre) to obtain gene deletion and which allows loss of function observation in real time (386). It was successfully applied in 2016 in *L. mexicana* to obtain deletion of the *cyclin-dependent protein kinase* (*CRK3*) gene (386). A null mutant was generated by (i) replacement of one genomic allele with a *CRK3*-version flanked by loxP sites (sites of diCre recognition), followed by replacement of the second copy by a cassette encoding two subunits of the Cre recombinase, fused to rapamycin binding domains (386). After strain generation, rapamycin was added leading to the dimerization of Cre subunits, forming a functional Cre recombinase that excised the remaining floxed

copy of the gene of interest (386). In *T. cruzi*, DiCre system efficiency in recombination was very low (387) and to improve it, further protocols were assessed with direct delivery of Cre recombinase fused to the C-terminus of *T. cruzi* histone H2B, and tested on epimastigotes and tissue culture-derived trypomastigotes transfected with reporter plasmid for Cre activity (388). Briefly, the gene coding for the fluorescent (tdTomato) protein flanked by loxP sites and in a head-to-head orientation in the reporter plasmid (unable to be transcribed) is delivered to the parasite (388). After Cre recombinase transfection, the tdTomato coding sequence reverted and transcription was turned on in up to 85% of parasites (388). Even though promising results were obtained with the inducible gene editing of the nitroreductase gene, the DiCre system still needs further optimization for endogenous gene evaluation and to be easily assessable in *T. cruzi*.

Regarding the subcellular localization, our microscopy analysis of the mNeonGreen-tagged ADKIN, RSKIN and ADRED revealed cytoplasmatic staining with strong labelling (specially in ADRED-tagged parasites) in rounded and large structures mainly located in the posterior region of epimastigotes of *T. cruzi*. This later morphological and subcellular distribution is compatible with typical storage organelles in epimastigotes named reservosomes (389,390). Further co-localization studies using specific markers for RE

 (*e.g.* Rab7, cysteine proteinases, among others) and endocytic ligands in the mNeonGreen-tagged parasites are needed to support the current subcellular location data. RE are acidic organelles and considered an endpoint of the endocytic pathway of a variety of studied substrates like proteins and lipids obtained from the surrounding medium along with proteolytic enzymes originating from the secretory pathway; acting at the same time as a storage organelle and as a lysosome-related organelle involved in substrate hydrolysis (389,390). It has been reported that endocytic vesicles budding off from the cytostome and the flagellar pocket of epimastigotes shuttle their cargo to RE (391). These organelles are stage-specific in *T. cruzi*, being gradually lost during metacyclogenesis. It has been proposed that nutrients in RE serve as main energy source for parasite differentiation (392). Further co-localization studies using specific markers for RE (*e.g.* Rab7, cysteine proteinases, among others) and endocytic ligands in the mNeonGreen-tagged parasites are needed to support the current subcellular location data.

Regarding RSKIN, recent subcellular proteomic studies demonstrated the presence of this enzyme in purified RE (390). The RE proteomic analysis by LC-MS/MS evidenced the presence of several other protein families including those related to lipid

metabolism arguing in favour that these organelles play a role in lipid synthesis. Also, enzymes related to signal transduction were located in these structures (*e.g.* protein tyrosine phosphatase, regulatory subunit of protein kinase A, casein kinase, activated protein kinase C receptor, protein kinase) including the serine/threonine protein kinase. In addition, several endosomal/lysosomal membrane proteins, proteins related to vesicular traffic, pumps and channel proteins, proteins involved in lipid, carbohydrate and protein metabolism, cell signaling proteins among others were also found the purified *T. cruzi* RE (390).

It is also possible that misfolded target-proteins due to fusion with MNeonGreen end up being degraded in RE, considering their function as endpoint of the endocytic pathway for protein degradation (389,390).

6.6   Conclusion

With the results obtained up to now, it can be concluded that the CRISPR/Cas9 gene editing technique was effective to precisely perform gene tagging studies and to obtain heterozygote KO clones for several GOI. Given their presumable essentiality, alternative methods to study null mutant phenotypes will be needed. Further analysis will be performed to confirm the heterozygous profile of the current clones and to evaluate protein expression changes of the GOI and assay their susceptibility to the studied compounds.

Part 3

Chapter 7: General discussion

Chapter 8: Concluding remarks

Chapter 9: Bibliography

Chapter 10: Appendix

7   GENERAL DISCUSSION

For decades, the international scientific community has been seeking for alternative treatments for kinetoplastid-caused diseases, addressed in the current thesis and with new alternatives delivered for some of them. A new entity fexinidazole is now used to treat HAT chronic stage and a pediatric formulation of benznidazole is now available for CD (152). The oral miltefosine used to VL since 2002 (134) was approved by United States Food and Drug Administration (FDA) in 2014 to treat CL caused by *L. braziliensis*, *L. guyanensis*, and *L. panamensis* (393), with reasonable efficacy and manageable toxicity when compared to other treatments (137). Still, the discovery of new drugs is not yet attained for *r*-HAT chronic stage, CD and CL, the two last deeply disregarded among NTDs in terms of drug R&D.

The target product profile (TPP) plays an important role in "effective optimization of drug candidates, decision-making within an organization, design of clinical research strategies, and constructive communication with regulatory authorities") (https://dndi.org/research-and-development/target-product-profiles/).

Some TPP topics are outlined in table 7.1. As for all diseases, the TPP of an ideal drug includes safety and efficacy against all disease stages, parasite species/strains to be used in all endemic regions, with preferably oral short treatment regimens and/or topical use in the case of CL. An acceptable drug profile needs to have, at least, the efficacy and safe profile of the current applied/approved drugs, also lacking genotoxicity and teratogenicity (392) for applicability in pregnant and lactating woman. Based on prior scientific knowledge in drug discovery, target candidate profile (TCP) is a set of criteria related to compound desirable features compiled from literature for multiple neglected diseases, describing physicochemical, antiparasitic, pharmacokinetic/pharmacodynamic (PK/PD) behavior, safety issues, and formulation properties of drug candidates to move from pre-clinical to clinical studies (218, 221, 394). When considered in early stage of drug discovery, the TCP defines goals for hit-to-lead candidates and enhances the chances of selecting promising agents and was therefore adopted in my research (218,221).

143

Table 7.1 Target product profile for cutaneous leishmaniasis, sleeping sickness and Chagas disease, retrieved from DNDi ((https://dndi.org/research-and-development/target-product-profiles/).

	Cutaneous leishmaniasis		Sleeping sickness		Chagas disease	
	Ideal	Acceptable	Ideal	Acceptable	Ideal	Acceptable
Target population	no restrictions	>9 months of age; no efficacy in immune-compromised patients; not for use in pregnancy	stages 1 and 2; melarsoprol refractory patients; pregnant and lactating women	stages 1 and 2	chronic and acute	acute
Target species	All	*L. tropica* *L. braziliensis*	Efficacy against both *T.b. gambiense* and *T.b. rhodesiense*	Efficacy against *T.b. gambiense* only	All regions with different DTUs	All regions with different DTUs
Efficacy	>95% patients with complete clinical cure:100% epithelialization of lesion(s) at 3 months from treatment onset; minimal scar; no relapse or development of Leishmaniasis recidivans or MCL (parasitological endpoint not required)	60% epithelialization of lesion(s) for *L. tropica* and 70% for *L. braziliensis* patients with complete cure Scar no worse than natural healing; <5% rate of relapse or development of Leishmaniasis recidivans or MCL at 1 year	Clinical efficacy > 95% at 18-month follow-up	Clinical efficacy > 95% at 18-month follow-up	>Bz standard dose in acute and chronic phases of disease	≥Bz standard dose (PC)
Safety/ tolerability	Well-tolerated	safety monitoring at PHC level; no major safety concerns: well-tolerated in >95% of patients treated. no treatment-induced mortality	<0.1% drug related mortality no monitoring for AEs	<1% possibly related mortality weekly simple lab testing (field testing) for AEs	< frequency of definitive treatment discontinuation than Bz by medical indication; not teratogenic or genotoxic; no pro-arrhythmic potential	< frequency of definitive treatment discontinuation than Bz by medical indication; not teratogenic or genotoxic; no pro-arrhythmic potential
Contra-indications	none	assessed at primary health care level	-	-	none	pregnancy
Formulation	Topical/ oral	Non-parenteral, or few doses if parenteral	adult and pediatric formulations		oral age-adapted	oral/parenteral age-adapted
Treatment regimen	Topical ≤ 14 days Oral < 7 days	Topical: 28 days Oral: twice daily for 28 days Parenteral ≤ 3 injections	<7 days oral once daily or <7 days intramuscular injection once daily	10 days oral or <10 days intramuscular injection	<30 days	Oral: any duration Parenteral: <7 days

Adverse events (AEs); Parasitological cure (PC); primary health care (PHC)

This thesis combines different screening approaches to identify prospective lead candidates. In fact, phenotypic screening plays a major role in first-in-class molecules

identification, followed by de MMOA exploration for molecule optimization and drug target discovery (210,211). Since trypanosomatids rely on host purine intermediates uptake to synthetize purines (245), a series of nucleoside analogues (**chapter 4)** were phenotypically screened against CD and HAT using *in vitro* and/or *in vivo* experimental models to select lead candidates, which were then further explored for their MoA (**chapters 6** and **7**).

Besides, natural libraries are important sources of new molecule entities to be further optimized by computer-aided drug design to facilitate drug screening (21,211–214) (**chapter 3**). In fact, a series of natural product-inspired phenyl sulfonyl derivatives (potent against *T. brucei* (214)) and nitroaromatic compounds based on a natural product-derived motif revealed potent leishmanicidal hits *in vitro* (Cp**6**, **7** and **30)** against CL. Moreover, active compounds such as the *in silico* shape-based hits Cp**1** and **2** (20) can also be directly identified by computer-aided drug design (211), using an active query compound as a starting point for the ligand-based shape screening, without the need of target crystal structure (215).

As described in **chapter 3**, three (two nitro-derivatives Cp**6** and Cp**7** and the adamantyl Cp**30)** presented promising characteristics *in vitro* based on TCP for CL: potency against intracellular forms within macrophages (IC_{50} = 4.57, 0.19 and 4 µM, respectively) besides displaying high SI (>109, >54 and >125 for Cp**6**, Cp**7** and Cp**30**, respectively) being at least 10-fold higher than the reference pentamidine. In fact, the criteria for TCP in terms of *in vitro* activity, selectivity and assay design were reached (129,221) for characterizing 'lead' candidates such as: (i) *in vitro* model that closely reproduces pathological conditions (220), (ii) short time of drug incubation (48 h instead of preconized 72h) to select fast-killing compounds (129,221), and (iii) >99% reduction of intracellular amastigote levels as compared to untreated control (129,221). These findings motivated us to move to *in vivo* studies using mice-CL model (**chapter 3)** complying to the CL-TPP acceptable criteria in terms of safety and oral treatment regimen less than the 28 days bid. (14 days bid. in CL-BALB/c model) using doses (10 mg/kg/day) lower than predicted for human (30 mg/kg/day) (126,218). *L. braziliensis* and *L. tropica* are the targeted species for acceptable TPP as presented in table 7.1, since they are considered the most frequent causative agent of CL in NW and OW respectively (395, 396). CL comprises a complexity of clinical manifestations with host-parasite interaction peculiarities for different species (397,398), being a species-specific limitation for drug development and thus it is unlikely to find a drug suitable for all species (ideal TPP) (221).

As discussed in **chapter 3**, we assessed *L. amazonensis* as the commonest *Leishmania* species in Brazil, causing a wide spectrum of disease manifestations, including very severe and diffuse cutaneous leishmaniasis and also represents a suitable laboratory model for CL drug screening (233). Unfortunately, *in vivo* analysis did not meet our *in vitro* expectations since none of the tested compounds was able to reduce the cutaneous lesions. However, the bulk of the *in vitro* leishmanicidal efficacy supports their use as templates for further compound optimization focusing on analogs that have the appropriate TPP for new CL drugs, as recommended (221).

As described in **chapter 4,** trypanosomatids are unable to produce purine *de novo* and depends on the uptake of host intermediates (250), which makes this pathway attractive for drug discovery (251). In that sense, a series of nucleoside analogues was screened against a panel of trypanosomatids and indeed revealed promising candidates, including the unmodified ribofuranose analogues **14** and **06**. They exhibited SI of at least 300 and activity at submicromolar range ($IC_{50}<10\mu M$) (218), were metabolically stable in the presence of Phase-I and Phase-II metabolic enzymes and microsomal fractions, justifying further analysis to be conducted on different *T. cruzi* DTUs (including Y strain) and host cells (such as CCs) prior to *in vivo* evaluation (225). Despite the outstanding *in vitro* activity of several nucleotide derivatives tested so far, parasite recrudescence was observed when assayed using ACD-murine model (Table 4.1) One of them, the 4-amino-5-(4-chlorophenyl)-N7-(3′-deoxy-β-D-ribofuranosyl)-pyrrolo[2,3-d]pyrimidine referred as Cpd**1** in **chapter 4** (265) was further characterized *in vitro* for relapse occurrence (by washout assays) and impact on parasite fitness (pre-treatment assays of trypomastigote forms prior to infection of cardiac cell cultures). In our assays, parasite recrudescence was observed *in vitro* and after an extended period of treatment *in vivo* (60 days). Indeed, dormant forms are intrinsically related to parasite resurgence and need to be tackled by pre-clinical candidates for sterile cure (399,400). These outcomes also highlight the importance to use predictive *in vitro* tools for parasite recrudesce complemented with *in vivo* analysis (241).

Another important subject is related to the physicochemical/pharmacological profile (DMPK) of novel compounds since potent activity is pursued but not at expense of poor DMPK properties. DMPK needs to be incorporated as soon as possible in preclinical studies to maximize the success and assess important drug characteristics such as solubility, permeability, acceptable formulation and bioavailability, among others (221). These properties include polar surface area, charge, partition coefficient (measured

as cLogP), molecular weight, and H bonding (401,402), which were presently predicted *in silico* as well as assayed *in vitro*.

In this sense, a drug candidate for kinetoplastids must: (a) be able to cross the BBB for HAT chronic stage treatment, (b) be permeable to the skin to reach the site of infection for topical CL therapy, (c) act in the macrophage acidic phagolysosome for leishmaniasis therapy, (d) target different organs and tissues for CD treatment (403,404).

In vitro metabolic stability evaluation, as performed for the nucleoside analogues **14** and **06 (chapter 4),** is essential knowledge prior to *in vivo* analysis (274). *In silico* tools were also applied to predict some critical ADME parameters for the CL candidates: nitro-derivatives **6** and **7** (62), sulfonyl Cp**30** (21) and the *in silico* shape-based hits Cp**1** and **2**. The predicted results are discussed below.

Cp **6** and **7** do not violate Lipinski's rule (62,405,406). The results showed that Cps **6** and **7** have relatively lower cLogP (2.97 and 2.13, respectively) in comparison to reference drug miltefosine (cLogP 5.68). MIL is zwitterionic and its relatively high cLogP is ideal for high intestinal absorption (405). For Cp**6** and Cp**7** respectively, sufficient intestinal adsorption was expected from oral gavage due to neutrality at physiological pH and low molecular weights of 324.34 and 297.27 g/mol. Moderate to high Caco-2 permeability (0.83 and 1.04, respectively) was also predicted from *in silico* ADME calculations. The predicted volume of distribution is high and ideal for tissue distribution for both. Cell proliferation assay using Hep G2 cells indicates that both compounds are not hepatotoxic at the tested concentrations (160-1.2 µM). However, the predicted unbound fraction for Cp**6** is relatively low (5%) and ideal for Cp**7** (21%). Both are predicted as CYP_{3A4} substrates, which suggest significant first-pass hepatic clearance and low overall plasma and tissue concentration. Therefore, a comparative pharmacokinetics study (oral and intravenous) can provide insights into plasma concentrations and bioavailability of both compounds in addition to determining the appropriate dosage and structural changes necessary for *in vivo* efficacy. As nitro-drugs are activated by *Leishmania* NTR2 (242), it is possible that **6** and **7** may be also activated in a similar way. Their *in vitro* leishmanicidal efficacy supports their use as templates for nitroimidazole-based antileishmanial drug discovery programs focusing on analogues that have the appropriate TPP for new CL drugs.

Cp**30**'s *in vivo* lack of activity against CL is potentially tied to its high lipophilicity (cLogP of 4.3), impairing its use at a higher dose (*e.g.* at 40 mg/kg as assayed for MIL).

(21). Ongoing work on analogues of Cp**30** to improve aqueous solubility is planned as well as assessing metabolic stability for improved bioavailability.

The predicted properties of the hits Cp**1** and Cp**2 (chapter 3)** showed compliance with 'Lipinski rule of five' and 'Jorgensen rule of tree' – including good permeability and solubility properties – therefore more likely to be orally available (20). They also displayed permissible range of bind affinity to serum albumin protein and good blood-brain barrier permeation *in silico* (20). Cp**1** and **2** activities against intracellular forms of *L. amazonensis* (IC$_{50}$ of 9.35±1.87 and 7.25±1.46 µM, respectively) (20) is in a similar range of the query compound GNF5343 against *L. donovani* (7.3 ± 0.6 µM) (222) but with insufficient selectivity to support *in vivo* evaluation (20). Currently, minor structural modifications of Cp**2** are underway to improve potency, selectivity and pharmacological profile, aiming to contribute to the discovery of new chemical entities for CL.

Finally, the last part of my PhD thesis aimed to add some new knowledge related to the mode-of-action of nucleoside derivatives on *T. brucei* and *T. cruzi*. The *T. brucei* RNA interference (RNAi) library is extensively studied, making it more accessible to induce genome modifications/knockdowns and to study genes involved in a wide range of processes (297,298,314). This technique was applied in the current study in an attempt to identify and validate cellular targets in *T. brucei* (**chapter 5**). On the other hand, *T. cruzi* gene manipulation is more complex, and selection of stable parasites remains difficult since *T. cruzi* has no RNAi machinery. Fortunately, protocols for rapid generation of gene knockout mutants using CRISPR-Cas9 technique are now accessible (343,366) and represents a faster and accurate technology to edit the genome in many organisms, including for *T. cruzi* (26,347–350). As observed in **chapter 4**, some of the nucleoside derivatives were highly active against both *T. cruzi* and *T. brucei* (Cpd**1**, **14** and **88,** (IC$_{50}$<2µM *T. brucei* and <0.5µM *T. cruzi*), enhancing the chances of similar modes-of-action in both species. The molecular studies using whole-genome RNAi screening revealed a wide panel of possible nucleoside targets in *T. brucei*, including EndG, FLA1-binding protein, HSP, UBE1 GRESAG 4 ADKIN, RSKIN and OXRED and, apart from ADKIN, none triggered substantial parasite resistance by target downregulation. Moreover, the transport of the presently studied nucleoside analogues was not exclusively associated to P2 unlike melarsoprol and Pt (317–319), a desired feature for future candidates (146).

Among the revealed putative targets, there are enzymes that perform essential functions in the purine metabolic pathways such as phosphorylation of substrates

(ADKIN and RSKIN) and NADP-dependent reduction and protection against oxidative stress (OXRED), supporting their role as both potential targets for nucleoside analogues. Next, these targets were extrapolated for *T. cruzi* MoA study by CRISPR/Cas9 assessing ADKIN, *RSKIN*, and *ADRED* orthologous genes in an attempt to generate double knockouts, as reported in **chapter 6**.

Regardless the applied strategy of single or double transfection, one of the wild-type ORF remained present in all clones analysed by diagnostic PCR, supporting their role as essential genes and promising targets. Preliminary PCR scrutiny pointed for single knockouts generation for all targets which need to be further confirmed and validated for gene essentiality. DiCre system is a promising molecular resource to confirm gene essentiality by null mutants generation, but still not fully standardized for *T. cruzi* (387). Plasmid shuffle could therefore be an extra indicative of gene essentiality (385). As debated in **chapter 7**, *T. cruzi* is a puzzling parasite which many aspects of its biology unrevealed. It is known that DNA repair is essential for survival, infection and may be involved in drug resistance (378) together with other unknown mechanisms of evasion and/or intrinsic resistance to the applied drug pressure.

In vitro growth curves performed with the heterozygous clones for ADKIN and ADRED showed a significant loss of fitness on the curve onset and parasitemia peak respectively, an extra evidence of gene essentiality. In an attempt to have insight into the subcellular localization, ADKIN, RSKIN and ADRED were tagged with the fluorescent mNeonGreen and parasites analysed microscopically. The analyses suggest that some targets (ADRED tagged parasites) may be localized intracellularly in reservosomes, the endpoint of the endocytic pathway. Those *T. cruzi* stage-organelles are important for molecule storage, degradation, and the main energy source for differentiation (392). To confirm this observation and eliminate any bias, such as the endpoint of misfolded target-proteins due to fusion with MNeonGreen, further co-localization studies will be performed to specifically mark the RE and the endocytic pathway of the tagged parasites.

In summary, this PhD thesis aggregates several *in silico*, *in vitro* and *in vivo* strategies to fully evaluate CL, HAT and CD new drug candidates by phenotypic screening, taking into consideration disease specificity and treatment demands, including TPP and TCP profiles, besides assessing compounds MoA and pharmacological profile, in line with the pressing need to offer a strong PoC in pre-clinical studies.

8   CONCLUDING REMARKS

The aim of this thesis was:

-To evaluate anti-parasitic activity (*in vitro* and *in vivo*) and pharmacological profile (*in vitro* and/or *in silico*) of different classes of molecules (in combination or not) using relevant pathological forms and suitable experimental models for CL, HAT and CD, combining both phenotypic and target-based approaches for drug discovery:

- 2 out of 32 GNF5343-base shaped hits (hit Cp**1** and GNF5343 analogue Cp**2**) were potent against *L. amazonensis* intracellular forms (IC$_{50}$ equal to 9.35 ± 1.87 and 7.25 ± 1.46 µM respectively), but with insufficient selectivity (<10) to justify *in vivo* analysis.

- 2 out of 7 nitroaromatic compounds (Cp**6** and Cp**7**) derived from natural motifs and 1 sulfonyl derivative out of 21 product-inspired synthetic products (Cp**30**) were potent (IC$_{50}$ <10µM) and selective against intracellular forms of *L. amazonensis* (SI>50) encouraging us to further analyze their performance in CL-mice experimental model. Cp**6,7** and **30** were not active *in vivo*, justifying the need of molecule optimization to improve pharmacological and activity profiles.

- 8 out of 16 new optimized 7-deazapurine nucleosides were highly active against intracellular forms of *T. cruzi* in L929 cells (IC$_{50}$<1 µM) and at least 20 times more selective towards mammalian cells. Among them, the metabolically stable leads Cpd**14** and Cpd**06** (IC$_{50}$=0.05 and 0.2 µM respectively) were at least 300x more selective against the amastigote forms in comparison to host cells, deserving an *in vivo* follow-up.

- When assayed against *T. brucei* spp, none of the 16 nucleoside derivatives exhibited a selectivity and/or potency higher than the reference drug suramin and other nucleoside counterparts described in literature (269) (IC$_{50\ T.\ rhodesiense}$= 0.015 and 0.00052 nM (269) respectively), hence not considered for *in vivo* follow-up evaluation.

- To analyze the impact of Cpd**1** on parasite fitness, full intracellular cure *in vitro* and to surpass parasite relapse *in vivo* by extended periods of treatment:

- Cpd**1** (7-Aryl-7-deazapurine 3′-deoxyribonucleside) impaired *T. cruzi* trypomastigote capacity to successfully establish intracellular infection of cardiac cultures but did not prevent recrudescence *in vivo* after long-term treatment (60 days) probably due to the presence of dormant cells subpopulation or genetic factors in persister parasites involved in natural drug resistance, corroborating the wash-out *in vitro* outcomes.

- Cpd**1** combined with suboptimal dose of Bz (addictive effect *in vitro*) supressed animal parasitemia *in vivo* but did not prevent mortality.

-To infer the mode-of-action of promising trypanocidal candidates (nucleoside analogues) in *T. brucei* and *T. cruzi* and identify potential targets in drug discovery:

- RNAi studies suggest the involvement of ADKIN in the nucleoside JB588 mode-of-action in *T. brucei*, not exclusively dependent of P2 transporter.

- Single target-gene deletion by CRISPR/Cas9 in *T. cruzi* revealed ADKIN, RSKIN and OXRED as promising drug targets which will be further validated for gene essentiality and protein expression, followed by nucleoside analogues MoA studies.

- Our studies generate new knowledge regarding drug candidates with antiparasitic potential against trypanosomatid parasites, aiming to contribute to drug discovery programs for neglected diseases.

9 BIBLIOGRAPHY

1. Kinoshita-Yanaga AT, Toledo MJDO, De Araújo SM, Vier BP, Gomes ML. Accidental infection by *Trypanosoma cruzi* follow-up by the polymerase chain reaction: Case report. Revista do Instituto de Medicina Tropical de Sao Paulo. 2009;51(5):295–8.

2. Rezende JM, Lauar K, Oliveira AR. Aspectos clínicos e radiológicos da aperistalsis do esôfago. Rev Bras Gastroenterol. 1960;12:147–262.

3. Rassi A, de Rezende JM, Luquetti AO, Rassi A. Clinical Phases and Forms of Chagas Disease. American Trypanosomiasis. 2010; 709–741.

4. Coura JR, Albajar Viñas P, Brum-Soares LM, de Sousa AS, Xavier SS. Morbidity of Chagas heart disease in the microregion of Rio Negro, Amazonian Brazil: A case-control study. Memorias do Instituto Oswaldo Cruz. 2013;108(8):1009–13.

5. Dias Negrão Murback N, Hans Filho G, Ayres Ferreira do Nascimento R, Regina De Oliveira Nakazato K, Elizabeth Moraes Cavalheiros Dorval M. American cutaneous leishmaniasis : clinical , epidemiological and laboratory studies conducted at a university teaching. An Bras Dermatol. 2011;86(1):55–63.

6. Vingerhoets LMA, Bauer MP, Hamminga EA, Verweij JJ, Visser LG. Treatment and follow-up using microscopy and polymerase chain reaction in East African sleeping sickness: a case report. Grand Rounds. 2011;11(1):12–6.

7. Hayes P, Varga V, Olego-Fernandez S, Sunter J, Ginger ML, Gull K. Modulation of a cytoskeletal calpain-like protein induces major transitions in trypanosome morphology. Journal of Cell Biology. 2014;206(3):377–84.

8. Santos CC, Lionel JR, Peres RB, Batista MM, da Silva PB, de Oliveira GM, *et al. In Vitro*, *in silico*, and *in vivo* analyses of novel aromatic amidines against *Trypanosoma cruzi*. Antimicrobial Agents and Chemotherapy. 2017;62(2):1–8.

9. De Souza W. Electron microscopy of trypanosomes - A historical view. Memorias do Instituto Oswaldo Cruz. 2008;103(4):313–25.

10. Rocha GM, Teixeira DE, Miranda K, Weissmüller G, Bisch PM, de Souza W. Structural changes of the paraflagellar rod during flagellar beating in *Trypanosoma cruzi*. PLoS ONE. 2010;5(6).

11. Vatarunakamura C, Ueda-Nakamura T, de Souza W. Visualization of the cytostome in *Trypanosoma cruzi* by high resolution field emission scanning electron microscopy using secondary and backscattered electron imaging. FEMS microbiology letters. 2005; 242(2):227–30.

12. Zuma AA, dos Santos Barrias E, de Souza W. Basic Biology of *Trypanosoma cruzi*. Current Pharmaceutical Design. 2020;27(14):1671–732.

13. de Souza W. Structural organization of T*rypanosoma cruzi.* Memorias do Instituto Oswaldo Cruz. 2009;104(SUPPL. 1):89–100.

14. Marinho FA, Gonçalves KCS, Oliveira SSC, Gonçalves DS, Matteoli FP, Seabra SH, *et al.* The calpain inhibitor MDL28170 induces the expression of apoptotic markers in *leishmania amazonensis* promastigotes. PLoS ONE. 2014;9(1).

15. Alberio SO, Dias SS, Faria FP, Mortara RA, Barbiéri CL, Haapalainen EF. Ultrastructural and cytochemical identification of megasome in *Leishmania* (Leishmania) *chagasi.* Parasitology Research. 2004;92(3):246–54.

16. El-Sayed NM, Myler PJ, Blandin G, Berriman M, Crabtree J, Aggarwal G, *et al.* Comparative genomics of trypanosomatid parasitic protozoa. Science (New York, NY). 2005 Jul;309(5733):404–9.

17. Ponte-Sucre A, Gamarro F, Dujardin JC, Barrett MP, López-Vélez R, García-Hernández R, *et al.* Drug resistance and treatment failure in leishmaniasis: A 21st century challenge. PLoS Neglected Tropical Diseases. 2017;11(12):1–24.

18. Maya JD, Cassels BK, Iturriaga-Vásquez P, Ferreira J, Faúndez M, Galanti N, *et al.* Mode of action of natural and synthetic drugs against *Trypanosoma cruzi* and their interaction with the mammalian host. Comparative Biochemistry and Physiology - A Molecular and Integrative Physiology. 2007;146(4):601–20.

19. Garcia-Salcedo JA, Unciti-Broceta JD, Valverde-Pozo J, Soriano M. New approaches to overcome transport related drug resistance in trypanosomatid parasites. Frontiers in Pharmacology. 2016;7:1–14.

20. Cardoso Santos C, Meuser Batista M, Inam Ullah A, Rama Krishna Reddy T, Soeiro M de NC. Drug screening using shape-based virtual screening and *in vitro* experimental models of cutaneous Leishmaniasis. Parasitology. 2021;148(1):98–104.

21. Santos CC, Zhang H, Batista MM, de Oliveira GM, Demarque KC, da Silva-Gomes NL, *et al. In vitro* and *in vivo* evaluation of an adamantyl-based phenyl sulfonyl acetamide against cutaneous leishmaniasis models of *Leishmania amazonensis.* Antimicrobial agents and chemotherapy. 2020;64(12).

22. Motta MCM, Martins A, Catta-preta C, Cristina M, Motta M, Cezar A, *et al.* Predicting the Proteins of *Angomonas deanei*, *Strigomonas culicis* and their respective endosymbionts reveals new aspects of the Trypanosomatidae. PLoS One. 2013;8(4):e60209.

23. Gutteridge WE, Davies MJ. Enzymes of purine salvage in *Trypanosoma cruzi*. FEBS letters. 1981;127(2):211–4.

24. Bouton J, Ferreira de Almeida Fiuza L, Cardoso Santos C, Mazzarella MA, Soeiro M de NC, Maes L, *et al*. Revisiting Pyrazolo[3,4-d]pyrimidine nucleosides as anti-*Trypanosoma cruzi* and antileishmanial agents. Journal of Medicinal Chemistry [Internet]. 2021; 64(7):4206–38.

25. Shi H, Chamond N, Djikeng A, Tschudi C, Ullu E. RNA interference in *Trypanosoma brucei*: role of the n-terminal RGG domain and the polyribosome association of argonaute. J Biol Chem. 2009;284(52):36511-36520.

26. Beneke T, Madden R, Makin L, Valli J, Sunter J, Gluenz E. A CRISPR Cas9 high-throughput genome editing toolkit for kinetoplastids. Royal Society Open Science. 2017;4(5):1–16.

27. WHO. Neglected tropical diseases [Internet]. [cited 2020 Jun 23]. Available from: https://www.who.int/neglected_diseases/diseases/en/

28. Hotez PJ, Lo NC. 27 - Neglected Tropical Diseases: Public Health Control Programs and Mass Drug Administration. In: Ryan ET, Hill DR, Solomon T, Aronson NE, Endy TPBT-HTM and EID (Tenth E, editors). 2020;209–13.

29. WHO. Preventive Chemotherapy and Transmission Control (PCT). [Internet]. [cited 2020 Jun 23]. Available from: https://www.who.int/neglected_diseases/preventive_chemotherapy/information/en/

30. WHO. Innovative and intensified disease management [Internet]. [cited 2020 Jun 23]. Available from: https://www.who.int/neglected_diseases/disease_management/Innovative_Intensified_Disease_Management/en/

31. Hotez PJ, Fenwick A, Molyneux DH. Collateral benefits of preventive chemotherapy - expanding the war on neglected tropical diseases. The New England journal of medicine. 2019;380(25):2389–91.

32. Rosenberg M, Utzinger J, Addiss DG. Preventive chemotherapy versus innovative and intensified disease management in neglected tropical diseases: a distinction whose shelf life has expired. PLoS Neglected Tropical Diseases. 2016;10(4):9–12.

33. Chagas C. Nova tripanozomiaze humana: estudos sobre a morfolojia e o ciclo evolutivo do *Schizotrypanum cruzi* n. gen., n. sp., ajente etiolojico de nova entidade morbida do homem. Memorias [Internet]. 1909;1(2):159–218.

34. Dias JCP, Ramos AN, Gontijo ED, Luquetti A, Shikanai-Yasuda MA, Coura JR,

et al. 2nd Brazilian Consensus on Chagas disease, 2015. Revista da Sociedade Brasileira de Medicina Tropical. 2016;49:3–60.

35.   Pacheco LV, Santana LS, Barreto BC, Santos E de S, Meira CS. Oral transmission of Chagas disease: A literature review. Research, Society and Development [Internet]. 2021 Feb 17;10(2 SE-):e31910212636.

36.   WHO. Chagas disease (also known as American trypanosomiasis) [Internet]. Key facts. 2021 [cited 2021 Jun 14]. Available from: https://www.who.int/news-room/fact-sheets/detail/chagas-disease-(american-trypanosomiasis)

37.   Coura JR. Chagas disease: what is known and what is needed - A background article. Memórias do Instituto Oswaldo Cruz. 2007;102(review):113–22.

38.   WHO. Chagas disease (also known as American trypanosomiasis) [Internet]. World Health Organization. 2021 [cited 2021 Aug 2]. Available from: https://www.who.int/news-room/fact-sheets/detail/chagas-disease-(american-trypanosomiasis)

39.   Pecoul B, Batista C, Stobbaerts E, Ribeiro I, Vilasanjuan R, Gascon J, *et al*. The BENEFIT trial: Where do we go from here? PLoS Neglected Tropical Diseases. 2016;10(2):2–5.

40.   Stanaway JD, Roth G. The burden of Chagas disease: estimates and challenges. Global heart. 2015 Sep;10(3):139–44.

41.   Coura JR, Dias JCP. Epidemiology, control and surveillance of Chagas disease - 100 years after its discovery. Memorias do Instituto Oswaldo Cruz. 2009;104(SUPPL. 1):31–40.

42.   Hotez PJ, Alvarado M, Basáñez M-G, Bolliger I, Bourne R, Boussinesq M, *et al*. The Global Burden of Disease Study 2010: Interpretation and implications for the neglected tropical diseases. PLOS Neglected Tropical Diseases [Internet]. 2014 Jul 24;8(7):e2865.

43.   Pinazo M-J, Pinto J, Ortiz L, Sánchez J, García W, Saravia R, *et al*. A strategy for scaling up access to comprehensive care in adults with Chagas disease in endemic countries: The Bolivian Chagas Platform. PLoS neglected tropical diseases. 2017;11(8):e0005770.

44.   WHO. Chagas disease in Latin America: an epidemiological update based on 2010 estimates. Releve epidemiologique hebdomadaire. 2015;90(6):33–43.

45.   Nunes MCP, Dones W, Morillo CA, Encina JJ, Ribeiro AL. Chagas disease: An overview of clinical and epidemiological aspects. Journal of the American College of Cardiology. 2013;62(9):767–76.

46. Lidani KCF, Andrade FA, Bavia L, Damasceno FS, Beltrame MH, Messias-Reason IJ, *et al.* Chagas disease: From discovery to a worldwide health problem. Journal of Physical Oceanography. 2019;49(6):1–13.

47. Nunes MCP, Beaton A, Acquatella H, Bern C, Bolger AF, Echeverría LE, *et al.* Chagas Cardiomyopathy: An Update of Current Clinical Knowledge and Management: A Scientific Statement From the American Heart Association. Vol. 138, Circulation. 2018. 169–209 p.

48. Steverding D. The history of leishmaniasis. Parasites and Vectors. 2017;10(1):1–10.

49. Leishman WB. On the possibility of the occurrence of trypanosomiasis in India. British Medical Journal. 1903;1(2213):1252–4.

50. Donovan C. On the possibility of the occurrence of trypanosomiasis in India. 1903. The National medical journal of India. 1994;7(4):196,201-202.

51. da Silva LJ. Vianna and the discovery of *Leishmania braziliensis*: the role of Brazilian parasitologists in the identification of Bauru's ulcer as American leishmaniasis. Parasitologia. 2005;47(3–4):335–41.

52. Thomaz-Soccol V, Lanotte G, Rioux JA, Pratlong F, Martini-Dumas A, Serres E. Monophyletic origin of the genus Leishmania Ross, 1903. Annales de parasitologie humaine et comparee. 1993;68(2):107–8.

53. Emro WHO. Infectious agent (s) WHO case definition Incubation period Communicability period Epidemiology and risk factors Situation in countries affected by crisis in Syria. 2020;1–7.

54. Dndi Annual Report. MEDICINES FOR THE PEOPLE [Internet]. 2020. Available from: https://dndi.org/wp-content/uploads/2021/08/DNDi-AnnualReport-2020.pdf

55. Arenas R, Torres-Guerrero E, Quintanilla-Cedillo MR, Ruiz-Esmenjaud J. Leishmaniasis: A review. F1000Research. 2017;6:1–15.

56. Alvar J, Vélez ID, Bern C, Herrero M, Desjeux P, Cano J, et al. Leishmaniasis worldwide and global estimates of its incidence. PLoS ONE. 2012;7(5).

57. WHO. Leishmaniasis [Internet]. Fact sheets. [cited 2021 Sep 16]. Available from: https://www.who.int/health-topics/leishmaniasis#tab=tab_1

58. Martins ALGP, Barreto JA, Lauris JRP, Martins ACGP. American tegumentary leishmaniasis: Correlations among immunological, histopathological and clinical parameters. Anais Brasileiros de Dermatologia. 2014;89(1):52–8.

59. David CV, Craft N. Cutaneous and mucocutaneous leishmaniasis. Dermatol Ther.

2009;22(6):491-502.

60. Bilgic-Temel A, Murrell DF, Uzun S. Cutaneous leishmaniasis: A neglected disfiguring disease for women. International Journal of Women's Dermatology [Internet]. 2019;5(3):158–65.

61. de Vries HJC, Reedijk SH, Schallig HDFH. Cutaneous leishmaniasis: recent developments in diagnosis and management. American Journal of Clinical Dermatology. 2015;16(2):99–109.

62. Santos CC, Zhang H, Batista MM, de Oliveira GM, Demarque KC, da Silva-Gomes NL, Moreira OC Ogungbe IV, Soeiro MdNC. Phenotypic investigation of 4 nitrophenylacetyl- and 4-nitro-1H-imidazoyl-based compounds as antileishmanial agents. Parasitology. 2022; 3:1-6.

63. Bailey F, Mondragon-Shem K, Haines LR, Olabi A, Alorfi A, Ruiz-Postigo JA, *et al*. Cutaneous leishmaniasis and co-morbid major depressive disorder: A systematic review with burden estimates. PLoS Neglected Tropical Diseases. 2019;13(2):1–22.

64. Steverding D. The history of African trypanosomiasis. Parasites and Vectors. 2008;1(1):1–8.

65. Kleine F. Positive infektionsversuche mit Trypanosoma brucei durch glossina palpalis. Deutsche Medizinische Wochenzeitschrift. 1909;11:469–470.

66. Stephens JWW, Fantham HB. On the peculiar morphology of a trypanosome from a case of sleeping sickness and the possibility of its being a new species (*T. rhodesiense*). Proc R Soc Lond B. 1910;83:28–33.

67. Drugs for Neglected disease initiative. Sleeping Sickness Factsheet. Making medical history with revolutionary treatments [Internet]. 2019 [cited 2021 Sep 23]. p. 1–2. Available from: https://dndi.org/wp-content/uploads/2020/10/DNDi-Factsheet-SleepingSickness-2019.pdf

68. Barrett MP, Burchmore RJS, Stich A, Lazzari JO, Frasch AC, Cazzulo JJ, *et al.* The trypanosomiases. Lancet (London, England). 2003 Nov;362(9394):1469–80.

69. Stich A, Abel PM, Krishna S. Human African trypanosomiasis. BMJ (Clinical research ed). 2002;325(7357):203–6.

70. Bottieau E, Clerinx J. Human African trypanosomiasis: progress and stagnation. Infectious disease clinics of North America. 2019;33(1):61–77.

71. Baker CH, Welburn SC. The long wait for a new drug for human african trypanosomiasis. Trends in parasitology. 2018;34(10):818–27.

72. Kennedy PGE. Update on human African trypanosomiasis (sleeping sickness).

Journal of neurology. 2019 Sep;266(9):2334–7.

73. World Health Organization. Trypanosomiasis, human African (sleeping sickness) [Internet]. Key facts. 2021 [cited 2021 Sep 23]. Available from: https://www.who.int/en/news-room/fact-sheets/detail/trypanosomiasis-human-african-(sleeping-sickness)

74. Deeks ED. Fexinidazole: First Global Approval. Drugs. 2019 Feb;79(2):215–20.

75. DNDi. Making treatment safer and more effective for people living. 2018;16.

76. Yun O, Priotto G, Tong J, Flevaud L, Chappuis F. NECT is next: implementing the new drug combination therapy for T*rypanosoma brucei gambiense* sleeping sickness. PLoS neglected tropical diseases. 2010 May;4(5):e720.

77. Matovu E, Mugasa CM, Waiswa P, Kitibwa A, Boobo A, Ndung'u JM. Haemoparasitic Infections in Cattle from a *Trypanosoma brucei Rhodesiense* Sleeping Sickness Endemic District of Eastern Uganda. Tropical Medicine and Infectious Disease. 2020;5(1):1–10.

78. Caljon G, De Baetselier P, Magez S. African trypanosomiasis. Medical Parasitology. 2009;161–70.

79. Latif AA, Ntantiso L, De Beer C. African animal trypanosomosis (nagana) in northern KwaZulu-Natal, South Africa: Strategic treatment of cattle on a farm in endemic area. Onderstepoort Journal of Veterinary Research. 2019;86(1):1–6.

80. Vodnala M, Ranjbarian F, Pavlova A, De Koning HP, Hofer A. *Trypanosoma brucei* methylthioadenosine phosphorylase protects the parasite from the antitrypanosomal effect of deoxyadenosine: Implications for the pharmacology of adenosine antimetabolites. Journal of Biological Chemistry. 2016;291(22):11717–26.

81. Bekele E. The current situation and diagnostic approach of nagana in africa: a review. 2015 Jan 1;

82. Borst P. Maxi-circles, glycosomes, gene transposition, expression sites, transsplicing, transferrin receptors and base J. Molecular and biochemical parasitology. 2016;205(1–2):39–52.

83. Leon W, Frasch AC, Hoeijmakers JH, Fase-Fowler F, Borst P, Brunel F, *et al.* Maxi-circles and mini-circles in kinetoplast DNA from *Trypanosoma cruzi*. Biochimica et biophysica acta. 1980 Apr;607(2):221–31.

84. Haag J, O'hUigin C, Overath P. The molecular phylogeny of trypanosomes: evidence for an early divergence of the Salivaria. Molecular and biochemical parasitology. 1998;91(1):37–49.

85. Teixeira SM, de Paiva RMC, Kangussu-Marcolino MM, DaRocha WD. Trypanosomatid comparative genomics: Contributions to the study of parasite biology and different parasitic diseases. Genetics and Molecular Biology. 2012;35(1):1–17.

86. Martínez-Calvillo S, Nguyen D, Stuart K, Myler PJ. Transcription initiation and termination on *Leishmania major* chromosome 3. Eukaryotic cell [Internet]. 2004;3(2):506–17.

87. Clayton C. Regulation of gene expression in trypanosomatids: living with polycistronic transcription. Open Biol. 2019 28;9(6):190072.

88. Günzl A, Bruderer T, Laufer G, Schimanski B, Tu L-C, Chung H-M, *et al.* RNA polymerase I transcribes procyclin genes and variant surface glycoprotein gene expression sites in *Trypanosoma brucei*. Eukaryotic cell. 2003 Jun;2(3):542–51.

89. Schier AC, Taatjes DJ. Structure and mechanism of the RNA polymerase II transcription machinery. Genes and Development. 2020;34(7–8):465–88.

90. LeBowitz JH, Smith HQ, Rusche L, Beverley SM. Coupling of poly(A) site selection and trans-splicing in Leishmania. Genes & development. 1993 Jun;7(6):996–1007.

91. Hajduk SL, Harris ME, Pollard VW. RNA editing in kinetoplastid mitochondria. FASEB journal : official publication of the Federation of American Societies for Experimental Biology. 1993;7(1):54–63.

92. El-Sayed NM, Myler PJ, Bartholomeu DC, Nilsson D, Aggarwal G, Tran A-N, *et al.* The genome sequence of *Trypanosoma cruzi*, etiologic agent of Chagas disease. Science (New York, NY). 2005 Jul;309(5733):409–15.

93. Sima N, McLaughlin EJ, Hutchinson S, Glover L. Escaping the immune system by DNA repair and recombination in African trypanosomes. Open biology. 2019 Nov;9(11):190182.

94. Olivier M, Gregory DJ, Forget G. Subversion mechanisms by which Leishmania parasites can escape the host immune response: A signaling point of view. Clinical Microbiology Reviews. 2005;18(2):293–305.

95. Callejas-Hernández F, Rastrojo A, Poveda C, Gironès N, Fresno M. Genomic assemblies of newly sequenced *Trypanosoma cruzi* strains reveal new genomic expansion and greater complexity. Scientific Reports. 2018;8(1):1–13.

96. Docampo R, de Souza W, Miranda K, Rohloff P, Moreno SNJ. Acidocalcisomes - conserved from bacteria to man. Nature reviews Microbiology. 2005 Mar;3(3):251–61.

97.   Halliday C, de Castro-Neto A, Alcantara CL, Cunha-e-Silva NL, Vaughan S, Sunter JD. Trypanosomatid flagellar pocket from structure to function. Trends in Parasitology [Internet]. 2021;37(4):317–29.

98.   Alcantara CL, de Souza W, Cunha E Silva NL. The cytostome-cytopharynx complex of intracellular and extracellular amastigotes of *Trypanosoma cruzi* exhibit structural and functional differences. Cellular microbiology. 2021;23(9):e13346.

99.   Rodríguez NE, Gaur U, Wilson ME. Role of caveolae in *Leishmania chagasi* phagocytosis and intracellular survival in macrophages. Cellular Microbiology. 2006;8(7):1106–20.

100.   Scianimanico S, Desrosiers M, Dermine JF, Méresse S, Descoteaux A, Desjardins M. Impaired recruitment of the small GTPase rab7 correlates with the inhibition of phagosome maturation by *Leishmania donovani* promastigotes. Cellular microbiology. 1999;1(1):19–32.

101.   Antoine JC, Prina E, Lang T, Courret N. The biogenesis and properties of the parasitophorous vacuoles that harbour Leishmania in murine macrophages. Trends in microbiology. 1998;6(10):392–401.

102.   Kane MM, Mosser DM. Leishmania parasites and their ploys to disrupt macrophage activation. Current opinion in hematology. 2000;7(1):26–31.

103.   Wanderley JLM, Benjamin A, Real F, Bonomo A, Moreira MEC, Barcinski MA. Apoptotic mimicry: An altruistic behavior in host/Leishmania interplay. Brazilian Journal of Medical and Biological Research. 2005;38(6):807–12.

104.   van Zandbergen G, Klinger M, Mueller A, Dannenberg S, Gebert A, Solbach W, *et al.* Cutting edge: neutrophil granulocyte serves as a vector for Leishmania entry into macrophages. The Journal of Immunology. 2004;173(11):6521–5.

105.   Ribeiro-de-Jesus A, Almeida RP, Lessa H, Bacellar O, Carvalho EM. Cytokine profile and pathology in human leishmaniasis. Brazilian Journal of Medical and Biological Research. 1998;31(1):143–8.

106.   Bates PA. Revising Leishmania's life cycle. Nature Microbiology [Internet]. 2018;3(5):529–30.

107.   CDC. Leishmaniasis [Internet]. Global Health, Division of Parasitic Diseases and Malaria. 2020 [cited 2021 Sep 26]. Available from: https://www.cdc.gov/dpdx/leishmaniasis/index.html

108.   Van Overtvelt L, Vanderheyde N, Verhasselt V, Ismaili J, De Vos L, Goldman M, *et al.* Trypanosoma cruzi infects human dendritic cells and prevents their

maturation: Inhibition of cytokines, HLA-DR, and costimulatory molecules. Infection and Immunity. 1999;67(8):4033–40.

109. Yoshida N. Molecular basis of mammalian cell invasion by *Trypanosoma cruzi*. Anais da Academia Brasileira de Ciencias. 2006 Mar;78(1):87–111.

110. de Souza W, de Carvalho TMU, Barrias ES. Review on *Trypanosoma cruzi*: Host Cell Interaction. International journal of cell biology. 2010;2010:295394.

111. Barrias E, Carvalho T, De Souza W. *Trypanosoma cruzi*: entry into mammalian host cells and parasitophorous vacuole formation. Front Immunol. 2013 Aug 1;4:186.

112. Cerbán FM, Stempin CC, Volpini X, Carrera Silva EA, Gea S, Motran CC. Signaling pathways that regulate *Trypanosoma cruzi* infection and immune response. Biochimica et Biophysica Acta (BBA) - Molecular Basis of Disease. 2020;1866(5):165707.

113. Schenkman S, Jiang MS, Hart GW, Nussenzweig V. A novel cell surface trans-sialidase of *Trypanosoma cruzi* generates a stage-specific epitope required for invasion of mammalian cells. Cell. 1991 Jun;65(7):1117–25.

114. Giorgi ME, de Lederkremer RM. The Glycan Structure of T. cruzi mucins Depends on the Host. Insights on the Chameleonic Galactose. Molecules. 2020;25(17).

115. Bartholomeu DC, de Paiva RMC, Mendes TAO, DaRocha WD, Teixeira SMR. Unveiling the intracellular survival gene kit of trypanosomatid parasites. PLoS Pathogens. 2014;10(12).

116. CDC. American Trypanosomiasis (also known as Chagas Disease) [Internet]. Global health, division of parasitic diseases and malaria. 2019 [cited 2021 Sep 27]. Available from: https://www.cdc.gov/parasites/chagas/biology.html

117. Muriel R. V. Notes on the life-history of Trypanosoma gambiense, with a brief reference to the cycles of *Trypanosoma nanum* and *Trypanosoma pecorum* in *Glossina palpalis*. Phil Trans R Soc Lond. 1913;203:161–84.

118. Rotureau B, Van Den Abbeele J. Through the dark continent: African trypanosome development in the tsetse fly. Frontiers in cellular and infection microbiology. 2013;3:53.

119. Dostálová A, Volf P. Leishmania development in sand flies: parasite-vector interactions overview. Parasites & Vectors. 2012;5(1):276.

120. Barry JD, Graham S V, Fotheringham M, Graham VS, Kobryn K, Wymer B. VSG gene control and infectivity strategy of metacyclic stage *Trypanosoma brucei*. Molecular and biochemical parasitology. 1998;91(1):93–105.

121. Vickerman K. Developmental cycles and biology of pathogenic trypanosomes. British medical bulletin. 1985;41(2):105–14.

122. Schuster S, Lisack J, Subota I, Zimmermann H, Reuter C, Müller T, *et al.* Unexpected plasticity in the life cycle of *Trypanosoma brucei.* eLife. 2021;10:1–23.

123. Batram C, Jones NG, Janzen CJ, Markert SM, Engstler M. Expression site attenuation mechanistically links antigenic variation and development in *Trypanosoma brucei*. eLife. 2014;3:e02324.

124. Wilkinson SR, Taylor MC, Horn D, Kelly JM, Cheeseman I. A mechanism for cross-resistance to nifurtimox and benznidazole in trypanosomes. Proceedings of the National Academy of Sciences of the United States of America. 2008;105(13):5022–7.

125. Chatelain E, Ioset JR. Drug discovery and development for neglected diseases: The DNDi model. Drug Design, Development and Therapy. 2011;(5):175–81.

126. Thomas J, Baker N, Hutchinson S, Dominicus C, Trenaman A, Glover L, *et al.* Insights into antitrypanosomal drug mode-of-action from cytology-based profiling. PLoS Neglected Tropical Diseases. 2018;12(11):1–19.

127. Field MC, Horn D, Fairlamb AH, Ferguson MAJ, Gray DW, Read KD, *et al.* Anti-trypanosomatid drug discovery: An ongoing challenge and a continuing need. Nature Reviews Microbiology. 2017;15(4):217–31.

128. Babokhov P, Sanyaolu AO, Oyibo WA, Fagbenro-Beyioku AF, Iriemenam NC. A current analysis of chemotherapy strategies for the treatment of human African trypanosomiasis. Pathogens and Global Health. 2013;107(5):242–52.

129. Van Bocxlaer K, Caridha D, Black C, Vesely B, Leed S, Sciotti RJ, *et al.* Novel benzoxaborole, nitroimidazole and aminopyrazoles with activity against experimental cutaneous leishmaniasis. International Journal for Parasitology: Drugs and Drug Resistance. 2019;11:129–38.

130. Zingales B, Andrade SG, Briones MRS, CAmBell DA, Chiari E, Fernandes O, *et al.* A new consensus for *Trypanosoma cruzi* intraspecific nomenclature: Second revision meeting recommends TcI to TcVI. Memorias do Instituto Oswaldo Cruz. 2009;104(7):1051–4.

131. Zingales B, Miles MA, Moraes CB, Luquetti A, Guhl F, Schijman AG, *et al.* Drug discovery for chagas disease should consider *Trypanosoma cruzi* strain diversity. Memorias do Instituto Oswaldo Cruz. 2014;109(6):828–33.

132. Rao SPS, Barrett MP, Dranoff G, Faraday CJ, Gimpelewicz CR, Hailu A, *et al.*

Drug Discovery for Kinetoplastid Diseases: Future Directions. ACS Infectious Diseases. 2019;5(2):152–7.

133. S Shirzadi MR. Lipsosomal amphotericin B: a review of its properties, function, and use for treatment of cutaneous leishmaniasis. Res Rep Trop Med. 2019;10:11-18.

134. Ouellette M, Drummelsmith J, Papadopoulou B. Leishmaniasis: drugs in the clinic, resistance and new developments. Drug resistance updates : reviews and commentaries in antimicrobial and anticancer chemotherapy. 2004;7(4–5):257–66.

135. Weisz G. Making Medical History. Bulletin of the History of Medicine. 2006;80(1):153–9.

136. Oliveira LF, Schubach AO, Martins MM, Passos SL, Oliveira R V, Marzochi MC, *et al*. Systematic review of the adverse effects of cutaneous leishmaniasis treatment in the New World. Acta Tropica. 2011;118(2):87–96.

137. Ware JM, O'Connell EM, Brown T, Wetzler L, Talaat KR, Nutman TB, *et al.* Efficacy and Tolerability of Miltefosine in the Treatment of Cutaneous Leishmaniasis. Clin Infect Dis. 2021;73(7):e2457-e2562.

138. Croft SL, Sundar S, Fairlamb AH. Drug resistance in leishmaniasis. Clinical Microbiology Reviews. 2006;19(1):111–26.

139. Hodiamont CJ, Kager PA, Bart A, de Vries HJC, van Thiel PPAM, Leenstra T, *et al.* Species-directed therapy for leishmaniasis in returning travellers: a comprehensive guide. PLoS neglected tropical diseases. 2014;8(5):e2832.

140. van Thiel PPAM, Leenstra T, Kager PA, de Vries HJ, van Vugt M, van der Meide WF, *et al.* Miltefosine treatment of *Leishmania major* infection: an observational study involving Dutch military personnel returning from northern Afghanistan. Clinical infectious diseases : an official publication of the Infectious Diseases Society of America. 2010;50(1):80–3.

141. Dastidar SKG. A new sodium antimony gluconate for the treatment of kala-azar. Journal of the Indian Medical Association. 1945;14:298.

142. Chakraborty AK, Majumder HK. Mode of action of pentavalent antimonials: specific inhibition of type I DNA topoisomerase of *Leishmania donovani.* Biochemical and biophysical research communications. 1988;152(2):605–11.

143. Haldar AK, Sen P, Roy S. Use of antimony in the treatment of leishmaniasis: current status and future directions. Majumder HK, editor. Molecular Biology International. 2011;2011:571242.

144. Fairlamb AH, Cerami A. Metabolism and functions of trypanothione in the Kinetoplastida. Annual review of microbiology. 1992;46:695–729.

145. Wyllie S, Cunningham ML, Fairlamb AH. Dual action of antimonial drugs on thiol redox metabolism in the human pathogen *Leishmania donovani*. The Journal of biological chemistry. 2004;279(38):39925–32.

146. Hefnawy A, Berg M, Dujardin JC, De Muylder G. Exploiting knowledge on Leishmania drug resistance to support the quest for new drugs. Trends in Parasitology. 2017;33(3):162–74.

147. Gourbal B, Sonuc N, Bhattacharjee H, Legare D, Sundar S, Ouellette M, *et al.* Drug uptake and modulation of drug resistance in Leishmania by an aquaglyceroporin. The Journal of biological chemistry. 2004;279(30):31010–7.

148. Rugani JN, Gontijo CMF, Frézard F, Soares RP, Do Monte-Neto RL. Antimony resistance in *Leishmania* (Viannia) *braziliensis* clinical isolates from atypical lesions associates with increased ARM56/ARM58 transcripts and reduced drug uptake. Memorias do Instituto Oswaldo Cruz. 2019;114(7):1–9.

149. do Monte-Neto RL, Coelho AC, Raymond F, Légaré D, Corbeil J, Melo MN, *et al.* Gene expression profiling and molecular characterization of antimony resistance in *Leishmania amazonensis*. PLoS Neglected Tropical Diseases. 2011;5(5).

150. Karima EF, Nadine M, Philippe L, Gaétan R, Chantal G, Nathalie T, *et al.* Role of the ABC Transporter MRPA (PGPA) in antimony resistance in *Leishmania infantum* axenic and intracellular amastigotes. Antimicrobial Agents and Chemotherapy. 2005;49(5):1988–93.

151. Mukherjee B, Mukhopadhyay R, Bannerjee B, Chowdhury S, Mukherjee S, Naskar K, *et al.* Antimony-resistant but not antimony-sensitive *Leishmania donovani* up-regulates host IL-10 to overexpress multidrug-resistant protein 1. Proc Natl Acad Sci U S A. 2013;110(7):E575-82.

152. Sundar S, Olliaro PL. Miltefosine in the treatment of leishmaniasis: Clinical evidence for informed clinical risk management. Therapeutics and clinical risk management. 2007;3(5):733–40.

153. Rijal S, Ostyn B, Uranw S, Rai K, Bhattarai NR, Dorlo TPC, *et al.* Increasing failure of miltefosine in the treatment of kala-azar in Nepal and the potential role of parasite drug resistance, reinfection, or noncompliance. Clinical Infectious Diseases [Internet]. 2013 Jun 1;56(11):1530–8.

154. Pérez-Victoria FJ, Sánchez-Cañete MP, Castanys S, Gamarro F. Phospholipid

translocation and miltefosine potency require both *L. donovani* miltefosine transporter and the new protein LdRos3 in Leishmania parasites. The Journal of biological chemistry. 2006;281(33):23766–75.

155. Dorlo TPC, Balasegaram M, Beijnen JH, de Vries PJ. Miltefosine: a review of its pharmacology and therapeutic efficacy in the treatment of leishmaniasis. The Journal of antimicrobial chemotherapy. 2012;67(11):2576–97.

156. Verma NK, Dey CS. Possible mechanism of miltefosine-mediated death of *Leishmania donovani*. Antimicrobial agents and chemotherapy. 2004 ;48(8):3010–5.

157. Pérez-Victoria FJ, Castanys S, Gamarro F. *Leishmania donovani* resistance to miltefosine involves a defective inward translocation of the drug. Antimicrobial agents and chemotherapy. 2003 Aug;47(8):2397–403.

158. Rakotomanga M, Saint-Pierre-Chazalet M, Loiseau PM. Alteration of fatty acid and sterol metabolism in miltefosine-resistant *Leishmania donovani* promastigotes and consequences for drug-membrane interactions. Antimicrobial agents and chemotherapy. 2005;49(7):2677–86.

159. Neves LO, Talhari AC, Gadelha EPN, Silva Júnior RM da, Guerra JA de O, Ferreira LC de L, *et al.* A randomized clinical trial comparing meglumine antimoniate, pentamidine and amphotericin B for the treatment of cutaneous leishmaniasis by *Leishmania guyanensis*. Anais brasileiros de dermatologia. 2011;86(6):1092–101.

160. Bray PG, Barrett MP, Ward SA, de Koning HP. Pentamidine uptake and resistance in pathogenic protozoa: past, present and future. Trends in parasitology. 2003;19(5):232–9.

161. Coelho AC, Beverley SM, Cotrim PC. Functional genetic identification of PRP1, an ABC transporter superfamily member conferring pentamidine resistance in *Leishmania major*. Molecular and biochemical parasitology. 2003;130(2):83–90.

162. Basselin M, Denise H, Coombs GH, Barrett MP. Resistance to pentamidine in *Leishmania mexicana* involves exclusion of the drug from the mitochondrion. Antimicrobial Agents and Chemotherapy. 2002;46(12):3731–8.

163. Laniado-Laborín R, Cabrales-Vargas MN. Amphotericin B: side effects and toxicity. Revista iberoamericana de micologia. 2009 Dec;26(4):223–7.

164. Eiras DP, Kirkman LA, Murray HW. Cutaneous leishmaniasis: current treatment practices in the usa for returning travelers. Current treatment options in infectious diseases. 2015;7(1):52–62.

165. Neumann A, Czub J, Baginski M. On the possibility of the amphotericin b-sterol complex formation in cholesterol- and ergosterol-containing lipid bilayers: a molecular dynamics study. The Journal of Physical Chemistry B. 2009;113(48):15875–85.

166. Chattopadhyay A, Jafurulla M. A novel mechanism for an old drug: amphotericin B in the treatment of visceral leishmaniasis. Biochemical and biophysical research communications. 2011;416(1–2):7–12.

167. Chawla B, Jhingran A, Panigrahi A, Stuart KD, Madhubala R. Paromomycin affects translation and vesicle-mediated trafficking as revealed by proteomics of paromomycin -susceptible -resistant *Leishmania donovani*. PLoS ONE. 2011;6(10).

168. Miranda-Verastegui C, Tulliano GF, Gyorkos TW, Calderon W, Rahme E, Ward B, *et al.* First-line therapy for human cutaneous leishmaniasis in Peru using the TLR7 agonist imiquimod in combination with pentavalent antimony. PLoS Neglected Tropical Diseases. 2009;3(7):1–10.

169. López L, Vélez I, Asela C, Cruz C, Alves F, Robledo S, *et al.* A phase II study to evaluate the safety and efficacy of topical 3% amphotericin B cream (Anfoleish) for the treatment of uncomplicated cutaneous leishmaniasis in Colombia. PLoS Neglected Tropical Diseases. 2018;12(7):1–12.

170. Valencia BM, Miller D, Witzig RS, Boggild AK, Llanos-Cuentas A. Novel low-cost thermotherapy for cutaneous leishmaniasis in peru. PLoS Neglected Tropical Diseases. 2013;7(5):1–9.

171. Sosa N, Pascale JM, Jiménez AI, Norwood JA, Kreishman-Detrick M, Weina PJ, *et al.* Topical paromomycin for New World cutaneous leishmaniasis. PLOS Neglected Tropical Diseases. 2019;13(5):e0007253.

172. Nagle A, Biggart A, Be C, Srinivas H, Hein A, Caridha D, *et al.* Discovery and Characterization of clinical candidate LXE408 as a Kinetoplastid-selective proteasome inhibitor for the treatment of leishmaniases. Journal of Medicinal Chemistry. 2020;63(19):10773–81.

173. Richie R. Chemotherapy of experimental acute Chagas disease in mice: beneficial effects of Ro 7-1051 on parasitemia and tissue parasitism. Prog Med. 1973;101:282.

174. Castro JA, De Mecca MM, Bartel LC. Toxic side effects of drugs used to treat Chagas' disease (American trypanosomiasis). Human and Experimental Toxicology. 2006;25(8):471–9.

175. Lascano F, Altcheh J. An evaluation of nifurtimox for Chagas disease in children. Expert Opinion on Orphan Drugs. 2021;9(5):139–49.

176. DNDi. Proposal for the inclusion of Benznidazol pediatric dosage form as treatment for Chagas disease in children younger than 2 years old in the World Health Organization model list of essential medicines for children. 2012;1–66. Available from: http://www.who.int/selection_medicines/committees/expert/19/applications/benz nidazole/en/

177. Olivera MJ, Cucunubá ZM, Álvarez CA, Nicholls RS. Safety profile of nifurtimox and treatment interruption for chronic chagas disease in Colombian adults. American Journal of Tropical Medicine and Hygiene. 2015;93(6):1224–30.

178. DNDi. Chagas disease: progress towards shorter, better treatments to stop a silent killer. Disease Factsheet.

179. Coura JR, Castro SL De. A critical review on Chagas Disease chemotherapy. 2002;97:3–24.

180. Soeiro MNC, de Castro SL. *Trypanosoma cruzi* targets for new chemotherapeutic approaches. Expert opinion on therapeutic targets. 2009 Jan;13(1):105–21.

181. Molina I, Salvador F, Sánchez-Montalvá A. Posaconazole versus Benznidazole for chronic Chagas' Disease. New England Journal of Medicine. 2014;371(10):965–6.

182. Berenstein AJ, Falk N, Moscatelli G, Moroni S, González N, Garcia-Bournissen F, *et al*. Adverse events associated with nifurtimox treatment for chagas disease in children and adults. Antimicrobial Agents and Chemotherapy. 2021;65(2).

183. Urbina JA, Docampo R. Specific chemotherapy of Chagas disease: Controversies and advances. Trends in Parasitology. 2003;19(11):495–501.

184. Maya JD, Cassels BK, Iturriaga-Vásquez P, Ferreira J, Faúndez M, Galanti N, *et al*. Mode of action of natural and synthetic drugs against *Trypanosoma cruzi* and their interaction with the mammalian host. Comparative biochemistry and physiology Part A, Molecular & integrative physiology. 2007;146(4):601–20.

185. Murta SM, Gazzinelli RT, Brener Z, Romanha AJ. Molecular characterization of susceptible and naturally resistant strains of *Trypanosoma cruzi* to benznidazole and nifurtimox. Molecular and biochemical parasitology. 1998 ;93(2):203–14.

186. Filardi LS, Brener Z. Susceptibility and natural resistance of *Trypanosoma cruzi* strains to drugs used clinically in Chagas disease. Transactions of the Royal Society of Tropical Medicine and Hygiene. 1987;81(5):755–9.

187. Camandaroba ELP, Reis EAG, Gonçalves MS, Reis MG, Andrade SG. *Trypanosoma cruzi*: Susceptibility to chemotherapy with benznidazole of clones isolated from the highly resistant Colombian strain. Revista da Sociedade Brasileira de Medicina Tropical. 2003;36(2):201–9.

188. Campos MCO, Leon LL, Taylor MC, Kelly JM. Benznidazole-resistance in *Trypanosoma cruzi*: Evidence that distinct mechanisms can act in concert. Molecular and Biochemical Parasitology [Internet]. 2014;193(1):17–9.

189. Mejía-Jaramillo AM, Fernández GJ, Montilla M, Nicholls RS, Triana-Chávez O. *Trypanosoma cruzi* strains resistant to benznidazole occurring in Colombia. Biomedica : revista del Instituto Nacional de Salud. 2012 Jun;32(2):196–205.

190. Nogueira FB, Krieger MA, Nirdé P, Goldenberg S, Romanha AJ, Murta SMF. Increased expression of iron-containing superoxide dismutase-A (TcFeSOD-A) enzyme in *Trypanosoma cruzi* population with *in vitro*-induced resistance to benznidazole. Acta tropica. 2006;100(1–2):119–32.

191. Murta SMF, Krieger MA, Montenegro LR, Campos FFM, Probst CM, Avila AR, *et al.* Deletion of copies of the gene encoding old yellow enzyme (TcOYE), a NAD(P)H flavin oxidoreductase, associates with *in vitro*-induced benznidazole resistance in *Trypanosoma cruzi*. Molecular and biochemical parasitology. 2006;146(2):151–62.

192. Díaz-Viraqué F, Chiribao ML, Trochine A, González-Herrera F, Castillo C, Liempi A, *et al*. Old Yellow Enzyme from *Trypanosoma cruzi* exhibits in vivo Prostaglandin F2α synthase activity and has a key role in parasite infection and drug susceptibility. Frontiers in Immunology. 2018; 9: 456.

193. Téllez J, Romero I, Romanha AJ, Steindel M. Drug transporter and oxidative stress gene expression in human macrophages infected with benznidazole-sensitive and naturally benznidazole-resistant *Trypanosoma cruzi* parasites treated with benznidazole. Parasites and Vectors. 2019;12(1):1–9.

194. Zingales B, Araujo RGA, Moreno M, Franco J, Aguiar PHN, Nunes SL, *et al*. A novel ABCG-like transporter of *Trypanosoma cruzi* is involved in natural resistance to benznidazole. Memorias do Instituto Oswaldo Cruz. 2015;110(3):433–44.

195. Rajão MA, Furtado C, Alves CL, Passos-Silva DG, de Moura MB, Schamber-Reis BL, *et al*. Unveiling benznidazole's mechanism of action through overexpression of DNA repair proteins in *Trypanosoma cruzi*. Environmental and molecular mutagenesis. 2014 May;55(4):309–21.

196. Drugs for Neglected Diseases initiative. R&D portifolio for Chagas disease [Internet]. What we have achieved. [cited 2021 Oct 6]. Available from: https://dndi.org/diseases/chagas/projects-achievements/

197. Pépin J, Milord F. The treatment of human African trypanosomiasis. Advances in parasitology. 1994;33:1–47.

198. Eperon G, Balasegaram M, Potet J, Mowbray C, Valverde O, Chappuis F. Treatment options for second-stage gambiense human African trypanosomiasis. Expert Review of Anti-Infective Therapy. 2014;12(11):1407–17.

199. Drugs for Neglected Diseases initiative. Newer, simpler treatments for sleeping sickness [Internet]. 2018 [cited 2021 Oct 7]. p. 15. Available from: https://dndi.org/wp-content/uploads/2018/09/DNDi_HAT_2018.pdf

200. Lindner AK, Lejon V, Chappuis F, Seixas J, Kazumba L, Barrett MP, *et al*. New WHO guidelines for treatment of gambiense human African trypanosomiasis including fexinidazole: substantial changes for clinical practice. The Lancet Infectious Diseases. 2020;20(2):e38–46.

201. Drugs for Neglected Diseases initiative. Sleeping sickness: Projects & achievements [Internet]. 2021 [cited 2021 Oct 7]. Available from: https://dndi.org/diseases/sleeping-sickness/projects-achievements/

202. Schweingruber ME. The melaminophenyl arsenicals melarsoprol and melarsen oxide interfere with thiamine metabolism in the fission yeast *Schizosaccharomyces pombe*. Antimicrobial Agents and Chemotherapy. 2004;48(9):3268–71.

203. Macedo JP, Currier RB, Wirdnam C, Horn D, Alsford S, Rentsch D. Ornithine uptake and the modulation of drug sensitivity in *Trypanosoma brucei*. FASEB Journal. 2017;31(10):4649–60.

204. Torreele E, Trunz BB, Tweats D, Kaiser M, Brun R, Mazué G, *et al.* Fexinidazole - a new oral nitroimidazole drug candidate entering clinical development for the treatment of sleeping sickness. PLoS Neglected Tropical Diseases. 2010;4(12):1–15.

205. Kaiser M, Bray MA, Cal M, Trunz BB, Torreele E, Brun R. Antitrypanosomal activity of fexinidazole, a new oral nitroimidazole drug candidate for treatment of sleeping sickness. Antimicrobial Agents and Chemotherapy. 2011;55(12):5602–8.

206. Alsford S, Eckert S, Baker N, Glover L, Sanchez-Flores A, Leung KF, *et al*. High-throughput decoding of antitrypanosomal drug efficacy and resistance. Nature. 2012;482(7384):232–6.

207. Graf FE, Ludin P, Wenzler T, Kaiser M, Brun R, Pyana PP, *et al.* Aquaporin 2

Mutations in *Trypanosoma brucei gambiense* field isolates correlate with decreased susceptibility to Pentamidine and Melarsoprol. PLoS Neglected Tropical Diseases. 2013;7(10):e2475.

208. Wiedemar N, Zwyer M, Zoltner M, Cal M, Field MC, Mäser P. Expression of a specific variant surface glycoprotein has a major impact on suramin sensitivity and endocytosis in *Trypanosoma brucei*. FASEB BioAdvances. 2019;1(10):595–608.

209. McGhee S, Gonzalez J, Nadeau C, Ortega J. Assessment and treatment of cutaneous leishmaniasis in the emergency department. Emerg Nurse. 2020; 28(2):36-41.

210. Swinney DC. Phenotypic vs. Target-based drug discovery for first-in-class medicines. Clinical Pharmacology and Therapeutics. 2013;93(4):299–301.

211. Swinney DC, Anthony J. How were new medicines discovered? Nature Reviews Drug Discovery. 2011;10(7):507–19.

212. Newman DJ, Cragg GM, Snader KM. Natural Products as Sources of New Drugs over the Period 1981−2002. Journal of Natural Products. 2003 1;66(7):1022–37.

213. Eder J, Herrling PL. Trends in Modern Drug Discovery. Handbook of experimental pharmacology. 2016;232:3–22.

214. Zhang H, Collins J, Nyamwihura R, Ware S, Kaiser M, Ogungbe IV. Discovery of a quinoline-based phenyl sulfone derivative as an antitrypanosomal agent. Bioorganic and Medicinal Chemistry Letters. 2018;28(9):1647–51.

215. Kumar A, Zhang KYJ. Advances in the development of shape similarity methods and their application in drug discovery. Frontiers in Chemistry. 2018;6:1–21.

216. Van Norman GA. Drugs, Devices, and the FDA: Part 1: An Overview of Approval Processes for Drugs. JACC: Basic to Translational Science. 2016;1(3):170–9.

217. Chatelain E, Konar N. Translational challenges of animal models in chagas disease drug development: A review. Drug Design, Development and Therapy. 2015;9:4807–23.

218. Katsuno K, Burrows JN, Duncan K, van Huijsduijnen RH, Kaneko T, Kita K, *et al.* Hit and lead criteria in drug discovery for infectious diseases of the developing world. Nature Reviews Drug Discovery. 2015;14(11):751–8.

219. Walker DM, Oghumu S, Gupta G, Mcgwire BS, Drew ME, Satoskar AR. Mechanisms of cellular invasion by intracellular parasites Mechanisms of host cell invasion in Leishmania. Cell Mol Life Sci. 2014;71(7):1245–63.

220. Stacey G. Primary Cell Cultures and Immortal Cell Lines. Encyclopedia of Life Sciences. 2006;1–6.

221. Caridha D, Vesely B, van Bocxlaer K, Arana B, Mowbray CE, Rafati S, *et al.* Route map for the discovery and pre-clinical development of new drugs and treatments for cutaneous leishmaniasis. International Journal for Parasitology: Drugs and Drug Resistance. 2019;11:106–17.

222. Khare S, Nagle AS, Biggart A, Lai YH, Liang F, Davis LC, *et al.* Proteasome inhibition for treatment of leishmaniasis, Chagas disease and sleeping sickness. Nature. 2016;537(7619):229–33.

223. El-Sayed ANM, Myler PJ, Blandin G, Berriman M, Aggarwal G, Caler E, *et al.* Comparative genomics of trypanosomatid parasitic protozoa. Science. 2005;309(5733):404-9.

224. Carothers S, Nyamwihura R, Collins J, Zhang H, Park H, Setzer WN, *et al.* Bauerenol acetate, the pentacyclic triterpenoid from *Tabernaemontana longipes*, is an antitrypanosomal agent. Molecules. 2018;23(2).

225. Romanha AJ, de Castro SL, Soeiro M de NC, Lannes-Vieira J, Ribeiro I, Talvani A, *et al. In vitro* and *in vivo* experimental models for drug screening and development for Chagas disease. Memorias do Instituto Oswaldo Cruz. 2010;105(2):233–8.

226. Feitosa LM, da Silva ER, Hoelz LVB, Souza DL, Come JAASS, Cardoso-Santos C, *et al.* New pyrazolopyrimidine derivatives as *Leishmania amazonensis* arginase inhibitors. Bioorganic and Medicinal Chemistry. 2019;27(14): 3061-3069.

227. Godinho JLP, Simas-Rodrigues C, Silva R, Ürmenyi TP, De Souza W, Rodrigues JCF. Efficacy of miltefosine treatment in *Leishmania amazonensis*-infected BALB/c mice. International Journal of Antimicrobial Agents. 2012;39(4):326–31.

228. Mikus J, Steverding D. A simple colorimetric method to screen drug cytotoxicity against Leishmania using the dye Alamar Blue®. Parasitology International. 2000;48(3):265–9.

229. Jorge TCA & Castro S. 18.2 Protocolos de cultura primária. In: Doença de chagas: manual para experimentação animal. Editora FIOCRUZ; 2000; p.298.

230. Rizk YS, Santos-Pereira S, Gervazoni L, Hardoim DJ, Cardoso FO, de Souza CSF, *et al.* Amentoflavone as an ally in the treatment of cutaneous leishmaniasis: analysis of its antioxidant/prooxidant mechanisms. Front. Cell. Infect. Microbiol. 2021; 11:615814.

231. Soeiro MNC, de Souza EM, da Silva CF, Batista D, Batista MM, Pavão BP, *et al. In vitro* and *in vivo* studies of the antiparasitic activity of sterol 14α-demethylase (CYP51) inhibitor VNI against drug-resistant strains of *Trypanosoma cruzi.*

Antimicrob Agents Chemother. 2013;57(9):4151-4163.

232. Ribeiro-Romão RP, Saavedra AF, Da-Cruz AM, Pinto EF, Moreira OC. Development of real-time PCR assays for evaluation of immune response and parasite load in golden hamster (*Mesocricetus auratus*) infected by *Leishmania* (Viannia) *braziliensis.* Parasites and Vectors. 2016;9(1):1–12.

233. Lainson R, Shaw JJ, Silveira FT, Souza AAA de, Braga RR, Ishikawa EAY. The dermal leishmaniases of Brazil, with special reference to the eco-epidemiology of the disease in Amazonia. Memórias do Instituto Oswaldo Cruz. 1994;89:435–43.

234. Chatelain E, Ioset JR. Drug discovery and development for neglected diseases: The DNDi model. Drug Design, Development and Therapy. 2011;(5):175–81.

235. Silva CF, Batista MM, Mota RA, de Souza EM, Stephens CE, Som P, *et al*. Activity of "reversed" diamidines against *Trypanosoma cruzi* "*in vitro*." Biochemical Pharmacology. 2007;73(12):1939–46.

236. Okwor I, Uzonna J. Social and economic burden of human leishmaniasis. American Journal of Tropical Medicine and Hygiene. 2016;94(3):489–93.

237. Ruoti M, Oddone R, Lampert N, Orué E, Miles MA, Alexander N, *et al.* Mucocutaneous leishmaniasis: Knowledge, attitudes, and practices among Paraguayan communities, patients, and health professionals. Journal of Tropical Medicine. 2013;2013:538629.

238. Hertweck C. Natural Products as Source of Therapeutics against Parasitic Diseases. Angewandte Chemie (International ed in English). 2015;54(49):14622–4.

239. Wink M. Medicinal plants: A source of anti-parasitic secondary metabolites. Molecules. 2012;17(11):12771–91.

240. De Rycker M, O'Neill S, Joshi D, Campbell L, Gray DW, Fairlamb AH (2012) A Static-Cidal Assay for *Trypanosoma brucei* to aid hit prioritisation for progression into drug discovery programmes. PLoS Negl Trop Dis 6(11): e1932.

241. Cal M, Ioset JR, Fügi MA, Mäser P, Kaiser M. Assessing anti-*T. cruzi* candidates *in vitro* for sterile cidality. International Journal for Parasitology: Drugs and Drug Resistance. 2016;6(3):165–70.

242. Wyllie S, Roberts AJ, Norval S, Patterson S, Foth BJ, Berriman M, *et al*. Activation of Bicyclic Nitro-drugs by a Novel Nitroreductase (NTR2) in Leishmania. PLoS Pathogens. 2016;12(11):1–22.

243. Drugs for Neglected Diseases initiative. Target product profile for cutaneous leishmaniasis [Internet]. 2021 [cited 2021 Jan 30]. Available from:

https://dndi.org/diseases/cutaneous-leishmaniasis/target-product-profile/

244. Baek KH, Piel L, Rosazza T, Prina E, Späth GF, No JH. Infectivity and Drug Susceptibility Profiling of different leishmania-host cell combinations. pathogens. 2020; 20;9(5):393.

245. Cardoso-Santos C, Ferreira L, Fiuza DA, Franc C, Hulpia F, Calenbergh S V, *et al*. 7-Aryl-7-deazapurine 30-deoxyribonucleoside derivative as a novel lead for Chagas' disease therapy: *in vitro* and *in vivo* pharmacology. JAC- Antimicrobial Resistance. 2021;3(4):1–9.

246. Chua SMH, Fraser JA. Surveying purine biosynthesis across the domains of life unveils promising drug targets in pathogens. 2020;819–31.

247. Borghi C, Narkiewicz K, Mancia G. Uric acid and xantine-oxidase inhibitors in patients with gout: A re-assessment and an update. Vol. 26, Cardiology journal. 2019. p. 99–101.

248. Wise M, Callen JP. Azathioprine: a guide for the management of dermatology patients. Dermatologic therapy. 2007;20(4):206–15.

249. Elion GB. The biochemistry and mechanism of action of acyclovir. The Journal of antimicrobial chemotherapy. 1983 Sep;12 Suppl B:9–17.

250. Arora K, Rai AK. Dependence of Leishmania parasite on host derived ATP: an overview of extracellular nucleotide metabolism in parasite. Journal of Parasitic Diseases. 2019;43(1):1–13.

251. Campagnaro GD, de Freitas Nascimento J, Girard RBM, Silber AM, de Koning HP. Cloning and characterisation of the Equilibrative Nucleoside Transporter family of *Trypanosoma cruzi*: ultra-high affinity and selectivity to survive in the intracellular niche. Biochimica et Biophysica Acta - General Subjects. 2018;1862(12):2750–63.

252. Freitas-Mesquita AL, Meyer-Fernandes JR. 3'nucleotidase/nuclease in protozoan parasites: Molecular and biochemical properties and physiological roles. Experimental parasitology. 2017 Aug;179:1–6.

253. Freitas-Mesquita AL, Gomes MT, Vieira DP, Paes-Vieira L, Nascimento MTC, Lopes AHCS, *et al*. Inhibitory effects promoted by 5'-nucleotides on the ecto-3'-nucleotidase activity of *Leishmania amazonensis*. Experimental parasitology. 2016 Oct;169:111–8.

254. Peres NT de A, Cunha LCS, Barbosa MLA, Santos MB, Oliveira FA de, Jesus AMR de, *et al*. Infection of human macrophages by *Leishmania infantum* is influenced by ecto-nucleotidases. Frontiers in Immunology. 2018;8:1954.

255. Acosta H, Burchmore R, Naula C, Gualdrón-López M, Quintero-Troconis E, Cáceres AJ, *et al*. Proteomic analysis of glycosomes from *Trypanosoma cruzi* epimastigotes. Molecular and Biochemical Parasitology. 2019;229:62–74.

256. Mazzeti AL, Diniz LDF, Gonçalves KR, Wondollinger RS, Assíria T, Ribeiro I. Synergic effect of allopurinol in combination with nitroheterocyclic compounds against *Trypanosoma cruzi*. Antimicrobial Agents and Chemotherapy. 2019;63(6):1–11.

257. Gallerano RH, Marr JJ, Sosa RR. Therapeutic efficacy of allopurinol in patients with chronic Chagas' disease. The American journal of tropical medicine and hygiene. 1990;43(2):159–66.

258. Coura JR. Present situation and new strategies for Chagas disease chemotherapy: a proposal. Memorias do Instituto Oswaldo Cruz. 2009;104(4):549–54.

259. Rassi A, Luquetti AO, Rassi AJ, Rassi GG, Rassi SG, DA Silva IG, *et al.* Specific treatment for *Trypanosoma cruzi*: lack of efficacy of allopurinol in the human chronic phase of Chagas disease. The American journal of tropical medicine and hygiene. 2007;76(1):58–61.

260. Martinez S, Gonzalez M, Vernaza ME. Treatment of cutaneous leishmaniasis with allopurinol and stibogluconate. Clinical infectious diseases: an official publication of the Infectious Diseases Society of America. 1997 Feb;24(2):165–9.

261. Herwaldt BL, Neva FA, Berman JD. Allopurinol in the treatment of American cutaneous leishmaniasis. The New England journal of medicine. United States; 1992;327: 498–9.

262. Ginel PJ, Lucena R, López R, Molleda JM. Use of allopurinol for maintenance of remission in dogs with leishmaniasis. The Journal of small animal practice. 1998;39(6):271–4.

263. Berens RL, Marr JJ, Steele da Cruz FS, Nelson DJ. Effect of allopurinol on *Trypanosoma cruzi*: metabolism and biological activity in intracellular and bloodstream forms. Antimicrobial agents and chemotherapy. 1982;22(4):657–61.

264. Perlíková P, Hocek M. Pyrrolo[2,3-d]pyrimidine (7-deazapurine) as a privileged scaffold in design of antitumor and antiviral nucleosides. Medicinal research reviews. 2017;37(6):1429–60.

265. Hulpia F, Van Hecke K, França Da Silva C, Da Gama Jaen Batista D, Maes L, Caljon G, *et al*. Discovery of Novel 7-Aryl 7-Deazapurine 3′-Deoxy-ribofuranosyl nucleosides with potent activity against *Trypanosoma cruzi*. Journal of Medicinal Chemistry. 2018;61(20):9287–300.

266. Lin C, Hulpia F, Da Silva CF, Batista DDGJ, Van Hecke K, Maes L, *et al*. Discovery of Pyrrolo[2,3- b]pyridine (1,7-Dideazapurine) nucleoside analogues as anti- *Trypanosoma cruzi* agents. Journal of Medicinal Chemistry. 2019;62(19):8847–65.

267. Rottenberg ME, Masocha W, Ferella M, Petitto-Assis F, Goto H, Kristensson K, *et al*. Treatment of African trypanosomiasis with cordycepin and adenosine deaminase inhibitors in a mouse model. The Journal of infectious diseases. 2005;192(9):1658–65.

268. Hulpia F, Campagnaro GD, Scortichini M, Van Hecke K, Maes L, de Koning HP, *et al.* Revisiting tubercidin against kinetoplastid parasites: Aromatic substitutions at position 7 improve activity and reduce toxicity. European Journal of Medicinal Chemistry. 2019;164(2019):689–705.

269. Hulpia F, Mabille D, Campagnaro GD, Schumann G, Maes L, Roditi I, *et al*. Combining tubercidin and cordycepin scaffolds results in highly active candidates to treat late-stage sleeping sickness. Nature Communications. 2019;10(1):1–11.

270. Hulpia F, Campagnaro GD, Alzahrani KJ, Alfayez IA, Ungogo MA, Mabille D, *et al*. Structure-activity relationship exploration of 3′-Deoxy-7-deazapurine nucleoside analogues as anti- *Trypanosoma brucei* agents. ACS Infectious Diseases. 2020;6(8):2045–56.

271. Lin C, Fiuza LFA, Santos CC, Nunes DF, Moreira OC, Bouton J, *et al.* 6-Methyl-7-Aryl-7-Deazapurine Nucleosides as anti-*Trypanosoma cruzi* agents: structure-activity relationship and *in vivo* efficacy. ChemMedChem. 2021;16(14):2231-2253.

272. Don R, Ioset J-R. Screening strategies to identify new chemical diversity for drug development to treat kinetoplastid infections. Parasitology. 2014 Jan;141(1):140–6.

273. Cos P, Vlietinck AJ, Berghe D Vanden, Maes L. Anti-infective potential of natural products: How to develop a stronger *in vitro* "proof-of-concept." Journal of Ethnopharmacology. 2006;106(3):290–302.

274. Masimirembwa CM, Bredberg U, Andersson TB. Metabolic stability for drug discovery and development: pharmacokinetic and biochemical challenges. Clinical pharmacokinetics. 2003;42(6):515–28.

275. Richardson SJ, Bai A, Kulkarni AA, Moghaddam MF. Efficiency in Drug Discovery: Liver S9 fraction assay as a screen for metabolic stability. Drug metabolism letters. 2016;10(2):83–90.

175

276. Buckner FS, Verlinde CLMJ, Flamme ACLA. Efficient Technique for Screening Drugs for Activity against *Trypanosoma cruzi* Using Parasites Expressing ^{N}L - Galactosidase. 1996;40(11):2592–7.

277. Kaiser M, Maes L, Tadoori LP, Spangenberg T, Ioset JR. Repurposing of the open access malaria box for kinetoplastid diseases identifies novel active scaffolds against trypanosomatids. Journal of Biomolecular Screening. 2015;20(5):634–45.

278. Kaminsky R, Brun R. *In vitro* and *in vivo* activities of trybizine hydrochloride against various pathogenic trypanosome species. 1998;42(11):2858–62.

279. Batista DDGJ, Batista MM, De Oliveira GM, Do Amaral PB, Lannes-Vieira J, Britto CC, *et al*. Arylimidamide DB766, a potential chemotherapeutic candidate for Chagas' disease treatment. Antimicrobial Agents and Chemotherapy. 2010;54(7):2940–52.

280. Meirelles MN, de Araujo-Jorge TC, Miranda CF, W de Souza W, Barbosa HS. Interaction of *Trypanosoma cruzi* with heart muscle cells: ultrastructural and cytochemical analysis of endocytic vacuole formation and effect upon myogenesis *in vitro*. European Journal of Cellular Biology. 1986;41(2):198–206.

281. Aprigliano O, Masuda MO, Meirelles MN, Pereira MC, Barbosa HS, Barbosa JC. Heart muscle cells acutely infected with *Trypanosoma cruzi:* characterization of electrophysiology and neurotransmitter responses. Journal of molecular and cellular cardiology. 1993;25(10):1265–74.

282. Timm BL, Da Silva PB, Batista MM, Farahat AA, Kumar A, Boykin DW, *et al. In vitro* investigation of the efficacy of novel diamidines against *Trypanosoma cruzi*. Parasitology. 2014;141(10):1272–6.

283. Coutinho L, Ferreira MA, Cosson A, Batista MM, Batista D da GJ, Minoprio P, *et al.* Inhibition of *Trypanosoma cruzi* proline racemase affects host-parasite interactions and the outcome of *in vitro* infection. Memorias do Instituto Oswaldo Cruz. 2009;104(8):1055–62.

284. Odds FC. Synergy, antagonism, and what the chequerboard puts between them. Journal of Antimicrobial Chemotherapy. 2003;52(1):1.

285. Trinconi CT, Reimão JQ, Coelho AC, Uliana SRB. Efficacy of tamoxifen and miltefosine combined therapy for cutaneous leishmaniasis in the murine model of infection with *Leishmania amazonensis*. Journal of Antimicrobial Chemotherapy. 2016;71(5):1314–22.

286. Duffy T, Cura CI, Ramirez JC, Abate T, Cayo NM, Parrado R, *et al*. Analytical performance of a Multiplex Real-Time PCR assay using TaqMan probes for

quantification of *Trypanosoma cruzi* Satellite DNA in blood samples. 2013;7(1):e2000.

287. Guedes-Da-Silva FH, Batista DGJ, Meuser MB, Demarque KC, Fulco TO, Araújo JS, *et al. In vitro* and *in vivo* trypanosomicidal action of novel arylimidamides against *Trypanosoma cruzi*. Antimicrobial Agents and Chemotherapy. 2016;60(4):2425–34.

288. Sanchez-Guillén MC, López-Colombo A, Ordóñez-Toquero G, Gomez-Albino I, Ramos-Jimenez J, Torres-Rasgado E *et al.* Clinical forms of *Trypanosoma cruzi* infected individuals in the chronic phase of Chagas disease in Puebla, Mexico Mem Inst Oswaldo Cruz.2006; 101(7): 733-739.

289. Franco CH, Alcântara LM, Chatelain E, Freitas-Junior L, Moraes CB. Drug discovery for chagas disease: impact of different host cell lines on assay performance and hit compound selection. Tropical Medicine and Infectious Disease. 2019;4(2):82.

290. Guedes-da-Silva FH, Batista D da GJ, Da Silva CF, Pavão BP, Batista MM, Moreira OC, *et al.* Successful aspects of the coadministration of sterol 14α-demethylase inhibitor VFV and Benznidazole in experimental mouse models of Chagas Disease caused by the drug-resistant strain of *Trypanosoma cruzi*. ACS infectious diseases. 2019 Mar;5(3):365–71.

291. Pinesi HT, Strabelli TMV, Aiello VD. Case 4/2019 - 26-year-old man with congenital chagas disease and heart transplantation. Arquivos Brasileiros de Cardiologia. 2019;113(2):286–93.

292. Perez CJ, Lymbery AJ, Thompson RCA. Reactivation of Chagas Disease: Implications for Global Health. Trends in parasitology. 2015;31(11):595–603.

293. Sun W, Sanderson PE, Zheng W. Drug combination therapy increases successful drug repositioning. Drug discovery today. 2016;21(7):1189–95.

294. Musa A, Khalil E, Hailu A, Olobo J, Balasegaram M, Omollo R, *et al*. Sodium stibogluconate (ssg) & paromomycin combination compared to ssg for visceral leishmaniasis in east africa: a randomised controlled trial. PLoS Neglected Tropical Diseases. 2012;6(6):e1674.

295. Urbina JA. Recent clinical trials for the etiological treatment of chronic chagas disease: Advances, challenges and perspectives. Journal of Eukaryotic Microbiology. 2015;62(1):149–56.

296. De Oliveira GM, Da Silva TM, Batista WS, Franco M, Schor N. Acute *Trypanosoma cruzi* experimental infection induced renal ischemic/reperfusion

lesion in mice. Parasitology Research. 2009;106(1):111–20.

297. Glover L, Alsford S, Baker N, Turner DJ, Sanchez-Flores A, Hutchinson S, *et al.* Genome-scale RNAi screens for high-throughput phenotyping in bloodstream-form African trypanosomes. Nature Protocols. 2015;10(1):106–33.

298. Setten RL, Rossi JJ, Han S. The current state and future directions of RNAi-based therapeutics. Nature Reviews Drug Discovery. 2019;18(6):421-446.

299. Wilson RC, Doudna JA. Molecular Mechanisms of RNA Interference. Annu Rev Biophys. 2013;42:217-39.

300. Mamta B, Rajam M V. RNAi technology: a new platform for crop pest control. Physiology and molecular biology of plants : an international journal of functional plant biology. 2017;23(3):487–501.

301. Fire A, Xu S, Montgomery MK, Kostas SA, Driver SE, Mello CC. Potent and specific genetic interference by double-stranded RNA in *Caenorhabditis elegans*. Nature. 1998;391(6669):806–11.

302. Napoli C, Lemieux C, Jorgensen R. Introduction of a chimeric chalcone synthase gene into petunia results in reversible co-suppression of homologous genes in trans. The Plant cell. 1990;2(4):279–89.

303. Romano N, Macino G. Quelling: transient inactivation of gene expression in *Neurospora crassa* by transformation with homologous sequences. Molecular microbiology. 1992;6(22):3343–53.

304. Montgomery MK. RNA interference: historical overview and significance. Methods in molecular biology (Clifton, NJ). 2004;265:3–21.

305. Setten RL, Rossi JJ, Han S. The current state and future directions of RNAi-based therapeutics. Nature Reviews Drug Discovery. 2019;18(6):421–46.

306. Ngô H, Tschudi C, Gull K, Ullu E. Double-stranded RNA induces mRNA degradation in *Trypanosoma brucei*. Proceedings of the National Academy of Sciences of the United States of America. 1998;95(25):14687–92.

307. Patrick KL, Luz PM, Ruan J-P, Shi H, Ullu E, Tschudi C. Genomic rearrangements and transcriptional analysis of the spliced leader-associated retrotransposon in RNA interference-deficient *Trypanosoma brucei*. Molecular microbiology. 2008 Jan;67(2):435–47.

308. Shi H, Tschudi C, Ullu E. An unusual Dicer-like1 protein fuels the RNA interference pathway in *Trypanosoma brucei*. RNA (New York, NY). 2006/10/19. 2006;12(12):2063–72.

309. Stortz JA, Serafim TD, Alsford S, Wilkes J, Fernandez-Cortes F, Hamilton G, *et*

al. Genome-wide and protein kinase-focused RNAi screens reveal conserved and novel damage response pathways in *Trypanosoma brucei*. PLoS pathogens. 2017 Jul;13(7):e1006477.

310. Morris JC, Wang Z, Drew ME, Englund PT. Glycolysis modulates trypanosome glycoprotein expression as revealed by an RNAi library. The EMBO journal. 2002 Sep;21(17):4429–38.

311. Drew ME, Morris JC, Wang Z, Wells L, Sanchez M, Landfear SM, *et al*. The adenosine analog tubercidin inhibits glycolysis in *Trypanosoma brucei* as revealed by an RNA interference library. The Journal of biological chemistry. 2003 Nov;278(47):46596–600.

312. Verner Z, Paris Z, Lukes J. Mitochondrial membrane potential-based genome-wide RNAi screen of *Trypanosoma brucei*. Parasitology research. 2010;106(5):1241–4.

313. Burkard G, Fragoso CM, Roditi I. Highly efficient stable transformation of bloodstream forms of *Trypanosoma brucei*. 2007;153:220–3.

314. Schumann Burkard G, Jutzi P, Roditi I. Genome-wide RNAi screens in bloodstream form trypanosomes identify drug transporters. Molecular and Biochemical Parasitology. 2011;175(1):91–4.

315. Mabille D, Cardoso Santos C, Hendrickx R, Claes M, Takac P, Clayton C, *et al.* 4E interacting protein as a potential novel drug target for nucleoside analogues in *Trypanosoma brucei.* Microorganisms. 2021;9(4):826.

316. Ho HTB, Wang J. The Nucleoside Transporters CNTs and ENTs. In: Drug Transporters Hoboken, NJ: John Wiley & Sons, Inc.; 2014. p. 107–26.

317. Geiser F, Lüscher A, de Koning HP, Seebeck T, Mäser P. Molecular pharmacology of adenosine transport in *Trypanosoma brucei*: P1/P2 revisited. Molecular pharmacology. 2005 Sep;68(3):589–95.

318. Carter NS, Fairlamb AH. Arsenical-resistant trypanosomes lack an unusual adenosine transporter. Nature. 1993 Jan;361(6408):173–6.

319. Carter NS, Berger BJ, Fairlamb AH. Uptake of diamidine drugs by the P2 nucleoside transporter in melarsen-sensitive and -resistant *Trypanosoma brucei brucei*. The Journal of biological chemistry. 1995;270(47):28153–7.

320. Gutteridge WE, Ross AM, Schweingruber A, Ma P, Pinar O, Munagala NR, *et al.* Adenosine kinase of *Trypanosoma brucei* and its role in susceptibility to adenosine antimetabolites. Parasitology. 2007;51(11):3895–901.

321. Lüscher A, Onal P, Schweingruber A-M, Mäser P. Adenosine kinase of

Trypanosoma brucei and its role in susceptibility to adenosine antimetabolites. Antimicrobial agents and chemotherapy. 2007;51(11):3895–901.

322. Vodnala M, Fijolek A, Rofougaran R, Mosimann M, Mäser P, Hofer A. Adenosine kinase mediates high affinity adenosine salvage in *Trypanosoma brucei*. The Journal of biological chemistry. 2008;283(9):5380–8.

323. Sun SY, Wang C, Yuan YA, He CY. An intracellular membrane junction consisting of flagellum adhesion glycoproteins links flagellum biogenesis to cell morphogenesis in *Trypanosoma brucei*. Journal of cell science. 2013;126(Pt 2):520–31.

324. Naguleswaran A, Gunasekera K, Schimanski B, Heller M, Hemphill A, Ochsenreiter T, *et al*. *Trypanosoma brucei* RRM1 is a nuclear RNA-binding protein and modulator of chromatin structure. mBio. 2015;6(2):e00114.

325. Florini F, Naguleswaran A, Gharib WH, Bringaud F, Roditi I. Unexpected diversity in eukaryotic transcription revealed by the retrotransposon hotspot family of *Trypanosoma brucei*. Nucleic acids research. 2019;47(4):1725–39.

326. Falk F, Marucha KK, Clayton C. Mechanisms of translation repression by the EIF4E1-4EIP cap-binding complex of *Trypanosoma brucei*: potential roles of the NOT complex and a terminal uridylyl transferase. bioRxiv. 2021.05.19;444837.

327. Jansen K, Heirbaut L, Verkerk R, Cheng JD, Joossens J, Cos P, *et al.* Extended Structure–Activity relationship and pharmacokinetic investigation of (4-Quinolinoyl)glycyl-2-cyanopyrrolidine inhibitors of Fibroblast Activation Protein (FAP). Journal of Medicinal Chemistry. 2014;57(7):3053–74.

328. Williams KM, Qie S, Atkison JH, Salazar-Arango S, Alan Diehl J, Olsen SK. Structural insights into E1 recognition and the ubiquitin-conjugating activity of the E2 enzyme Cdc34. Nature Communications. 2019;10(1):3296.

329. Bijlmakers M-J. Ubiquitination and the proteasome as drug targets in trypanosomatid diseases. Frontiers in chemistry. 2020;8:630888.

330. Boer DR, Bijlmakers M-J. Differential Inhibition of human and trypanosome ubiquitin E1S by TAK-243 offers possibilities for parasite selective inhibitors. Scientific reports. 2019;9(1):16195.

331. Salmon D, Vanwalleghem G, Morias Y, Denoeud J, Krumbholz C, Lhommé F, *et al.* Adenylate cyclases of *Trypanosoma brucei* inhibit the innate immune response of the host. Science (New York, NY). 2012;337(6093):463–6.

332. Makin L, Gluenz E. cAMP signalling in trypanosomatids: role in pathogenesis and as a drug target. Trends in Parasitology. 2015;31(8):373–9.

333. Reis-cunha JL, Valdivia HO, Bartholomeu DC. Gene and chromosomal copy number variations as an adaptive mechanism towards a parasitic lifestyle in trypanosomatids. 2018; 19(2):87-97..

334. Vanwalleghem G, Fontaine F, Lecordier L, Tebabi P, Klewe K, Nolan DP, *et al.* Coupling of lysosomal and mitochondrial membrane permeabilization in trypanolysis by APOL1. Nature Communications. 2015;6(1):8078.

335. Surve SV, Jensen BC, Heestand M, Mazet M, Smith TK, Bringaud F, *et al.* NADH dehydrogenase of *Trypanosoma brucei* is important for efficient acetate production in bloodstream forms. Molecular and biochemical parasitology. 2017 Jan;211:57–61.

336. Fang J, Wang Y, Beattie DS. Isolation and characterization of complex I, rotenone-sensitive NADH: ubiquinone oxidoreductase, from the procyclic forms of Trypanosoma brucei. European journal of biochemistry. 2001;268(10):3075–82.

337. Reis-Cunha JL, Rodrigues-Luiz GF, Valdivia HO, Baptista RP, Mendes TAO, de Morais GL, *et al.* Chromosomal copy number variation reveals differential levels of genomic plasticity in distinct *Trypanosoma cruzi* strains. BMC Genomics. 2015;16(1):1–15.

338. Reis-Cunha JL, Baptista RP, Rodrigues-Luiz GF, Coqueiro-dos-Santos A, Valdivia HO, de Almeida LV, *et al*. Whole genome sequencing of *Trypanosoma cruzi* field isolates reveals extensive genomic variability and complex aneuploidy patterns within TcII DTU. BMC Genomics 2018; 19: 816.

339. Wang W, Peng D, Baptista RP, Li Y, Kissinger JC, Tarleton RL.. Strain-specific genome evolution in *Trypanosoma cruzi*, the agent of Chagas disease. 2021;17(1):e1009254.

340. De Pablos LM. Editorial:New Insights into the Genomes of Kinetoplastid Parasites. Current genomics. 2018;19(2):77.

341. Teixeira SMR. Control of gene expression in Trypanosomatidae. Brazilian Journal Of Medical And Biological Research. 1998;31:1503–16.

342. Almeida RF De, Fernandes M, Martins L, Godoy F De. An updated map of *Trypanosoma cruzi* histone post-translational modifications. 2021;1–10.

343. Burle-Caldas GA, Grazielle-Silva V, Laibida LA, DaRocha WD, Teixeira SMR. Expanding the tool box for genetic manipulation of *Trypanosoma cruzi.* Molecular and Biochemical Parasitology. 2015;203(1–2):25–33.

344. Behan FM, Iorio F, Picco G, Gonçalves E, Beaver CM, Migliardi G, *et al.* Prioritization of cancer therapeutic targets using CRISPR-Cas9 screens. Nature.

2019;568(7753):511–6.

345. Frangoul H, Altshuler D, Cappellini MD, Chen Y-S, Domm J, Eustace BK, et al. CRISPR-Cas9 Gene Editing for Sickle Cell Disease and β-Thalassemia. The New England journal of medicine. 2021 Jan;384(3):252–60.

346. Khan FA, Pandupuspitasari NS, Chun-Jie H, Ao Z, Jamal M, Zohaib A, *et al.* CRISPR/Cas9 therapeutics: a cure for cancer and other genetic diseases. Oncotarget. 2016 Aug;7(32):52541–52.

347. Burle-Caldas GA, Soares-Simões M, Lemos-Pechnicki L, DaRocha WD, Teixeira SMR. Assessment of two CRISPR-Cas9 genome editing protocols for rapid generation of *Trypanosoma cruzi* gene knockout mutants. International Journal for Parasitology [Internet]. 2018;48(8):591–6. Available from: https://doi.org/10.1016/j.ijpara.2018.02.002

348. Yagoubat A, Corrales RM, Bastien P, Lévêque MF, Sterkers Y. Gene editing in Trypanosomatids : Tips and tricks in the CRISPR-Cas9 Era. 2020;

349. Peng D, Kurup SP, Yao PY, Minning TA, Tarleton RL. CRISPR-Cas9-mediated single-gene and gene family disruption in *Trypanosoma cruzi.* mBio. 2014;6(1):1–11.

350. Costa FC, Francisco AF, Jayawardhana S, Calderano SG, Lewis MD, Olmo F, *et al*. Expanding the toolbox for *Trypanosoma cruzi*: A parasite line incorporating a bioluminescence-fluorescence dual reporter and streamlined CRISPR/Cas9 functionality for rapid *in vivo* localisation and phenotyping. PLoS Neglected Tropical Diseases. 2018;12(4):1–21.

351. Jansen R, Embden JDA Van, Gaastra W, Schouls LM. Identification of genes that are associated with DNA repeats in prokaryotes. 2002;43:1565–75.

352. Mojica FJM, Juez G. Transcription at different salinities of Haloferax mediterranei sequences adjacent to partially modified Psfl sites. 1993;9:613–21.

353. Mojica FJM, Ferrer C, Juez G. Long stretches of short tandem repeats are present in the largest replicons of the Archaea Haloforax mediterranei and Haloferax volcanii and could be involved in replicon partitioning. 1995;17:85–93.

354. Mojica F, Díez-Villaseñor C, Soria E, Juez G. Biological significance of a family of regularly spaced repeats in the genomes of Archaea, Bacteria and mitochondria. Molecular Microbiology. 2000;36:244–6.

355. Mojica FJM, Díez-Villaseñor C, García-Martínez J, Soria E. Intervening sequences of regularly spaced prokaryotic repeats derive from foreign genetic elements. Journal of molecular evolution. 2005 Feb;60(2):174–82.

356. Pourcel C, Salvignol G, Vergnaud G. CRISPR elements in Yersinia pestis acquire new repeats by preferential uptake of bacteriophage DNA, and provide additional tools for evolutionary studies. Microbiology (Reading, England). 2005 Mar;151(Pt 3):653–63.

357. Bolotin A, Quinquis B, Sorokin A, Ehrlich SD. Clustered regularly interspaced short palindrome repeats (CRISPRs) have spacers of extrachromosomal origin. 2005;1066:2551–61.

358. Brouns SJJ, Jore MM, Lundgren M, Westra ER, Slijkhuis RJH, Snijders APL, *et al.* Small CRISPR RNAs Guide Antiviral Defense in Prokaryotes. Science. 2008 15;321(5891):960 LP – 964.

359. Marraffini LA, Sontheimer EJ. CRISPR interference limits horizontal gene transfer in staphylococci by targeting DNA. Science (New York, NY). 2008 Dec;322(5909):1843–5.

360. Sapranauskas R, Gasiunas G, Fremaux C, Barrangou R, Horvath P, Siksnys V. The Streptococcus thermophilus CRISPR/Cas system provides immunity in Escherichia coli. Nucleic acids research. 2011 Nov;39(21):9275–82.

361. Barrangou R, Fremaux C, Deveau H, Richards M, Boyaval P, Moineau S, *et al.* CRISPR provides acquired resistance against viruses in prokaryotes. Science (New York, NY). 2007 Mar;315(5819):1709–12.

362. Deltcheva E, Chylinski K, Sharma CM, Gonzales K. Europe PMC Funders Group Europe PMC Funders Author Manuscripts CRISPR RNA maturation by trans - encoded small RNA and host factor RNase III. 2011;471(7340):602–7.

363. Gasiunas G, Barrangou R, Horvath P, Siksnys V. Cas9-crRNA ribonucleoprotein complex mediates specific DNA cleavage for adaptive immunity in bacteria. Proceedings of the National Academy of Sciences of the United States of America. 2012 Sep;109(39):E2579-86.

364. Jinek M, Chylinski K, Fonfara I, Hauer M, Doudna JA, Charpentier E. A programmable dual-RNA–guided DNA endonuclease in adaptive bacterial Immunity. Science. 2012;337(6096):816 LP – 821.

365. Lander N, Chiurillo M, Storey M, Vercesi A, Docampo R. CRISPR / Cas9-mediated endogenous C-terminal tagging of *Trypanosoma cruzi* Genes reveals the acidocalcisome localization of the inositol 1 , 4 , 5-trisphosphate receptor. The Journal of biological chemistry. 2016;291(49):25505–15.

366. Medeiros LCS, South L, Peng D, Bustamante JM, Wang W, Bunkofske M, *et al.* Rapid, selection-free, high-efficiency genome editing in protozoan parasites using

CRISPR-Cas9 ribonucleoproteins. mBio. 2017;8(6):e01788-17..

367. Martel D, Beneke T, Gluenz E, Späth GF, Rachidi N. Characterisation of Casein Kinase 1.1 in *Leishmania donovani* Using the CRISPR Cas9 Toolkit. Nakayasu ES, editor. BioMed Research International. 2017;2017:4635605.

368. Wittner M, Squillante L, Nadler JP, Tanowitz HB. *Trypanosoma cruzi*: colony formation and clonal growth in agar. Exp Parasitol. 1982;53(2):255-61.

369. Aslett M, Aurrecoechea C, Berriman M, Brestelli J, Brunk BP, Carrington M, e*t al.* TriTrypDB: A functional genomic resource for the Trypanosomatidae. Nucleic Acids Research. 2009;38(SUPPL.1):457–62.

370. Berg M, Van der Veken P, Goeminne A, Haemers A, Augustyns K. Inhibitors of the purine salvage pathway: a valuable approach for antiprotozoal chemotherapy? Current Medicinal Chemistry. 2010;17(23):2456–81.

371. Koning HP De, Bridges DJ, Burchmore RJS. Purine and pyrimidine transport in pathogenic protozoa : From biology to therapy. 2005;29:987–1020.

372. Merritt C, Silva LE, Tanner AL, Stuart K, Pollastri MP. Kinases as druggable targets in trypanosomatid protozoan parasites. Chemical Reviews. 2014;114(22):11280–304.

373. De Vas MG, Portal P, Alonso GD, Schlesinger M, Flawiá MM, Torres HN, *et al.* The NADPH–cytochrome P450 reductase family in *Trypanosoma cruzi* is involved in the sterol biosynthesis pathway. International Journal for Parasitology. 2011;41(1):99–108.

374. Leroux AE, Krauth-Siegel RL. Thiol redox biology of trypanosomatids and potential targets for chemotherapy. Molecular and Biochemical Parasitology [Internet]. 2016;206(1-2):67-74.

375. Fernandez-Cortes F, Serafim TD, Wilkes JM, Jones NG, Ritchie R, McCulloch R, et al. RNAi screening identifies *Trypanosoma brucei* stress response protein kinases required for survival in the mouse. Scientific Reports. 2017;7(1):6156.

376. Al-salabi MI, Koning HP De. Purine nucleobase transport in amastigotes of *Leishmania mexicana* : Involvement in Allopurinol Uptake. 2005;49(9):3682–9.

377. Kidder GW. Adenosine kinase from *Trypanosoma cruzi.* Biochemical and biophysical research communications. 1982;107(1):381–8.

378. Aguiar PHN, Furtado C, Repolês BM, Ribeiro GA, Mendes IC, Peloso EF, *et al.* Oxidative stress and DNA lesions: the role of 8-oxoguanine lesions in *Trypanosoma cruzi* cell viability. PLoS neglected tropical diseases. 2013;7(6):e2279.

379. Rose E, Lott J, Hecht M. Mechanisms of DNA repair in *Trypanosoma cruzi* : What do we know so far ? DNA Repair (Amst). 2020;91-92:102873.

380. Genois M, Paquet ER, Laffitte MN, Maity R, Ouellette M, Masson J. DNA repair pathways in trypanosomatids: from DNA repair to drug resistance. Microbiol Mol Biol Rev. 2014;78(1):40-73.

381. Hanukoglu I. Adrenodoxin reductase of mitochondrial cytochrome P450 systems: structure and regulation of expression. In: Curti B, Ronchi S, Zanetti G, editors. De Gruyter; 2019;859–64.

382. Müller JJ, Lapko A, Bourenkov G, Ruckpaul K, Heinemann U. Adrenodoxin reductase-adrenodoxin complex structure suggests electron transfer path in steroid biosynthesis. The Journal of biological chemistry. 2001;276(4):2786–9.

383. Szczebara FM, Chandelier C, Villeret C, Masurel A, Bourot S, Duport C, *et al.* Total biosynthesis of hydrocortisone from a simple carbon source in yeast. Nature Biotechnology. 2003;21(2):143–9.

384. Cordeiro AT. NADPH producing enzymes as promising drug targets for Chagas Disease. Current medicinal chemistry. 2019;26(36):6564–71.

385. Jones NG, Catta-Preta CMC, Lima APCA, Mottram JC. Genetically validated drug targets in leishmania: current knowledge and future prospects. ACS Infectious Diseases. 2018;4(4):467–77.

386. Duncan SM, Myburgh E, Philipon C, Brown E, Meissner M, Brewer J, *et al.* Conditional gene deletion with DiCre demonstrates an essential role for CRK3 in *Leishmania mexicana* cell cycle regulation. Molecular Microbiology. 2016;100(6):931–44.

387. Kangussu-Marcolino MM, Cunha AP, Avila AR, Herman J-P, DaRocha WD. Conditional removal of selectable markers in *Trypanosoma cruzi* using a site-specific recombination tool: proof of concept. Molecular and biochemical parasitology. 2014 ;198(2):71–4.

388. Pacheco-Lugo LA, Sáenz-García JL, Díaz-Olmos Y, Netto-Costa R, Brant RSC, DaRocha WD. CREditing: a tool for gene tuning in *Trypanosoma cruzi*. International Journal for Parasitology [Internet]. 2020;50(13):1067–77.

389. Soares MJ. The reservosome of *Trypanosoma cruzi* epimastigotes: an organelle of the endocytic pathway with a role on metacyclogenesis. Memorias do Instituto Oswaldo Cruz. 1999;94(SUPPL. 1):139–41.

390. Sant'Anna C, Nakayasu ES, Pereira MG, Lourenço D, De Souza W, Almeida IC, *et al.* Subcellular proteomics of *Trypanosoma cruzi* reservosomes. Proteomics.

2009;9(7):1782–94.

391. Soares MJ, de Souza W. Endocytosis of gold-labeled proteins and LDL by *Trypanosoma cruzi.* Parasitology research. 1991;77(6):461–8.

392. Soares MJ, Souto-Padrón T, Bonaldo MC, Goldenberg S, de Souza W. A stereological study of the differentiation process in *Trypanosoma cruzi.* Parasitology research. 1989;75(7):522–7.

393. Monge-Maillo B, López-Vélez R, Saravolatz LD. Miltefosine for visceral and cutaneous leishmaniasis: drug characteristics and evidence-based treatment recommendations. Clinical Infectious Diseases. 2015;60(9):1398–404.

394. Kratz NJ. Drug discovery for Chagas disease: A viewpoint. Acta Tropica. 2019; 198: 105107.

395. Pinart M, Rueda JR, Romero GA, Pinzón-Flórez CE, Osorio-Arango K, Silveira Maia-Elkhoury AN, *et al*. Interventions for American cutaneous and mucocutaneous leishmaniasis. Cochrane Database Syst Rev. 2020; 8(8):CD004834.

396. Sharma NL, Mahajan VK, Kanga A, Sood A, Katoch VM, Mauricio I, *et al.* Localized cutaneous leishmaniasis due to *Leishmania donovani* and *Leishmania tropica*: Preliminary findings of the study of 161 new cases from a new endemic focus in Himachal Pradesh, India. American Journal of Tropical Medicine and Hygiene. 2005;72(6):819–24.

397. Gabriel Á, Valério-Bolas A, Palma-Marques J, Mourata-Gonçalves P, Ruas P, Dias-Guerreiro T, *et al.* Cutaneous Leishmaniasis: the complexity of host's effective immune response against a polymorphic parasitic disease. Journal of immunology research. 2019;2019:2603730.

398. De Oliveira CI, Brodskyn CI. The immunobiology of *Leishmania braziliensis* infection. Frontiers in Immunology. 2012;3(JUN):1–9.

399. Barrett MP, Kyle DE, Sibley LD, Radke JB, Tarleton RL. Protozoan persister-like cells and drug treatment failure. Nature Reviews Microbiology. 2019;17(10):607–20.

400. Bustamante JM, Sanchez-Valdez F, Padilla AM, White B, Wang W, Tarleton RL. A modified drug regimen clears active and dormant trypanosomes in mouse models of Chagas disease. Science translational medicine. 2020;12(567).

401. Lombardo F, Desai P V, Arimoto R, Desino KE, Fischer H, Keefer CE, *et al. In silico* Absorption, Distribution, Metabolism, Excretion, and Pharmacokinetics (ADME-PK): utility and best practices. An Industry Perspective from the

International Consortium for Innovation through Quality in Pharmaceutical Development. Journal of medicinal chemistry. 2017;60(22):9097–113.

402. Lipinski CA, Lombardo F, Dominy BW, Feeney PJ. Experimental and computational approaches to estimate solubility and permeability in drug discovery and development settings. Advanced drug delivery reviews. 2001;46(1–3):3–26.

403. Molina HA, Kierszenbaum F. Kinetics of development of inflammatory lesions in myocardial and skeletal muscle in experimental *Trypanosoma cruzi* infection. The Journal of parasitology. 1988;74(3):370–4.

404. Buckner FS, Wilson AJ, Van Voorhis WC. Detection of live *Trypanosoma cruzi* in tissues of Infected mice by using histochemical stain for β-galactosidase. Infection and Immunity. 1999;67(1):403–9.

405. Gleeson MP. Generation of a set of simple, interpretable ADMET rules of thumb. Journal of Medicinal Chemistry. 2008;51(4):817–34.

406. Pires DEV, Blundell TL, Ascher DB. pkCSM: Predicting small-molecule pharmacokinetic and toxicity properties using graph-based signatures. Journal of Medicinal Chemistry. 2015;58(9):4066–72.

10 APPENDIX

10.1 Curriculum vitae

Camila Cardoso Santos
<u>Address:</u> Belo Horizonte City, Minas Gerais, Brazil
<u>E-mail:</u> santos.camila1036@gmail.com
www.linkedin.com/in/camila-santos-17a8a284
https://www.researchgate.net/profile/Camila-Santos-30
http://lattes.cnpq.br/9532466893381461

10.1.1 Education

PhD. Sc. **Doctorate's degree in Parasite Biology and Biomedical Sciences.** Oswaldo Cruz Foundation- FIOCRUZ, Rio de Janeiro City, Rio de Janeiro State, Brazil, and University of Antwerp (UA), Antwerp, Belgium.

Special program for pedagogical training for teachers (690 h). Candido Mendes University. Rio de Janeiro City, Rio de Janeiro State, Brazil. Year of conclusion: 2017.

M.Sc. **Master's degree in Parasite Biology.** Oswaldo Cruz Foundation- FIOCRUZ, Rio de Janeiro City, Rio de Janeiro skate, Brazil. Year of conclusion: 2016.

B.A. **Biological Sciences.** Federal University of Minas Gerais (UFMG). Minas Gerais State, Brazil. Year of conclusion: 2013.

Undergraduate Exchange Program *Science Without Borders*. University of Bristol (UoB), Bristol City, UK. One year at **Cellular and Molecular Medicine** Bachelor Course. 2012-2013.

Bachelor national mobility program between Brazilian Federal Universities. Federal University of Rio Grande do Norte (UFRN) Natal City, Rio Grande do Norte state. One semester of Marine Biology. 2011.

10.1.2 Language skills

• Native Portuguese
• Professional English
• Elementary Spanish

10.1.3 Experiences

- Multidisciplinary pre-clinical studies involving synthetic compounds against cutaneous leishmaniasis, American and African trypanosomiasis. LBC/FIOCRUZ/Brazil & LMPH, UAntwerp/ Belgium.   2015/2021

- Periodic review in International Journal for Parasitology: Drugs and drug resistance.   2021

- Voluntary biology teacher for University Entrance Exam at EDUCAFRO MINAS - Franciscan Center for the Defense of Rights. 1 year.   2014

- Internship: multitasking activities related to drug repurposing in Leishmaniasis. Cellular and Molecular Parasitology Laboratory (LBCM). Rene Rachou Research Center CPqRR/FIOCRUZ. Belo Horizonte City, MG State, Brazil. 1 year.   2014

- Internship: proteomic analysis Department of Virology. Dengue Virus research group. University of Bristol (UoB).   2013

- Internship: innate immunology and oral vaccine for cattle. Laboratory of Molecular Genetics of Protozoan Parasites LGMPP. UFMG. 1 year.   2012

- Internship: management, rehabilitation, environmental education, protection and turtle research. Projeto Tamar/ICMBio, Ubatuba, Sao Paulo State, Brazil. 216 h.   Feb, 2012

- Internship: Dengue epidemiology surveillance applying molecular methods in the Laboratory of Molecular Genetics of Protozoan Parasites (LGMPP/UFMG/Brazil) in a partnership with ECOVEC enterprise. 5 months.   2011

10.1.4 Events participation

- Attended course: Synthetic Biology of Microorganisms Applied to Industrial Biotechnology, promoted by the Brazilian Center for Research in Energy and Materials (CNPEM).   3rd, 4th Aug 2021

- Remote talk for annual scientific initiation meeting (RAIC) at Fiocruz. Joint PhD: the progress in scientific research and personal development.   June 2021

- Attended course: Topics in contemporaneous protozoology (20 h), promoted by the Brazilian Society of Protozoology (BSP).   August 2020

• Poster presentation / flash talk BSP Spring Meeting 2019. Manchester. Nucleoside analogues against trypanosomatid parasites: phenotypic screening and mechanism-of-action.	April 2019
• Science activities ministered during school vacation, on Saturdays: studying and learning by playing. Workshop: "Discovering Chagas disease" by memory game.	July 2018
• 5ª Edition of the Carlos chagas cycle of lectures. (Symposium). Publication in the proceedings: Optimizing compound screening: the use of computational tools to predict heterocyclic aromatic amidines behaviour.	April 2017

10.1.5 Technical and software skills

- Solid background in parasitology, including cellular and molecular biology

- Experience in cell culture, drug screening, *in vivo* animal models, confocal, scanning and electron microscopy, conventional and real-time PCR, qPCR, gene editing by RNAi and CRISPR/Cas9.

- Computer skills: GraphPad prism, Microsoft office pack, Chemdraw, G suite, adobe apps including Photoshop, Microsoft Windows and Mac OS X operating systems.

10.1.6 Scientific publications

10.1.6.1 From masters and undergraduate thesis:

- **Santos CC,** Lionel JR, Peres RB, Batista MM, da Silva PB, de Oliveira, GM, da Silva CF, Batista D, Souza S, Andrade CH, Neves BJ, Braga RC, Patrick DA, Bakunova SM, Tidwell RR, Soeiro MNC. *In vitro*, *in silico*, and *in vivo* analyses of novel aromatic amidines against *Trypanosoma cruzi*. *Antimicrobial agents and chemotherapy*. **2018**; *62*(2), e02205-17.

- Sandes S, Alvim L, Silva B, Acurcio L, Campos M, **Santos C**, Nicoli J, Neumann E, Nunes Á. Selection of new lactic acid bacteria strains bearing probiotic features from mucosal microbiota of healthy calves: looking for immunobiotics through *in vitro* and *in vivo* approaches for immunoprophylaxis applications. Microbiol Res. **2017**; 200:1 – 13.

- De Araújo JS, da Silva PB, Batista MM, Peres RB, **Cardoso-Santos C**, Kalejaiye TD, Munday JC, De Heuvel E, Sterk GJ, Augustyns K, Salado IG, Matheeussen A, De Esch I, De Koning HP, Leurs R, Maes L, Soeiro MNC. Evaluation of

190

phthalazinone phosphodiesterase inhibitors with improved activity and selectivity against *Trypanosoma cruzi*. J Antimicrob Chemother. **2020**; *75*(4): 958-967.

- Feitosa LM.; Da Silva ER, Hoelz LVB, Souza DL, Come JAASS, **Santos CC**; Batista MM, Soeiro, MNC, Boechat N, Pinheiro LCS. New pyrazolopyrimidine derivatives as *Leishmania amazonensis* arginase inhibitors. Bioorganic & Medicinal Chemistry. **2019**; 27: 3061 - 3069.

- Simões-Silva MR, De Araújo JS, Oliveira GM, Demarque KC, Peres RB, D'Almeida-Melo I, Batista DGJ, Da Silva CF, **Cardoso-Santos C**, Da Silva PB, Batista MM, Bahia MT², Soeiro MNC. 2017. Drug repurposing strategy against *Trypanosoma cruzi* infection: *In vitro* and *in vivo* assessment of the activity of metronidazole in mono- and combined therapy. Biochem Pharmacol. **2017**; 145: 46 – 53.

10.1.6.2 During PhD, as first author:

- **Santos CC**, Zhang H, Batista MM, de Oliveira GM, Demarque KC, da Silva-Gomes NL, Moreira OC Ogungbe IV, Soeiro MdNC. Phenotypic investigation of 4 nitrophenylacetyl- and 4-nitro-1H-imidazoyl-based compounds as antileishmanial agents. Parasitology. Accepted Dec 2021, published Feb **2022**; 3:1-6.

- **Cardoso-Santos C**, Fiuza LFA, da Silva CF, Mazzeti AL, Girão RD, Oliveira GM, Batista DGJ, Moreira OC, Gomes NLS, Maes L, Caljon G, Hulpia F, Van Calenbergh S, Soeiro MNC. 2121. 7-Aryl-7-deazapurine 3'-deoxyribonucleoside derivative as novel lead for chagas disease therapy: *in vitro* and *in vivo* pharmacology. JAC Antimicrob Resist. **2121**; 3(4):dlab168.

- **Santos CC**, Batista MM, Ullah AI, Reddy TRK, Soeiro MdeNC. Drug screening using shape-based virtual screening and *in vitro* experimental models of cutaneous Leishmaniasis. Parasitology. **2021**; 148. 98–104.

- **Cardoso Santos C**, Zhang H, Batista MM, de Oliveira GM, Demarque KC, da Silva-Gomes NL, Moreira OC, Ogungbe IV, Soeiro MdNC. *In vitro* and *in vivo* evaluation of an adamantyl based phenyl sulfonyl acetamide against cutaneous leishmaniasis models of *Leishmania amazonensis*. Antimicrob Agents Chemother. **2020**; 64:e01188-20.

- **Cardoso Santos C**; Zhang H; Batista MM; de Oliveira GM; Demarque KC; da Silva-Gomes NL; Moreira OC; Ogungbe IV, Soeiro MdNC. Phenotypic investigation of 4 nitrophenylacetyl- and 4-nitro-1H-imidazoyl-based compounds as antileishmanial agents. Parasitology. 2022 Feb 3:1-6. doi: 10.1017/S0031182021002079.

10.1.6.3 During PhD, as co-author:

- Mabille D, **Santos CC**, Hendrickx R, Claes M, Takac P, Clayton C, Hendrickx S, Hulpia F, Maes L, Van Calenbergh S, Caljon G. 4E interacting protein as a potential novel drug target for nucleoside analogues in *Trypanosoma brucei*. Microorganisms. **2021**; 9(4): 826.

- Bouton J, Ferreira de Almeida Fiuza L, **Santos CC**, Mazzarella MA, Soeiro MNC, Maes L, Karalic I, Caljon G, Van Calenbergh S. Revisiting pyrazolo[3,4 *d*]pyrimidine

nucleosides as anti-*Trypanosoma cruzi* and antileishmanial agents. J Med Chem. **2021**; 64(7): 4206-4238.

• Lin C, Ferreira de Almeida Fiuza L, **Santos CC**, Ferreira Nunes D, Cruz Moreira O, Bouton J, Karalic I, Maes L, Caljon G, Hulpia F, de Nazaré C Soeiro M, Van Calenbergh S. 6-Methyl-7-Aryl-7-deazapurine nucleosides as Anti-*Trypanosoma cruzi* agents: structure-activity relationship and *in vivo* efficacy. Biochem Pharmacol. **2021**; 16(14): 2231-2253.

10.2 Files of published papers during PhD

p. 195

Paper 1: Santos CC, Batista MM, Ullah AI, Reddy TRK, Soeiro MdeNC. Drug screening using shape-based virtual screening and *in vitro* experimental models of cutaneous Leishmaniasis. Parasitology 2021; 148. 98–104.
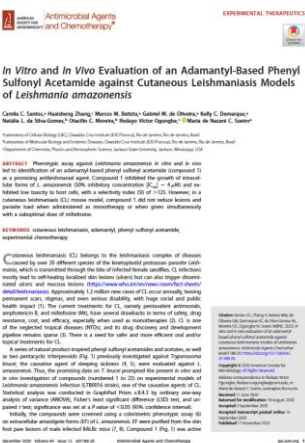
p. 202

Paper 2: Santos CC, Zhang H, Batista MM, de Oliveira GM, Demarque KC, da Silva-Gomes NL, Moreira OC, Ogungbe IV, Soeiro MdNC**.** *In vitro* and *in vivo* evaluation of an adamantyl based phenyl sulfonyl acetamide against cutaneous leishmaniasis models of *Leishmania amazonensis*. 2020; Antimicrob Agents Chemother 64:e01188-20.

Paper 3: Santos CC, Zhang H; Batista MM; de Oliveira GM; Demarque KC; da Silva-Gomes NL; Moreira OC, Ogungbe IV, Soeiro MNC Phenotypic investigation of 4 nitrophenylacetyl- and 4-nitro-1H-imidazoyl-based compounds as antileishmanial agents. Parasitology. 2022; 3:1-6

p. 208

Paper 4: Cardoso-Santos C, Fiuza LFA, da Silva CF, Mazzeti AL, Girão RD, Oliveira GM, Batista DGJ, Moreira OC, Gomes NLS, Maes L, Caljon G, Hulpia F, Van Calenbergh S, Soeiro MNC. 7-Aryl-7-Deazapurine 3′-Deoxyribonucleoside derivative as novel lead for chagas disease therapy: *In vitro* and *In vivo* pharmacology. JAC Antimicrob Resist. 2021; 3(4):dlab168.

p. 214
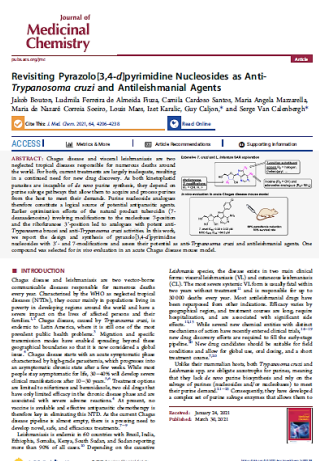
Paper 5: Bouton J, Fiuza LFA, **Santos CC**, Mazzarella MA, Soeiro MNC, Maes L, Karalic I, Caljon G, Calenbergh SV. Revisiting pyrazolo[3,4 d]pyrimidine nucleosides as anti-Trypanosoma cruzi and antileishmanial agents. J Med Chem. 2021; 64(7): 4206-4238.

p. 223

p. 256

Paper 6: Lin C, Fiuza LFA, Cardoso Santos C, Nunes DF, Moreira OC, Bouton J, Karalic I, Maes L, Caljon G, Hulpia F, Soeiro MNC, Calenbergh SV. 6-Methyl-7-Aryl-7-deazapurine nucleosides as anti-*Trypanosoma cruzi* agents: structure-activity relationship and *in vivo* efficacy. Biochem Pharmacol. 2021; 16(14): 2231-2253.

p. 280

Paper 7: Mabille D**, Santos CC**, Hendrickx R, Claes M, Takac P, Clayton C, Hendrickx S, Hulpia F, Maes L, Calenbergh SV, Caljon G. 4E interacting protein as a potential novel drug target for nucleoside analogues in *Trypanosoma brucei*. Microorganisms 2021; 9(4): 826.

Drug screening using shape-based virtual screening and *in vitro* experimental models of cutaneous Leishmaniasis

Camila Cardoso Santos[1], Marcos Meuser Batista[1], Asma Inam Ullah[2],
Tummala Rama Krishna Reddy[2] and Maria de Nazaré Correia Soeiro[1] 🆔

[1]Laboratory of Cellular Biology (LBC), Oswaldo Cruz Institute (IOC/FIOCRUZ), CEP21040-360, Rio de Janeiro, RJ, Brazil and [2]The Medicines Research Group, School of Health, Sport and Bioscience, College of Applied Health and Communities, University of East London, Stratford Campus, Water Lane, London, UK

Abstract

Cutaneous leishmaniasis (CL) is one of the most disregarded tropical neglected disease with the occurrence of self-limiting ulcers and triggering mucosal damage and stigmatizing scars, leading to huge public health problems and social negative impacts. Pentavalent antimonials are the first-line drug for CL treatment for over 70 years and present several drawbacks in terms of safety and efficacy. Thus, there is an urgent need to search for non-invasive, non-toxic and potent drug candidates for CL. In this sense, we have implemented a shape-based virtual screening approach and identified a set of 32 hit compounds. *In vitro* phenotypic screenings were conducted using these hit compounds to check their potential leishmanicidal effect towards *Leishmania amazonensis* (*L. amazonensis*). Two (Cp1 and Cp2) out of the 32 compounds revealed promising antiparasitic activities, exhibiting considerable potency against intracellular amastigotes present in peritoneal macrophages (IC$_{50}$ values of 9.35 and 7.25 μM, respectively). Also, a sterile cidality profile was reached at 20 μM after 48 h of incubation, besides a reasonable selectivity ($\approx$8), quite similarly to pentamidine, a diamidine still in use clinically for leishmaniasis. Cp1 with an oxazolo[4,5-b]pyridine scaffold and Cp2 with benzimidazole scaffold could be developed by lead optimization studies to enhance their leishmanicidal potency.

CAMBRIDGE
UNIVERSITY PRESS

Introduction

Cutaneous leishmaniasis (CL) is a vector-borne tropical neglected disease caused by over 20 different species of kinetoplastid parasites of the genus *Leishmania*. This disfiguring and stigmatizing disease occurs through the injection of promastigote forms into the mammalians by infected female sandflies, triggering ulcers and permanent scars on the skin and/or oral and nasal mucosa injuries, thus contributing to high social stigmatization and public health issue (Bilgic-Temel *et al*., 2019; WHO, 2020). Although about 1.2 million new cases occur annually, CL does not have adequate treatment that are mostly based on old and highly toxic drugs besides the occurrence of high number of parasite species with drug-resistance profile (Alvar *et al*., 2012; de Vries *et al*., 2015; Bailey *et al*., 2019; ; Van Bocxlaer *et al*., 2019).

Computer-aided drug design is an efficient strategy to identify active compounds. Shape-based screening has been successfully employed for the development of anti-fungal and anti-bacterial agents (Swinney and Anthony, 2011). The purpose of the shape-based screening is to identify chemically diverse compounds that show similar biological activity as the query compound. This is based on the principle that diverse structures that share similar shape and electrostatic potential surface or topology will have highest probability to bind to the same pocket and consequently share a similar activity (Kumar and Zhang, 2018).

Due to the limited information on targeted proteins of *Leishmania amazonensis*, we have chosen ligand-based shape screening approach for the hit identification process. The main advantages of this approach are that it only needs a single active compound as the starting point, and that a target crystal structure is not a requirement. This approach aids in the identification of diverse scaffolds other than the query compound scaffold, hence patent issues associated with the chemical space can be avoided.

Ligand-based shape screening was carried out using an active compound GNF5343 (Fig. 1) that displayed activity against the kinetoplastid parasites *Trypanosoma cruzi*, *Trypanosoma brucei* and *Leishmania donovani* (Khare *et al*., 2016). To our knowledge, GNF5343 activity against *L. amazonensis* has not yet been reported. It has been suggested that the kinetoplastid parasites (*Leishmania* species and *Trypanosoma* species) share comparative genomic features (EI-Sayed *et al*., 2005). GNF5343 activity against the three parasites suggests that this compound could be acting through a common receptor target. Hence, we have hypothesized that compounds that show shape similarity with GNF5343 should inhibit the common target and display activity against the *L. amazonensis*. Based on this hypothesis, we presently used GNF5343 as a query compound.
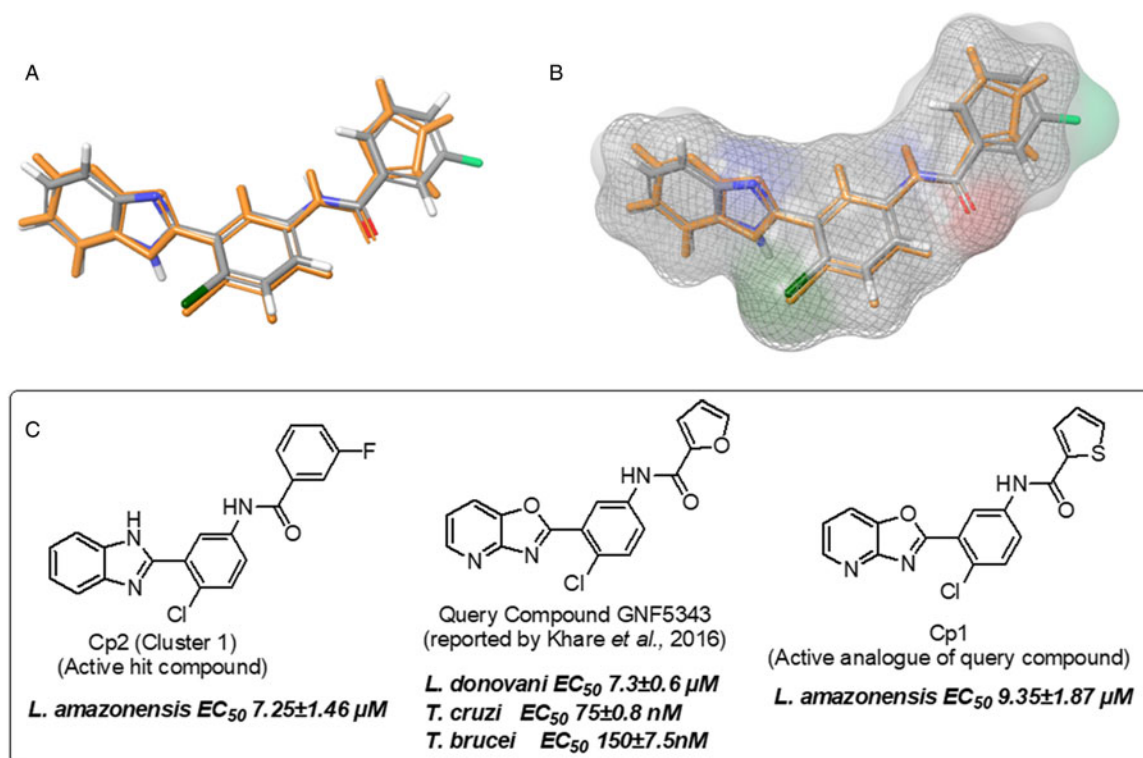
Fig. 1. Shape-based virtual screening results. (A) Illustrating the good alignment of query compound GNF5343 (orange sticks) with compound **2** (atom type coloured sticks). (B) Displaying maximum volume overlap that indicates good shape complementarity between the query compound (represented with mesh with an area of 300 Å^2) and the compound **2** (represented with van der Waals molecular surface area of 326.5 Å^2). (C) Molecular structures and their associated activity data. 1a and 1b images are generated using Phase-Schrödinger drug design software.

Thus, the urgent need for safer and selective potent drugs associated with promising aspects of identified diverse hit compounds from our ligand-based shape-screening programme encouraged us to perform *in vitro* phenotypic screening on amastigotes of *L. amazonensis*, which is one of the main agents of CL in the Americas (Martins *et al*., 2014; de Vries *et al*., 2015).

Methods

Compounds

All 32 identified hit compounds (Figs 1 and 2) that were purchased from Asinex commercial vendor and the reference drug, pentamidine (Pt), were dissolved in 99.99% dimethyl sulphoxide (DMSO) (stock solutions at 20 mM) and fresh dilutions prepared extemporaneously, with the final concentration never exceeding 0.6% DMSO for *in vitro* experiments, which does not induce host cell toxicity (Santos *et al*., 2018).

Parasite strain and mammalian host cell cultures

Leishmania amazonensis (strain *LTB0016*) was used throughout the study. Male BALB/c mice were infected (10^6 amastigotes $20 \mu L^{-1}$ culture medium, *via* subcutaneous) at their foot paws, using a BD ultrafine^{TM} 6 mm syringe ($15/64''$) × 31 G, following previous reported protocol, with minor modifications (Van Bocklaer *et al*., 2019). After 30 days post infection, the animal skin lesions were aseptically removed, and the parasites obtained by mechanic dissociation (pipetting). The purified amastigotes were then assayed directly with the studied compounds to check the activity upon free amastigote (FA) forms, or used to infect primary cultures of peritoneal macrophages (PMM) to investigate their potency against intracellular forms (IA) (Feitosa *et al*., 2019). Swiss male mice (18–20 g) were inoculated with 3% thioglycolate

and after 4 days, PMM collected by rinsing the animals' peritoneum with RPMI 1640. Mammalian cells were seeded at 24 (3×10^5 cells well^{-1}) and 96-well (5×10^4 cells well^{-1}) plates and used for *in vitro* infection and host cell cytotoxicity analysis, respectively. The cultures were sustained at 37°C with 5% CO_2 atmosphere in RPMI 1-640 medium (pH 7.2−7.4) without phenol red (Gibco BRL) but supplemented with 1% L-glutamine, penicillin−streptomycin 10 000 U mL^{-1}, 10% fetal bovine serum (FBS). Assays using FA were also maintained at 32°C using the same RPMI culture medium but adding 5% FBS instead of 10%.

Cytotoxicity upon mammalian host cells and leishmanicidal analysis

For cytotoxicity analysis, PMM were incubated for 48 h with increasing concentrations of the tested compounds (up to 500 μM). Cellular viability was evaluated by AlamarBlue tests (Invitrogen) following the manufacturer's instructions (Da Silva *et al*., 2007; Romanha *et al*., 2010). The leishmanicidal activity was explored in two steps: in the first set of assays, amastigotes (10^6 parasites per well in 0.2 mL) purified from animal lesions (FA) were exposed for 48 h using a fixed concentration (10 μM) and then, drug activity assessed by AlamarBlue tests (Mikus & Sterverding, 2000). Then, in a second set of phenotypic screenings, the activity of the compounds was further validated on IA. In these assays, PMM (3×10^5) were infected with amastigotes (9×10^5 amastigotes) using multiplicity of infection (MOI) 3:1 (Van Bocxlaer *et al*., 2019). After 48 h of compound incubation (0–20 μM), infected PMM were rinsed with saline buffered with phosphate (PBS), fixed with Bouin's solution and stained with Giemsa for light microscopy analysis (Santos *et al*., 2018). Then, the percentage of infected host cells and the number of parasites per infected cells were scored for determination of the corresponding infection index (II) that represents the
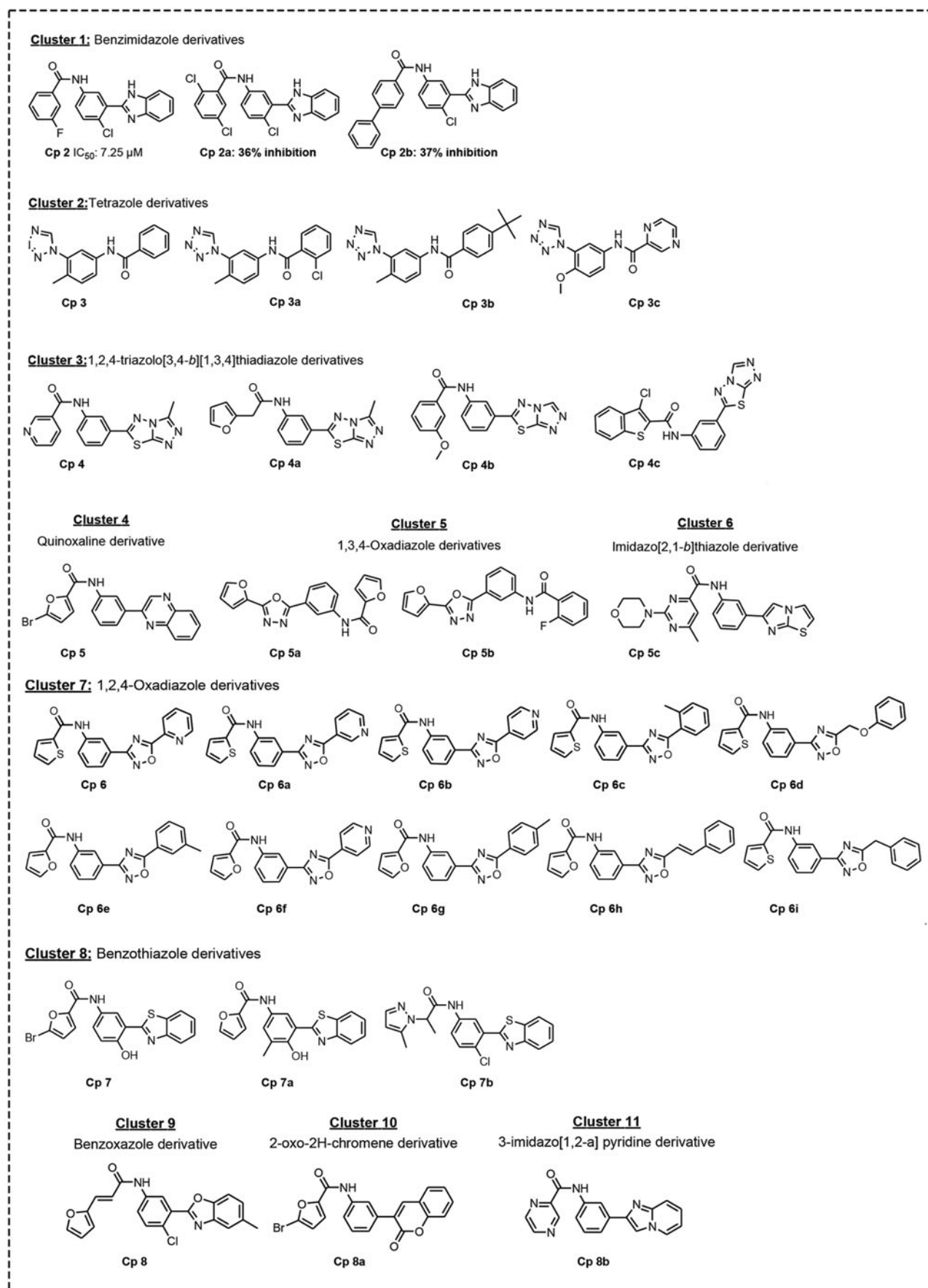
Fig. 2. Clusters of hit compounds identified by shape-based virtual screening strategy. Cp 2a and Cp2b: % inhibition at $10\,\mu\text{M}$.

multiplication factor of both parameters. Only characteristic parasite nuclei and kinetoplasts were counted as surviving parasites since irregular structures could mean parasites undergoing death. The results were expressed as % of reduction of the parasite burden and the IC_{50} and IC_{90} calculated (Santos *et al.*, 2018). All assays were run in at least twice in three independent repeats.

Compound database preparation

Using the LigPrep module of the Schrödinger drug design software, a database (Asinex gold) of commercially available compounds was prepared by performing two-dimensional (2D) to three-dimensional (3D) conversion, addition of hydrogens, generation of ionization states, tautomeric states, stereoisomers and ring conformations at the physiological pH 7.0 ± 2.0. Further, energy minimization of all the compounds was carried out using the molecular mechanics OPLS3 force field (Harder *et al.*, 2016). Compound selection was carried out by applying the Lipinski filter (molecular weight (mol. wt.) ≤ 500; calculated log P (cLogP) ≤ 5; H-bond acceptors (HBA) ≤ 10; H-bond donors (HBD) ≤ 5), besides removing the compounds with nitro groups and reactive functional groups (QikProp, Schrödinger release, 2017). A database was computed with a final set of 60 000 compounds.

Shape-based screening approach

The shape screening was performed using the phase module (Schrödinger-Phase, 2017). We used single 3D structure of GNF5343 compound as the query structure (Fig. 1). Compounds were screened by using the pharmacophore volume scoring setting which treats each compound as a collection of pharmacophore features. These features are aromatic groups, HBA groups, HBD groups, hydrophobic groups, positive charge groups and negative charge groups. Pharmacophoric tolerance was represented by a sphere of radius 2 Å. During the screening, 100 conformers were generated for each compound and the best 10 conformers were retained for matching pharmacophore features similarity. Phase similarity score (phase sim score) was computed based on the maximum aligned features for these conformers.

Cluster analysis

Schrödinger Canvas module was used to perform the cluster analysis as described (Schrödinger-Canvas manual, 2017). All the 31 compounds (Fig. 2) were processed using the hierarchical clustering algorithm with tanimoto similarity as a distance matrix. 2D fingerprints and atom pairs were used as metrics to quantify the chemical diversity.

Results

A subset of 31 compounds was selected based on the structural diversity and phase similarity score. Phase similarity score was computed from the maximum overlapping pharmacophore features as described in the method section. Clustering analysis was carried out on the selected subset of 31 compounds using a hierarchical clustering algorithm. A total of 11 clusters were identified (Fig. 2), of which five were singletons with diverse chemical structures such as quinoxaline derivative (cluster 4), imidazo [2,1-b]thiazole derivative (cluster 6), benzoxazole derivative (cluster 9), 2-oxo-2H-chromene derivative (cluster 10) and 3-imidazo [1,2-a] pyridine derivative (cluster 11). As the query compound GNF5343 was not available for purchase, we have selected one of its close analogue Cp1 (Fig. 1) for the comparative studies along with the selected set of 31 hit compounds. Cp1 differs from GNF5343 in having a thiophenyl ring substitution instead of furyl ring. All 32 compounds were purchased from Asinex and assayed using different protocols *in vitro*. A fixed concentration ($10 \mu M$) was first assessed on FA and findings demonstrated that two (Cp1 and Cp2) out of the 32 compounds reduced ($\geq 50\%$) the number of live parasites. Analogues of Cp2 from

cluster 1 (Fig. 1: Cps 2a and 2b) displayed weak inhibition (Fig. 2). Compounds from other clusters did not show any activity. While Cp1 is a close analogue of query compound, Cp2 is structurally diverse from GNF5343 in having benzimidazole scaffold. These active compounds (Cp1 and Cp2) and the reference drug pentamidine (Pt) were further analysed against FA using increasing concentrations of the tested compounds and Pt. The findings showed moderate leishmanicidal effect, with IC_{50} values of 13.03 ± 2.69 and $14.09 \pm 2.25 \mu M$ for Cp1 and Cp2, respectively, being less potent than Pt ($0.71 \pm 0.05 \mu M$).

In the second round of assays, the compounds were further evaluated against IA present in the cytoplasm of PPM, which represent the gold models for *in vitro* screening of leishmanicidal agents (DNDi, 2018). Our data showed that both compounds were active upon IA, exhibiting IC_{50} values of 9.35 ± 1.87 and $7.25 \pm 1.46 \mu M$, respectively, while Pt yielded $1.94 \pm 0.50 \mu M$. Against the IA, Cp1 and Cp2 reached low IC_{90} values ($17.25 \pm 0.21 \mu M$ and $18.54 \pm 0.96 \mu M$), exhibiting a leishmanicidal profile since both drastically dropped the number of parasites per cell as well as the percentage of infected PMM (Fig. 3). Regarding the mammalian host cell toxicity, we found that after 48 h of exposure, Cp1 and Cp2 were about 3-fold less toxic as compared to Pt, giving IC_{50} of 62.75 ± 0.27 and 65.39 ± 0.61, with selectivity indexes of 6 and 9, respectively, in similar range than the reference drug (SI = 8).

In silico assessment of drug likeness and drug metabolism and pharmacokinetics (DMPK) properties is the most effective way in reducing time, expenses and maximizes the success in drug discovery process (Lombardo *et al.*, 2017). Therefore, drug likeness and DMPK properties were predicted for both Cp1 and Cp2 using the QikProp module (QikProp, Schrödinger release 2017–2). Recommended compliance scores are given in Table 1. The predicted properties of Cp1 and Cp2 showed compliance with 'Lipinski rule of five'. According to 'Jorgensen rule of three' any compound that met the recommended criteria (Table 1) are more likely to be orally available. The predicted properties of both Cp1 and Cp2 displayed compliance with 'Jorgensen rule of three'. Hence, these compounds could show good permeability and solubility properties. Both these properties are crucial for good oral bioavailability. QPPMDCK values are the prediction of MDCK cell permeability (nm/s), which is a good mimic for blood–brain permeation. According to this, both compounds displayed good blood–brain permeation. The efficiency of a drug may be affected by the extent at which it binds to human plasma protein. If compounds show high binding affinity to serum albumin this could lead to poor efficacy. Hence it is very crucial to understand the binding characteristics of Cp1 and Cp2. The predicted human serum albumin binding values (Table 1) for both Cp1 and Cp2 are within the permissible range indicating a lower binding affinity to the serum albumin protein.

Discussion

Compound GNF5343, an oxazolo[4,5-b]pyridine derivative (Fig. 1) was reported to display activity against *L. donovani* with an EC_{50} of $7.3 \pm 0.6 \mu M$, *T. cruzi* with an EC_{50} of 75 ± 0.8 nM and *T. brucei* with an EC_{50} of 150 ± 7.5 nM (Khare *et al.*, 2016). This active compound was used as a query compound to perform the shape-based virtual screening of a set of 60 000 chemically diverse compounds from the Asinex database. Compounds were ranked based on the phase similarity score. Phase similarity scores range from 0 (minimum similarity) to 1 (maximum similarity). Compounds with a phase similarity score above 0.85 were not considered in the selection as compounds with high similarity scores could be the close analogues of the query compounds.
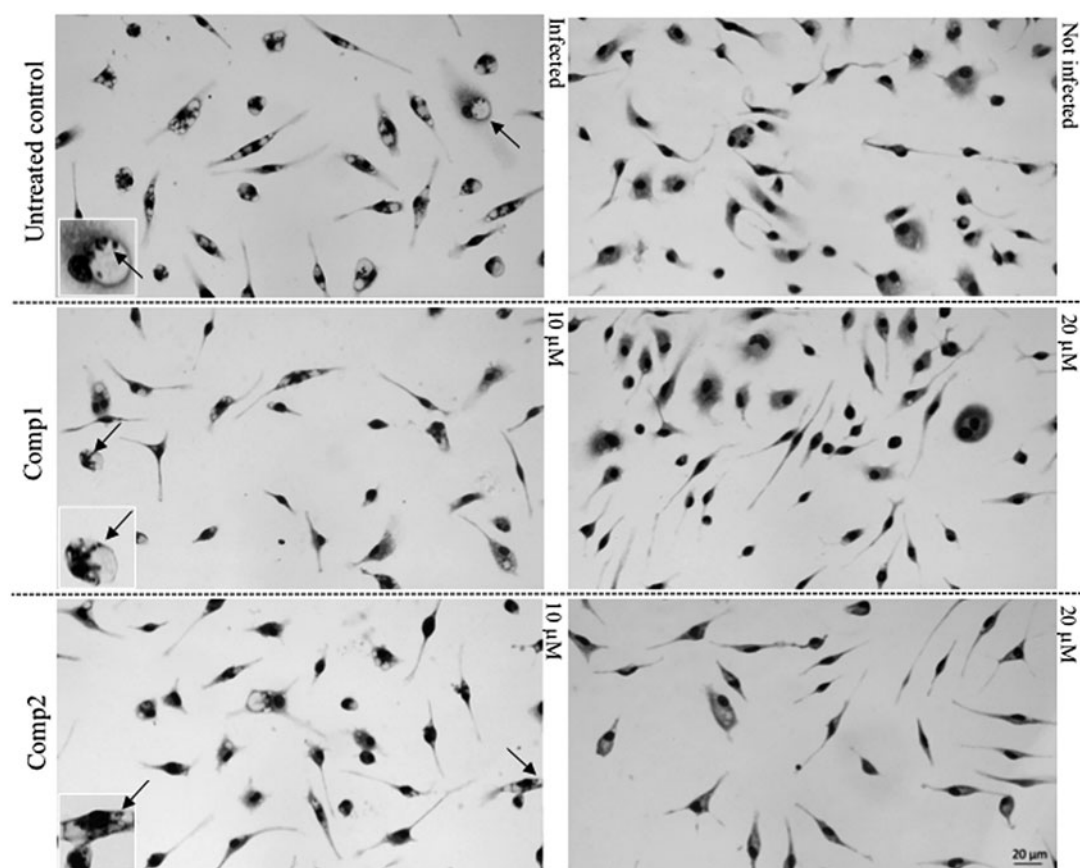
Fig. 3. Light microscopy images of Giemsa-stained uninfected and infected PMM exposed or not (untreated control) to 10 and 20 μm of Cp1 and Cp2, demonstrating parasite sterilization at 20 μm. Arrows: intracellular parasites.

Table 1. *In silico* assessment of drug likeness and predicted DMPK properties of Cp1 and Cp2

		Recommended compliance score (range for 95% of drugs)	Compound ID	
			Cp1	Cp2
Lipinski rule of five	Mol. wt.	≤500	355.80	365.794
	HBD	≤5	1	2
	HBA	≤10	4	2
	cLogP	≤5	3.36	4.59
Jorgensen rule of three	QPlogS	−6.5 to 0.5	−5.380	−6.289
	QPCaco	<25 poor, >500 great	1403	1721
	Primary metabolites	<7	3	0
% Human oral absorption	–	>80% is high, <25% is low	100	100
QPPMDCK	–	>500 great, <25 poor	2650	3285
QPlogKhsa	–	−1.5 to 1.5	0.243	0.616

Mol. wt: molecular weight; HBD: hydrogen bond donor; HBA: hydrogen bond acceptor; cLogP: calculated logarithm of partition coefficient; QPlogS: the logarithm of aqueous solubility; QPCaco: Caco-2 cell permeability in nm/s, model for the gut−blood barrier; QPPMDCK: Madin−Darby canine kidney (MDCK) cell permeability in nm/s, model for the blood−brain barrier; QPlogKhsa: the logarithm of predicted binding constant to human serum albumin.

Compounds that are chemically diverse but similar shape to query compound GNF5343 with a shape similarity score between 0.85 and 0.6 were chosen for further analysis. These compounds were visually inspected to assess their structural diversity and synthetic accessibility. Compounds that showed poor shape similarity (phase similarity score less than 0.6) to query compound GNF5343 were not considered in the selection. Cp1 and Cp2 are the two active compounds identified from the selected set of 32 compounds as described under the results. Analysis of the predicted alignments of these two compounds indicate that the root-mean-square deviation (RMSD) value for the maximum common structure between GNF5343 and Cp1 is 0.147 Å (figure not shown) and the RMSD value for the Cp2 is 1.569 Å (Fig. 1a). Both GNF5343 and Cp2 displayed maximum volume overlap (Fig. 1b) indicating that these two compounds are having similar topology to form similar van der Waals surface interactions at the same region. It is interesting to note the varied distribution of HBD, HBA and hydrophobicity between the basic scaffolds

(oxazolo[4,5-b]pyridine *vs* benzimidazole) of GNF5343 and Cp2. Both Cp1 and Cp2 displayed activity against *L. amazonensis* (Fig. 1c) with an EC_{50} of $9.35 \pm 1.87\,\mu M$ and EC_{50} of $7.25 \pm 1.46\,\mu M$, respectively.

This activity of both Cp1 and Cp2 supports our hypothesis. Herein, we report two novel compounds active against *L. amazonensis*.

Currently, our analysis was performed using primary cultures of PMM infected with *L. amazonensis* since professional phagocytes are the main source of host cells for those obligate intracellular parasites (Walker *et al.*, 2014). This *in vitro* standardized experimental model for CL is claimed to closely reproduce *in vivo* conditions (Stacey, 2006), therefore, contributing to novel drug candidate screenings for this neglected illness (Chatelain and Ioset, 2011; Caridha *et al.*, 2019). Another interesting point to be addressed is the use of protocols that enable the identification of antiparasitic drugs that induces rapid parasite lysis (Da Silva *et al.*, 2007). This is especial characteristic as most of the CL patients live in very poor areas with difficult access to public health assistance and then, frequently display advanced pathologies, demanding a fast *killer* drug (Ruoti *et al.*, 2013; Okwor and Uzonna, 2016). Aiming to fulfill this demand, we established a period of 48 h of drug exposure while testing the parasites and host mammalian cells, a shorter period of incubation as compared with others reported in the current literature for CL *in vitro* models (Van Bocklaer *et al.*, 2019).

This study explored the leishmanicidal effect of Cp1 (an analogue of GNF5343) and Cp2 (a benzimidazole analogue) identified using shape-based virtual screening approach. Both Cp1 and Cp2 achieved quite relevant potency against amastigotes, especially those lodged inside macrophages, reaching IC_{50} values below $10\,\mu M$, a considerable characteristic preconized for a hit compound with anti-leishmania effect (Katsuno *et al.*, 2015). Remarkably, clearance on *L. amazonensis* infection was found at $20\,\mu M$ in the infected PMM, a relevant feature to mitigate the possible occurrence of parasite drug resistance and relapses after ceasing the drug administration (Cal *et al.*, 2016). The Cp1 and Cp2 were less toxic than the reference drug (pentamidine) still in use for Leishmaniasis but their selectivity indexes (<10) discouraged to move them for *in vivo* proof of concept. However, their chemical optimization for a wider therapeutic window and promotion of potency is largely desirable to continue further studies using these compounds. Currently, we are performing structural modifications of Cp2 aiming to improve its potency, selectivity and satisfactory pharmacological profile, favouring future phenotypic studies in order to move its derivatives forward to new *in vitro* screening and *in vivo* evaluation, aiming to contribute for drug discovery process of new therapeutic approaches for CL. These analogues will also be tested against other kinetoplastid parasites to assess their activity.

Conflicts of interest. None.

Ethical standards. All procedures were carried out in accordance with the guidelines established by the FIOCRUZ Committee of Ethics for the Use of Animals (CEUA L038/2017).

References

Alvar J, Vélez ID, Bern C, Herrero M, Desjeux P, Cano, J, Jannin, J and den Boer, M., & WHO Leishmaniasis Control Team (2012) Leishmaniasis worldwide and global estimates of its incidence. *PLoS ONE* **7**, e35671.

Bailey F, Mondragon-Shem K, Haines LR, Olabi A, Alorfi A, Ruiz-Postigo JA, Alvar J, Hotez P, Adams ER, Vélez ID, Al-Salem W, Eaton J, Acosta-Serrano Á and Molyneux DH (2019) Cutaneous leishmaniasis and co-morbid major depressive disorder: a systematic review with burden estimates. Cutaneous leishmaniasis and co-morbid major depressive disorder: a systematic review with burden estimates. *PLoS Neglected Tropical Diseases* **13**, e0007092.

Bilgic-Temel A, Murrell, DF and Uzun S (2019) Cutaneous leishmaniasis: a neglected disfiguring disease for women. *International Journal of Women's Dermatology* **5**, 158–165.

Cal M, Ioset J-R, Fügi MA, Mäser P and Kaiser M (2016) Assessing anti-*T. cruzi* candidates in vitro for sterile cidality. *International Journal for Parasitology: Drugs and Drug Resistance* **6**, 165–170.

Canvas (2017) Schrödinger Release 2017–2: Maestro, Schrödinger, LLC, New York, NY.

Caridha D, Vesely B, van Bocxlaer K, Arana B, Mowbray CE, Rafati S, Uliana S, Reguera R, Kreishman-Deitrick M, Sciotti R, Buffet P and Croft SL (2019) Route map for the discovery and pre-clinical development of new drugs and treatments for cutaneous leishmaniasis. *International Journal for Parasitology: Drugs and Drug Resistance* **11**, 106–117.

Chatelain E and Ioset JR (2011) Drug discovery and development for neglected diseases: the DNDi model. *Drug Design, Development and Therapy* **16**, 175–81.

Da Silva CF, Batista MM, Mota RA, de Souza EM, Stephens CE, Som P, Boykin DW and Soeiro Mde N (2007) Activity of "reversed" diamidines against *Trypanosoma cruzi* "in Vitro". *Biochemical Pharmacology* **73**, 1939–46.

de Vries HJ, Reedijk SH and Schallig HD (2015) Cutaneous leishmaniasis: recent developments in diagnosis and management. *American Journal of Clinical Dermatology* **16**, 99–109.

DNDi Annual report (2018) Making medical history. Available at https://www.dndi.org/wp-content/uploads/2019/07/DNDi_2018_AnnualReport.pdf (Accessed 8 March 2020).

El-Sayed N, Myler P, Blandin G, Berriman M, Crabtree J, Aggarwal G, Caler E, Renauld H, Worthey E, Hertz-Fowler C, Ghedi E, Peacock C, Bartholomeu D, Haas B, Tran A, Wortman J, Alsmark Ucm, Angiuoli S, Anupama A, Badger J, Bringaud F, Cadag E, Carlton J, Cerqueira G, Creasy T, Delcher A, Djikeng A, Embley T, Hauser C, Ivens A, Kummerfeld S, Pereira-Leal J, Nilsson D, Peterson J, Salzberg S, Shallom J, Silva J, Sundaram J, Westenberger S, White O, Metville S, Donelson J, Andersson B, Stuart K and Hall N (2005) Comparative genomics of trypanosomatid parasitic protozoa. *Science* **309**, 404–409.

Feitosa LM, da Silva ER, Hoelz LVB, Souza DL, Come JAASS, Cardoso-Santos C, Batista MM, Soeiro MNC, Boechat N and Pinheiro LCS (2019) New pyrazolopyrimidine derivatives as *Leishmania amazonensis* arginase inhibitors. *Bioorganic & Medical Chemistry* **27**, 3061–3069.

Harder E, Damm W, Maple J, Wu C, Reboul M, Xiang JY, Wang L, Lupyan D, Dahlgren MK, Knight JL, Kaus JW, Cerutti DS, Krilov G, Jorgensen WL, Abel R and Friesner RA (2016) OPLS3: a force field providing broad coverage of drug-like small molecules and proteins. *Journal of Chemical Theory and Computation* **12**, 281–296.

Katsuno K, Burrows JN, Duncan K, van Huijsduijnen RH and Kaneko T (2015) Hit and lead criteria in drug discovery for infectious diseases of the developing world. *Nature Reviews Drug Discovery* **14**, 751–758.

Khare S, Nagle AS, Biggart A, Lai YH, Liang F, Davis LC, Barnesn SW, Mathison CJN, Myburgh E, Gao MY, Gillespie JR, Liu X, Tan JL, Stinson M, Rivera IC, Ballard J, Yeh V, Groessl T, Federe G, Koh HXY, Venable JD, Bursulaya B, Shapiro M, Mishra PK, Spraggon G, Brock A, Mottram JC, Buckner FS, Rao SPS, Wen BG, Walker JR, Tuntland T, Molteni V, Glynne RJ and Supek F (2016) Proteasome inhibition for treatment of Leishmaniasis, Chagas disease and sleeping sickness. *Nature* **537**, 229–233.

Kumar A and Zhang KYJ (2018) Advances in the development of shape similarity methods and their application in drug discovery. *Frontiers in Chemistry* **6**, 315.

Lombardo F, Desai PV, Arimoto R, Desino KE, Fischer H, Keefer CE, Petersson C, Winiwarter S and Broccatelli F (2017) In silico absorption, distribution, metabolism, excretion, and pharmacokinetics (ADME-PK): utility and best practices. An industry perspective from the international

consortium for innovation through quality in pharmaceutical development. *Journal of Medical Chemistry* **60**, 9097–9113.

Martins AL, Barreto JA, Lauris JR and Martins AC (2014) American tegumentary leishmaniasis: correlations among immunological, histopathological and clinical parameters. *Anais Brasileiros de Dermatologia* **89**, 52–58.

Mikus J and Sterverding D (2000) A simple colorimetric to screen drug cytotoxicity against Leishmania using the dye Alamar blue. *Parasitology international* **48**, 265–269.

Okwor I and Uzonna J (2016) Social and economic burden of human leishmaniasis. *American Journal of Tropical Medical Hygiene* **94**, 489–493.

QikProp (2017) Virtual screening workflow, Schrödinger Release 2017-2: Maestro, Schrödinger, LLC, New York, NY.

Romanha AJ, Castro SL, Soeiro Mde N, Lannes-Vieira J, Ribeiro I, Talvani A, Bourdin B, Blum B, Olivieri B, Zani C, Spadafora C, Chiari E, Chatelain E, Chaves G, Calzada JE, Bustamante JM, Freitas-Junior LH, Romero LI, Bahia MT, Lotrowska M, Soares M, Andrade SG, Armstrong T, Degrave W and Andrade Zde A (2010) *In vitro* and *in vivo* experimental models for drug screening and development for Chagas disease. *Memórias do Instituto Oswaldo Cruz* **105**, 233–238.

Ruoti M, Oddone R, Lampert N, Orué E, Miles MA, Alexander N, Rehman AM, Njord R, Shu S, Brice S, Sinclair B and Krentel A (2013) Mucocutaneous leishmaniasis: knowledge, attitudes, and practices among Paraguayan communities, patients, and health professionals. *Journal of Tropical Medicine* **2013**, 538629. https://doi.org/10.1155/2013/538629

Santos CC, Lionel JR, Peres RB, Batista MM, da Silva PB, de Oliveira GM, da Silva CF, Batista D, Souza S, Andrade CH, Neves BJ, Braga RC, Patrick DA, Bakunova SM, Tidwell RR and Soeiro M (2018) *In vitro*, *in silico*, and *in vivo* analyses of novel aromatic amidines against *Trypanosoma cruzi*. *Antimicrobial Agents and Chemotherapy*, **62**: e02205–17.

Stacey G (2006) Primary cell cultures and immortal cell lines. *Encyclopedia of Life Sciences*. doi:10.1038/npg.els.0003960.

Swinney DC and Anthony J (2011) How were new medicines discovered? *Nature Reviews Drug Discovery* **10**, 507–519.

Van Bocxlaer K, Caridha D, Black C, Vesely B, Leed S, Sciotti RJ, Wijnant GJ, Yardley V, Braillard S, Mowbray CE, Ioset JR and Croft SL (2019) Novel benzoxaborole, nitroimidazole and aminopyrazoles with activity against experimental cutaneous leishmaniasis. *International Journal for Parasitology: Drugs and Drug Resistance* **11**, 129–138. doi: 10.1016/j.ijpddr.2019.02.002

Walker DM, Oghumu S, Gupta G, McGwire BS, Drew ME and Satoskar AR (2014) Mechanisms of cellular invasion by intracellular parasites. *Cellular and Molecular Life Sciences* **71**, 1245–1263.

World Health Organization (2020) Leishmaniasis factsheet – 2015 (last update 2 March 2020) Brazil. Available at https://www.who.int/en/news-room/fact-sheets/detail/leishmaniasis (Accessed 8 March 2020).

In Vitro and *In Vivo* Evaluation of an Adamantyl-Based Phenyl Sulfonyl Acetamide against Cutaneous Leishmaniasis Models of *Leishmania amazonensis*

Camila C. Santos,[a] Huaisheng Zhang,[c] Marcos M. Batista,[a] Gabriel M. de Oliveira,[a] Kelly C. Demarque,[a] Natália L. da Silva-Gomes,[b] Otacílio C. Moreira,[b] Ifedayo Victor Ogungbe,[c] ![ORCID] Maria de Nazaré C. Soeiro[a]

[a]Laboratory of Cellular Biology (LBC), Oswaldo Cruz Institute (IOC/Fiocruz), Rio de Janeiro, Rio de Janeiro, Brazil
[b]Laboratory of Molecular Biology and Endemic Diseases, Oswaldo Cruz Institute (IOC/Fiocruz), Rio de Janeiro, Rio de Janeiro, Brazil
[c]Department of Chemistry, Physics and Atmospheric Science, Jackson State University, Jackson, Mississippi, USA

ABSTRACT Phenotypic assay against *Leishmania amazonensis in vitro* and *in vivo* led to identification of an adamantyl-based phenyl sulfonyl acetamide (compound 1) as a promising antileishmanial agent. Compound 1 inhibited the growth of intracellular forms of *L. amazonensis* (50% inhibitory concentration [IC_{50}] = 4 μM) and exhibited low toxicity to host cells, with a selectivity index (SI) of >125. However, in a cutaneous leishmaniasis (CL) mouse model, compound 1 did not reduce lesions and parasite load when administered as monotherapy or when given simultaneously with a suboptimal dose of miltefosine.

KEYWORDS cutaneous leishmaniasis, adamantyl, phenyl sulfonyl acetamide, experimental chemotherapy

Cutaneous leishmaniasis (CL) belongs to the leishmaniasis complex of diseases caused by over 20 different species of the kinetoplastid protozoan parasite *Leishmania*, which is transmitted through the bite of infected female sandflies. CL infections mostly lead to self-healing localized skin lesions (ulcers) but can also trigger disseminated ulcers and mucosa lesions (https://www.who.int/en/news-room/fact-sheets/detail/leishmaniasis). Approximately 1.2 million new cases of CL occur annually, leaving permanent scars, stigmas, and even serious disability, with huge social and public health impact (1). The current treatments for CL, namely pentavalent antimonials, amphotericin B, and miltefosine (Mt), have several drawbacks in terms of safety, drug resistance, cost, and efficacy, especially when used as monotherapies (2). CL is one of the neglected tropical diseases (NTDs), and its drug discovery and development pipeline remains sparse (3). There is a need for safer and more efficient oral and/or topical treatments for CL.

A series of natural product-inspired phenyl sulfonyl acetamides and acetates, as well as two pentacyclic triterpenoids (Fig. 1) previously investigated against *Trypanosoma brucei*, the causative agent of sleeping sickness (4, 5), were evaluated against *L. amazonensis*. Thus, the promising data on *T. brucei* prompted the present *in vitro* and *in vivo* investigation of compounds (numbered 1 to 23) on experimental models of *Leishmania amazonensis* infection (LTB0016 strain), one of the causative agents of CL. Statistical analysis was conducted in GraphPad Prism v.8.4.3 by ordinary one-way analysis of variance (ANOVA), Fisher's least significant difference (LSD) test, and unpaired *t* test; significance was set at a *P* value of <0.05 (95% confidence interval).

Initially, the compounds were screened using a colorimetric phenotypic assay (6) on extracellular amastigote forms (EF) of *L. amazonensis*. EF were purified from the skin foot paw lesions of male infected BALBc mice (7, 8). Compound 1 (Fig. 1) was active

Address correspondence to Ifedayo Victor Ogungbe, ifedayo.v.ogungbe@jsums.edu, or Maria de Nazaré C. Soeiro, soeiro@ioc.fiocruz.br.
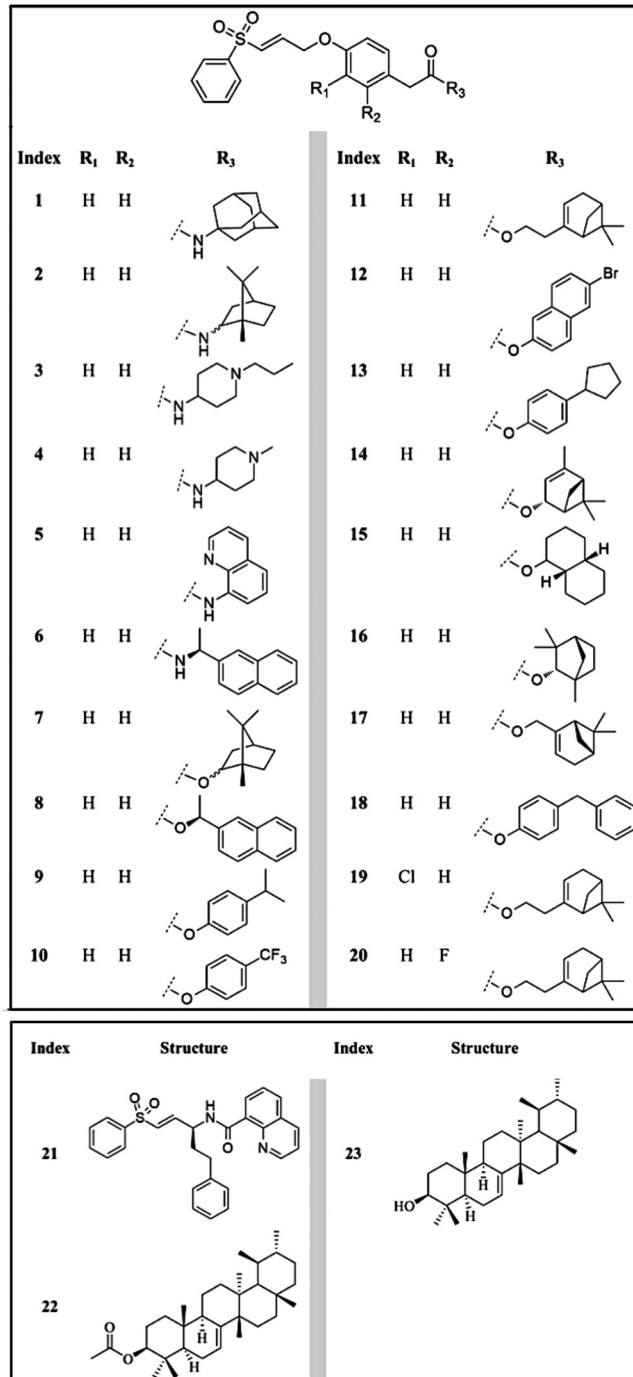
FIG 1 Chemical structures of tested compounds.

against EF (Fig. 2A). After 48 h of treatment, 5 μM compound 1 led to a 44% reduction in viable EF, and the 50% inhibitory concentration (IC$_{50}$) was determined to be 12.07 $\pm$ 1.78 μM (Fig. 2A). Due to this promising profile, compound 1 was further evaluated by light microscopy against intracellular forms (IF) localized in primary cultures of peritoneal macrophages (PMM) (9). The intracellular forms are the relevant forms in mammalian infections. Compound 1 (IC$_{50}$ = 4.00 $\pm$ 1.79 μM) was about 3-fold more potent (P = 0.0367) against IF than miltefosine (IC$_{50}$ = 13.3 $\pm$ 3.03 μM), with no observable toxicity against PMM up to 500 μM and with a selectivity index (SI) of >125 (Fig. 2A). The relatively high SI of compound 1 makes it a good hit compound for CL

203

A

Compound	IC$_{50}$ EF	IC$_{50}$ IF	IC$_{50}$ PPM	SI EF	SI IF
1	12.07±1.78	4.00±1.79	>500	>41.42	>125
Miltefosine	4.37±0.11	13.3±3.03	169.69±5.07	38.83	12.76

B   **C**   **D**
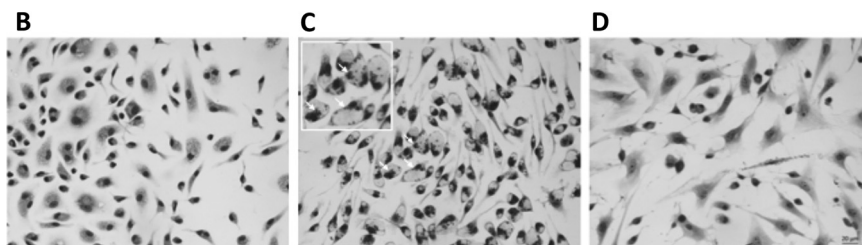
FIG 2 (A) Compound 1 and miltefosine activity expressed as 50% inhibitory concentration (IC$_{50}$) on *L. amazonensis* (LTB0016 strain) after 48 h of drug exposure against extracellular amastigote forms purified from animal lesion (EF) and intracellular forms (IF) within primary cultures of peritoneal macrophages (PMM), host cell toxicity, and respective selectivity indexes (SI). (B to D) Light microscopy images of Giemsa-stained uninfected (B) and infected PMM (C) subjected or not to 10 μM compound 1 (D), demonstrating parasite sterilization due to drug exposure. Arrows indicate intracellular parasites.

(10). Moreover, analysis by light microscopy clearly demonstrate that compound 1 has a cidal rather than a static effect upon the intracellular forms, since it reduced not only the number of parasites per host cell but also the percentage of infected PMM, leading to cell culture sterilization (0% infection) at 10 μM (Fig. 2B and C).

The leishmanicidal activity of compound 1 and with its relatively low IC$_{90}$ (7.16 μM; IF) are desirable features to avoid parasitic relapses and drug resistance (11). According to the international target product profile recommended for novel drug candidates for leishmaniasis (10, 12), the sum of these phenotypic findings encouraged us to move compound 1 to LC mouse experimental models. *In vivo* assays were conducted using a CL mouse model by the left foot paw subcutaneous infection of BALBc male mice (18 to 20 g) with 2×10^5 amastigotes of *L. amazonensis* (BT0016 strain) as described by Feitosa and coworkers in 2019 (7) (full details are provided in the supplemental material). The drug treatment started at 15 days postinfection (dpi), on the onset of the lesions measuring 200 mm³, corresponding to a 3- to 4-mm diameter (3). Compound 1 at 10 mg/kg was given twice a day (b.i.d.), alone or in coadministration with a suboptimal dose of Milteforan (Mt) 4 mg/kg once a day (q.d.), for 14 days. As a positive control, Mt was administered at 40 mg/kg q.d. The animals were monitored daily, and the lesion size was regularly measured until the endpoint of 31 dpi. Thereafter, the animals were euthanized and their skin lesions collected for imprinting Giemsa analysis by light microscopy, as well as for parasite load quantification by quantitative PCR (qPCR), as reported previously (11, 13). All procedures were carried out in accordance with the guidelines established by the Fiocruz Committee of Ethics for the Use of Animals (CEUA L038/2017).

The *in vivo* infection led to a gradual increase in the size of the skin lesions of mice treated with the drug vehicle alone, which reached 438.8 $\pm$ 42.05 mm³ at the endpoint (Fig. 3A). Compound 1 given alone (10 mg/kg b.i.d. for 14 days) led to a mild increase (19%; $P = 0.0328$) in lesion sizes, with a mean value of 550.7 $\pm$ 23.15 mm³. When compound 1 was coadministered with a suboptimal dose of Mt (10 mg/kg of compound 1 plus 4 mg/kg of Mt, q.d. for 14 days), the lesions decreased by 20% ($P = 0.0934$). Mt alone at the optimal dose (40 mg/kg q.d. for 14 days) led to about a 72% significant reduction ($P < 0.0001$) in the size of the lesions, thereby reverting the clinical condition (Fig. 3A and B).

For qPCR, standard curves were constructed using DNA samples extracted from mouse skin fragments spiked with 10^6 amastigotes of *L. amazonensis*. Parasite load

204
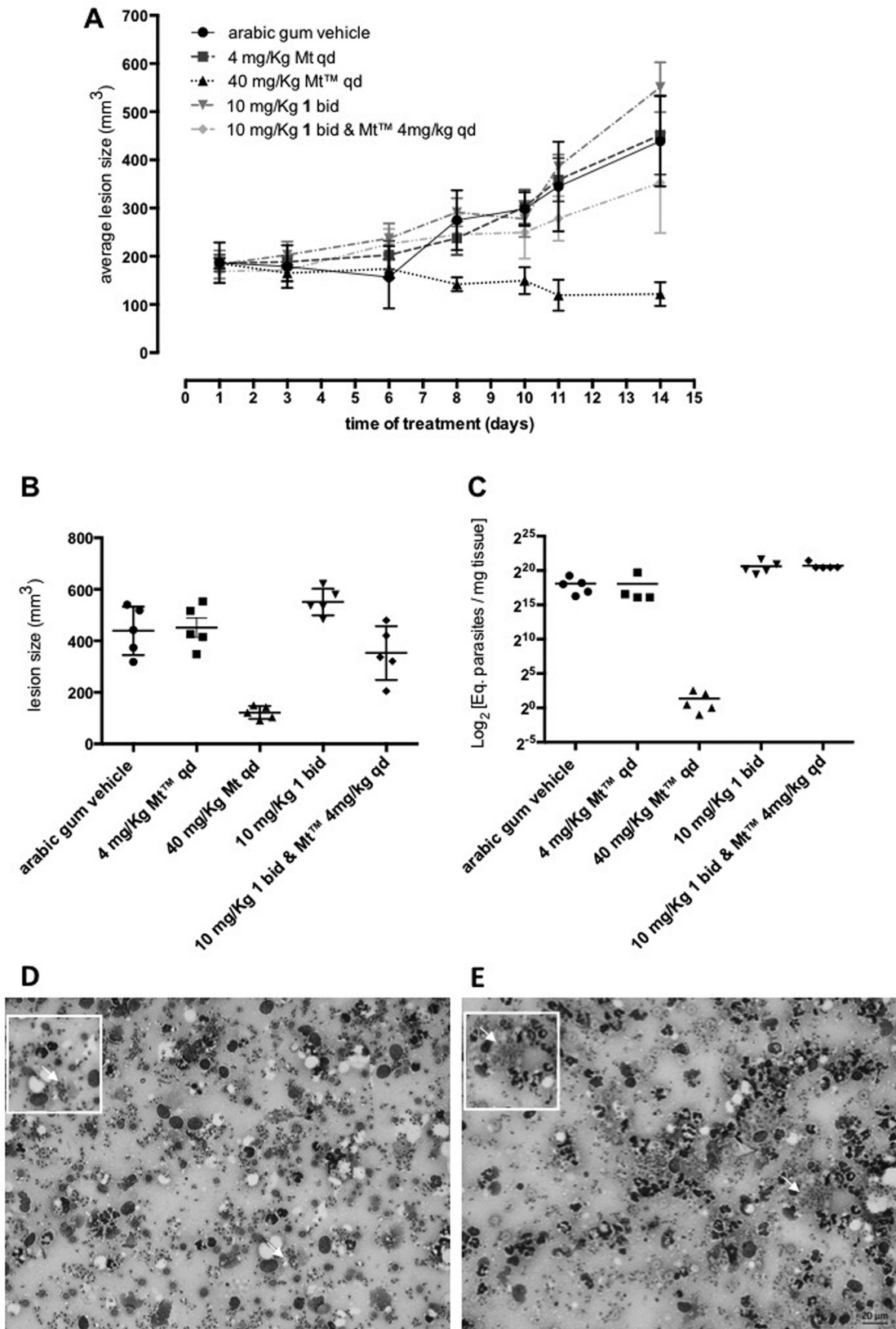
FIG 3 Activity of compound 1 in the *L. amazonensis*-BALBc model of CL. The graphics show average lesion size during treatment (A) and average lesion size (B) and parasite load by quantitative PCR (qPCR) at 31 days postinfection (C), according to each experimental group. Light microscopy of lesion imprints of infected mice treated with vehicle (D) and after oral (p.o.) administration of compound 1 at 10 mg/kg b.i.d. (E). Arrows indicates intracellular parasites.

expressed as equivalents of parasite DNA/mg tissue (eq par/mg tissue) showed a 93.2% efficiency for the target 18S rRNA gene in *Leishmania*, with a linearity coefficient of 0.98 (Fig. S1A). For the mouse glyceraldehyde-3-phosphate dehydrogenase (GAPDH) target, an efficiency of 91.4% was observed, with a linearity coefficient of 0.99 (Fig. S1B), confirming the sensitivity and accuracy of parasite detection and quantification (13). The molecular readout showed that mice treated with compound 1 alone (160,496 ± 45,419 eq par/mg tissue) or in coadministration with Mt (170,706 ± 28,584 eq par/mg tissue) led to an increase in parasite load (6- to 7-fold; $P = 0.0018$ and 0.0010, respectively) compared to that in the vehicle-treated group (27,753 ± 9,539 eq par/mg tissue) at 31 dpi (Fig. 3C). As expected, Mt given at 40 mg/kg suppressed parasite load (0.256 ± 0.102 eq par/mg tissue, 99.99%; $P = 0.00196$) in infected mice (8).

Analysis of lesion imprints on Giemsa-stained slides using light microscopy (Fig. 3D and E) showed that vehicle-treated mice (Fig. 3D) have numerous intracellular parasites (arrow) in macrophages besides the inflammatory diffuse infiltrates. Compound 1 lesions (Fig. 3E) also revealed a similar pattern, exhibiting high parasitemia, while the Mt group displayed only a few nonviable parasites. Our findings revealed that compound 1 has leishmanicidal activity *in vitro* but lacks *in vivo* efficacy under the treatment conditions used in this study. The lack of efficacy is potentially tied to compound 1's lipophilicity. Its relatively high lipophilicity (cLogP of 4.3) actually impaired its use at a higher dose such as the one used for the reference drug Mt (40 mg/kg). Drugs in clinical use for leishmaniasis generally have high aqueous solubility. Thus, ongoing work on analogues of compound 1 is aimed at improving aqueous solubility and using absorption, distribution, metabolism, and excretion (ADME) experiments to reduce obvious metabolic liabilities. Analogues of compound 1 with improved bioavailability could potentially contribute to the drug discovery and development pipeline of leishmaniasis.

Finally, although it did not reach successfully *in vivo* outcomes, our present phenotypic study brings novel knowledge to the field of drug discovery for LC, which aims to achieve a future delivery of new therapies for patients suffering from this disregarded neglected tropical disease.

SUPPLEMENTAL MATERIAL

Supplemental material is available online only.
SUPPLEMENTAL FILE 1, PDF file, 0.4 MB.

REFERENCES

1. Alvar J, Vélez ID, Bern C, Herrero M, Desjeux P, Cano J, Jannin J, den Boer M, WHO Leishmaniasis Control Team. 2012. Leishmaniasis worldwide and global estimates of its incidence. PLoS One 7:1–12. https://doi.org/10.1371/journal.pone.0035671.

2. Drugs for Neglected Diseases initiative. 2018. Making medical history to meet the needs of neglected patients. Drugs for Neglected Diseases initiative, Geneva, Switzerland. https://www.dndi.org/wp-content/uploads/2019/07/DNDi_2018_AnnualReport.pdf.

206

3. Van Bocxlaer K, Caridha D, Black C, Vesely B, Leed S, Sciotti RJ, Wijnant GJ, Yardley V, Braillard S, Mowbray CE, Ioset JR, Croft SL. 2019. Novel benzoxaborole, nitroimidazole and aminopyrazoles with activity against experimental cutaneous leishmaniasis. Int J Parasitol Drugs Drug Resist 11:129–138. https://doi.org/10.1016/j.ijpddr.2019.02.002.

4. Zhang H, Collins J, Nyamwihura R, Ware S, Kaiser M, Ogungbe IV. 2018. Discovery of a quinoline-based phenyl sulfone derivative as an antitrypanosomal agent. Bioorg Med Chem Lett 28:1647–1651. https://doi.org/10.1016/j.bmcl.2018.03.039.

5. Carothers S, Nyamwihura R, Collins J, Zhang H, Park H, Setzer WN, Ogungbe IV. 2018. Bauerenol acetate, the pentacyclic triterpenoid from *Tabernaemontana longipes*, is an antitrypanosomal agent. Molecules 23:355. https://doi.org/10.3390/molecules23020355.

6. Mikus J, Steverding D. 2000. A simple colorimetric to screen drug cytotoxicity against *Leishmania* using the dye Alamar Blue. Parasitol Int 48:265–269. https://doi.org/10.1016/s1383-5769(99)00020-3.

7. Feitosa LM, da Silva ER, Hoelz LVB, Souza DL, Come JAASS, Cardoso-Santos C, Batista MM, Soeiro M. d N C, Boechat N, Pinheiro LCS. 2019. New pyrazolopyrimidine derivatives as *Leishmania amazonensis* arginase inhibitors. Bioorg Med Chem 27:3061–3069. https://doi.org/10.1016/j.bmc.2019.05.026.

8. Godinho JL, Simas-Rodrigues C, Silva R, Ürmenyi TP, de Souza W, Rodrigues JC. 2012. Efficacy of miltefosine treatment in *Leishmania amazonensis*-infected BALB/c mice. Int J Antimicrob Agents 39:326–331. https://doi.org/10.1016/j.ijantimicag.2011.11.008.

9. Santos CC, Lionel JR, Peres RB, Batista MM, da Silva PB, de Oliveira GM, da Silva CF, Batista D, Souza S, Andrade CH, Neves BJ, Braga RC, Patrick DA, Bakunova SM, Tidwell RR, Soeiro M. 2017. *In vitro*, *in silico*, and *in vivo* analyses of novel aromatic amidines against *Trypanosoma cruzi*. Antimicrob Agents Chemother 62:e02205-17. https://doi.org/10.1128/AAC.02205-17.

10. Katsuno K, Burrows JN, Duncan K, Hooft van Huijsduijnen R, Kaneko T, Kita K, Mowbray CE, Schmatz D, Warner P, Slingsby BT. 2015. Hit and lead criteria in drug discovery for infectious diseases of the developing world. Nat Rev Drug Discov 14:751–758. https://doi.org/10.1038/nrd4683.

11. Cal M, Ioset J-R, Fügi MA, Mäser P, Kaiser M. 2016. Assessing anti-*T. cruzi* candidates *in vitro* for sterile cidality. Int J Parasitol Drugs Drug Resist 6:165–170. https://doi.org/10.1016/j.ijpddr.2016.08.003.

12. Caridha D, Vesely B, van Bocxlaer K, Arana B, Mowbray CE, Rafati S, Uliana S, Reguera R, Kreishman-Deitrick M, Sciotti R, Buffet P, Croft SL. 2019. Route map for the discovery and pre-clinical development of new drugs and treatments for cutaneous leishmaniasis. Int J Parasitol Drugs Drug Resist 11:106–117. https://doi.org/10.1016/j.ijpddr.2019.06.003.

13. Ribeiro-Romão RP, Saavedra AF, Da-Cruz AM, Pinto EF, Moreira OC. 2016. Development of real-time PCR assays for evaluation of immune response and parasite load in golden hamster (*Mesocricetus auratus*) infected by *Leishmania (Viannia) braziliensis*. Parasit Vectors 9:361. https://doi.org/10.1186/s13071-016-1647-6.

207

Authors for correspondence:
Ifedayo Victor Ogungbe,
E-mail: ifedayo.v.ogungbe@jsums.edu;
Maria de Nazaré Correia Soeiro,
E-mail: soeiro@ioc.fiocruz.br

Phenotypic investigation of 4-nitrophenylacetyl- and 4-nitro-1H-imidazoyl-based compounds as antileishmanial agents

Camila C. Santos[1], Huaisheng Zhang[2], Marcos M. Batista[1], Gabriel M. de Oliveira[1], Kelly C. Demarque[1], Natália L. da Silva[3], Otacílio C. Moreira[3], Ifedayo Victor Ogungbe[2] and Maria de Nazaré Correia Soeiro[1]

[1]Laboratory of Cellular Biology (LBC), Oswaldo Cruz Institute (IOC/FIOCRUZ), 21040-360 Rio de Janeiro, RJ, Brazil; [2]Department of Chemistry, Jackson State University, Jackson, MS 39217-0510, USA and [3]Laboratory of Molecular Biology and Endemic Diseases, Oswaldo Cruz Institute (IOC/FIOCRUZ), 21040-360 Rio de Janeiro, RJ, Brazil

Abstract

Cutaneous leishmaniasis (CL) is a spectrum of clinical manifestations characterized by severe skin ulcerations that leads to social stigma. There are limited treatment options for CL, and the available drugs are becoming less efficacious due to drug resistance. More efficacious and safer antileishmanial drugs are needed. In this study, the biological effect of seven synthetically accessible nitroaromatic compounds was evaluated *in vitro* against amastigotes of *Leishmania amazonensis*, followed by *in vivo* evaluation using mouse models of CL. Two compounds (**6** and **7**) were active against amastigotes *in vitro* [half-maximal effective concentration (EC_{50}): 4.57 ± 0.08 and $9.19 \pm 0.68\,\mu M$, respectively], with selectivity indexes >50, and the other compounds were not selective. *In vivo*, compounds **6** and **7** ($10\,mg\,kg^{-1}$, twice a day for 14 days) failed to reduce skin lesion sizes and parasite loads determined by light microscopy of lesion *imprints* and quantitative polymerase chain reaction. Nevertheless, the *in vitro* leishmanicidal efficacy sustained their use as templates for nitroimidazole-based antileishmanial drug discovery programmes focusing on analogues with more suitable properties.

Introduction

Cutaneous leishmaniasis (CL) comprises a broad spectrum of clinical manifestations caused by over 20 different kinetoplastid *Leishmania* species transmitted by female sandflies (WHO, 2020). In Asia and Africa, most CL cases are caused by *Leishmania major* and *Leishmania tropica*, leading to self-limiting ulcers. In the Americas, the disease is caused by several species, including *Leishmania braziliensis*, *Leishmania mexicana*, *Leishmania guyanensis*, *Leishmania naiffi* and *Leishmania amazonensis*. The clinical presentations range from self-healing localized skin lesions to disfiguring mucocutaneous ulcerations (Martins *et al.*, 2014; de Vries *et al.*, 2015). Annually, about 1.2 million new CL cases are reported, and a significant number of patients develop severely disfiguring permanent scars, which results in social stigma and loss of economic productivity (Alvar *et al.*, 2012; Baileyid *et al.*, 2019). CL is one of the most mistreated illnesses among neglected tropical diseases (NTDs). The large variation of drug susceptibility among the diverse parasite species makes the drug discovery process even more difficult (de Vries *et al.*, 2015; Van Bocxlaer *et al.*, 2019).

The first-line treatment for CL includes pentavalent antimonials: sodium stibogluconate and meglumine antimoniate. Antimonials present several drawbacks in terms of efficacy, safety (cardiotoxicity and hepatotoxicity) and protracted periods of drug administration (Weisz, 2006). Alternative systemic agents include miltefosine, amphotericin B, pentamidine isethionate, paromomycin and granulocyte-macrophage colony-stimulating factor, limited by severe adverse effects (de Vries *et al.*, 2015). There is a need for safer, more selective and easily accessible therapies for CL.

A few new small molecules are currently in preclinical and clinical development against *Leishmania*. One example is the first-in-class kinetoplastid-selective proteasome inhibitor compound LXE408. LXE408 was discovered by Novartis with financial support from the Wellcome Trust. LXE408 is efficacious in the murine model of CL, and it is under clinical trial for the treatment of visceral leishmaniasis (Nagle *et al.*, 2020). Partnerships between not-for-profit research and private pharmaceutical companies for the research and development of new treatments for NTDs such as leishmaniasis are increasing (Katsuno *et al.*, 2015).

Some of the compounds in development include nitroaromatic compounds, which are historically used to treat several diseases caused by protozoans, for example, DNDI-8219, DNI-VL2098 and DNDI-0690 (Van Bocxlaer *et al.*, 2019). In this study, we envision that scaffold-driven and easily synthesizable nitroaromatic compounds based on prior art can facilitate rapid phenotypic screenings using *in vitro* and *in vivo* experimental models. The scaffolds were selected based on our ongoing research on the use of natural product-derived motifs in the design and development of antiprotozoal agents (Zhang *et al.*, 2018). The compounds were evaluated against the free amastigote forms (AFs) of *L. amazonensis* (strain *LTB0016*),

purified from paw lesion, followed by evaluation against the intracellular forms as well as on peritoneal macrophages (PMMs). The most selective were evaluated in *L. amazonensis*-infected BALB/c mice. The methods and results are presented below.

Materials and methods

Compounds: Dimethyl sulphoxide (DMSO, Merck) solutions (30 mM) of the compounds (Fig. 1) and miltefosine ≥98% (Sigma-Aldrich, St. Louis, USA) were diluted just before the *in vitro* experiments into RPMI-1640 medium (pH: 7.2–7.4) without phenol red (Sigma-Aldrich (St. Louis, USA), R7509) but supplemented with 1% L-alanyl-L-glutamine (GLUTAMAX I, Gilbco™), 1% penicillin–streptomycin 5000 U mL^{-1} (Gibco™, PEN-STR) and 10% heat-inactivated sterile-filtered fetal bovine serum (FBS), from Cultilab, Brazil. The concentration of DMSO was <0.6% for all *in vitro* experiments to prevent non-specific toxicity to host cells (Romanha *et al.*, 2010). For *in vivo* assays, compounds **6** and **7** were prepared daily in a solution composed of 5% Gum Arabic from acacia tree (Sigma-Aldrich, St. Louis, USA), 6% DMSO and 3% Tween™ 80 Surfact-Amps™ detergent solution (Thermo Scientific™). The reference drug, Milteforan™ (Mt™), was dissolved in sterile deionized water.

Parasite strain and mammalian host cell cultures

Leishmania amazonensis (strain *LTB0016*) was used throughout the study. AFs were purified from male BALB/c mice. Briefly, the foot paws were inoculated (subcutaneously) with 20 μL containing 10^6 amastigotes, and the animal skin lesions were aseptically removed 30 days post-infection (dpi). The parasites in the lesions were mechanically dispersed by pipetting and used for the assays. The compounds were tested on (1) extracellular AFs; (2) intracellular amastigote forms (IA) in PMMs and (3) BALB/c mouse models infected with amastigotes as recently described (Cardoso Santos *et al.*, 2021). PMMs were obtained from Swiss male mice (18–20 g) inoculated with 3% Brewer thioglycollate medium (Merck) previously diluted in water and autoclaved. After 4 days of stimulation, the cells were collected by rinsing the animals' peritoneum with RPMI 1640. The cells were subsequently seeded in 24- (3×10^5 cells well^{-1}) and 96-well (5×10^4 cells well^{-1}) plates for analysis of infection and cytotoxicity assays, respectively. Cell cultures were maintained at 37°C, 5% CO$_2$ atmosphere in RPMI 1640 medium (pH: 7.2–7.4) without phenol red, but supplemented with 1% L-glutamine, 1% (PEN-STR) and 10% FBS. Assays using AF were maintained at 32°C using RPMI culture medium containing 5% FBS.

Cytotoxicity and in vitro leishmanicidal analysis

The toxicity of the compounds on host cells was evaluated 24 h after PMMs were seeded into culture plates. The compounds (0–500 μM) were added to the wells and incubated as described above for 48 h, and cellular viability was evaluated using the AlamarBlue test (Invitrogen) according to the manufacturer's recommendations. The effect of the compounds (0–20 μM) on AFs was evaluated using 10^6 parasites per well (0.2 mL) for 48 h, and parasite viability assessed with AlamarBlue tests as reported (Mikus and Steverding, 2000; Santos *et al.*, 2020). Phenotypic screenings against IAs were performed by infecting 3×10^5 PMMs with 9×10^5 amastigotes, multiplicity of infection being 3. After 48 h of drug treatment, cultures were rinsed with saline, fixed 5 min with Bouin and stained for 15 min with Giemsa solution (Sigma-Aldrich (St. Louis, USA), 32884), filtered and diluted five times in distilled water (Santos *et al.*, 2018; Feitosa *et al.*, 2019). Samples were subsequently evaluated by

light microscopy and photographs were obtained by using a Zeiss AxioObserver MI microscope (Oberkochen, Germany). The percentage of infected host cells, the number of parasites per infected cell and the corresponding infection index were obtained. Parasites with well-defined nuclei and kinetoplasts were counted as surviving since irregular structures could mean parasites undergoing death. The results were expressed as % reduction in parasite burden, and the half-maximal effective concentration (EC$_{50}$) and 90% maximal effective concentration (EC$_{90}$) were calculated by non-linear regression analysis using GraphPad Prism v.9.1.2. All assays were run at least twice with three independent replicates each time.

Hep G2 viability assay

Hep G2 (CRL-11997™) cells were grown in complete growth medium (Dulbecco's modified Eagle medium: F12 containing L-glutamine and sodium bicarbonate, 10% FBS and 1% penicillin/streptomycin) incubated at 37°C in a 5% CO$_2$ environment. Cells were seeded into 96-well plates at 5×10^5 cells mL^{-1} and incubated for about 24 h. Cells were treated with the compounds prepared in DMSO for 72 h at a final concentration range of 160–1.2 μM in triplicates. Cell viability was assessed using the 3-(4,5-dimethylthiazol-2-yl)-2,5-diphenyl-2*H*-tetrazolium bromide assay as previously described (Zhang *et al.*, 2018). Podophyllotoxin was used as cytotoxicity control, and sodium dodecyl sulphate (10%) was used as assay control.

In vivo efficacy analysis

Male BALB/c mice (18–20 g) obtained from the animal facilities of ICTB (Institute of Science and Biomodels Technology, Fiocruz, RJ, Brazil) were housed five per cage, kept in a room at 20–24°C under a 12-light and 12-h dark cycle and provided with sterile water and chow ad libitum. Animals were subcutaneously inoculated with 5×10^5 amastigotes on the left foot paw (Godinho *et al.*, 2012). The treatment started 15 dpi, corresponding to the lesion onset (size diameter of 3–4 mm) (Van Bocxlaer *et al.*, 2019). The compounds were given for 14 days by oral gavage (100 μL) at 10 mg kg^{-1}, twice a day (q12h). Mt™ was administered at a standardized dose (40 mg kg^{-1}) once a day (q24h). The lesions were measured regularly in three dimensions (height, width and depth), and animals were euthanized at 31 dpi. Skin lesions aseptically removed were used for molecular analysis of parasite load by quantitative polymerase chain reaction (qPCR) and light microscopy inspections of *imprints* (Ribeiro-Romão *et al.*, 2016). All procedures were carried out in accordance with the guidelines established by the FIOCRUZ Committee of Ethics for the Use of Animals (CEUA L038/2017). Statistical analysis was conducted in GraphPad Prism v.9.1.2 by analysis of variance (ANOVA): (1) one-way Fisher's LSD test or (2) two-way unpaired *t*-test with Welch's correction, significance $P < 0.05$ [95% confidence interval (CI)].

Results

All experimental details are fully described in the Supplementary material. The compounds (Fig. 1) were synthesized as shown in Fig. S1 and diluted just before the *in vitro* experiments. First, the compounds were screened at 10 μM against extracellular amastigotes of *L. amazonensis* purified from male BALB/c paw lesions (Feitosa *et al.*, 2019) using colorimetric assays (AlamarBlue test, Invitrogen) (Mikus and Steverding, 2000; Godinho *et al.*, 2012). Two (**6** and **7**) out of the seven compounds caused a significant decline in the total number of live parasites (≥50% decrease compared to untreated parasites) with only 48 h of drug exposition.
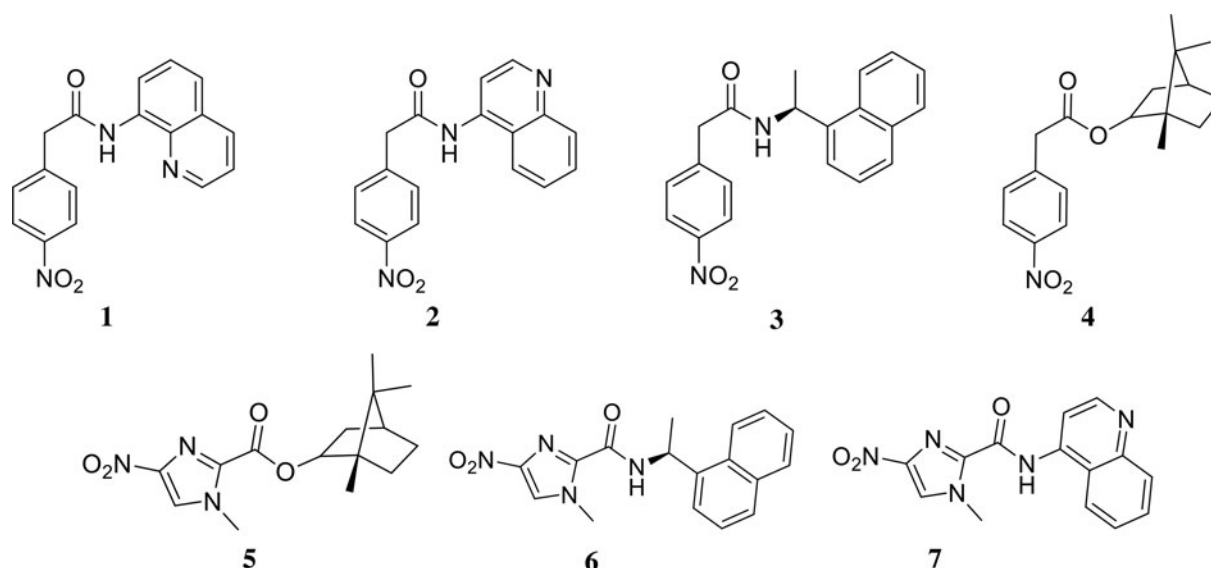
Fig. 1. Structures of the tested compounds.

Table 1. Phenotypic studies of compounds **6** and **7** against *Leishmania amazonensis* and their toxicity profile

Compound	EC_{50} $(\mu M)_{AF}$	EC_{50} $(\mu M)_{IA}$	CC_{50} $(\mu M)_{PMM}$	SI_{AF}	SI_{IA}	CC_{50} (μM) Hep G2
6	10.78 ± 0.80	4.57 ± 0.08 ($P = 0.027$)[a]	>500	>46	>109	>160
7	13.12 ± 1.70	9.19 ± 0.68	>500	>38	>54	>160
Miltefosine	4.37 ± 0.11	13.30 ± 3.03[a]	169.69 ± 5.07	>38	>12	–

AF, amastigote forms of *L. amazonensis* (LTB0016 strain) purified from animal lesions; IA, intracellular forms in peritoneal macrophages; SI, selective index.
EC_{50} is reported as mean and s.d. values.
[a]Statistical analysis was performed with GraphPad prism v.9.1.2 by ordinary ANOVA test.

Next, **6** and **7** were further analysed in dose–response assays. The EC_{50} values obtained were 10.78 ± 0.80 and 13.12 ± 1.70 μM, respectively (Table 1). Host cell viability showed that compounds did not exhibit any toxicity up to the highest tested concentration, leading to $CC_{50\ PMM}$ values >500 μM. Also, when cellular viability was assessed using Hep G2 cultures, no toxicity was observed ($CC_{50\ Hep}$ values >160 μM, Table 1). The selective antiparasitic activity was encouraging, and we decided to evaluate the compounds on intracellular amastigotes (IA) in PMMs (9×10^5 IA: 3×10^5 PMMs well^{-1}), which mimics typical infection in mammalian cells. Light microscopy analysis showed that **6** was about 3-fold more active compared to the reference drug (miltefosine, $P = 0.0273$). Its EC_{50} was 4.57 μM, and it is quite selective [selective index (SI) > 100]. Compound **6** also displayed low EC_{90} (9.14 μM) and caused a 92% decrease in PMM infection at 10 μM. Compound **7** is slightly less potent ($EC_{50} = 9.19$ μM and $EC_{90} = 17.2$ μM) with an SI of >50 (Table 1). Both compounds displayed an impressive leishmanicidal effect due to a drastic decrease in the number of parasites per cell and the ratio of infected cells at 20 μM (Fig. S2). These favourable results prompted us to conduct preliminary *in vivo* proof of concepts using both hit compounds.

In the *in vivo* experiment, we observed a gradual increase in skin lesion size of mice treated with the vehicle alone, attaining 438.8 ± 42.05 mm^3 at the endpoint (Fig. 2). Mice treated with compound **6** displayed similar lesions size (443.7 ± 47.76 mm^3, $P = 0.4798$), whereas a slight increase was observed using **7** (550.9 ± 30.23 mm^3, $P = 0.2398$), as compared to the vehicle-treated group. Mt™ achieved a 72% decrease in the size of skin lesions and significantly improved the clinical condition ($P < 0.0001$ (Fig. 2A and B). The qPCR standardization curves achieved all the desired efficiency and linearity coefficient criteria,

ranging between 93.2–91.4% and 0.98–0.99% for the parasite kDNA amplification (Fig. S3A) and mice GAPDH target (Fig. S3B), respectively. At 31 dpi, qPCR readout expressed as DNA equivalents per mg of tissue (14) showed a 5–10-fold increase in the parasite load of mice treated with **6** ($276\,526 \pm 40\,519$ eq. par mg^{-1} tissue, $P = 0.0208$) and **7** ($153\,765 \pm 54\,932$ eq. par mg^{-1} tissue, $P = 0.0829$) as compared to the vehicle-treated group ($27\,753 \pm 9539$ eq. par mg^{-1} tissue) (Fig. 2B). Mt™ completely suppressed (99.99%) parasite load (0.256 ± 0.1022 eq. par mg^{-1} tissue, $P = 0.0437$). The qPCR showed that the hit compounds lacked *in vivo* efficacy, and it was corroborated by a qualitative light microscopy analysis of lesions *imprints* (Fig. 2C). The findings clearly showed that both **6**- and **7**-treated animal groups have high parasitaemia coupled with the presence of lymphomononuclear diffuse infiltrates and several parasite niches inside mononuclear host cells (Fig. 2).

The lack of *in vivo* efficacy suggests low bioavailability of the compounds in mice. Low bioavailability is generally caused by impaired absorption or high clearance of compounds. Therefore, an *in silico* tool, pkCSM, was used to predict some critical absorption, distribution and metabolism parameters of **6** and **7**, comparing to miltefosine (Gleeson, 2008; Pires *et al.*, 2015). Compounds **6** and **7** do not violate Lipinski's rule. The $cLog\,Ps$ of **6** and **7** are 2.97 and 2.13, respectively, while that of miltefosine is 5.68 (Table 2). Since miltefosine is zwitterionic, its relatively high $cLog\,P$ is ideal for high intestinal absorption. Similarly, since compounds **6** and **7** have low molecular weights (324.34 and 297.27 g mol^{-1}, respectively) and are neutral molecules at physiological pH with relatively low $cLog\,P$, sufficient intestinal adsorption was expected from oral gavage. The predicted high intestinal absorption further supports this in addition to the
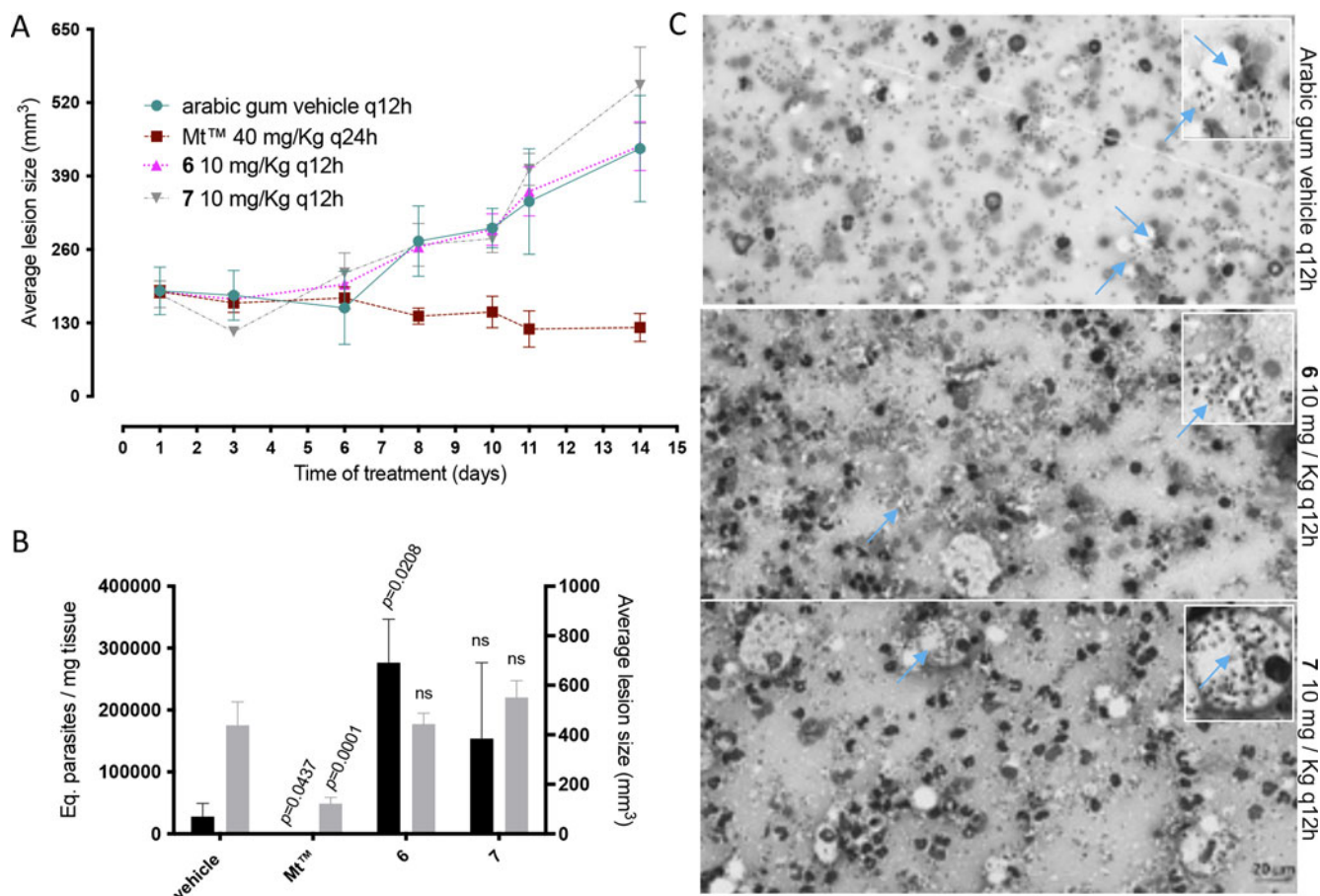
Fig. 2. Effect of **6** and **7** in CL experimental mouse models using BALB/c mice infected with *Leishmania amazonensis*. The graphics show: average lesion size during treatment (A), the correlation between parasite load by qPCR (black bars) and average lesion size measurements (grey bars) at 31 dpi (B), according to each experimental group. Light microscopy of lesion imprints of infected mice treated with vehicle and after administration of compounds **6** and **7** at 10 mg kg^{-1} q12h po (C). Arrow: intracellular parasites. Statistical analysis was performed with GraphPad prism v.9.1.2 by ANOVA test (95% CI). When *P* value ⩾0.05 = not significant (ns).

Table 2. Predicted ADME properties of **6**, **7** and miltefosine

Compound	cLog *P*	Caco2-permeability	Intestinal absorption[a]	VD$_{ss}$[a]	Fraction unbound[a]	CYP3A4 substrate
6	2.97	0.83	90.23	1.28	0.05	Yes
7	2.13	1.043	90.03	0.81	0.21	Yes
Miltefosine	5.68	1.049	92.02	0.36	0.16	Yes

[a]The predicted values are for humans.

predicted moderate to high Caco-2 permeability (0.83 and 1.04, respectively) from *in silico* Absorption, Distribution, Metabolism, and Excretion (ADME) calculations. Oral gavage was selected for this study because oral administration is the preferred route for the clinical use of new antileishmanial drugs. The predicted volume of distribution (VD$_{ss}$) is high and ideal for tissue distribution for both compounds. However, the predicted unbound fraction for **6** is relatively low (5%) and ideal for **7** (21%). Both compounds are predicted as CYP3A4 substrates, which suggest significant first-pass hepatic clearance and low overall plasma and tissue concentration. Therefore, a comparative pharmacokinetics study (oral and intravenous) can provide insight into plasma concentrations and bioavailability of both compounds in addition to determining the appropriate dosage and structural changes necessary for *in vivo* efficacy. Also, *in silico* toxicological analysis of both compounds suggests probable mutagenicity (positive for Ames tests) and potential to inhibit hERG II and that **6** is potentially hepatotoxic. However, animals treated

with compounds **6** and **7** did not show any observable side-effects. A cell proliferation assay using Hep G2 cells indicates that the compounds are not hepatotoxic at the tested concentrations (160–1.2 μM).

Discussion

Leishmania amazonensis is one of the most common *Leishmania* species in Brazil, known to cause a wide spectrum of pathologies, including highly severe and diffuse CL (Lainson *et al.*, 1994). Most CL patients live in impoverished communities with limited access to primary healthcare facilities (Okwor and Uzonna, 2016). The lack of access to primary healthcare typically means that the disease is usually at an advanced stage before medical intervention is sought, if available (Ruoti *et al.*, 2013). In this study, we explored the *in vitro* and *in vivo* leishmanicidal effects of compounds derived from two nitroaromatics scaffolds (4-nitrophenylacetyl and 4-nitro-1*H*-imidazolyl). The *in vitro* data demonstrated that

two 4-nitro-1*H*-imidazolyl compounds have acceptable selectivity indices (>50 for intracellular forms of *L. amazonensis*) as previously discussed by Caridha *et al.* (2019) as well as by Alcântara *et al.* (2018). Therefore, their antileishmanial activities were investigated further. The compounds were administered to BALB/c mouse models of CL for 14 days at a relatively low dose, starting at the onset of lesions (Godinho *et al.*, 2012). The results showed that the *in vitro* potency of the hit compounds **6** and **7** did not translate to desired *in vivo* efficacy. The measurements of the mouse lesions (using a paquimeter) and the molecular analysis of animal parasitism (qPCR) demonstrated a lack of *in vivo* activity of both compounds, whereas Mt™ suppressed both parameters, as reported (Van Bocxlaer *et al.*, 2019). The lack of *in vivo* efficacy of the tested compounds could be, at least in part, due to low bioavailability and/or high metabolic clearance. Nevertheless, as nitro-drugs are activated by *Leishmania* nitroreductases (NTR2) (Wyllie *et al.*, 2016), it is possible that **6** and **7** may be also activated in a similar way, and thus, the *in vitro* leishmanicidal efficacy supports their use as templates for nitroimidazole-based antileishmanial drug discovery programmes focusing on analogues that have the appropriate Target Product Profile (TPP) for new CL drugs, as recommended (Drugs for Neglected Diseases Initiative, 2020).

Supplementary material. The supplementary material for this article can be found at https://doi.org/10.1017/S0031182021002079

Conflict of interest. None.

Ethical standards. All procedures were carried out in accordance with the guidelines established by the FIOCRUZ Committee of Ethics for the Use of Animals (CEUA L038/2017).

References

Alcântara LM, Ferreira TC, Gadelha FR and Miguel DC (2018) Challenges in drug discovery targeting TriTryp diseases with an emphasis on leishmaniasis. *International Journal for Parasitology: Drugs and Drug Resistance* **8**, 430–439.

Alvar J, Vélez ID, Bern C, Herrero M, Desjeux P, Cano J, Jannin J and de Boer M (2012) Leishmaniasis worldwide and global estimates of its incidence. *PLoS ONE* **7**, e35671. doi: 10.1371/journal.pone.0035671

Baileyid F, Mondragon-Shem K, Haines LR, Olabi A, Alorfi A, Ruiz-Postigo JA, Alvar J, Hotez P, Adams ER, Vélez ID, Al-Salem W, Eaton J, Acosta-Serrano Á and Molyneux DH (2019) Cutaneous leishmaniasis and co-morbid major depressive disorder: a systematic review with burden estimates. *PLoS Neglected Tropical Diseases* **13**, 1–22.

Cardoso Santos C, Meuser Batista M, Inam Ullah A, Rama Krishna Reddy T and Soeiro MdNC (2021) Drug screening using shape-based virtual screening and *in vitro* experimental models of cutaneous leishmaniasis. *Parasitology* **148**, 98–104.

Caridha D, Vesely B, Van Bocxlaer K, Arana B, Mowbray CE, Rafati S, Uliana S, Reguera R, Kreishman-Deitrick M, Sciotti R and Buffet P (2019) Route map for the discovery and pre-clinical development of new drugs and treatments for cutaneous leishmaniasis. *International Journal for Parasitology: Drugs and Drug Resistance* **11**, 106–117.

de Vries HJC, Reedijk SH and Schallig HDFH (2015) Cutaneous leishmaniasis: recent developments in diagnosis and management. *American Journal of Clinical Dermatology* **16**, 99–109.

Drugs for Neglected Diseases Initiative (2020) Target product profile for cutaneous leishmaniasis. Retrieved from DNDi website: https://dndi.org/diseases/cutaneous-leishmaniasis/target-product-profile/ (accessed 30 January 2021).

Feitosa LM, da Silva ER, Hoelz LVB, Souza DL, Come JAASS, Cardoso-Santos C, Batista MM, Soeiro MDNC, Boechat N and Pinheiro LCS (2019) New pyrazolopyrimidine derivatives as *Leishmania amazonensis* arginase inhibitors. *Bioorganic and Medicinal Chemistry* **27**, 3061–3069. doi: 10.1016/j.bmc.2019.05.026

Gleeson MP (2008) Generation of a set of simple, interpretable ADMET rules of thumb. *Journal of Medicinal Chemistry* **51**, 817–834.

Godinho JLP, Simas-Rodrigues C, Silva R, Ürmenyi TP, De Souza W and Rodrigues JCF (2012) Efficacy of miltefosine treatment in *Leishmania amazonensis*-infected BALB/c mice. *International Journal of Antimicrobial Agents* **39**, 326–331.

Katsuno K, Burrows JN, Duncan K, van Huijsduijnen RH, Kaneko T, Kita K, Mowbray CE, Schmatz D, Warner P and Slingsby BT (2015) Hit and lead criteria in drug discovery for infectious diseases of the developing world. *Nature Reviews Drug Discovery* **14**, 751–758. doi: 10.1038/nrd4683

Lainson R, Shaw JJ, Silveira FT, de Souza AAA, Braga RR and Ishikawa EAY (1994) The dermal leishmaniases of Brazil, with special reference to the eco-epidemiology of the disease in Amazonia. *Memorias do Instituto Oswaldo Cruz* **89**, 435–443.

Martins ALGP, Barreto JA, Lauris JRP and Martins ACGP (2014) American tegumentary leishmaniasis: correlations among immunological, histopathological and clinical parameters. *Anais Brasileiros de Dermatologia* **89**, 52–58.

Mikus J and Steverding D (2000) A simple colorimetric method to screen drug cytotoxicity against Leishmania using the dye Alamar Blue®. *Parasitology International* **48**, 265–269.

Nagle A, Biggart A, Be C, Srinivas H, Hein A, Caridha D, Sciotti RJ, Pybus B, Kreishman-Deitrick M, Bursulaya B, Lai YH, Gao MY, Liang F, Mathison CJN, Liu X, Yeh V, Smith J, Lerario I, Xie Y, Chianelli D, Gibney M, Berman A, Chen YL, Jiricek J, Davis LC, Liu X, Ballard J, Khare S, Eggimann FK, Luneau A, Groessl T, Shapiro M, Richmond W, Johnson K, Rudewicz PJ, Rao SPS, Thompson C, Tuntland T, Spraggon G, Glynne RJ, Supek F, Wiesmann C and Molteni V (2020) Discovery and characterization of clinical candidate LXE408 as a kinetoplastid-selective proteasome inhibitor for the treatment of leishmaniases. *Journal of Medicinal Chemistry* **63**, 10773–10781.

Okwor I and Uzonna J (2016) Social and economic burden of human leishmaniasis. *American Journal of Tropical Medicine and Hygiene* **94**, 489–493.

Pires DEV, Blundell TL and Ascher DB (2015) pkCSM: predicting small-molecule pharmacokinetic and toxicity properties using graph-based signatures. *Journal of Medicinal Chemistry* **58**, 4066–4072.

Ribeiro-Romão RP, Saavedra AF, Da-Cruz AM, Pinto EF and Moreira OC (2016) Development of real-time PCR assays for evaluation of immune response and parasite load in golden hamster (*Mesocricetus auratus*) infected by *Leishmania* (*Viannia*) *braziliensis*. *Parasites and Vectors* **9**, 1–12.

Romanha AJ, de Castro SL, Soeiro M, Lannes-Vieira J, Ribeiro I, Talvani A, Bourdin B, Blum B, Olivieri B, Zani C, Spadafora C, Chiari E, Chatelain E, Chaves G, Calzada JE, Bustamante JM, Freitas-Junior LH, Romero LI, Bahia MT, Lotrowska M, Soares M, Andrade SG, Armstrong T, Degrave W and Andrade ZdA (2010) *In vitro* and *in vivo* experimental models for drug screening and development for Chagas disease. *Memorias do Instituto Oswaldo Cruz* **105**, 233–238.

Ruoti M, Oddone R, Lampert N, Orué E, Miles MA, Alexander N, Rehman AM, Njord R, Shu S, Brice S, Sinclair B and Krentel A (2013) Mucocutaneous leishmaniasis: knowledge, attitudes, and practices among Paraguayan communities, patients, and health professionals. *Journal of Tropical Medicine*, ID 538629. doi: 10.1155/2013/538629

Santos CC, Lionel JR, Peres RB, Batista MM, da Silva PB, de Oliveira GM, da Silva CF, Batista DGJ, Souza SMO, Andrade CH, Neves BJ, Braga RC, Patrick DA, Bakunova SM, Tidwell RR and Soeiro MdNC (2018) *In vitro*, *in silico*, and *in vivo* analyses of novel aromatic amidines against *Trypanosoma cruzi*. *Antimicrobial Agents and Chemotherapy* **62**, e02205-17.

Santos CC, Zhang H, Batista MM, de Oliveira GM, Demarque KC, da Silva-Gomes NL, Moreira OC, Ogungbe IV and Soeiro MdNC (2020) *In vitro* and *in vivo* evaluation of an adamantyl-based phenyl sulfonyl acetamide against cutaneous leishmaniasis models of *Leishmania amazonensis*. *Antimicrobial Agents and Chemotherapy* **64**, e01188-20.

Van Bocxlaer K, Caridha D, Black C, Vesely B, Leed S, Sciotti RJ, Wijnant GJ, Yardley V, Braillard S, Mowbray CE, Ioset JR and Croft SL (2019) Novel benzoxaborole, nitroimidazole and aminopyrazoles with activity against experimental cutaneous leishmaniasis. *International Journal for Parasitology: Drugs and Drug Resistance* **11**, 129–138.

Weisz G (2006) Making medical history. *Bulletin of the History of Medicine* **80**, 153–159.

World Health Organization, Regional Office for the Eastern Mediterranean (2020) *Infectious agent (s) WHO case definition incubation period communicability period epidemiology and risk factors Situation in countries affected by crisis in Syria*. pp. 1–7.

Wyllie S, Roberts AJ, Norval S, Patterson S, Foth BJ, Berriman M, Read KD and Fairlamb AH (2016) Activation of bicyclic nitro-drugs by a novel nitroreductase (NTR2) in *Leishmania*. *PLoS Pathogens* **12**, e1005971.

Zhang H, Collins J, Nyamwihura R, Ware S, Kaiser M and Ogungbe IV (2018) Discovery of a quinoline-based phenyl sulfone derivative as an antitrypanosomal agent. *Bioorganic and Medicinal Chemistry Letters* **28**, 1647–1651.

JAC-Antimicrobial Resistance

7-Aryl-7-deazapurine 3′-deoxyribonucleoside derivative as a novel lead for Chagas' disease therapy: *in vitro* and *in vivo* pharmacology

Camila Cardoso-Santos[1,2], Ludmila Ferreira de Almeida Fiuza[1], Cristiane França da Silva[1], Ana Lia Mazzeti[1], Roberson Donola Girão[1], Gabriel Melo de Oliveira[1], Denise da Gama Jaen Batista[1], Otacilio Cruz Moreira[3], Natália Lins da Silva Gomes[3], Louis Maes[2], Guy Caljon [iD] [2], Fabian Hulpia[4]†, Serge V. Calenbergh[4]‡ and Maria de Nazaré Correia Soeiro[1]*‡

[1]Laboratory of Cellular Biology (LBC), Oswaldo Cruz Institute (IOC/FIOCRUZ), 21040-360 Rio de Janeiro, RJ, Brazil; [2]Laboratory of Microbiology, Parasitology and Hygiene (LMPH), University of Antwerp, 2610 Wilrijk, Antwerp, Belgium; [3]Real Time PCR Platform RPT09A, Laboratory of Molecular Biology and Endemic Diseases, Oswaldo Cruz Institute (IOC/FIOCRUZ), Rio de Janeiro, RJ, Brazil; [4]Laboratory for Medicinal Chemistry (Campus Heymans), Ghent University, Ottergemsesteenweg 460, 9000 Gent, Belgium

*Corresponding author. E-mail: soeiro@ioc.fiocruz.br
†Present address: Janssen Pharmaceutica N.V., Turnhoutseweg 30, 2340 Beerse, Belgium.
‡Both authors made an equal contribution to the article.

Background: The protozoan *Trypanosoma cruzi* is auxotrophic for purines and causes Chagas' disease (CD), a neglected illness affecting >6 million people. Combining the 3-deoxyribofuranose part of cordycepin with the modified purine ring of a nucleoside 'hit' led to the discovery of 4-amino-5-(4-chlorophenyl)-N7-(3′-deoxy-β-D-ribofuranosyl)-pyrrolo[2,3-d]pyrimidine (Cpd**1**), revealing promising anti-*T. cruzi* activity.

Objectives: To further evaluate Cpd**1** *in vitro* and *in vivo* to fully assess its therapeutic potential against CD, covering cell culture sterilization through washout assays, drug combination with benznidazole and long-term administration in *T. cruzi*-infected mice.

Results: Although less susceptible to Cpd**1** than amastigotes, trypomastigotes present an impaired capacity to successfully establish intracellular infection of cardiac cultures. Combination of benznidazole with Cpd**1** indicated no interaction (additive effect) (FIC index = 0.72) while administration to mice at one-tenth of the optimal dose (2.5 mg/kg and 10 mg/kg for Cpd**1** and benznidazole, respectively) suppressed parasitaemia but failed to avoid mortality. Long-term treatment (60 days) gave a rapid drop of the parasitaemia (>98% decline) and 100% mice survival but only 16% cure. *In vitro* washout experiments demonstrated that although parasite release into the supernatant of infected cardiac cultures was reduced by >94%, parasite recrudescence did occur after treatment.

Conclusions: Parasite recrudescence did occur after treatment corroborating the hypothesis of therapeutic failure due to subpopulations of dormant forms and/or genetic factors in persister parasites involved in natural drug resistance.

Introduction

American trypanosomiasis, known as Chagas' disease (CD), was discovered in 1909 by Carlos Chagas and is largely ignored in terms of R&D investment.[1] CD is caused by the protozoan *Trypanosoma cruzi* and has two clinical disease stages. The asymptomatic or oligosymptomatic acute phase lasts up to 2 months and is characterized by patent parasitaemia. Due to an efficient host immune response, the parasitism is controlled but not eliminated and the disease moves to the chronic stage in which most infected people will present an asymptomatic profile. After years or even decades for reasons not fully known yet, 30%–40% develop progressive cardiac and/or digestive complications with fatal outcome.[2–4] The nature of the host–parasite interaction as well as the host's and parasite's genetic backgrounds may play a role in these symptomatic manifestations.[5] Also, comorbidity with the new coronavirus SARS-CoV-2 is a threat for chagasic patients.[6]

Substantial improvement in vector control was achieved in several endemic countries, and the number of new cases dropped considerably. However, it still poses a public concern due to remaining/new triatome foci,[7] besides congenital and oral transmissions.[8]

Only two old nitro-derivative drugs are available: benznidazole and nifurtimox.[9] Both have low efficacy in the chronic stage, limiting a therapeutic benefit for millions of infected individuals.[10,11] Also, they require long-term administration and elicit several side effects leading to low patient adherence or discontinuation of treatment. Finally, the nitro-drugs are contraindicated in pregnant women and in people suffering from liver or kidney failure or neurological disorders.[9,12,13] Novel, safer and more efficacious drugs are therefore mandatory.[14]

Like other trypanosomatid protozoa, *T. cruzi* depends on uptake of host purines as it is not able to synthetize purine rings *de novo*, rendering interference with the purine salvage attractive.[15,16] In fact, purine nucleoside analogues have a wide spectrum of activity, including antiviral,[17] antitumoral[18] and antibacterial.[19] Some nucleoside derivatives exhibit nano- and submicromolar *in vitro* activity against African trypanosomes,[20] *Leishmania* spp.[21] and *T. cruzi*.[22,23]

After revisiting the anti-trypanosomatid activity of the natural nucleoside antibiotic tubercidin and a series of C-7 modified analogues, phenyl-substituted compounds showed encouraging efficacy against intracellular forms of *T. cruzi,* being more potent than benznidazole, which motivated us to combine 7-substituted 7-deazapurine moieties with the carbohydrate group of cordycepin.[22,23] After rounds of optimization, compound **1** (Cpd**1**) or 4-amino-5-(4-chlorophenyl)-N7-(3′-deoxy-β-D-ribofuranosyl)-pyrrolo[2,3-d]pyrimidine (Figure 1) revealed outstanding efficacy in an acute mouse model of CD, however, without resulting in parasitological cure.[23]

In the present study, additional *in vitro* and *in vivo* protocols were performed to assess and improve the efficacy of Cpd**1**, including drug combination approaches with benznidazole, washout assays, pretreatment of trypomastigotes prior to incubation with host cells, and dose-titration and long-term (60 days) drug administration experiments in mice aiming to control parasite relapses.

Materials and methods

Compounds

Benznidazole (LAFEPE, Brazil) was used as reference drug. Cpd**1** (Figure 1) was synthesized as described by Hulpia *et al.*[23] The identity and purity of Cpd**1** was confirmed via ^1H NMR, ^{13}C, HRMS and analytical LC/MS respectively. The analytical data match those previously reported.[23] Purity of Cpd**1** was >95%. Stock solutions of benznidazole and Cpd**1** were prepared in 100% DMSO, with the final in-test concentration never exceeding 0.6% for *in vitro* experiments to avoid non-specific toxicity.[24]

Mammalian cell culture

Primary cultures of mouse embryonic cardiac cells (CC) were obtained as described.[25,26] L929 cell lines were cultivated (4.000 cells/well) in 96-well microplates at 37 °C in RPMI 1640 medium (Sigma–Aldrich).[27]

Parasites

Bloodstream trypomastigotes (BT) of Y strain (DTU II) were obtained as reported.[24] The trypomastigote forms of Tulahuen strain (DTU VI) expressing the *Escherichia coli* β-galactosidase gene were collected from the supernatant of L929 cell cultures previously infected (host: parasite cell ratio 10:1).[27] For both strains, purified parasites were added to RPMI 1640 medium supplemented with 5% FBS to perform assays at 37 °C in 5% CO_2.

In vitro assays

The infections were performed using parasite: host cell ratio 10:1, at least two assays in biological duplicate. Half inhibitory concentration (EC_{50}) and statistical analysis (95% CI of SD) were obtained through non-linear regression analysis by GraphPad Prism Version 9.1.0.

Pretreated BT forms

Bloodstream trypomastigotes were incubated for 24 h with Cpd**1** and benznidazole at their corresponding EC_{50} (23 ± 4 and 11.5 ± 1.1 µM, respectively).[23] Parasites were rinsed to remove compound, and the number of live and motile parasites determined by light microscopic quantification to adjust the parasite: host cell ratio. After 24 h of interaction, the infected CC were rinsed to get rid of non-internalized parasites, fixed with Bouin or submitted to additional incubation up to 72 h.[28] After fixation and staining with Giemsa, light microscopic analysis was performed to determine the number of infected host cells, parasites per infected cell and infection index (percentage of infected cells multiplied by the average number of intracellular parasites per infected host cell).

Washout assays

After 24 h of plating, CC were infected for 24 h at 37 °C with BT (Y strain). The cultures were rinsed to remove free parasites and treated for 168 h at 37 °C with the compounds at the non-toxic concentration of 5 µM in culture medium that was replaced every 48 h. After 168 h of drug exposure, the cultures were rinsed using PBS and drug-free culture medium was added for another 168 h of incubation. Parasites released into the medium were quantified using light microscopy.[22]
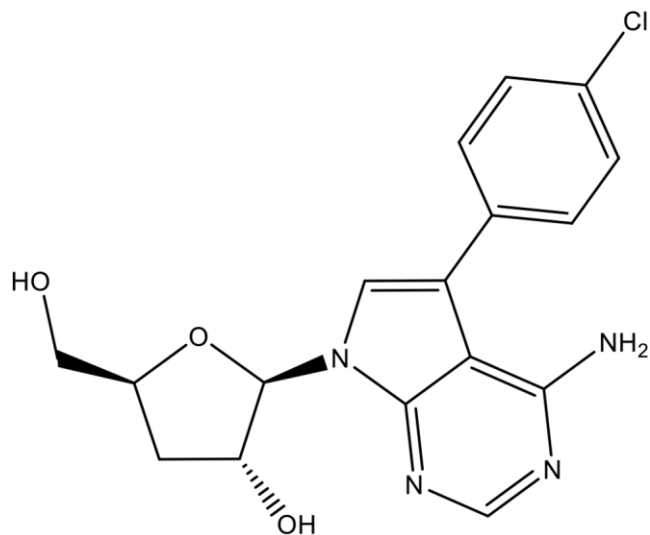
Figure 1. Chemical structure of Cpd**1**: 4-amino-5-(4-chlorophenyl)-N7-(3′-deoxy-β-D-ribofuranosyl)-pyrrolo[2,3-d]pyrimidine.

Drug combination assays

The association of benznidazole + Cpd**1** was assessed by colorimetric read-out using L929 cells that were infected for 2 h with trypomastigote forms (Tulahuen-β-gal strain), followed by rinsing the cultures to remove non-internalized parasites and further incubated for 24 h before drug administration using a fixed-ratio method.[29,30] Predetermined EC_{50} values were used to determine the top concentrations of each drug ensuring that EC_{50} fell at the midpoint of a seven-point 2-fold dilution series. The fixed ratios of 5:0, 4:1, 3:2, 2:3, 1:4 and 0:5 were used.[30,31] At least two independent experiments in triplicate were performed. The FIC index (FICI) at the EC_{50} of each drug was calculated as EC_{50} when in combination/EC_{50} of drug alone. The sum of FICI of each compound (ΣFICI) was obtained.[31] The mean ΣFICI (xΣFICI) was calculated as the average of ΣFICI. Isobolograms were built by plotting the FICI values. The ΣFICI was used to classify the nature of interaction as recommended by Odds:[30] synergy for xΣFICI ≤0.5, no interaction for xΣFICI 0.5–4 and antagonism for xΣFICI >4.

In vivo activity

Male Swiss Webster mice (18–20 g, 4–5 weeks of age) obtained from the animal facilities of the Institute of Science and Biomodels Technology (ICTB) Fiocruz were housed at a maximum of six per cage, kept in a specific-pathogen-free room at 20 °C to 24 °C under a 12 h light and 12 h darkness cycle, and provided sterilized water and chow *ad libitum*. The animals were acclimated for 7 days before starting the experiments. Infection was performed by intraperitoneal (IP) injection of 10^4 bloodstream trypomastigotes (BT) (Y strain). The animals were divided into the following groups ($n \geq 5$): untreated (infected but treated only with citrate buffer vehicle) and treated (infected and treated with the compounds). *T. cruzi* (Y strain)-infected mice were treated by oral gavage for 60 consecutive days (except for weekends) starting at 5 days post-infection (dpi), which corresponds to the parasitaemia onset, using 0.25–25 mg/kg (q12h) of Cpd**1** or 100 mg/kg/day benznidazole. Co-administration for 11 days at suboptimal doses of Cpd**1** (2.5 mg/kg/day) + benznidazole (10 mg/kg/day) was also performed. Benznidazole at 100 mg/kg/day as the optimal dose was run in parallel. Cpd**1** was diluted in 10% (v/v) EtOH, 0.1 M aqueous citrate buffer (pH 3.02, 1.8 mg/mL and then dosed according to body weight of the animals and drug concentration). The drug formulations were freshly prepared before each administration. Only mice with positive parasitaemia were used in the infected groups. Parasitaemia was individually checked by direct microscopic counting of parasites in 5 μL blood, and mice were examined daily for mortality until 261 dpi when blood was collected from surviving animals for qPCR analysis. Animal survival is expressed as the percentage survival rate at the endpoint. For blood qPCR analysis, 500 μL of blood was diluted in a 1:2 volume of guanidine solution and heated for 60 s in boiling water, followed by DNA purification using a High Pure PCR Template Preparation Kit (Roche Applied Science) and quantitative Realtime multiplex PCR assays. TaqMan probes were used for quantification of both *T. cruzi* satellite nuclear DNA and internal amplification control (IAC) (Figure S1, available as Supplementary data at *JAC-AMR* Online).[32] Standard curves were constructed for absolute quantification through the serial dilution of total DNA, ranging from 10^5 parasite equivalents to 1 parasite equivalents per mL of blood, obtained with a negative blood sample in guanidine-EDTA. Parasite load was then expressed as equivalent of parasite DNA per mL of blood.[33] All animal studies were carried out in strict accordance with the guidelines established by the FIOCRUZ Committee of Ethics for the Use of Animals (CEUA L038-2017).

Statistical analysis

Statistical analysis was performed using ANOVA with the level of significance set at $P \leq 0.05$.

Results

Pretreatment of BT

BT were incubated with EC_{50} of Cpd**1** or benznidazole. Drug-treated and untreated parasites were rinsed, and live and motile trypomastigotes quantified before infection of CC. After 24 h, infected cultures were rinsed to remove non-internalized trypomastigotes and followed-up for up to 72 h (Figure 2). Although not presenting high potency, Cpd**1** induced morphological alterations (round-shape like phenotype) suggestive of impaired fitness. When treated parasites were used to infect CC, although no major effect could be found after 24 h post-infection (hpi), a high and statistically significant ($P < 0.025$) drop in all parameters (percentage of infected host cells, parasites per infected cell and infection index rates) was observed for Cpd**1** pretreated trypomastigotes after 48 and 72 h of CC infection. With benznidazole pretreated parasites, the mean parasites per infected cell values gave a statistically relevant decrease ($P = 0.0135$) only at 48 hpi, while after 72 h all parameters were reduced ($P \leq 0.0093$) (Figure 2a–d). Cpd**1** and benznidazole interfere with parasite fitness, impairing the parasite's ability to successfully establish and sustain infection *in vitro*, affecting the proliferative capacity as clearly shown at 72 hpi with earlier and greater reduction rates triggered by Cpd**1** leading to >90% decrease in the infection indexes (Figure 2c).

Drug combination

In vitro effect of co-treatment of Cpd**1**[23] and benznidazole was assessed by colorimetric readout, using L929 cells infected with β-gal Tulahuen strain with a fixed-ratio method.[29–31] The result of xΣFICI equal to 0.72 obtained from Cpd**1** and benznidazole combination confers the status of a merely additive effect (Figure 3). The most promising results were obtained with the drug ratio of 1:4 (Cpd**1**: benznidazole) leading to the lowest IC_{50} and ΣFICI = 0.27 revealing a synergistic profile (Figure 3a). The isobolograms (Figure 3b) show the drug interaction profile with almost all ratios below the graphic threshold, except for 4:1 Cpd**1**: benznidazole ratio (ΣFICI = 1.11).

A proof-of-concept *in vivo* co-administration study was conducted with Cpd**1** and benznidazole in male Swiss mice infected with Y strain (five per group).[27] The chosen drug ratio was near to that which gave the best results *in vitro* (synergy profile reached at 1:4 of Cpd**1**: benznidazole ratio). The treatment started on the onset of parasitaemia (5 dpi) and was given orally for 11 days q12h for Cpd**1** and q24h for benznidazole. Mice also received each drug alone (Cpd**1** at 2.5 mg/kg and benznidazole 10 mg/kg), benznidazole at its optimal dose (100 mg/kg) or just vehicle.

Cpd**1**, benznidazole and their combination gave similar declines in parasite load, reaching ≥94% at peak on 8 dpi (Figure 3c). Cpd**1** (2.5 mg/kg) given alone resulted in 60% of animal survival. However, mice treated with benznidazole + Cpd**1** showed increased death rates (80% mortality) and enhanced toxicity, exhibiting urination impairment, prostatic and hunched postures with weight loss. All surviving mice in the different groups showed parasite relapse after interrupting drug administration. Based on the still promising results of Cpd**1** in monotherapy at 2.5 mg/kg producing >97% reduction in blood parasitaemia, follow-up experiments were conducted adopting dose-dependent analysis with reduced Cpd**1** doses and introducing long-term drug
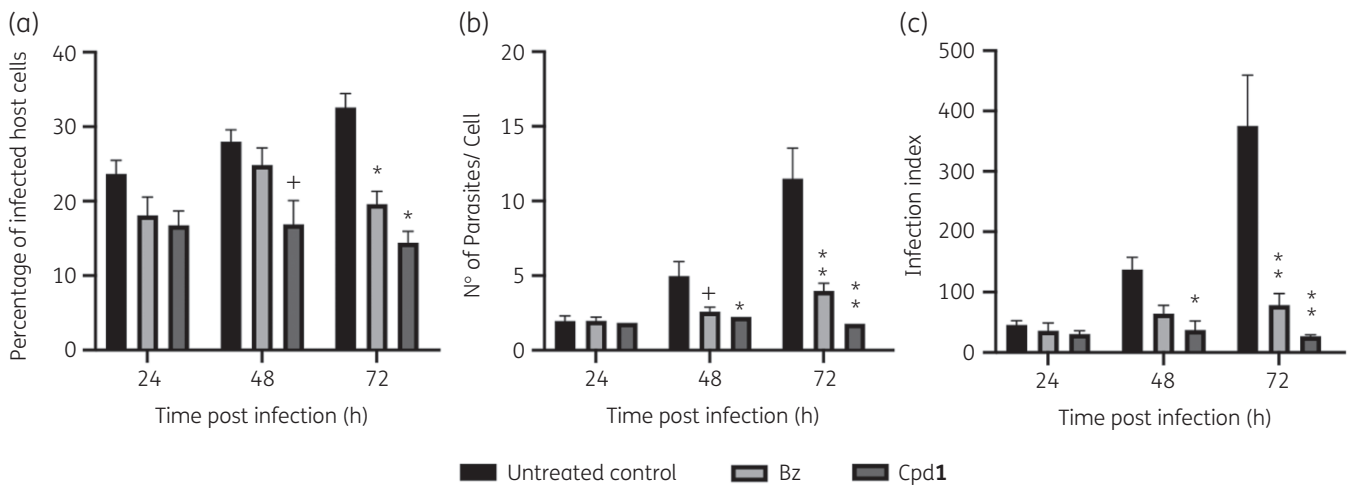
Figure 2. Pretreatment assays of *T. cruzi* (Y strain) with Cpd**1** or benznidazole (Bz) before parasite–host cell interaction. BT were treated or not (untreated control) for 24 h with the compounds (corresponding EC_{50}), rinsed and used to infect cardiac cell cultures (moi 10:1) in drug-free medium. The mean and standard deviation values were plotted according to percentage of infected host cells (a), number of parasites/cell (b) and infection index (c), at each timepoint. Statistical analysis was performed by two-way multiple comparison ANOVA Tukey's test ($P < 0.05$, 95% CI). $^{+}P < 0.05$, $^{*}P < 0.01$ and $^{**}P < 0.001$.

(a)

Drug ratio	EC_{50} (µM) Mean±SD		FICI		ΣFICI	xΣFICI
	Cpd1	Bz	Cpd1	Bz		
5:0	0.246±0.097					
4:1	0.101±0.064	1.396±0.097	0.41	0.70	1.11	
3:2	0.082±0.059	1.059±0.064	0.33	0.53	0.86	
2:3	0.056±0.045	0.695±0.059	0.23	0.35	0.57	0.72
1:4	0.028±0.024	0.319±0.045	0.11	0.16	0.27	
0:5		2.006±1.024				

(b)

(c)

Figure 3. *In vitro* (a and b) and *in vivo* (c) analysis of Cpd**1** and benznidazole (Bz) combination. Isobolograms (b) of FICI values (a) were calculated based on the *in vitro* activity (EC_{50}) against intracellular forms of *T. cruzi* after 168 h of drug exposure. (c) *In vivo* evaluation of Cpd**1** in *T. cruzi* mouse model of acute infection displaying parasitaemia levels of animal groups. Male Swiss mice were infected (IP) with 10^4 BT (Y strain) and drug administration (11 days) started at 5 dpi. Benznidazole alone was given at 100 mg/kg (q24h, orally) as a reference drug given at the optimal dose. Co-administration of benznidazole (10 mg/kg, q24h, orally) and Cpd**1** (2.5 mg/kg, q12h) is depicted (c). Control group received only vehicle (citrate buffer, q12h).
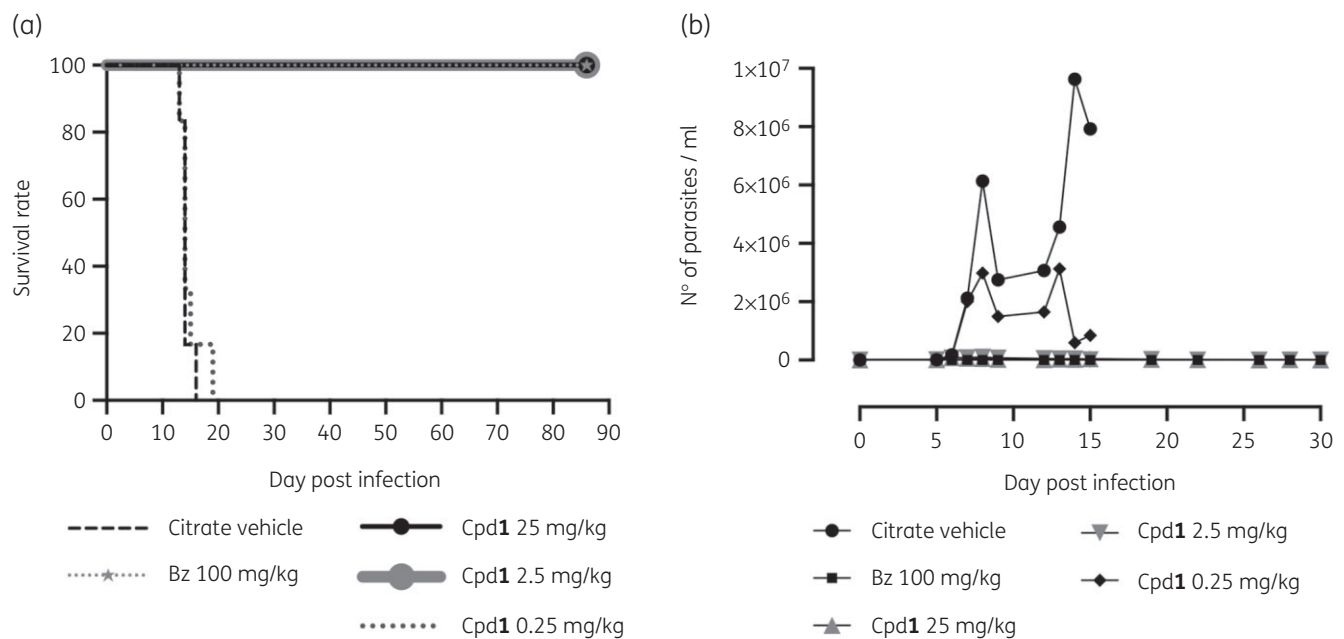
Figure 4. *In vivo* evaluation of Cpd**1** in a mouse model of *T. cruzi* acute infection. (a) Survival rates (b) and parasitaemia levels of animal groups. Male Swiss mice were infected (IP) with 10^4 BT (Y strain). Cpd**1** administration (0.25–25 mg/kg, q12h, orally) was initiated at 5 dpi and given for 60 days. Benznidazole (Bz) was included as a reference drug (100 mg/kg, once a day, orally). Control group received only vehicle (citrate buffer, q12h).

administration (60 days) aiming to check whether sterile cure could be achieved.

In vivo dose-titration and long-term drug administration

To check for parasite sterilization, an extended and dose-response protocol of drug administration (Cpd**1** at 0.25–25 mg/kg for 60 days, excluding weekends) was used in the same mouse model of acute *T. cruzi* infection. Cpd**1** showed a dose-dependent decrease in both parasitaemia levels and mortality rates (Figure 4a and b). At 25 and 2.5 mg/kg, a sharp drop (>98%) in blood parasite load was reached similarly to benznidazole at 100 mg/kg (Figure 4a). Cpd**1** at 0.25 mg/kg resulted in >50% of parasitaemia decline although was not able to prevent animal mortality (Figure 4a and b). Blood analysis by qPCR of the surviving animals[33] showed that the standard curves ranged from 10^5 to 1 parasite equivalents per mL of blood. Parasite load referred as equivalent of parasite DNA per mL of blood sample (parasite equivalents/mL) showed 76% efficiency for the satellite nuclear DNA target with a linearity coefficient of 0.996 (Figure S1b), confirming the sensitivity and accuracy of parasite detection and quantification. When infected mice were treated with benznidazole, three out of five animals presented negative blood qPCR (60% of cure) while another showed very low amplification (0.0247 parasite equivalents/mL) (Figure 5). Doses of 25 and 2.5 mg/kg of Cpd**1** also decreased the blood parasite load but to a lesser extent than benznidazole, with the one animal from the 25 mg/kg group displaying negative qPCR (17% cure) (Figure 5). Statistical analysis indicated no significant differences between the groups (ANOVA $P > 0.31$).

Washout assays

The number of released parasites into the supernatant of the infected CC cultures was quantified by light microscopy at different timepoints (Figure 6a).

Both benznidazole and Cpd**1**-treated cultures sustained a marked and significant ($P \leq 0.001$) reduction in the number of released parasites compared with the untreated samples, which showed a continuous discharge of trypomastigotes into the culture medium peaking at 144 h with >200 parasites/mL (Figure 6a and b). Before drug withdrawal, Cpd**1** fully suppressed parasitism (light microscopy observation) while benznidazole resulted in a minor parasite release ($\approx$8 parasites/mL) at 144 hpi (Figure 6a). After medium washout at 168 h, benznidazole and Cpd**1** were able to sustain the absence of parasites into the culture supernatant for 24 h, while untreated cultures exhibited >75 parasites/mL. However, trypomastigotes were identified from the fourth day of drug removal (at 264 h) in benznidazole as well as Cpd**1**-treated cultures. Benznidazole and Cpd**1** incubation resulted in comparable parasitism (6 and 10 parasites/mL, respectively) that was at least 19-fold lower than the untreated group (180 parasites/mL). At the last timepoint (312 h or sixth day post-drug withdrawal), the number of released parasites reached 15 (Cpd**1**) and 13 (benznidazole) parasites/mL, being about 15-fold lower than the untreated control (>210 parasites/mL). Washout assays demonstrated a similar capacity of Cpd**1** and benznidazole to temporarily arrest parasite growth, ensuing a reduced number of released parasites into the supernatant of infected CC cultures. Cpd**1** could not provide definite sterile cure (Figure 6) even upon using long-term drug administration (Figures 4 and 5).
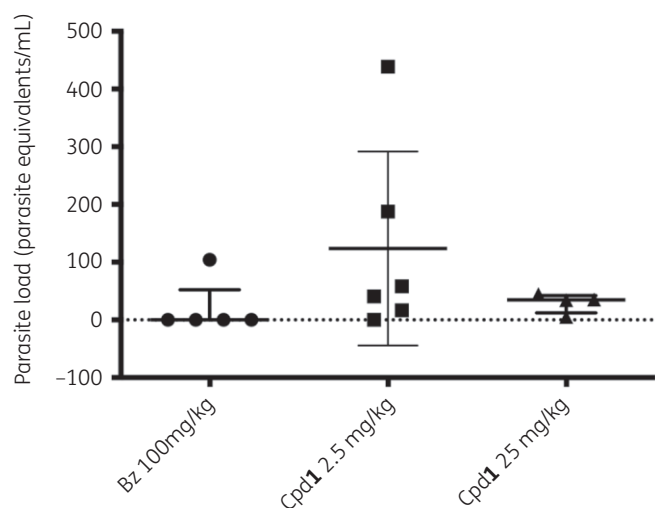
Figure 5. Blood qPCR analysis of surviving Swiss male mice infected with *T. cruzi* (Y strain) and orally treated with Cpd**1** (25 and 2.5 mg/kg, q12h) and benznidazole (Bz) (100 mg/kg, q24h). Parasite load is referred as number of parasite equivalents per mL. Each symbol on the scatter dot plots represents an individual value. Bars represent the median values and whiskers represent the IQR. Statistical analysis was performed by one-way multiple comparison ANOVA Tukey's test between the experimental groups ($P < 0.05$, 95% CI), all displaying no significant (ns) difference: $0.31 < P < 0.43$.
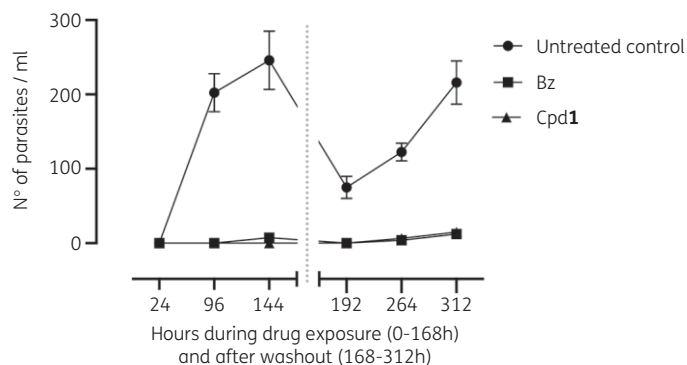
Figure 6. Washout experiments of *T. cruzi*-infected cardiac cell cultures. Number of culture-released trypomastigotes as a function of incubation time. Infected cultures (Y strain) were incubated for 168 h with Cpd**1** or benznidazole (Bz) and then another 168 h with drug-free medium before assay readout. Data represent mean $\pm$ SD of two independent experiments. The grey dotted line indicates the timepoint at which compound exposure is halted by changing to drug-free medium. Statistically significant values between control and treated groups were calculated by Welsh multiple non-parametric *t*-test ($P < 0.05$, 95% CI) and *P* values ranging $0.000009 \leq P < 0.002$.

Discussion

After more than five decades since their introduction into clinical use, the two old nitro-heterocyclic drugs benznidazole and nifurtimox still represent the only available therapeutic arsenal to treat CD patients who mostly belong to a vulnerable socioeconomic group.[34,35] This scenario has become even worse under the COVID-19 syndemic since the 30%–40% of chronic chagasic patients are more vulnerable to have a health outcome harmed or worsened by SARS-CoV-2

infection.[36] Despite these serious challenges, some recent improvement has been achieved based on the development of a paediatric formulation of benznidazole[37] and the potential adoption of a shorter benznidazole treatment regimen.[38] Fexinidazole, a 5-nitroimidazole derivative recently approved for sleeping sickness therapy[39] is under repurposing analysis in chronic chagasic patients.[40] However, no novel chemical entity has yet been discovered or implemented for this silent disease although some pre-clinical studies have reported promising drug candidates for CD, including nucleoside derivatives that act on the purine salvage pathway.[41] Our group reassessed the natural antibiotic tubercidin and a series of 7-substituted analogues aiming to identify novel hits against *Trypanosoma brucei*, the agent of human African trypanosomiasis.[42] Besides being very active against *T. brucei*, some phenyl-substituted analogues also presented high *in vitro* potency against *T. cruzi*, which motivated us to explore related 7-substituted 7-deazapurine moieties with the carbohydrate group of cordycepin (i.e. 3′-deoxy-D-ribofuranose). Some of these derivatives, such as Cpd**1**, showed an acceptable safety and efficacy profile in mouse models of *T. cruzi* infection.[23] Cpd**1** also presented desirable drug-like properties, such as good oral bioavailability and *in vitro* metabolic stability, which are essential characteristics to meet the target product profile (TPP) and allow potential clinical translation. The current criteria for 'hit' and 'lead' candidate selection for CD comprises definition of compound profile activity (preferably trypanocidal),[43] efficacy against different *T. cruzi* discrete type units (DTUs) and parasite forms relevant for human infection,[44,45] host–parasite interaction exploitation,[14] capacity to sustain sterile cure *in vitro*[43] and parasitaemia suppression and survival rates with sterile cure *in vivo*.[46] Most of these criteria were investigated for Cpd**1**, which proved highly potent against intracellular forms from different parasite strains and DTUs, displayed very high selectivity indices and was metabolically stable in the presence of mouse, human, rat and dog S9 microsomal fractions.[23] Unfortunately, no sterile cure could be achieved despite its high capacity to fully suppress parasitaemia and provide 100% survival in mouse models of *T. cruzi* infection.[23] As observed with other purine nucleoside analogues,[22,47,48] Cpd**1** was inactive against BT despite its outstanding intracellular activity in infected CC cultures ($EC_{50} = 0.029 \pm 0.006 \, \mu M$) and L929 cell lines ($EC_{50} = 0.25 \pm 0.17 \, \mu M$).[23] At that time, the lack of *in vivo* sterilization by Cpd**1** was attributed at least in part to its inefficacy towards BT and/or to the short treatment period (only 5 days) adopted in the initial *in vivo* study.

Our present study demonstrated that although Cpd**1** is not potent to induce a rapid lysis of the trypomastigotes, it induced morphological alterations (round-shape like phenotype) suggestive of impaired fitness. To check if these treated and surviving parasites were able to invade host cells and differentiate into intracellular amastigotes, a pretreatment assay on BT before infection was performed, revealing impairment of the parasite's ability to develop successfully in CC. The pre-incubation of BT with Cpd**1** followed by rinsing and quantification of the live and motile forms to normalize the parasite: host cell ratio resulted in reduced infection indices (>90%) as compared with the infected untreated parasites.

When evaluated in a mouse model of acute *T. cruzi* infection under extended drug administration (60 days), Cpd**1** could control parasitaemia but was unable to induce sterile cure as confirmed by qPCR analysis. *In vitro* washout assays corroborated these findings as Cpd**1** was unable to accomplish sterilization even though
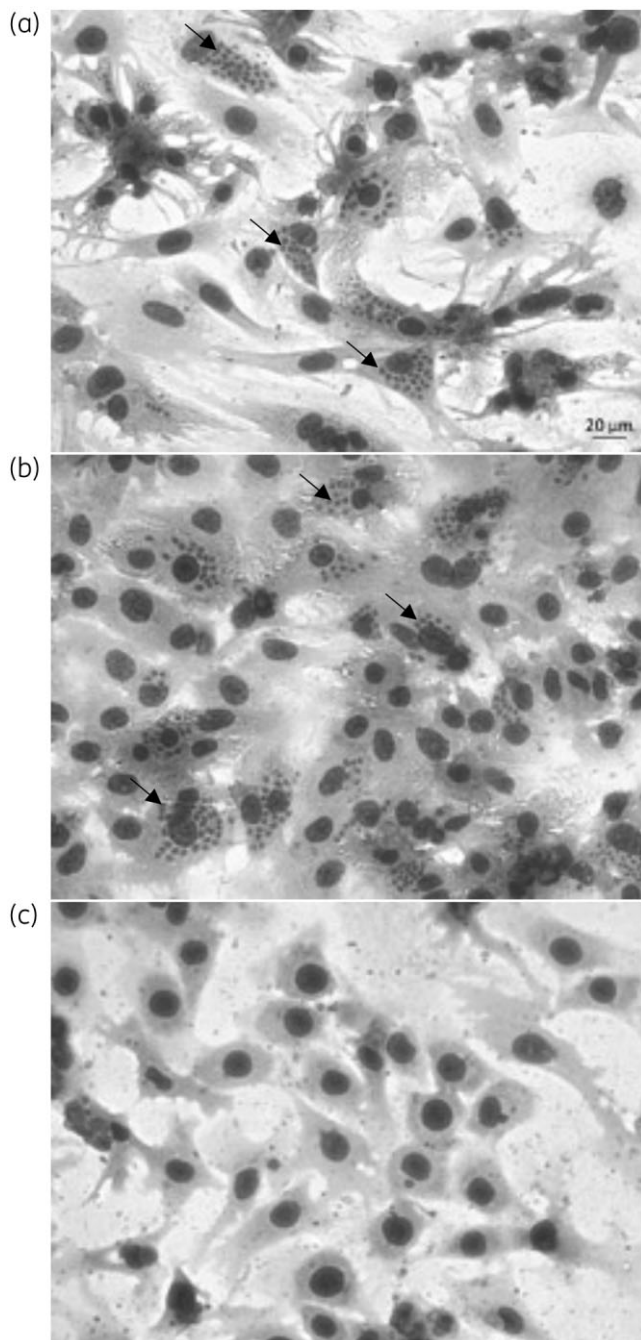
Figure 7. Light microscopy of cardiac cell cultures infected with *T. cruzi* (Y strain). (a) Untreated and treated with 1 µM (b) benznidazole (Bz) and (c) Cpd**1**. Arrows: intracellular amastigotes.

the number of released trypomastigotes was >90% lower than in untreated controls. As proposed in immunocompromised CD patients, it is probable that trypomastigotes can flourish from 'dormant forms' located in different organs, including the gastrointestinal tract.[49,50] Our present assays argue in favour of dormant forms since even though it was not able to lyse trypomastigotes, Cpd**1** impairs their ability to establish a successful *in vitro* infection. Despite outstanding efficacy against intracellular forms (Figure 7),

Cpd**1** is not able to induce *in vitro* sterilization possibly due to its inefficacy against low metabolic latent (e.g. dormant) parasites.

Drug combinations have largely been encouraged to find more efficient, shorter and safer therapies for different diseases, thereby also mitigating drug resistance.[51] For more than one decade, combinations of nifurtimox/eflornithine (NECT)[52] and sodium stibogluconate/paromomycin (SSG&PM)[53] have been successfully used for human African trypanosomiasis and cutaneous leishmaniasis, respectively, but no combination therapy is yet available for CD.[54] Our data indicated an additive interaction profile when benznidazole + Cpd**1** was used *in vitro*. *In vivo* co-administration using suboptimal doses of both agents did not improve the outcomes of each compound used separately. Conversely, an unexpected toxic profile (urination impairment) was noted that could be related to the exacerbation of renal injuries induced by *T. cruzi* infection.[55]

Our drug research complies with current criteria for drug discovery programmes of neglected tropical diseases (NTDs) caused by kinetoplastids, seeking robust proof-of-concept in preclinical trials to infer the ability of novel compounds to eliminate residual parasite nests and avoid relapses. The excellent efficacies of Cpd**1** on intracellular amastigote forms and on trypomastigote fitness were not enough to achieve *in vitro* nor *in vivo* sterilization, possibly due to the presence of dormant forms of *T. cruzi.* It remains attractive to evaluate nucleoside prodrugs to check for improved permeability and/or improved *in vivo* efficacy as novel drug candidates for NTDs like CD.

Transparency declarations

None to declare.

Supplementary data

Figure S1 is available as Supplementary data at *JAC-AMR* Online.

References

1 Coura JR, Dias JCP. Epidemiology, control and surveillance of Chagas disease:- 100 years after its discovery. *Mem Inst Oswaldo Cruz* 2009; **104**: 31–40.

2 World Health Organization. Key Facts. Chagas Disease (Also Known as American Trypanosomiasis). https://www.who.int/news-room/fact-sheets/detail/chagas-disease-(american-trypanosomiasis)

3 Rassi A Jr, Rassi A, Marcondes de Rezende J. American trypanosomiasis (Chagas disease). *Infect Dis Clin North Am* 2012; **26**: 275–91.

4 Dias JCP, Ramos AN Jr, Gontijo ED *et al.* 2nd Brazilian Consensus on Chagas disease, 2015. *Rev Soc Bras Med Trop* 2016; **49** Suppl 1: 3–60.

5 Pérez-Mazliah D, Ward AI, Lewis MD. Host-parasite dynamics in Chagas disease from systemic to hyper-local scales. *Parasite Immunol* 2021; **43**: e12786.

6 Zaidel EJ, Forsyth CJ, Novick G *et al.* COVID-19: implications for people with Chagas disease. *Glob Heart* 2020; **15**: 69.

7 Dias JVL, Queiroz DRM, Martins HR *et al.* Spatial distribution of triatomines in domiciles of an urban area of the Brazilian Southeast region. *Mem Inst Oswaldo Cruz* 2016; **111**: 43–50.

8 Drugs for Neglected Diseases Initiative. Annual Report 2018. Making Medical History to Meet the Needs of Neglected Patients. https://www.dndial. org/wp-content/uploads/2020/03/DNDi_2018_AnnualReport.pdf?x96328.

9 Castro JA, De Mecca MM, Bartel LC. Toxic side effects of drugs used to treat Chagas' disease (American trypanosomiasis). *Hum Exp Toxicol* 2006; **25**: 471–9.

10 Olivera MJ, Cucunubá ZM, Álvarez CA *et al.* Safety profile of nifurtimox and treatment interruption for chronic chagas disease in Colombian adults. *Am J Trop Med Hyg* 2015; **93**: 1224–30.

11 Drugs for Neglected Diseases Initiative. Disease Factsheet. Chagas Disease: Progress Towards Shorter, Better Treatments to Stop a Silent Killer. https://dndi.org/wp-content/uploads/2020/10/DNDi-Factsheet-Chagas-2019. pdf.

12 Berenstein AJ, Falk N, Moscatelli G *et al.* Adverse events associated with nifurtimox treatment for Chagas disease in children and adults. *Antimicrob Agents Chemother* 2021; **65**: e01135-20.

13 Urbina JA, Docampo R. Specific chemotherapy of Chagas disease: controversies and advances. *Trends Parasitol* 2003; **19**: 495–501.

14 Rao SPS, Barrett MP, Dranoff G *et al.* Drug discovery for kinetoplastid diseases: future directions. *ACS Infect Dis* 2019; **5**: 152–7.

15 Berg M, Van der Veken P, Goeminne A *et al.* Inhibitors of the purine salvage pathway: a valuable approach for antiprotozoal chemotherapy? *Curr Med Chem* 2010; **17**: 2456–81.

16 Ceron CR, Caldas RD, Felix CR *et al.* Purine metabolism in trypanosomatids. *J Protozool* 1979; **26**: 479–83.

17 Jordheim LP, Durantel D, Zoulim F *et al.* Advances in the development of nucleoside and nucleotide analogues for cancer and viral diseases. *Nat Rev Drug Discov* 2013; **12**: 447–64.

18 Galmarini CM, Mackey JR, Dumontet C. Nucleoside analogues and nucleobases in cancer treatment. *Lancet Oncol* 2002; **3**: 415–24.

19 Seki JI. Nucleoside analogues. *Nippon Nogeikagaku Kaishi* 1992; **66**: 1349–53.

20 Hulpia F, Campagnaro GD, Alzahrani KJ *et al.* Structure-activity relationship exploration of 3′-deoxy-7-deazapurine nucleoside analogues as anti-*Trypanosoma brucei* agents. *ACS Infect Dis* 2020; **6**: 2045–56.

21 Azzouz S, Lawton P. *In vitro* effects of purine and pyrimidine analogues on *Leishmania donovani* and *Leishmania infantum* promastigotes and intracellular amastigotes. *Acta Parasitol* 2017; **62**: 582–8.

22 Lin C, Hulpia F, Da Silva CF *et al.* Discovery of pyrrolo[2,3- b]pyridine (1,7-dideazapurine) nucleoside analogues as anti- *Trypanosoma cruzi* agents. *J Med Chem* 2019; **62**: 8847–65.

23 Hulpia F, Van Hecke K, França Da Silva C *et al.* Discovery of novel 7-aryl 7-deazapurine 3′-deoxy-ribofuranosyl nucleosides with potent activity against *Trypanosoma cruzi*. *J Med Chem* 2018; **61**: 9287–300.

24 Batista DDGJ, Batista MM, De Oliveira GM *et al.* Arylimidamide DB766, a potential chemotherapeutic candidate for Chagas' disease treatment. *Antimicrob Agents Chemother* 2010; **54**: 2940–52.

25 Meirelles MN, de Araujo-Jorge TC, Miranda CF *et al.* Interaction of *Trypanosoma cruzi* with heart muscle cells: ultrastructural and cytochemical analysis of endocytic vacuole formation and effect upon myogenesis *in vitro*. *Eur J Cell Biol* 1986; **41**: 198–206.

26 Timm BL, Da Silva PB, Batista MM *et al.* *In vitro* investigation of the efficacy of novel diamidines against *Trypanosoma cruzi*. *Parasitology* 2014; **141**: 1272–6.

27 Romanha AJ, de Castro SL, Soeiro M de NC *et al.* *In vitro* and *in vivo* experimental models for drug screening and development for Chagas disease. *Mem Inst Oswaldo Cruz* 2010; **105**: 233–8.

28 Coutinho L, Ferreira MA, Cosson A *et al.* Inhibition of *Trypanosoma cruzi* proline racemase affects host-parasite interactions and the outcome of *in vitro* infection. *Mem Inst Oswaldo Cruz* 2009; **104**: 1055–62.

29 Santos CC, Lionel JR, Peres RB *et al.* *In vitro*, *in silico*, and *in vivo* analyses of novel aromatic amidines against *Trypanosoma cruzi*. *Antimicrob Agents Chemother* 2018; **62**: e02205-17.

30 Odds FC. Synergy, antagonism, and what the chequerboard puts between them. *J Antimicrob Chemother* 2003; **52**: 1.

31 Trinconi CT, Reimão JQ, Coelho AC *et al.* Efficacy of tamoxifen and miltefosine combined therapy for cutaneous leishmaniasis in the murine model of infection with *Leishmania amazonensis*. *J Antimicrob Chemother* 2016; **71**: 1314–22.

32 Duffy T, Cura CI, Ramirez JC *et al.* Analytical performance of a multiplex real-time PCR assay using TaqMan probes for quantification of *Trypanosoma cruzi* satellite DNA in blood samples. *PLoS Negl Trop Dis* 2013; **7**: e2000.

33 Guedes-Da-Silva FH, Batista DDGJ, Meuser MB *et al.* *In vitro* and *in vivo* trypanosomicidal action of novel arylimidamides against *Trypanosoma cruzi*. *Antimicrob Agents Chemother* 2016; **60**: 2425–34.

34 Ben Beard C. Forgotten people, forgotten diseases: the neglected tropical diseases and their impact on global health and development. *Emerg Infect Dis* 2009; **15**: 510–1.

35 Hotez PJ, Damania A, Bottazzi ME. Central Latin America: two decades of challenges in neglected tropical disease control. *PLoS Negl Trop Dis* 2020; **14**: e0007962.

36 Nishiga M, Wang DW, Han Y *et al.* COVID-19 and cardiovascular disease: from basic mechanisms to clinical perspectives. *Nat Rev Cardiol* 2020; **17**: 543–58.

37 Drugs for Neglected Dieseases Initiative. LAFEPE Benznidazol 12,5 mg. Pediatric Dosage Form of Benznidazole. https://dndi.org/wp-content/uploads/ 2009/03/Product_launch_PaedBenz_dossier_ENG.pdf.

38 Molina-Morant D, Fernández ML, Bosch-Nicolau P *et al.* Efficacy and safety assessment of different dosage of benznidazol for the treatment of Chagas disease in chronic phase in adults (MULTIBENZ study): study protocol for a multicenter randomized Phase II non-inferiority clinical trial. *Trials* 2020; **21**: 328.

39 Lindner AK, Lejon V, Chappuis F *et al.* New WHO guidelines for treatment of gambiense human African trypanosomiasis including fexinidazole: substantial changes for clinical practice. *Lancet Infect Dis* 2020; **20**: e38–46.

40 Deeks ED. Fexinidazole: first global approval. *Drugs* 2019; **79**: 215–20.

41 Mazzeti AL, Capelari-oliveira P, Bahia MT *et al.* Review on experimental treatment strategies against *Trypanosoma cruzi*. *J Exp Pharmacol* 2021; **13**: 409–32.

42 Hulpia F, Mabille D, Campagnaro GD *et al.* Combining tubercidin and cordycepin scaffolds results in highly active candidates to treat late-stage sleeping sickness. *Nat Commun* 2019; **10**: 5564.

43 Cal M, Ioset JR, Fügi MA *et al.* Assessing anti-*T. cruzi* candidates *in vitro* for sterile cidality. *Int J Parasitol Drugs Drug Resist* 2016; **6**: 165–70.

44 Katsuno K, Burrows JN, Duncan K *et al.* Hit and lead criteria in drug discovery for infectious diseases of the developing world. *Nat Rev Drug Discov* 2015; **14**: 751–8.

45 Franco CH, Alcântara LM, Chatelain E *et al*. Drug discovery for Chagas disease: impact of different host cell lines on assay performance and hit compound selection. *Trop Med Infect Dis* 2019; **4**: 82.

46 Guedes-da-Silva FH, Batista DDGJ, Da Silva CF *et al*. Successful aspects of the coadministration of sterol 14α-demethylase inhibitor VFV and benznidazole in experimental mouse models of Chagas disease caused by the drug-resistant strain of *Trypanosoma cruzi*. *ACS Infect Dis* 2019; **5**: 365–71.

47 Lin C, Fiuza LFA, Santos CC *et al*. 6-Methyl-7-aryl-7-deazapurine nucleosides as anti-*Trypanosoma cruzi* agents: structure-activity relationship and *in vivo* efficacy. *ChemMedChem* 2021; **16**: 2231–53.

48 Bouton J, Ferreira de Almeida Fiuza L, Cardoso Santos C *et al*. Revisiting pyrazolo[3,4-d]pyrimidine nucleosides as anti-*Trypanosoma cruzi* and anti-leishmanial agents. *J Med Chem* 2021; **64**: 4206–38.

49 Pinesi HT, Strabelli TMV, Aiello VD. Case 4/2019 - 26-year-old man with congenital Chagas disease and heart transplantation. *Arq Bras Cardiol* 2019; **113**: 286–93.

50 Perez CJ, Lymbery AJ, Thompson RCA. Reactivation of Chagas disease: implications for global health. *Trends Parasitol* 2015; **31**: 595–603.

51 Sun W, Sanderson PE, Zheng W. Drug combination therapy increases successful drug repositioning. *Drug Discov Today* 2016; **21**: 1189–95.

52 Yun O, Priotto G, Tong J *et al*. NECT is next: implementing the new drug combination therapy for *Trypanosoma brucei gambiense* sleeping sickness. *PLoS Negl Trop Dis* 2010; **4**: e720.

53 Musa A, Khalil E, Hailu A *et al*. Sodium stibogluconate (SSG) & paromomycin combination compared to SSG for visceral leishmaniasis in East Africa: a randomised controlled trial. *PLoS Negl Trop Dis* 2012; **6**: e1674.

54 Urbina JA. Recent clinical trials for the etiological treatment of chronic Chagas disease: advances, challenges and perspectives. *J Eukaryot Microbiol* 2015; **62**: 149–56.

55 De Oliveira GM, Da Silva TM, Batista WS *et al*. Acute *Trypanosoma cruzi* experimental infection induced renal ischemic/reperfusion lesion in mice. *Parasitol Res* 2009; **106**: 111–20.

Revisiting Pyrazolo[3,4-d]pyrimidine Nucleosides as Anti-Trypanosoma cruzi and Antileishmanial Agents

Jakob Bouton, Ludmila Ferreira de Almeida Fiuza, Camila Cardoso Santos, Maria Angela Mazzarella, Maria de Nazaré Correia Soeiro, Louis Maes, Izet Karalic, Guy Caljon,* and Serge Van Calenbergh*

ACCESS | Metrics & More | Article Recommendations | Supporting Information

ABSTRACT: Chagas disease and visceral leishmaniasis are two neglected tropical diseases responsible for numerous deaths around the world. For both, current treatments are largely inadequate, resulting in a continued need for new drug discovery. As both kinetoplastid parasites are incapable of *de novo* purine synthesis, they depend on purine salvage pathways that allow them to acquire and process purines from the host to meet their demands. Purine nucleoside analogues therefore constitute a logical source of potential antiparasitic agents. Earlier optimization efforts of the natural product tubercidin (7-deazaadenosine) involving modifications to the nucleobase 7-position and the ribofuranose 3′-position led to analogues with potent anti-*Trypanosoma* brucei and anti-*Trypanosoma cruzi* activities. In this work, we report the design and synthesis of pyrazolo[3,4-d]pyrimidine nucleosides with 3′- and 7-modifications and assess their potential as anti-*Trypanosoma cruzi* and antileishmanial agents. One compound was selected for *in vivo* evaluation in an acute Chagas disease mouse model.

Extensive *T. cruzi* and *L. infantum* SAR exploration

ribofuranose 3′-modifications: R₁ = OH, H, F

7-position substituent screen R₂ = halogen, (hetero)aryl, ...

Inosine (R₃ = OH) and adenosine analogues (R₃= NH₂)
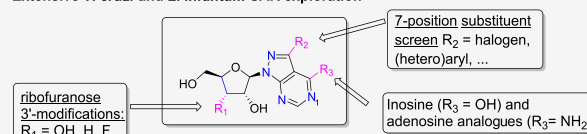
In vivo evaluation in acute Chagas disease mouse model

T. cruzi IC₅₀: 0.32 ± 0.02 μM
MRC-5SV2 IC₅₀: >64.0 μM

99% parasitemia reduction
83% survival rate
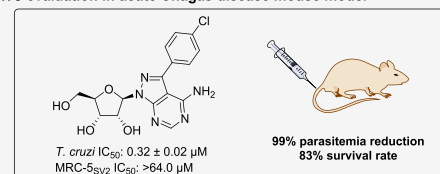
INTRODUCTION

Chagas disease and leishmaniasis are two vector-borne communicable diseases responsible for numerous deaths every year. Characterized by the WHO as neglected tropical diseases (NTDs), they occur mainly in populations living in poverty in developing regions around the world and have a severe impact on the lives of affected persons and their families.[1,2] Chagas disease, caused by *Trypanosoma cruzi*, is endemic to Latin America, where it is still one of the most prevalent public health problems.[3] Migration and specific transmission modes have enabled spreading beyond these geographical boundaries so that it is now considered a global issue.[4] Chagas disease starts with an acute symptomatic phase characterized by high-grade parasitemia, which progresses into an asymptomatic chronic state after a few weeks. While most people stay asymptomatic for life, 30−40% will develop severe clinical manifestations after 10−30 years.[5,6] Treatment options are limited to nifurtimox and benznidazole, two old drugs that have only limited efficacy in the chronic disease phase and are associated with severe adverse reactions.[4] At present, no vaccine is available and effective antiparasitic chemotherapy is therefore key in eliminating this NTD. As the current Chagas disease pipeline is almost empty, there is a pressing need to develop novel, safe, and efficacious treatments.[7−9]

Leishmaniasis is endemic in 60 countries with Brazil, India, Ethiopia, Somalia, Kenya, South Sudan, and Sudan reporting more than 90% of all cases.[10] Depending on the causative

Leishmania species, the disease exists in two main clinical forms: visceral leishmaniasis (VL) and cutaneous leishmaniasis (CL). The most severe systemic VL form is usually fatal within two years without treatment[11] and is responsible for up to 30 000 deaths every year. Most antileishmanial drugs have been repurposed from other indications. Efficacy varies by geographical region, and treatment courses are long, require hospitalization, and are associated with significant side effects.[12,13] While several new chemical entities with distinct mechanisms of action have recently entered clinical trials,[14−19] new drug discovery efforts are required to fill the early-stage pipeline.[20] New drug candidates should be suitable for field conditions and allow for global use, oral dosing, and a short treatment course.[7,20]

Unlike their mammalian hosts, both *Trypanosoma cruzi* and *Leishmania* spp. are obligate auxotrophs for purines, meaning that they lack *de novo* purine biosynthesis and rely on the salvage of purines (nucleosides and/or nucleobases) to meet their purine demand.[21−23] Consequently, they have developed a complex set of purine salvage enzymes that allows them to
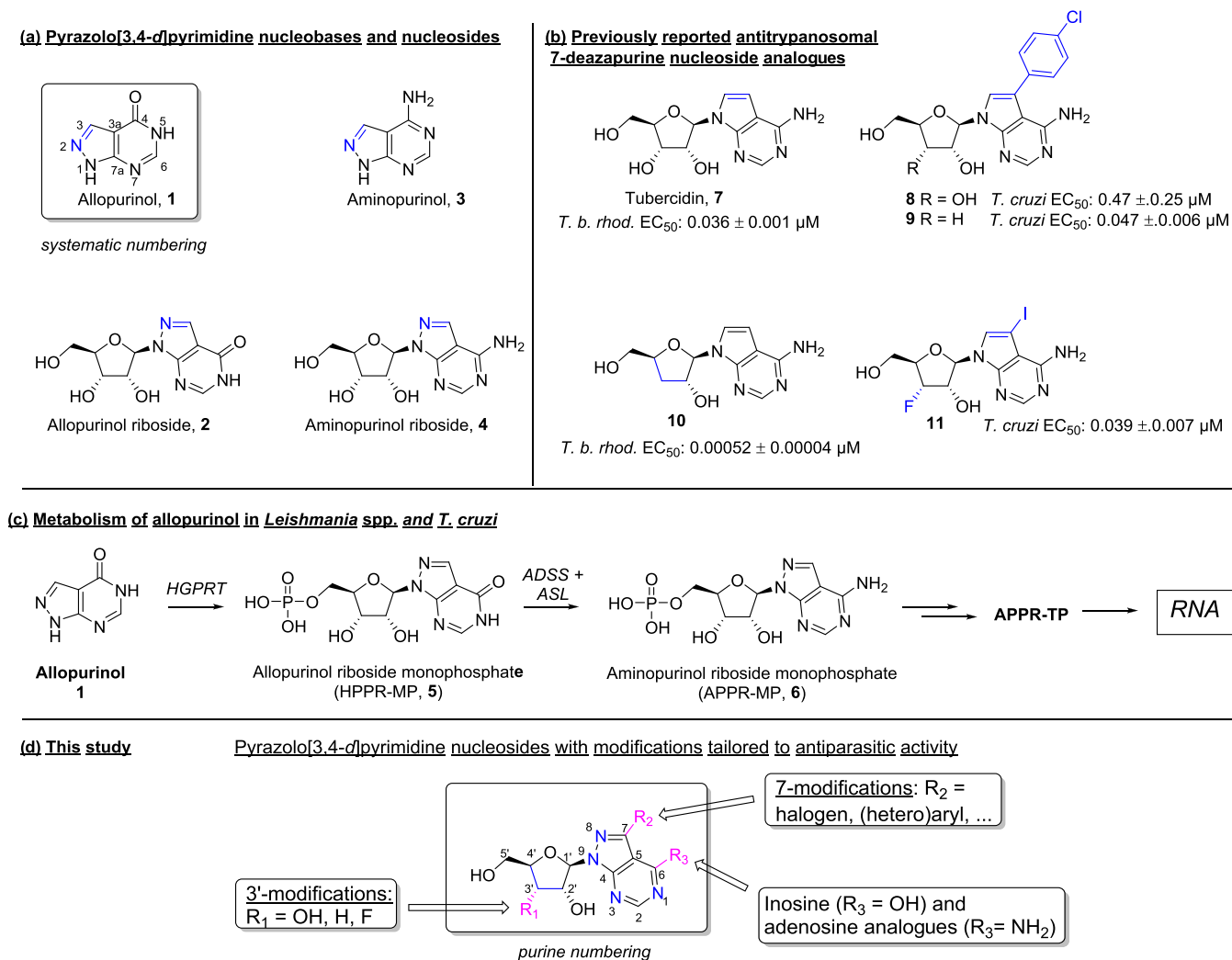
Figure 1. (a) Structures of pyrazolo[3,4-d]pyrimidines. (b) Antitrypanosomal 7-deazapurine nucleosides previously reported by our group. (c) Metabolism of allopurinol in *Leishmania* spp. and *T. cruzi*. (c, d) Pyrazolo[3,4-d]pyrimidine nucleosides reported in this study. Throughout the text, purine numbering is used as shown in Figure 1d, while in the experimental part, systematic numbering is employed.

acquire and process purines from their hosts. Purine (nucleoside) analogues therefore constitute an interesting pool of potential antiparasitic agents. Indeed, several analogues have been reported that act as inhibitors of enzymes of the purine salvage pathway or as "subversive substrates", which are selectively activated by salvage enzymes of the invading parasite.[24−26]

An example of such a subversive substrate is allopurinol (**1**) (Figure 1a). Next to its use as a treatment for gout, allopurinol inhibits the growth of several *Leishmania* and *Trypanosoma* species[27] in which its mechanism of action has been well-investigated.[28,29] It is selectively metabolized by the parasite to inosine- and adenosine-like nucleotide derivatives **5** and **6** and ultimately to an ATP analogue (i.e., APPR-TP) that is incorporated in RNA (Figure 1c).[28−30] Allopurinol has been evaluated in humans for VL treatment with mixed results. Although it achieved full cures in some patients, it was not satisfactory in monotherapy as first-line treatment due to its static rather than cidal character.[31] Nevertheless, allopurinol is still used in certain combination regimens for the treatment of CL,[11,32,33] and it is the treatment of choice for VL and CL in dogs.[34] Allopurinol has also been investigated for the treatment of Chagas disease with mixed outcomes.[35−37] For example, it

proved effective in treating reactivation after heart transplantation.[38,39] Both in leishmaniasis[33,40−42] and in Chagas disease,[43−45] allopurinol has demonstrated synergism with currently used drugs, demonstrating that a nucleobase/nucleoside analogue could be a valuable addition to the therapeutic arsenal. The *in vitro* antileishmanial activity of the ribonucleoside of allopurinol (**2**) is several times higher than allopurinol, but **2** was not further evaluated *in vivo* due to production difficulties and limited benefit over allopurinol.[46−48] The 6-amino congeners aminopurinol **3** and riboside derivative **4** (Figure 1a) were generally more active *in vitro* than allopurinol and **2**,[46,49,50] which may be due to faster conversion to the same active triphosphate. However, **3** and **4** suffered from cytotoxicity and selectivity concerns. Yet, Avila et al. found aminopurinol to be effective in animal models of both VL and Chagas disease at dosages as much as 300-fold lower than used for allopurinol and well below the toxic dose in humans.[46,51] Despite these promising data, neither aminopurinol **3** nor its ribonucleoside **4** was further evaluated for the treatment of leishmaniasis or Chagas disease.

Our group recently reported several 7-deazapurine nucleosides derived from the natural product tubercidin (**7**) that display potent activity against *Typanosoma brucei* and *T. cruzi*

Scheme 1. Synthesis of Ribofuranose-Modified Pyrazolo[3,4-d]pyrimidine Nucleosides[a]
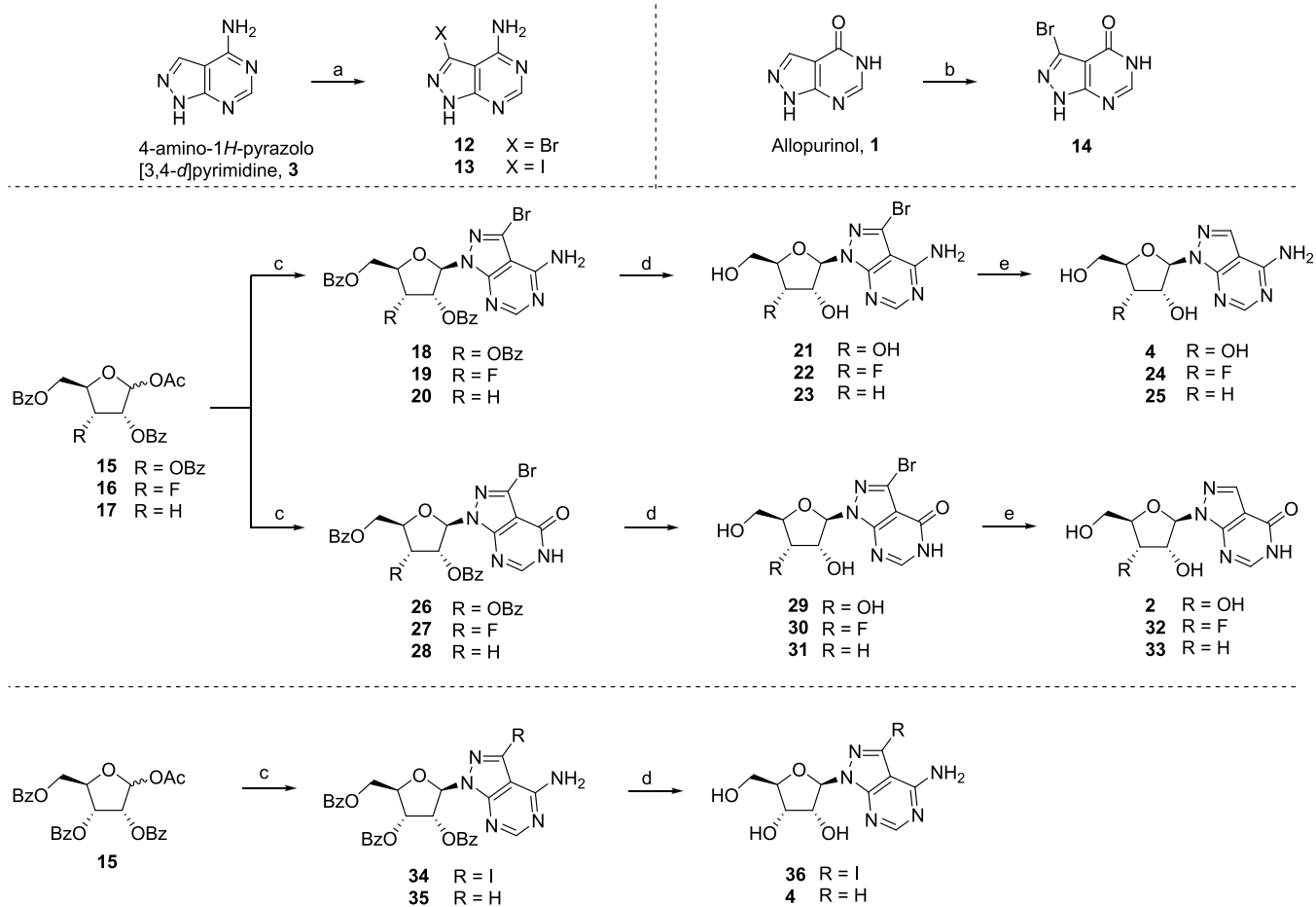
[a]Reagents and conditions: (a) NBS, DMF, 60 °C, 91% (for **12**), NIS, DMF, 80 °C, 93% (for **13**); (b) NBS, water, 90 °C, 87%; (c) **12** (for **18**–**20**), **14** (for **26**–**28**), or **13** (for **34**) BF₃·OEt₂, MeNO₂, reflux, 77% (**34**); (d) 0.5 M NaOMe in MeOH, 70% over 2 steps (**21**), 19% over 2 steps (**22**), 20% over 2 steps (**23**), 38% over 2 steps (**29**), 11% over 2 steps (**30**), 6% over 2 steps (**31**), 64% (**36**); (e) Pd/C, H₂, 1 M aq. NaOAc, MeOH, 61% (**4**), 82% (**24**), 66% (**25**), 54% (**2**), 83% (**32**), 80% (**33**).

([Figure 1]b).[52−56] The introduction of selected substituents on the 7-position (as in **8, 9**) led to selective anti-*T. cruzi* and anti-*T. brucei* agents.[52] Further deletion of the hydroxyl group on position 3′ afforded compound **10**, which was able to fully cure mice with CNS-stage sleeping sickness,[55] and **9**, which displayed high potency against *T. cruzi*.[53] A fluorine atom in position 3′ also proved favorable, with **11** displaying high anti-*T. cruzi* activity.[57] Compound **9** was evaluated in a Chagas mouse model but failed to deliver sterile cure. Furthermore, none of these 7-deazapurine nucleosides displayed selective activity against the phylogenetically related *Leishmania*, which is remarkable given that several nucleoside analogues display antileishmanial potential,[47,48,58−61] and many nucleosides combine antichagasic and antileishmanial activities.[46,48,61] Nevertheless, known antileishmanial nucleoside analogues (*e.g.*, the pyrazolo[3,4-d]pyrimidines (*vide supra*), carbocyclic inosine,[62] 9-deazainosine,[58] Formycin B[58]) contain nucleobase surrogates other than 7-deazapurine, leading us to assume that a 7-deazapurine base is detrimental for antileishmanial activity.

In the search for nucleoside analogues with improved antileismanial activity, we decided to explore nucleosides featuring a pyrazolo[3,4-d]pyrimidine (8-aza-7-deazapurine) nucleobase. Next to 7-deazapurines, pyrazolo[3,4-d]-pyrimidines are the only purine isosteres that allow

derivatization *via* 7-modifications,[63,64] such as the ones found beneficial to increase the potency and selectivity of (3′-deoxy)tubercidin. Compared to tubercidin **1**,[65] aminopurinol riboside **4** is significantly less toxic.[51] Although several 7-modified and 3′-modified pyrazolo[3,4-d]pyrimidine nucleosides have been reported,[66−68] they have not been explored for antiparasitic activity. One exception is 7-bromo-allopurinol riboside, which proved more potent than allopurinol.[69]

In this study, we describe the synthesis and initial evaluation of a library of 7-substituted and ribofuranose-modified pyrazolo[3,4-d]pyrimidine nucleosides, comprising both inosine-like (allopurinol riboside) and adenosine-like (aminopurinol riboside) analogues. The structure−activity relationships for anti-*T. cruzi* and antileishmanial activity are discussed, and one analogue was evaluated in an acute Chagas disease mouse model.

■ RESULTS AND DISCUSSION

Chemistry. The required brominated and iodinated nucleobase analogues **12** and **13** were readily obtained from aminopurinol **3** *via* reaction with *N*-bromosuccinimide (NBS) or *N*-iodosuccinimide (NIS) in *N,N*-dimethylformamide (DMF) at elevated temperature ([Scheme 1]). While we were also interested in the chloro and fluoro derivatives,

225

Scheme 2. Reagents and Conditions: (a) NBS, DMF, 50 °C; (b) NaOMe, MeOH, 70 °C, 51% Over 2 steps; (c) 38, KOH, TDA-1, MeCN, 8%; (d) 7 N NH$_3$ in MeOH, 90 °C, 76%; (e) H$_2$, Pd(OH)$_2$/C, NaOAc, MeOH, 46%
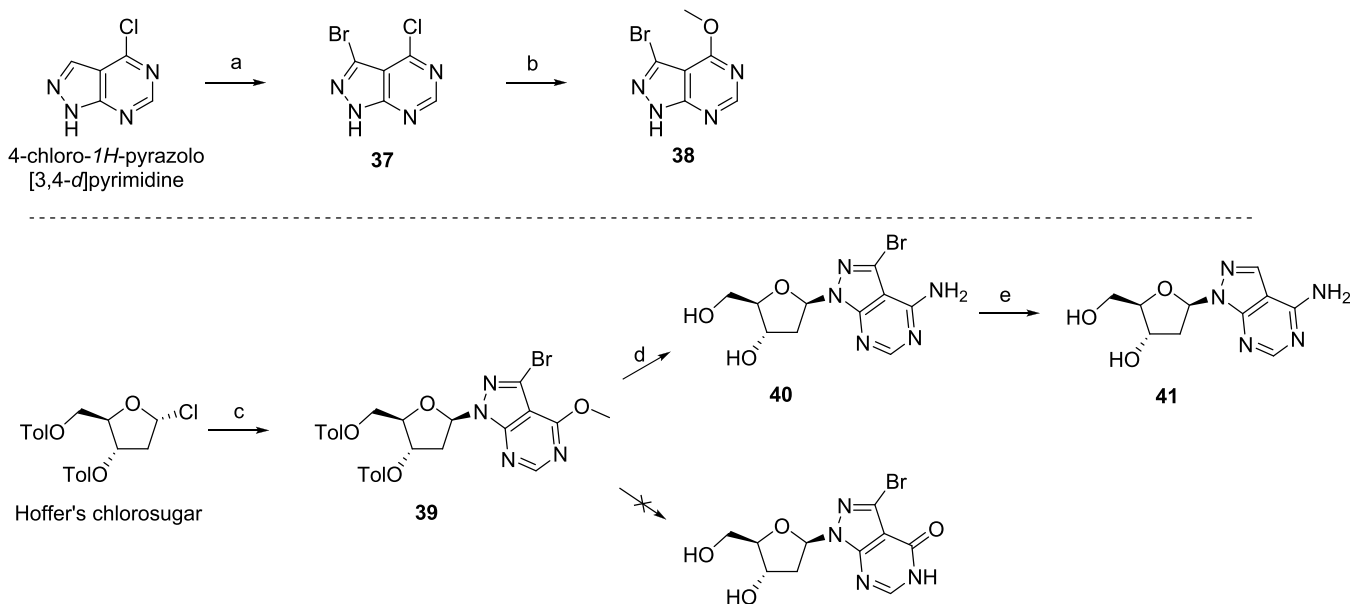
chlorination of aminopurinol **3** with N-chlorosuccinimide (NCS) or fluorination with diethylaminosulfur trifluoride (DAST) failed to deliver the desired halogenated heterocycles. Bromination of allopurinol with bromine in water at 90 °C afforded **14**.

7-Bromoallopurinol **14** and 7-bromoaminopurinol **12** were coupled with 1-O-acetyl-2,3,5-tri-O-benzoyl-β-D-ribofuranose, its 3′-deoxy counterpart **17**,[53] and 3′-deoxy-3′-fluoro analogue **16**.[57] Coupling of these three donors with 7-bromoaminopurinol **12** was performed with BF$_3$·OEt$_2$ in refluxing nitromethane, as described for **18**.[69] For the 7-bromoaminopurinol nucleosides **18**−**20**, a single product was obtained and no regioisomers were observed. Deprotection with sodium methoxide resulted in **21**−**23**, and reductive dehalogenation with H$_2$ and Pd/C in buffered methanol afforded **4**, **24**, and **25**. Remarkably, the combined glycosylation-deprotection yields were much lower (~20%) for the 3′-modified analogues compared to that of the ribofuranose **4** (~70%). The correct regiochemistry of the final compounds was confirmed via comparison of the ^{13}C NMR spectra of **24** and **25** with that of the literature compound **4**. The chemical shifts of C-7 (~133 ppm) and C-5 (~154 ppm) (systematic numbering) were identical to reported values, whereas in the N-8 regioisomer, C-7 would be shifted upfield about 10 ppm and C-5 shifted downfield about 5−6 ppm.[70,71] In the ^{1}H-^{13}C HMBC spectra, H-1′−C-7 coupling was absent, providing further evidence of the desired N-9 regiochemistry.

7-Bromoallopurinol **14** was glycosylated under the same conditions, but for each donor three different products with the same mass were observed on thin-layer chromatography (TLC), corresponding to the N-9, N-8, and N-1 regioisomers. The higher-running, less polar spot was the major product and was presumed to be the correct regioisomer[72] and was isolated. Glycosylation yields were generally lower (~50%) than for the corresponding aminopurinols. The correct regiochemistries of **32** and **33** were verified via comparison of their ^{13}C NMR spectra with that of **2**.[72] Compared to the 6-aminonucleosides, the upfield shift of C-7 in the N-8 isomer is reported to be less pronounced,[72] but the values of C-7 (~135 ppm) and C-5

(~148 ppm) (systematic numbering) were again very similar. Similarly, in this case, H-1′−C-7 coupling was again absent in the ^{1}H-^{13}C HMBC spectra, further confirming N-9 attachment of the heterocycle.

Glycosylation of **15** with 7-iodoaminopurinol afforded **34** in high yield, and deprotection in methanolic ammonia furnished **36**. Both **34** and **36** were used for further modifications (vide infra). Compound **4** could also be obtained from direct glycosylation of 4-aminopyrazolo[3,4-d]pyrimidine, followed by deprotection.

The 2′-deoxy analogues were prepared as described by Seela et al. (Scheme 2).[64,73−75] Compound **38** was obtained efficiently by bromination of 4-chloro-1H-pyrazolo[3,4-d]-pyrimidine with NBS, followed by nucleophilic aromatic substitution with sodium methoxide. Anion glycosylation of **38** with commercially available Hoffer's chlorosugar afforded **39** in 8% yield. Simultaneous deprotection and introduction of the 6-amino group to afford **40** was achieved by overnight heating in methanolic ammonia. Reductive dehalogenation via hydrogenation over Pd/C in buffered methanol afforded **41**. Attempted conversion of **39** to the corresponding 6-oxo congener in dilute NaOH solution, as described by Seela for the 3-unsubstituted analogue,[71] resulted in glycosidic bond breakage.

Further modifications focused on the introduction of substituents on the 7-position of **21**. Different phenyl rings were introduced via aqueous Suzuki coupling reactions with the appropriate arylboronic acids to furnish **42**−**63** (Scheme 3). Reaction with 4-chloro-3-cyano-phenylboronic acid gave rise to significant amounts of biphenyl product **75**, which was also isolated. Except for the 2-pyridyl and 2-thiophene substituents in **65** and **67**, which were introduced via Stille coupling, other heterocyclic substituents were also introduced under aqueous Suzuki coupling conditions to furnish **64**, **66**, and the substituted 2-thienyl analogues **68**−**70**. The vinyl- and isopropenyl-compounds **71** and **72** were synthesized via the Suzuki reaction with the respective potassium trifluoroborate salts, while trans-2-vinylphenylboronic acid was used to obtain **73**. The synthesis of **74** required multiple additions of

Scheme 3. Reagents and Conditions: (a) Boronic Acid or Trifluoroborate Salt, Pd(OAc)$_2$, TPPTS, Na$_2$CO$_3$ (in the Case of a Boronic Acid) or Cs$_2$CO$_3$ (When a Trifluoroborate Salt Was Used), MeCN/H$_2$O 1:2, 16−81% (For All Compounds Except for 67 and 65); (b) Tributylstannylated Heterocycle, Pd(PPh$_3$)$_4$, CuI, DMF, 24% (67)*, 66% (65)*; (c) H$_2$, Pd(OH)$_2$/C, MeOH, 81%

227
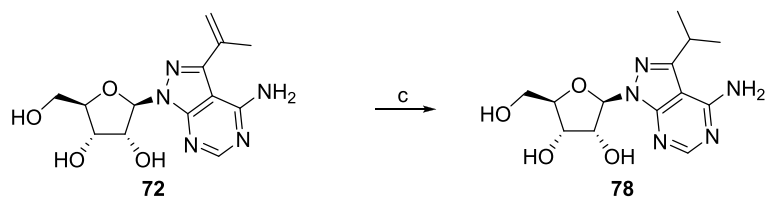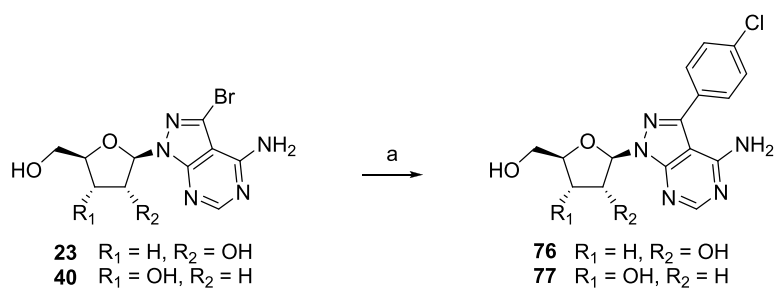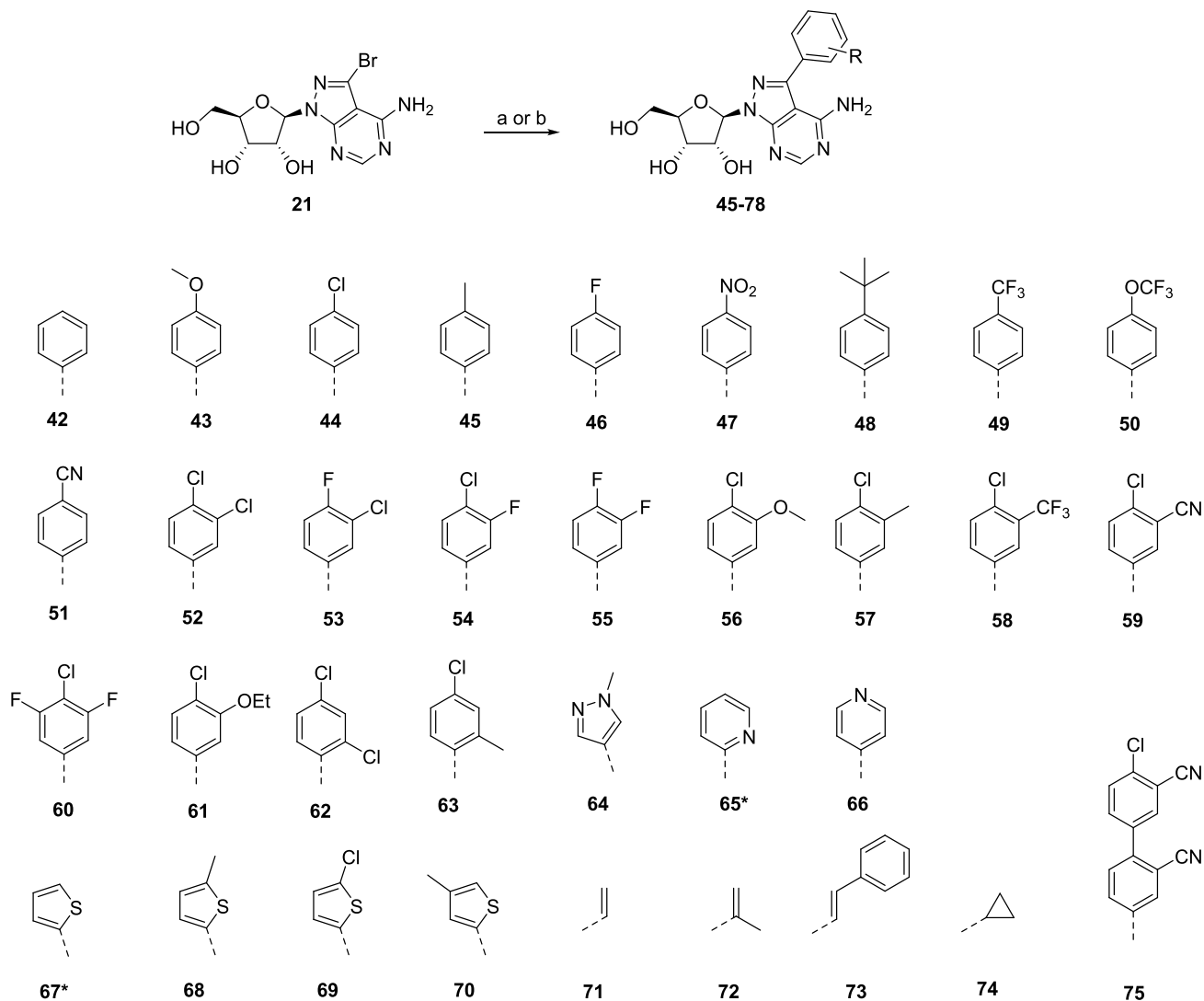
Scheme 4. Reagents and Conditions: (a) Phenol (for 79) or 4-Chlorophenol (for 80), CuI, N,N-Dimethylglycine, Cs$_2$CO$_3$, DMA, 120 °C, 5% (79), 3% (80); (b) CuCl, aq. NH$_4$OH (for 81) or aq. NHMe (for 82) or Pyrrolidine, 1,4-Dioxane/H$_2$O 1:2 (for 83), 120 °C, 19% (81), 5% (82), 16% (83); (c) Me$_4$NCl, Cu$_2$O, L-Proline, 2-Methoxyethanol, 120 °C, 7 days; (d) 0.5 M NaOMe in MeOH, 34% Over 2 Steps
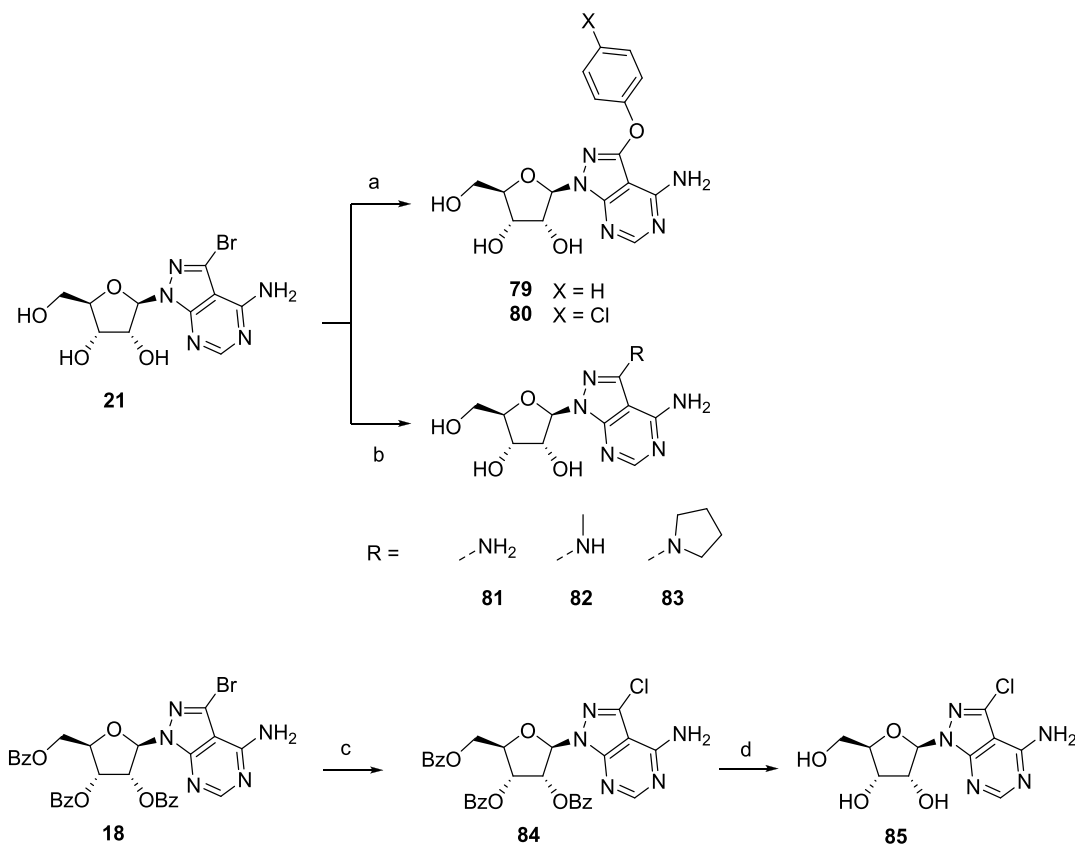
cyclopropylboronic acid, since reaction with potassium cyclopropyltrifluoroborate proved unsuccessful. Likewise, the 3′-deoxy and 2′-deoxy bromonucleosides **23** and **40** were subjected to the Suzuki reaction with 4-chlorophenylboronic acid to afford **76** and **41**. Finally, the isopropenyl group of previously obtained **72** was reduced *via* catalytic hydrogenation to afford **78**.

Ullman coupling of **21** with phenol or 4-chlorophenol under conditions described for other pyrazolo[3,4-*d*]pyrimidines[76] afforded **79** and **80**, respectively (Scheme 4). The yields were very low (5 and 3%) but provided sufficient amounts of product for preliminary evaluation. The synthesis of **81** *via* Ullman coupling in aqueous ammonia has already been described,[69] and methylamine and pyrrolidine could be coupled under similar conditions to furnish **82** and **83**. To introduce a 7-chloro, **18** was subjected to a copper-catalyzed *retro*-Finkelstein reaction.[77] Although this reaction was sluggish, **85** was obtained in decent yield after deprotection.

The 7-iodo analogue **36** served as a useful precursor for another set of analogues (Scheme 5). The Sonogashira reaction with phenylacetylene furnished **86**, which was further reduced to **87** *via* catalytic hydrogenation. The Sonogashira reaction with ethynyltrimethylsilane yielded **88**, which was either further reduced to **89** or reacted with azidotrimethylsilane in a copper(I)-catalyzed azide-alkyne cycloaddition to **90**. A nitrile substituent was introduced *via* a palladium-catalyzed coupling reaction with Zn(CN)$_2$ to furnish **91**.[66] The nitrile group was further transformed to a tetrazole **92** *via* a 1,3-dipolar cycloaddition reaction or reduced to the aminomethyl

analogue **93** *via* hydrogenation over Raney nickel. Alternatively, hydration of the nitrile in basic hydrogen peroxide solution furnished **94**. Attempted hydrolysis of nitrile **91**[66] failed to deliver the carboxylic acid but resulted in cleavage of the N-glycosidic bond instead. A trifluoromethyl substituent was introduced *via* a cross-coupling reaction with *in situ*-formed CuCF$_3$[56,78] to afford **95**. Deprotection using sodium methoxide then furnished **96**.

To gain access to the methyl-substituted base **98**, 5-amino-4-cyano-3-methyl-1*H*-pyrazole **97** was synthesized *de novo* from malononitrile and acetyl chloride according to the method of Haneman (Scheme 6).[79] Ring closure of **97** with thioacetamide instead of formamide furnished the bismethylated heterocycle **99**. Glycosylation of **98** afforded **100**, which was deprotected to **101**. Unfortunately, attempted glycosylation of **99** under the same conditions was not successful.

Since a carboxylic acid could not be obtained from the cyano analogue **91**, we looked at other methods to introduce a carbonyl group on the 7-position. Vilsmeier−Haack formylation of **35** failed and only led to N-formylation of the 6-amino group. Palladium-catalyzed carbonylation reactions of **34** with different CO equivalents were also unsuccessful.[80−82] Finally, we tried to convert a vinyl substituent into the corresponding aldehyde (Scheme 7). To minimize side reactions, we chose to start from the benzoyl-protected iodide precursor **36**. Suzuki reaction with potassium vinyl trifluoroborate[83] afforded **102** in acceptable yields. Oxidative cleavage of the vinyl group **102** was accomplished *via* the Lemieux−Johnson oxidation to afford aldehyde **103**. The carboxylic acid analogue **108** could

Scheme 5. Reagents and Conditions: (a) Phenylacetylene, PdCl$_2$(PPh$_3$)$_2$, CuI, DMF/Et$_3$N 4:1, 40%; (b) H$_2$, Pd(OH)$_2$/C, MeOH, 89% (87), 74% (89); (c) (i) Ethynyltrimethylsilane, PdCl$_2$(PPh$_3$)$_2$, CuI, DMF/Et$_3$N 4:1; (ii) 7 N NH$_3$ in MeOH, 19%; (d) TMSN$_3$, CuI, DMF/MeOH 9:1, 100 °C, 40%; (e) Zn(CN)$_2$, Pd$_2$(dba)$_3$, dppf, DMF, 150 °C, 28%; (f) NaN$_3$, NH$_4$Cl, LiCl, DMF, 100 °C, 25%; (g) H$_2$, Raney Nickel, MeOH, 10%; (h) NH$_4$OH, H$_2$O$_2$, 25%; (i) TMSCF$_3$, CuI, KF, DMF/NMP 1:1, Reflux; (j) 0.5 M NaOMe in MeOH, 14% Over 2 Steps
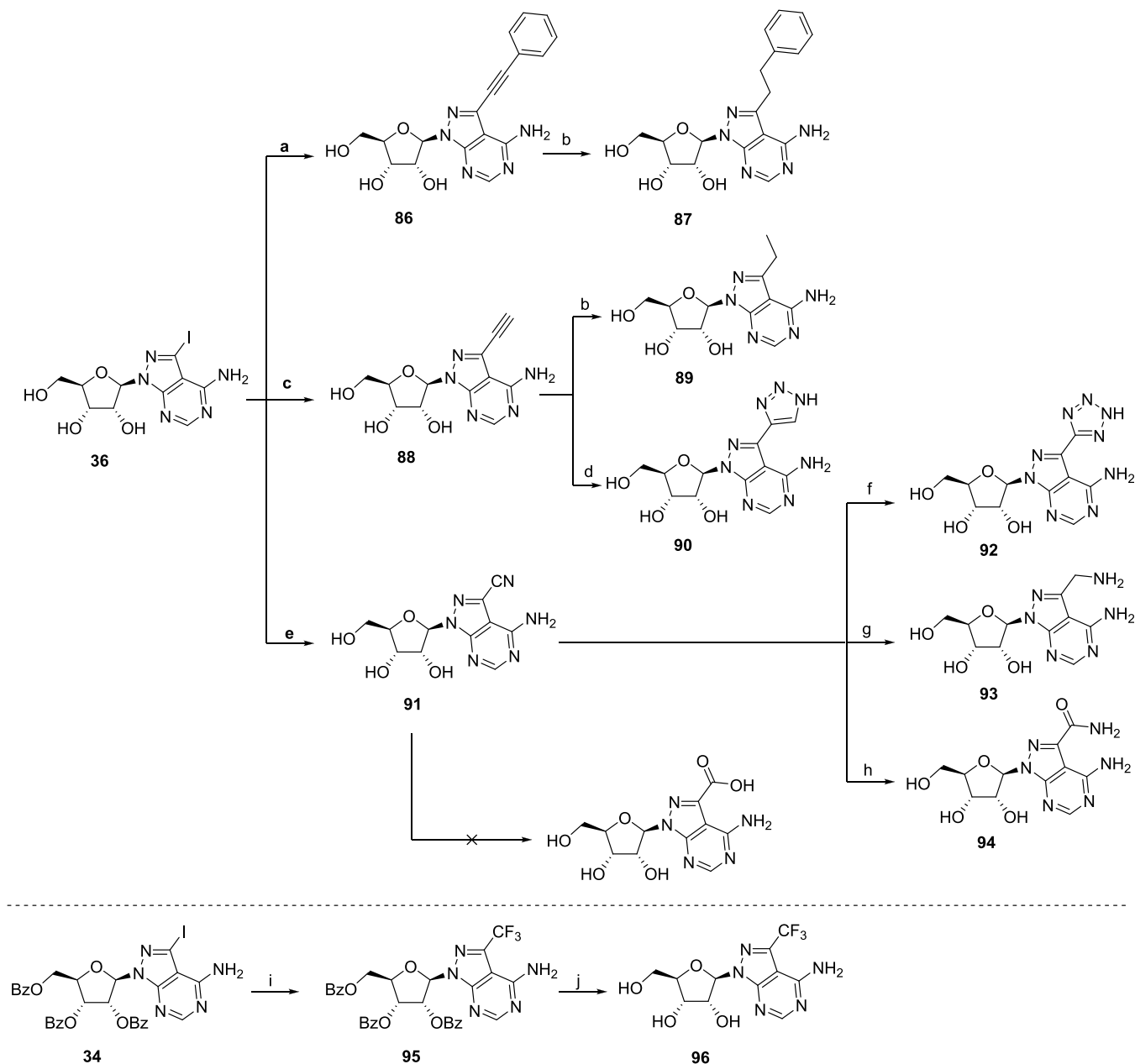
now efficiently be obtained *via* the Pinnick oxidation of **103**. Alternatively, the aldehyde functionality of **103** was further elaborated to a methyl-*N*-morpholino substituent *via* reductive amination (**104**) or to a difluoromethyl substituent *via* reaction with DAST (**106**). Deprotection under basic conditions afforded **105** and **107**. The carboxylic acid functionality was further derivatized to different amides *via* HCTU-mediated coupling to afford analogues **113**−**116** after benzoate deprotection. Attempted cyclopropanation of **102** with *in situ*-generated difluorocarbene (from BrCF$_2$CO$_2$Na[84]) or dichlorocarbene (generated from CHCl$_3$ and NaOH) failed.

Biological Evaluation. The prepared nucleoside analogues were evaluated *in vitro* for their activity against *T. cruzi* and

Leishmania infantum. Cytotoxicity was assayed against MRC-5$_{SV2}$ cells (*T. cruzi* host cell) and primary mouse macrophages (PMM, *L. infantum* host cell) (Table 1).

Although the anti-*T. cruzi* and antileishmanial activities of allopurinol (**1**), aminopurinol (**3**), and their ribonucleosides **2** and **4** are already known, they were included in this study as reference compounds. In accordance with various literature reports,[46,51,85] **1** and **3** displayed good activity against *T. cruzi* and *L. infantum*. Yet, the 20-fold higher activity and selectivity of aminopurinol (**3**) compared to allopurinol (**1**) against *L. infantum* is striking. As mentioned before, **3** has never been evaluated in an *in vivo* VL model although it is known to be safe at low doses.[46,51] Introduction of a bromo substituent in

Scheme 6. Reagents and Conditions: (a)(i) NaH, AcCl, Tetrahydrofuran (THF), 0 °C to RT, (ii) Dimethyl Sulfate, Reflux, (iii) H$_2$NNH$_2$·H$_2$O, Et$_3$N, 38% Over 3 Steps; (b) Formamide, 180 °C, 23%; (c) Thioacetamide, Reflux, 36%; (d) 98, BF$_3$·OEt$_2$, MeNO$_2$, Reflux; (e) 0.5 M NaOMe in MeOH, 21% Over 2 Steps
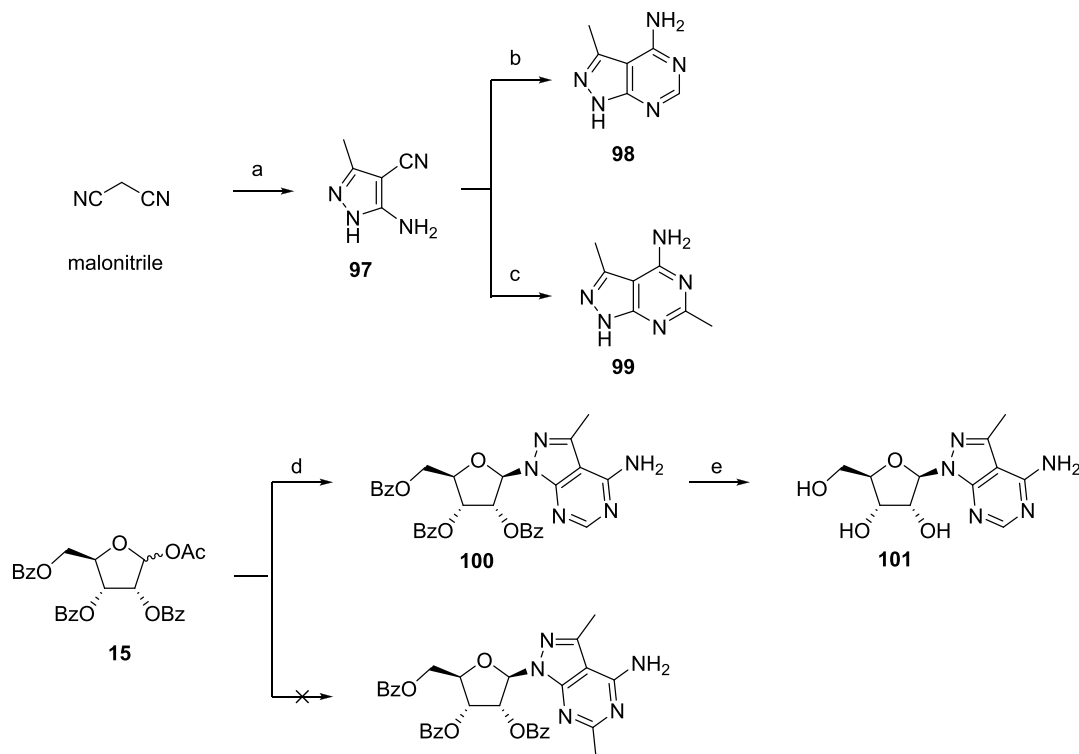
position 7 of allopurinol (**1**) or aminopurinol (**3**) led to a drastic drop in activity, possibly due to impeded conversion by PRTases, which are essential for the activation of nucleobase analogues. The 4-APP ribonucleoside **4** displayed potent activity against both *T. cruzi* and *L. infantum* intracellular amastigotes, as could be expected from literature reports on its activity against *T. cruzi* epimastigotes and *Leishmania* promastigotes.[49,50] In both MRC-5$_{SV2}$ cells and PMM cells, **4** failed to show cytotoxicity up to 64 μM, but similar to **3**, it has never been evaluated *in vivo*. Introduction of a halogen atom on the 7-position of **4** (compounds **21** and **36**) led to a severe decrease in activity against *T. cruzi* and *L. infantum*. This is different from earlier reported results in *T. cruzi* epimastigotes and *Leishmania* promastigotes, where the activity was more comparable to the parent compound **4**.[49,50] Activity of allopurinol ribonucleoside **2** was comparable to allopurinol.[85] In our hands, introduction of a bromide on the 7-position of **2** (compound **29**) rendered the compound inactive, which conflicts with a report stating it to be more active than **2** against *L. tropica* intracellular amastigotes.[69]

The combination of aminopurinol (**3**) and allopurinol (**1**) with a 3′-deoxy-3′-fluororibofuranose moiety (**24** and **32**) resulted in inactive compounds. Introduction of a bromide on the 3-position of **24** rendered the compound highly cytotoxic (**22**). It did not display any selective activity, contrasting with the matched 7-deazapurine nucleoside.[57] The same was true for the 3′-deoxynucleosides **23**, **25**, **31**, and **33**. While the inactivity of **33** was already noted by Moorman et al.,[86] the inactivity of **25** was more surprising, as removal of the 3′-hydroxy group resulted in a major increase in activity against *T. brucei* or *T. cruzi* in earlier 7-deazapurine nucleoside series.[53,55] Again, the introduction of a 7-bromo substituent (**23**) afforded a cytotoxic compound without any specific antiparasitic

activity. The 2′-deoxynucleosides **41** and **40** were also inactive, as was already reported for **41**.[46]

Based on the structure−activity relationship (SAR) of earlier nucleoside series,[52,53,57,78] which demonstrated that modifications of the 7-position could improve activity, we performed an extensive substituent screen. In a first set of analogues, different substituted phenyl rings were introduced on the 7-position (Table 2). Remarkably, also in this series, a 4-chlorophenyl (**44**) proved to confer the best antitrypanosomal activity (IC$_{50}$ = 0.32 μM) and was about 50-fold more active than the 7-phenyl analogue **42**. The second most potent para-substituted analogue was the 4-methylphenyl substituted compound **45**. Further substitution of the 4-chlorophenyl substituent with a 3-fluoro (**53**), methyl (**57**), or methoxy group (**56**) failed to potentiate its activity. The 2,4-substituted analogues **62** and **63** were less active than the 3,4-disubstituted analogues. Strikingly, the superiority of this 4-chlorophenyl modification has also been observed for other 7-deazapurine nucleosides and suggests that the chloro substituent is involved in a crucial interaction with a parasitic target or transporter, rather than just reducing the electron density of the phenyl ring. Removal of the 3′-OH group as in **76** was expected to result in increased anti-*T. cruzi* activity, based on earlier observations with 7-deazapurine nucleosides,[53] but surprisingly led to a compound that was 3-fold less active than **44**. Nevertheless, **44** is more potent than its 7-deazapurine congener[52] and displays an improved selectivity profile, with no *in vitro* toxicity in MRC-5$_{SV2}$ or PMM cells in concentrations up to 64 μM. The 2′-deoxy analogue **77** displayed reasonably good anti-*T. cruzi* activity but was less potent than both **44** and **76**. All phenyl-substituted analogues displayed in Table 2 were inactive against *L. infantum*.

Scheme 7. Reagents and Conditions: (a) Potassium Vinyl Trifluoroborate, Pd(OAc)$_2$, PPh$_3$, Cs$_2$CO$_3$, DMF/H$_2$O 9:1, 100 °C, 38%; (b) K$_2$OsO$_4$·2H$_2$O, NaIO$_4$, 2,6-Lutidine, 1,4-Dioxane/H$_2$O 3:1, 48%; (c) Morpholine, NaBH$_3$CN, AcOH, MeOH/THF 2:1; (d) 0.5 M NaOMe in MeOH, 64% Over 2 Steps (105), 58% Over 2 Steps (107), 29% Over 2 Steps (113), 28% Over 2 Steps (114), 61% Over 2 Steps (115), 44% Over 2 Steps (116); (e) NaClO$_2$, NaH$_2$PO$_4$, H$_2$O$_2$, THF/H$_2$O 6:1, 94%; (f) DAST, CH$_2$Cl$_2$; (g) Aq. NHMe (109), Pyrrolidine (110), Aniline (111), or Benzylamine (112), HCTU, N,N-Diisopropylethylamine (DIPEA), DMF
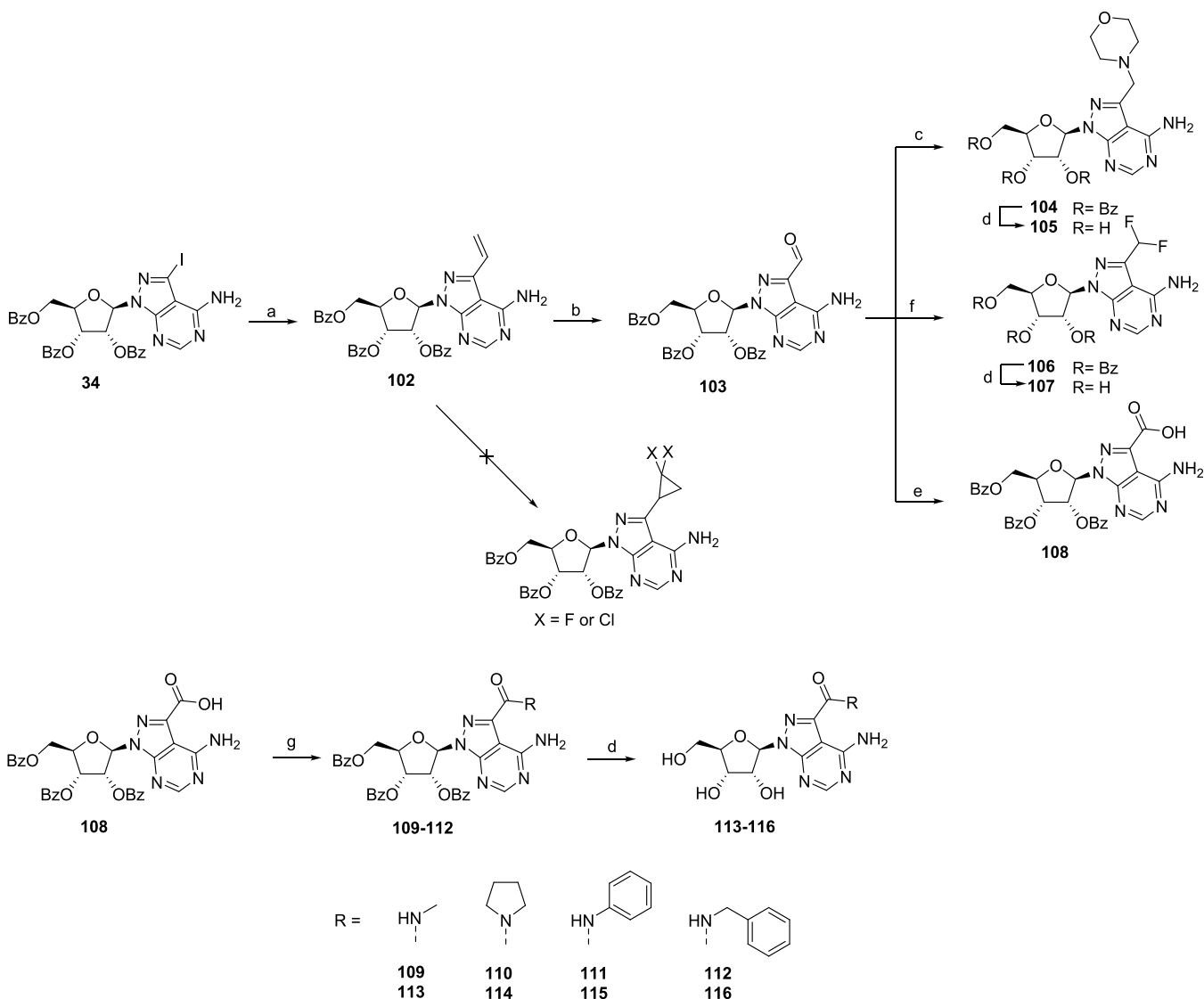
Bioisosteric replacement of the phenyl ring by a thiophene resulted in a loss of activity (67−70) (Table 3). The 5-chlorothiophene and 5-methylthiophene analogues 69 and 68 were 5−10-fold less active than their phenyl counterparts and displayed lower selectivity. Introducing an extra atom or linker between the nucleobase and the phenyl ring was also not tolerated, as illustrated by the inactivity of the phenoxy analogues 79 and 80 and the low activity of elongated phenyl analogues 86, 73, and 87. None of these analogues showed any activity against *L. infantum*. A number of nitrogen-containing heterocycles were also introduced on the 7-position (64−66, 90, and 92). A 2- or 4-pyridyl substituent (65 and 66), an *N*-methylpyrazole (64), and tetrazole (92) did not lead to any specific activity against *T. cruzi* or *L. infantum*. While 64 and 92 were devoid of MRC-5$_{SV2}$ cytotoxicity, the triazole analogue 90 was highly cytotoxic and also did not display any specific antiparasitic activity.

Among a series of analogues with small substituents on the 7-position, a nitrile (91) led to reasonable activity against both *T. cruzi* and *L. infantum* (Table 4). The chloro analogue 85 was less active against *T. cruzi* but displayed higher selectivity toward MRC-5$_{SV2}$ cells. A trifluoromethyl (96) or difluoromethyl (107) substituent resulted in cytotoxic compounds that did not display selective antiparasitic activity. Among the carbon-based substituents, the methyl analogue 101 and the ethynyl analogue 88 displayed moderate anti-*T. cruzi* activity. A vinyl (71), ethyl (89), or cyclopropyl (74) substituent led to inactive compounds, while an isopropenyl (72) or isopropyl (78) group resulted in cytotoxic compounds with no specific antiparasitic activity. An amine (81), methylamine (82), or pyrrolidine group (83) on the 7-position did not lead to any significant antiparasitic activity, as was the case for an aminomethyl (93) or morpholinomethyl (105) substituent. The activity of the amide-substituted nucleosides (94, 113−

Table 1. Evaluation of Drug Sensitivity of Ribofuranose-Modified Nucleoside Analogues against *T. cruzi* and *L. inf.*[a]
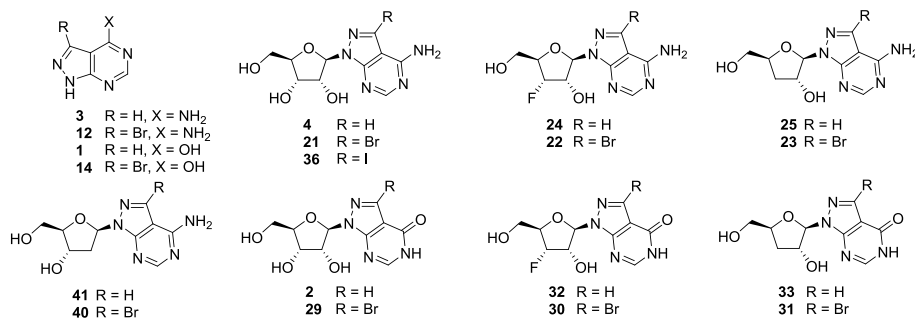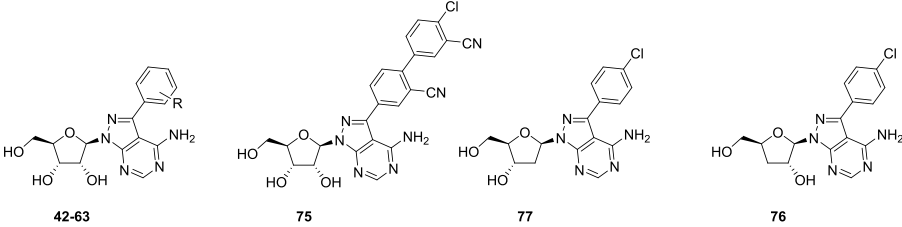
cpd.	structure	*T. cruzi* IC$_{50}$ (μM)	MRC-5 CC$_{50}$ (μM)	SI	*L. infantum.* IC$_{50}$ (μM)	PMM CC$_{50}$ (μM)	SI
Nucleobases							
3	R = H	0.57	2.46	5	0.18	>64.0	>355
12	R = Br	38.1	>64.0	>1	22.6	>64.0	>2
1	R = H	9.75 ± 1.75	>64.0	>7	3.51 ± 1.77	>64.0	>18
14	R = Br	>64.0	>64.0		>64.0	>64.0	
Ribonucleosides							
4	X = H	0.29 ± 0.03	>64.0	>219	1.06 ± 0.35	>64.0	>60
21	X = Br	4.37 ± 0.55	>64.0	>15	29.4 ± 21.4	>64.0	>2
36	R = I	12.62	25.4	2	25.4	>64.0	>2
2	R = H	7.18 ± 3.66	>64.0	9	6.66 ± 4.66	>64.0	10
29	R = Br	>64.0	>64.0		>64.0	>64.0	
3′-Deoxy-3′-Fluoronucleosides							
24	X = H	>64.0	>64.0		>64.0	>64.0	
22	X = Br	1.06	0.23	0	0.08	0.13	1
32	X = H	>64.0	>64.0		>64.0	>64.0	
30	R = Br	>64.0	>64.0		>64.0	>64.0	
3′-Deoxynucleosides							
25	R = H	>64.0	>64.0		>64.0	>64.0	
23	R = Br	38.5	2.2	0	>64.0	>64.0	
33	R = H	>64.0	>64.0		>64.0	>64.0	
31	R = Br	>64.0	>64.0		>64.0	>64.0	
2′-Deoxynucleosides							
41	R = H	>64.0	>64.0		>64.0	>64.0	
40	R = Br	53.2 ± 10.8	24.9 ± 14.0	0	>64.0	>64.0	

[a]Cytotoxicity Was Assayed against Human MRC-5$_{SV2}$ Cells and Primary Mouse Macrophages (PMMs). Values represent mean ± SEM, which originate from 2−3 independent experiments and are expressed in μM. Values in italics represent the result of a single determination because of inactivity or overt cytotoxicity. SI: *in vitro* selectivity index is the ratio of CC$_{50}$ for the host cell (MRC-5$_{SV2}$ for *T. cruzi*, PMM for *L. inf.*) and IC$_{50}$ of the parasite. Benznidazole was included as a reference for *T. cruzi* (IC$_{50}$ = 2.02 ± 0.28 μM) and miltefosine as a reference for *L. infantum* (IC$_{50}$ = 7.47 ± 2.23 μM).

116) varied: a carboxamide group (94) again resulted in a cytotoxic compound, while adding a methyl group on the amide nitrogen (113) removed all cytotoxic effects and provided a compound with moderate anti-*T. cruzi* activity. Amide analogues with bigger groups (114−116) were inactive.

Overall, the SAR of the pyrazolo[3,4-*d*]pyrimidine nucleosides for anti-*T. cruzi* and anti-*L. infantum* activities turned out to be completely different from previously reported 7-deazapurine[52,53,57] and 1,7-dideazapurine[78] nucleoside series. As already known from several literature reports, the parent nucleosides aminopurinol riboside 4 and allopurinol riboside 2 displayed good *in vitro* activity against both *T. cruzi* and *L. infantum*. Introduction of a halogen atom on the 7-position had a detrimental effect on the activity against both *T. cruzi* and *L. infantum* and modifications at the 3′-position of the ribose moiety, expected to result in more potent compounds based on SAR studies of earlier nucleoside series, completely abolished activity, or resulted in cytotoxic compounds. A substituent screen of the 7-position of 4 revealed highly varying effects on

the antiparasitic activity and cytotoxicity to MRC-5$_{SV2}$ and PMM. A 4-chlorophenyl substituent resulted in a compound with potent anti-*T. cruzi* activity and devoid of cytotoxic effects in MRC-5$_{SV2}$ or PMM at concentrations up to 64 μM. Contrary to expectations, removal of the 3′-hydroxyl group of 44 resulted in a compound that was 2−3-fold less potent (76). The insertion of a linker (oxygen, carbon-based, amide) between the oxygen and the phenyl ring was not tolerated. Bioisosteric replacement of the phenyl ring with a thiophene was also not tolerated and resulted in a 10-fold decrease in activity. Other heterocycles in the 7-position resulted in compounds with low antiparasitic activity. The effect of other, smaller substituents varied greatly. Some resulted in moderate anti-*T. cruzi* activity (*e.g.*, chloride, methyl, ethynyl), while other substituents afforded highly cytotoxic nonselective compounds. Overall, none of the 7-modified analogues displayed good activity against *L. infantum*, suggesting that, regardless of the nature of the heterocyclic nucleobase, substituents on this position are not tolerated. 44 was the

Table 2. Evaluation of Drug Sensitivity of 7-Modified Nucleoside Analogues against *T. cruzi* and *L. infantum*[a]

cpd.	structure (R =)	*T. cruzi* IC$_{50}$ (μM)	MRC-5 CC$_{50}$ (μM)	SI	*L. inf.* IC$_{50}$ (μM)	PMM CC$_{50}$ (μM)	SI
42	H	*13.1*	*>64.0*	>5	*>64.0*	*>64.0*	
43	4-OMe	18.2	*>64.0*	>4	*>64.0*	*>64.0*	
44	4-Cl	0.32 ± 0.02	*>64.0*	>197	*>64.0*	*>64.0*	
45	4-Me	1.77 ± 0.92	*>64.0*	>36	*>64.0*	*>64.0*	
46	4-F	3.36 ± 1.88	*>64.0*	>19	*>64.0*	*>64.0*	
47	4-NO$_2$	10.3 ± 5.8	*>64.0*	>6	*>64.0*	*>64.0*	
48	4-*t*-Bu	*>64.0*	*>64.0*		*>64.0*	*>64.0*	
49	4-CF$_3$	6.34 ± 1.90	*>64.0*	>10	57.0 ± 9.3	*>64.0*	>1
50	4-OCF$_3$	15.6 ± 6.2	*>64.0*	>4	*>64.0*	*>64.0*	
51	4-CN	*32.0*	*>64.0*	>2	*>64.0*	*>64.0*	
52	3,4-diCl	2.82 ± 1.94	*>64.0*	>23	*>64.0*	*>64.0*	
53	3-Cl-4-F	4.66 ± 2.71	*>64.0*	>14	*>64.0*	*>64.0*	
54	4-Cl-3-F	1.19 ± 0.92	*>64.0*	>54	*>64.0*	*>64.0*	
55	3,4-diF	4.24 ± 1.55	*>64.0*	>15	*>64.0*	*>64.0*	
56	4-Cl-3-OMe	1.14 ± 1.02	*>64.0*	>56	*>64.0*	*>64.0*	
57	4-Cl-3-Me	0.81 ± 0.13	*>64.0*	>79	*>64.0*	*>64.0*	
58	4-Cl-3-CF$_3$	*43.8*	*>64.0*	>1	*>64.0*	*>64.0*	
59	4-Cl-3-CN	*>64.0*	*>64.0*		*>64.0*	*>64.0*	
60	4-Cl-3,5-diF	1.33 ± 0.51	*>64.0*	>17	*>64.0*	*>64.0*	
61	4-Cl-3-OEt	45.3	*>64.0*	>1	*>64.0*	*>64.0*	
62	2,4-diCl	6.06 ± 2.69	*>64.0*	>11	52.8 ± 11.2	*>64.0*	>1
63	4-Cl-2-Me	3.76 ± 0.61	*>64.0*	>17	*>64.0*	*>64.0*	
75		*>64.0*	*>64.0*		*>64.0*	*>64.0*	
77		2.49 ± 0.42	*>64.0*	>22	[32.5, >64.0]	[32.0, >64.0]	1
76		1.04 ± 0.32	*>64.0*	>61	*>64.0*	*>64.0*	

[a]Cytotoxicity was assayed against human MRC-5SV2 cells and primary mouse macrophages (PMMs). Values represent mean ± SEM, which originate from 2−3 independent experiments and are expressed in μM. Values in parentheses represent the values of the different determinations, as no correct average can be calculated. Values in italics represent the result of a single determination because of inactivity or overt cytotoxicity. SI: *in vitro* selectivity index is the ratio of CC$_{50}$ for the host cell (MRC-5$_{SV2}$ for *T. cruzi*, PMM for *L. inf.*) and IC$_{50}$ of the parasite. Benznidazole was included as a reference for *T. cruzi* (IC$_{50}$ = 2.02 ± 0.28 μM) and miltefosine as a reference for *L. infantum* (IC$_{50}$ = 7.47 ± 2.23 μM).

most potent analogue for *T. cruzi* and was more active and more selective than its matched 7-deazapurine nucleoside congener.[52] Because of its potent anti-*T. cruzi* activity and favorable selectivity profile, **44** was selected for further evaluation in an acute Chagas disease mouse model.

Metabolic Stability of Compound 44. The *in vitro* metabolic stability of **44** was evaluated using male mice and pooled human liver microsomes (S9 fraction) (Table 5). Compound **44** was not susceptible to Phase-I and Phase-II metabolism in both mouse and human microsomes with 100% of the parent drug remaining after 60 min. These results favored further evaluation of **44** in an *in vivo* laboratory rodent model.

***In Vivo* Evaluation of Compound 44.** To determine its efficacy *in vivo*, **44** was evaluated in an acute Chagas disease model using the Y strain of *T. cruzi* in Swiss male mice.[92,93] **44** was evaluated at 0.25, 2.5, or 25 mg/kg b.i.d or in combination with benznidazole (**44** at 2.5 mg/kg b.i.d + benznidazole at 10 mg/kg q.d.). Compounds were administered orally for 5 consecutive days, starting the administration at parasitemia onset on day 6 postinfection (dpi), which peaked at 8 dpi in untreated animals. **44** at 25 mg/kg gave 99% reduction in the parasitemia peak at 8 dpi, which was similar to the optimal q.d. dose of benznidazole at 100 mg/kg. Lower dosages (0.25 and 2.5 mg/kg) only gave partial reduction of parasitemia (43%). Coadministration of **44** (2.5 mg/kg) and benznidazole (10 mg/kg) reached 71% reduction, which was slightly better than benznidazole alone. However, no mice sustained negative parasitemia, hence failing parasitological cure. In the 2.5 mg/mk and 25 mg/kg treatment groups, 5 out of 6 mice (83%) survived until the end of the experiment (34 dpi), similar to benznidazole at 10 mg/kg. In the benznidazole 100 mg/kg group, all mice survived. In the untreated control group, all mice succumbed to the infection by day 27. In the 0.25 mg/kg, only one mouse survived at 34 dpi (Figure 2).

As the *in vitro T. cruzi* screening was performed with the Tulahuen strain (DTU IV) and *in vivo* assays with the Y strain (DTU II), additional *in vitro* screens were conducted with the latter. The findings confirmed the high potency of **44** against intracellular forms (IC$_{50}$ = 0.26 ± 0.03 μM, SI > 1900) present in cardiomyocytes (Table 6), similar to the values obtained with the Tulahuen strain intracellular amastigotes. In addition,

233

Table 3. Evaluation of Drug Sensitivity of 7-Modified Pyrazolo[3,4-d]pyrimidine Nucleoside Analogues against $T.\ cruzi$ and $L.\ infantum$[a]
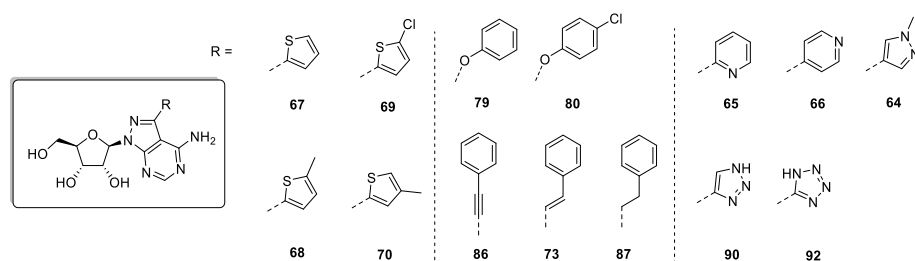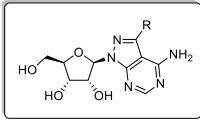
cpd.	$T.\ cruzi$ IC$_{50}$ (μM)	MRC-5 CC$_{50}$ (μM)	SI	$L.\ infantum.$ IC$_{50}$ (μM)	PMM CC$_{50}$ (μM)	SI
Thiophenes						
67	*10.4*	*32*	*3*	*>64.0*	*>64.0*	
69	2.56 ± 1.12	47.3 ± 6.12	14	*>64.0*	*>64.0*	
68	7.10 ± 4.2	*>64.0*	*>9*	*[32.0,>64.0]*	*>64.0*	*>1*
70	*32*	*>64.0*	*>2*	*>64.0*	*>64.0*	
Elongated phenyls						
79	*>64.0*	*>64.0*		*32*	*>64.0*	*>2*
80	*>64.0*	*>64.0*		*>64.0*	*>64.0*	
86	29.4 ± 11.1	*>64.0*	*>2*	49.4 ± 8.7	*>64.0*	*>1*
73	*16.5*	*>64.0*	*>4*	*50.8*	*>64.0*	*>1*
87	*52.3*	*>64.0*	*>1*	*>64.0*	*>64.0*	
Nitrogen-containing heterocycles						
65	30.1 ± 17.8	36.4 ± 4.1	1	*[50.8, >64.0, >64.0]*	*>64.0*	1
66	*21.5*	*>64.0*	*>3*	*25.4*	*>64.0*	*>3*
64	*45.3*	*>64.0*	*>1*	*>64.0*	*>64.0*	
90	*0.43*	*0.6*	1	*43.1*	*>64.0*	*>1*
92	*>64.0*	*>64.0*		*>64.0*	*>64.0*	

[a]Cytotoxicity was assayed against human MRC-5$_{SV2}$ cells and primary mouse macrophages (PMMs). Values represent mean ± SEM, which originate from 2−3 independent experiments and are expressed in μM. Values in parentheses represent the values of the different determinations, as no correct average can be calculated. Values in italics represent the result of a single determination because of inactivity or overt cytotoxicity. SI: *in vitro* selectivity index is the ratio of CC$_{50}$ for the host cell (MRC-5$_{SV2}$ for $T.\ cruzi$, PMM for $L.\ inf.$) and IC$_{50}$ of the parasite. Benznidazole was included as a reference for $T.\ cruzi$ (IC$_{50}$ = 2.02 ± 0.28 μM) and miltefosine as a reference for $L.\ infantum$ (IC$_{50}$ = 7.47 ± 2.23 μM).

44 did not exert cardiotoxicity in two-dimensional (2D) and three-dimensional (3D) cardiac cell cultures, giving CC$_{50}$ values up to 500 and 200 μM, respectively. After discarding the potential impact of parasite strain on the *in vitro* and *in vivo* outcomes, we next evaluated the activity of **44** (as well as **4**) against the nondividing and highly infective bloodstream trypomastigote form. Both compounds proved to be inactive (IC$_{50}$ > 81 μM), while benznidazole gave an IC$_{50}$ of 5.7 ± 0.6 μM. These results corroborate former studies using pyrrolo-[2,3-b]pyridine (1,7-dideazapurine) nucleoside analogues that failed to achieve parasitological cure in treated mice despite parasitemia suppression and high animal survival rates.[78] The inability to kill bloodstream trypomastigotes may explain the parasitemia recrudescence and thus lack of sterile cure, as has also been reported for other nucleoside analogues.[53,78] The lack or low activity against bloodstream trypomastigotes resembles that of the azole ergosterol biosynthesis inhibitors that failed in clinical trials for Chagas disease,[87,88] raising the potential relevance of targeting both the intracellular multiplicative amastigotes and the nonreplicative trypomastigote forms. Recent findings also highlighted the role of metabolic heterogeneity in drug efficacy upon recalcitrant $T.\ cruzi$ infection.[89] The authors reported that limiting exogenous glutamine impairs ergosterol biosynthesis inhibitors (azoles) to act upon intracellular amastigotes. In addition to the occurrence of nonreplicative forms (like dormant amastigotes and trypomastigotes), the impact of metabolic and environ-

mental heterogeneity must be considered in the search for novel anti-$T.\ cruzi$ agents as these factors can modulate drug efficacy.

Effect of the $T.\ cruzi$ Host Cell on Drug Sensitivity to Compound 44. To investigate whether host cell permeability could be a limiting factor for the *in vivo* $T.\ cruzi$ efficacy or lack of antileishmanial activity of compound **44**, we evaluated the effect of **44** against $T.\ cruzi$ in PMM host cells (Table 7). Surprisingly, **44** was completely inactive against $T.\ cruzi$ in PMM cells, while benznidazole retained its activity in both cell types. To rule out drug efflux as the cause of this effect, the experiment was repeated in the presence of the ABC transporter inhibitors verapamil, cyclosporine A, and probenecid. In all cases, **44** was inactive, indicating that its inactivity in PMM cells is likely due to permeability issues. These findings might offer further explanation as to why **44** was not able to fully clear $T.\ cruzi$ infection *in vivo*. Tissue tropism in Chagas disease has been demonstrated to play an important role in persistence,[90−92] and limited permeability in certain tissues has also been implicated in the ineffectivity of Posaconazole in curing $T.\ cruzi$ infections.[93] These results could also offer an explanation as to why several of the herein-reported nucleoside analogues, as well as others that were previously found to display potent anti-$T.\ cruzi$ activity, are inactive when evaluated against $L.\ infantum$ intracellular amastigotes in PMM host cells.[52,94] The origins of this lack of permeability in PMM cells are currently unclear and require further study. Furthermore, it

Table 4. Evaluation of Drug Sensitivity of 7-Modified Nucleoside Analogues against *T. cruzi* and *L. infantum*[a]

cpd.	*T. cruzi* IC$_{50}$ (μM)	MRC-5 CC$_{50}$ (μM)	SI	*L. infantum.* IC$_{50}$ (μM)	PMM CC$_{50}$ (μM)	SI
85	2.89 ± 0.23	>64.0	>22	>64.0	>64.0	>1
91	*0.95*	*34.6*	*36*	*8*	*>64.0*	*>8*
96	*27*	*13.3*	*<1*	*>64.0*	*>64.0*	
107	*8.3*	*2.42*	*<1*	*0.25*	*0.25*	*1*
101	4.68 ± 1.33	57.5 ± 6.5	12	32.7 ± 15.5	40.0 ± 12	1
88	2.78 ± 0.04	[46.5, >64.0]	20	10.4 ± 2.3	[8.00, >64.0]	1
71	*>64.0*	*>64.0*		*12.7*	*32*	*3*
89	*>64.0*	*>64.0*		*>64.0*	*>64.0*	
74	*>64.0*	*>64.0*		*>64.0*	*>64.0*	
72	*29.5*	*0.35*	*<1*	*24.1*	*32*	*1*
78	*>64.0*	*10.6*	*<1*	*>64.0*	*>64.0*	
81	*7.64*	*23*	*3*	*6.82*	*8*	*1*
82	*>64.0*	*>64.0*		*50.8*	*>64.0*	*>1*
83	*>64.0*	*>64.0*		*>64.0*	*>64.0*	
93	*11.1*	*59.3*	*5*	*2*	*8*	*4*
105	*>64.0*	*>64.0*		*>64.0*	*>64.0*	
94	*0.25*	*0.25*	*1*	*8.11*	*8*	*1*
113	*4*	*>64.0*	*16*	*>64.0*	*>64.0*	
114	*>64.0*	*>64.0*		*>64.0*	*>64.0*	
115	*>64.0*	*>64.0*		*32.5*	*32*	*1*
116	*>64.0*	*>64.0*		*>64.0*	*>64.0*	

[a]Cytotoxicity was assayed against human MRC-5$_{SV2}$ cells and primary mouse macrophages (PMMs). Values represent mean ± SEM, which originate from 2−3 independent experiments and are expressed in μM. Values in parentheses represent the values of the different determinations, as no correct average can be calculated. Values in italics represent the result of a single determination because of inactivity or overt cytotoxicity. SI: *in vitro* selectivity index is the ratio of CC$_{50}$ for the host cell (MRC-5$_{SV2}$ for *T. cruzi*, PMM for *L. inf.*) and IC$_{50}$ of the parasite. Benznidazole was included as a reference for *T. cruzi* (IC$_{50}$ = 2.02 ± 0.28 μM) and miltefosine as a reference for *L. infantum* (IC$_{50}$ = 7.47 ± 2.23 μM).

Table 5. *In Vitro* Metabolic Stability of Compound 44 Using Male Mouse and Pooled Human S9 Microsomal Fractions[a]

		mouse % 44 remaining		human % 44 remaining	
phase-I/II	time	mean	STDEV	mean	STDEV
CYP450-NADPH	0	100		100	
	15	103	11.4	102	10.3
	30	103	12.8	101	7.8
	60	108	16.1	101	8.5
UGT enzymes	0	100		100	
	15	103	3.2	100	2.8
	30	115	0.3	106	9.5
	60	115	3.0	104	7.2

[a]The depicted values are the percentage of remaining parent compound at the various time points of incubation (0−15−30−60 min). Data originate from two independent experiments of two biological replicates. Diclofenac (susceptible to Phase-I and Phase-II metabolism) was included as reference to ensure proper assay performance (data not shown).

would be worthwhile to evaluate if certain nucleoside prodrugs could lead to improved permeability and/or improved *in vivo* efficacy.

■ CONCLUSIONS

We described the design and synthesis of a library of pyrazolo[3,4-*d*]pyrimidine nucleosides that were evaluated for *in vitro* activity against *T. cruzi* and *L. infantum* intracellular amastigotes. SAR trends were highly different from earlier reported nucleoside series. Modifications of the 3′-position of the parent adenosine- and inosine-like analogues aminopurinol riboside **4** and allopurinol riboside **2** were detrimental to activity and led to inactive compounds. The introduction of a halogen atom on the 7-position led to a significant decrease in activity. An extensive screen of substituents on the 7-position **4** revealed varying effects on antiparasitic activity and selectivity toward MRC-5$_{SV2}$ and PMM cells. A 4-chlorophenyl substituent on the 7-position (**44**) afforded good anti-*T. cruzi* activity and selectivity and was also metabolically stable in human and mouse liver microsomes. **44** was next evaluated in an acute Chagas disease model, resulting in a rapid, almost complete reduction in parasitemia. Treatment with **44** led to the survival of 5 out of 6 mice but failed to induce sterile parasitological cure. None of the new analogues showed good *in vitro* activity against *L. infantum*, which could potentially be attributed to limited permeability in the PMM host cell.
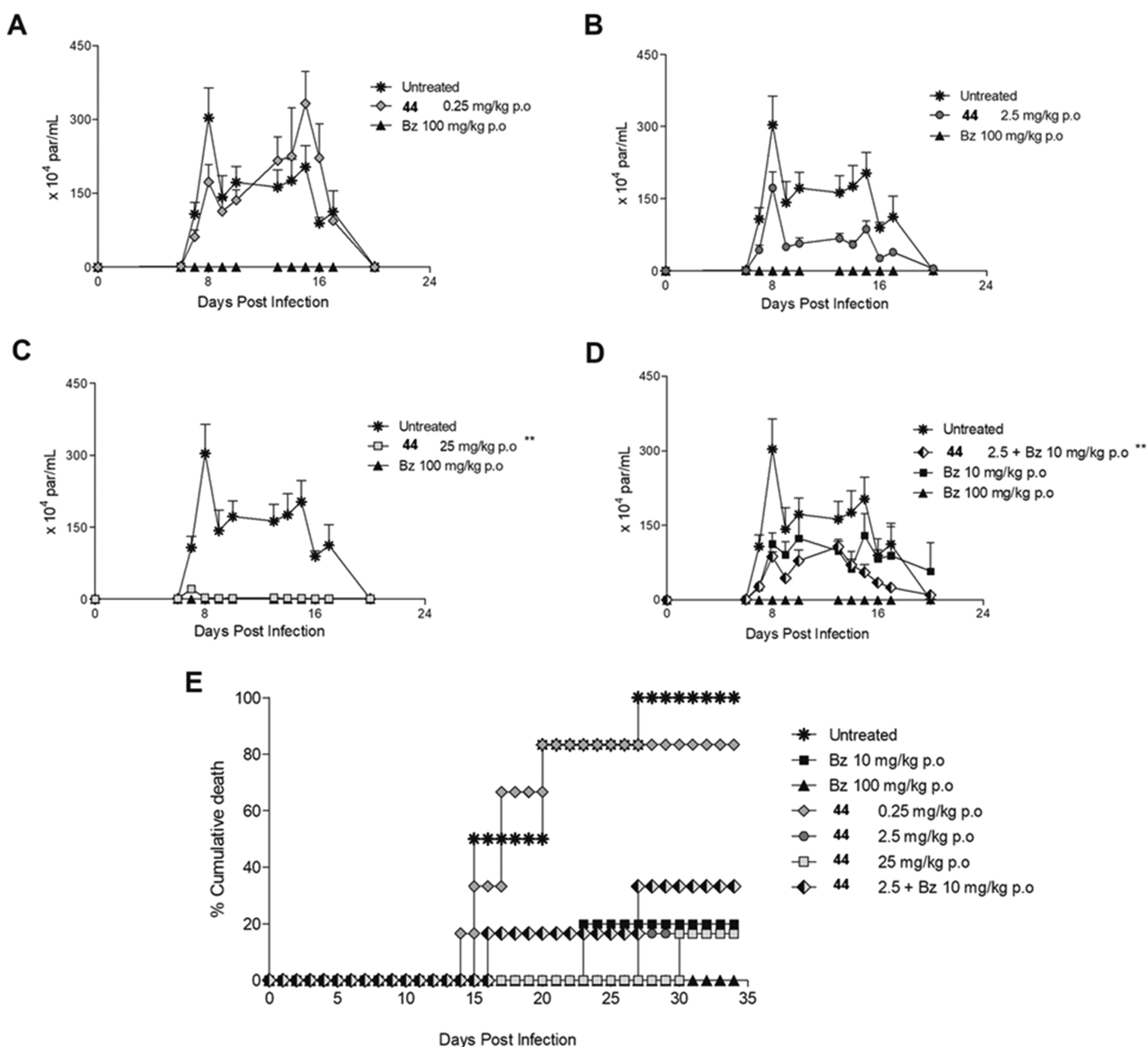
Figure 2. *In vivo* efficacy of **44** administered orally for 5 days in Swiss mice infected with the Y strain of *T. cruzi*. Parasitemia curve for **44** at (A) 0.25 mg/kg/b.i.d, (B) 2.5 mg/kg/b.i.d, (C) 25 mg/kg/b.i.d, and (D) coadministration of **44** at 2.5 mg/kg + benznidazole (Bz) at 10 mg/kg/b.i.d. Mortality rates were up to 35 dpi (E). ** p value ≤ 0.05.

Table 6. *In Vitro* Efficacy of 4 and 44 against *T. cruzi* Y-Strain Bloodstream Trypomastigotes and Intracellular Amastigotes in Cardiac Cells[a]

cpd.	*T. cruzi* Y bloodstream trypomastigotes IC_{50} (μM)	*T. cruzi* Y intracellular amastigotes IC_{50} (μM)	primary cardiac cells LC_{50} (μM)
4	>81	2.46 ± 0.3	>500
44	>81	0.26 ± 0.03	500

[a]IC_{50} values are depicted as means ± SEM of two independent determinations, using duplicates.

EXPERIMENTAL SECTION

Chemistry. *General.* All reagents and solvents were obtained from standard commercial sources and were of analytical grade. Unless otherwise specified, they were used as received. All moisture-sensitive reactions were carried out under an argon atmosphere. Reactions were carried out at ambient temperature, unless otherwise indicated. Reactions were monitored *via* analytical TLC or analytical LCMS. Analytical TLC was performed on Machery—Nagel precoated F254 aluminum plates and visualized by UV followed by staining with basic aq. $KMnO_4$, cerium-molybdate, or sulfuric acid-anisaldehyde spray. Analytical LCMS was performed on a Waters AutoPurification system

Table 7. Evaluation of Drug Sensitivity of 44 and Benznidazole (Bz) against *T. cruzi* in PMM Host Cells, Alone or with Coadministration of Verapamil (8 μM), Probenecid (700 μM), or Cyclosporin A (2 μM)

cpd.	*T. cruzi* (MRC-5) IC_{50} (μM)	*T. cruzi* (PMM) IC_{50} (μM)	*T. cruzi* (PMM) + verapamil IC_{50} (μM)	*T. cruzi* (PMM) + probenecid IC_{50} (μM)	*T. cruzi* (PMM) + cyclosporin A IC_{50} (μM)
44	0.32 ± 0.02	>64.0	>64.0	>64.0	>64.0
Bz	2.02 ± 0.28	1.96 ± 0.25			

(equipped with ACQUITY QDa (mass; 100−1000 amu)) and 2998 Photodiode Array (220−400 nm) using a Waters Cortecs C18 (2.7 μm, 100 mm × 4.6mm) column and a gradient system of HCOOH in H$_2$O (0.2%, v/v)/MeCN at a flow rate of 1.44 mL/min (95:05−00:100 in 6.5 min or 50:50−00:100 in 6.5 min), or a Waters Alliance XE separation module using a Phenomenex Kinetix C8 (2.6 μm, 50 mm × 2.10 mm) column and the same gradient system. Preparative HPLC was performed on the same system, using a Phenomenex Luna Omega Polar column (250 mm × 21 mm, 5 μm) and a gradient system of 0.2% formic acid in water/MeCN at a flow rate of 20 mL/min (gradients are specified in the individual procedures). Column chromatography was performed manually using Machery−Nagel 60 M silica gel (40−63 μm) or on a Reveleris X2 (Grace/Büchi) automated flash unit employing prepacked silica columns. Exact mass measurements were performed on a Waters LCT Premier XE time-of-flight (ToF) mass spectrometer equipped with a standard electrospray (ESI) and a modular Lockspray interface. Samples were infused in a MeCN/water (1:1) + 0.1% formic acid mixture at 100 μL/min. NMR spectra were recorded on a Varian Mercury 300 MHz spectrometer or a Bruker Avance Neo 400 MHz spectrometer. Chemical shifts (δ) are given in ppm, and spectra are referenced to the residual solvent peak. Coupling constants are given in Hz. Systematic numbering is employed for NMR assignments in the individual procedures. Melting points were determined on a Büchi-545 apparatus and are uncorrected. Purity was assessed by means of liquid chromatography−mass spectrometry (LCMS). All obtained final compounds had purity >95%, as assayed by analytical HPLC (UV), unless otherwise indicated.

General Procedure A: Large-Scale BF$_3$·OEt$_2$-Mediated Glycosylation with Commercially Available 1-O-Acetyl-2,3,5-tri-O-benzoyl-β-D-ribofuranose. The respective pyrazolo[3,4-d]pyrimidine (1.0 equiv) and 1-O-acetyl-tri-O-benzoyl-β-D-ribofuranose (1.5 equiv) were added to dry nitromethane (2.5 mL/mmol). The mixture was heated to reflux, when BF$_3$·OEt$_2$ (1.5 equiv) was added, upon which the solids started to dissolve. After 90 min of heating at reflux, the solvent was removed *in vacuo*. The resulting oil was dissolved in CH$_2$Cl$_2$ (sonicate until fully dissolved) and directly poured on a silica column (preconditioned with CH$_2$Cl$_2$). The column was eluted with 100% CH$_2$Cl$_2$ until all excess 1-O-acetyl-tri-O-benzoyl-β-D-ribofuranose had eluted and then with 5% acetone in CH$_2$Cl$_2$ to collect the product.

General Procedure B: Small-Scale BF$_3$·OEt$_2$-Mediated Glycosylation with Protected Ribose Derivative. The respective pyrazolo[3,4-d]pyrimidine (1.1 equiv) and ribose derivative (1.0 equiv) were added to dry nitromethane (2.5 mL/mmol). The mixture was heated to reflux, when BF$_3$·OEt$_2$ (1.0 equiv) was added, upon which the solids started to dissolve. After 90 min of heating at reflux, the solvent was removed *in vacuo*. The resulting oil was dissolved in CH$_2$Cl$_2$, celite (1.5 g/g starting material) was added, and the solvent was removed *in vacuo*. The resulting solid was purified by flash column chromatography to afford the protected nucleoside.

General Procedure C: Deprotection with NaOMe. Protected nucleoside (1.0 equiv) was dissolved in CH$_2$Cl$_2$ (0.5 mL/mmol). MeOH (5 mL/mmol) was added, followed by NaOMe in MeOH (5.4 M, 0.2 mL/mmol). The mixture was stirred at room temperature or 60 °C (for **36**) until TLC analysis (20% MeOH in CH$_2$Cl$_2$) indicated completion of the reaction. The reaction was neutralized to pH 7 *via* the addition of 4 N HCl, celite (1.5 g/g starting material) was added, and the solvents were removed *in vacuo*. The solid residue was brought onto a silica column and eluted with a mixture of MeOH and CH$_2$Cl$_2$ to isolate the final product.

General Procedure D: Catalytic Hydrogenation in Buffered MeOH. The nucleoside analogue was dissolved in a mixture of MeOH (8 mL/mmol) and aq. 1M NaOAc (2 mL/mmol). The flask was placed under a nitrogen atmosphere, and a catalytic amount of Pd/C was added. The atmosphere was exchanged for H$_2$ and the mixture was stirred until TLC analysis (20% MeOH in CH$_2$Cl$_2$) indicated completion of the reaction. The mixture was then filtered over celite, celite was added to the filtrate, and the solvents were removed *in*

vacuo. The resulting solid was purified *via* flash column chromatography to afford the final product.

General Procedure E: Suzuki Reaction. Compound **21** (1 equiv) or **23** (in the case of **76**, 1 equiv), boronic acid (1.5 equiv) or trifluoroborate salt (1.5 equiv) Na$_2$CO$_3$ (when a boronic acid was used, 3 equiv) or Cs$_2$CO$_3$ (when a trifluoroborate salt was used, 3 equiv), Pd(OAc)$_2$ (0.05 equiv), and TPPTS (0.12 equiv) were added to a 10 mL round-bottom flask, equipped with a stir bar. Next, the flask was evacuated and refilled with argon. This procedure was repeated three times in total. Next, MeCN (2 mL/mmol SM) and H$_2$O (4 mL/mmol SM) were added to the solids under argon. After 5 min of stirring, the mixture was heated to reflux. When the starting material was fully consumed (usually 1−3 h; as monitored by LCMS analysis), the mixture was cooled to ambient temperature and neutralized (pH ~ 7) with 4 M aq. HCl. Celite (5 g/mmol) was added, and the mixture was concentrated *in vacuo*. The residue was purified by flash column chromatography.

General Procedure F: Amide Coupling. The nucleoside carboxylic acid (1.0 equiv) was dissolved in DMF (10 mL/mmol). DIPEA (3.0 equiv) was added, followed by HCTU (2.5 equiv). After 5 min, the respective amine (5.0 equiv) was added and the reaction mixture was stirred overnight. When TLC or LCMS analysis indicated full conversion, the reaction mixture was diluted with excess EtOAc and transferred to a separation funnel. The organic phase was washed with 1 N HCl, aq. sat. NaHCO$_3$, and brine sequentially. The organic phase was then dried over Na$_2$SO$_4$ and concentrated *in vacuo*. The residue was used directly in the next reaction, without purification.

3-Bromo-4-amino-1H-pyrazolo[3,4-d]pyrimidine (12). 4-Amino-1H-pyrazolo[3,4-d]pyrimidine **3** (8.26 g, 61.1 mmol, 1.0 equiv) was dissolved in DMF (60 mL). NBS (11.4 g, 64.2 mmol, 1.05 equiv) was added, and the mixture was heated at 60 °C overnight. The mixture was cooled to room temperature and poured into ice-cold water (350 mL). The resulting suspension was stirred for 10 min at 0 °C and filtered overnight. The solids were collected and dried under a high vacuum overnight to afford **12** (11.9 g, 55.7 mmol, 91% yield) as an off-white solid. ^{1}H NMR (300 MHz, DMSO-d_6) δ 6.91 (1H, br. s, NH$_2$′), 7.72 (1H, br. s, NH$_2$″), 8.16 (1H, s, C-6), 13.75 (1H, br. s, NH) ppm. HRMS (ESI): calcd for C$_5$H$_5$BrN$_5$ ([M + H]$^+$): 213.9728, found: 213.9731.

3-Iodo-4-amino-1H-pyrazolo[3,4-d]pyrimidine (13). 4-Amino-1H-pyrazolo[3,4-d]pyrimidine **3** (5.68 g, 42.1 mmol, 1.0 equiv) was dissolved in DMF (40 mL). NIS (10.4 g, 46.3 mmol, 1.1 equiv) was added, and the mixture was heated at 80 °C overnight. The mixture was cooled to room temperature and poured into ice-cold water (350 mL). The resulting suspension was stirred for 10 min at 0 °C and filtered overnight. The solids were collected and dried under a high vacuum overnight to afford **13** (10.2 g, 39.1 mmol, 93% yield) as a white solid. ^{1}H NMR (300 MHz, DMSO-d_6) δ 8.16 (1H, s, C-6), 13.80 (1H, br. s, NH) ppm. HRMS (ESI): calcd for C$_5$H$_5$IN$_5$ ([M + H]$^+$): 261.9590, found: 261.9594.

3-Bromo-allopurinol (14). Allopurinol (4.55 g, 33.4 mmol, 1.0 equiv) was suspended in water (300 mL). Bromine (4.29 mL, 83.6 mmol, 2.5 equiv) was added carefully, and a reflux cooler with a septum was placed on top of the flask. The reflux cooler was connected *via* vacuum tubing to a large flask containing excess aq. 2 M Na$_2$S$_2$O$_3$ solution. The reaction mixture was heated at 90 °C overnight and cooled down to room temperature. A mixture of aq. sat. NaHCO$_3$ (75 mL) and aq. 2 M Na$_2$S$_2$O$_3$ (75 mL) was added through the reflux cooler, after which the reaction mixture turned white. The suspension was cooled down further to 0 °C, stirred for 10 min, and filtered. The solids were washed with ice-cold water (3×), collected, and dried over a high vacuum overnight to afford **14** (6.26 g, 29.1 mmol, 87%) as a light-yellow solid. ^{1}H NMR (300 MHz, DMSO-d_6) δ 8.04 (1H, d, J = 3.8 Hz), 12.22 (1H, br. s.), 13.98 (1H, br. s) ppm. ^{13}C NMR (75 MHz, DMSO-d_6) δ 104.5 (C-3a), 121.9 (C-3), 149.4 (C-7a), 154.6 (C-6), 157.0 (C-4) ppm. HRMS (ESI): calcd for C$_5$H$_4$BrN$_4$O ([M + H]$^+$): 214.9568, found: 214.9572.

3-Bromo-4-amino-1-(2′,3′,5′-tri-O-benzoyl-β-D-ribofuranosyl)-pyrazolo[3,4-d]pyrimidine[69] *(18).* Compound **12** (10.3 g, 48.1 mmol, 1.0 equiv) and 1-O-acetyl-tri-O-benzoyl-β-D-ribofuranose

(36.4 g, 72.2 mmol, 1.5 equiv) were subjected to general procedure A to afford **18** (20.3 g, 30.8 mmol, 64% yield) as a brown oil. ^{1}H NMR (300 MHz, DMSO-d_6) δ 4.51–4.67 (2 H, m, H-5′, H-5″), 4.82–4.89 (1H, m, H-4′), 6.10 (1H, t, J = 5.7 Hz, H-3′), 6.25 (1H, dd, J = 5.4, 3.4 Hz, H-2′), 6.67 (1H, d, J = 3.2 Hz, H-1′), 7.38–7.70 (9H, m, H$_{Phe}$), 7.84–8.05 (6H, m, H$_{Phe}$), 8.24 (1H, s, H-6) ppm. ^{13}C NMR (75 MHz, DMSO-d_6) δ 63.6 (C-5′), 71.3 (C-3′), 74.2 (C-2′), 79.5 (C-4′), 86.4 (C-1′), 100.3 (C-3a), 121.2 (C-3) 128.8 (C$_{Phe}$), 129.0 (C$_{Phe}$), 129.2 (C$_{Phe}$), 129.2 (C$_{Phe}$), 129.7 (C$_{Phe}$), 129.8 (C$_{Phe}$), 129.8 (C$_{Phe}$), 129.8 (C$_{Phe}$), 133.9 (C$_{Phe}$), 134.3 (C$_{Phe}$), 134.4(C$_{Phe}$), 155.5 (C-7a), 157.7 (C-6), 157.8 (C-4), 165.0 (C=O), 165.1 (C=O), 165.9 (C=O) ppm. HRMS (ESI): calcd for C$_{31}$H$_{25}$BrN$_5$O$_7$ ([M + H]$^+$): 658.0937, found: 658.0925.

3-Bromo-4-amino-1-(2′,5′-di-O-benzoyl-3′-deoxy-3′-fluoro-β-D-ribofuranosyl)pyrazolo[3,4-d]pyrimidine (19). Compound **12** (0.330 g, 1.54 mmol, 1.1 equiv) and compound **16** (0.563 g, 1.40 mmol) were subjected to general procedure B. Purification by flash column chromatography (automated, 0 → 5% MeOH in CH$_2$Cl$_2$) afforded semipure **19**, which was used as such in the next reaction. HRMS (ESI): calcd for C$_{24}$H$_{20}$BrFN$_5$O$_5$ ([M + H]$^+$): 556.0632, found: 556.0590.

3-Bromo-4-amino-1-(2′,5′-di-O-benzoyl-3′-deoxy-β-D-ribofuranosyl)pyrazolo[3,4-d]pyrimidine (20). Compound **12** (0.395 g, 1.84 mmol, 1.1 equiv) and compound **17** (0.643 g, 1.67 mmol, 1.0 equiv) were subjected to general procedure B. Purification by flash column chromatography (automated, 0 → 5% MeOH in CH$_2$Cl$_2$) afforded semipure **20**, which was used as such in the next reaction. HRMS (ESI): calcd for C$_{24}$H$_{21}$BrN$_5$O$_5$ ([M + H]$^+$): 538.726, found: 538.0706.

3-Bromo-4-amino-1-β-D-ribofuranosylpyrazolo[3,4-d]pyrimidine (21). Compound **18** (12.7 g, 19.4 mmol) was subjected to general procedure C (reaction time: 2 h). Purification was performed *via* flash column chromatography (manual, first 5% MeOH in CH$_2$Cl$_2$ to remove higher-running impurities, and then 15% MeOH in CH$_2$Cl$_2$) to isolate **21** (4.68 g, 13.5 mmol, 70% yield) as a white solid. ^{1}H NMR (300 MHz, DMSO-d_6) δ 3.38–3.47 (1H, m, H-5′), 3.50–3.60 (1H, m, H-5″), 3.89 (1H, dd, J = 10.0, 4.7 Hz, H-4′), 4.16 (1H, dd, J = 9.4, 4.7 Hz, H-3′), 4.55 (1H, dd, J = 10.8, 5.6 Hz, H-2′), 4.81 (1H, t, J = 5.9 Hz, OH), 5.16 (1H, d, J = 5.3 Hz, OH), 5.40 (1H, d, J = 5.9 Hz, OH), 6.06 (1H, d, J = 5.0 Hz, H-1′), 8.24 (1H, s, H-6) ppm. ^{13}C NMR (75 MHz, DMSO-d_6) δ 62.2 (C-5′), 70.6 (C-3′), 72.9 (C-2′), 85.3 (C-4′), 88.1 (C-1′), 99.7 (C-3a), 119.3 (C-3), 155.0 (C-7a), 157.0 (C-6), 157.4 (C-4) ppm. HRMS (ESI): calcd for C$_{10}$H$_{13}$BrN$_5$O$_4$ ([M + H]$^+$): 330.0202, found: 330.0198.

3-Bromo-4-amino-1-(3′-deoxy-3′-fluoro-β-D-ribofuranosyl)-pyrazolo[3,4-d]pyrimidine (22). Compound **19** (used directly from the previous reaction) was subjected to general procedure C (reaction time: 90 min). Purification *via* flash column chromatography (automated, 0 →10% MeOH in CH$_2$Cl$_2$) afforded **22** (97 mg, 0.279 mmol, 20% yield over 2 steps) as a white solid. ^{1}H NMR (300 MHz, DMSO-d_6) δ 3.47–3.54 (2H, m, H-5′, H-5″), 4.11–4.27 (1H, m, H-4′), 4.84–5.18 (3H, m, H-3′, H-2′, OH), 5.87 (1H, d, J = 6.7 Hz, OH), 6.06 (1H, d, J = 7.3 Hz, H-1′) ppm, 6.99 (1H, br. s, OH), 8.09 (1H, br. s, OH), 8.24 (1H, s, H-6). ^{13}C NMR (75 MHz, DMSO-d_6) δ 61.4 (d, J = 10.4 Hz, C-5′), 71.6 (d, J = 16.1 Hz, C-2′), 83.8 (d, J = 20.7 Hz, C-4′), 87.5 (C-1′), 92.9 (d, J = 182.0 Hz, C-3′), 100.5 (C-3a), 120.2 (C-3), 155.9 (C-7a), 157.6 (C-6), 157.9 (C-4) ppm. ^{19}F NMR (282 MHz, DMSO-d_6) δ −198.19 (1F, dt, J = 54.1, 25.2 Hz) ppm. HRMS (ESI): calcd for C$_{10}$H$_{12}$BrFN$_5$O$_3$ ([M + H]$^+$): 348.0108, found: 348.0090.

3-Bromo-4-amino-1-(3′-deoxy-β-D-ribofuranosyl)pyrazolo[3,4-d]pyrimidine (23). Compound **20** (used directly from the previous reaction) was subjected to general procedure C (reaction time: 2 h). Flash column chromatography (automated, 2 → 20% MeOH in CH$_2$Cl$_2$) afforded **23** (0.106 g, 0.321 mmol, 19% yield over 2 steps). ^{1}H NMR (300 MHz, DMSO-d_6) δ 1.98 (1H, ddd, J = 12.7, 6.3, 2.1 Hz, H-3′), 2.25 (1H, ddd, J = 12.8, 9.0, 5.7 Hz, H-3″), 3.38–3.50 (2H, m, H-5′, H-5″), 4.31 (1H, ddd, J = 11.6, 9.3, 5.8 Hz, H-4′), 4.55 (1H, dt, J = 5.4, 1.8 Hz, H-2′), 6.11 (1H, d, J = 1.8 Hz, H-1′), 8.24 (1H, s, H-6) ppm. ^{13}C NMR (75 MHz, DMSO-d_6) δ 36.3 (C-3′),

64.4 (C-5′), 74.6, (C-2′) 81.6 (C-4′), 91.0 (C-1′), 99.8 (C-3a), 119.6 (C-3), 155.0 (C-7a), 157.5 (C-6), 157.7 (C-4) ppm. HRMS (ESI): calcd for C$_{10}$H$_{13}$BrN$_5$O$_3$ ([M + H]$^+$): 330.0202, found: 330.0195.

4-Amino-1-β-D-ribofuranosylpyrazolo[3,4-d]pyrimidine[70] *(4).* Compound **21** (120 mg, 0.347 mmol) was subjected to general procedure D (reaction time: 2 h). Flash column chromatography (automated, 4 → 20% MeOH in CH$_2$Cl$_2$) afforded **4** (57 mg, 0.213 mmol, 61% yield) as a white solid. ^{1}H NMR (300 MHz, DMSO-d_6) δ 3.38–3.64 (2H, m, H-5′, H-5″), 3.87–3.96 (1H, m, H-4′), 4.22 (1H, dd, J = 9.7, 4.4 Hz, H-3′), 4.60 (1H, dd, J = 10.0, 5.0 Hz, H-2′), 4.88 (1H, t, J = 5.9 Hz, OH), 5.14 (1H, d, J = 4.7 Hz, OH), 5.36 (1H, d, J = 6.4 Hz, OH), 6.09 (1H, d, J = 4.7 Hz, H-1′), 8.18 (1H, s, H-3), 8.20 (1H, s, H-6) ppm. ^{13}C NMR (101 MHz, DMSO-d_6) δ 62.5 (C-5′), 71.0 (C-2′), 73.2 (C-3′), 85.1 (C-4′), 88.6 (C-1′), 100.5 (C-3a), 133.5 (C-3), 154.1 (C-7a), 156.2 (C-6), 158.1 (C-4) ppm. HRMS (ESI): calcd for C$_{10}$H$_{14}$N$_5$O$_4$ ([M + H]$^+$): 268.1046, found: 268.1032. Spectral data are in accordance with literature values.[70]

4-Amino-1-(3′-deoxy-3′-fluoro-β-D-ribofuranosyl)pyrazolo[3,4-d]pyrimidine (24). Compound **22** (0.058 g, 0.167 mmol) was subjected to general procedure D (reaction time: 15 min). Purification *via* flash column chromatography (automated, 2 → 15% MeOH in CH$_2$Cl$_2$) afforded **24** (37 mg, 0.137 mmol, 82% yield) as a white solid. ^{1}H NMR (300 MHz, DMSO-d_6) δ 3.47–3.65 (2H, m, H-5′, H-5″), 4.21 (1H, dt, J = 24.9, 4.7 Hz, H-4′), 4.93–5.31 (3H, m, H-3′, H-2′, OH), 5.83 (1H, d, J = 6.4 Hz, OH), 6.10 (1H, d, J = 7.0 Hz, H-1′), 7.50–8.07 (2H, m, NH$_2$), 8.20 (2H, s, H-6, H-3) ppm. ^{13}C NMR (75 MHz, DMSO-d_6) δ 61.2 (d, J = 10.4 Hz, C-5′), 71.3 (d, J = 17.3 Hz, C-2′), 83.2 (d, J = 21.9 Hz, C-4′), 87.7 (C-1′), 92.7 (d, J = 182.0 Hz, C-3′), 100.8 (C-3a), 133.6 (C-3), 154.3 (C-7a), 156.2 (C-6), 158.1 (C-4) ppm. ^{19}F NMR (282 MHz, DMSO-d_6) δ −198.52 (1F, dt, J = 54.1, 25.2 Hz) ppm. HRMS (ESI): calcd for C$_{10}$H$_{13}$FN$_5$O$_3$ ([M + H]$^+$): 270.1002, found: 270.0998.

4-Amino-1-(3′-deoxy-β-D-ribofuranosyl)pyrazolo[3,4-d]-pyrimidine (25). Compound **23** (0.050 g, 0.151 mmol) was subjected to general procedure D (reaction time: 3 h). Purification *via* flash column chromatography (automated, 2 → 15% MeOH in CH$_2$Cl$_2$) afforded **25** (26 mg, 0.100 mmol, 66% yield) as a white solid. ^{1}H NMR (300 MHz, DMSO-d_6) δ 1.98 (1H, ddd, J = 12.7, 6.2, 2.2 Hz, H-3′), 2.33 (1H, ddd, J = 12.7, 9.1, 5.7 Hz, H-3″), 3.36–3.53 (2H, m, H-5′, H-5″), 4.32 (1H, ddd, J = 11.4, 9.1, 5.9 Hz, H-4′), 4.51–4.61 (1H, m, H-2′), 4.74 (1H, t, J = 5.7 Hz, OH), 5.53 (1H, d, J = 3.8 Hz, OH), 6.14 (1H, d, J = 1.5 Hz, H-1′), 7.50–7.98 (2H, br. m, NH$_2$), 8.15 (1H, s, H-3), 8.19 (1H, s, H-6) ppm. ^{13}C NMR (75 MHz, DMSO-d_6) δ 36.1 (C-3′), 64.2 (C-5′), 74.5 (C-2′), 81.0 (C-4′), 90.7 (C-1′), 100.1 (C-3a), 133.2 (C-3a), 153.7 (C-7a), 156.1 (C-6), 158.0 (C-4) ppm. HRMS (ESI): calcd for C$_{10}$H$_{14}$N$_5$O$_3$ ([M + H]$^+$): 252.1079, found: 252.1075.

3-Bromo-4-oxo-1-(2′,3′,5′-tri-O-benzoyl-β-D-ribofuranosyl)-pyrazolo[3,4-d]pyrimidine[69] *(26).* Compound **14** (6.45 g, 30.0 mmol, 1.0 equiv) and 1-O-acetyl-tri-O-benzoyl-β-D-ribofuranose (22.7 g, 45.0 mmol, 1.5 equiv) were subjected to general procedure A to afford, after recrystallization from MeOH, **26** (6.26 g, 9.49 mmol, 32% yield) as a white solid. ^{1}H NMR (400 MHz, CDCl$_3$) δ 4.66 (1H, dd, J = 12.2, 4.6 Hz, H-5′), 4.80 (1H, dd, J = 12.3, 3.8 Hz, H-5″), 4.84–4.89 (1H, m, H-4′), 6.26 (1H, dd, J = 6.1, 5.3 Hz, H-3′), 6.34 (1H, dd, J = 5.3, 3.0 Hz, H-2′), 6.72 (1H, d, J = 2.9 Hz, H-1), 7.34–7.62 (9H, m, H$_{Phe}$), 7.94–8.15 (7H, m, H$_{Phe}$, H-6), 11.91 (1H, br. s., NH) ppm. ^{13}C NMR (101 MHz, CDCl$_3$) δ 63.5 (C-5′), 71.6 (C-2′), 74.6 (C-3′), 80.4 (C-4′), 87.2 (C-1′), 106.0 (C-3a), 124.5 (C-3), 128.5 (C$_{Phe}$), 128.5 (C$_{Phe}$), 128.5 (C$_{Phe}$), 128.6 (C$_{Phe}$), 128.7 (C$_{Phe}$), 129.5 (C$_{Phe}$), 129.8 (C$_{Phe}$), 129.8 (C$_{Phe}$), 129.9 (C$_{Phe}$), 133.2 (C$_{Phe}$), 133.6 (C$_{Phe}$), 133.7 (C$_{Phe}$), 148.1 (H-7a), 153.9 (H-6), 158.5 (H-4), 165.1 (C=O), 165.2 (C=O), 166.3 (C=O) ppm. HRMS (ESI): calcd for C$_{31}$H$_{24}$BrN$_4$O$_8$ ([M + H]$^+$): 659.0778, found: 659.0774.

3-Bromo-4-oxo-1-(2′,5′-tri-O-benzoyl-3′-deoxy-3′-fluoro-β-D-ribofuranosyl)pyrazolo[3,4-d]pyrimidine (27). Compounds **14** (0.338 g, 1.57 mmol, 1.1 equiv) and **16** (0.575 g, 1.43 mmol, 1.0 equiv) were subjected to general procedure B. TLC analysis (5% MeOH in CH$_2$Cl$_2$) indicated the presence of a major apolar spot and two smaller more polar spots. The major apolar spot was presumed to

be the desired N-1 regioisomer[72] **27** and was isolated *via* flash chromatography (automated, 0 → 5% MeOH in CH$_2$Cl$_2$) and used as such in the next reaction. HRMS (ESI): calcd for C$_{24}$H$_{19}$BrFN$_4$O$_6$ ([M + H]$^+$): 557.0472, found: 557.0457.

3-Bromo-4-oxo-1-(2′,5′-tri-O-benzoyl-3′-deoxy-β-D-ribofuranosyl)pyrazolo[3,4-d]pyrimidine (28). Compounds **14** (0.348 g, 1.62 mmol, 1.1 equiv) and **17** (0.565 g, 1.47 mmol, 1.0 equiv) were subjected to general procedure B. TLC analysis (5% MeOH in CH$_2$Cl$_2$) indicated the presence of a major apolar spot and two smaller more polar spots. The major apolar spot was presumed to be the desired N-1 regioisomer[72] **28** and was isolated *via* flash chromatography (automated, 0 → 5% MeOH in CH$_2$Cl$_2$) and used as such in the next reaction. HRMS (ESI): calcd for C$_{24}$H$_{20}$BrN$_4$O$_6$ ([M + H]$^+$): 539.0566, found: 539.0552.

3-Bromo-4-oxo-1-β-D-ribofuranosyl-pyrazolo[3,4-d]pyrimidine[69] *(29).* Compound **26** (0.530 g, 0.804 mmol) was subjected to general procedure C (reaction time: 1 h). Purification *via* flash column chromatography (automated, 4 → 20% MeOH in CH$_2$Cl$_2$) afforded **29** (105 mg, 0.302 mmol, 38% yield) as a white solid. ^{1}H NMR (300 MHz, DMSO-d_6) δ 3.36−3.47 (1H, m, H-5′), 3.48−3.59 (1H, m, H-5″), 3.88 (1H, dd, J = 10.3, 4.7 Hz, H-4′), 4.10−4.18 (1H, m, H-3′), 4.44−4.53 (1H, m, H-2′), 4.66−4.80 (1H, m, OH), 5.16 (1H, br. s., OH), 5.42 (1H, br. s., OH), 6.00 (1H, d, J = 5.0 Hz, H-1′), 8.15 (1H, s, H-6), 12.41 (1H, br. s., NH) ppm. HRMS (ESI): calcd for C$_{10}$H$_{12}$BrN$_4$O$_5$ ([M + H]$^+$): 346.9991, found: 347.0004. Spectral data are in accordance with literature values.[69]

3-Bromo-4-oxo-1-(3′-deoxy-3′-fluoro-β-D-ribofuranosyl)-pyrazolo[3,4-d]pyrimidine (30). Compound **27** (used directly from the previous step) was subjected to general procedure C (reaction time: 3 h). Flash column chromatography (automated, 2 → 12% MeOH in CH$_2$Cl$_2$), followed by an additional purification *via* preparative RP-HPLC (0.2% formic acid in H$_2$O/MeCN 98:02 to 0:100 in 18 min) afforded **30** (56 mg, 0.160 mmol, 11% yield over 2 steps) as a white solid. ^{1}H NMR (300 MHz, DMSO-d_6) δ 3.44−3.62 (2H, m, H-5′, H-5″), 4.21 (1H, dt, J = 25.8, 5.3 Hz, H-4′), 4.90 (1H, ddd, J = 24.6, 7.0, 4.4 Hz, H-2′), 5.08 (1H, dd, J = 54.2, 4.1 Hz, H-3′), 6.03 (1H, d, J = 7.0 Hz, H-1′), 8.18 (1H, s, H-6), 12.43 (1H, br. s, NH) ppm. ^{13}C NMR (75 MHz, DMSO-d_6) δ 60.9 (d, J = 10.4 Hz, C-5′), 71.5 (d, J = 16.1 Hz, C-2′), 83.6 (d, J = 20.7 Hz, C-4′), 87.0 (C-1′), 92.3 (d, J = 183.1 Hz, C-3′), 105.4 (C-3a), 122.8 (C-3), 150.3 (C-7a), 154.5 (C-6), 156.3 (C-4) ppm. ^{19}F NMR (282 MHz, DMSO-d_6) δ −198.39 (1F, dt, J = 54.1, 25.2 Hz) ppm. HRMS (ESI): calcd for C$_{10}$H$_{11}$BrFN$_4$O$_4$ ([M + H]$^+$): 348.9948, found: 348.9996.

3-Bromo-4-oxo-1-(3′-deoxy-β-D-ribofuranosyl)pyrazolo[3,4-d]-pyrimidine (31). Compound **28** (used directly from the previous step) was subjected to general procedure C (reaction time: 3 h). Flash column chromatography (automated, 2 → 15% MeOH in CH$_2$Cl$_2$), followed by an additional purification *via* preparative RP-HPLC (0.2% formic acid in H$_2$O/MeCN 98:02 to 30:70 in 18 min) afforded **31** (31 mg, 0.093 mmol, 6% yield over 2 steps) as a white solid. ^{1}H NMR (300 MHz, CD$_3$OD) δ 2.10 (1H, ddd, J = 13.1, 6.4, 1.9 Hz, H-3′), 2.48 (1H, ddd, J = 13.2, 9.4, 5.6 Hz, H-3″), 3.62 (1H, dd, J = 11.7, 5.9 Hz, H-5′), 3.70 (1H, dd, J = 11.7, 4.1 Hz, H-5″), 4.46−4.56 (1H, m, H-4′), 4.67 (1H, dt, J = 5.6, 1.6 Hz, H-2′), 6.24 (1H, d, J = 1.5 Hz, H-1′), 8.05 (1H, s, H-6) ppm. ^{13}C NMR (75 MHz, CD$_3$OD) δ 37.0 (C-3′), 66.1 (C-5′), 77.3 (C-2′), 83.6 (C-4′), 93.3 (C-1′), 107.0 (C-3a), 124.4 (C-3), 150.5 (C-7a), 155.5 (C-6), 159.1 (C-4) ppm. HRMS (ESI): calcd for C$_{10}$H$_{12}$BrN$_4$O$_4$ ([M + H]$^+$): 331.0042, found: 331.0047.

4-Oxo-1-β-D-ribofuranosylpyrazolo[3,4-d]pyrimidine (Allopurinol Riboside)[72] *(2).* Compound **29** (65 mg, 0.187 mmol) was submitted to general procedure D (reaction time: 1 h). Flash column chromatography (automated, 10 → 35% MeOH in CH$_2$Cl$_2$) afforded **2** (27 mg, 0.101 mmol, 54% yield) as a white solid. ^{1}H NMR (300 MHz, DMSO-d_6) δ 3.43 (1H, dd, J = 11.7, 5.9 Hz, H-5′), 3.57 (1H, dd, J = 11.7, 4.4 Hz, H-5″), 3.91 (1H, dd, J = 10.0, 5.0 Hz, H-4′), 4.21 (1H, t, J = 4.8 Hz, H-3′), 4.54 (1H, m, J = 4.5, 4.5 Hz, H-2′), 4.77 (1H, br. s., OH), 4.96−5.63 (2H, m, OH, OH), 6.07 (1H, d, J = 4.4 Hz, H-1′), 8.13 (1H, s, H-3), 8.17 (1H, s, H-6), 12.37 (1H, br. s, NH) ppm. HRMS (ESI): calcd for C$_{10}$H$_{13}$N$_4$O$_5$ ([M + H]$^+$):

269.0886, found: 269.0891. Spectral data are in accordance with literature values.[72]

4-Oxo-1-(3′-deoxy-3′-fluoro-β-D-ribofuranosyl)pyrazolo[3,4-d]-pyrimidine (32). Compound **30** (0.031 g, 0.089 mmol) was subjected to general procedure D (reaction time: 30 min). Purification *via* flash column chromatography afforded **32** (20 mg, 0.074 mmol, 83% yield) as a white solid. ^{1}H NMR (300 MHz, DMSO-d_6) δ 3.47−3.57 (2H, m, H-5′, H-5″), 4.13−4.29 (1H, m, H-4′), 4.89−5.22 (2H, m, H-3′, H-2′), 6.09 (1H, d, J = 7.0 Hz, H-1′), 8.15 (1H, s, H-6), 8.22 (1H, s, H-4), 12.22 (1H, br. s, NH) ppm. ^{13}C NMR (75 MHz, DMSO-d_6) δ 61.0 (d, J = 10.4 Hz, C-5′), 71.6 (d, J = 16.1 Hz, C-2′), 83.4 (d, J = 20.7 Hz, C-4′), 87.1 (C-1′), 92.5 (d, J = 182.0 Hz, C-3′), 106.6 (C-3a), 135.8 (C-3), 148.9 (C-7a), 153.5 (C-6), 157.0 (C-4) ppm. ^{19}F NMR (282 MHz, DMSO-d_6) δ −198.82 (1F, dt, J = 54.1, 24.8 Hz) ppm. HRMS (ESI): calcd for C$_{10}$H$_{12}$FN$_4$O$_4$ ([M + H]$^+$): 271.0843, found: 271.0834.

4-Oxo-1-(3′-deoxy-β-D-ribofuranosyl)pyrazolo[3,4-d]pyrimidine (33). Compound **31** (0.023 g, 0.069 mmol) was subjected to general procedure D (reaction time: 30 min). Purification *via* flash column chromatography afforded **33** (14 mg, 0.056 mmol, 80% yield) as a white solid. ^{1}H NMR (300 MHz, DMSO-d_6) δ 1.91−2.05 (1H, m, H-3′), 2.23−2.37 (1H, m, H-3″), 3.33−3.56 (2H, m, H-5′, H-5″), 4.25−4.42 (1H, m, H-4′), 4.49−4.63 (1H, m, H-2′), 4.85 (1H, br. s, OH), 5.59 (1H, br. s, OH), 6.12 (1H, s, H-1′), 8.13 (1H, s, H-3), 8.14 (1H, s, H-6), 12.2 (1H, s, NH) ppm. ^{13}C NMR (75 MHz, DMSO-d_6) δ 36.0 (C-3′), 64.1 (C-5′), 74.7 (C-2′), 81.4 (C-4′), 90.7 (C-1′), 105.9 (C-3a), 135.4 (C-3), 148.5 (C-7a), 152.4 (C-6), 157.1 (C-4) ppm. HRMS (ESI): calcd for C$_{10}$H$_{13}$N$_4$O$_4$ ([M + H]$^+$): 253.0937, found: 253.0921.

3-Iodo-4-amino-1-(2′,3′,5′-tri-O-benzoyl-β-D-ribofuranosyl)-pyrazolo[3,4-d]pyrimidine[95] *(34).* Compound **13** (10.1 g, 39.1 mmol, 1.0 equiv) and 1-O-acetyl-2,3,5-tri-O-benzoyl-β-D-ribofuranose (29.6 g, 58.7 mmol, 1.5 equiv) were subjected to general procedure A to afford **34** (21.2 g, 30.0 mmol, 77% yield) as a yellow oil. ^{1}H NMR (300 MHz, CDCl$_3$) δ 4.56−4.90 (3H, m, H-5′, H-5″, H-4′), 6.20 (1H, t, J = 5.6 Hz, H-3′), 6.36 (1H, dd, J = 5.0, 3.2 Hz, H-2′), 6.76 (1H, d, J = 2.9 Hz, H-2′), 7.35−7.62 (9H, m, H$_{Phe}$), 7.91−8.14 (6H, m, H$_{Phe}$), 8.34 (1H, s, H-6) ppm. HRMS (ESI): calcd for C$_{31}$H$_{25}$IN$_5$O$_7$ ([M + H]$^+$): 706.0799, found: 706.0824. Spectral data are in accordance with literature values.[95]

4-Amino-1-(2′,3′,5′-tri-O-benzoyl-β-D-ribofuranosyl)pyrazolo-[3,4-d]pyrimidine[70] *(35).* 4-Aminopyrazolo[3,4-d]pyrimidine **3** (3.16 g, 23.4 mmol, 1.0 equiv) and 1-O-acetyl-2,3,5-tri-O-benzoyl-β-D-ribofuranose (17.7 g, 35.1 mmol, 1.5 equiv) were subjected to general procedure A to afford **35** (8.06 g, 13.9 mmol, 59% yield) as a colorless foam. ^{1}H NMR (300 MHz, DMSO-d_6) δ ppm 4.54 (1H, dd, J = 12.3, 4.4 Hz, H-5′), 4.68 (1H, dd, J = 12.3, 3.5 Hz, H-5″), 4.89−4.95 (1H, m, H-4′), 6.17−6.33 (2H, m, H-2′, H-3′), 6.75 (1H, d, J = 2.6 Hz, H-1′), 7.40−7.56 (6H, m, H$_{Phe}$), 7.59−7.72 (3H, m, H$_{Phe}$), 7.87−8.03 (6H, m, H$_{Phe}$), 8.47 (1H, br. s, NH$_2$), 8.40 (1H, s, H-3), 8.43 (1H, s, H-6), 9.13 (1H, br. s., NH$_2$′) ppm. ^{13}C NMR (75 MHz, DMSO-d_6) δ 63.2 (C-5′), 71.0 (C-2′), 74.2 (C-3′), 79.1 (C-4′), 86.2 (C-1′), 100.3 (-3a), 128.4 (C$_{Phe}$), 128.5 (C$_{Phe}$), 128.6 (C$_{Phe}$), 128.7 (C$_{Phe}$), 128.8 (C$_{Phe}$), 129.2 (C$_{Phe}$), 129.3 (C$_{Phe}$), 129.4 (C$_{Phe}$), 133.5 (C$_{Phe}$), 133.9 (C$_{Phe}$), 134.0 (C$_{Phe}$), 135.7 (C-3), 152.0 (C-7a), 152.8 (C-6), 154.5 (C-4), 164.6 (C=O), 164.7 (C=O), 165.4 (C=O) ppm. HRMS (ESI): calcd for C$_{31}$H$_{26}$N$_5$O$_7$ ([M + H]$^+$): 580.1832, found: 580.1793. Spectral data are in accordance with literature values.[70]

3-Iodo-4-amino-1-β-D-ribofuranosylpyrazolo[3,4-d]pyrimidine[95] *(36).* Compound **34** (7.43 g, 10.5 mmol) was subjected to general procedure C, with the exception that the temperature was raised to 60 °C to aid dissolution, (reaction time: 2 h). Purification *via* flash column chromatography (manual, 5% MeOH in CH$_2$Cl$_2$ to remove higher-running impurities and then 15% MeOH in CH$_2$Cl$_2$) afforded **36** (2.63 g, 6.69 mmol, 64% yield) as an off-white solid. ^{1}H NMR (300 MHz, DMSO-d_6) δ 3.43 (1H, dd, J = 11.7, 5.6 Hz, H-5′), 3.55 (1H, dd, J = 11.7, 4.4 Hz, H-5″), 3.89 (1H, dd, J = 10.0, 4.4 Hz, H-4′), 4.16 (1H, t, J = 4.7 Hz, H-3′), 4.53−4.60 (1H, m, H-2′), 4.82 (1H, br. s, OH), 5.15 (1H, br. s, OH), 5.38 (1H, br. s, OH), 6.03 (1H, d, J = 5.0 Hz, H-1′), 8.23 (1H, s, H-6) ppm. ^{13}C NMR (75

MHz, DMSO-d_6) δ 62.7 (C-5'), 71.1 (C-2'), 73.3 (C-3'), 85.7 (C-4'), 88.7 (C-1'), 103.9 (C-3a), 121.0 (C-3), 154.9 (C-7a), 156.8 (C-6), 158.2 (C-4) ppm. HRMS (ESI): calcd for $C_{10}H_{13}IN_5O_4$ ([M + H]$^+$): 394.0012, found: 394.0021.

3-Bromo-4-chloropyrazolo[3,4-d]pyrimidine (37). 4-Chloropyrazolo[3,4-d]pyrimidine (5.00 g, 32.4 mmol, 1.0 equiv) was dissolved in DMF (50 mL). NBS (6.33 g, 35.6 mmol, 1.1 equiv) was added, and the mixture was heated at 50 °C for 3 h. H$_2$O (100 mL) was added, and the mixture was extracted with EtOAc (3 ×150 mL). The combined organic phases were dried over Na$_2$SO$_4$ and concentrated *in vacuo*. The residue was used crude in the next reaction. HRMS (ESI): calcd for $C_5H_2BrClN_4$ ([M + H]$^+$): 232.9230, found: 232.9242.

3-Bromo-4-methoxypyrazolo[3,4-d]pyrimidine[73] (38). Compound 37 (crude) was dissolved in MeOH (50 mL). NaOMe (5.4 M in MeOH, 20 mL) was added, and the mixture was heated at 70 °C for 2 h. The reaction was quenched *via* the addition of aq. sat. NH$_4$Cl (200 mL) and H$_2$O (50 mL). The mixture was extracted with EtOAc (3 × 250 mL), and the combined organic phases were dried over Na$_2$SO$_4$ and concentrated *in vacuo*. The residue was purified by flash column chromatography (manual, petroleum ether/EtOAc 60:40) to afford 38 (3.76 g, 16.4 mmol, 51% yield over 2 steps) as an off-white solid. ^{1}H NMR (400 MHz, DMSO-d_6) δ 4.10 (3H, s, CH$_3$), 8.56 (1H, s, H-6), 14.27 (1H, br. s., NH) ppm. ^{13}C NMR (101 MHz, DMSO-d_6) δ 54.4 (C-5'), 101.4 (C-3a), 118.1 (C-3), 156.0 (C-7a), 156.4 (C-6), 163.0 (C-4) ppm. HRMS (ESI): calcd for $C_6H_6BrN_4O$ ([M + H]$^+$): 228.9725, found: 228.9738. Spectral data are in accordance with literature values.[73]

3-Bromo-4-methoxy-1-(2'-deoxy-3',5'-di-O-(p-toluoyl)-β-D-ribofuranosyl)pyrazolo[3,4-d]pyrimidine[73] (39). Powdered KOH (1.60 g, 28.6 mmol, 4.0 equiv) and TDA-1 (0.227 mL, 0.71 mmol, 0.1 equiv) were added to a suspension of 38 (1.64 g, 7.14 mmol, 1.0 equiv) in MeCN (250 mL). The mixture was stirred for 20 min before Hoffer's chlorosugar (2.64 g, 6.78 mmol, 0.95 equiv) was added. The mixture was stirred for another 30 min and filtered over celite. The filtrate was concentrated *in vacuo*, and the residue was adsorbed onto celite and purified *via* flash column chromatography (automated, 5 → 35% EtOAc in petroleum ether) to afford 39 (310 mg, 0.55 mmol, 8% yield) as a white solid. ^{1}H NMR (400 MHz, CDCl$_3$) δ 2.41 (3H, s, CH$_{3\ toluoyl}$), 2.44 (3H, s, CH$_{3\ toluoyl}$), 2.67 (1H, ddd, J = 14.3, 6.4, 3.0 Hz, H-2'), 3.52 (1H, dt, J = 14.0, 6.8 Hz, H-2''), 4.19 (3H, s, OCH$_3$), 4.47−4.68 (3H, m, H-5', H-5'', H-4'), 5.80−5.92 (1H, m, H-3'), 6.91 (1H, t, J = 6.7 Hz, H-1'), 7.18−7.33 (4H, m, H$_{toluoyl}$), 7.88−7.99 (2H, m, H$_{toluoyl}$), 8.00−8.07 (2H, m, H$_{toluoyl}$), 8.51−8.63 (1H, s, H-6) ppm. ^{13}C NMR (101 MHz, CDCl$_3$) δ 21.7 (2 × CH$_{3\ toluoyl}$), 35.8 (OCH$_3$), 54.6 (C-2'), 64.1 (C-5'), 75.4 (C-3'), 82.8 (C-4'), 85.0 (C-1'), 103.8 (C-3a), 120.4 (C-3), 126.6 (C$_{toluoyl}$), 127.0 (C$_{toluoyl}$), 129.1 (C$_{toluoyl}$), 129.2 (C$_{toluoyl}$), 129.8 (C$_{toluoyl}$), 129.9 (C$_{toluoyl}$), 143.7 (C$_{toluoyl}$), 144.3 (C$_{toluoyl}$), 156.4 (-6), 163.9 (C-4), 165.9 (C=O), 166.3 (C=O) ppm. HRMS (ESI): calcd for $C_{27}H_{26}BrN_4O_6$ ([M + H]$^+$): 581.1036, found: 581.1009. Spectral data are in accordance with literature values.[73]

4-Amino-3-bromo-1-(2'-deoxy-β-D-ribofuranosyl)pyrazolo[3,4-d]pyrimidine[64] (40). Compound 39 (0.310 g, 0.48 mmol) was stirred in 7 N NH$_3$ in MeOH (20 mL) in a pressure tube at 90 °C for 24 h. The reaction vessel was cooled down to room temperature before it was opened, and its contents were transferred to a pear-shaped flask. The volatiles were removed *in vacuo*, and the residue was adsorbed onto celite and purified by flash column chromatography (automated, 2 → 10% MeOH in CH$_2$Cl$_2$ + 1% NH$_4$OH) to afford 40 (120 mg, 0.363 mmol, 76% yield) as a white solid. ^{1}H NMR (400 MHz, DMSO-d_6) δ 2.25 (1H, m, J = 13.3, 6.8, 4.2 Hz, H-2'), 2.74 (1H, dt, J = 13.0, 6.3 Hz, H-2''), 3.36 (1H, dt, J = 11.6, 5.9 Hz, H-5'), 3.50 (1H, dt, J = 11.4, 5.6 Hz, H-5''), 3.80 (1H, td, J = 5.7, 3.6 Hz, H-4'), 4.34−4.46 (1H, m, H-3'), 4.75 (1H, t, J = 5.8 Hz, OH), 5.27 (1H, d, J = 4.6 Hz, OH), 6.51 (1H, t, J = 6.4 Hz, H-1'), 8.23 (1H, s, H-6) ppm. ^{13}C NMR (101 MHz, DMSO-d_6) δ 37.8 (C-2'), 62.3 (C-5'), 70.8 (C-3'), 83.9 (C-4'), 87.7 (C-1'), 99.8 (C-3a), 119.0 (C-3), 154.5 (C-7a), 157.0 (C-6), 157.4 (C-4) ppm. HRMS (ESI): calcd for

$C_{10}H_{13}BrN_5O_3$ ([M + H]$^+$): 330.0202, found: 330.0231. Spectral data are in accordance with literature values.[64]

4-Amino-1-(2'-deoxy-β-D-ribofuranosyl)pyrazolo[3,4-d]-pyrimidine[74] (41). Compound 40 (72 mg, 0.218 mmol) was subjected to general procedure D (reaction time: 30 min). Purification *via* flash column chromatography (automated, 5 → 15% MeOH in CH$_2$Cl$_2$) afforded 41 (52 mg, 0.100 mmol, 46% yield) as a white solid. ^{1}H NMR (400 MHz, DMSO-d_6) δ 2.23 (1H, ddd, J = 13.1, 6.7, 3.9 Hz, H-2'), 2.80 (1H, dt, J = 13.0, 6.3 Hz, H-2''), 3.33−3.41 (1H, m, H-5', partially under water peak), 3.52 (1H, dd, J = 11.4, 5.3 Hz, H-5''), 3.81 (1H, td, J = 5.6, 3.5 Hz, H-4'), 4.43 (1H, br. s., H-3'), 4.80 (1H, br. s., OH), 5.24 (1H, br. s., OH), 6.54 (1H, t, J = 6.5 Hz, H-1'), 7.45−7.98 (2H, m, NH$_2$), 8.15 (1H, s, H-3), 8.19 (1H, s, H-6) ppm. ^{13}C NMR (101 MHz, DMSO-d_6) δ 38.0 (C-2'), 62.5 (C-5'), 71.1 (C-3'), 84.0 (C-4'), 87.6 (C-1'), 100.5 (C-3a), 133.1 (C-3), 153.7 (C-7a), 156.0 (C-6), 158.0 (C-4) ppm. HRMS (ESI): calcd for $C_{10}H_{14}N_5O_3$ ([M + H]$^+$): 252.1097, found: 252.1084. Spectral data are in accordance with literature values.[96]

3-Phenyl-4-amino-1-β-D-ribofuranosylpyrazolo[3,4-d]-pyrimidine[97] (42). Compound 21 (0.132 g, 0.38 mmol) was subjected to general procedure E, using phenylboronic acid as the coupling partner and Na$_2$CO$_3$ as the base. Purification *via* flash column chromatography (automated, 2 → 15% MeOH in CH$_2$Cl$_2$), followed by an additional purification by preparative RP-HPLC (0.2% formic acid in H$_2$O/MeCN 0:100 to 49:51 in 18 min) afforded 42 (44 mg, 0.118 mmol, 34% yield) as a white solid. ^{1}H NMR (300 MHz, DMSO-d_6) δ 3.42−3.53 (1H, m, H-5'), 3.55−3.67 (1H, m, H-5''), 3.93 (1H, dd, J = 10.0, 4.7 Hz, H-4'), 4.22−4.30 (1H, m, H-3'), 4.60−4.70 (1H, m, H-2'), 4.77−4.89 (1H, m, OH), 5.06−5.20 (1H, m, OH), 5.33−5.49 (1H, m, OH), 6.19 (1H, d, J = 4.7 Hz, H-1'), 7.47−7.62 (3H, m, H$_{Phe}$), 7.65−7.72 (2H, m, H$_{Phe}$), 8.29 (1H, s, H-6) ppm. HRMS (ESI): calcd for $C_{16}H_{18}N_5O_4$ ([M + H]$^+$): 344.1359, found: 344.1356. Spectral data are in accordance with literature values.[97]

3-(4-Methoxyphenyl)-4-amino-1-β-D-ribofuranosylpyrazolo[3,4-d]pyrimidine (43). Compound 21 (0.087 g, 0.25 mmol) was subjected to general procedure E, using 4-methoxyphenylboronic acid as the coupling partner and Na$_2$CO$_3$ as the base. Purification *via* flash column chromatography (automated, 1 → 12% MeOH in CH$_2$Cl$_2$), followed by an additional purification by preparative RP-HPLC (0.2% formic acid in H$_2$O/MeCN 98:02 to 41:59 in 10.5 min) afforded 43 (42 mg, 0.112 mmol, 45% yield) as a white solid. ^{1}H NMR (300 MHz, DMSO-d_6) δ 3.46 (1H, dd, J = 11.7, 5.6 Hz, H-5'), 3.60 (1H, dd, J = 11.7, 4.1 Hz, H-5''), 3.84 (3H, s, CH$_3$), 3.93 (1H, dd, J = 9.6, 4.7 Hz, H-4'), 4.26 (1H, t, J = 4.8 Hz, H-3'), 4.65 (1H, t, J = 4.8 Hz, H-2'), 6.18 (1H, d, J = 4.7 Hz, H-1'), 7.05−7.19 (2H, m, H$_{Phe}$), 7.55−7.67 (2H, m, H$_{Phe}$), 8.27 (1H, s, H-6) ppm. ^{13}C NMR (75 MHz, DMSO-d_6) δ 55.7 (CH$_3$), 62.8 (C-5'), 71.4 (C-2'), 73.7 (C-3'), 85.6 (C-4'), 88.8 (C-1'), 98.2 (C-3a), 115.1 (C$_{Phe}$), 125.3 (C$_{Phe}$), 130.0 (C$_{Phe}$), 145.2 (C-3), 155.7 (C-7a), 156.4 (C-6), 158.7 (C-4), 160.3 (C$_{Phe}$) ppm. HRMS (ESI): calcd for $C_{17}H_{20}N_5O_5$ ([M + H]$^+$): 374.1464, found: 374.1455.

3-(4-Chlorophenyl)-4-amino-1-β-D-ribofuranosylpyrazolo[3,4-d]pyrimidine (44). Compound 21 (0.087 g, 0.25 mmol) was subjected to general procedure E, using 4-chlorophenylboronic acid as the coupling partner and Na$_2$CO$_3$ as the base. Purification *via* flash column chromatography (automated, 1 → 12% MeOH in CH$_2$Cl$_2$), followed by an additional purification by preparative RP-HPLC (0.2% formic acid in H$_2$O/MeCN 0:100 to 41:59 in 10.5 min) afforded 44 (38 mg, 0.101 mmol, 40% yield) as a white solid. ^{1}H NMR (300 MHz, DMSO-d_6) δ 3.44 (1H, dd, J = 11.7, 5.6 Hz, H-5'), 3.58 (1H, dd, J = 12.0, 4.7 Hz, H-5''), 3.91 (1H, dd, J = 10.0, 5.0 Hz, H-4'), 4.25 (1H, t, J = 4.7 Hz, H-3'), 4.63 (1H, t, J = 4.8 Hz, H-2'), 4.86 (1H, br. s, OH), 5.33 (2H, br. s, OH, OH), 6.17 (1H, d, J = 4.4 Hz, H-1'), 6.99 (2H, br. s, NH$_2$), 7.57−7.70 (4H, m, H$_{Phe}$), 8.26 (1H, s, H-6) ppm. ^{13}C NMR (75 MHz, DMSO-d_6) δ 62.3 (C-5'), 70.8 (C-2'), 73.2 (C-3'), 85.2 (C-4'), 88.4 (C-1'), 97.8 (C-3a), 129.2 (C$_{Phe}$), 130.0 (C$_{Phe}$), 131.4 (C$_{Phe}$), 133.7 (C$_{Phe}$), 143.8 (C-3), 155.4 (C-7a), 156.1 (C-6), 158.2 (C-4) ppm. HRMS (ESI): calcd for $C_{16}H_{17}ClN_5O_4$ ([M + H]$^+$): 378.0969, found: 378.0981.

3-(4-Methylphenyl)-4-amino-1-β-D-ribofuranosylpyrazolo[3,4-d]pyrimidine (45). Compound **21** (0.094 g, 0.27 mmol) was subjected to general procedure E, using 4-methylphenylboronic acid as the coupling partner and Na_2CO_3 as the base. Purification *via* flash column chromatography (automated, 2 → 15% MeOH in CH_2Cl_2), followed by an additional purification by preparative RP-HPLC (0.2% formic acid in H_2O/MeCN 98:02 to 41:59 in 10.5 min) afforded **45** (40 mg, 0.112 mmol, 42% yield) as a white solid. ^{1}H NMR (300 MHz, DMSO-d_6) δ 2.40 (3H, s, CH_3), 3.40–3.52 (1H, m, H-5′), 3.54–3.67 (1H, m, H-5″), 3.93 (1H, dd, J = 9.1, 5.0 Hz, H-4′), 4.27 (1H, q, J = 4.7 Hz, H-3′), 4.65 (1H, q, J = 5.0 Hz, H-2′), 4.85 (1H, t, J = 5.7 Hz, OH), 5.14 (1H, d, J = 5.3 Hz, OH), 5.41 (1H, d, J = 5.6 Hz, OH), 6.19 (1H, d, J = 4.4 Hz, H-1′), 7.38 (2H, d, J = 7.9 Hz, H_{Phe}), 7.57 (2H, d, J = 7.9 Hz, H_{Phe}), 8.27 (1H, s, H-6) ppm. ^{13}C NMR (75 MHz, DMSO-d_6) δ 20.9 (CH_3), 62.4 (C-5′), 70.9 (C-2′), 73.2 (C-3′), 85.2 (C-4′), 88.4 (C-1′), 97.8 (C-3a), 128.1 (C_{Phe}), 129.8 (C_{Phe}), 138.4 (C_{Phe}), 144.9 (C-3), 155.3 (C-7a), 156.0 (C-6), 158.2 (C-4) ppm. HRMS (ESI): calcd for $C_{17}H_{20}N_5O_4$ ([M + H]$^+$): 358.1515, found: 358.1500.

3-(4-Fluorophenyl)-4-amino-1-β-D-ribofuranosylpyrazolo[3,4-d]pyrimidine (46). Compound **21** (0.120 g, 0.35 mmol) was subjected to general procedure E, using 4-fluorophenylboronic acid as the coupling partner and Na_2CO_3 as the base. Purification *via* flash column chromatography (automated, 2 → 15% MeOH in CH_2Cl_2), followed by an additional purification by preparative RP-HPLC (0.2% formic acid in H_2O/MeCN 98:02 to 32:68 in 12 min) afforded **46** (66 mg, 0.183 mmol, 52% yield) as a white solid. ^{1}H NMR (300 MHz, DMSO-d_6) δ 3.46 (1H, dd, J = 11.9, 5.7 Hz, H-5′), 3.60 (1H, dd, J = 11.7, 4.4 Hz, H-5″), 3.93 (1H, dd, J = 10.0, 4.4 Hz, H-4′), 4.26 (1H, t, J = 4.7 Hz, H-3′), 4.65 (1H, t, J = 4.7 Hz, H-2′), 4.85 (1H, br. s, OH), 5.13 (1H, br. s, OH), 5.40 (1H, br. s, OH), 6.18 (1H, d, J = 4.4 Hz, H-1′), 6.97 (2H, br. s, NH_2), 7.32–7.47 (2H, m, H_{Phe}), 7.63–7.76 (2H, m, H_{Phe}), 8.28 (1H, s, H-6) ppm. ^{13}C NMR (75 MHz, DMSO-d_6) δ 62.8 (C-5′), 71.3 (C-2′), 73.6 (C-3′), 85.6 (C-4′), 88.8 (C-1′), 98.3 (C-3a), 116.6 (d, J = 21.9 Hz, C-3$_{Phe}$, C-5$_{Phe}$), 129.5 (d, J = 3.5 Hz, C-1$_{Phe}$), 130.9 (d, J = 9.2 Hz, C-2$_{Phe}$, C-6$_{Phe}$), 144.4 (C-3), 155.8 (C-7a), 156.5 (C-6), 158.6 (C-4), 163.0 (d, J = 245.0 Hz, C-4$_{Phe}$) ppm. ^{19}F NMR (282 MHz, DMSO-d_6) δ −113.07 to −112.95 (1F, m) ppm. HRMS (ESI): calcd for $C_{16}H_{17}FN_5O_4$ ([M + H]$^+$): 362.1265, found: 362.1265.

3-(4-Nitrophenyl)-4-amino-1-β-D-ribofuranosylpyrazolo[3,4-d]pyrimidine (47). Compound **21** (0.120 g, 0.35 mmol) was subjected to general procedure E, using 4-nitrophenylboronic acid as the coupling partner and Na_2CO_3 as the base. Purification *via* flash column chromatography (automated, 2 → 15% MeOH in CH_2Cl_2), followed by an additional purification by preparative RP-HPLC (0.2% formic acid in H_2O/MeCN 98:02 to 32:68 in 12 min) afforded **47** (70 mg, 0.181 mmol, 52% yield) as a light-brown solid. ^{1}H NMR (300 MHz, DMSO-d_6) δ 3.47 (1H, dd, J = 11.7, 5.9 Hz, H-5′), 3.61 (1H, dd, J = 11.7, 4.7 Hz, H-5″), 3.95 (1H, dd, J = 10.0, 4.7 Hz, H-4′), 4.28 (1H, t, J = 4.4 Hz, H-3′), 4.67 (1H, br. s, H-2′), 4.84 (1H, br. s, OH), 5.16 (1H, br. s, OH), 5.43 (1H, br. s, OH), 6.22 (1H, d, J = 4.7 Hz, H-1′), 7.94 (2H, d, J = 8.8 Hz, H_{Phe}), 8.31 (1H, s, H-6), 8.37−8.45 (2H, m, H_{Phe}) ppm. ^{13}C NMR (75 MHz, DMSO-d_6) δ 62.3 (C-5′), 70.8 (C-2′), 73.2 (C-3′), 85.3 (C-4′), 88.5 (C-1′), 98.0 (C-3a), 124.3 (C-3$_{Phe}$, C-5$_{Phe}$), 129.6 (C-2$_{Phe}$, C-6$_{Phe}$), 138.9 (C-1$_{Phe}$), 143.1 (C-3), 147.4 (C-4$_{Phe}$), 155.6 (C-7a), 156.2 (C-6), 158.1 (C-4) ppm. HRMS (ESI): calcd for $C_{16}H_{17}N_6O_6$ ([M + H]$^+$): 389.1210, found: 389.1211.

3-(4-tert-Butylphenyl)-4-amino-1-β-D-ribofuranosylpyrazolo[3,4-d]pyrimidine (48). Compound **21** (0.120 g, 0.35 mmol) was subjected to general procedure E, using 4-*tert*-butylphenylboronic acid as the coupling partner and Na_2CO_3 as the base. Purification *via* flash column chromatography (automated, 2 → 15% MeOH in CH_2Cl_2), followed by an additional purification by preparative RP-HPLC (0.2% formic acid in H_2O/MeCN 98:02 to 33:67 in 12 min) afforded **48** (55 mg, 0.138 mmol, 39% yield) as a white solid. ^{1}H NMR (300 MHz, DMSO-d_6) δ 1.35 (9H, s, 3 × CH_3), 3.45 (1H, dd, J = 11.7, 5.9 Hz, H-5′), 3.61 (1H, dd, J = 11.7, 4.1 Hz, H-5″), 3.95 (1H, dd, J = 9.7, 4.7 Hz, H-4′), 4.27 (1H, t, J = 4.7 Hz, H-3′), 4.64

(1H, t, J = 5.0 Hz, H-2′), 4.86 (1H, br. s, OH), 5.17 (1H, br. s, OH), 5.44 (1H, br. s, OH), 6.19 (1H, d, J = 4.4 Hz, H-1′), 7.54−7.68 (4H, m, H_{Phe}), 8.28 (1H, s, C-6) ppm. ^{13}C NMR (75 MHz, DMSO-d_6) δ 31.0 (CH(CH_3)$_3$), 34.5 (<u>C</u>H(CH_3)$_3$), 62.4 (C-5′), 70.9 (C-2′), 73.3 (C-3′), 85.2 (C-4′), 88.4 (C-1′), 97.8 (C-3a), 126.0 (C-3$_{Phe}$, C-5$_{Phe}$), 127.9 (C-2$_{Phe}$, C-6$_{Phe}$), 129.8 (C-1$_{Phe}$), 144.8 (C-3), 151.4 (C-4$_{Phe}$), 155.3 (C-7a), 156.0 (C-6), 158.2 (C-4) ppm. HRMS (ESI): calcd for $C_{20}H_{26}N_5O_4$ ([M + H]$^+$): 400.1985, found: 400.1972.

3-(4-Trifluoromethylphenyl)-4-amino-1-β-D-ribofuranosylpyrazolo[3,4-d]pyrimidine (49). Compound **21** (0.120 g, 0.35 mmol) was subjected to general procedure E, using 4-trifluoromethylphenylboronic acid as the coupling partner and Na_2CO_3 as the base. Purification *via* flash column chromatography (automated, 2 → 15% MeOH in CH_2Cl_2), followed by an additional purification by preparative RP-HPLC (0.2% formic acid in H_2O/MeCN 98:02 to 33:67 in 12 min) afforded **49** (67 mg, 0.163 mmol, 47% yield) as a white solid. ^{1}H NMR (300 MHz, DMSO-d_6) δ 3.48 (1H, dd, J = 11.7, 5.0 Hz, H-5′), 3.60 (1H, dd, J = 11.4, 3.5 Hz, H-5″), 3.94 (1H, dd, J = 10.0, 4.7 Hz, H-4′), 4.27 (1H, t, J = 4.5 Hz, H-3′), 4.66 (1H, t, J = 4.5 Hz, H-2′), 4.84 (1H, br. s., OH), 5.18 (1H, br. s., OH), 5.45 (1H, br. s., OH), 6.21 (1H, d, J = 4.4 Hz, H-1′), 7.86−7.96 (4H, m, H_{Phe}), 8.30 (1H, s, H-6) ppm. ^{13}C NMR (75 MHz, DMSO-d_6) δ 62.8 (C-5′), 71.3 (C-2′), 73.7 (C-3′), 85.7 (C-4′), 88.9 (C-1′), 98.3 (C-3a), 126.5 (q, J = 3.5 Hz, C-3Phe, C-5Phe), 129.4 (q, J = 32.2 Hz, C-4Phe), 129.5 (C-2Phe, C-6Phe), 137.0 (C-4Phe), 144.0 (C-3), 156.0 (C-7a), 156.6 (C-6), 158.6 (C-4) ppm. 1 quaternary carbon (<u>C</u>F$_3$) missing. ^{19}F NMR (282 MHz, DMSO-d_6) δ −61.06 (1F, s) ppm. HRMS (ESI): calcd for $C_{17}H_{17}F_3N_5O_4$ ([M + H]$^+$): 412.1233, found: 412.1225.

3-(4-Trifluoromethoxyphenyl)-4-amino-1-β-D-ribofuranosylpyrazolo[3,4-d]pyrimidine (50). Compound **21** (0.120 g, 0.35 mmol) was subjected to general procedure E, using 4-trifluoromethoxyphenylboronic acid as the coupling partner and Na_2CO_3 as the base. Purification *via* flash column chromatography (automated, 4 → 15% MeOH in CH_2Cl_2), followed by an additional purification by preparative RP-HPLC (0.2% formic acid in H_2O/MeCN 98:02 to 0:100 in 18 min) afforded **50** (40 mg, 0.094 mmol, 27% yield) as a white solid. ^{1}H NMR (300 MHz, DMSO-d_6) δ 3.37−3.50 (1H, m, H-5′), 3.53−3.66 (1H, m, H-5″), 3.93 (1H, dd, J = 10.0, 5.6 Hz, H-4′), 4.26 (1H, dd, J = 7.0, 5.0 Hz, H-3′), 4.65 (0 H, dd, J = 8.2, 4.1 Hz, H-2′), 4.84 (1H, t, J = 5.3 Hz, OH), 5.18 (1H, br. s., OH), 5.45 (1H, d, J = 4.4 Hz, OH), 6.19 (1H, d, J = 4.7 Hz, H-1′), 7.54 (2H, dd, J = 8.8, 0.9 Hz, H_{Phe}), 7.71−7.89 (2H, m, H_{Phe}), 8.29 (1H, s, H_{Phe}) ppm. ^{13}C NMR (75 MHz, DMSO-d_6) δ 62.8 (C-5′), 71.3 (C-2′), 73.7 (C-3′), 85.7 (C-4′), 88.9 (C-1), 98.3 (C-3a), 120.60 (q, J = 255.0 Hz, <u>C</u>F$_3$), 122.1 (C-3$_{Phe}$, C-5$_{Phe}$), 130.7 (C-2$_{Phe}$, C-6$_{Phe}$), 132.3 (C-1), 144.1 (C-3), 149.1 (C-4$_{Phe}$), 155.9 (C-7a), 156.5 (C-6), 158.7 (C-4) ppm. ^{19}F NMR (282 MHz, DMSO-d_6) δ −56.61 (1F, s) ppm. HRMS (ESI): calcd for $C_{17}H_{17}F_3N_5O_5$ ([M + H]$^+$): 428.1182, found: 428.1204.

3-(4-Cyanophenyl)-4-amino-1-β-D-ribofuranosylpyrazolo[3,4-d]pyrimidine (51). Compound **21** (0.120 g, 0.35 mmol) was subjected to general procedure E, using 4-cyanophenylboronic acid as the coupling partner and Na_2CO_3 as the base. Purification *via* flash column chromatography (automated, 4 → 15% MeOH in CH_2Cl_2), followed by an additional purification by preparative RP-HPLC (0.2% formic acid in H_2O/MeCN 98:02 to 33:67 in 12 min) afforded **51** (56 mg, 0.152 mmol, 43% yield) as a white solid. ^{1}H NMR (400 MHz, DMSO-d_6) δ 3.46 (1H, dd, J = 10.9, 5.2 Hz, H-5′), 3.60 (1H, dd, J = 11.6, 3.6 Hz, H-5″), 3.94 (1H, dd, J = 9.9, 4.8 Hz, H-4′), 4.27 (1H, dd, J = 8.6, 3.6 Hz, H-3′), 4.65 (1H, dd, J = 8.6, 4.9 Hz, H-2′), 4.75−4.90 (1H, m, OH), 5.16 (1H, d, J = 4.0 Hz, OH), 5.43 (1H, d, J = 5.4 Hz, OH), 6.21 (1H, d, J = 4.5 Hz, H-1′), 7.07 (2H, br. s, NH_2), 7.85 (2H, d, J = 8.3 Hz, H-3$_{Phe}$, H-5$_{Phe}$), 8.02 (2H, d, J = 8.3 Hz, H-2$_{Phe}$, H-6$_{Phe}$), 8.30 (1H, s, H-6) ppm. ^{13}C NMR (101 MHz, DMSO-d_6) δ 62.3 (C-5′), 70.9 (C-2′), 73.3 (C-3′), 85.3 (C-4′), 88.5 (C-1′), 97.9 (C-3a), 111.3 (C-4$_{Phe}$), 118.8 (<u>C</u>N), 129.1 (C-2$_{Phe}$, C-6$_{Phe}$), 133.1 (C-3$_{Phe}$, C-5$_{Phe}$), 137.1 (C-1$_{Phe}$), 143.4 (C-3), 155.6 (C-7a), 156.2 (C-6), 158.2 (C-4) ppm. HRMS (ESI): calcd for $C_{17}H_{17}N_6O_4$ ([M + H]$^+$): 369.1311, found: 369.1241.

241

3-(3,4-Dichlorophenyl)-4-amino-1-β-D-ribofuranosylpyrazolo-[3,4-d]pyrimidine (52). Compound **21** (0.118 g, 0.34 mmol) was subjected to general procedure E, using 3,4-dichlorophenylboronic acid as the coupling partner and Na_2CO_3 as the base. Purification *via* flash column chromatography (automated, 0 → 15% MeOH in CH_2Cl_2), followed by an additional purification by preparative RP-HPLC (0.2% formic acid in H_2O/MeCN 98:02 to 41:59 in 10.5 min) afforded **52** (45 mg, 0.109 mmol, 32% yield) as a white solid. ^{1}H NMR (300 MHz, DMSO-d_6) δ 3.40–3.52 (1H, m, H-5′), 3.55–3.65 (1H, m, H-5″), 3.93 (1H, dd, J = 9.7, 4.7 Hz, H-4′), 4.26 (1H, t, J = 4.5 Hz, H-3′), 4.65 (1H, t, J = 3.8 Hz, H-2′), 4.83 (1H, br. s., OH), 5.17 (1H, br. s., OH), 5.43 (1H, br. s., OH), 6.18 (1H, d, J = 4.7 Hz, H-1′), 6.95–7.37 (2H, m, NH_2), 7.63 (1H, dd, J = 8.2, 2.1 Hz, H-6_{Phe}), 7.81 (1H, d, J = 8.5 Hz, H-5_{Phe}), 7.85 (1H, d, J = 2.1 Hz, H-2_{Phe}), 8.29 (1H, s, H-6) ppm. ^{13}C NMR (75 MHz, DMSO-d_6) δ 62.2 (C-5′), 70.8 (C-2′), 73.2 (C-3′), 85.2 (C-4′), 88.4 (C-1′), 97.8 (C-3a), 128.5 (C-6_{Phe}), 130.1 (C-2_{Phe}), 131.3 (C-5_{Phe}), 131.6 (C-3_{Phe}) 131.7 (C-4_{Phe}), 133.1 (C-1_{Phe}), 142.6 (C-3), 155.4 (C-7a), 156.1 (C-6), 158.2 (C-4) ppm. HRMS (ESI): calcd for $C_{16}H_{16}Cl_2N_5O_4$ ([M + H]$^+$): 412.0579, found: 412.0575.

3-(3-Chloro-4-fluorophenyl)-4-amino-1-β-D-ribofuranosylpyrazolo[3,4-d]pyrimidine (53). Compound **21** (0.120 g, 0.35 mmol) was subjected to general procedure E, using 3-chloro-4-fluorophenylboronic acid as the coupling partner and Na_2CO_3 as the base. Purification *via* flash column chromatography (automated, 0 → 15% MeOH in CH_2Cl_2), followed by an additional purification by preparative RP-HPLC (0.2% formic acid in H_2O/MeCN 98:02 to 32:68 in 12 min) afforded **53** (75 mg, 0.197 mmol, 56% yield) as a white solid. ^{1}H NMR (300 MHz, DMSO-d_6) δ 3.40–3.51 (1H, m, H-5′), 3.54–3.67 (1H, m, H-5″), 3.93 (1H, dd, J = 10.0, 5.3 Hz, H-4′), 4.26 (1H, dd, J = 10.0, 5.0 Hz, H-3′), 4.64 (1H, dd, J = 10.5, 5.6 Hz, H-2′), 4.82 (1H, t, J = 5.9 Hz, OH), 5.14 (1H, d, J = 5.6 Hz, OH), 5.40 (1H, d, J = 5.9 Hz, OH), 6.18 (1H, d, J = 4.4 Hz, H-1′), 6.79–7.38 (2H, br. s, NH_2), 7.52–7.69 (2H, m, H-5_{Phe}, H-6_{Phe}), 7.80 (1H, dd, J = 7.0, 2.1 Hz, H-2_{Phe}), 8.28 (1H, s, H-6) ppm. ^{13}C NMR (75 MHz, DMSO-d_6) δ 62.2 (C-5′), 70.8 (C-2′), 73.2 (C-3′), 85.2 (C-4′), 88.4 (C-1′), 97.8 (C-3a), 117.5 (d, J = 21.9 Hz, C-5_{Phe}), 120.1 (d, J = 20.7 Hz, C-3_{Phe}), 129.1 (d, J = 8.1 Hz, C-6_{Phe}), 130.3 (d, J = 3.5 Hz, C-1_{Phe}), 130.4 (C-2_{Phe}), 142.8 (C-3), 155.4 (C-7a), 156.1 (C-6), 158.2 (C-4) ppm. 1 quaternary carbon (C-4_{Phe}) missing. ^{19}F NMR (282 MHz, DMSO-d_6) δ −118.16 to −115.34 (142 F, m) ppm. HRMS (ESI): calcd for $C_{16}H_{16}ClFN_5O_4$ ([M + H]$^+$): 396.0875, found: 396.0891.

3-(3-Fluoro-4-chlorophenyl)-4-amino-1-β-D-ribofuranosylpyrazolo[3,4-d]pyrimidine (54). Compound **21** (0.120 g, 0.35 mmol) was subjected to general procedure E, using 3-fluoro-4-chlorophenylboronic acid as the coupling partner and Na_2CO_3 as the base. Purification *via* flash column chromatography (automated, 0 → 15% MeOH in CH_2Cl_2), followed by an additional purification by preparative RP-HPLC (0.2% formic acid in H_2O/MeCN 98:02 to 33:67 in 12 min) afforded **54** (82 mg, 0.207 mmol, 59% yield) as a white solid. ^{1}H NMR (300 MHz, DMSO-d_6) δ 3.39–3.52 (1H, m, H-5′), 3.59 (1H, dt, J = 12.0, 4.7 Hz, H-5″), 3.93 (1H, q, J = 4.7 Hz, H-4′), 4.26 (1H, q, J = 5.0 Hz, H-3′), 4.65 (1H, q, J = 5.2 Hz, H-2′), 4.82 (1H, t, J = 5.7 Hz, OH), 5.14 (1H, d, J = 5.6 Hz, OH), 5.41 (1H, d, J = 5.9 Hz, OH), 6.18 (1H, d, J = 4.4 Hz, H-1′), 7.20 (2H, br. s, NH_2), 7.51 (1H, ddd, J = 8.2, 2.1, 0.6 Hz, H-5_{Phe}), 7.63 (1H, dd, J = 10.1, 2.1 Hz, H-2_{Phe}), 7.76 (1H, t, J = 8.1 Hz, H-6_{Phe}), 8.28 (1H, s, H-6) ppm. ^{13}C NMR (75 MHz, DMSO-d_6) δ 62.3 (C-5′), 70.8 (C-2′), 73.3 (C-3′), 84.8 (C-4′), 88.3 (C-1′) 97.8 (C-3a), 116.8 (d, J = 20.7 Hz, C-2_{Phe}), 120.0 (d, J = 18.4 Hz, C-4_{Phe}), 125.5 (d, J = 3.5 Hz, C-5_{Phe}), 131.3 (C-6_{Phe}), 133.4 (d, J = 8.1 Hz, C-1_{Phe}), 142.9 (C-3), 155.4 (C-7a), 156.1 (C-6), 158.1 (C-4), 157.4 (d, J = 244.5 Hz, C-3_{Phe}) ppm. ^{19}F NMR (282 MHz, DMSO-d_6) δ −115.13 (dd, J = 10.2, 7.8 Hz) ppm. HRMS (ESI): calcd for $C_{16}H_{16}ClFN_5O_4$ ([M + H]$^+$): 396.0875, found: 396.0860.

3-(3,4-Difluorophenyl)-4-amino-1-β-D-ribofuranosylpyrazolo-[3,4-d]pyrimidine (55). Compound **21** (0.120 g, 0.35 mmol) was subjected to general procedure E, using 3,4-difluorophenylboronic acid as the coupling partner and Na_2CO_3 as the base. Purification *via*

flash column chromatography (automated, 0 → 15% MeOH in CH_2Cl_2), followed by an additional purification by preparative RP-HPLC (0.2% formic acid in H_2O/MeCN 98:02 to 33:67 in 12 min) afforded **55** (66 mg, 0.174 mmol, 50% yield) as a white solid. ^{1}H NMR (300 MHz, DMSO-d_6) δ 3.40–3.51 (1H, m, H-5′), 3.58 (1H, d, J = 3.8 Hz, H-5″), 3.93 (1H, dd, J = 10.0, 5.3 Hz, H-4′), 4.26 (1H, t, J = 4.5 Hz, H-3′), 4.64 (1H, t, J = 4.7 Hz, H-2′), 4.74–4.88 (1H, m, OH), 5.03–5.29 (1H, m, OH), 5.33–5.51 (1H, m, OH), 6.18 (1H, d, J = 4.4 Hz, H-1′), 6.90–7.33 (2H, m, H_{Phe}), 7.40–7.55 (1H, m, H_{Phe}), 7.55–7.73 (1H, m, H_{Phe}), 8.28 (1H, s, H-6) ppm. ^{13}C NMR (75 MHz, DMSO-d_6) δ 62.3 (C-5′), 70.4 (C-2′), 73.3 (C-3′) 85.2 (C-4′), 88.4 (C-1′), 97.8 (C-3a), 117.3–118.7 (C_{Phe}), 124.9–125.9 (C_{Phe}), 129.5–130.4 (C_{Phe}), 143.0 (d, J = 2.3 Hz, C-3), 147.9–148.8 (C_{Phe}), 151.3 (C-7a), 155.0–155.6 (C_{Phe}), 156.1 (C-6), 158.1 (C-4) ppm. ^{19}F NMR (282 MHz, DMSO-d_6) δ −138.90 to −138.66 (1F, m), −137.66 to −137.43 (1F, m) ppm. HRMS (ESI): calcd for $C_{16}H_{16}F_2N_5O_4$ ([M + H]$^+$): 380.1170, found: 380.1185.

3-(3-Methoxy-4-chlorophenyl)-4-amino-1-β-D-ribofuranosylpyrazolo[3,4-d]pyrimidine (56). Compound **21** (0.120 g, 0.35 mmol) was subjected to general procedure E, using 3-methoxy-4-chlorophenylboronic acid as the coupling partner and Na_2CO_3 as the base. Purification *via* flash column chromatography (automated, 0 → 15% MeOH in CH_2Cl_2), followed by an additional purification by preparative RP-HPLC (0.2% formic acid in H_2O/MeCN 98:02 to 33:67 in 12 min) afforded **56** (86 mg, 0.211 mmol, 60% yield) as a white solid. ^{1}H NMR (300 MHz, DMSO-d_6) δ 3.47 (1H, dd, J = 11.0, 5.4 Hz, H-5′), 3.61 (1H, dd, J = 11.0, 4.7 Hz, H-5″), 3.82–4.04 (4H, m, H-4′, C$\underline{H}_3$), 4.27 (1H, t, J = 4.7 Hz, H-3′), 4.66 (1H, t, J = 4.7 Hz, H-2′), 4.85 (1H, br. s., OH), 5.03–5.24 (1H, m, OH), 5.31–5.57 (1H, m, OH), 6.19 (1H, d, J = 4.7 Hz, H-1′), 7.25 (1H, dd, J = 8.1, 1.9 Hz, H-6_{Phe}), 7.36 (1H, d, J = 1.8 Hz, H-2_{Phe}), 7.59 (1H, d, J = 7.9 Hz, H-5_{Phe}), 8.28 (1H, s, H-6) ppm. ^{13}C NMR (75 MHz, DMSO-d_6) δ 56.0 (CH_3), 62.3 (C-5′), 70.8 (C-2′), 73.2 (C-3′), 85.2 (C-4′), 88.5 (C-1′), 97.8 (C-3a), 112.8 (C-2_{Phe}), 121.0 (C-6_{Phe}), 121.7 (C-4_{Phe}), 130.5 (C-5_{Phe}), 132.6 (C-1_{Phe}), 144.0 (C-3), 154.8 (C-7a), 155.3 (C-3_{Phe}), 156.0 (C-6), 158.2 (C-4) ppm. HRMS (ESI): calcd for $C_{17}H_{19}ClN_5O_5$ ([M + H]$^+$): 408.1075, found: 408.1099.

3-(3-Methyl-4-chlorophenyl)-4-amino-1-β-D-ribofuranosylpyrazolo[3,4-d]pyrimidine (57). Compound **21** (0.120 g, 0.35 mmol) was subjected to general procedure E, using 3-methyl-4-chlorophenylboronic acid as the coupling partner and Na_2CO_3 as the base. Purification *via* flash column chromatography (automated, 2 → 15% MeOH in CH_2Cl_2), followed by an additional purification by preparative RP-HPLC (0.2% formic acid in H_2O/MeCN 98:02 to 33:67 in 12 min) afforded **57** (88 mg, 0.224 mmol, 64% yield) as a white solid. ^{1}H NMR (300 MHz, DMSO-d_6) δ 2.56 (3H, s, CH_3), 3.54 (1H, dt, J = 11.8, 6.0 Hz, H-5′), 3.68 (1H, dt, J = 12.0, 4.7 Hz, H-5″), 4.01 (1H, dd, J = 9.4, 4.7 Hz, H-4′), 4.34 (1H, q, J = 5.2 Hz, H-3′), 4.73 (1H, q, J = 5.2 Hz, H-2′), 4.92 (1H, t, J = 5.9 Hz, OH), 5.22 (1H, d, J = 5.6 Hz, OH), 5.48 (1H, d, J = 5.9 Hz, OH), 6.26 (1H, d, J = 4.7 Hz, H-1′), 6.57–7.45 (2H, m, NH_2), 7.55–7.77 (3H, m, H_{Phe}), 8.36 (1H, s, H-6) ppm. ^{13}C NMR (75 MHz, DMSO-d_6) δ 19.8 (CH_3), 62.3 (C-5′), 70.8 (C-2′), 73.2 (C-3′), 85.2 (C-4′), 88.4 (C-1′), 97.8 (C-3a), 127.4 (C_{Phe}), 129.6 (C_{Phe}), 130.9 (C_{Phe}), 131.4 (C_{Phe}), 134.0 (C_{Phe}), 136.3 (C_{Phe}), 143.9 (C-3), 155.4 (C-7a), 156.1 (C-6), 158.1 (C-4) ppm. HRMS (ESI): calcd for $C_{17}H_{19}ClN_5O_4$ ([M + H]$^+$): 392.1126, found: 392.1073.

3-(3-Trifluoromethyl-4-chlorophenyl)-4-amino-1-β-D-ribofuranosylpyrazolo[3,4-d]pyrimidine (58). Compound **21** (0.120 g, 0.35 mmol) was subjected to general procedure E, using 3-trifluoromethyl-4-chlorophenylboronic acid as the coupling partner and Na_2CO_3 as the base. Purification *via* flash column chromatography (automated, 2 → 15% MeOH in CH_2Cl_2), followed by an additional purification by preparative RP-HPLC (0.2% formic acid in H_2O/MeCN 98:02 to 33:67 in 12 min) afforded **58** (50 mg, 0.112 mmol, 32% yield) as a white solid. ^{1}H NMR (300 MHz, DMSO-d_6) δ 3.46 (1H, dd, J = 11.6, 5.7 Hz, H-5′), 3.60 (1H, dd, J = 11.7, 4.1 Hz, H-5″), 3.94 (1H, dd, J = 9.7, 5.0 Hz, H-4′), 4.27 (1H, t, J = 4.5 Hz, H-3′), 4.66 (1H, t, J = 4.4 Hz, H-2′), 4.83 (1H, br. s., OH), 5.16 (1H, br.

s., OH), 5.40 (1H, br. s., OH), 6.20 (1H, d, J = 4.7 Hz, H-1′), 7.23 (2H, br. s., NH$_2$), 7.77–8.10 (3H, m, H$_{Phe}$), 8.30 (1H, s, H-6) ppm. ^{13}C NMR (75 MHz, DMSO-d_6) δ 62.2 (C-5′), 70.8 (C-2′), 73.2 (C-3′), 85.3 (C-4′), 88.5 (C-1′), 97.9 (C-3a), 122.7 (q, J = 275.0 Hz, $\underline{C}$F$_3$), 127.0 (C$_{Phe}$), 127.5 (d, J = 4.6 Hz, C$_{Phe}$), 131.1 (C$_{Phe}$), 132.0 (C$_{Phe}$), 132.4 (C$_{Phe}$), 133.6 (C$_{Phe}$), 142.6 (C-3), 155.5 (C-7a), 156.1 (C-6), 158.2 (C-4) ppm. ^{19}F NMR (377 MHz, DMSO-d_6) δ −61.4 (s) ppm. HRMS (ESI): calcd for C$_{17}$H$_{16}$F$_3$ClN$_5$O$_4$ ([M + H]$^+$): 446.0843, found: 446.0853.

3-(3-Cyano-4-chlorophenyl)-4-amino-1-β-ᴅ-ribofuranosylpyrazolo[3,4-d]pyrimidine (59). Compound **21** (0.120 g, 0.35 mmol) was subjected to general procedure E, using 3-cyano-4-chlorophenylboronic acid as the coupling partner and Na$_2$CO$_3$ as the base. Purification *via* flash column chromatography (automated, 2 → 15% MeOH in CH$_2$Cl$_2$), followed by an additional purification by preparative RP-HPLC (0.2% formic acid in H$_2$O/MeCN 98:02 to 40:60 in 12 min) afforded **59** (25 mg, 0.062 mmol, 18% yield) as a white solid and **75** (7 mg, 0.014 mmol, 4% yield) as a white solid. Analytical data **59**: ^{1}H NMR (400 MHz, DMSO-d_6) δ 3.37–3.51 (1H, m, H-5′), 3.59 (1H, ddd, J = 11.5, 9.6, 4.3 Hz, H-5″), 3.93 (1H, q, J = 4.8 Hz, H-4′), 4.26 (1H, q, J = 4.8 Hz, H-3′), 4.65 (1H, q, J = 5.0 Hz, H-2′), 4.82 (1H, t, J = 5.8 Hz, OH), 5.15 (1H, d, J = 5.4 Hz, OH), 5.42 (1H, d, J = 5.6 Hz, OH), 6.19 (1H, d, J = 4.5 Hz, H-1′), 6.79–7.65 (2H, m, NH$_2$), 7.90 (1H, d, J = 8.1 Hz, H$_{Phe}$), 7.96 (H, dd, J = 8.3, 2.4 Hz, H$_{Phe}$), 8.17 (1H, d, J = 2.0 Hz, H$_{Phe}$), 8.29 (1H, s, H-6) ppm. ^{13}C NMR (101 MHz, DMSO-d_6) δ 60.3 (C-5′), 70.8 (C-2′), 73.2 (C-3′), 85.2 (C-4′), 88.4 (C-1′), 97.9 (C-3a), 112.9 (C$_{Phe}$), 116.0 (C$_{Phe}$), 130.7 (C$_{Phe}$), 132.3 (C$_{Phe}$), 134.2 (C$_{Phe}$), 134.4 (C$_{Phe}$), 135.6 (C$_{Phe}$), 142.1 (C-3), 155.5 (C-7a), 156.2 (C-6), 158.1 (C-4) ppm. HRMS (ESI): calcd for C$_{17}$H$_{16}$ClN$_6$O$_4$ ([M + H]$^+$): 403.0922, found: 403.0929. Analytical data **75**: ^{1}H NMR (400 MHz, DMSO-d_6) δ 3.41–3.53 (1H, m, H-5′), 3.61 (1H, dt, J = 11.8, 4.8 Hz, H-5″), 3.95 (1H, dd, J = 10.0, 4.9 Hz, H-4′), 4.29 (1H, dd, J = 10.4, 5.1 Hz, H-3′), 4.65 (1H, dd, J = 10.3, 5.0 Hz, H-2′), 4.82 (1H, t, J = 5.4 Hz, OH), 5.16 (1H, d, J = 5.6 Hz, OH), 5.43 (1H, d, J = 5.8 Hz, OH), 6.22 (1H, d, J = 4.4 Hz, H-1′), 7.15 (2H, br. s, NH$_2$), 7.84–8.23 (5H, m, H$_{Phe}$), 8.30 (1H, d, J = 2.0 Hz, H$_{Phe}$), 8.32 (1H, s, H-6) ppm. ^{13}C NMR (101 MHz, DMSO-d_6) δ 62.2 (C-5′), 70.8 (C-2′), 73.3 (C-3′), 85.2 (C-4′), 88.4 (C-1′), 98.0 (C-3a), 111.3 (C$_{Phe}$), 112.6 (C$_{Phe}$), 115.6 (C$_{Phe}$), 118.0 (C$_{Phe}$), 130.6 (C$_{Phe}$), 131.0 (C$_{Phe}$), 133.1 (C$_{Phe}$), 133.4 (C$_{Phe}$), 133.4 (C$_{Phe}$), 134.7 (C$_{Phe}$), 135.1 (C$_{Phe}$), 136.0 (C$_{Phe}$), 137.3 (C$_{Phe}$), 141.1 (C$_{Phe}$), 142.5 (C-3), 155.5 (C-7a), 156.2 (C-6), 158.2 (C-4) ppm. HRMS (ESI): calcd for C$_{24}$H$_{19}$ClN$_7$O$_4$ ([M + H]$^+$): 504.1187, found: 504.1199.

3-(3,5-Difluoro-4-chlorophenyl)-4-amino-1-β-ᴅ-ribofuranosylpyrazolo[3,4-d]pyrimidine (60). Compound **21** (0.120 g, 0.35 mmol) was subjected to general procedure E, using 3,5-difluoro-4-chlorophenylboronic acid as the coupling partner and Na$_2$CO$_3$ as the base. Purification *via* flash column chromatography (automated, 2 → 15% MeOH in CH$_2$Cl$_2$), followed by an additional purification by preparative RP-HPLC (0.2% formic acid in H$_2$O/MeCN 98:02 to 33:67 in 12 min) afforded **60** (70 mg, 0.169 mmol, 48% yield) as a white solid. ^{1}H NMR (300 MHz, DMSO-d_6) δ 3.40–3.52 (1H, m, H-5′), 3.60 (1H, dt, J = 11.8, 4.8 Hz, H-5″), 3.93 (1H, dd, J = 10.0, 4.7 Hz, H-4′), 4.27 (1H, dd, J = 10.0, 5.0 Hz, H-3′), 4.65 (1H, dd, J = 10.5, 5.3 Hz, H-2′), 4.82 (1H, t, J = 5.9 Hz, OH), 5.14 (1H, d, J = 5.6 Hz, OH), 5.41 (1H, d, J = 5.9 Hz, OH), 6.18 (1H, d, J = 4.7 Hz, H-1′), 7.24 (2H, br. s., NH$_2$), 7.46–7.65 (2H, m, H$_{Phe}$), 8.28 (H-6) ppm. ^{13}C NMR (75 MHz, DMSO-d_6) δ 62.2 (C-5′), 70.8 (C-2′), 73.2 (C-3′), 85.2 (C-4′), 88.5 (C-1′), 97.9 (C-3a), 108.8 (t, J = 20.7 Hz, C$_{Phe}$), 112.8 (dd, J = 23.0, 2.3 Hz, C$_{Phe}$), 133.1 (t, J = 10.4 Hz, C$_{Phe}$), 142.1 (d, J = 2.3 Hz, C-3), 155.7 (C-7a), 156.2 (C-6), 156.6 (d, J = 3.5 Hz, C$_{Phe}$), 158.0 (C-4), 159.9 (d, J = 4.6 Hz) ppm. ^{19}F NMR (282 MHz, DMSO-d_6) δ −112.93 (2F, d, J = 7.2 Hz) ppm. HRMS (ESI): calcd for C$_{16}$H$_{15}$ClF$_2$N$_5$O$_4$ ([M + H]$^+$): 414.0781, found: 414.0733.

3-(3-Ethoxy-4-chlorophenyl)-4-amino-1-β-ᴅ-ribofuranosylpyrazolo[3,4-d]pyrimidine (61). Compound **21** (0.120 g, 0.35 mmol) was subjected to general procedure E, using 3-ethoxy-4-chlorophenylboronic acid as the coupling partner and Na$_2$CO$_3$ as

the base. Purification *via* flash column chromatography (automated, 2 → 15% MeOH in CH$_2$Cl$_2$) afforded **61** (108 mg, 0.256 mmol, 73% yield) as a white solid. ^{1}H NMR (300 MHz, DMSO-d_6) δ 1.40 (3H, t, J = 6.9 Hz, CH$_3$), 3.60 (1H, ddd, J = 12.0, 10.0, 4.7 Hz, H-5′), 3.94 (1H, dd, J = 10.0, 4.4 Hz, H-5″), 4.20 (2H, q, J = 6.9 Hz, CH$_2$), 4.27 (1H, dd, J = 10.0, 5.0 Hz, H-4′), 4.66 (1H, dd, J = 10.3, 5.0 Hz, H-3′), 4.85 (1H, dd, J = 6.4, 5.6 Hz, H-2′), 5.14 (1H, d, J = 5.6 Hz, OH), 5.40 (1H, d, J = 5.9 Hz, OH), 6.19 (1H, d, J = 4.4 Hz, OH), 6.69–7.23 (2H, m, NH$_2$), 7.24 (1H, dd, J = 8.2, 1.8 Hz, H-6$_{Phe}$), 7.34 (1H, d, J = 1.8 Hz, H-2$_{Phe}$), 7.59 (1H, d, J = 8.2 Hz, H-5$_{Phe}$), 8.28 (1H, s, H-6) ppm. ^{13}C NMR (75 MHz, DMSO-d_6) δ 14.6 (CH$_3$), 62.3 (C-5′), 64.3 (CH$_2$), 70.8 (C-2′), 73.2 (C-3′), 85.3 (C-4′), 88.5 (C-5′), 97.8 (C-3a), 113.6 (C-2$_{Phe}$), 120.9 (C-6$_{Phe}$), 121.9 (C-4$_{Phe}$), 130.5 (C-5$_{Phe}$), 132.5 (C-1$_{Phe}$), 144.1 (C-3), 154.1 (C-3), 155.3 (C-7a), 156.0 (C-6), 158.2 (C-4) ppm. HRMS (ESI): calcd for C$_{18}$H$_{21}$ClN$_5$O$_5$ ([M + H]$^+$): 422.1231, found: 422.1141.

3-(2,4-Dichlorophenyl)-4-amino-1-β-ᴅ-ribofuranosylpyrazolo[3,4-d]pyrimidine (62). Compound **21** (0.120 g, 0.35 mmol) was subjected to general procedure E, using 2,4-dichlorophenylboronic acid as the coupling partner and Na$_2$CO$_3$ as the base. Purification *via* flash column chromatography (automated, 2 → 15% MeOH in CH$_2$Cl$_2$), followed by an additional purification by preparative RP-HPLC (0.2% formic acid in H$_2$O/MeCN 98:02 to 33:67 in 12 min) afforded **62** (42 mg, 0.102 mmol, 29% yield) as a white solid. ^{1}H NMR (300 MHz, DMSO-d_6) δ 3.37–3.48 (1H, m, H-5′), 3.52–3.63 (1H, m, H-5″), 3.92 (1H, dd, J = 10.0, 4.8 Hz, H-4′), 4.22 (1H, dd, J = 9.7, 5.0 Hz, H-3′), 4.61 (1H, dd, J = 9.7, 4.7 Hz, H-2′), 4.82 (1H, t, J = 5.9 Hz, OH), 5.14 (1H, d, J = 5.6 Hz, OH), 5.41 (1H, d, J = 5.9 Hz, OH), 6.16 (1H, d, J = 4.4 Hz, H-1′), 7.52 (1H, d, J = 8.5 Hz, H-3$_{Phe}$), 7.57 (1H, dd, J = 8.2, 2.1 Hz, H-5$_{Phe}$), 7.79 (1H, d, J = 2.1 Hz, H-6$_{Phe}$), 8.25 (1H, s, H-6) ppm. ^{13}C NMR (75 MHz, DMSO-d_6) δ 62.4 (C-5′), 70.9 (C-2′), 73.2 (C-3′), 85.2 (C-4′), 88.6 (C-1′), 99.4 (C-3a), 127.8 (C-3$_{Phe}$), 129.7 (C-6$_{Phe}$), 130.3 (C-1$_{Phe}$), 133.2 (C-2$_{Phe}$), 133.9 (C-5$_{Phe}$), 134.7 (C-4$_{Phe}$), 141.2 (C-3), 154.7 (C-7a), 156.2 (C-6), 157.8 (C-4) ppm. HRMS (ESI): calcd for C$_{16}$H$_{16}$Cl$_2$N$_5$O$_4$ ([M + H]$^+$): 412.0579, found: 412.0586.

3-(2-Methyl-4-chlorophenyl)-4-amino-1-β-ᴅ-ribofuranosylpyrazolo[3,4-d]pyrimidine (63). Compound **21** (0.120 g, 0.35 mmol) was subjected to general procedure E, using 2-methyl-4-chlorophenylboronic acid as the coupling partner and Na$_2$CO$_3$ as the base. Purification *via* flash column chromatography (automated, 2 → 15% MeOH in CH$_2$Cl$_2$) afforded **63** (83 mg, 0.212 mmol, 61% yield) as a white solid. ^{1}H NMR (300 MHz, DMSO-d_6) δ 2.18–2.37 (3H, m, CH$_3$), 3.42 (1H, dd, J = 11.7, 5.9 Hz, H-5′), 3.58 (1H, dd, J = 11.7, 4.4 Hz, H-5″), 3.93 (1H, dd, J = 9.1, 4.7 Hz, H-4′), 4.23 (1H, t, J = 5.0 Hz, H-3′), 4.60 (1H, t, J = 4.5 Hz, H-2′), 6.19 (1H, d, J = 4.1 Hz, H-1′), 7.30–7.45 (2H, m, NH$_2$, H$_{Phe}$), 7.49 (1H, s, H$_{Phe}$), 8.30 (1H, s, H-6) ppm. ^{13}C NMR (101 MHz, DMSO-d_6) δ 19.9 (CH$_3$), 62.8 (C-5′), 71.4 (C-2′), 73.9 (C-3′), 85.6 (C-4′), 88.9 (C-1′), 99.4 (C-3a), 126.7 (C$_{Phe}$), 131.0 (C$_{Phe}$), 132.1 (C$_{Phe}$), 134.1 (C$_{Phe}$), 139.8 (C$_{Phe}$), 143.8 (C-3), 155.0 (C-7a), 156.0 (C-6), 157.9 (C-4) ppm. HRMS (ESI): calcd for C$_{17}$H$_{19}$ClN$_5$O$_4$ ([M + H]$^+$): 392.1126, found: 392.1077.

3-(1-Methylpyrazol-4-yl)-4-amino-1-β-ᴅ-ribofuranosylpyrazolo[3,4-d]pyrimidine (64). Compound **21** (0.120 g, 0.35 mmol) was subjected to general procedure E, using 1-methylpyrazole-4-boronic acid as the coupling partner and Na$_2$CO$_3$ as the base. Purification *via* flash column chromatography (automated, 2 → 15% MeOH in CH$_2$Cl$_2$) afforded **64** (65 mg, 0.187 mmol, 53% yield) as a white solid. ^{1}H NMR (300 MHz, DMSO-d_6) δ 3.45 (1H, dt, J = 11.2, 5.4 Hz, H-5′), 3.59 (1H, dt, J = 12.0, 4.2 Hz, H-5″), 3.80–4.02 (4H, m, CH$_3$, H-4′), 4.24 (1H, dd, J = 9.7, 5.0 Hz, H-3′), 4.62 (1H, dd, J = 9.7, 5.1 Hz, H-2′), 4.86 (1H, t, J = 5.2 Hz, OH), 5.12 (1H, d, J = 5.3 Hz, OH), 5.38 (1H, d, J = 5.9 Hz, OH), 6.13 (1H, d, J = 4.7 Hz, H-1′), 6.67–7.46 (2H, m, NH$_2$), 7.74 (1H, s, H-5$_{pyrazole}$), 8.10 (1H, s, H-3$_{pyrazole}$), 8.24 (1H, s, H-6) ppm. ^{13}C NMR (75 MHz, DMSO-d_6) δ 62.4 (C-5′), 70.9 (C-2′), 73.1 (C-3′), 85.2 (C-4′), 88.4 (C-1′), 98.1 (C-3a), 113.3 (C-4$_{pyrazole}$), 130.4 (C-5$_{pyrazole}$), 137.7 (C-3$_{pyrazole}$), 155.0 (C-7a), 156.0 (C-6), 158.3 (C-4) ppm. 1 quaternary carbon (C-3)

missing. HRMS (ESI): calcd for $C_{14}H_{18}N_7O_4$ ([M + H]$^+$): 348.1420, found: 348.1418.

3-(Pyridin-2-yl)-4-amino-1-β-D-ribofuranosylpyrazolo[3,4-d]-pyrimidine, Formic Acid Salt (65). Compound **21** (0.173 g, 0.50 mmol, 1.0 equiv), Pd(PPh$_3$)$_4$ (0.087 g, 0.075 mmol, 0.15 equiv), and CuI (0.010 g, 0.05 mmol, 0.1 equiv) were dissolved in dry degassed DMF (2 mL) under argon. 2-(Tributylstannyl)pyridine was added, and the mixture was warmed to 100 °C. After 2 h, LCMS analysis indicated completion of the reaction. The mixture was cooled to room temperature, diluted with MeOH (15 mL) and MeCN (15 mL), and washed with hexanes (2 × 15 mL). The MeOH/MeCN phase was concentrated *in vacuo*. The residue was adsorbed onto celite and purified by flash column chromatography (automated, 4 → 15% MeOH in CH$_2$Cl$_2$), followed by an additional purification by preparative HPLC (0.2% formic acid in H$_2$O/MeCN 98:02 to 33:67 in 12 min) to afford **67** (80 mg, 0.232 mmol, 66% yield) as a white solid. NMR analysis showed the presence of an extra proton, indicating that **65** was isolated as its formic acid salt. ^{1}H NMR (300 MHz, DMSO-d_6) δ 3.43−3.58 (1H, m, H-5′), 3.60−3.74 (1H, m, H-5″), 3.97 (1H, dd, J = 9.7, 4.7 Hz, H-4′), 4.27−4.41 (1H, m, H-3′), 4.60−4.74 (1H, m, H-2′), 4.88 (1H, br. s., OH), 5.17 (1H, br. s., OH), 5.47 (1H, br. s., OH), 6.21 (1H, d, J = 4.4 Hz, H-1′), 7.51 (1H, ddd, J = 7.5, 5.1, 1.2 Hz, H-4$_{pyr}$), 8.04 (1H, td, J = 7.8, 1.8 Hz, H-5$_{pyr}$), 8.11 (1H, d, J = 3.2 Hz), 8.24 (1H, s, H-6), 8.28 (1H, d, J = 7.9 Hz, H-3$_{pyr}$), 8.74 (1H, dd, J = 4.1, 0.9 Hz, H-6$_{pyr}$), 9.93 (1H, d, J = 3.8 Hz, NH) ppm. ^{13}C NMR (75 MHz, DMSO-d_6) δ 62.4 (C-5′), 71.0 (C-2′), 73.4 (C-3′), 85.4 (C-4′), 88.6 (C-1′), 98.5 (C-3a), 121.0 (C-3$_{pyr}$), 124.1 (C-5$_{pyr}$), 138.3 (C-3), 143.7 (C-4$_{pyr}$), 148.5 (C-6$_{pyr}$), 150.7 (C-2$_{pyr}$), 155.7 (C-7a), 156.6 (C-6), 158.8 (C-4)ppm. HRMS (ESI): calcd for $C_{15}H_{17}N_6O_4$ ([M + H]$^+$): 345.1311, found: 345.1312.

3-(Pyridin-4-yl)-4-amino-1-β-D-ribofuranosylpyrazolo[3,4-d]-pyrimidine (66). Compound **21** (0.120 g, 0.35 mmol) was subjected to general procedure E, using pyridine-4-boronic acid as the coupling partner and Na$_2$CO$_3$ as the base. Purification *via* flash column chromatography (automated, 2 → 15% MeOH in CH$_2$Cl$_2$) afforded **66** (37 mg, 0.056 mmol, 16% yield) as a white solid. ^{1}H NMR (300 MHz, DMSO-d_6) δ 3.39−3.55 (1H, m, H-5′), 3.55−3.70 (1H, m, H-5″), 3.94 (1H, dd, J = 9.7, 4.8 Hz, H-4′), 4.28 (1H, dd, J = 10.0, 5.2 Hz, H-3′), 4.66 (1H, dd, J = 9.7, 5.0 Hz, H-2′), 4.84 (1H, t, J = 5.9 Hz, OH), 5.16 (1H, d, J = 5.6 Hz, OH), 5.43 (1H, d, J = 5.6 Hz, OH), 6.21 (1H, d, J = 4.4 Hz, H-1′), 7.18 (2H, br. s., NH$_2$), 7.67 (2H, d, J = 5.9 Hz, H-3$_{pyr}$, H-5$_{pyr}$), 8.31 (1H, s, H-6), 8.74 (2H, d, J = 5.3 Hz, H-2$_{pyr}$, H-6$_{pyr}$) ppm. ^{13}C NMR (75 MHz, DMSO-d_6) δ 62.3 (C-5′), 70.8 (C-2′), 73.2 (C-3′), 85.3 (C-4′), 88.6 (C-1′), 97.9 (C-3a), 122.8 (C-3$_{pyr}$, C-5$_{pyr}$), 139.8 (C-3), 142.6 (C-4$_{pyr}$), 150.3 (C-2$_{pyr}$, C-6$_{pyr}$), 155.6 (C-7a), 156.2 (C-6), 158.1 (C-4) ppm. HRMS (ESI): calcd for $C_{15}H_{17}N_6O_4$ ([M + H]$^+$): 345.1311, found: 345.1317.

3-(Thiophen-2-yl)-4-amino-1-β-D-ribofuranosylpyrazolo[3,4-d]-pyrimidine (67). Compound **21** (0.173 g, 0.50 mmol, 1.0 equiv), Pd(PPh$_3$)$_4$ (0.087 g, 0.075 mmol, 0.15 equiv), and CuI (0.010 g, 0.05 mmol, 0.1 equiv) were dissolved in dry degassed DMF (2 mL) under argon. 2-(Tributylstannyl)thiophene (0.238 mL, 0.75 mmol, 1.5 equiv) was added, and the mixture was warmed to 100 °C. After 2 h, LCMS analysis indicated completion of the reaction. The mixture was cooled to room temperature, diluted with MeOH (15 mL) and MeCN (15 mL), and washed with hexanes (2 × 15 mL). The MeOH/MeCN phase was concentrated *in vacuo*. The residue was adsorbed onto celite and purified by flash column chromatography (automated, 4 → 15% MeOH in CH$_2$Cl$_2$), followed by an additional purification by preparative HPLC (0.2% formic acid in H$_2$O/MeCN 98:02 to 33:67 in 12 min) to afford **67** (42 mg, 0.120 mmol, 24% yield) as a white solid. ^{1}H NMR (300 MHz, DMSO-d_6) δ 3.46 (1H, dt, J = 11.4, 5.4 Hz, H-5′), 3.60 (1H, dt, J = 11.7, 3.8 Hz, H-5″), 3.93 (1H, dd, J = 10.0, 4.7 Hz, H-4′), 4.14−4.31 (1H, m, H-3′), 4.62 (1H, dd, J = 7.3, 3.2 Hz, H-2′), 4.84 (1H, t, J = 6.2 Hz, OH), 5.16 (1H, br. s., OH), 5.42 (1H, br. s., OH), 6.16 (1H, d, J = 4.7 Hz, H-1′), 6.83−7.19 (2H, m, NH$_2$), 7.25 (2H, dd, J = 5.0, 3.5 Hz, C-4$_{Het}$), 7.50 (1H, dd, J = 3.7, 1.0 Hz, C-3$_{Het}$), 7.72 (1H, dd, J = 5.1, 1.0 Hz, C-5$_{Het}$), 8.28 (1H, s, H-6) ppm. ^{13}C NMR (75 MHz, DMSO-d_6) δ 62.9 (C-

5′), 71.3 (C-2′), 73.6 (C-3′), 85.8 (C-4′), 88.9 (C-1′), 98.1 (C-3a), 128.3 (C-3$_{Het}$), 128.5(C-4$_{Het}$), 128.9 (C-5$_{Het}$), 134.3 (C-2$_{Het}$), 139.4 (C-3), 155.7 (C-7a), 156.6 (C-6), 158.6 (C-4) ppm. HRMS (ESI): calcd for $C_{14}H_{16}N_5O_4S$ ([M + H]$^+$): 350.0923, found: 350.0932.

3-(5-Methylthiophen-2-yl)-4-amino-1-β-D-ribofuranosylpyrazolo[3,4-d]pyrimidine (68). Compound **21** (0.120 g, 0.35 mmol) was subjected to general procedure E, using 5-methylthiophene-2-boronic acid as the coupling partner and Na$_2$CO$_3$ as the base. Purification *via* flash column chromatography (automated, 2 → 15% MeOH in CH$_2$Cl$_2$) afforded **64** (65 mg, 0.187 mmol, 53% yield) as a white solid. ^{1}H NMR (300 MHz, DMSO-d_6) δ 3.34 (3H, s, CH$_3$), 3.44 (1H, dt, J = 11.9, 6.1 Hz, H-5′), 3.59 (1H, dt, J = 11.4, 4.7 Hz, H-5″), 3.91 (1H, dd, J = 9.7, 4.7 Hz, H-4′), 4.23 (1H, dd, J = 10.0, 5.0 Hz, H-3′), 4.58 (1H, dd, J = 9.7, 5.0 Hz, H-2′), 4.82 (1H, t, J = 5.9 Hz, OH), 5.13 (1H, d, J = 5.6 Hz, OH), 5.40 (1H, d, J = 5.9 Hz, OH), 6.13 (1H, d, J = 4.7 Hz, H-1′), 6.82−6.97 (1H, m, C-4$_{Het}$), 6.99−7.21 (2H, m, NH$_2$), 7.27 (1H, d, J = 3.5 Hz, C-3$_{Het}$), 8.25 (1H, s, H-6) ppm. ^{13}C NMR (75 MHz, DMSO-d_6) δ 14.9 (CH$_3$), 62.5 (C-5′), 70.9 (C-2′), 73.2 (C-3′), 85.3 (C-4′), 88.4 (C-1′), 97.5 (C-3a), 126.8 (C-4$_{Het}$), 128.0 (C-5$_{Het}$), 131.5 (C-3$_{Het}$), 139.1 (C-2$_{Het}$), 141.3 (C-3), 155.2 (C-7a), 156.2 (C-6), 158.1 (C-4) ppm. HRMS (ESI): calcd for $C_{15}H_{18}N_5O_4S$ ([M + H]$^+$): 364.1079, found: 364.1088.

3-(5-Chlorothiophen-2-yl)-4-amino-1-β-D-ribofuranosylpyrazolo[3,4-d]pyrimidine (69). Compound **21** (0.120 g, 0.35 mmol) was subjected to general procedure E, using 5-chlorothiophene-2-boronic acid as the coupling partner and Na$_2$CO$_3$ as the base. Purification *via* flash column chromatography (automated, 2 → 15% MeOH in CH$_2$Cl$_2$), followed by an additional purification by preparative RP-HPLC (0.2% formic acid in H$_2$O/MeCN 98:02 to 40:60 in 12 min) afforded **69** (55 mg, 0.143 mmol, 41% yield) as a white solid. ^{1}H NMR (400 MHz, DMSO-d_6) δ 3.36−3.51 (1H, m, H-5′), 3.59 (1H, dt, J = 11.6, 5.0 Hz, H-5″), 3.92 (1H, dd, J = 10.3, 5.1 Hz, H-4′), 4.23 (1H, dd, J = 10.0, 5.1 Hz, H-3′), 4.60 (1H, dd, J = 10.0, 5.0 Hz, H-2′), 4.82 (1H, t, J = 5.8 Hz, OH), 5.15 (1H, d, J = 5.6 Hz, OH), 5.42 (1H, d, J = 5.9 Hz, OH), 6.15 (1H, d, J = 4.5 Hz, H-1′), 7.25 (2H, d, J = 4.0 Hz, H-4$_{Het}$), 7.35 (1H, d, J = 3.9 Hz, H-3$_{Het}$), 8.28 (1H, s, H-6) ppm. ^{13}C NMR (101 MHz, DMSO-d_6) δ 62.3 (C-5′), 70.9 (C-2′), 73.2 (C-3′), 85.3 (C-4′), 88.4 (C-1′), 97.5 (C-3a), 128.0 (C-3$_{Het}$), 128.2 (C-5$_{Het}$), 129.3 (C-4$_{Het}$), 132.8 (C-2$_{Het}$), 138.1 (C-3), 155.3 (C-7a), 156.3 (C-6), 158.2 (C-4) ppm. HRMS (ESI): calcd for $C_{14}H_{15}ClN_5O_4S$ ([M + H]$^+$): 384.0533, found: 384.0550.

3-(4-Methylthiophen-2-yl)-4-amino-1-β-D-ribofuranosylpyrazolo[3,4-d]pyrimidine (70). Compound **21** (0.120 g, 0.35 mmol) was subjected to general procedure E, using 4-methylthiophene-2-boronic acid as the coupling partner and Na$_2$CO$_3$ as the base. Purification *via* flash column chromatography (automated, 2 → 15% MeOH in CH$_2$Cl$_2$), followed by an additional purification by preparative RP-HPLC (0.2% formic acid in H$_2$O/MeCN 98:02 to 40:60 in 12 min) afforded **70** (38 mg, 0.105 mmol, 30% yield) as a white solid. ^{1}H NMR (400 MHz, DMSO-d_6) δ 2.29 (3H, d, J = 0.5 Hz, CH$_3$), 3.40−3.50 (1H, m, H-5′), 3.59 (1H, dt, J = 11.9, 4.8 Hz, H-5″), 3.92 (1H, dd, J = 10.1, 4.9 Hz, H-4′), 4.24 (1H, dd, J = 10.3, 5.0 Hz, H-3′), 4.61 (1H, dd, J = 9.9, 5.1 Hz, H-2′), 4.83 (1H, t, J = 5.8 Hz, OH), 5.15 (1H, d, J = 5.6 Hz, OH), 5.41 (1H, d, J = 5.9 Hz, OH), 6.15 (1H, d, J = 4.5 Hz, H-1′), 7.28 (1H, t, J = 1.1 Hz, H-3$_{Het}$), 7.30 (1H, d, J = 1.1 Hz, H-5$_{Het}$), 8.27 (1H, s) ppm. ^{13}C NMR (101 MHz, DMSO-d_6) δ 15.5 (CH$_3$), 62.4 (C-5′), 70.9 (C-2′), 73.1 (C-3′), 85.3 (C-4′), 88.4 (C-1′), 97.5 (C-3a), 122.8 (C-5$_{Het}$), 130.0 (C-3$_{Het}$), 133.5 (C-4$_{Het}$), 138.5 (C-3), 139.1 (C-2$_{Het}$), 155.2 (C-7a), 156.2 (C-6), 158.1 (C-4) ppm. HRMS (ESI): calcd for $C_{15}H_{18}N_5O_4S$ ([M + H]$^+$): 364.1079, found: 364.1081.

3-Vinyl-4-amino-1-β-D-ribofuranosylpyrazolo[3,4-d]pyrimidine (71). Compound **21** (0.118 g, 0.34 mmol) was subjected to general procedure E, using potassium vinyl trifluoroborate as the coupling partner and Cs$_2$CO$_3$ as the base. Purification *via* flash column chromatography (automated, 2 → 15% MeOH in CH$_2$Cl$_2$), followed by an additional purification by preparative RP-HPLC (0.2% formic acid in H$_2$O/MeCN 98:02 to 33:67 in 12 min) afforded **71** (60 mg,

0.205 mmol, 58% yield) as a white solid. ^{1}H NMR (400 MHz, DMSO-d_6) δ 3.41–3.50 (1H, m, H-5′), 3.60 (1H, dt, J = 11.6, 4.8 Hz, H-5″), 3.92 (1H, dd, J = 9.4, 4.8 Hz, H-4′), 4.24 (1H, dd, J = 9.9, 5.5 Hz, h-3′), 4.57 (1H, dd, J = 10.1, 5.0 Hz, H-2′), 4.87 (1H, t, J = 5.8 Hz, OH), 5.12 (1H, d, J = 5.4 Hz, OH), 5.36 (1H, d, J = 5.9 Hz, OH), 5.46 (1H, dd, J = 11.8, 1.0 Hz, CH=C$\underline{H}_2$), 6.05 (1H, dd, J = 17.1, 1.0 Hz, CH=C$\underline{H}_2$), 6.12 (1H, d, J = 4.3 Hz, H-1′), 7.28 (1H, dd, J = 17.1, 11.0 Hz, C$\underline{H}$=CH$_2$), 7.54 (2H, br. s, NH$_2$), 8.18 (1H, s, H-6) ppm. ^{13}C NMR (101 MHz, DMSO-d_6) δ 62.4 (C-5′), 70.9 (C-2′), 73.2 (C-3′), 85.3 (C-4′), 88.5 (C-1′), 98.1 (C-3a), 118.5 (CH=$\underline{C}$H$_2$), 127.3 (C$\underline{H}$=CH$_2$), 141.9 (C-3), 155.0 (C-7a), 155.9 (C-6), 158.1 (C-4) ppm. HRMS (ESI): calcd for C$_{12}$H$_{16}$N$_5$O$_4$ ([M + H]$^+$): 294.1202, found: 294.1213.

3-Isopropenyl-4-amino-1-β-D-ribofuranosylpyrazolo[3,4-d]-pyrimidine (72). Compound **21** (0.250 g, 0.72 mmol) was subjected to general procedure E, using potassium isopropenyltrifluoroborate as the coupling partner and Cs$_2$CO$_3$ as the base. Purification *via* flash column chromatography (automated, 2 → 15% MeOH in CH$_2$Cl$_2$) afforded **72** (170 mg, 0.553 mmol, 77% yield) as a white solid. ^{1}H NMR (300 MHz, DMSO-d_6) δ 2.18 (3H, s, C$\underline{H}_3$C=CH$_2$), 3.45 (1H, dt, J = 11.6, 5.9 Hz, H-5′), 3.55–3.65 (1H, m, H-5″), 3.92 (1H, dd, J = 9.7, 4.4 Hz, H-4′), 4.23 (1H, dd, J = 9.7, 4.7 Hz, H-3′), 4.59 (1H, dd, J = 9.4, 5.0 Hz, H-2′), 4.84 (1H, t, J = 5.6 Hz, OH), 5.12 (1H, d, J = 5.3 Hz, OH), 5.29–5.45 (2H, m, OH, CH$_3$C=C$\underline{H}_2$), 5.53 (1H, br. s., CH$_3$C=C$\underline{H}_2$), 6.13 (1H, d, J = 4.1 Hz, H-1′), 7.16 (2H, br. s., NH$_2$), 8.23 (1H, s, H-6) ppm. ^{13}C NMR (75 MHz, DMSO-d_6) δ 21.7 ($\underline{C}$H$_3$C=CH$_2$), 62.4 (C-5′), 70.9 (C-2′), 73.2 (C-3′), 85.2 (C-4′), 88.5 (C-1′), 97.3 (C-3a), 118.6 (CH$_3$C=$\underline{C}$H$_2$), 137.2 (CH$_3$$\underline{C}$=CH$_2$), 146.2 (C-3), 154.9 (C-7a), 155.9 (C-6), 158.2 (C-4) ppm. HRMS (ESI): calcd for C$_{13}$H$_{18}$N$_5$O$_4$ ([M + H]$^+$): 308.1359, found: 308.1367.

3-(E-Styryl)-4-amino-1-β-D-ribofuranosylpyrazolo[3,4-d]-pyrimidine (73). Compound **21** (0.120 g, 0.35 mmol) was subjected to a slightly modified general procedure E, using *trans*-2-vinyl-phenylboronic acid as the coupling partner and Na$_2$CO$_3$ as the base. Purification *via* flash column chromatography (automated, 2 → 15% MeOH in CH$_2$Cl$_2$), followed by an additional purification by preparative RP-HPLC (0.2% formic acid in H$_2$O/MeCN 98:02 to 33:67 in 12 min) afforded **72** (55 mg, 0.149 mmol, 43% yield) as a white solid. ^{1}H NMR (300 MHz, DMSO-d_6) δ 3.48 (1H, dd, J = 11.7, 5.9 Hz, H-5′), 3.62 (1H, dd, J = 11.7, 4.4 Hz, H-5″), 3.92 (1H, dd, J = 10.0, 4.7 Hz, H-4′), 4.26 (1H, t, J = 4.7 Hz, H-3′), 4.65 (1H, t, J = 5.0 Hz, H-2′), 6.12 (1H, d, J = 4.7 Hz, H-1′), 7.26–7.49 (4H, m, H$_{Phe}$), 7.53–7.71 (3H, m, NH$_2$, H$_{Phe}$), 7.74–7.83 (2H, m, 2 × H$_{vinyl}$), 8.18 (1H, s, H-6) ppm. ^{13}C NMR (75 MHz, DMSO-d_6) δ 62.4 (C-5′), 70.9 (C-2′), 73.1 (C-3′), 85.3 (C-4′), 88.6 (C-1′), 98.5 (C-3a), 118.0 (C$_{vinyl}$), 127.4 (C$_{Phe}$), 128.0 (C$_{Phe}$), 128.3 (C$_{Phe}$), 128.6 (C$_{Phe}$), 132.2 (C$_{vinyl}$), 141.8 (C-3), 155.1 (C-7a), 155.9 (C-6), 158.1 (C-4) ppm. HRMS (ESI): calcd for C$_{18}$H$_{20}$N$_5$O$_4$ ([M + H]$^+$): 370.1515, found: 370.1509.

3-Cyclopropyl-4-amino-1-β-D-ribofuranosylpyrazolo[3,4-d]-pyrimidine (74). Compound **21** (0.120 g, 0.35 mmol) was subjected to a slightly modified general procedure E, using cyclopropylboronic acid as the coupling partner and Na$_2$CO$_3$ as the base. After 8 h, a second portion of cyclopropylboronic acid (1.5 equiv) was added, and the reaction was stirred for another 16 h, before LCMS analysis indicated full conversion. Purification *via* flash column chromatography (automated, 2 → 15% MeOH in CH$_2$Cl$_2$) afforded **74** (72 mg, 0.234 mmol, 67% yield) as a white solid. ^{1}H NMR (300 MHz, DMSO-d_6) δ 0.77–1.07 (4H, m, 2 × CH$_2$ $_{cyclopropyl}$), 2.39–2.48 (1H, m, CH$_{cyclopropyl}$), 3.40 (1H, dt, J = 12.0, 6.0 Hz, H-5′), 3.57 (1H, dt, J = 11.7, 4.7 Hz, H-5″), 3.87 (1H, dd, J = 9.7, 4.7 Hz, H-4′), 4.20 (1H, dd, J = 10.0, 5.2 Hz, H-3′), 4.49 (1H, dd, J = 10.0, 5.0 Hz, H-2′), 4.81 (1H, dd, J = 6.6, 5.1 Hz, OH), 5.06 (1H, d, J = 5.9 Hz, OH), 5.30 (1H, d, J = 5.9 Hz, OH), 6.01 (1H, d, J = 4.4 Hz, H-1′), 7.41 (2H, br. s., NH$_2$), 8.15 (1H, s, H-6) ppm. ^{13}C NMR (75 MHz, DMSO-d_6) δ 7.7 (C$_{cyclopropyl}$), 7.9 (C$_{cyclopropyl}$), 8.5 (C$_{cyclopropyl}$), 62.4 (C-5′), 71.0 (C-2′), 73.2 (C-3′), 85.0 (C-4′), 88.4 (C-1′), 99.5 (C-3a), 147.0 (C-3), 154.9 (C-7a), 155.9 (C-6), 158.3 (C-4) ppm. HRMS (ESI): calcd for C$_{13}$H$_{18}$N$_5$O$_4$ ([M + H]$^+$): 308.1359, found: 308.1342.

3-(4-Chlorophenyl)-4-amino-1-(3′-deoxy-β-D-ribofuranosyl)-pyrazolo[3,4-d]pyrimidine (76). Compound **23** (0.026 g, 0.079 mmol) was subjected to general procedure E, using 4-chlorophe-nylboronic acid as the coupling partner and Na$_2$CO$_3$ as the base. Purification *via* flash column chromatography (automated, 0 → 10% MeOH in CH$_2$Cl$_2$ + 1% NH$_4$OH) afforded **76** (23 mg, 0.064 mmol, 81% yield) as a white solid. ^{1}H NMR (400 MHz, DMSO-d_6) δ 2.00 (1H, ddd, J = 12.3, 6.2, 1.6 Hz, H-3′), 2.28–2.46 (1H, m, H-3″), 3.39–3.58 (2H, m, H-5′, H-5″), 4.29–4.41 (1H, m, H-2′), 4.62 (1H, br. s., H-4′), 4.75 (1H, t, J = 5.7 Hz, OH), 5.59 (1H, d, J = 3.8 Hz, OH), 6.24 (1H, s, H-1′), 7.61 (2H, d, J = 8.4 Hz, H$_{Phe}$), 7.67 (2H, d, J = 8.4 Hz, H$_{Phe}$), 8.28 (1H, s, H-6) ppm. ^{13}C NMR (101 MHz, DMSO-d_6) δ 36.1 (C-3′), 64.1 (C-5′), 74.5 (C-2′), 81.2 (C-4′), 90.6 (C-1′), 97.5 (C-3a), 129.2 (C$_{Phe}$), 130.0 (C$_{Phe}$), 131.5 (C$_{Phe}$), 133.6 (C$_{Phe}$), 143.7 (C-3), 155.0 (C-7a), 156.1 (C-6), 158.2 (C-4) ppm. HRMS (ESI): calcd for C$_{16}$H$_{17}$ClN$_5$O$_3$ ([M + H]$^+$): 362.1020, found: 362.0999.

3-(4-Chlorophenyl)-4-amino-1-(2′-deoxy-β-D-ribofuranosyl)-pyrazolo[3,4-d]pyrimidine (77). Compound **23** (0.042 g, 0.127 mmol) was subjected to general procedure E, using 4-chlorophe-nylboronic acid as the coupling partner and Na$_2$CO$_3$ as the base. Purification *via* flash column chromatography (automated, 1 → 8% MeOH in CH$_2$Cl$_2$ + 1% NH$_4$OH) afforded **76** (28 mg, 0.098 mmol, 81% yield) as a white solid. ^{1}H NMR (400 MHz, DMSO-d_6) δ 2.29 (1H, ddd, J = 13.2, 6.8, 4.3 Hz, H-2′), 2.85 (1H, dt, J = 12.9, 6.0 Hz, H-2″), 3.40 (1H, dt, J = 11.7, 6.0 Hz, H-5′), 3.55 (1H, dt, J = 11.4, 5.5 Hz, H-5″), 3.84 (1H, td, J = 5.4, 3.6 Hz, H-4′), 4.42–4.51 (1H, m, H-3′), 4.77 (1H, t, J = 5.8 Hz, OH), 5.27 (1H, d, J = 4.6 Hz, OH), 6.64 (1H, t, J = 6.4 Hz, H-1′), 7.58–7.64 (2H, m, H$_{Phe}$), 7.65–7.72 (2H, m, H$_{Phe}$), 8.27 (1H, s, H-6) ppm. ^{13}C NMR (101 MHz, DMSO-d_6) δ 38.0 (C-2′), 62.4 (C-5′), 71.1 (C-3′), 83.9 (C-4′), 87.7 (C-1′), 97.8 (C-3a), 129.2 (C$_{Phe}$), 130.0 (C$_{Phe}$), 131.5 (C$_{Phe}$), 133.6 (C$_{Phe}$), 143.6 (C-3), 155.0 (C-7a), 156.0 (C-6), 158.1 (C-4) ppm. HRMS (ESI): calcd for C$_{16}$H$_{17}$ClN$_5$O$_3$ ([M + H]$^+$): 362.1020, found: 362.1004.

3-Isopropyl-4-amino-1-β-D-ribofuranosylpyrazolo[3,4-d]-pyrimidine (78). Compound **72** (0.060 g, 0.195 mmol) was dissolved in MeOH (5 mL). The flask was placed under a nitrogen atmosphere, and a catalytic amount of Pd(OH)$_2$/C was added. The atmosphere was exchanged for H$_2$, and the mixture was stirred for 1 h until TLC analysis (10% MeOH in CH$_2$Cl$_2$) indicated completion of the reaction. The mixture was filtered over celite, celite was added to the filtrate, and the solvents were removed under reduced pressure. The solid residue was purified *via* flash column chromatography (automated, 4 → 20% MeOH in CH$_2$Cl$_2$) to afford **78** (49 mg, 0.158 mmol, 81% yield) as a white solid. ^{1}H NMR (300 MHz, DMSO-d_6) δ 1.26 (6H, d, J = 6.7 Hz, CH(C$\underline{H}_3$)$_2$), 3.38–3.65 (3H, m, H-5′, H-5″, C$\underline{H}$(CH$_3$)$_2$), 3.90 (1H, dd, J = 9.4, 4.7 Hz, H-4′), 4.25 (1H, dd, J = 10.3, 5.0 Hz, H-3′), 4.56 (1H, dd, J = 10.0, 5.3 Hz, H-2′), 4.85 (1H, dd, J = 6.7, 5.0 Hz, OH), 5.07 (1H, d, J = 5.6 Hz, OH), 5.32 (1H, d, J = 5.9 Hz, OH), 6.06 (1H, d, J = 4.4 Hz, H-1′), 7.30 (2H, br. s, NH$_2$), 8.15 (1H, s, H-6) ppm. ^{13}C NMR (75 MHz, DMSO-d_6) δ 22.3 (CH($\underline{C}$H$_3$)$_2$), 27.4 ($\underline{C}$H(CH$_3$)$_2$), 63.0 (C-5′), 71.5 (C-2′), 73.7 (C-3′), 85.6 (C-4′), 89.1 (C-1′), 98.6 (C-3a), 151.6 (C-3), 155.5 (C-7a), 156.2 (C-6), 158.5 (C-4) ppm. HRMS (ESI): calcd for C$_{13}$H$_{20}$N$_5$O$_4$ ([M + H]$^+$): 310.1515, found: 310.1494.

3-O-Phenyl-4-amino-1-β-D-ribofuranosylpyrazolo[3,4-d]-pyrimidine (79). Compound **21** (0.220 g, 0.64 mmol, 1.0 equiv), phenol (0.090 g, 0.96 mmol, 1.5 equiv), CuI (0.024 g, 0.13 mmol, 0.2 equiv), N,N-dimethylglycine (0.040 g, 0.38 mmol, 0.6 equiv), and Cs$_2$CO$_3$ (0.417 g, 1.28 mmol, 2.0 equiv) were dissolved in dry degassed DMA (4 mL) under argon. The reaction was heated at 120 °C overnight, cooled down to room temperature, and concentrated *in vacuo*. The residue was taken up in MeOH, celite was added, and the mixture was concentrated under reduced pressure. The solid residue was purified by flash column chromatography (automated, 2 → 15% MeOH in CH$_2$Cl$_2$) to afford **79** (12 mg, 0.033 mmol, 5% yield) as a white solid. ^{1}H NMR (300 MHz, DMSO-d_6) δ 3.34–3.42 (1H, m, H-5′, underwater peak), 3.48 (1H, dd, J = 12.0, 4.4 Hz, H-5″), 3.84 (1H, dd, J = 10.3, 4.7 Hz, H-4′), 4.07 (1H, t, J = 4.8 Hz, H-3′), 4.43 (1H, t, J = 4.7 Hz, H-2′), 6.02 (1H, d, J = 4.1 Hz, H-1′), 7.14–7.26 (1H, m,

H$_{Phe}$), 7.33–7.49 (4H, m, H$_{Phe}$), 8.22 (1H, br. s, H-6) ppm. ^{13}C NMR (101 MHz, DMSO-d_6) δ 62.3 (C-5′), 70.7 (C-2′), 73.1 (C-3′), 84.9 (C-4′), 88.1 (C-1′), 119.1 (C$_{Phe}$), 124.5 (C$_{Phe}$), 129.6 (C$_{Phe}$), 152.8 (C$_{Phe}$), 154.7 (C-7a), 155.0 (C-6), 157.4 (C-4), 157.4 (C-3) ppm. Two quaternary carbons missing (C-3, C-3a). HRMS (ESI): calcd for C$_{16}$H$_{18}$N$_5$O$_5$ ([M + H]$^+$): 360.1308, found: 360.1308.

3-O-(4-Chlorophenyl)-4-amino-1-β-D-ribofuranosylpyrazolo[3,4-d]pyrimidine (80). Compound **21** (0.220 g, 0.64 mmol, 1.0 equiv), 4-chlorophenol (0.123 g, 0.96 mmol, 1.5 equiv), CuI (0.024 g, 0.13 mmol, 0.2 equiv), *N*,*N*-dimethylglycine (0.040 g, 0.38 mmol, 0.6 equiv), and Cs$_2$CO$_3$ (0.417 g, 1.28 mmol, 2.0 equiv) were dissolved in dry degassed DMA (4 mL) under argon. The reaction was heated at 120 °C overnight, cooled down to room temperature, and concentrated *in vacuo*. The residue was taken up in MeOH, celite was added, and the mixture was concentrated under reduced pressure. The solid residue was purified by flash column chromatography (automated, 2 → 15% MeOH in CH$_2$Cl$_2$), followed by an additional purification *via* preparative RP-HPLC (0.2% formic acid in H$_2$O/MeCN 98:02 to 33:67 in 12 min) to afford **80** (8 mg, 0.020 mmol, 3% yield) as a white solid. ^{1}H NMR (300 MHz, DMSO-d_6) δ 3.34–3.42 (1H, m, H-5′), 3.46–3.54 (1H, m, H-5″.), 3.84 (1H, dd, *J* = 10.0, 5.3 Hz, H-4′), 4.02–4.16 (1H, m, H-3′), 4.31–4.52 (1H, m, H-2′), 4.64–4.75 (1H, m, OH), 4.96–5.18 (1H, m, OH), 5.26–5.50 (1H, m, OH), 6.02 (1H, d, *J* = 4.1 Hz, H-1′), 7.48 (4H, s, H$_{Phe}$), 8.21 (1H, s, H$_{Phe}$) ppm. ^{13}C NMR (75 MHz, DMSO-d_6) δ 62.1 (C-5′), 70.6 (C-2′), 73.0 (C-3′), 84.8 (C-4′), 88.0 (C-1′), 89.8 (C-3a), 120.9 (C$_{Phe}$), 128.2 ($_{CPhe}$), 129.3 (C$_{Phe}$), 152.3 (C$_{Phe}$), 153.4 (C-7a), 154.9 (C-6), 157.3 (C-4), 157.4 (C-3) ppm. HRMS (ESI): calcd for C$_{16}$H$_{17}$ClN$_5$O$_5$ ([M + H]$^+$): 394.0918, found: 394.0927.

3,4-Diamino-1-β-D-ribofuranosylpyrazolo[3,4-d]pyrimidine[69] (81). A mixture of **21** (145 mg, 0.42 mmol, 1.0 equiv), CuCl (0.006 g, 0.042 mmol, 0.1 equiv), and aq. NH$_4$OH (20–30% wt, 30 mL) was heated in a pressure reactor at 130 °C overnight. The vessel was cooled to room temperature, and the contents were diluted with MeOH and transferred to a pear-shaped flask. Celite was added, and the mixture was concentrated *in vacuo* slowly (NH$_3$ evolution!). The solid residue was purified by flash column chromatography (4 → 20% MeOH in CH$_2$Cl$_2$), followed by an additional purification by preparative RP-HPLC (0.2% formic acid in H$_2$O/MeCN 98:02 to 40:60 in 12 min) to afford **81** (23 mg, 0.082 mmol, 19% yield) as a white solid. ^{1}H NMR (300 MHz, DMSO-d_6) δ 3.32–3.45 (1H, m, H-5′), 3.54 (1H, dd, *J* = 11.7, 4.1 Hz, H-5″), 3.81 (1H, dd, *J* = 9.4, 4.4 Hz, H-4′), 4.11 (1H, t, *J* = 4.8 Hz, H-3′), 4.44 (1H, t, *J* = 5.0 Hz, H-2′), 4.82 (1H, br. s, OH), 5.03 (1H, br. s, OH), 5.23 (1H, br. s, OH), 5.84 (2H, br. s, NH$_2$), 5.93 (1H, d, *J* = 4.7 Hz, H-1′), 7.29 (2H, br. s., NH$_2$), 8.02 (1H, s, H-6) ppm. ^{13}C NMR (75 MHz, DMSO-d_6) δ 62.7 (C-5′), 71.0 (C-2′), 72.6 (C-3′), 84.5 (C-4′), 87.4 (C-1′), 90.6 (C-3a), 148.1 (C-3), 155.0 (C-7a), 156.1 (C-6), 157.8 (C-4) ppm. Spectral data are in accordance with literature values.[69] HRMS (ESI): calcd for C$_{10}$H$_{15}$N$_6$O$_4$ ([M + H]$^+$): 283.1155, found: 283.1179.

3-N-Methylamino-4-amino-1-β-D-ribofuranosylpyrazolo[3,4-d]pyrimidine (82). A mixture of **21** (150 mg, 0.43 mmol, 1.0 equiv), CuCl (0.006 g, 0.043 mmol, 0.1 equiv), and aqueous methylamine (40%, 30 mL) was heated in a pressure reactor at 130 °C over the weekend. The vessel was cooled to room temperature, and the contents were diluted with MeOH and transferred to a pear-shaped flask. Celite was added, and the mixture was concentrated *in vacuo* slowly (NHMe evolution!). The solid residue was purified by flash column chromatography (4 → 20% MeOH in CH$_2$Cl$_2$), followed by an additional purification by preparative RP-HPLC (0.2% formic acid in H$_2$O/MeCN 98:02 to 33:67 in 12 min) to afford **82** (6 mg, 0.020 mmol, 5% yield) as a white solid. ^{1}H NMR (300 MHz, D$_2$O) δ 2.85 (3H, s, CH$_3$), 3.76 (1H, dd, *J* = 12.6, 4.1 Hz, H-5′), 3.82–3.92 (1H, m, H-5″), 4.17 (1H, dd, *J* = 7.0, 3.8 Hz, H-4′), 4.45 (1H, dd, *J* = 5.0, 3.8 Hz, H-3′), 4.71–4.80 (1H, m, H-2′, partially underwater peak), 6.07 (1H, d, *J* = 5.0 Hz, H-1′), 8.04 (1H, s, H-6) ppm. A qualitative ^{13}C NMR spectrum could not be obtained from the amount of product available. HRMS (ESI): calcd for C$_{11}$H$_{17}$N$_6$O$_4$ ([M + H]$^+$): 297.1311, found: 297.1318.

3-(1-Pyrrolidin-yl)-4-amino-1-β-D-ribofuranosylpyrazolo[3,4-d]pyrimidine (83). A mixture of **21** (150 mg, 0.43 mmol, 1.0 equiv), CuCl (0.006 g, 0.043 mmol, 0.1 equiv), pyrrolidine (0.706 mL, 8.60 mmol, 20.0 equiv) in 1,4-dioxane (1.5 mL) and H$_2$O (3 mL) was heated in at 120 °C over the weekend. The mixture was cooled to room temperature and diluted with MeOH. Celite was added, and the mixture was concentrated *in vacuo*. The solid residue was purified by flash column chromatography (4 → 20% MeOH in CH$_2$Cl$_2$), followed by an additional purification by preparative RP-HPLC (0.2% formic acid in H$_2$O/MeCN 98:02 to 33:67 in 12 min) to afford **83** (23 mg, 0.068 mmol, 16% yield) as a white solid. ^{1}H NMR (300 MHz, DMSO-d_6) δ 1.83–1.96 (4H, m, 2 × CH$_2$$_{pyrrolidine}$), 3.29–3.40 (4H, m, 2 × CH$_2$$_{pyrrolidine}$), 3.45 (1H, dd, *J* = 11.7, 5.6 Hz, H-5′), 3.59 (1H, dd, *J* = 11.7, 4.1 Hz, H-5″), 3.87 (1H, dd, *J* = 9.7, 4.7 Hz, H-4′), 4.21 (1H, t, *J* = 4.8 Hz, H-3′), 4.50 (1H, t, *J* = 4.5 Hz, H-2′), 4.81 (1H, br. s, OH), 5.02 (1H, br. s, OH), 5.28 (1H, br. s, OH), 6.02 (1H, d, *J* = 4.4 Hz, H-1′), 6.98 (2H, br. s, NH$_2$), 8.09 (1H, s, H-6) ppm. ^{13}C NMR (75 MHz, DMSO-d_6) δ 24.7 (2 × C$_{pyrrolidine}$), 50.3 (2 × C$_{pyrrolidine}$), 62.6 (C-5′), 71.1 (C-2′), 73.1 (C-3′), 84.9 (C-4′), 87.9 (C-1′), 92.1 (C-3a), 150.7 (C-3), 155.4 (C-7a), 155.8 (C-6), 157.8 (C-4) ppm. HRMS (ESI): calcd for C$_{14}$H$_{21}$N$_6$O$_4$ ([M + H]$^+$): 337.1624, found: 337.1630.

3-Chloro-4-amino-1-(2′,3′,5′-tri-O-benzoyl-β-D-ribofuranosyl)-pyrazolo[3,4-d]pyrimidine (84). Compound **18** (0.223 g, 0.339 mmol, 1.0 equiv), Cu$_2$O (0.012 g, 0.085 mmol, 0.25 equiv), Me$_4$NCl (0.111 g, 1.02 mmol, 3.0 equiv), and L-proline (0.020 g, 0.17 mmol, 0.5 equiv) were suspended in dry degassed 2-methoxy-ethanol (2 mL) under argon. The mixture was heated at 120 °C for 7 days until LCMS analysis indicated ~80% conversion and further progression had ceased. The mixture was cooled to room temperature and concentrated *in vacuo*. The residue was used crude in the next reaction. HRMS (ESI): calcd for C$_{31}$H$_{25}$ClN$_5$O$_7$ ([M + H]$^+$): 614.1443, found: 614.2593.

3-Chloro-4-amino-1-β-D-ribofuranosylpyrazolo[3,4-d]pyrimidine (85). The crude **84** from the previous reaction was subjected to general procedure C (reaction time: 1 h). Flash column chromatography (automated, 4 → 20% MeOH in CH$_2$Cl$_2$), followed by an additional purification *via* preparative RP-HPLC (0.2% formic acid in H$_2$O/MeCN 98:02 to 88:12 in 4 min, then to 77:23 in 5 min, and then to 33:67 in 3 min) afforded **85** (35 mg, 0.116 mmol, 34% yield) as a white solid. ^{1}H NMR (300 MHz, DMSO-d_6) δ 3.42 (1H, dt, *J* = 12.0, 5.9 Hz, H-5′), 3.55 (1H, dt, *J* = 11.7, 5.0 Hz, H-5″), 3.89 (1H, dd, *J* = 9.7, 4.7 Hz, H-4′), 4.16 (1H, dd, *J* = 9.7, 4.7 Hz, H-3′), 4.54 (1H, dd, *J* = 10.5, 5.3 Hz, H-2′), 4.80 (1H, t, *J* = 5.7 Hz, OH), 5.16 (1H, d, *J* = 5.3 Hz, OH), 5.40 (1H, d, *J* = 5.9 Hz, OH), 6.05 (1H, d, *J* = 4.7 Hz, OH), 7.23 (1H, br. s, NH), 8.03 (1H, s, NH), 8.24 (1H, s, H-6) ppm. ^{13}C NMR (75 MHz, DMSO-d_6) δ 62.2 (C-5′), 70.6 (C-2′), 72.9 (C-3′), 85.2 (C-4′), 88.0 (C-1′), 97.5 (C-3a), 132.0 (C-3), 155.1 (C-7a), 157.2 (C-6), 157.3 (C-4) ppm. HRMS (ESI): calcd for C$_{10}$H$_{13}$ClN$_5$O$_4$ ([M + H]$^+$): 302.0656, found: 302.0652.

3-Phenylethynyl-4-amino-1-β-D-ribofuranosylpyrazolo[3,4-d]-pyrimidine (86). Compound **36** (0.250 g, 0.636 mmol, 1.0 equiv), PdCl$_2$(PPh$_3$)$_2$ (0.022 g, 0.032 mmol, 0.05 equiv), and CuI (0.012 g, 0.1 equiv) were added to a 10 mL round-bottom flask. The flask was evacuated and backfilled with argon three times. Then, anhydrous, degassed DMF (2 mL), Et$_3$N (0.5 mL), and phenylacetylene (0.105 mL, 0.96 mmol, 1.5 equiv) were added. The resulting solution was stirred at room temperature for 3 h until LCMS analysis indicated completion of the reaction. The mixture was concentrated *in vacuo*, and the residue was taken up in MeOH, adsorbed onto celite, and purified *via* flash column chromatography (automated, 2 → 12% MeOH in CH$_2$Cl$_2$) to afford **86** (93 mg, 0.253 mmol, 40% yield) as a white solid. ^{1}H NMR (300 MHz, DMSO-d_6) δ 3.46 (1H, dt, *J* = 11.8, 6.0 Hz, H-5′), 3.59 (1H, dt, *J* = 11.9, 4.9 Hz, H-5″), 3.93 (1H, dd, *J* = 9.7, 4.7 Hz, H-4′), 4.21 (1H, dd, *J* = 9.4, 5.0 Hz, H-3′), 4.63 (1H, dd, *J* = 10.8, 5.0 Hz, H-2′), 4.86 (1H, t, *J* = 5.9 Hz, OH), 5.18 (1H, d, *J* = 5.6 Hz, OH), 5.43 (1H, d, *J* = 6.2 Hz, OH), 6.13 (1H, d, *J* = 5.0 Hz, H-1′), 7.27–7.55 (3H, m, H$_{Phe}$), 7.67–7.84 (2H, m, H$_{Phe}$), 8.28 (1H, s, H-6) ppm. ^{13}C NMR (75 MHz, DMSO-d_6) δ 62.7 (C-5′), 71.2 (C-2′), 73.5 (C-3′), 81.1 (C$_{ethynyl}$), 85.8 (C-4′), 88.9 (C-1′), 94.1

(C$_{ethynyl}$), 101.2 (C-3a), 121.5 (C-3), 127.3 (C$_{Phe}$), 129.1 (C$_{Phe}$), 130.1 (C$_{Phe}$), 132.4 (C$_{Phe}$), 154.7 (C-7a), 157.2 (C-6), 158.2 (C-4) ppm. HRMS (ESI): calcd for C$_{18}$H$_{18}$N$_5$O$_4$ ([M + H]$^+$): 368.1359, found: 368.1355.

3-Phenylethyl-4-amino-1-β-D-ribofuranosylpyrazolo[3,4-d]-pyrimidine (87). Compound **86** (0.051 g, 0.139 mmol) was dissolved in MeOH (5 mL). The flask was placed under a nitrogen atmosphere, and a catalytic amount of Pd(OH)$_2$/C was added. The atmosphere was exchanged for H$_2$ and the mixture was stirred for 1 h until TLC analysis (20% MeOH in CH$_2$Cl$_2$) indicated completion of the reaction. The mixture was filtered over celite, celite was added to the filtrate, and the solvents were removed under reduced pressure. The solid residue was purified *via* flash column chromatography (automated, 2 → 20% MeOH in CH$_2$Cl$_2$) to afford **87** (46 mg, 0.124 mmol, 89% yield) as a white solid.

^{1}H NMR (300 MHz, DMSO-d_6) δ 3.02 (2H, dd, J = 8.6, 7.0 Hz, CH$_2$), 3.28 (2H, dd, J = 9.2, 7.0 Hz, CH$_2$), 3.42 (1H, dt, J = 12.2, 6.3 Hz, H-5′), 3.58 (1H, dt, J = 11.7, 4.7 Hz, H-5″), 3.89 (1H, dd, J = 10.3, 4.6 Hz, H-4′), 4.22 (1H, dd, J = 10.5, 5.0 Hz, H-3′), 4.54 (1H, dd, J = 10.3, 5.0 Hz, H-2′), 4.83 (1H, dd, J = 6.4, 5.3 Hz, OH), 5.08 (1H, d, J = 5.6 Hz, OH), 5.31 (1H, d, J = 5.9 Hz, OH), 6.06 (1H, d, J = 4.4 Hz, H-1′), 7.15−7.32 (5H, m, H$_{Phe}$), 8.16 (1H, s, H-6) ppm. ^{13}C NMR (75 MHz, DMSO-d_6) δ 29.4 (CH$_2$), 33.4 (CH$_2$), 62.6 (C-5′), 71.0 (C-2′), 73.2 (C-3′), 85.0 (C-4′), 88.3 (C-1′), 98.8 (C-3a), 125.8 (C$_{Phe}$), 128.1 (C$_{Phe}$), 128.5 (C$_{Phe}$), 141.1 (C$_{Phe}$), 145.2 (C-3), 155.0 (C-7a), 155.8 (C-6), 158.3 (C-4) ppm. HRMS (ESI): calcd for C$_{18}$H$_{22}$N$_5$O$_4$ ([M + H]$^+$): 372.1672, found: 372.1684.

3-Ethynyl-4-amino-1-β-D-ribofuranosylpyrazolo[3,4-d]-pyrimidine (88). Compound **36** (0.250 g, 0.636 mmol, 1.0 equiv), PdCl$_2$(PPh)$_3$ (0.022 g, 0.032 mmol, 0.05 equiv), and CuI (0.012 g, 0.1 equiv) were added to a 10 mL round-bottom flask. The flask was evacuated and backfilled with argon three times. Then, anhydrous, degassed DMF (2 mL), Et$_3$N (0.5 mL), and ethynyltrimethylsilane (0.881 mL, 6.36 mmol, 10 equiv) were added. The resulting solution was stirred at room temperature for 3 h until LCMS analysis indicated completion of the reaction. The mixture was concentrated *in vacuo*, and the residue was taken up in MeOH, adsorbed onto celite, and purified *via* flash column chromatography (automated, 2 → 12% MeOH in CH$_2$Cl$_2$). The intermediate TMS-ethynyl nucleoside was stirred overnight in 7 N NH$_3$ in MeOH (10 mL). The mixture was concentrated *in vacuo*, and the residue was purified again by flash column chromatography (automated, 2 → 12% MeOH in CH$_2$Cl$_2$) to afford **88** (35 mg, 0.120 mmol, 19% yield) as a white solid. ^{1}H NMR (300 MHz, DMSO-d_6) δ 3.43 (1H, dt, J = 11.7, 6.0 Hz, H-5′), 3.57 (1H, dt, J = 11.7, 5.0 Hz, H-5″), 3.91 (1H, dd, J = 9.7, 4.7 Hz, H-4′), 4.19 (1H, dd, J = 9.7, 4.7 Hz, H-3′), 4.57 (1H, dd, J = 10.7, 5.2 Hz, H-2′), 4.70 (1H, s, H$_{ethynyl}$), 4.83 (1H, t, J = 5.9 Hz, OH), 5.16 (1H, d, J = 5.3 Hz, OH), 5.41 (1H, d, J = 6.2 Hz, OH), 6.09 (1H, d, J = 4.7 Hz, H-1′), 6.79 (2H, br. s, NH$_2$), 8.25 (1H, s, H-6) ppm. ^{13}C NMR (75 MHz, DMSO-d_6) δ 62.2 (C-5′), 70.7 (C-2′), 73.0 (C-3′), 74.9 (C$_{ethynyl}$), 85.4 (C-4′), 86.7 (C$_{ethynyl}$), 88.4 (C-1′), 101.1 (C-3a), 126.3 (C-3), 154.0 (C-7a), 156.8 (C-6), 157.7 (C-4) ppm. HRMS (ESI): calcd for C$_{12}$H$_{14}$N$_5$O$_4$ ([M + H]$^+$): 292.1046, found: 292.1049.

3-Ethyl-4-amino-1-β-D-ribofuranosylpyrazolo[3,4-d]pyrimidine (89). Compound **88** (47 mg, 0.161 mmol) was dissolved in MeOH (5 mL). The flask was placed under a nitrogen atmosphere, and a catalytic amount of Pd(OH)$_2$/C was added. The atmosphere was exchanged for H$_2$ and the mixture was stirred for 1 h until TLC analysis (20% MeOH in CH$_2$Cl$_2$) indicated completion of the reaction. The mixture was filtered over celite, celite was added to the filtrate, and the solvents were removed under reduced pressure. The solid residue was purified *via* flash column chromatography (automated, 2 → 20% MeOH in CH$_2$Cl$_2$) to afford **87** (35 mg, 0.119 mmol, 74% yield) as a white solid. ^{1}H NMR (300 MHz, DMSO-d_6) δ 1.22 (3H, t, J = 7.5 Hz, CH$_2$C$\underline{H}_3$), 2.96 (2H, q, J = 7.5 Hz, C$\underline{H}_2$CH$_3$), 3.43 (1H, dt, J = 12.0, 6.0 Hz, H-5′), 3.59 (1H, dt, J = 12.0, 4.7 Hz, H-5″), 3.89 (1H, dd, J = 9.7, 4.5 Hz, H-4′), 4.21 (1H, dd, J = 10.3, 5.3 Hz, H-3′), 4.57 (1H, dd, J = 10, 5.0 Hz, H-2′), 4.86 (1H, t, J = 6.0 Hz, OH), 5.08 (1H, d, J = 5.6 Hz, OH), 5.30 (1H, d, J

= 5.9 Hz, OH), 6.04 (1H, d, J = 4.7 Hz, H-1′), 7.32 (2H, br. s., NH$_2$), 8.15 (1H, s, H-6) ppm. ^{13}C NMR (75 MHz, DMSO-d_6) δ 13.0 (CH$_2$C$\underline{H}_3$), 21.4 (C$\underline{H}_2$CH$_3$), 62.5 (C-5′), 70.9 (C-2′), 73.0 (C-3′), 85.0 (C-4′), 88.3 (C-1′), 98.6 (C-3a), 147.2 (C-3), 155.1 (C-7a), 155.9 (C-6), 158.2 (C-4) ppm. HRMS (ESI): calcd for C$_{12}$H$_{18}$N$_5$O$_4$ ([M + H]$^+$): 296.1359, found: 296.1363.

3-(1H-1,2,3-Triazol-4-yl)-4-amino-1-β-D-ribofuranosylpyrazolo-[3,4-d]pyrimidine (90). Compound **88** (0.125 g, 0.429 mmol, 1.0 equiv) and CuI (0.004 g, 0.021 mmol, 0.05 equiv) were dissolved in MeOH (0.2 mL) and DMF (1.8 mL). TMSN$_3$ (0.085 mL, 0.644 mmol, 1.5 equiv) was added, and the mixture was heated at 100 °C overnight. The mixture was cooled to room temperature and concentrated *in vacuo*. The residue was dissolved in MeOH, celite was added, and the solvents were removed under reduced pressure. The solid residue was purified by flash column chromatography (4 → 20% MeOH in CH$_2$Cl$_2$) to afford **90** (57 mg, 0.170 mmol, 40% yield) as a light-brown solid. ^{1}H NMR (300 MHz, DMSO-d_6) δ 3.48 (1H, dt, J = 12.0, 5.6 Hz, H-5′), 3.62 (1H, dt, J = 12.0, 4.7 Hz, H-5″), 3.93 (1H, dd, J = 9.4, 4.6 Hz, H-4′), 4.26 (1H, dd, J = 10.0, 5.0 Hz, H-3′), 4.66 (1H, dd, J = 10.3, 5.2 Hz, H-2′), 4.88 (1H, t, J = 5.6 Hz, OH), 5.13 (1H, d, J = 5.6 Hz, OH), 5.43 (1H, d, J = 5.9 Hz, OH), 6.14 (1H, d, J = 5.0 Hz, H-1′), 8.14 (1H, br. s., CH$_{triazole}$), 8.25 (1H, s, H-6), 8.54 (1H, br. s, NH) ppm. ^{13}C NMR (75 MHz, DMSO-d_6) δ 62.4 (C-5′), 70.9 (C-2′), 73.0 (C-3′), 85.4 (C-4′), 88.8 (C-), 98.0 (C-3a), 131.1 (C$_{triazole}$), 136.3 (C-3), 140.3 (C$_{triazole}$), 155.1 (C-7a), 156.7 (C-6), 158.4 (C-4) ppm. HRMS (ESI): calcd for C$_{12}$H$_{15}$N$_8$O$_4$ ([M + H]$^+$): 335.1216, found: 335.1205.

3-Cyano-4-amino-1-β-D-ribofuranosylpyrazolo[3,4-d]-pyrimidine[66] *(91).* Compound **36** (2.73 g, 6.95 mmol, 1.0 equiv), Pd$_2$(dba)$_3$ (0.382 g, 0.417 mmol, 0.06 equiv), dppf (0.771 g, 1.39 mmol, 0.2 equiv), and Zn(CN)$_2$ (0.490 g, 4.17 mmol, 0.6 equiv) were dissolved in dry degassed DMF (30 mL) in a flame-dried flask under argon. The mixture was stirred at 150 °C for 90 min until LCMS analysis indicated completion of the reaction. The mixture was cooled to room temperature and concentrated *in vacuo*. The residue was taken up in MeOH, celite was added, and the solvents were removed under reduced pressure. The solid residue was purified first by manual flash column chromatography (5 → 20% MeOH in CH$_2$Cl$_2$) and then by automated flash column chromatography (4 → 20% MeOH in CH$_2$Cl$_2$) to afford **91** (570 mg, 1.95 mmol, 28% yield) as a white solid. ^{1}H NMR (300 MHz, DMSO-d_6) δ 3.45 (1H, dt, J = 11.7, 5.9 Hz, H-5′), 3.58 (1H, dt, J = 12.0, 5.0 Hz, H-5″), 3.95 (1H, dd, J = 9.7, 4.7 Hz, H-4′), 4.22 (1H, dd, J = 9.7, 5.0 Hz, H-3′), 4.60 (1H, dd, J = 10.3, 5.2 Hz, H-2′), 4.82 (1H, t, J = 5.9 Hz, OH), 5.23 (1H, d, J = 5.6 Hz, OH), 5.50 (1H, d, J = 5.9 Hz, OH), 6.17 (1H, d, J = 5.0 Hz, H-1′), 8.35 (1H, s, H-6) ppm. ^{13}C NMR (101 MHz, DMSO-d_6) δ 62.0 (C-5′), 70.6 (C-2′), 73.3 (C-3′), 85.8 (C-4′), 89.1 (C-1′), 101.2 (C-3), 113.0 (CN), 116.9 (C-3a), 154.4 (C-7a), 157.1 (C-6), 157.4 (C-4) ppm. HRMS (ESI): calcd for C$_{11}$H$_{13}$N$_6$O$_4$ ([M + H]$^+$): 293.0998, found: 293.1002. Spectral data are in accordance with literature values.[66]

3-(1H-Tetrazol-5-yl)-4-amino-1-β-D-ribofuranosylpyrazolo[3,4-d]pyrimidine (92). Compound **91** (0.074 g, 0.253 mmol), NaN$_3$ (0.021 g, 0.329 mmol, 1.3 equiv), NH$_4$Cl (0.018 g, 0.329 mmol, 1.3 equiv), and a catalytic amount of LiCl were suspended in DMF (3 mL). The mixture was heated at 100 °C overnight, cooled down to room temperature, and concentrated *in vacuo*. The residue was taken up in MeOH, adsorbed onto celite, and purified by flash column chromatography (2 → 40% MeOH in CH$_2$Cl$_2$ + 0.1% AcOH) to afford **92** (21 mg, 0.063 mmol, 25% yield) as a white solid. ^{1}H NMR (300 MHz, DMSO-d_6) δ 3.50 (1H, dd, J = 11.7, 6.2 Hz, H-5′), 3.65 (1H, dd, J = 11.9, 4.5 Hz, H-5″), 3.97 (1H, dd, J = 10.3, 5.0 Hz, H-4′), 4.34 (1H, t, J = 4.8 Hz, H-3′), 4.70 (1H, t, J = 4.8 Hz, H-2′), 6.20 (1H, d, J = 4.4 Hz, H-1′), 8.34 (1H, s, H-6), 8.45 (1H, br. s., H$_{tetrazole}$), 9.12 (1H, br. s., NH$_{tetrazole}$) ppm. ^{13}C NMR (75 MHz, DMSO-d_6) δ 62.4 (C-5′), 70.7 (C-2′), 73.1 (C-3′), 85.7 (C-4′), 89.1 (C-1′), 98.6 (C-3a), 131.3 (C-3), 150.4 (C$_{tetrazole}$), 155.0 (C-7a), 156.4 (C-6), 157.5 (C-4) ppm. HRMS (ESI): calcd for C$_{11}$H$_{14}$N$_9$O$_4$ ([M + H]$^+$): 336.1169, found: 336.1176.

3-Aminomethyl-4-amino-1-β-D-ribofuranosylpyrazolo[3,4-d]-pyrimidine (93). 88 (47 mg, 0.161 mmol) was dissolved in MeOH (5 mL). The flask was placed under a nitrogen atmosphere, and Raney nickel (slurry in H_2O, 1 mL) was added. The atmosphere was exchanged for H_2 and the mixture was stirred for 1 h until TLC analysis (20% MeOH in CH_2Cl_2) indicated completion of the reaction. The mixture was filtered over celite, celite was added to the filtrate, and the solvents were removed under reduced pressure. The solid residue was purified via flash column chromatography (automated, NH_4OH/MeOH/CH_2Cl_2 1/0/99 → 1/25/74), followed by an additional purification via preparative RP-HPLC (0.2% formic acid in H_2O/MeCN 95:05 to 68:32 in 6 min) to afford 93 (5 mg, 0.017 mmol, 10% yield) as a white solid. ^1H NMR (300 MHz, CD_3OD) δ 2.66 (2H, s, C$\underline{H}_2NH_2$), 3.69 (1H, dd, J = 12.3, 4.4 Hz, H-5′), 3.81 (1H, dd, J = 12.3, 3.2 Hz, H-5″), 4.10 (1H, dd, J = 7.9, 3.5 Hz, H-4′), 4.38−4.51 (1H, m, H-3′), 4.73−4.80 (1H, m, H-2′), 6.23 (1H, d, J = 4.7 Hz, H-1′), 8.20 (1H, s, H-6), 8.50 (4H, br. s., 2 × NH_2) ppm. A qualitative ^{13}C NMR spectrum could not be obtained from the amount of product available. HRMS (ESI): calcd for $C_{11}H_{17}N_6O_4$ ([M + H]$^+$): 297.1311, found: 297.1314.

3-Carboxamido-4-amino-1-β-D-ribofuranosylpyrazolo[3,4-d]-pyrimidine[66] (94). Compound 91 (55 mg, 0.188 mmol) was dissolved in aq. NH_4OH (28−30% wt 4 mL). Aq. H_2O_2 (30% w/w, 1 mL) was added, and the mixture was stirred for 2 h until LCMS analysis indicated full conversion. The residue was diluted with MeOH, celite was added, and the solvents were removed under reduced pressure. The solid residue was purified by flash column chromatography (automated, 2 → 40% MeOH in CH_2Cl_2 + 0.1% AcOH) to afford 92 (21 mg, 0.063 mmol, 25% yield) as a brown solid. ^1H NMR (300 MHz, DMSO-d_6) δ 3.47 (1H, dt, J = 12.0, 6.2 Hz, H-5′), 3.62 (1H, dt, J = 12.0, 5.3 Hz, H-5″), 3.93 (1H, dd, J = 10.3, 4.7 Hz, H-4′), 4.30 (1H, dd, J = 10.3, 4.7 Hz, H-3′), 4.68 (1H, dd, J = 10.5, 5.3 Hz, H-2′), 4.84 (1H, t, J = 5.9 Hz, OH), 5.08 (1H, d, J = 5.6 Hz, OH), 5.44 (1H, d, J = 5.9 Hz, OH), 6.14 (1H, d, J = 4.7 Hz, H-1′), 7.99 (1H, s, NH_2), 8.07 (1H, br. s., NH_2), 8.19 (1H, br. s., NH_2), 8.24 (1H, s, H-6), 8.86 (1H, br. s., NH_2) ppm. ^{13}C NMR (101 MHz, DMSO-d_6) δ 62.3 (C-5′), 70.8 (C-2′), 73.1 (C-3′), 85.7 (C-4′), 88.9 (C-1′), 99.5 (C-3a), 139.0 (C-3), 155.4 (C-7a), 156.9 (C-6), 158.2 (C-4), 163.8 (C=O) ppm. HRMS (ESI): calcd for $C_{11}H_{15}N_6O_5$ ([M + H]$^+$): 311.1104, found: 311.1110. Spectral data are in accordance with literature values.[66]

3-Trifluoromethyl-4-amino-1-(2′,3′,5′-tri-O-benzoyl)-β-D-ribofuranosylpyrazolo[3,4-d]pyrimidine (95). TMSCF$_3$ (0.315 mL, 2.13 mmol, 3.0 equiv) was added dropwise over the course of 1 h to a suspension of CuI (0.406 g, 2.13 mmol, 3.0 equiv) and KF (0.124 g, 2.13 mmol, 3.0 equiv) in a mixture of dry degassed DMF/NMP 1:1 (3 mL). When all solids had dissolved, 34 (0.500 g, 0.709 mmol, 1.0 equiv) in dry degassed DMF/NMP 1:1 (3 mL) was added, and the mixture was heated to reflux. After 3 h, LC/MS analysis showed full conversion of the starting material, and the reaction was cooled to room temperature. The mixture was diluted with EtOAc (15 mL) and water (5 mL), and the solids were filtered off over Celite. The filter cake was washed extensively with additional EtOAc (3 × 25 mL), and the combined filtrates were transferred to a separation funnel. Additional water (40 mL) was added, the phases were separated, and the organic phase was washed twice more with water (25 mL). The organic layer was dried over Na_2SO_4 and concentrated in vacuo. The residue was used as such in the next reaction. HRMS (ESI): calcd for $C_{32}H_{25}F_3N_5O_7$ ([M + H]$^+$): 648.1706, found: 648.1723.

3-Trifluoromethyl-4-amino-1-β-D-ribofuranosylpyrazolo[3,4-d]-pyrimidine (96). Crude 95 was subjected to general procedure C (reaction time: 1 h). Purification by flash column chromatography (4 → 20% MeOH in CH_2Cl_2), followed by additional purification by preparative RP-HPLC (0.2% formic acid in H_2O/MeCN 98:02 to 33:67 in 12 min) afforded 96 (33 mg, 0.098 mmol, 14% yield over 2 steps) as a white solid. ^1H NMR (300 MHz, DMSO-d_6) δ 3.44 (1H, dt, J = 12.0, 5.6 Hz, H-5′), 3.58 (1H, dt, J = 12.0, 4.7 Hz, H-5″), 3.94 (1H, dd, J = 9.7, 5.0 Hz, H-4′), 4.22 (1H, dd, J = 8.5, 4.1 Hz, H-3′), 4.61 (1H, dd, J = 9.4, 4.7 Hz, H-2′), 4.83 (1H, t, J = 5.6 Hz, OH), 5.23 (1H, d, J = 5.0 Hz, OH), 5.48 (1H, d, J = 5.6 Hz, OH), 6.18

(1H, d, J = 4.7 Hz, H-1′), 8.36 (1H, s, H-6) ppm. ^{13}C NMR (101 MHz, DMSO-d_6) δ 62.1 (C-5′), 70.7 (C-2′), 73.1 (C-3′), 85.7 (C-4′), 88.8 (C-1′), 96.6 (C-3a), 120.7 (q, J = 269.0 Hz, CF$_3$), 132.8 (q, J = 38.5 Hz, C-3), 155.6 (C-7a), 156.7 (C-6), 157.2 (C-4). ^{19}F NMR (282 MHz, DMSO-d_6) δ −59.61 (1F, s) ppm. HRMS (ESI): calcd for $C_{11}H_{13}F_3N_5O_4$ ([M + H]$^+$): 336.0920, found: 336.0917.

5-Amino-3-methyl-1H-pyrazole-4-carbonitrile[98] (97). A solution of malonitrile (1.11 mL, 20.0 mmol, 1.0 equiv) in THF (20 mL) was cooled to 0 °C. NaH (60% wt in mineral oil, 1.60 g, 40.0 mmol, 2.0 equiv) was added slowly, and the mixture was stirred for 10 min. Acetyl chloride (1.43 mL, 20.0 mmol, 1.0 equiv) was added, and the mixture was gradually warmed to room temperature. After 1 h, dimethyl sulfate (2.28 mL, 24.0 mmol, 1.2 equiv) was added and the mixture was heated to reflux. After 3 h, the mixture was cooled down to room temperature, and Et$_3$N (6.97 mL, 50.0 mmol, 2.0 equiv) was added, followed by hydrazine hydrate (1.0 mL, 20.0 mmol, 1.0 equiv). The mixture was again heated at reflux temperature for 1 h and cooled down to room temperature. The mixture was concentrated in vacuo, diluted with H_2O and EtOAc, and transferred to a separation funnel. The phases were separated, and the aqueous phase was extracted twice more with EtOAc. The combined organic phases were dried over Na_2SO_4 and concentrated in vacuo. The residue was taken up in MeCN, celite was added, and the solvent was removed under reduced pressure. The solid residue was purified by flash column chromatography (manual, petroleum ether/EtOAc 1:1 and 3:7) to afford 97 (0.930 g, 7.61 mmol, 38% yield) as a yellow sticky foam. ^1H NMR (300 MHz, DMSO-d_6) δ 2.12 (3H, br. s.), 5.72 (2H, br. s), 11.51 (1H, br. s) ppm. HRMS (ESI): calcd for $C_5H_7N_4$ ([M + H]$^+$): 123.0671, found: 123.0662. Spectral data are in accordance with literature values.[98]

3-Methyl-4-amino-1H-pyrazolo[3,4-d]pyrimidine[99] (98). Compound 97 (0.441 g, 3.61 mmol, 1.0 equiv) was dissolved in formamide (2 mL). The mixture was heated at 180 °C for 24 h and cooled down to room temperature by pouring into ice-cold water (25 mL). The resulting solids were filtered off and dried under a high vacuum overnight to afford 98 (126 mg, 0.84 mmol, 23% yield) as a brown solid. ^1H NMR (300 MHz, DMSO-d_6) δ 2.52 (3H, s, CH$_3$), 7.15 (2H, br. s., NH_2), 8.09 (1H, s, H-6), 12.91 (1H, br. s., NH) ppm. ^{13}C NMR (75 MHz, DMSO-d_6) δ 14.9 (CH$_3$), 98.8 (C-3a), 141.3 (C-3), 156.1 (C-7a), 156.3 (C-6), 158.8 (C-4) ppm. HRMS (ESI): calcd for $C_6H_8N_5$ ([M + H]$^+$): 150.0780, found: 150.0768. Spectral data are in accordance with literature values.[99]

3,6-Dimethyl-4-amino-1H-pyrazolo[3,4-d]pyrimidine (99). Compound 97 (0.206 g, 1.69 mmol, 1.0 equiv) was dissolved in 2-methoxy-ethanol (3 mL). Thioacetamide (0.253 g, 3.37 mmol, 2.0 equiv) was added, and the mixture was heated at reflux overnight. The mixture was cooled down to room temperature, and the solvent was removed in vacuo. The residue was taken up in MeOH, adsorbed onto celite, and purified by flash column chromatography (manual, 10% MeOH in CH_2Cl_2) to afford 99 (100 mg, 0.61 mmol, 36% yield) as a light-purple solid. ^1H NMR (300 MHz, DMSO-d_6) δ 2.06 (3H, s, CH$_3$), 2.36 (3H, s, CH$_3$), 7.14 (2H, br. s, NH_2), 12.80 (1H, br. s, NH) ppm. ^{13}C NMR (75 MHz, DMSO-d_6) δ 14.6 (CH$_3$) 21.8 (CH$_3$), 97.0 (C-3a), 141.1 (C-3), 157.3 (C-7a), 158.5 (C-4), 164.9 (C-6) ppm. HRMS (ESI): calcd for $C_7H_{10}N_5$ ([M + H]$^+$): 164.0936, found: 164.0914.

3-Methyl-4-amino-1-(2′,3′,5′-tri-O-benzoyl-1-β-D-ribofuranosyl)-pyrazolo[3,4-d]pyrimidine (100). Compound 98 (0.100 g, 0.67 mmol) and 1-O-acetyl-2,3,5-tri-O-benzoyl-β-D-ribofuranose (0.406 g, 0.8 mmol, 1.2 equiv) were subjected to general procedure B. Purification by flash column chromatography (automated, 0 → 5% MeOH in CH_2Cl_2) afforded 100, which was used as such in the next reaction. HRMS (ESI): calcd for $C_{32}H_{28}N_5O_7$ ([M + H]$^+$): 594.1989, found: 594.2010.

3-Methyl-4-amino-1-β-D-ribofuranosyl-pyrazolo[3,4-d]-pyrimidine (101). Compound 98 (used directly from the previous reaction) was subjected to general procedure C (reaction time: 1 h). Purification by flash column chromatography (automated, 4 → 20% MeOH in CH_2Cl_2) afforded 101 (40 mg, 0.142 mmol, 21% yield over 2 steps) as a white solid. ^1H NMR (300 MHz, DMSO-d_6) δ 2.53 (3H,

s, CH$_3$), 3.42 (1H, dt, J = 11.9, 6.1 Hz, H-5′), 3.56 (1H, dt, J = 11.4, 4.7 Hz, H-5″), 3.87 (1H, dd, J = 9.7, 4.7 Hz, H-4′), 4.17 (1H, dd, J = 10.0, 5.0 Hz, H-3′), 4.56 (1H, dd, J = 10.5, 5.3 Hz, H-2′), 4.86 (1H, t, J = 5.9 Hz, OH), 5.10 (1H, d, J = 5.3 Hz, OH), 5.30 (1H, d, J = 5.9 Hz, OH), 6.02 (1H, d, J = 4.7 Hz, H-1′), 7.35 (2H, br. s., NH$_2$), 8.14 (1H, s, H-6) ppm. ^{13}C NMR (75 MHz, DMSO-d_6) δ 14.5 (CH$_3$), 62.4 (C-5′), 70.8 (C-2′), 72.8 (C-3′), 84.9 (C-4′), 88.0 (C-1′), 99.3 (C-3a), 141.9 (C-3), 155.1 (C-7a), 156.0 (C-6), 158.4 (C-4) ppm. HRMS (ESI): calcd for C$_{11}$H$_{16}$N$_5$O$_4$ ([M + H]$^+$): 282.1202, found: 282.1216.

3-Vinyl-4-amino-1-(2′,3′,5′-tri-O-benzoyl-β-D-ribofuranosyl)-pyrazolo[3,4-d]pyrimidine (102). Compound **34** (5.66 g, 8.03 mmol, 1.0 equiv), Pd(OAc)$_2$ (0.090 g, 0.40 mmol, 0.05 equiv), PPh$_3$ (0.316 g, 1.20 mmol, 0.15 equiv), potassium vinyl trifluoroborate (2.92 g, 10.0 mmol, 1.25 equiv), and Cs$_2$CO$_3$ (7.85 g, 24.1 mmol, 3.0 equiv) were dissolved in degassed DMF/H$_2$O 9:1 (20 mL) under argon. The mixture was stirred at 100 °C for 72 h, cooled down to room temperature, and transferred to a separation funnel. Water (50 mL) was added, and the mixture was extracted with CH$_2$Cl$_2$ (3 × 100 mL). The combined organic phases were dried over Na$_2$SO$_4$ and concentrated *in vacuo*. The residue was purified by flash column chromatography (automated, 40 → 100% EtOAc in petroleum ether) to afford **102** (1.85 g, 3.05 mmol, 38% yield) as a colorless oil. ^{1}H NMR (300 MHz, CDCl$_3$) δ 4.64 (1H, dd, J = 11.7, 4.7 Hz, H-5′), 4.73−4.89 (2H, m, H-5″, H-4′), 5.66 (1H, dd, J = 11.1, 1.2 Hz, HC=CH$_2$), 5.98 (1H, dd, J = 17.7, 1.2 Hz, HC=CH$_2$), 6.10 (2H, br. s, NH$_2$), 6.34 (1H, t, J = 5.7 Hz, H-3′), 6.44 (1H, dd, J = 5.3, 3.2 Hz, H-2′), 6.87 (1H, d, J = 3.2 Hz, H-1′), 6.87 (1H, dd, J = 17.9, 11.4 Hz, HC=CH$_2$), 7.30−7.45 (6H, m, H$_{Bz}$), 7.48−7.61 (3H, m, H$_{Bz}$), 7.92−8.03 (4H, m, H$_{Bz}$), 8.05−8.14 (2H, m, H$_{Bz}$), 8.35 (1H, s, H-6) ppm. ^{13}C NMR (75 MHz, CDCl$_3$) δ 64.0 (C-5′), 72.0 (C-2′), 74.5 (C-3′), 80.0 (C-4′), 86.7 (C-1′), 98.9 (C-3a), 121.8 (HC=CH$_2$), 128.2 (HC=CH$_2$), 128.3 (C$_{Bz}$), 128.4 (C$_{Bz}$), 128.4 (C$_{Bz}$), 128.8 (C$_{Bz}$), 128.9 (C$_{Bz}$), 129.6 (C$_{Bz}$), 129.8 (C$_{Bz}$), 129.8 (C$_{Bz}$), 133.0 (C$_{Bz}$), 133.5 (C$_{Bz}$), 133.6 (C$_{Bz}$), 144.3 (C-3), 155.4 (C-7a), 155.4 (C-6), 157.5 (C-4), 165.1 (C=O), 165.3 (C=O), 166.2 (C=O) ppm. HRMS (ESI): calcd for C$_{33}$H$_{28}$N$_5$O$_7$ ([M + H]$^+$): 606.1989, found: 606.1978.

4-Amino-1-(2′,3′,5′-tri-O-benzoyl-β-D-ribofuranosyl)pyrazolo-[3,4-d]pyrimidine-3-carbaldehyde (103). Compound **102** (1.53 g, 2.52 mmol, 1.0 equiv) and K$_2$OsO$_4$·2H$_2$O (0.019 g, 0.05 mmol, 0.02 equiv) were dissolved in a mixture of dioxane (18.9 mL, 7.5 mL/mmol) and water (6.3 mL, 2.5 mL/mmol). 2.6-Lutidine (0.584 mL, 5.04 mmol, 2.0 equiv) and NaIO$_4$ (2.16 g, 10.1 mmol, 4.0 equiv) were added, and the mixture was stirred for 3 h until TLC analysis (petroleum ether/EtOAc 50:50) indicated full conversion. Aq. sat. Na$_2$SO$_3$ (25 mL) was added, and the mixture was stirred for 1 more hour before it was transferred to a separation funnel. The mixture was extracted with CH$_2$Cl$_2$ (3 × 60 mL). The combined organic fractions were dried over Na$_2$SO$_4$ and concentrated *in vacuo*. The residue was purified by flash column chromatography (automated, 15 → 70% EtOAc in petroleum ether) to afford 103 (0.731 g, 1.20 mmol, 48% yield) as a white solid. ^{1}H NMR (300 MHz, CDCl$_3$) δ 4.62 (1H, dd, J = 13.2, 5.3 Hz, H-5′), 4.85−4.94 (2H, m, H-5″, H-4′), 6.32 (1H, t, J = 5.6 Hz, H-3′), 6.49 (1H, dd, J = 5.4, 3.7 Hz, H-2′), 6.58 (1H, br. s, NH$_2$), 6.91 (1H, d, J = 3.5 Hz, H-1′), 7.34−7.47 (6H, m, H$_{Bz}$), 7.52−7.63 (3H, m, H$_{Bz}$), 7.90 (1H, br. s, NH$_2$), 7.94−8.05 (4H, m, H$_{Bz}$), 8.05−8.16 (2H, m, H$_{Bz}$), 8.40 (1H, s, H-6), 9.70 (1H, s, CHO) ppm. ^{13}C NMR (75 MHz, CDCl$_3$) δ 63.3 (C-5′), 71.8 (C-2′), 74.3 (C-3′), 80.8 (C-4′), 87.3 (C-1′), 99.4 (C-3a), 128.4 (C$_{Phe}$), 128.5 (C$_{Phe}$) (C$_{Phe}$), 129.6 (C$_{Phe}$), 129.8 (C$_{Phe}$), 129.8 (C$_{Phe}$), 133.3 (C$_{Phe}$), 133.7 (C$_{Phe}$), 133.8 (C$_{Phe}$), 144.9 (C-3), 156.1 (C-7a), 156.7 (C-6), 157.5 (C-4), 165.1 (C=O), 165.3 (C=O), 166.0 (C=O), 187.9 (CHO) ppm. HRMS (ESI): calcd for C$_{32}$H$_{26}$N$_5$O$_8$ ([M + H]$^+$): 608.1781, found: 608.1792.

3-(Morpholinomethyl)-4-amino-1-(2′,3′,5′-tri-O-benzoyl-β-D-ribofuranosyl)pyrazolo[3,4-d]pyrimidine (104). Compound **103** (0.125 g, 0.206 mmol, 1.0 equiv) was dissolved in a mixture of MeOH (2 mL) and THF (1 mL). Morpholine (0.089 mL, 1.03 mmol, 5.0 equiv) and AcOH (0.236 mL, 4.12 mmol, 20.0 equiv) were added,

followed by NaBH$_3$CN (0.039 g, 0.62 mmol, 3.0 equiv). After 2 h, LCMS analysis indicated completion of the reaction. The reaction mixture was diluted with water (15 mL) and extracted with EtOAc (3 × 25 mL). The combined organic phases were dried over Na$_2$SO$_4$, concentrated *in vacuo*, and used crude in the next reaction. HRMS (ESI): calcd for C$_{36}$H$_{35}$N$_6$O$_8$ ([M + H]$^+$): 679.2516, found: 679.2631.

3-(Morpholinomethyl)-4-amino-1-(β-D-ribofuranosyl)pyrazolo-[3,4-d]pyrimidine (105). Compound **104** (crude) was subjected to general procedure C (reaction time: 90 min). Purification by flash column chromatography (automated, 4 → 20% MeOH in CH$_2$Cl$_2$) afforded **105** (48 mg, 0.131 mmol, 64% yield over 2 steps) as a white solid. ^{1}H NMR (300 MHz, DMSO-d_6) δ 2.38−2.58 (4H, m, 2 × CH$_2$ morpholine, under DMSO peak), 3.42 (1H, dt, J = 10.5, 5.0 Hz, H-5′), 3.49−3.69 (5H, m, H-5″, 2 × CH$_2$ morpholine), 3.75 (1H, d, J = 14.4 Hz, CH$_2$N), 3.80 (1H, d, J = 14.4 Hz, CH$_2$N), 3.88 (1H, dd, J = 9.4, 4.7 Hz, H-4′), 4.18 (1H, dd, J = 8.2, 4.4 Hz, H-3′), 4.58 (1H, dd, J = 9.7, 3.8 Hz, H-2′), 4.87 (1H, t, J = 6.2 Hz, OH), 5.10 (1H, d, J = 3.5 Hz, OH), 5.31 (1H, d, J = 4.1 Hz, OH), 6.02 (1H, d, J = 5.0 Hz, H-1′), 7.79 (1H, br. s., NH$_2$), 8.17 (1H, s, H-6), 8.55 (1H, br. s., NH$_2$) ppm. ^{13}C NMR (75 MHz, DMSO-d_6) δ 52.9 (2 × CH$_2$ morpholine), 56.1 (CH$_2$N), 62.4 (C-5′), 66.0 (2 × CH$_2$ morpholine), 70.8 (C-2′), 72.8 (C-3′), 85.1 (C-4′), 88.4 (C-1′), 99.4 (C-3a), 143.5 (C-3), 155.2 (C-7a), 156.2 (C-6), 158.6 (C-4) ppm. HRMS (ESI): calcd for C$_{15}$H$_{23}$N$_6$O$_5$ ([M + H]$^+$): 367.1730, found: 367.1727.

3-Difluoromethyl-4-amino-1-(2′,3′,5′-tri-O-benzoyl-β-D-ribofuranosyl)pyrazolo[3,4-d]pyrimidine (106). Compound **103** (0.143 g, 0.235 mmol, 1.0 equiv) was dissolved in CH$_2$Cl$_2$ (5 mL). DAST (0.155 mL, 1.18 mmol, 5.0 equiv) was added, and the mixture was stirred overnight at room temperature. The reaction was quenched *via* the slow addition of aq. sat. NaHCO$_3$ (20 mL) and extracted with CH$_2$Cl$_2$ (3 × 25 mL). The combined organic phases were dried over Na$_2$SO$_4$ and concentrated *in vacuo*. The residue was taken up in CH$_2$Cl$_2$, adsorbed onto celite, and purified *via* flash column chromatography (5 → 65% EtOAc in petroleum ether). The obtained product was used directly in the next reaction. HRMS (ESI): calcd for C$_{32}$H$_{26}$F$_2$N$_5$O$_7$ ([M + H]$^+$): 630.1800, found: 630.1808.

3-Difluoromethyl-4-amino-1-(β-D-ribofuranosyl)pyrazolo[3,4-d]-pyrimidine (107). Compound **106** (used directly from the previous reaction) was subjected to general procedure C (reaction time: 30 min). Purification *via* flash column chromatography (4 → 20% MeOH in CH$_2$Cl$_2$) afforded **107** (43 mg, 0.136 mmol, 58% yield over 2 steps) as a white solid. ^{1}H NMR (300 MHz, DMSO-d_6) δ 3.44 (1H, dt, J = 11.8, 6.0 Hz, H-5′), 3.57 (1H, dt, J = 11.7, 5.0 Hz, H-5″), 3.93 (1H, dd, J = 10.0, 4.7 Hz, H-2′), 4.20 (1H, dd, J = 10.0, 5.0 Hz, H-3′), 4.61 (1H, dd, J = 10.5, 5.3 Hz, H-2′), 4.84 (1H, t, J = 5.7 Hz, OH), 5.19 (1H, d, J = 5.3 Hz, OH), 5.43 (1H, d, J = 5.9 Hz, OH), 6.14 (1H, d, J = 4.7 Hz, H-1′), 6.72 (1H, br. s), 7.42 (1H, t, J = 53.3 Hz), 7.94 (1H, br. s), 8.32 (1H, s) ppm. ^{13}C NMR (75 MHz, DMSO-d_6) δ 62.6 (C-5′), 71.2 (C-2′), 73.4 (C-3′), 85.9 (C-4′), 89.0 (C-1′) 97.4 (C-3a), 111.5 (t, J = 232.6 Hz, CF$_2$H), 138.5 (t, J = 28.8 Hz, C-3), 155.8 (C-7a), 157.2 (C-6), 157.6 (C-4) ppm. ^{19}F NMR (282 MHz, DMSO-d_6) δ −110.91 (2F, d, J = 52.9 Hz) ppm. HRMS (ESI): calcd for C$_{11}$H$_{14}$F$_2$N$_5$O$_4$ ([M + H]$^+$): 318.1014, found: 318.1019.

4-Amino-1-(2′,3′,5′-tri-O-benzoyl-β-D-ribofuranosyl)pyrazolo-[3,4-d]pyrimidine-3-carboxylic Acid (108). Compound **103** (0.588 g, 0.968 mmol, 1.0 eq) and NaH$_2$PO$_4$ (0.035 g, 0.291 mmol, 0.3 equiv) were dissolved in a mixture of THF (9 mL) and H$_2$O (1.5 mL). Aq. H$_2$O$_2$ (30% w/w, 0.110 mL, 0.968 mmol, 1.0 equiv) was added, followed by dropwise addition of a solution of NaClO$_2$ (0.123 g, 1.36 mmol, 1.4 equiv) in H$_2$O (1.5 mL). The reaction mixture was stirred overnight, diluted with 0.5 M HCl (20 mL), and extracted with EtOAc (3 × 50 mL). The combined organic phases were dried over Na$_2$SO$_4$ and concentrated *in vacuo*. The residue was taken up in CH$_2$Cl$_2$ and adsorbed onto celite. The solid residue was purified by flash column chromatography (0 → 10% MeOH in CH$_2$Cl$_2$ + 0.1% HOAc) to afford **108** (0.570 g, 0.914 mmol, 94%) as a colorless oil. ^{1}H NMR (300 MHz, CDCl$_3$) δ 4.72 (1H, dd, J = 13.2, 6.4 Hz, H-5′), 4.82−4.94 (2H, m, H-5″, H-4′), 6.32 (1H, t, J = 5.6 Hz, H-3′), 6.58 (1H, dd, J = 5.3, 4.1 Hz, H-2′), 6.83 (1H, d, J = 3.8 Hz, H-1′), 7.31−

7.70 (9H, m, H$_{Bz}$), 7.89–8.13 (6H, m, H$_{Bz}$), 8.18 (1H, s, H-6), 11.50 (2H, br. s, NH$_2$), 12.60 (1H, br. s, COOH) ppm. ^{13}C NMR (75 MHz, CDCl$_3$) δ 63.8 (C-5′), 71.8 (C-2′), 74.1 (C-3′), 80.7 (C-4′), 89.1 (C-1′), 101.0 (C-3a), 128.4 (C$_{Bz}$), 128.5 (C$_{Bz}$), 128.6 (C$_{Bz}$), 128.8 (C$_{Bz}$), 129.5 (C$_{Bz}$), 129.8 (C$_{Bz}$), 129.9 (C$_{Bz}$), 132.0 (C$_{Bz}$), 132.2 (C$_{Bz}$), 133.2 (C$_{Bz}$), 133.6 (C$_{Bz}$), 133.7 (C$_{Bz}$), 147.0 (C-3), 152.5 (C-7a), 154.1 (C-6), 155.7 (C-4), 165.0 (COOH), 165.1 (C=O), 166.1 (C=O) ppm. HRMS (ESI): calcd for C$_{32}$H$_{26}$N$_5$O$_9$ ([M + H]$^+$): 624.1731, found: 624.1745.

3-Methylamido-4-amino-1-(β-D-ribofuranosyl)pyrazolo[3,4-d]-pyrimidine (113). Compound **108** (0.125 g, 0.20 mmol) was subjected to general procedure F, with methylamine (40% wt in H$_2$O) as the coupling partner. The obtained residue was subjected to general procedure C (reaction time: 1 h). Purification *via* flash column chromatography (automated, 4 → 20% MeOH in CH$_2$Cl$_2$) afforded **113** (0.019 g, 0.059 mmol, 29% yield over 2 steps) as a white solid. ^{1}H NMR (300 MHz, DMSO-d_6) δ 2.85 (3H, s, CH$_3$) 3.35–3.50 (1H, m, H-5′, partially underwater peak), 3.63 (1H, dd, J = 12.0, 4.7 Hz, H-5′), 3.93 (2H, dd, J = 10.3, 4.7 Hz, H-4′), 4.30 (1H, t, J = 4.7 Hz, H-3′), 4.67 (2H, t, J = 4.7 Hz, H-2′), 6.13 (1H, d, J = 4.7 Hz, H-1′), 8.24 (1H, s, H-6) ppm. ^{13}C NMR (75 MHz, DMSO-d_6) δ 26.0 (CH$_3$), 62.4 (C-5′), 70.8 (C-2′), 73.1 (C-3′), 85.7 (C-4′), 89.0 (C-1′), 99.3 (C-3a), 139.0 (C-3), 155.4 (C-7a), 157.0 (C-6), 158.1 (C-4), 162.1 (C=O) ppm. HRMS (ESI): calcd for C$_{12}$H$_{17}$N$_6$O$_5$ ([M + H]$^+$): 325.1260, found: 325.1265.

3-Pyrrolidinamido-4-amino-1-(β-D-ribofuranosyl)pyrazolo[3,4-d]pyrimidine (114). Compound **108** (0.080 g, 0.128 mmol) was subjected to general procedure F, with pyrrolidine as the coupling partner. The obtained residue was subjected to general procedure C (reaction time: 1 h). Purification *via* flash column chromatography (automated, 1 → 15% MeOH in CH$_2$Cl$_2$) afforded **114** (0.006 g, 0.016 mmol, 28% yield over 2 steps) as a white solid. ^{1}H NMR (300 MHz, CD$_3$OD) δ 1.90–2.12 (4H, m, 2 × CH$_2$ $_{pyrrolidine}$), 3.60–3.74 (3H, m, H-5′, CH$_2$ $_{pyrrolidine}$), 3.78 (1H, dd, J = 12.3, 3.2 Hz, H-5″), 4.05–4.21 (3H, m, H-4′, CH$_2$ $_{pyrrolidine}$), 4.50 (1H, t, J = 5.1 Hz, H-3′), 4.75 (1H, t, J = 4.7 Hz, H-2′) 6.34 (1H, d, J = 3.8 Hz, H-1′), 8.20 (1H, s, H-6) ppm. A qualitative ^{13}C NMR spectrum could not be obtained from the amount of product available. HRMS (ESI): calcd for C$_{15}$H$_{21}$N$_6$O$_5$ ([M + H]$^+$): 365.1573, found: 365.1567.

3-Anilinamido-4-amino-1-β-D-ribofuranosylpyrazolo[3,4-d]-pyrimidine (115). Compound **108** (0.125 g, 0.20 mmol) was subjected to general procedure F, with aniline as the coupling partner. The obtained residue was subjected to general procedure C (reaction time: 1 h). Purification *via* flash column chromatography (automated, 1 → 15% MeOH in CH$_2$Cl$_2$) afforded **115** (0.047 g, 0.122 mmol, 61% yield over 2 steps) as a white solid. ^{1}H NMR (300 MHz, DMSO-d_6) δ 3.52 (1H, dt, J = 11.6, 6.0 Hz, H-5′), 3.68 (1H, dt, J = 11.7, 5.0 Hz, H-5″), 3.97 (1H, dd, J = 8.8, 4.4 Hz, H-4′), 4.33 (1H, dd, J = 9.1, 4.7 Hz, H-3′), 4.75–5.00 (2H, m, H-2′, OH), 5.15 (1H, d, J = 5.6 Hz, OH), 5.46 (1H, d, J = 5.9 Hz, OH), 6.19 (1H, d, J = 5.0 Hz, H-1′), 7.20 (1H, t, J = 7.3 Hz, H-4$_{aniline}$), 7.41 (2H, t, J = 7.8 Hz, H-2$_{aniline}$, H-6$_{aniline}$), 7.78 (2H, d, J = 7.9 Hz, H-3$_{aniline}$, H-5$_{aniline}$), 8.20 (1H, br. s., NH$_2$′), 8.29 (1H, s, H-6), 8.54 (1H, br. s., NH$_2$), 10.45 (1H, s, NH) ppm. ^{13}C NMR (75 MHz, DMSO-d_6) δ 62.1 (C-5′), 70.7 (C-2′), 72.8 (C-3′), 85.9 (C-4′), 89.4 (C-1′), 99.7 (C-3a), 121.7 (C-2$_{aniline}$, C-6$_{aniline}$), 124.8 (C-4$_{aniline}$), 128.7 (C-3$_{aniline}$, C-5$_{aniline}$), 137.4 (C-1aniline), 138.7 (C-3), 155.5 (C-7a), 157.0 (C-6), 158.1 (C-4), 160.4 (C=O) ppm. HRMS (ESI): calcd for C$_{17}$H$_{19}$N$_6$O$_5$ ([M + H]$^+$): 387.1417, found: 387.1422.

3-Benzylamido-4-amino-1-β-D-ribofuranosylpyrazolo[3,4-d]-pyrimidine (116). Compound **108** (0.125 g, 0.20 mmol) was subjected to general procedure F, with benzylamine as the coupling partner. The obtained residue was subjected to general procedure C (reaction time: 1 h). Purification *via* flash column chromatography (automated, 1 → 15% MeOH in CH$_2$Cl$_2$) afforded **116** (0.035 g, 0.087 mmol, 44% yield over 2 steps) as a white solid. ^{1}H NMR (300 MHz, DMSO-d_6) δ 3.48 (1H, dt, J = 12.3, 6.2 Hz, H-5′), 3.63 (1H, dt, J = 12.0, 5.3 Hz, H-5″), 3.94 (1H, dd, J = 9.7, 4.7 Hz, H-4′), 4.32 (1H, dd, J = 10.3, 5.0 Hz, H-3′), 4.46–4.63 (2H, m, CH$_2$ $_{benzyl}$), 4.72 (1H, dd, J = 10.3, 5.0 Hz, H-2′), 4.85 (1H, t, J = 6.2 Hz, OH), 5.10

(1H, d, J = 5.9 Hz, OH), 5.47 (1H, d, J = 5.9 Hz, OH), 6.16 (1H, d, J = 5.0 Hz, H-1′), 7.19–7.38 (5H, m, H$_{Phe}$), 8.11 (1H, d, J = 3.2 Hz, NH$_2$), 8.26 (1H, s, H-6), 8.80 (1H, d, J = 3.2 Hz, NH$_2$′), 9.38 (1H, t, J = 6.2 Hz, NH) ppm. ^{13}C NMR (75 MHz, DMSO-d_6) δ 42.3 (CH$_2$ $_{benzyl}$), 62.3 (C-5′), 70.7 (C-2′), 73.0 (C-3′), 85.7 (C-4′), 89.0 (C-1′), 99.4 (C-3a), 126.9 (C-4$_{Phe}$), 127.3 (C-2$_{Phe}$, C-6$_{Phe}$), 128.4 (C-3$_{Phe}$, C-5$_{Phe}$), 138.7 (C-1$_{Phe}$), 139.1 (C-3), 155.4 (C-7a), 156.9 (C-6), 158.1 (C-4), 161.7 (C=O) ppm. HRMS (ESI): calcd for C$_{17}$H$_{19}$N$_6$O$_5$ ([M + H]$^+$): 401.1573, found: 401.1571.

Biological Evaluation. All animal experiments were conducted in compliance with institutional guidelines.

Drug Sensitivity Assays. Compound stock solutions were prepared at 20 mM in 100% dimethyl sulfoxide (DMSO). The compounds were serially prediluted (2-fold or 4-fold) in DMSO followed by a further (intermediate) dilution in demineralized water to assure a final in-test DMSO concentration of <1%. Compounds were assayed in 10 concentrations of a 4-fold compound dilution series starting at 64 μM.

L. infantum. L. infantum [MHOM/MA(BE)/67] was used. This strain was maintained in golden hamsters (*Mesocricetus auratus*) obtained from Janvier (Le Genest Saint Isle, France) following approval by the Ethical Committee of the University of Antwerp (ECD2019–10). Amastigotes were collected from the spleens of infected donor hamsters as described elsewhere,[100] and spleen parasite burdens were assessed using the Stauber technique. Primary peritoneal mouse macrophages (PMMs) were used as host cells and obtained from Swiss mice (Janvier; ethical approval ECD2019–10) after a 2-day peritoneal stimulation with a 2% potato starch suspension. All cultures and assays were conducted at 37 °C under an atmosphere of 5% CO$_2$. Assays were performed in 96-well microtiter plates, each well containing 10 μL of the compound dilutions together with 190 μL of macrophage/parasite inoculum (3 × 10^4 cells + 4.5 × 10^5 parasites/well). The inoculum was prepared in RPMI-1640 medium, supplemented with 200 mM L-glutamine, 16.5 mM NaHCO$_3$, and 5% inactivated fetal calf serum. The macrophages were infected after 48 h. The compounds were added after 2 h of infection. Parasite multiplication was compared to untreated-infected controls (100% growth) and uninfected controls (0% growth). After 5 days incubation, parasite burdens (mean number of amastigotes/macrophage) were microscopically assessed after staining with a 10% Giemsa solution. The results were expressed as % reduction in parasite burden compared to untreated control wells, and an IC$_{50}$ value was calculated.

PMM Cytotoxicity. PMM toxicity was assessed during the *in vitro Leishmania* susceptibility assays *via* microscopic evaluation of cell detachment, lysis, and granulation. Evaluation was done by semi-quantitative scoring (no exact counting was performed) of at least 500 cells distributed over adjacent microscopic fields. The results were expressed as % reduction in normal cells compared to untreated control wells, and a CC$_{50}$ value was determined.

T. cruzi. The β-galactosidase expressing *T. cruzi* Tulahuen CL2 strain (nifurtimox-sensitive) was used. This strain was maintained in MRC-5$_{SV2}$ (human lung fibroblast) cells in MEM medium, supplemented with 200 mM L-glutamine, 16.5 mM NaHCO$_3$, and 5% inactivated fetal calf serum. All cultures and assays were conducted at 37 °C under an atmosphere of 5% CO$_2$.

Assays were performed in sterile 96-well microtiter plates, each well containing 10 μL of the watery compound dilutions together with 190 μL of MRC-5$_{SV2}$ cell/parasite inoculum (4 × 10^3 cells/well + 4 × 10^4 parasites/well). For some assays, PMMs were used as *T. cruzi* host cells. For this purpose, 3 × 10^4 cells were plated per well and infected two days later with 1.5 × 10^4 parasites. To explore the involvement of ABC transporters, compound exposure was also combined with established inhibitors verapamil (8 μM), probenecid (700 μM), or cyclosporine A (2 μM). *T. cruzi* growth was compared to untreated-infected controls (100% growth) and noninfected controls (0% growth) after 7 days incubation at 37 °C and 5% CO$_2$. Parasite burdens were assessed after adding the substrate CPRG (chlorophenolred ß-D-galactopyranoside): 50 μL/well of a stock solution containing 15.2 mg of CPRG + 250 μL of Nonidet in 100 mL of PBS.

The change in color was measured spectrophotometrically at 540 nm after 4 h incubation at 37 °C. The results were expressed as % reduction in parasite burdens compared to control wells, and an IC_{50} value was calculated.

MRC-5$_{SV2}$ Cytotoxicity. MRC-5$_{SV2}$ cells were cultured in MEM + Earl's salts-medium, supplemented with L-glutamine, NaHCO$_3$, and 5% inactivated fetal calf serum. All cultures and assays were conducted at 37 °C under an atmosphere of 5% CO$_2$. Assays were performed in sterile 96-well microtiter plates, each well containing 10 μL of the watery compound dilutions together with 190 μL of MRC-5$_{SV2}$ inoculum (1.5 × 10^5 cells/mL). Cell growth was compared to untreated control wells (100% cell growth) and medium-control wells (0% cell growth). After 3 days incubation, cell viability was assessed fluorimetrically after addition of 50 μL of resazurin per well. After 4 h at 37 °C, fluorescence was measured (λ_{ex} 550 nm, λ_{em} 590 nm). The results were expressed as % reduction in cell growth/viability compared to control wells, and an IC_{50} value was determined.

Metabolic Stability. Male mouse and pooled human liver microsomes were purchased from a commercial source (Corning) and stored at −80 °C. NADPH generating system solutions A and B and UGT reaction mix solutions A and B (Corning) were kept at −20 °C. The test compound and the reference compound diclofenac were formulated in DMSO at 10 mM. The microsomal stability assay was carried out based on the BD Biosciences Guidelines for Use (TF000017 Rev1.0) with minor adaptations. The metabolic stability of the compounds was studied through the CYP450 superfamily (Phase-I metabolism) by fortification with reduced nicotinamide adenine dinucleotide phosphate (NADPH) and through uridine glucuronosyl-transferase (UGT) enzymes (Phase-II metabolism) by fortification with uridine diphosphate glucuronic acid (UDPGA). For the CYP450 and other NADPH-dependent enzymes, both compounds were incubated at 5 μM together with 0.5 mg/mL liver microsomes in potassium phosphate buffer in a reaction started by the addition of 1 mM NADPH and stopped at the above-listed sampling times. At these time points, 20 μL was withdrawn from the reaction mixture and 80 μL of cold acetonitrile (ACN), containing the internal standard tolbutamide, was added to inactivate the enzymes and precipitate the protein. The mixture was vortexed for 30 s and centrifuged at 4 °C for 5 min at 15 000 rpm. The supernatant was stored at −80 °C until analysis. For the UGT enzymes, both compounds were incubated at 5 μM together with 0.5 mg/mL liver microsomes in a reaction started by the addition of 2 mM UDPGA cofactor. The corresponding loss of the parent compound was determined using liquid chromatography (UPLC) (Waters Aquity) coupled with tandem quadrupole mass spectrometry (MS^2) (Waters Xevo), equipped with an electrospray ionization (ESI) interface and operated in the multiple reaction monitoring (MRM) mode. The optimal MS parameters and control of the chromatographic separation conditions were tuned in a preceding experiment.

T. cruzi Y-Strain Bloodstream Trypomastigote Activity. Bloodstream trypomastigotes of the Y strain were obtained by cardiac puncture of infected Swiss Webster mice on the parasitaemia peak, and drug sensitivity assays were performed as described.[53]

T. cruzi Y-Strain Intracellular Amastigote Activity. After 24 h of plating, 2D cardiac cell cultures were infected for 24 h at 37 °C with bloodstream trypomastigotes of *T. cruzi* (Y strain) employing a parasite/host cell ratio of 10:1. Then, the cultures were washed to remove free parasites and treated for 48 h at 37 °C with a serial dilution of the compound in culture medium. After drug exposure, the cultures were rinsed using phosphate-buffered saline, fixed, and stained with Giemsa as described previously.[78,101] The mean numbers of infected host cells and of parasites per infected cell were scored in 200 host cells in two independent experiments each run in duplicate. Only characteristic parasite nuclei and kinetoplasts were considered as surviving parasites since irregular structures could represent parasites undergoing cell death. The compound activity was estimated by calculating the inhibition levels of the inhibition index (II, percentage of infected cells vs the mean number of parasites per infected cell).

Cytotoxicity on Cardiac Cells. Cardiac 2D and 3D cell cultures were obtained from the heart of Swiss Webster mice embryos, as reported.[102] To prepare the three-dimensional cultures, isolated cardiac cells were seeded in 96-well U plates (25 × 10^3 cell/well), previously coated with 1% agarose. Both cardiac cultures were sustained in Dulbecco's modified Eagle's medium (DMEM; without phenol red; Sigma-Aldrich) supplemented with 5% fetal bovine serum, 2.5 mM CaCl$_2$, 1 mM L-glutamine, streptomycin, and 2% chicken embryo extract, at 37 °C. Noninfected cultures were incubated for 48 h at 37 °C with crescent concentrations of **44** diluted in supplemented DMEM medium. Morphology was evaluated by light microscopy, and cellular viability was determined using PrestoBlue.[53] The results are expressed as the difference in reduction between treated and nontreated cultures adopting the manufacturer's instructions. The CC$_{50}$ (minimum concentration that reduces 50% of the cellular viability) was then determined.[102]

In Vivo Evaluation. Compounds. Bz (2-nitroimidazole; Laboratório Farmacêutico do Estado de Pernambuco [LAFEPE], Brazil) was used as a reference drug and was formulated using 3% Tween 80 in distilled water. The nucleoside analogue **44** was diluted using 10% Tween 80 in sterile water.

Mouse Infection and Treatment. Male Swiss Webster mice (18−20 g; 4−5 weeks of age) were obtained from the animal facilities of ICTB (Institute of Science and Biomodels Technology/Fiocruz/RJ/Brazil). Housing of animals was with a maximum of 6 animals per cage, in a specific-pathogen-free (SPF) room at 20−24 °C under a 12 h light and 12 h dark cycle. All animals were provided sterilized water and chow ad libitum. The animals were acclimatized for 7 days before the experiments. On the day of infection (0 dpi), animals were infected by i.p. administration of 10^4 bloodstream trypomastigotes (Y strain) originating from an infected donor mouse. Noninfected control mice were age-matched and housed under identical conditions.[53] Each experimental group consisted of six animals: untreated (infected vehicle-treated control) and treated (infected and treated with 44 or with benznidazole). Treatment was initiated at the onset of parasitemia (6 dpi) only using mice with detectable parasitemia. **44** was administered by oral gavage for five consecutive days at 25, 2.5, and 0.25 mg/kg twice daily. Benznidazole treatments at 10 mg/kg and at the optimal dose (100 mg/kg p.o.) were run in parallel. The efficacy of **44** in coadministration with benznidazole was also evaluated (**44** at 2.5 mg/kg b.i.d + benznidazole at 10 mg/kg/day). All treatments followed a 5-day (6th to 10th dpi) dosing regimen, and all compound formulations were freshly prepared before administration. Parasitemia levels in *T. cruzi* assays were individually checked by light microscopic counting of parasites in 5 μL of blood, and mortality rates were checked daily until 34 dpi and expressed as a percentage of cumulative mortality, as described previously.[95]

■ ASSOCIATED CONTENT

ⓈI Supporting Information

The Supporting Information is available free of charge at https://pubs.acs.org/doi/10.1021/acs.jmedchem.1c00135.

> HPLC traces of selected final compounds and copies of ^{1}H and ^{13}C NMR spectra of synthesized compounds (PDF)

> Molecular formula strings (CSV)

■ AUTHOR INFORMATION

Corresponding Authors

Guy Caljon − *Laboratory of Microbiology, Parasitology and Hygiene (LMPH), University of Antwerp, B-2610 Wilrijk, Belgium*; Phone: +32 (0)3 265 26 01; Email: Guy.Caljon@uantwerpen.be

Serge Van Calenbergh − *Laboratory for Medicinal Chemistry (Campus Heymans), Ghent University, B-9000 Gent, Belgium*; ⓘ orcid.org/0000-0002-4201-1264; Phone: +32 (0)9 264 81 24; Email: Serge.VanCalenbergh@UGent.be; Fax: +32 (0)9 264 81 46

Authors

Jakob Bouton − *Laboratory for Medicinal Chemistry (Campus Heymans), Ghent University, B-9000 Gent, Belgium*

Ludmila Ferreira de Almeida Fiuza − *Laboratório de Biologia Celular, Instituto Oswaldo Cruz (FIOCRUZ), Fundação Oswaldo Cruz, 21040-360 Rio de Janeiro, Brazil*

Camila Cardoso Santos − *Laboratório de Biologia Celular, Instituto Oswaldo Cruz (FIOCRUZ), Fundação Oswaldo Cruz, 21040-360 Rio de Janeiro, Brazil*

Maria Angela Mazzarella − *Department of Pharmaceutical Sciences, University of Perugia, Perugia 06100, Italy*

Maria de Nazaré Correia Soeiro − *Laboratório de Biologia Celular, Instituto Oswaldo Cruz (FIOCRUZ), Fundação Oswaldo Cruz, 21040-360 Rio de Janeiro, Brazil*

Louis Maes − *Laboratory of Microbiology, Parasitology and Hygiene (LMPH), University of Antwerp, B-2610 Wilrijk, Belgium*

Izet Karalic − *Laboratory for Medicinal Chemistry (Campus Heymans), Ghent University, B-9000 Gent, Belgium*

Complete contact information is available at:
https://pubs.acs.org/10.1021/acs.jmedchem.1c00135

Notes

The authors declare no competing financial interest.

■ ABBREVIATIONS

APP(R), aminopyrazolo[3,4-*d*]pyrimidine (riboside); Bz, benznidazole; CL, cutaneous leishmaniasis; DTU, discrete typing unit; PMM, primary mouse macrophage; PRTase, phosphoribosyltransferase; *L. infantum*, *Leishmania infantum*; SI, selectivity index; T. cruzi, *Trypanosoma cruzi*; TDA-1, tris[2-(2-methoxyethoxy)ethyl]amine; TPPTS, triphenylphosphine-3,3′,3″-trisulfonic acid trisodium salt; VL, visceral leishmaniasis

■ REFERENCES

(1) Molyneux, D. Neglected Tropical Diseases. *Community Eye Health* **2013**, *26*, 21−24.

(2) Houweling, T. A. J.; Karim-Kos, H. E.; Kulik, M. C.; Stolk, W. A.; Haagsma, J. A.; Lenk, E. J.; Richardus, J. H.; Vlas, S. J. de. Socioeconomic Inequalities in Neglected Tropical Diseases: A Systematic Review. *PLoS Neglected Trop. Dis.* **2016**, *10*, No. e0004546.

(3) Lee, B. Y.; Bacon, K. M.; Bottazzi, M. E.; Hotez, P. J. Global Economic Burden of Chagas Disease: A Computational Simulation Model. *Lancet Infect. Dis.* **2013**, *13*, 342−348.

(4) Lidani, K. C. F.; Andrade, F. A.; Bavia, L.; Damasceno, F. S.; Beltrame, M. H.; Messias-Reason, I. J.; Sandri, T. L. Chagas Disease: From Discovery to a Worldwide Health Problem. *Front. Public Health* **2019**, *7*, 166.

(5) Chatelain, E.; Konar, N. Translational Challenges of Animal Models in Chagas Disease Drug Development: A Review. *Drug Des. Dev. Ther.* **2015**, *9*, 4807−4823.

(6) Pérez-Molina, J. A.; Molina, I. Chagas Disease. *Lancet* **2018**, *391*, 82−94.

(7) Rao, S. P. S.; Barrett, M. P.; Dranoff, G.; Faraday, C. J.; Gimpelewicz, C. R.; Hailu, A.; Jones, C. L.; Kelly, J. M.; Lazdins-Helds, J. K.; Mäser, P.; Mengel, J.; Mottram, J. C.; Mowbray, C. E.; Sacks, D. L.; Scott, P.; Späth, G. F.; Tarleton, R. L.; Spector, J. M.; Diagana, T. T. Drug Discovery for Kinetoplastid Diseases: Future Directions. *ACS Infect. Dis.* **2019**, *5*, 152−157.

(8) Field, M. C.; Horn, D.; Fairlamb, A. H.; Ferguson, M. A. J.; Gray, D. W.; Read, K. D.; De Rycker, M.; Torrie, L. S.; Wyatt, P. G.; Wyllie, S.; Gilbert, I. H. Anti-Trypanosomatid Drug Discovery: An Ongoing Challenge and a Continuing Need. *Nat. Rev. Microbiol.* **2017**, *15*, 217−231.

(9) De Rycker, M.; Baragaña, B.; Duce, S. L.; Gilbert, I. H. Challenges and Recent Progress in Drug Discovery for Tropical Diseases. *Nature* **2018**, *559*, 498−506.

(10) WHO. *Regional Strategic Framework for Elimination of Kala-Azar from the Sout-East Asia Region (2005-2015)*; New Delhi, 2005.

(11) Burza, S.; Croft, S. L.; Boelaert, M. Leishmaniasis. *Lancet* **2018**, *392*, 951−970.

(12) Sundar, S.; Singh, A. Chemotherapeutics of Visceral Leishmaniasis: Present and Future Developments. *Parasitology* **2018**, *145*, 481−489.

(13) Chakravarty, J.; Sundar, S. Current and Emerging Medications for the Treatment of Leishmaniasis. *Expert Opin. Pharmacother.* **2019**, *20*, 1251−1265.

(14) DNDi. 2019 R&D portfolio in review: Leishmaniasis − DNDi. https://www.dndi.org/2020/media-centre/news-views-stories/news/leishmaniasis-rnd-portfolio-update/ (accessed Apr 20, 2020).

(15) Nagle, A.; Biggart, A.; Be, C.; Srinivas, H.; Hein, A.; Caridha, D.; Sciotti, R. J.; Pybus, B.; Kreishman-Deitrick, M.; Bursulaya, B.; Lai, Y. H.; Gao, M.-Y.; Liang, F.; Mathison, C. J. N.; Liu, X.; Yeh, V.; Smith, J.; Lerario, I.; Xie, Y.; Chianelli, D.; Gibney, M.; Berman, A.; Chen, Y.-L.; Jiricek, J.; Davis, L. C.; Liu, X.; Ballard, J.; Khare, S.; Eggimann, F. K.; Luneau, A.; Groessl, T.; Shapiro, M.; Richmond, W.; Johnson, K.; Rudewicz, P. J.; Rao, S. P. S.; Thompson, C.; Tuntland, T.; Spraggon, G.; Glynne, R. J.; Supek, F.; Wiesmann, C.; Molteni, V. Discovery and Characterization of Clinical Candidate LXE408 as a Kinetoplastid-Selective Proteasome Inhibitor for the Treatment of Leishmaniases. *J. Med. Chem.* **2020**, *63*, 10773−10781.

(16) Thomas, M. G.; De Rycker, M.; Ajakane, M.; Albrecht, S.; Álvarez-Pedraglio, A. I.; Boesche, M.; Brand, S.; Campbell, L.; Cantizani-Perez, J.; Cleghorn, L. A. T.; Copley, R. C. B.; Crouch, S. D.; Daugan, A.; Drewes, G.; Ferrer, S.; Ghidelli-Disse, S.; Gonzalez, S.; Gresham, S. L.; Hill, A. P.; Hindley, S. J.; Lowe, R. M.; MacKenzie, C. J.; MacLean, L.; Manthri, S.; Martin, F.; Miguel-Siles, J.; Nguyen, V. L.; Norval, S.; Osuna-Cabello, M.; Woodland, A.; Patterson, S.; Pena, I.; Quesada-Campos, M. T.; Reid, I. H.; Revill, C.; Riley, J.; Ruiz-Gomez, J. R.; Shishikura, Y.; Simeons, F. R. C.; Smith, A.; Smith, V. C.; Spinks, D.; Stojanovski, L.; Thomas, J.; Thompson, S.; Underwood, T.; Gray, D. W.; Fiandor, J. M.; Gilbert, I. H.; Wyatt, P. G.; Read, K. D.; Miles, T. J. Identification of GSK3186899/ DDD853651 as a Preclinical Development Candidate for the Treatment of Visceral Leishmaniasis. *J. Med. Chem.* **2019**, *62*, 1180−1202.

(17) Wyllie, S.; Thomas, M.; Patterson, S.; Crouch, S.; De Rycker, M.; Lowe, R.; Gresham, S.; Urbaniak, M. D.; Otto, T. D.; Stojanovski, L.; Simeons, F. R. C.; Manthri, S.; MacLean, L. M.; Zuccotto, F.; Homeyer, N.; Pflaumer, H.; Boesche, M.; Sastry, L.; Connolly, P.; Albrecht, S.; Berriman, M.; Drewes, G.; Gray, D. W.; Ghidelli-Disse, S.; Dixon, S.; Fiandor, J. M.; Wyatt, P. G.; Ferguson, M. A. J.; Fairlamb, A. H.; Miles, T. J.; Read, K. D.; Gilbert, I. H. Cyclin-Dependent Kinase 12 Is a Drug Target for Visceral Leishmaniasis. *Nature* **2018**, *560*, 192−197.

(18) Khare, S.; Nagle, A. S.; Biggart, A.; Lai, Y. H.; Liang, F.; Davis, L. C.; Barnes, S. W.; Mathison, C. J. N.; Myburgh, E.; Gao, M.-Y.; Gillespie, J. R.; Liu, X.; Tan, J. L.; Stinson, M.; Rivera, I. C.; Ballard, J.; Yeh, V.; Groessl, T.; Federe, G.; Koh, H. X. Y.; Venable, J. D.; Bursulaya, B.; Shapiro, M.; Mishra, P. K.; Spraggon, G.; Brock, A.; Mottram, J. C.; Buckner, F. S.; Rao, S. P. S.; Wen, B. G.; Walker, J. R.; Tuntland, T.; Molteni, V.; Glynne, R. J.; Supek, F. Proteasome Inhibition for Treatment of Leishmaniasis, Chagas Disease and Sleeping Sickness. *Nature* **2016**, *537*, 229−233.

(19) Van den Kerkhof, M.; Mabille, D.; Chatelain, E.; Mowbray, C. E.; Braillard, S.; Hendrickx, S.; Maes, L.; Caljon, G. In Vitro and in Vivo Pharmacodynamics of Three Novel Antileishmanial Lead Series. *Int. J. Parasitol. Drugs Drug Resist.* **2018**, *8*, 81−86.

(20) Katsuno, K.; Burrows, J. N.; Duncan, K.; Van Huijsduijnen, R. H.; Kaneko, T.; Kita, K.; Mowbray, C. E.; Schmatz, D.; Warner, P.; Slingsby, B. T. Hit and Lead Criteria in Drug Discovery for Infectious Diseases of the Developing World. *Nat. Rev. Drug Discovery* **2015**, *14*, 751−758.

(21) Berens, R. L.; Marr, J. J.; LaFon, S. W.; Nelson, D. J. Purine Metabolism in Trypanosoma Cruzi. *Mol. Biochem. Parasitol.* **1981**, *3*, 187−196.

(22) Carter, N. S.; Yates, P.; Arendt, C. S.; Boitz, J. M.; Ullman, B. Purine and Pyrimidine Metabolism in Leishmania. In *Drug Targets in Kinetoplastid Parasites*; Majumder, H. K., Ed.; Springer: New York, NY, 2008; pp 141−154.

(23) Boitz, J. M.; Ullman, B.; Jardim, A.; Carter, N. S. Purine Salvage in Leishmania: Complex or Simple by Design? *Trends Parasitol.* **2012**, *28*, 345−352.

(24) Berg, M.; Van der Veken, P.; Goeminne, A.; Haemers, A.; Augustyns, K. Inhibitors of the Purine Salvage Pathway: A Valuable Approach for Antiprotozoal Chemotherapy? *Curr. Med. Chem.* **2010**, *17*, 2456−2481.

(25) El Kouni, M. H. Potential Chemotherapeutic Targets in the Purine Metabolism of Parasites. *Pharmacol. Ther.* **2003**, *99*, 283−309.

(26) Datta, A. K.; Datta, R.; Sen, B. Antiparasitic Chemotherapy. In *Drug Targets in Kinetoplastid Parasites*; Majumder, H. K., Ed.; Advances In Experimental Medicine and Biology; Springer: New York, NY, 2008; pp 116−132.

(27) Pfaller, M. A.; Marr, J. J. Antileishmanial Effect of Allopurinol. *Antimicrob. Agents Chemother.* **1974**, *5*, 469−472.

(28) Looker, D. L.; Marr, J. J.; Berens, R. L. Mechanisms of Action of Pyrazolopyrimidines in Leishmania Donovani. *J. Biol. Chem.* **1986**, *261*, 9412−9415.

(29) Berens, R. L.; Marr, J. J.; Steele da Cruz, F. S.; Nelson, D. J. Effect of Allopurinol on Trypanosoma Cruzi: Metabolism and Biological Activity in Intracellular and Bloodstream Forms. *Antimicrob. Agents Chemother.* **1982**, *22*, 657−661.

(30) Nelson, D. J.; Bugge, C. J.; Elion, G. B.; Berens, R. L.; Marr, J. J. Metabolism of Pyrazolo(3,4-d)Pyrimidines in Leishmania Braziliensis and Leishmania Donovani. Allopurinol, Oxipurinol, and 4-Aminopyrazolo(3,4-d)Pyrimidine. *J. Biol. Chem.* **1979**, *254*, 3959−3964.

(31) Kager, P. A.; Rees, P. H.; Wellde, B. T.; Hockmeyer, W. T.; Lyerly, W. H. Allopurinol in the Treatment of Visceral Leishmaniasis. *Trans. R. Soc. Trop. Med. Hyg.* **1981**, *75*, 556−559.

(32) Martinez, S.; Marr, J. J. Allopurinol in the Treatment of American Cutaneous Leishmaniasis. *N. Engl. J. Med.* **1992**, *326*, 741−744.

(33) Yaich, S.; Charfeddine, K.; Masmoudi, A.; Masmoudi, M.; Zaghdhane, S.; Turki, H.; Hachicha, J. Atypical Presentation of Cutaneous Leishmaniasis in a Renal Transplant Recipient Successfully Treated with Allopurinol and Fluconazole. *Ann. Saudi Med.* **2013**, *33*, 187−191.

(34) Travi, B. L.; Cordeiro-da-Silva, A.; Dantas-Torres, F.; Miró, G. Canine Visceral Leishmaniasis: Diagnosis and Management of the Reservoir Living among Us. *PLoS Neglected Trop. Dis.* **2018**, *12*, No. e0006082.

(35) Gallerano, R. H.; Marr, J. J.; Sosa, R. R. Therapeutic Efficacy of Allopurinol in Patients with Chronic Chagas' Disease. *Am. J. Trop. Med. Hyg.* **1990**, *43*, 159−166.

(36) Rassi, A.; Luquetti, A. O.; Rassi, A.; Rassi, G. G.; Rassi, S. G.; DA Silva, I. G.; Rassi, A. G. Specific Treatment for Trypanosoma Cruzi: Lack of Efficacy of Allopurinol in the Human Chronic Phase of Chagas Disease. *Am. J. Trop. Med. Hyg.* **2007**, *76*, 58−61.

(37) Apt, W.; Arribada, A.; Zulantay, I.; Solari, A.; Sánchez, G.; Mundaca, K.; Coronado, X.; Rodríguez, J.; Gil, L. C.; Osuna, A. Itraconazole or Allopurinol in the Treatment of Chronic American Trypanosomiasis: The Results of Clinical and Parasitological Examinations 11 Years Post-Treatment. *Ann. Trop. Med. Parasitol.* **2005**, *99*, 733−741.

(38) Almeida, D. R.; Carvalho, A. C.; Branco, J. N.; Pereira, A. P.; Correa, L.; Vianna, P. V.; Buffolo, E.; Martinez, E. E. Chagas' Disease Reactivation after Heart Transplantation: Efficacy of Allopurinol Treatment. *J. Heart Lung Transplant. Off. Publ. Int. Soc. Heart Transplant.* **1996**, *15*, 988−992.

(39) Bestetti, R. B.; Theodoropoulos, T. A. D. A Systematic Review of Studies on Heart Transplantation for Patients with End-Stage Chagas' Heart Disease. *J. Card. Failure* **2009**, *15*, 249−255.

(40) Martinez, S.; Looker, D. L.; Berens, R. L.; Marr, J. J. The Synergistic Action of Pyrazolopyrimidines and Pentavalent Antimony against Leishmania Donovani and L. braziliensis. *Am. J. Trop. Med. Hyg.* **1988**, *39*, 250−255.

(41) Chunge, C. N.; Gacmra, G.; Muigai, R.; Wasunna, K.; Rashid, J. R.; Chulay, J. D.; Anabwani, G.; Oster, C. N.; Bryceson, A. D. M. Visceral Leishmaniasis Unresponsive to Antimonial Drugs III. Successful Treatment Using a Combination of Sodium Stibogluconate plus Allopurinol. *Trans. R. Soc. Trop. Med. Hyg.* **1985**, *79*, 715−718.

(42) Torrus, D.; Boix, V.; Massa, B.; Portilla, J.; Pérez-Mateo, M. Fluconazole plus Allopurinol in Treatment of Visceral Leishmanlasis. *J. Antimicrob. Chemother.* **1996**, *37*, 1042−1043.

(43) Grosso, N. L.; Alarcon, M. L.; Bua, J.; Laucella, S. A.; Riarte, A.; Fichera, L. E. Combined Treatment with Benznidazole and Allopurinol in Mice Infected with a Virulent Trypanosoma Cruzi Isolate from Nicaragua. *Parasitology* **2013**, *140*, 1225−1233.

(44) Perez-Mazliah, D. E.; Alvarez, M. G.; Cooley, G.; Lococo, B. E.; Bertocchi, G.; Petti, M.; Albareda, M. C.; Armenti, A. H.; Tarleton, R. L.; Laucella, S. A.; Viotti, R. Sequential Combined Treatment with Allopurinol and Benznidazole in the Chronic Phase of Trypanosoma Cruzi Infection: A Pilot Study. *J. Antimicrob. Chemother.* **2013**, *68*, 424−437.

(45) Rial, M. S.; Scalise, M. L.; López Alarcón, M.; Esteva, M. I.; Búa, J.; Benatar, A. F.; Prado, N. G.; Riarte, A. R.; Fichera, L. E. Experimental Combination Therapy Using Low Doses of Benznidazole and Allopurinol in Mouse Models of Trypanosoma Cruzi Chronic Infection. *Parasitology* **2019**, *146*, 305−313.

(46) Avila, J. L.; Casanova, M. A. Comparative Effects of 4-Aminopyrazolopyrimidine, Its 2′-Deoxyriboside Derivative, and Allopurinol on in Vitro Growth of American Leishmania Species. *Antimicrob. Agents Chemother.* **1982**, *22*, 380−385.

(47) Berman, J. D.; Lee, L. S.; Robins, R. K.; Revankar, G. R. Activity of Purine Analogs against Leishmania Tropica within Human Macrophages in Vitro. *Antimicrob. Agents Chemother.* **1983**, *24*, 233−236.

(48) Marr, J. Purine Analogs as Chemotherapeutic Agents in Leishmaniasis and American Trypanosomiasis. *J. Lab. Clin. Med.* **1991**, *118*, 111−119.

(49) Avila, J.; Polegre, M. A.; Robins, R. K. Biological Action of Pyrazolopyrimidine Derivatives against Trypanosoma Cruzi. Studies in Vitro and in Vivo. *Comp. Biochem. Physiol., Part C: Comp. Pharmacol.* **1987**, *86*, 49−54.

(50) Avila, J.; Polegre, M. A.; Avila, A.; Robins, R. K. Action of Pyrazolopyrimidine Derivatives on American Leishmania Spp. Promastigotes. *Comp. Biochem. Physiol., Part C: Comp. Pharmacol.* **1986**, *83*, 285−289.

(51) Avila, J.; Avila, A.; Muñoz, E.; Monzón, H. Trypanosoma Cruzi: 4-Aminopyrazolopyrimidine in the Treatment of Experimental Chagas' Disease. *Exp. Parasitol.* **1983**, *56*, 236−240.

(52) Hulpia, F.; Campagnaro, G. D.; Scortichini, M.; Van Hecke, K.; Maes, L.; de Koning, H. P.; Caljon, G.; Van Calenbergh, S. Revisiting Tubercidin against Kinetoplastid Parasites: Aromatic Substitutions at Position 7 Improve Activity and Reduce Toxicity. *Eur. J. Med. Chem.* **2019**, *164*, 689−705.

(53) Hulpia, F.; Van Hecke, K.; França da Silva, C.; da Gama Jaen Batista, D.; Maes, L.; Caljon, G.; de Nazaré C. Soeiro, M.; Van Calenbergh, S. Discovery of Novel 7-Aryl 7-Deazapurine 3′-Deoxy-Ribofuranosyl Nucleosides with Potent Activity against Trypanosoma Cruzi. *J. Med. Chem.* **2018**, *61*, 9287−9300.

(54) Hulpia, F.; Campagnaro, G. D.; Alzahrani, K. J.; Alfayez, I. A.; Ungogo, M. A.; Mabille, D.; Maes, L.; de Koning, H. P.; Caljon, G.; Van Calenbergh, S. Structure−Activity Relationship Exploration of 3′-Deoxy-7-Deazapurine Nucleoside Analogues as Anti-Trypanosoma Brucei Agents. *ACS Infect. Dis.* **2020**, *6*, 2045−2056.

(55) Hulpia, F.; Mabille, D.; Campagnaro, G. D.; Schumann, G.; Maes, L.; Roditi, I.; Hofer, A.; de Koning, H. P.; Caljon, G.; Van Calenbergh, S. Combining Tubercidin and Cordycepin Scaffolds Results in Highly Active Candidates to Treat Late-Stage Sleeping Sickness. *Nat. Commun.* **2019**, *10*, No. 5564.

(56) Hulpia, F.; Bouton, J.; Campagnaro, G. D.; Alfayez, I. A.; Mabille, D.; Maes, L.; de Koning, H. P.; Caljon, G.; Van Calenbergh, S. C6−O-Alkylated 7-Deazainosine Nucleoside Analogues: Discovery of Potent and Selective Anti-Sleeping Sickness Agents. *Eur. J. Med. Chem.* **2020**, *188*, No. 112018.

(57) Bouton, J.; Furquim d'Almeida, A.; Maes, L.; Caljon, G.; Van Calenbergh, S.; Hulpia, F. Synthesis and Evaluation of 3′-Fluorinated 7-Deazapurine Nucleosides as Antikinetoplastid Agents. *Eur. J. Med. Chem.* **2021**, *216*, No. 113290.

(58) Berman, J. D.; Hanson, W. L.; Lovelace, J. K.; Waits, V. B.; Jackson, J. E.; Chapman, W. L.; Klein, R. S. Activity of Purine Analogs against Leishmania Donovani in Vivo. *Antimicrob. Agents Chemother.* **1987**, *31*, 111−113.

(59) Berman, J. D.; Keenan, C. M.; Lamb, S. R.; Hanson, W. L.; Waits, V. B. Leishmania Donovani: Oral Efficacy and Toxicity of Formycin B in the Infected Hamster. *Exp. Parasitol.* **1983**, *56*, 215−221.

(60) Rainey, P.; Nolan, P. A.; Townsend, L. B.; Robins, R. K.; Fox, J. J.; Secrist, J. A., III; Santi, D. V. Inosine Analogs as Anti-Leishmanial Agents. *Pharm. Res.* **1985**, *02*, 217−220.

(61) Marr, J. J.; Berens, R. L.; Cohn, N. K.; Nelson, D. J.; Klein, R. S. Biological Action of Inosine Analogs in *Leishmania* and *Trypanosoma Spp. Antimicrob. Agents Chemother.* **1984**, *25*, 292−295.

(62) Morishige, K.; Aji, T.; Ishii, A.; Yasuda, T.; Wataya, Y. Leishmania Donovani: Pilot Study for Evaluation of Therapeutic Effects of Inosine Analogs against Amastigotes in Vitro and in Vivo. *Exp. Parasitol.* **1995**, *80*, 665−671.

(63) Seela, F.; Becher, G. Synthesis of 7-Halogenated 8-Aza-7-Deaza-2′-Deoxyguanosines and Related Pyrazolo[3,4-d]Pyrimidine 2′-Deoxyribonucleosides. *Synthesis* **1998**, *1998*, 207−214.

(64) Seela, F.; Zulauf, M. Synthesis of 7-Alkynylated 8-Aza-7-Deaza-2′-Deoxyadenosines via the Pd-Catalysed Cross-Coupling Reaction. *J. Chem. Soc., Perkin Trans. 1* **1998**, 3233−3240.

(65) Mihich, E.; Simpson, C. L.; Mulhern, A. I. Comparative Study of the Toxicologic Effects of 7-Deazaadenosine (Tubercidin) and 7-Deazainosine. *Cancer Res.* **1969**, *29*, 116−123.

(66) Earl, R. A.; Townsend, L. B. Pyrazolopyrimidine Nucleosides. Part VII. The Synthesis of Certain Pyrazolo [3,4-d] Pyrimidine Nucleosides Related to the Nucleoside Antibiotics Toyocamycin and Sangivamycin. *J. Heterocycl. Chem.* **1974**, *11*, 1033−1039.

(67) Hecht, S. M.; Frye, R. B.; Werner, D.; Fukui, T.; Hawrelak, S. D. Synthesis and Biological Activity of Pyrazolo[3,4-d]Pyrimidine Nucleosides and Nucleotides Related to Tubercidin, Toyocamycin, and Sangivamycin. *Biochemistry* **1976**, *15*, 1005−1015.

(68) Bhat, G. A.; Montero, J. L. G.; Panzica, R. P.; Wotring, L. L.; Townsend, L. B. Pyrazolopyrimidine Nucleosides. 12. Synthesis and Biological Activity of Certain Pyrazolo[3,4-d]Pyrimidine Nucleosides Related to Adenosine. *J. Med. Chem.* **1981**, *24*, 1165−1172.

(69) Cottam, H. B.; Petrie, C. R.; McKernan, P. A.; Goebel, R. J.; Kent Dailey, N.; Davidson, R. B.; Robins, R. K.; Revanka, G. R. Synthesis and Biological Activity of Certain 3,4-Disubstituted Pyrazolo[3,4-d]Pyrimidine Nucleosides1. *J. Med. Chem.* **1984**, *27*, 1119−1127.

(70) Lin, W.; Li, H.; Ming, X.; Seela, F. 1,N6-Etheno-7-Deaza-2,8-Diazaadenosine: Syntheses, Properties and Conversion to 7-Deaza-2,8-Diazaadenosine. *Org. Biomol. Chem.* **2005**, *3*, 1714−1718.

(71) Seela, F.; Steker, H. Facile Synthesis of 2′-Deoxyribofuranosides of Allopurinol and 4-Amino-1H-Pyrazolo[3,4-d]Pyrimidine via Phase-Transfer Glycosylation. *Helv. Chim. Acta* **1985**, *68*, 563−570.

(72) Lichtenthaler, F. W.; Cuny, E. Nucleosides, 381) The Ribonucleosides of Allopurinol. *Chem. Ber.* **1981**, *114*, 1610−1623.

(73) Seela, F.; Zulauf, M.; Becher, G. Unexpected Dehalogenation of 3-Bromopyrazolo[3,4-d]Pyrimidine Nucleosides during Nucleobase-Anion Glycosylation. *Nucleosides Nucleotides* **1997**, *16*, 305−314.

(74) Seela, F.; Kaiser, K. 8-Aza-7-deazaadenine N8- and N8-(B-D-2′-Deoxyribofuranosides): Building Blocks for Automated DNA Synthesis and Properties of Oligodeoxyribonucleotides. *Helv. Chim. Acta* **1988**, *71*, 1813−1823.

(75) Seela, F.; Winter, H.; Möller, M. Pyrazolo[3,4-d]Pyrimidine 2′-Deoxy- and 2′,3′ -Dideoxyribonucleosides: Studies on the Glycosylation of 4-Methoxypyrazolo[3,4-d]Pyrimidine. *Helv. Chim. Acta* **1993**, *76*, 1450−1458.

(76) Rutaganira, F. U.; Barks, J.; Dhason, M. S.; Wang, Q.; Lopez, M. S.; Long, S.; Radke, J. B.; Jones, N. G.; Maddirala, A. R.; Janetka, J. W.; El Bakkouri, M.; Hui, R.; Shokat, K. M.; Sibley, L. D. Inhibition of Calcium Dependent Protein Kinase 1 (CDPK1) by Pyrazolopyrimidine Analogs Decreases Establishment and Reoccurrence of Central Nervous System Disease by Toxoplasma Gondii. *J. Med. Chem.* **2017**, *60*, 9976−9989.

(77) Feng, X.; Qu, Y.; Han, Y.; Yu, X.; Bao, M.; Yamamoto, Y. Copper-Catalyzed Conversion of Aryl and Heteroaryl Bromides into the Corresponding Chlorides. *Chem. Commun.* **2012**, *48*, 9468−9470.

(78) Lin, C.; Hulpia, F.; da Silva, C. F.; Batista, D. d. G. J.; Van Hecke, K.; Maes, L.; Caljon, G.; Soeiro, M. d. N. C.; Van Calenbergh, S. Discovery of Pyrrolo[2,3-b]Pyridine (1,7-Dideazapurine) Nucleoside Analogues as Anti-Trypanosoma Cruzi Agents. *J. Med. Chem.* **2019**, *62*, 8847−8865.

(79) Hanefeld, U.; Rees, C. W.; White, A. J. P.; Williams, D. J. One-Pot Synthesis of Tetrasubstituted Pyrazoles—Proof of Regiochemistry. *J. Chem. Soc., Perkin Trans. 1* **1996**, *28*, 1545−1552.

(80) Wu, F. P.; Peng, J. B.; Qi, X.; Wu, X. F. Palladium-Catalyzed Carbonylative Transformation of Organic Halides with Formic Acid as the Coupling Partner and CO Source: Synthesis of Carboxylic Acids. *J. Org. Chem.* **2017**, *82*, 9710−9714.

(81) Ueda, T.; Konishi, H.; Manabe, K. Trichlorophenyl Formate: Highly Reactive and Easily Accessible Crystalline CO Surrogate for Palladium-Catalyzed Carbonylation of Aryl/Alkenyl Halides and Triflates. *Org. Lett.* **2012**, *14*, 5370−5373.

(82) Ueda, T.; Konishi, H.; Manabe, K. Palladium-Catalyzed Fluorocarbonylation Using N-Formylsaccharin as CO Source: General Access to Carboxylic Acid Derivatives. *Org. Lett.* **2013**, *15*, 5370−5373.

(83) Molander, G. A.; Brown, A. R. Suzuki−Miyaura Cross-Coupling Reactions of Potassium Vinyltrifluoroborate with Aryl and Heteroaryl Electrophiles. *J. Org. Chem.* **2006**, *71*, 9681−9686.

(84) Oshiro, K.; Morimoto, Y.; Amii, H. Sodium Bromodifluoroacetate: A Difluorocarbene Source for the Synthesis of Gem-Difluorocyclopropanes. *Synthesis* **2010**, *99*, 2080−2084.

(85) Berens, R. L.; Marr, J. J.; Nelson, D. J.; Lafon, S. W. Antileishmanial Effect of Allopurinol and Allopurinol Ribonucleoside on Intracellular Forms of Leishmania Donovani. *Biochem. Pharmacol.* **1980**, *29*, 2397−2398.

(86) Moorman, A. R.; LaFon, S. W.; Nelson, D. J.; Carter, H. H.; Marr, J. J.; Berens, R. L. Antiprotozoal Activity of 3′-Deoxyinosine. *Biochem. Pharmacol.* **1991**, *42*, 207−212.

(87) Soeiro, M. d. N. C.; de Souza, E. M.; da Silva, C. F.; Batista, D. d. G. J.; Batista, M. M.; Pavão, B. P.; Araújo, J. S.; Aiub, C. A. F.; da Silva, P. B.; Lionel, J.; Britto, C.; Kim, K.; Sulikowski, G.; Hargrove, T. Y.; Waterman, M. R.; Lepesheva, G. I. In Vitro and In Vivo Studies of the Antiparasitic Activity of Sterol 14α-Demethylase (CYP51) Inhibitor VNI against Drug-Resistant Strains of Trypanosoma Cruzi. *Antimicrob. Agents Chemother.* **2013**, *57*, 4151−4163.

(88) Chatelain, E.; Ioset, J.-R. Phenotypic Screening Approaches for Chagas Disease Drug Discovery. *Expert Opin. Drug Discovery* **2018**, *13*, 141−153.

(89) Dumoulin, P. C.; Vollrath, J.; Tomko, S. S.; Wang, J. X.; Burleigh, B. Glutamine Metabolism Modulates Azole Susceptibility in Trypanosoma Cruzi Amastigotes. *eLife* **2020**, *9*, No. e60226.

(90) Nagajyothi, F.; Machado, F. S.; Burleigh, B. A.; Jelicks, L. A.; Scherer, P. E.; Mukherjee, S.; Lisanti, M. P.; Weiss, L. M.; Garg, N. J.; Tanowitz, H. B. Mechanisms of Trypanosoma Cruzi Persistence in Chagas Disease. *Cell. Microbiol.* **2012**, *14*, 634−643.

(91) Fernandes, M. C.; Andrews, N. W. Host Cell Invasion by Trypanosoma Cruzi: A Unique Strategy That Promotes Persistence. *FEMS Microbiol. Rev.* **2012**, *36*, 734−747.

(92) Matos Ferreira, A. V.; Segatto, M.; Menezes, Z.; Macedo, A. M.; Gelape, C.; de Oliveira Andrade, L.; Nagajyothi, F.; Scherer, P. E.; Teixeira, M. M.; Tanowitz, H. B. Evidence for Trypanosoma Cruzi in Adipose Tissue in Human Chronic Chagas Disease. *Microbes Infect.* **2011**, *13*, 1002−1005.

(93) Francisco, A. F.; Lewis, M. D.; Jayawardhana, S.; Taylor, M. C.; Chatelain, E.; Kelly, J. M. Limited Ability of Posaconazole To Cure Both Acute and Chronic Trypanosoma Cruzi Infections Revealed by Highly Sensitive In Vivo Imaging. *Antimicrob. Agents Chemother.* **2015**, *59*, 4653−4661.

(94) Bouton, J.; Maes, L.; Karalic, I.; Caljon, G.; Van Calenbergh, S. Synthesis and Evaluation of a Collection of Purine-like C-Nucleosides as Antikinetoplastid Agents. *Eur. J. Med. Chem.* **2021**, *212*, No. 113101.

(95) Cottam, H. B.; Wasson, D. B.; Shih, H. C.; Raychaudhuri, A.; Di Pasquale, G.; Carson, D. A. New Adenosine Kinase Inhibitors with Oral Antiinflammatory Activity: Synthesis and Biological Evaluation. *J. Med. Chem.* **1993**, *36*, 3424−3430.

(96) Zhao, H.; Leonard, P.; Guo, X.; Yang, H.; Seela, F. Silver-Mediated Base Pairs in DNA Incorporating Purines, 7-Deazapurines, and 8-Aza-7-Deazapurines: Impact of Reduced Nucleobase Binding Sites and an Altered Glycosylation Position. *Chem. − Eur. J.* **2017**, *23*, 5529−5540.

(97) Kraybill, B. C.; Elkin, L. L.; Blethrow, J. D.; Morgan, D. O.; Shokat, K. M. Inhibitor Scaffolds as New Allele Specific Kinase Substrates. *J. Am. Chem. Soc.* **2002**, *124*, 12118−12128.

(98) Gao, Y.; Lam, Y. Synthesis of Pyrazolo[5,1-d][1,2,3,5]-Tetrazine-4(3H)-Ones. *J. Comb. Chem.* **2010**, *12*, 69−74.

(99) Kulkarni, A.; Quang, P.; Curry, V.; Keyes, R.; Zhou, W.; Cho, H.; Baffoe, J.; Török, B.; Stieglitz, K. 1,3-Disubstituted-4-Amino-pyrazolo [3, 4-d] Pyrimidines, a New Class of Potent Inhibitors for Phospholipase D. *Chem. Biol. Drug Des.* **2014**, *84*, 270−281.

(100) Hendrickx, S.; Caljon, G.; Maes, L. In Vitro Growth Inhibition Assays of Leishmania Spp. In *Trypanosomatids: Methods and Protocols*; Michels, P. A. M.; Ginger, M. L.; Zilberstein, D., Eds.; Springer: New York, NY, 2020; pp 791−800.

(101) Batista, D. G. J.; Pacheco, M. G. O.; Kumar, A.; Branowska, D.; Ismail, M. A.; Hu, L.; Boykin, D. W.; Soeiro, M. N. C. Biological, Ultrastructural Effect and Subcellular Localization of Aromatic Diamidines in Trypanosoma Cruzi. *Parasitology* **2010**, *137*, 251−259.

(102) Timm, B. L.; da Silva, P. B.; Batista, M. M.; da Silva, F. H. G.; da Silva, C. F.; Tidwell, R. R.; Patrick, D. A.; Jones, S. K.; Bakunov, S. A.; Bakunova, S. M.; Maria de Nazaré, C. S. In Vitro and In Vivo Biological Effects of Novel Arylimidamide Derivatives against Trypanosoma Cruzi. *Antimicrob. Agents Chemother.* **2014**, *58*, 3720−3726.

Check for updates

Chemistry
Europe

European Chemical
Societies Publishing

6-Methyl-7-Aryl-7-Deazapurine Nucleosides as Anti-*Trypanosoma cruzi* Agents: Structure-Activity Relationship and *in vivo* Efficacy

Cai Lin[+],[a] Ludmila Ferreira de Almeida Fiuza[+],[b] Camila Cardoso Santos,[b]
Daniela Ferreira Nunes,[c] Otacílio Cruz Moreira,[c] Jakob Bouton,[a] Izet Karalic,[a] Louis Maes,[d]
Guy Caljon,[d] Fabian Hulpia,*[a, e] Maria de Nazaré C. Soeiro,*[b] and Serge Van Calenbergh*[a]

Chagas disease is a tropical infectious disease resulting in progressive organ-damage and currently lacks efficient treatment and vaccine options. The causative pathogen, *Trypanosoma cruzi*, requires uptake and processing of preformed purines from the host because it cannot synthesize these *de novo*, instigating the evaluation of modified purine nucleosides as potential trypanocides. By modifying the pyrimidine part of a previously identified 7-aryl-7-deazapurine nucleoside, we found that substitution of a 6-methyl for a 6-amino group allows retaining *T. cruzi* amastigote growth inhibitory activity but confers improved selectivity towards mammalian cells. By

keeping the 6-methyl group unaltered, and introducing different 7-aryl groups, we identified several analogues with sub-micromolar antitrypanosomal activity. The 7-(4-chlorophenyl) analogue **14**, which was stable in microsomes, was evaluated in an acute mouse model. Oral administration of 25 mg/kg b.i.d. suppressed peak parasitemia and protected mice from infection-related mortality, gave similar reductions as the reference drug of blood parasite loads determined by qPCR, but as benznidazole failed to induce sterile cure in the short time period of drug exposure (5 days).

[a]   C. Lin,[+] J. Bouton, I. Karalic, Dr. F. Hulpia, Prof. S. Van Calenbergh
      Laboratory for Medicinal Chemistry (Campus Heymans)
      Ghent University
      Ottergemsesteenweg 460
      9000 Gent (Belgium)
      E-mail: fhulpia@its.jnj.com
            Serge.VanCalenbergh@UGent.be
[b]   L. Ferreira de Almeida Fiuza,[+] C. Cardoso Santos,
       Prof. M. de Nazaré C. Soeiro
      Laboratório de Biologia Celular
      Instituto Oswaldo Cruz (FIOCRUZ)
      Fundação Oswaldo Cruz, Rio de Janeiro
      Avenida Brasil 4365, Manguinhos
      21040-360 Rio de Janeiro (Brazil)
      E-mail: soeiro@ioc.fiocruz.br
[c]   Dr. D. Ferreira Nunes, Dr. O. Cruz Moreira
      Plataforma de PCR em Tempo Real RPT09A-Laboratório de Biologia
      Molecular e Doenças Endêmicas
      Instituto Oswaldo Cruz (FIOCRUZ)
      Fundação Oswaldo Cruz, Rio de Janeiro
      Avenida Brasil 4365, Manguinhos
      21040-360 Rio de Janeiro (Brazil)
[d]   Prof. L. Maes, Prof. G. Caljon
      Laboratory of Microbiology
      Parasitology and Hygiene
      University of Antwerp
      Universiteitsplein 1
      2610 Wilrijk (Belgium)
[e]   Dr. F. Hulpia
      Janssen Pharmaceutica NV
      Turnhoutseweg 30
      2340 Beerse (Belgium)
      E-mail: fhulpia@its.jnj.com

[+] These authors contributed equally to this work.

  Supporting information for this article is available on the WWW under
  https://doi.org/10.1002/cmdc.202100144

Introduction

Chagas disease (CD) is a neglected tropical disease that is endemic in the Latin American countries.[1–2] CD is caused by the kinetoplastid parasite *Trypanosoma cruzi* (*T. cruzi*) and is transmitted primarily in endemic regions via triatomine bugs. While taking a bloodmeal this vector defecates, releasing *T. cruzi* trypomastigotes which then establish an infection into the vertebrate mammalian host.[3] Notwithstanding the vector-mediated transmission route in endemic areas being most important, CD may also be contracted by ingesting contaminated food or drinks (oral route). Additionally, a diverse range of non-vector mediated transmission routes, such as congenital infection, blood transfusion or organ transplantation, plays a major role in non-endemic countries.[4] This is particularly worrisome in light of increased migration, often accompanied by an unawareness of infection status, rendering CD a global health concern.[5–6]

There are two stages in the progression of CD: the acute and chronic stage. The initial clinical manifestation in the acute phase is mild or even oligosymptomatic, but the parasite can typically be observed through blood examination. If no treatment is provided, the disease enters into a chronic phase and may remain asymptomatic for years and decades, displaying a subpatent parasitism due to an effective host's immune system. In the later chronic phase, for reasons not yet well known, some patients (30–40%) develop a progressive cardiomyopathy and/or digestive disorders besides neurological dysfunction.[7–9] The continuous damage of the heart muscle ultimately results in heart failure and sometimes sudden death.[10] Currently, no vaccine is available, making chemotherapy the only option.

These are not the final page numbers! ↗↗

ChemMedChem

Full Papers
doi.org/10.1002/cmdc.202100144

**Chemistry
Europe**
European Chemical
Societies Publishing

Benznidazole (BZ) and nifurtimox are two nitro-containing drugs used for the treatment of CD. However, both drugs suffer from several limitations such as low efficacy mainly at the later chronic stage, and significant side effects besides the occurrence of parasite strains that are naturally resistant to both nitro derivatives. Drug toxicity is particularly important as it contributes to poor patient compliance and premature treatment cessation, thus contributing to the persistence of the parasitism.[11–13] Therefore, the discovery and development of new treatment options are of critical importance.[14–15]

An attractive drug discovery paradigm is to exploit certain parasitic auxotrophies. Particularly, *T. cruzi* cannot synthesize purine rings from amino acids, resulting in their reliance on salvage[16–18] of preformed purine rings from the host for growth and proliferation, thereby increasing the likeliness for (modified) purine analogues as potential antiparasitic agents.[19–20]

Tubercidin, a natural antibiotic, displays attractive inhibitory potency against multiple pathogenic organisms, but its application is limited because of toxic effects on mammalian cells.[21–22] Selectivity improvement of 7-deazapurine nucleoside analogues has been achieved via modifications at C6[23] and/or C7.[22,24] Introduction of a 4-chlorophenyl substituent (analogue **2**, Figure 1) at C7 of tubercidin was found to confer potent anti-*T. cruzi* activity *in vitro*[22,25] and *in vivo*,[25] while decreasing cytotoxicity. Several other nucleoside analogues with modifications in the pyrimidine part of the purine were reported to exhibit potent activity against *T. cruzi*, including puromycin aminonucleoside (**3**),[26] 7-iodo-1,7-dideazaadenosine (**4**),[27] 3-

deazaguanosine (**5**)[28] and 2-amino-6-chloro-7-deazaadenosine (**6**) (Figure 1a).[29]

In this study, we set out to explore the structure-activity-relationship (SAR) of analogue **2** with particular attention to modifications of the pyrimidine part of the 7-deazapurine system. After having identified a favourable 6-methyl modification, we combined this modification with different C7 modifications (Figure 1b). One promising analogue with favourable *in vitro* metabolic stability was selected for efficacy evaluation in an experimental mouse model of *T. cruzi* infection.

Results and Discussion

Biological evaluation

In vitro evaluation

All prepared compounds were evaluated *in vitro* for their antitrypanosomal activity against *T. cruzi*, employing different parasite strains belonging to distinct DTUs (Tulahuen expressing β-galactosidase and Y strains, DTU VI and II, respectively) and parasite forms relevant for mammalian host (intracellular amastigotes and bloodstream trypomastigotes) always comparing to the findings obtained with BZ as a reference drug. In parallel, the *in vitro* cytotoxicity of the compounds was assessed in different host cells including the MRC-5 human fibroblast cell line and primary cardiac cell cultures grown as 2 and 3-D matrices (Tables 1–3, 6).
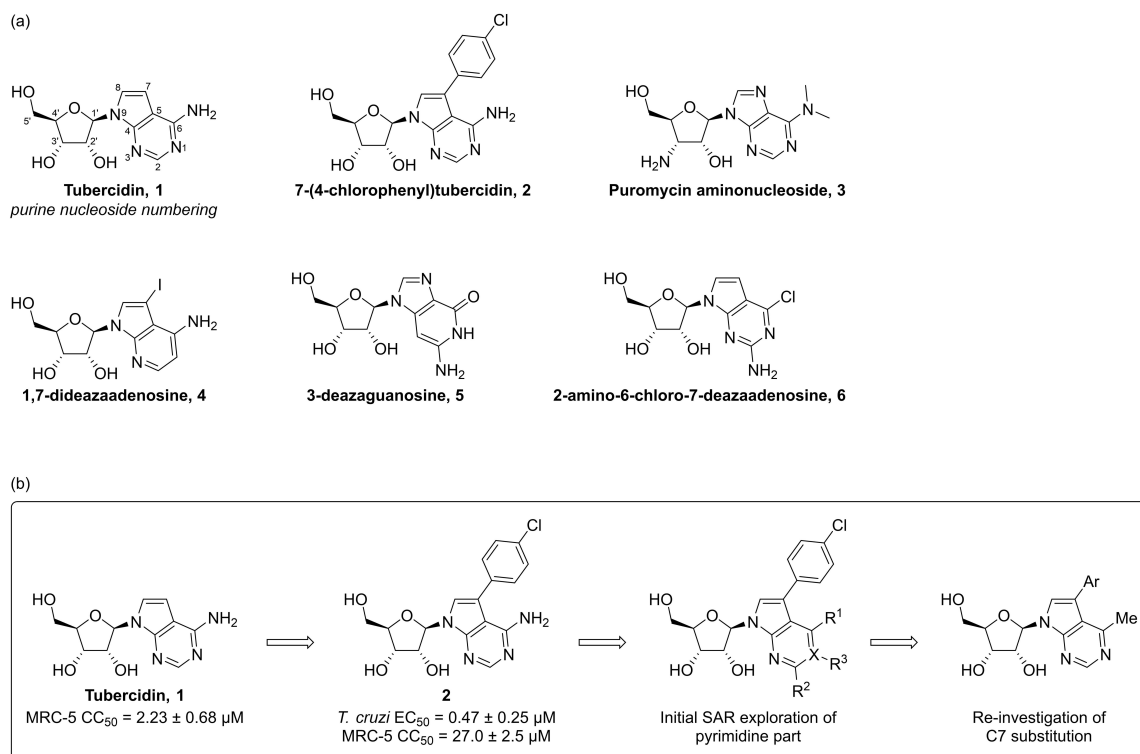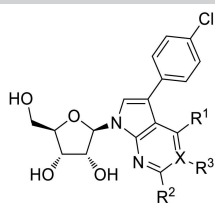
Figure 1. (a) Representative antitrypanosomal nucleoside analogues with C7 or pyrimidine ring modifications; (b) SAR exploration of the pyrimidine ring of **2** and exploration of C7-aryl modified 6-methyl-7-deazapurinecleoside.

ChemMedChem

Full Papers
doi.org/10.1002/cmdc.202100144

Chemistry Europe
European Chemical
Societies Publishing

Table 1. < Activity of 7-(*para*-chlorophenyl) nucleoside analogues with modifications in pyrimidine moieties against intracellular *T. cruzi* amastigotes.

Cpd.	X	R^1	R^2	R^3	*T. cruzi*[a] EC$_{50}$ [μM]	MRC-5[b] EC$_{50}$ [μM]	SI[c]
2[22,25]	N	NH$_2$	H	–	0.47 ± 0.25	27.0 ± 2.5	57
7	N	NHMe	H	–	41.6	> 64.0	> 1.54
8	N	NMe$_2$	H	–	33.4	> 64.0	> 1.92
9	N	OH	H	–	> 64.0	> 64.0	N.D.[d]
10[30]	N	OMe	H	–	43.1	61.1	1.42
11	N	OEt	H	–	26.3	50.4	1.92
12	N	SMe	H	–	20.3	> 64.0	> 3.15
13	N	H	H	–	11.9	> 64.0	> 5.38
14	N	Me	H	–	0.85 ± 0.21	> 64.0	> 75
15	N	Et	H	–	35.3	36.3	1.03
16	N	Ph	H	–	> 64.0	> 64.0	N.D.
17	N	OH	NH$_2$	–	> 64.0	> 64.0	N.D.
18	N	OMe	NH$_2$	–	30.6	22.5	0.74
19[31]	C	NH$_2$	H	H	> 64.0	> 64.0	N.D.
20	C	Me	H	H	9.76 ± 0.45	> 64.0; 20.2	N.D.
21	C	H	H	F	24.1	18.2	0.76
22	C	H	H	Cl	7.80	50.8	6.51
23	C	H	H	NO$_2$	8.45 ± 0.12	> 64.0	> 7.57
24	C	H	H	NH$_2$	> 64.0	> 64.0	N.D.
25	C	H	H	Me	9.98	23.4	2.34
BZ					2.28 ± 0.05	N.D.	N.D.

[a]Concentration of compound inhibiting growth by 50% (EC$_{50}$) of intracellular *T. cruzi* amastigotes (Tulahuen strain-expressing β-galactosidase). EC$_{50}$ values are described as mean ± SE of 2 or 4 independent experiments. Where SE is not provided, values (EC$_{50}$ > 10 μM) were determined in a single experiment; [b] Concentration of compound inhibiting growth by 50% (EC$_{50}$) of MRC-5 fibroblasts; [c] SI = selectivity index, EC$_{50}$ (MRC-5)/EC$_{50}$ (*T. cruzi*); [d] N.D.: not determined.

First, the activity against intracellular forms (Tulahuen strain) was investigated. Substitution of the 6-amino group of **2** by alternative groups (**7**–**12**) failed to give analogues with improved or comparable anti-*T. cruzi* activity. Likewise, complete removal of the 6-NH$_2$ (**13**) or its replacement by a phenyl (**16**) was not tolerated. Only the 6-methyl analogue **14** displayed sub-micromolar anti-*T. cruzi* activity, comparable to **2**. This analogue does not exhibit toxicity to the MCR-5 host cells at the highest concentration tested (> 64 μM), marking **14** as an interesting hit. Remarkably, homologation to a 6-ethyl analogue (**15**) resulted in complete loss of antiparasitic activity. Both deazaguanosine analogues **17** and **18** were devoid of anti-*T. cruzi* activity.

Then, we assessed the importance of N1, as we have previously shown that 1,7-dideazapurine analogues may display interesting anti-*T. cruzi* activity.[27] In this series, however, the combination of a 6-amino group with the 7-*para*-chlorophenyl (**19**) previously proved detrimental for activity.[27] Remarkably, replacing the 6-amino group of **19** by a methyl group (**20**) restored the anti-*T. cruzi* activity (EC$_{50}$ ~ 10 μM). However, this 1,7-dideaza analogue remained 10-fold less active than its 7-deaza congener **14**. Removal of the N1 nitrogen atom allows modifications at this position which were hardly explored before. 1-Chloro or nitro analogues showed modest activities (EC$_{50}$ < 10 μM), while the 1-amino analogue **24** was inactive.
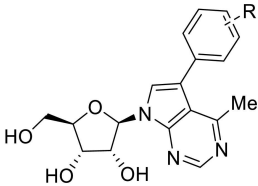
Having identified a 6-methyl group as a potential 6-amino isostere, we decided to further investigate the SAR of the 7-substituent of **14** (Table 2).

Removal of the chloro-substituent (**26**) led to a substantial activity drop, indicating the importance of *para* substitution. Several alternative substituents resulted in less potent analogues (**27**–**35**), including 4-F (**27**), 4-CF$_3$ (**28**) and 4-Me (**32**) that retained low micromolar anti-*T. cruzi* activity, similar to BZ. Shifting the halogen to the *meta* (**36**, **37**) or *ortho* (**38**) position reduced the anti-*T. cruzi* activity, in line with previous SAR observations with the 6-amino analogues.[22,25]

Generally, 3,4-disubstituted analogues (**39**, **40**) were more potent than 2,4-disubstituted (**44**, **45**) or 3,5-disubstituted analogues (**46**). Introduction of a fluoro (**40**) or a methoxy group (**43**) in the *meta* position of **14** gave a slight activity improvement. Selected bicyclic analogues of **26** (e.g. **49** and **53**) also showed reasonable activity. However, the effect of the aryl substituents on the activity did not show a clear trend. The fact that the observed SAR is in line with previous findings for 3′-deoxy-7-aryl tubercidin analogues,[25] suggests a similar target engagement.
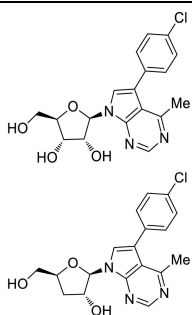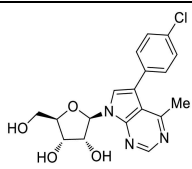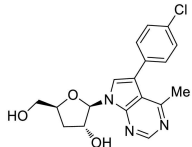
Finally, we investigated the effect of 3′-deoxygenation (Table 3), previously shown to significantly improve antitrypanosomal activity.[25,32–33] However, the 3′-deoxy analogue **54**

These are not the final page numbers! ↗↗

258

Table 2. Activity of 7-aromatic-deazapurine nucleoside analogues against intracellular *T. cruzi* amastigotes.[a]

Cpd.	R or structure	*T. cruzi*[a] EC$_{50}$ [μM]	MRC-5[b] EC$_{50}$ [μM]	SI[c]
14	4-Cl	0.85 ± 0.21	> 64.0	> 75
26	H	40.3	> 64.0	> 1.5
27	4-F	2.89 ± 0.35	> 64.0	> 22
28	4-CF$_3$	2.55 ± 0.11	> 64.0	> 25
29	4-OCF$_3$	31.5	> 64.0	> 2.0
30	4-CN	33.5	> 64.0	> 1.9
31	4-NO$_2$	13.4	> 64.0	> 4.7
32	4-Me	2.83 ± 0.03	> 64.0	> 22
33	4-Et	42.3	> 64.0	> 1.5
34	4-OMe	44.7	> 64.0	> 1.4
35	4-OH	7.47 ± 0.01	> 64.0	> 8.5
36	3-Cl	12.9 ± 0.78	> 64.0	> 4.9
37	3-F	12.7	> 64.0	> 5.0
38	2-Cl	9.27 ± 0.06	> 64.0	> 6.9
39	3,4-2Cl	1.58 ± 0.70	> 64.0	> 40
40	3-F-4-Cl	0.61 ± 0.04	> 64.0	> 104
41	3-CF$_3$-4-Cl	> 64.0	> 64.0	N.D.[d]
42	3-Me-4-Cl	1.61 ± 0.26	> 64.0	> 39
43	3-OMe-4-Cl	0.59 ± 0.02	> 64.0	> 108
44	2,4-2Cl	10.3 ± 0.09	> 64.0	> 6.2
45	2-F-4-Cl	1.51 ± 0.70	> 64.0	> 42
46	3,5-2Cl	10.9 ± 0.36	> 64.0	> 5.8
47	3,5-2F-4-Cl	2.49 ± 0.11	> 64.0	> 25
48	4-Ph	10.8 ± 2.52	> 64.0	> 5.9
49	2-naphthalene	3.06 ± 0.16	29.6; > 64.0	N.D.
50	5-(benzo[d][1,3]dioxole)	60.9	> 64	1
51	6-(2,3-dihydrobenzo[b][1,4]dioxine)	> 64	> 64	N.D.
52	6-1H-indole	> 64	> 64	N.D.
53	6-(1-methyl-1H-indole)	3.34	44.30	13
BZ		2.28 ± 0.05	N.D.	N.D.

[a] Concentration of compound inhibiting growth by 50% (EC$_{50}$) of intracellular *T. cruzi* amastigotes (Tulahuen strain-expressing β-galactosidase). EC$_{50}$ values are described as mean ± SE of 2 or 4 independent experiments. Where SE is not provided, values (EC$_{50}$ > 10 μM) were determined in a single experiment; [b] Concentration of compound inhibiting growth by 50% (EC$_{50}$) of MRC-5 fibroblasts; [c] SI = selectivity index, EC$_{50}$ (MRC-5)/EC$_{50}$ (*T. cruzi*); [d] N.D.: not determined.

Table 3. Comparison of activity of compound 14 and the corresponding 3'-deoxy- analogue against intracellular *T. cruzi* amastigotes.[a]

Cpd.	Structure	*T. cruzi*[a] EC$_{50}$ [μM]	MRC-5[b] EC$_{50}$ [μM]	SI[c]
14		0.85 ± 0.21	> 64.0	> 75
54		2.58 ± 0.67	> 64.0	> 25

[a] Concentration of compound inhibiting growth by 50% (EC$_{50}$) of intracellular *T. cruzi* amastigotes (Tulahuen strain-expressing β-galactosidase). EC$_{50}$ values are described as mean ± SE of 2 or 4 independent experiments; [b] Concentration of compound inhibiting growth by 50% (EC$_{50}$) of MRC-5 fibroblasts; [c] SI = selectivity index, EC$_{50}$ (MRC-5)/EC$_{50}$ (*T. cruzi*).

ChemMedChem

Full Papers
doi.org/10.1002/cmdc.202100144

Chemistry Europe
European Chemical
Societies Publishing

elicited a 3-fold weaker anti-*T. cruzi* activity than its ribose congener **14**.

In summary, a new series of 6-methyl 7-aryl-7-deazapurine nucleosides with activity against *T. cruzi* was discovered. SAR efforts showed that the 6-methyl group can function as a suitable bioisostere for the amino functionality, typically present in purines. Such replacement was previously exploited for antiviral[23,31,34–35] and cytotoxic nucleoside analogues.[23] Noteworthy is the complete lack of cytotoxicity against MRC-5 fibroblasts observed for almost all of the 6-methyl-7-(substituted) phenyl nucleosides, which represents a benefit compared to our previously reported analogue **7**.[22,25] It is noteworthy that the most promising analogues of this study (**14**, **40** and **43**) all possess a (modified) 7-(4-chlorophenyl) substituent, as summarized in Figure 2. Given that these three analogues display comparable *in vitro* antitrypanosomal activity, the lowest molecular weight compound **14** was selected for further evaluation (Tables 4-6). Compound **14** was not cardiotoxic ($CC_{50} > 400\ \mu M$) and presented a high potency against intracellular forms (Y strain) present within primary cardiac cell cultures ($EC_{50} = 0.77 \pm 0.05\ \mu M$) (Table 6). Also, the analogue continued to exert a promising biological effect when assessed in cardiac spheroids. The low cardiotoxicity profile of **14** was confirmed in 3D matrices ($CC_{50} > 200\ \mu M$) and it displayed similar trypanocidal effects at a 10 μM concentration as BZ, reducing the *T. cruzi* (Y strain) parasite loads in cardiac spheroids by 77.5 ± 6.4 and $87 \pm 4.2\%$ for **14** and BZ respectively, as evidenced by qPCR analysis.
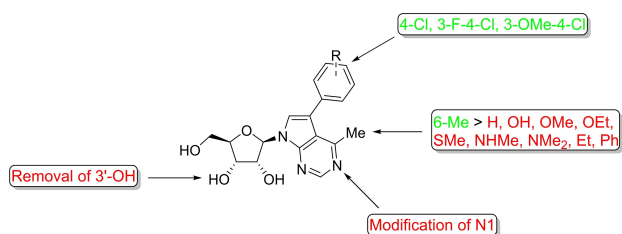
Figure 2. Summary of SAR trends for *T. cruzi*

In vitro metabolic stability of 14

The metabolic stability of **14** in the presence of mouse and human liver microsomal fractions was evaluated (Table 4). The percentage of remaining parent compound was monitored at three time points and compared to the start of the assay, indicating that **14** remained largely unaffected in the presence of either NADPH fortification (phase I) or UGT fortification (phase II). Hence, this analogue was further evaluated in a mouse model of acute *T. cruzi* infection.

In vivo evaluation of 14

The *in vivo* effect of **14** was evaluated in a stringent Y-strain *T. cruzi* acute male Swiss mouse model.[36]

Dose titration schedules of the different treatment groups are summarized Table 5. The nucleoside analogue **14** was administered at 0.25, 2.5, 25 mg/kg b.i.d. by oral gavage for 5 consecutive days, respectively, while BZ was administered orally at 10 or 100 mg/kg s.i.d. as suboptimal and optimal doses, for 5 consecutive days as a positive control. Two animal control groups (untreated and uninfected, as well as untreated and infected) were also included. To investigate the potential benefit of a combination treatment regimen, **14** (2.5 mg/kg) and BZ (10 mg/kg) were co-administered in a separate group (G6, Table 5).

Treatment was initiated at the onset of parasitemia (5 days post-infection (dpi)) and the peak parasitemia readout was performed at 8 dpi. **14** showed a concentration-dependent effect (Figure 3). It exerted a peak parasitemia reduction of 47%, 60% and 92% at 8 dpi in treatment regimens of 0.25, 2.5, 25 mg/kg b.i.d., respectively. The efficacy of **14** at 25 mg/kg b.i.d. (92%) approached that of BZ at 100 mg/kg s.i.d. (> 99%), when measured at 8 dpi and indistinguishable from BZ at 10 dpi and onwards. No toxic effects could be noticed in mice treated with **14**. Unexpectedly, co-administration of **14** (at 2.5 mg/kg) and BZ (at 10 mg/kg) led to a weaker parasitemia reduction than either compound separately. Treatment with **14** at 25 mg/kg gave 83.3% survival at 34 dpi, whereas lower doses (0.25, 2.5 mg/kg) did not protect against mortality (Figure 3 (E) and Table 5). All co-administered animals succumbed to the

Table 4. Evaluation of *in vitro* metabolic stability of 14 in the presence of male mouse and pooled human S9 microsomal fractions.[a]

| Phase I or II | Time [min] | Cpd. 14 remaining [%] | | | |
		MOUSE mean	SD	HUMAN mean	SD
CYP − NADPH	0	100	–	100	–
	15	93	2.7	104	5.8
	30	88	5.0	95	10.7
	60	86	0.7	96	5.4
UGT Enzymes	0	100	–	100	–
	15	98	0.6	97	1.8
	30	94	1.1	91	6.1
	60	97	0.8	93	3.0

[a] Values represent percentages of remaining parent compound. Four time points (0–15–30–60 min) of incubation were monitored. Values are reported as means and SD of two independent experiments. The reference drug was diclofenac, susceptible to phase I and phase II metabolism (data not shown).

260

ChemMedChem

Full Papers
doi.org/10.1002/cmdc.202100144

Chemistry
Europe
European Chemical
Societies Publishing
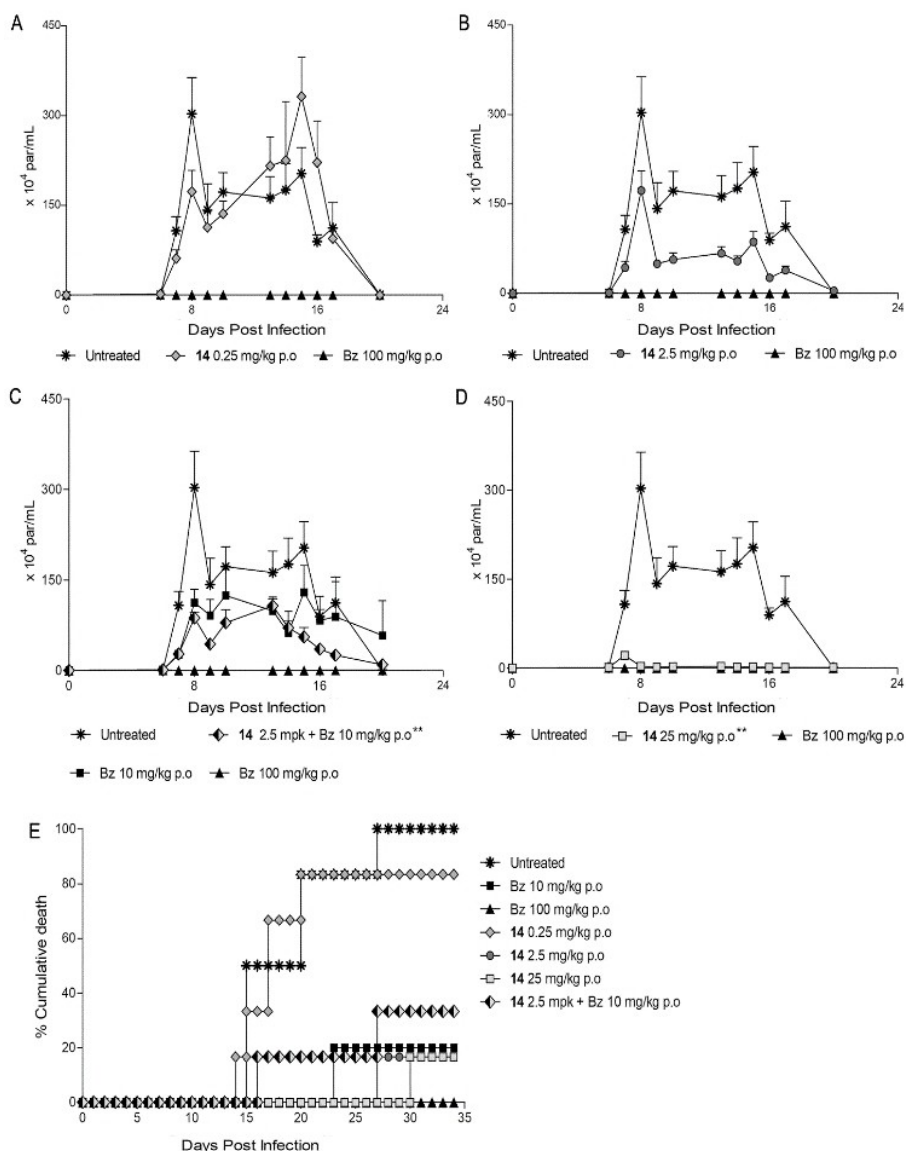
Figure 3. *In vivo* efficacy of **14** was evaluated in the mouse model of acute infection with Y-strain *T. cruzi*. (A–D) Blood parasitemia levels were measured via direct microscopic counting of the number of parasites in the blood (5 μL) from a tail vein puncture. (E) Cumulative mortality rate of the animals was recorded until 34 dpi. All treatments were for 5 consecutive days and were initiated at the onset of parasitemia (5 dpi).

Table 5. Administration and efficacy of 14 and BZ in acute CD mice model.[a]				
Group	Compound	Dose [mg/kg]	Doses per day	Survival
G1	–	Uninfected	–	6/6
G2	–	Untreated (vehicle)	–	0/6
G3	**14**	0.25	2	1/6
G4	**14**	2.5	2	0/6
G5	**14**	25	2	5/6
G6	**14+BZ**	2.5+10 (**BZ**)	(2+1)	0/6
G7	**BZ**	10	1	4/5
G8	**BZ**	100	1	5/5
[a] All treatments were executed at the onset of parasitemia (5 dpi) and treated for 5 consecutive days (p.o.).				

infection, in line with the parasitemia reduction trend. Unfortunately, none of treated animals had negative parasitemia at 34 dpi, indicating a lack of sterile cure at the used dosing regimens.

These are not the final page numbers! ↗↗

261

According to our previous work, the potential reason for *in vivo* failure may be the lack of activity against the bloodstream form (BF) trypomastigotes, since **14** was not active against BF trypomastigotes (Y strain) after 2 and 24 hours of incubation. Compound **14** displayed EC_{50} values > 81 μM, while BZ gave 11.5 μM (Table 6). Also, the lack of cure may be due to the short period of drug exposure in this proof of concept study (only 5 days of drug therapy). Under this treatment scheme, BZ also failed to provide sterile cure: all surviving **14**- and BZ-treated animals displayed positive blood parasitism evaluated by qPCR. Accordingly, the qPCR findings demonstrated a similar blood parasite load when both groups were analysed, reaching mean values of 83.9 ± 129.4 and 84.1 ± 90.7 par. eq./mL for **14** and BZ, respectively.

Chemistry

The synthesis of several 6-modified 7-chlorophenyl-7-deaza nucleoside analogues is depicted in Schemes 1–3. First, **55**[37] was reacted with different nucleophiles to effect 6-substitution and concomitant deprotection[38] (Scheme 1), providing the 7-iodo nucleoside intermediates **56–60**. Then, aqueous Suzuki coupling[22,24–25] allowed to construct the target 7-(4-chlorophenyl) derivatives **7–8**, **10–12**. To access inosine analogue **9**, **10** was demethylated with in situ generated TMSI.[37–38] 7-(4-chlorophen-

yl)-7-deazaguanosine (**17**) was prepared from the known **61**[23,39] using the same sequence of Suzuki coupling and *O*-demethylation.

Catalytic dechlorination of **62**[38] afforded **63**. **62** also served as a precursor for the introduction of a 6-methyl (**65**) or 6-ethyl group[40] (**66**) (Scheme 2). C7 halogenation was accomplished with the appropriate halosuccinimides. Subsequent ammonolysis and Suzuki coupling furnished the desired 4-chlorophenyl analogues **13**, **14** and **15**.

For the synthesis of the 6-phenyl analogue **16**, the phenyl group was first introduced on 6-chloro-7-deazapurine (Scheme 3). After iodination in DMF, heterocycle **70** was glycosylated under Vorbrüggen conditions[37] to give 7-iodo **71** after subsequent deprotection. Final introduction of the *para*-chlorophenyl at C7 via Pd-based cross coupling gave the desired **16**.

To probe the importance of the N1 nitrogen, several pyrrolo[2,3-*b*]pyridine (1,7-dideazapurine) nucleoside analogues were prepared (Scheme 4). First, 6-methyl analogue **72**[27] was subjected to standard aqueous Suzuki coupling to introduce the 4-chlorophenyl group. To obtain several 1-substituted nucleoside analogues, commercially available 5-substituted pyrrolo[2,3-*b*]pyridines were employed as the starting material. Bromination at C3 was effected by NBS/DMF to yield substituted heterocyclic analogues **73–76**.[41–42] Vorbrüggen glycosylation[27] afforded the desired analogues **77–80** after direct deprotection in saturated

Table 6. Activity of 14 against *T. cruzi* (Y strain) bloodstream trypomastigotes and intracellular amastigotes in 2D primary cardiac cells.[a]

Cpd.	Bloodstream trypomastigotes EC_{50} [μM]	Intracellular Amastigotes[b] EC_{50} [μM]	2D primary cardiac cells CC_{50} [μM]
14	> 81	0.77 ± 0.05	481.9
BZ	$11.5 \pm 1.1^*$	5.76 ± 0.09	> 1000

[a] EC_{50} values are described as means $\pm$ SD of 2 independent experiments; [b] The activities of analogues against intracellular amastigotes are estimated as the reduction of infection index (percentage of infected host cells × number of parasites per host cell); * Hulpia et al., 2018.[25]
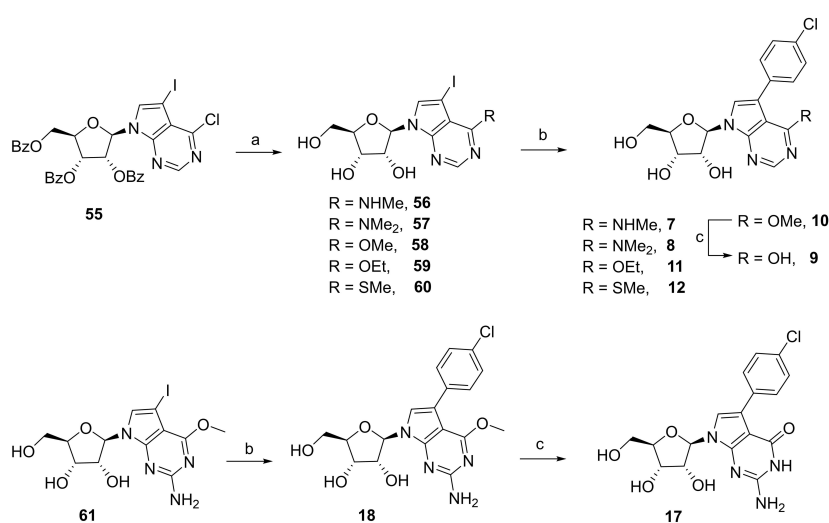
Scheme 1. Reagents and conditions: (a) methylamine (40% W/V in water), 82% (**56**); dimethylamine (40% W/V in water), 72% (**57**); 0.5 M NaOMe/MeOH or NaOEt/EtOH, 50°C, 68% (**58**); 51% (**59**); NaSMe, EtOH, r.t., 79% (**60**); (b) (4-chlorophenyl)boronic acid, Pd(OAc)₂, TPPTS, Na₂CO₃, MeCN/water (1:2 ratio), 100°C, 39% (**7**), 13% (**8**), 36% (**10**), 33% (**11**), 34% (**12**), 18% (**18**); (c) NaI, TMSCl, MeCN, 74% (**9**), 68% (**17**).

ChemMedChem

Full Papers
doi.org/10.1002/cmdc.202100144

Chemistry Europe
European Chemical
Societies Publishing
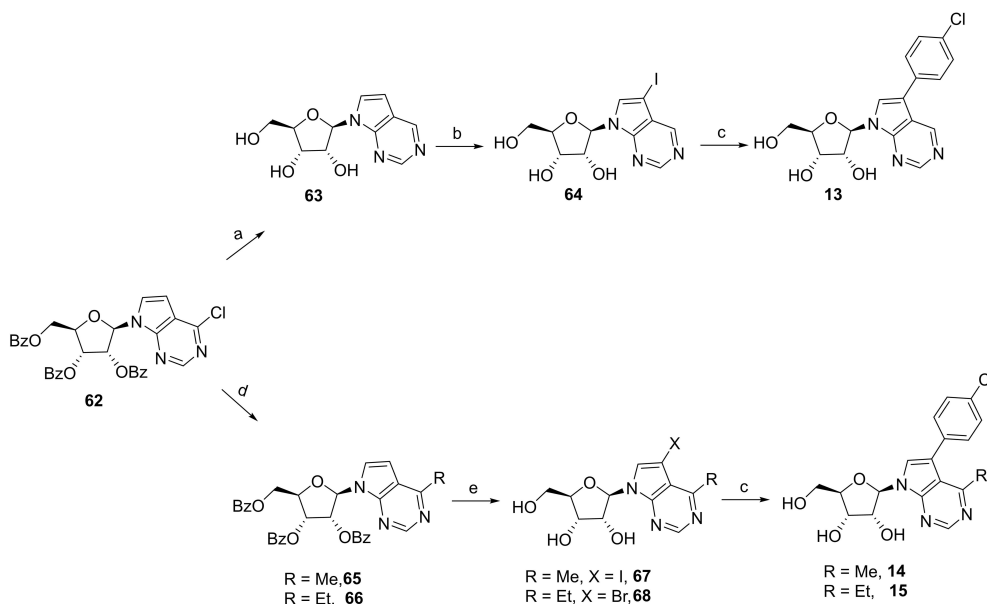
Scheme 2. Reagents and conditions: (a) Pd(OH)$_2$/C, H$_2$, K$_2$CO$_3$, MeOH, 84%; (b) NIS, DMF, 38%; (c) (4-chlorophenyl)boronic acid, Pd(OAc)$_2$, TPPTS, Na$_2$CO$_3$, MeCN/water (1:2 ratio), 100°C, 32% (**13**), 63% (**14**), 49% (**15**); (d) Me$_3$Al or Et$_3$Al, Pd(PPh$_3$)$_4$, THF, 100°C, 93% (**65**), 65% (**66**); (e) (i) NIS for **65**, NBS for **66**, DMF; (ii) 7 N NH$_3$/MeOH, 61% (**67**), 64% (**68**) for two steps.
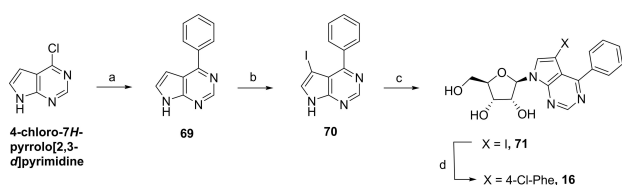
Scheme 3. Reagents and conditions: (a) phenylboronic acid, Pd(PPh$_3$)$_4$, K$_2$CO$_3$, toluene, 100°C, 95%; (b) NIS, DMF, 85%; (c) (i) 1-O-acetyl-2,3,5-tri-O-benzoyl-β-D-ribofuranose, BSA, TMSOTf, MeCN, 80°C; (ii) 7 N NH$_3$/MeOH, 22% for two steps; (d) (4-chlorophenyl)boronic acid, Pd(OAc)$_2$, TPPTS, Na$_2$CO$_3$, MeCN/water (1:2 ratio), 100°C, 23%.

methanolic ammonia. The desired *para*-chlorophenyl group was then introduced via Suzuki reaction to yield nucleoside analogues **21**, **23** and **25**. For the synthesis of **22**, a different Pd-catalyst system was used to reduce the formation the 7-dehalogenated product of **78**, which was difficult to remove from the desired **22**. To gain access to 1-amino derivative **24**, the 1-nitro group of **79** was reduced by catalytic hydrogenation (Pt/C) without concomitant dechlorination.

Encouraged by the observed SAR, various aromatic substituents were introduced at position 7 via Pd-based cross coupling of the 6-methyl-7-iode precursor **67** (Scheme 5).

To gain access to a 3'-deoxyribofuranose analogue, a Vorbrüggen reaction was performed involving 4-chloro-5-iodo-pyrrolo[2,3-*d*]pyrimidine[43] and 1-O-acetyl-2,5-di-O-benzoyl-3-deoxy-α/β-D-ribofuranose[25,32–33] to give **81**[33] (Scheme 6). A magnesium-iodine exchange with the Knochel reagent (iPrMgCl·LiCl)[23,32] and subsequent aqueous workup also removed the 7-iodo group. Palladium catalysed C6 methylation of the resulting intermediate with Al$_3$Me gave **82**. Subsequent removal of the benzoyl groups, introduction of a 7-bromo

group with NBS/DMF afforded **84**, which was converted to the desired **54**.

Conclusion

In a first set of *in vitro* assays of this study, we have investigated the influence of modifying the pyrimidine part of a previously reported 7-deazapurine nucleoside analogue on *T. cruzi* intracellular amastigotes. We found that a 6-methyl group acts as a suitable bioisostere and conferred a better selectivity. Next, keeping the 6-methyl group unaltered, we investigated alternative 7-substituents and found two 3,4-substituted phenyl analogues **40** and **43** that are equipotent to **14**. Nucleoside **14** showed a high potency against intracellular forms belonging to different strains and DTUs (Y and Tulahuen strains) and a low cardiotoxic profile in primary cardiac cell cultures. Our analyses employing a variety of *in vitro* models (fibroblast cell lines, 2D and 3D cardiac cell cultures and parasite strains belonging to distinct DTUs) is desirable since the metabolism of mammalian cells and parasite strains and host-parasite interactions have an impact on anti-*T. cruzi* compound activity.[44] In fact, using different *in vitro* assays in the drug discovery pipeline may better predict *in vivo* outcomes since the parasite invades different mammalian host cell types, and thus compounds must be effective in a range of host cell environments. The inclusion of cardiac organoids for anti-*T. cruzi* drug evaluation is recommended as the heart is one of the main target organs for infection and inflammation in CD and the drug responses may be influenced by the host cellular metabolism.[44–45]

In addition, we also tested the toxicity and anti-*T. cruzi* activity of compound **14** using cardiac spheroids that corrobo-

ChemMedChem

Full Papers
doi.org/10.1002/cmdc.202100144

Chemistry Europe
European Chemical
Societies Publishing
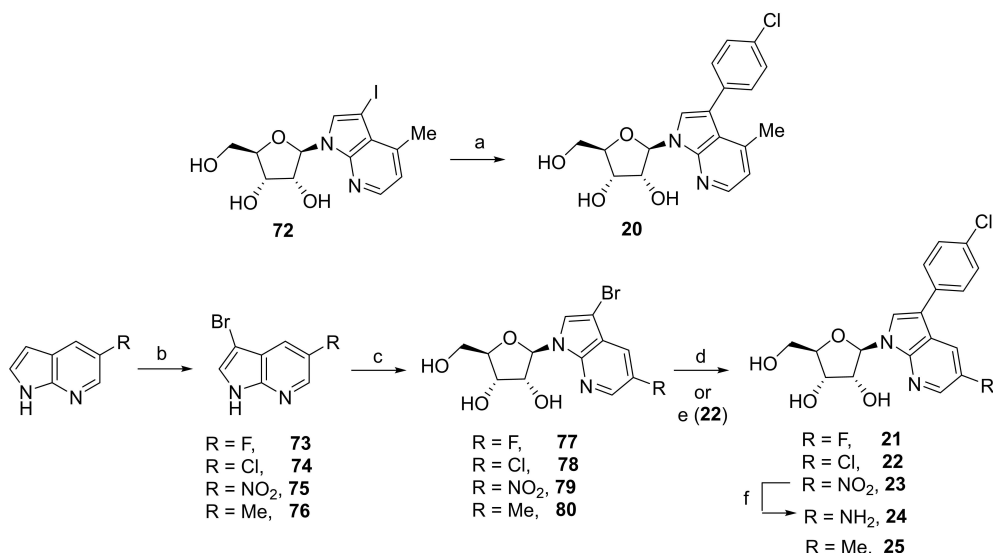
Scheme 4. Reagents and conditions: (a) (4-chlorophenyl)boronic acid, Pd(OAc)$_2$, TPPTS, Na$_2$CO$_3$, MeCN/water (1:2 ratio), 100 °C, 61%; (b) NBS, DMF, 95% (**73**), 92% (**74**), 84% (**75**), 81% (**76**); (c) (i) 1-O-acetyl-2,3,5-tri-O-benzoyl-β-ᴅ-ribofuranose, BSA, TMSOTf, MeCN, 80 °C; (ii) 7 N NH$_3$/MeOH, r.t., 24% (**77**), 32% (**78**), 79% (**79**), 61% (**80**) for two steps; (d) (4-chlorophenyl)boronic acid, Pd(OAc)$_2$, TPPTS, Na$_2$CO$_3$, MeCN/water (1:2 ratio), 100 °C, 13% (**21**), 15% (**23**), 14% (**25**); (e) Pd (PPh$_3$)$_4$, K$_2$CO$_3$, 1,4-dioxane/water (1:1 ratio), 100 °C, 24% (**22**); (f) Pt/C, H$_2$, MeOH, 68%.
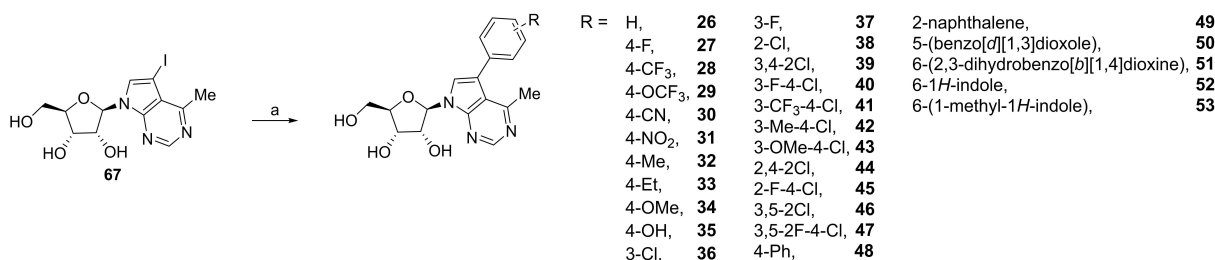
Scheme 5. Reagents and conditions: (a) arylboronic acid, Pd(OAc)$_2$, TPPTS, Na$_2$CO$_3$, MeCN/water (1:2 ratio), 100 °C, 21%–77%.
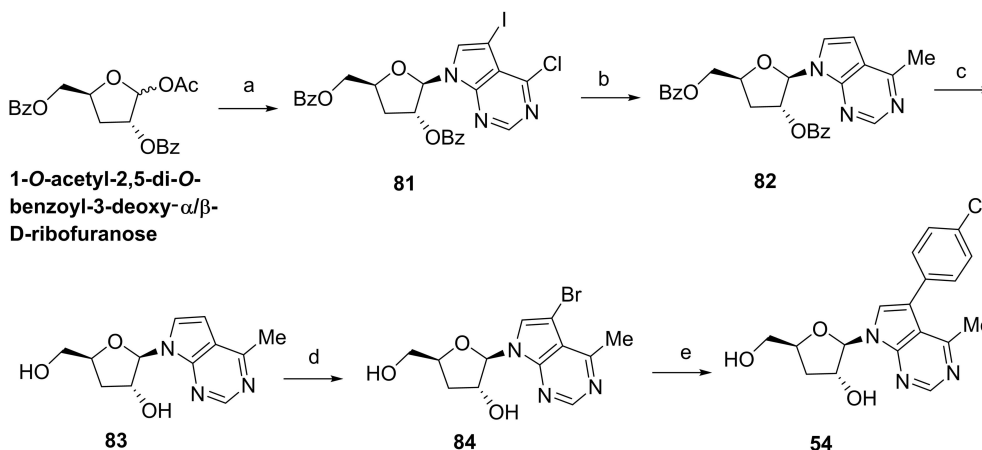
Scheme 6. Reagents and conditions: (a) 1-O-acetyl-2,3,5-tri-O-benzoyl-α/β-ᴅ-ribofuranose, BSA, TMSOTf, MeCN, 80 °C, 74%; (b) (i) iPrMgCl·LiCl, THF, −10 °C; (ii) 0.5 M aq. HCl, 0 °C; (ii) Me$_3$Al, Pd(PPh$_3$)$_4$, THF, 100 °C, 66% for three steps; (c) 0.1 M NaOMe/MeOH, 83%; (d) NBS, DMF, 50 °C, 73%; (e) 4-chlorophenylboronic acid, Pd(OAc)$_2$, TPPTS, Na$_2$CO$_3$, MeCN/water (1:2 ratio), 100 °C, 36%.

rated the cardiac 2-D assays, demonstrating lack of cardiotoxicity and similar antiparasitic effect of **14** as compared to the reference drug. The use of cardiac spheroids represents a very promising approach since 3-D cultures more closely reproduce

ChemMedChem

Full Papers
doi.org/10.1002/cmdc.202100144

Chemistry
Europe
European Chemical
Societies Publishing

the cellular microenvironments in *in vivo* systems and has gained great interest in drug discovery programs due to its cost-effectiveness.[46] Our *in vivo* data endorsed the use of 3-D cardiac cells as a sensitive *in vitro* model for drug evaluation of novel trypanosomicidal agents as reported.[45]

Following confirmation of metabolic stability *in vitro*, compound **14** was evaluated in a mouse model of acute experimental CD. At the highest dose (25 mg/kg p.o. b.i.d. for 5 days), it elicited comparable peak parasitemia reduction as the positive control BZ, and treated animals were protected from infection-caused mortality. Unfortunately, at 34 dpi, none of the surviving animals showed negative parasitemia evaluated by light microscopy. qPCR analysis at the endpoint showed that treatment with BZ at 100 mg/kg and **14** at 25 mg/kg resulted in similar blood parasite loads, demonstrating comparable efficacies under the tested treatment regimens. However, as already noticed using other nucleoside analogues,[25] a lack of activity was found when **14** was assayed against bloodstream trypomastigotes which may explain at least in part, the failure of sterile cure. As a new drug should be active against a heterogeneity of intracellular multiplicative amastigotes, non-replicative trypomastigotes and dormant forms,[44] we hoped that introducing additional modifications may have led to highly potent antitrypanosomal agents to be further evaluated in pre-clinical studies.

Experimental Section

Chemistry

All commercially available reagents and solvents were purchased in an analytical grade without further purification. All reactions were monitored under TLC analysis or HRMS or analytical LC–MS. Precoated F254 aluminium plates from Macherey-Nagel® were used and visualized by UC for TLC analysis. For analytical LC-MS, the conditions were that: a C18 column (2.7 mm, 100×4.6 mm) from Waters Cortecs; a gradient system consisting of 0.2% formic acid in H_2O (v/v)/MeCN; a gradient from 95:5 to 0:100 in 10 min with a flow rate of 1.44 mL/min. All purification was completed via silica gel column chromatography or preparative RP-HPLC. The 60 M silica gel (40–63 μm) from Macherey-Nagel® or an automated flash unit (Reveleris X2) from Grace/Büchi® with prepacked silica columns were used for silica gel column chromatography. For preparative RP-HPLC, the conditions were that: a Luna Omega Polar column (5 μm, 250×21 mm) from Phenomenex®; a gradient system consisting of 0.2% formic acid in H_2O (v/v)/ MeCN; a flow rate of 20 mL/min. a Waters AutoPurification system was applied in both of analytical LC–MS and preparative RP-HPLC, equipped with ACQUITY QDa (mass; 100–1000 amu) and 2998 Photodiode Array (220–400 nm). A LCT Premier XE time-of-flight (ToF) mass spectrometer from Waters was applied in exact mass measurements, equipped with a standard electrospray (ESI) and modular interface from Lockspray®. A 300 MHz spectrometer from Varian Mercury or a 400 MHz spectrometer from Bruker Avance Neo was used for NMR spectra. ^1H-^1H 2D NOESY and ^1H-^{13}C gHMBC were used respectively to ascertain the stereochemistry at C-1'. A Büchi-545 apparatus (uncorrected) was used for melting points measurements. Purity of final compounds was measured through integration of UV signal (total UV chromatogram and wavelength selected at 254 nm) in analytical LC-MS. Purity of all target compounds was at least 95%.

Nucleoside analogue **2**, **10** were prepared as described previously.[27,47]

In this section, the IUPAC nomenclature and numbering were applied in the pyrrolo[2,3-*d*]pyrimidine system, differing with the purine numbering in the body of the text.

General procedure A for Suzuki coupling reaction (as described in reference[24–25,48])

Iodo-derivative or **bromo-derivative** (1 eq.), boronic acid (1.5 eq.), Pd(OAc)$_2$ (0.05 eq.), TPPTS (0.15 eq.) and Na$_2$CO$_3$ (9 eq.) were added to a 10 mL round-bottom flask, equipped with a stir bar. Then, the flask was purged with argon thrice after removal of the air *in vacuo*. A mixture of MeCN/water (1/2 ratio, 6 mL/mmol SM) was added into the mixture via syringes. The reaction mixture was stirred at ambient temperature for 5 min, and then heated at 100 °C. When the consumption of SM was observed by HRMS (~1 to 2 h), the reaction was cooled to ambient temperature. Then, 0.5 M aq. HCl was added to neutralize the mixture. The solution was evaporated *in vacuo*, and the residue resuspended in MeOH and evaporated three times. Then the residue was adsorbed onto Celite® (from MeOH) and eluted over a short silica pad (~5 cm) with 20% MeOH/DCM. The resulting solution was evaporated till dryness and purified by column chromatography (MeOH/DCM gradient).

4-Methylamino-5-iodo-N7-(β-D–ribofuranosyl)-7*H*-pyrrolo[2,3-*d*]-pyrimidine (56[23]**).** **55**[23] (600 mg, 0.83 mmol) was dissolved in 1,4-dioxane (1 mL) and stirred in a 10 mL pressure tube. Methylamine solution (40% W/V solution in water, 5 mL) was added and then the reaction mixture was stirred at 100 °C overnight. After cooling to room temperature, the reaction mixture was evaporated till dryness, and purified by flash column chromatography (0→20% MeOH/DCM) to afford **56** (273 mg, 0.67 mmol) as a yellow foam in 82% yield. ^1H NMR (300 MHz, DMSO-d_6) δ: 3.03 (d, J=4.7 Hz, 3 H, NHCH_3), 3.49–3.56 (m, 1 H, H-5''), 3.58–3.65 (m, 1 H, H-5'), 3.88 (q, J=3.5 Hz, 1 H, H-4'), 4.06 (q, J=4.2 Hz, 1 H, H-3'), 4.35 (q, J=6.1 Hz, 1 H, H-2'), 5.10–5.16 (m, 2 H, OH-5' and OH-3'), 5.30 (d, J=6.2 Hz, 1 H, OH-2'), 6.03 (d, J=6.2 Hz, 1 H, H-1'), 6.44 (q, J=4.4 Hz, 1 H, NH), 7.65 (s, 1 H, H-6), 8.19 (s, 1 H, H-2). HRMS (ESI): calculated for $C_{12}H_{16}IN_4O_4$ ([M+H]$^+$): 407.0211, found: 407.0230.

4-Dimethylamino-5-iodo-N7-(β-D–ribofuranosyl)-7*H*-pyrrolo[2,3-*d*]-pyrimidine (57[23]**).** **55**[23] (600 mg, 0.83 mmol) was dissolved in 1,4-dioxane (1 mL) and stirred in a 10 mL pressure tube. Dimethylamine solution (40% W/V solution in water, 5 mL) was added and then the reaction mixture was stirred at 100 °C overnight. After cooling to room temperature, the reaction mixture was evaporated till dryness, and purified by flash column chromatography (0→20% MeOH/DCM) to afford **57** (250 mg, 0.60 mmol) as a yellow foam in 72% yield. ^1H NMR (300 MHz, DMSO-d_6) δ: 3.16 (s, 6 H, 2CH_3), 3.52–3.56 (m, 1 H, H-5''), 3.60–3.64 (m, 1 H, H-5'), 3.89 (q, J=3.5 Hz, 1 H, H-4'), 4.06–4.08 (m, 1 H, H-3'), 4.36 (t, J=5.3 Hz, 1 H, H-2'), 5.12 (br. s., 2 H, OH-5' and OH-3'), 5.32 (br. s., 1 H, OH-2'), 6.11 (d, J=6.1 Hz, 1 H, H-1'), 7.86 (s, 1 H, H-6), 8.24 (s, 1 H, H-2).). HRMS (ESI): calculated for $C_{13}H_{18}IN_4O_4$ ([M+H]$^+$): 421.0367, found: 421.0346.

4-Methoxy-5-iodo-N7-(β-D–ribofuranosyl)-7*H*-pyrrolo[2,3-*d*]-pyri-midine (58[23]**).** **55**[23] (600 mg, 0.83 mmol) was dissolved in 0.5 M NaOMe in MeOH (10 mL) and the reaction mixture was stirred at 50 °C for 3 h. Then, the reaction was cooled to room temperature. Then, 0.5 M aq. HCl solution was added to neutralize the reaction solution. The resulting mixture was evaporated till dryness, and purified by flash column chromatography (0→10% MeOH/DCM) to afford **58** (230 mg, 0.56 mmol) as a white solid in 68% yield. ^1H NMR (400 MHz, DMSO-d_6) δ: 3.53–3.57 (m, 1 H, H-5''), 3.62–3.66 (m, 1 H, H-5'), 3.91 (dd, J=3.0, 1.9 Hz, 1 H, H-4'), 4.06–4.09 (m, 4 H, H-3'

ChemMedChem

Full Papers
doi.org/10.1002/cmdc.202100144

Chemistry
Europe
European Chemical
Societies Publishing

and OCH$_3$), 4.35–4.38 (m, 1 H, H-2′), 5.07–5.09 (m, 1 H, OH-5′), 5.15 (br. s., 1 H, OH-3′), 5.36 (d, $J = 5.4$ Hz, 1 H, OH-2′), 6.13 (dd, $J = 6.2$, 1.8 Hz, 1 H, H-1′), 7.88 (d, $J = 2.0$ Hz, 1 H, H-6), 8.44 (d, $J = 2.1$ Hz, 1 H, H-2). HRMS (ESI): calculated for C$_{12}$H$_{15}$IN$_3$O$_5$ ([M + H]$^+$): 408.0051, found: 408.0063.

4-Ethoxy-5-iodo-N7-(β-D–ribofuranosyl)-7H-pyrrolo[2,3-d]-pyrimidine (59). 55[23] (300 mg, 0.41 mmol) was dissolved in 0.5 M NaOEt in EtOH (10 mL) and the reaction mixture was stirred at 50 °C for 3 h. Then, the reaction was cooled to room temperature. Then, 0.5 M aq. HCl solution was added to neutralize the reaction solution. The resulting mixture was evaporated till dryness, and purified by flash column chromatography (0→10% MeOH/DCM) to afford **59** (88 mg, 0.21 mmol) as a white solid in 51% yield. ^{1}H NMR (300 MHz, DMSO-d_6) δ: 1.40 (t, $J = 7.2$ Hz, 3 H, CH$_3$), 3.54 (ddd, $J = 12.0$, 5.6, 4.0 Hz, 1 H, H-5″), 3.63 (ddd, $J = 12.0$, 5.4, 4.0 Hz, 1 H, H-5′), 3.90 (q, $J = 3.5$ Hz, 1 H, H-4′), 4.08 (td, $J = 4.8$, 3.2 Hz, 1 H, H-3′), 4.34–4.40 (m, 1 H, H-2′), 4.53 (q, $J = 7.0$ Hz, 2 H, CH$_2$), 5.08 (t, $J = 5.6$ Hz, 1 H, OH-5′), 5.15 (d, $J = 4.7$ Hz, 1 H, OH-3′), 5.35 (d, $J = 6.2$ Hz, 1 H, OH-2′), 6.12 (d, $J = 6.2$ Hz, 1 H, H-1′), 7.86 (s, 1 H, H-6), 8.41 (s, 1 H, H-2). HRMS (ESI): calculated for C$_{13}$H$_{17}$IN$_3$O$_5$ ([M + H]$^+$): 422.0207, found: 422.0199.

4-Methylsulfanyl-5-iodo-N7-(β-D–ribofuranosyl)-7H-pyrrolo[2,3-d]-pyrimidine (60[23]). 55[23] (600 mg, 0.83 mmol) and sodium thiomethoxide (126 mg, 1.83 mmol, 2.2 eq.) was added in EtOH (10 mL) and the reaction mixture was stirred at ambient temperature for 4 h. Then, the resulting mixture was evaporated till dryness, and purified by flash column chromatography (0→10% MeOH/DCM) to afford **60** (273 mg, 0.66 mmol) as a white solid in 79% yield. ^{1}H NMR (300 MHz, DMSO-d_6) δ: 2.64 (s, 3 H, CH$_3$), 3.51–3.58 (m, 1 H, H-5″), 3.60–3.67 (m, 1 H, H-5′), 3.91 (q, $J = 3.5$ Hz, 1 H, H-4′), 4.36 (q, $J = 5.9$ Hz, 1 H, H-3′), 5.07 (t, $J = 5.4$ Hz, 1 H, H-2′), 5.16 (d, $J = 5.0$ Hz, 1 H, OH-5′), 5.37 (d, $J = 6.4$ Hz, 1 H, OH-3′), 6.15 (d, $J = 6.2$ Hz, 1 H, OH-2′), 7.99 (s, 1 H), 8.62 (s, 1 H). HRMS (ESI): calculated for C$_{12}$H$_{15}$IN$_3$O$_4$S ([M + H]$^+$): 423.9822, found: 423.9809.

4-Methylamino-5-(4-chloro-phenyl)-N7-(β-D–ribofuranosyl)-7H-pyrrolo[2,3-d]-pyrimidine (7). 7 was prepared according to General procedure A. **56** (210 mg, 0.52 mmol) gave rise to **7** (80 mg, 0.077 mmol) as a white solid in 13% yield. Melting point: 122 °C. ^{1}H NMR (300 MHz, DMSO-d_6) δ: 2.91 (d, $J = 4.7$ Hz, 3 H, CH$_3$), 3.43–3.57 (m, 1 H, H-5″), 3.58–3.71 (m, 1 H, H-5′), 3.90 (q, $J = 3.5$ Hz, 1 H, H-4′), 4.03–4.19 (m, 1 H, H-3′), 4.45 (t, $J = 5.6$ Hz, 1 H, H-2′), 5.17 (br. s., 2 H, OH-5′ and OH-3′), 5.32 (br. s., 1 H, OH-2′), 5.74 (q, $J = 4.6$ Hz, 1 H, HN), 6.12 (d, $J = 6.2$ Hz, 1 H, H-1′), 7.38–7.49 (m, 2 H, H–Ph, 7.49–7.60 (m, 3 H, H–Ph and H-6), 8.24 (s, 1 H, H-2). ^{13}C NMR (75 MHz, DMSO-d_6) δ: 28.0 (CH$_3$), 61.6 (C-5′), 70.6 (C-3′), 73.8 (C-2′), 85.1 (C-4′), 87.0 (C-1′), 100.5 (C-4a), 115.0 (C-5), 121.3 (C-6), 128.9 (2 C, C-3$_{Ph}$ and C-5$_{Ph}$), 130.0 (2 C, C-2$_{Ph}$ and C-6$_{Ph}$), 131.4 (C-4$_{Ph}$), 133.3 (C-1$_{Ph}$), 150.2 (C-7a), 151.6 (C-2), 156.8 (C-4). HRMS (ESI): calculated for C$_{18}$H$_{20}$ClN$_4$O$_4$ ([M + H]$^+$): 391.1168, found: 391.1159.

4-Dimethylamino-5-(4-chloro-phenyl)-N7-(β-D–ribofuranosyl)-7H-pyrrolo[2,3-d]-pyrimidine (8). 8 was prepared according to General procedure A. **57** (250 mg, 0.59 mmol) gave rise to **8** (30 mg, 0.20 mmol) as a white solid in 39% yield. Melting point: 75 °C. ^{1}H NMR (300 MHz, DMSO-d_6) δ: 2.75 (s, 6 H, 2CH$_3$), 3.48–3.57 (m, 1 H, H-5″), 3.58–3.70 (m, 1 H, H-5′), 3.90 (q, $J = 3.5$ Hz, 1 H, H-4′), 4.06–4.15 (m, 1 H, H-3′), 4.46 (q, $J = 6.0″$ Hz, 1 H, H-2′), 5.04–5.19 (m, 2 H, OH-5′ and OH-3′), 5.33 (d, $J = 6.4$ Hz, 1 H, OH-2′), 6.18 (d, $J = 6.2$ Hz, 1 H, H-1′), 7.36–7.56 (m, 4 H, H–Ph), 7.71 (s, 1 H, H-6), 8.29 (s, 1 H, H-2). ^{13}C NMR (75 MHz, DMSO-d_6) δ: 40.7 (2 C, CH$_3$), 61.6 (C-5′), 70.5 (C-3′), 73.8 (C-2′), 85.1 (C-4′), 86.8 (C-1′), 102.0 (C-4a), 115.7 (C-5), 122.1 (C-6), 128.5 (2 C, C–Ph), 129.7 (2 C, C–Ph), 131.1 (C-4$_{Ph}$), 134.6 (C-1$_{Ph}$), 150.3 (C-2), 152.3 (C-7a), 160.0 (C-4). HRMS (ESI): calculated for C$_{19}$H$_{22}$ClN$_4$O$_4$ ([M + H]$^+$): 405.1324, found: 405.1323.

4-Ethoxy-5-(4-chloro-phenyl)-N7-(β-D–ribofuranosyl)-7H-pyrrolo[2,3-d]-pyrimidine (11). 11 was prepared according to General procedure A. **59** (110 mg, 0.26 mmol) gave rise to **11** (35 mg, 0.086 mmol) as a white solid in 33% yield. Melting point: 138 °C. ^{1}H NMR (300 MHz, DMSO-d_6) δ: 1.36 (t, $J = 7.0$ Hz, 3 H, CH$_3$), 3.56 (ddd, $J = 11.9$, 5.8, 4.2 Hz, 1 H, H-5″), 3.66 (ddd, $J = 12.0$, 5.2, 4.2 Hz, 1 H, H-5′), 3.93 (q, $J = 4.0$ Hz, 1 H, H-4′), 4.08–4.20 (m, 1 H, H-3′), 4.41–4.57 (m, 3 H, H-2′ and CH$_2$), 5.08 (t, $J = 5.6$ Hz, 1 H, OH-5′), 5.16 (d, $J = 5.0$ Hz, 1 H, OH-3′), 5.37 (d, $J = 6.4$ Hz, 1 H, OH-2′), 6.22 (d, $J = 6.2$ Hz, 1 H, H-1′), 7.40–7.52 (m, 2 H, H–Ph), 7.67–7.79 (m, 2 H, H–Ph), 7.93 (s, 1 H, H-6), 8.45 (s, 1 H, H-2). ^{13}C NMR (75 MHz, DMSO-d_6) δ: 14.2 (CH$_3$), 61.5 (C-5′), 62.2 (CH$_2$), 70.4 (C-3′), 74.0 (C-2′), 85.2 (C-4′), 86.9 (C-1′), 102.6 (C-4a), 115.1 (C-5), 122.9 (C-6), 128.0 (2 C, C-3$_{Ph}$ and C-5$_{Ph}$), 130.2 (2 C, C-2$_{Ph}$ and C-6$_{Ph}$), 131.1 (C-4$_{Ph}$), 132.5 (C-1$_{Ph}$), 150.9 (C-2), 152.7 (C-7a), 162.2 (C-4). HRMS (ESI): calculated for C$_{19}$H$_{21}$ClN$_3$O$_5$ ([M + H]$^+$): 406.1144, found: 406.1156.

4-Oxo-5-(4-chloro-phenyl)-N7-(β-D–ribofuranosyl)-7H-pyrrolo[2,3-d]-pyrimidine (9). 10 (70 mg, 0.18 mmol) and NaI (135 mg, 0.90 mmol, 5 eq.) were placed in anhydrous MeCN (5 mL). Next, TMSCl (114 μL, 0.90 mmol, 5 eq.) was slowly added into the reaction mixture, and the mixture was stirred at ambient temperature for 2 h. The precipitate was filtered, washed with MeCN, and dissolved in water. Then, aq. sat. NaHCO$_3$ was added to neutralize the solution. The mixture was evaporated till dryness, and purified by flash column chromatography (0→20% MeOH/DCM) to afford **9** (50 mg, 0.13 mmol) as a white solid in 74% yield. Melting point: 75 °C. ^{1}H NMR (300 MHz, DMSO-d_6) δ: 3.55 (ddd, $J = 11.8$, 5.6, 4.2 Hz, 1 H, H-5″), 3.65 (ddd, $J = 12.0$, 5.4, 4.0 Hz, 1 H, H-5′), 3.90 (q, $J = 3.8$ Hz, 1 H, H-4′), 4.07–4.16 (m, 1 H, H-3′), 4.38 (q, $J = 6.0$ Hz, 1 H, H-2′), 5.04 (t, $J = 5.6$ Hz, 1 H, OH-5′), 5.14 (d, $J = 5.0$ Hz, 1 H, OH-3′), 5.36 (d, $J = 6.2$ Hz, 1 H, OH-2′), 6.10 (d, $J = 6.2$ Hz, 1 H, H-1′), 7.38–7.41 (m, 1 H, H–Ph), 7.41–7.45 (m, 1 H, H–Ph), 7.78 (s, 1 H, H-6), 7.95–7.98 (m, 2 H, H–Ph and H-2), 7.98–8.02 (m, 1 H, H–Ph), 12.10 (br. s., 1 H, NH). ^{13}C NMR (75 MHz, DMSO-d_6) δ: 61.4 (C-5′), 70.4 (C-3′), 74.1 (C-2′), 85.1 (C-4′), 86.8 (C-1′), 105.0 (C-4a), 119.0 (C-5), 119.2 (C-6), 127.9 (2 C, C-3$_{Ph}$ and C-5$_{Ph}$), 129.6 (2 C, C-2$_{Ph}$ and C-6$_{Ph}$), 130.7 (C-4$_{Ph}$), 132.5 (C-1$_{Ph}$), 144.3 (C-2), 149.0 (C-7a), 158.4 (C-4). HRMS (ESI): calculated for C$_{17}$H$_{17}$ClN$_3$O$_5$ ([M + H]$^+$): 378.0851, found: 378.0840.

4-Methylsulfanyl-5-(4-chloro-phenyl)-N7-(β-D–ribofuranosyl)-7H-pyrrolo[2,3-d]-pyrimidine (12). 12 was prepared according to General procedure A. **60** (260 mg, 0.61 mmol) gave rise to **12** (85 mg, 0.21 mmol) as a white solid in 34% yield. Melting point: 209 °C. ^{1}H NMR (300 MHz, DMSO-d_6) δ: 2.55 (s, 3 H, CH$_3$), 3.55 (ddd, $J = 12.0$, 5.6, 4.0 Hz, 1 H, H-5″), 3.64 (ddd, $J = 12.0$, 5.2, 4.2 Hz, 1 H, H-5′), 3.93 (q, $J = 3.8$ Hz, 1 H, H-4′), 4.05–4.21 (m, 1 H, H-3′), 4.45 (q, $J = 5.8$ Hz, 1 H, H-2′), 5.04 (t, $J = 5.6$ Hz, 1 H, OH-5′), 5.17 (d, $J = 5.0$ Hz, 1 H, OH-3′), 5.39 (d, $J = 6.2$ Hz, 1 H, OH-2′), 6.25 (d, $J = 6.2$ Hz, 1 H, H-1′), 7.40–7.57 (m, 4 H, H–Ph), 7.85 (s, 1 H, H-6), 8.68 (s, 1 H, H-2). ^{13}C NMR (75 MHz, DMSO-d_6) δ: 11.9 (CH$_3$), 61.4 (C-5′), 70.5 (C-3′), 74.1 (C-2′), 85.2 (C-4′), 86.7 (C-1′), 114.0 (C-4a), 115.4 (C-5), 124.5 (C-6), 127.9 (2 C, C–Ph), 131.7 (2 C, C–Ph), 132.1 (C-4$_{Ph}$), 132.4 (C-1$_{Ph}$), 148.7 (C-7a), 150.4 (C-2), 161.1 (C-4). HRMS (ESI): calculated for C$_{18}$H$_{19}$ClN$_3$O$_4$S ([M + H]$^+$): 408.0779, found: 408.0795.

2-Amino-4-methoxy-5-(4-chloro-phenyl)-N7-(β-D–ribofuranosyl)-7H-pyrrolo[2,3-d]-pyrimidine (18). 18 was prepared according to General procedure A, except for the use of 90 °C instead of 100 °C. **61** (300 mg, 0.71 mmol) gave rise to **18** (53 mg, 0.13 mmol) as a white solid in 18% yield. Melting point: 202 °C. ^{1}H NMR (300 MHz, DMSO-d_6) δ: 3.44–3.56 (m, 1 H, H-5″), 3.56–3.69 (m, 1 H, H-5′), 3.84 (q, $J = 4.0$ Hz, 1 H, H-4′), 3.91 (s, 3 H, OCH$_3$), 4.02–4.15 (m, 1 H, H-3′), 4.37 (q, $J = 6.0$ Hz, 1 H, H-2′), 5.00 (t, $J = 5.6$ Hz, 1 H, OH-5′), 5.05 (d, $J = 4.4$ Hz, 1 H, OH-3′), 5.26 (d, $J = 6.2$ Hz, 1 H, OH-2′), 6.05 (d, $J = 6.2$ Hz, 1 H, H-1′), 6.32 (br. s., 2 H, NH$_2$), 7.36–7.41 (m, 2 H, H–Ph and H-6), 7.42–7.47 (m, 1 H, H–Ph), 7.59–7.63 (m, 1 H, H–Ph), 7.64–7.68 (m, 1 H, H–Ph). ^{13}C NMR (75 MHz, DMSO-d_6) δ: 53.0 (OCH$_3$), 61.6 (C-

266

ChemMedChem

Full Papers
doi.org/10.1002/cmdc.202100144

Chemistry
Europe
European Chemical
Societies Publishing

5′), 70.5 (C-3′), 73.4 (C-2′), 84.7 (C-4′), 85.8 (C-1′), 95.0 (C-4a), 115.5 (C-5), 118.4 (C-6), 128.0 (2 C, C-3$_{Ph}$ and C-5$_{Ph}$), 129.5 (2 C, C-2$_{Ph}$ and C-6$_{Ph}$), 130.5 (C-4$_{Ph}$), 133.5 (C-1$_{Ph}$), 155.7 (C-7a), 159.4 (C-2), 163.2 (C-4). HRMS (ESI): calculated for $C_{18}H_{20}ClN_4O_5$ ([M+H]$^+$): 407.1117, found: 407.1134.

2-Amino-4-oxo-5-(4-chloro-phenyl)-N7-(β-D–ribofuranosyl)-7H-pyrrolo[2,3-d]-pyrimidine (17). 18 (53 mg, 0.13 mmol) and NaI (98 mg, 0.65 mmol, 5 eq.) were placed in anhydrous MeCN (5 mL). Next, TMSCl (82 μL, 0.65 mmol, 5 eq.) was slowly added into the reaction mixture, and the mixture was stirred at ambient temperature for 2 h. The precipitate was filtered, washed with MeCN, and dissolved in water. Then, aq. sat. NaHCO$_3$ was added to neutralize the solution. The mixture was evaporated till dryness, and purified by flash column chromatography (0→20% MeOH/DCM) to afford 17 (35 mg, 0.089 mmol) as a white solid in 68% yield. Melting point: 249 °C. ^{1}H NMR (300 MHz, DMSO-d_6) δ: 3.45–3.55 (m, 1 H, H-5″), 3.56–3.68 (m, 1 H, H-5′), 3.82 (q, J=4.1 Hz, 1 H, H-4′), 4.00–4.12 (m, 1 H, H-3′), 4.31 (q, J=6.2 Hz, 1 H, H-2′), 4.97 (t, J=5.6 Hz, 1 H, OH-5′), 5.04 (d, J=4.4 Hz, 1 H, OH-3′), 5.26 (d, J=6.2 Hz, 1 H, OH-2′), 5.94 (d, J=6.2 Hz, 1 H, H-1′), 6.32 (br. s, 2 H, NH$_2$), 7.32–7.35 (m, 1 H, H–Ph), 7.35–7.37 (m, 1 H, H–Ph), 7.38 (s, 1 H, H-6), 7.96–8.00 (m, 1 H, H–Ph), 8.00–8.03 (m, 1 H, H–Ph), 10.48 (s, 1 H, NH). ^{13}C NMR (75 MHz, DMSO-d_6) δ: 61.6 (C-5′), 70.4 (C-3′), 73.5 (C-2′), 84.6 (C-4′), 85.8 (C-1′), 97.2 (C-4a), 115.8 (C-6), 118.7 (C-5), 127.8 (2 C, C-3$_{Ph}$ and C-5$_{Ph}$), 129.1 (2 C, C-2$_{Ph}$ and C-6$_{Ph}$), 130.1 (C-4$_{Ph}$), 133.2 (C-1$_{Ph}$), 152.6 (C-7a), 152.7 (C-2), 158.8 (C-4). HRMS (ESI): calculated for $C_{17}H_{18}ClN_4O_5$ ([M+H]$^+$): 393.0960, found: 393.0976.

N7-(β-D–ribofuranosyl)-7H-pyrrolo[2,3-d]-pyrimidine (63). 62[23,49] (200 mg, 0.33 mmol) was dissolved in MeOH (5 mL), and solid K$_2$CO$_3$ (91 mg, 0.66 mmol, 2 eq.) was added. The flask was purged with N$_2$, and a cat. amount of Pd(OH)$_2$/C was added. Then, the N$_2$ gas was exchanged with H$_2$ (balloon; bubbling). The reaction mixture was stirred at room temperature until HRMS showed full consumption of the SM (2 h). Then, the H$_2$ balloon was removed and K$_2$CO$_3$ (136 mg, 0.99 mmol, 3 eq.) was added, and the resulting mixture stirred at ambient temperature until all benzoyl groups of the SM were removed (3 h). 0.5 M aq. HCl solution was added to neutralize the mixture, after which the solution was filtered over Celite®. The filtrate was evaporated till dryness and purified by column chromatography (0→10% MeOH/DCM) to afford 63 (70 mg, 0.28 mmol) as a white solid in 84% yield. ^{1}H NMR (300 MHz, DMSO-d_6) δ: 3.55 (ddd, J=12.0, 5.6, 4.0 Hz, 1 H, H-5″), 3.64 (ddd, J=12.0, 5.4, 4.2 Hz, 1 H, H-5′), 3.93 (q, J=3.7 Hz, 1 H, H-4′), 4.10–4.15 (m, 1 H, H-3′), 4.41–4.47 (m, 1 H, H-2′), 5.06 (t, J=5.4 Hz, 1 H, OH-5′), 5.17 (d, J=5.0 Hz, 1 H, OH-3′), 5.36 (d, J=6.4 Hz, 1 H, OH-2′), 6.22 (d, J=6.2 Hz, 1 H, H-1′), 6.71 (d, J=3.8 Hz, 1 H, H-5), 7.87 (d, J=3.8 Hz, 1 H, H-6), 8.80 (s, 1 H, H-2), 9.03 (s, 1 H, H-4). HRMS (ESI): calculated for $C_{11}H_{14}N_3O_4$ ([M+H]$^+$): 252.0979, found: 252.0970.

5-Iodo-N7-(β-D–ribofuranosyl)-7H-pyrrolo[2,3-d]-pyrimidine (64). 63 (470 mg, 1.87 mmol) was dissolved in DMF (5 mL), and NIS (631 mg, 2.81 mmol, 1.5 eq.) was added. The resulting mixture was stirred at 50 °C for 2 h. Then, the mixture was evaporated till dryness and purified by column chromatography (0→10% MeOH/DCM) to afford 64 (270 mg, 0.71 mmol) as a white solid in 38% yield. ^{1}H NMR (400 MHz, DMSO-d_6) δ: 3.53–3.58 (m, 1 H, H-5″), 3.62–3.67 (m, 1 H, H-5′), 3.93 (q, J=3.6 Hz, 1 H, H-4′), 4.11 (q, J=4.2 Hz, 1 H, H-3′), 4.42 (q, J=5.8 Hz, 1 H, H-2′), 5.08 (t, J=5.4 Hz, 1 H, OH-5′), 5.18 (d, J=4.8 Hz, 1 H, OH-3′), 5.40 (d, J=6.4 Hz, 1 H, OH-2′), 6.21 (d, J=6.3 Hz, 1 H, H-1′), 8.12 (s, 1 H, H-6), 8.77 (s, 1 H, H-2), 8.87 (s, 1 H, H-4). HRMS (ESI): calculated for $C_{11}H_{13}IN_3O_4$ ([M+H]$^+$): 377.9945, found: 377.9954.

5-(4-Chloro-phenyl)-N7-(β-D–ribofuranosyl)-7H-pyrrolo[2,3-d]-pyrimidine (13). 13 was prepared according to General procedure A. 64 (260 mg, 0.69 mmol) gave rise to 13 (80 mg, 0.22 mmol) as a

grey solid in 32% yield. Melting point: 65 °C. ^{1}H NMR (300 MHz, DMSO-d_6) δ: 3.58 (ddd, J=11.8, 5.8, 4.4 Hz, 1 H, H-5″), 3.68 (ddd, J=12.0, 5.4, 4.2 Hz, 1 H, H-5′), 3.95 (q, J=4.0 Hz, 1 H, H-4′), 4.09–4.22 (m, 1 H, H-3′), 4.51 (q, J=6.0 Hz, 1 H, H-2′), 5.08 (t, J=5.6 Hz, 1 H, OH-5′), 5.20 (d, J=5.0 Hz, 1 H, OH-3′), 5.42 (d, J=6.2 Hz, 1 H, OH-2′), 6.28 (d, J=5.9 Hz, 1 H, H-1′), 7.41–7.58 (m, 2 H, H–Ph), 7.74–7.92 (m, 2 H, H–Ph), 8.31 (s, 1 H, H-6), 8.89 (s, 1 H, H-2), 9.38 (s, 1 H, H-4). ^{13}C NMR (75 MHz, DMSO-d_6) δ: 61.5 (C-5′), 70.5 (C-3′), 73.9 (C-2′), 85.3 (C-4′), 86.5 (C-1′), 114.0 (C-5), 116.7 (C-4a), 124.9 (C-6), 128.2 (2 C, C-2$_{Ph}$ and C-6$_{Ph}$), 129.0 (2 C, C-3$_{Ph}$ and C-5$_{Ph}$), 131.2 (C-4$_{Ph}$), 132.0 (C-1$_{Ph}$), 149.1 (C-4), 151.3 (C-2), 151.5 (C-7a). HRMS (ESI): calculated for $C_{17}H_{17}ClN_3O_4$ ([M+H]$^+$): 362.0902, found: 362.0922.

4-Methyl-N7-(2′,3′,5′-tri-O-benzoyl-β-D–ribofuranosyl)-7H-pyrrolo[2,3-d]-pyrimidine (65). 62[23,49] (9.27 g, 15.5 mmol) and Pd(PPh$_3$)$_4$ (358 mg, 0.31 mmol, 0.02 eq.) were placed into a 250 mL round bottom flask. The flask was purged with argon thrice after removal of the air in vacuo. Next, anhydrous THF (62 mL, 4 mL/mmol) was added via syringe, and AlMe$_3$ solution (2 M in toluene, 9.3 mL, 18.6 mmol, 1.2 eq.) was added dropwise. After the mixture was stirred for 15 min at ambient temperature, the reaction was refluxed at 100 °C until TLC analysis showed the SM was consumed completely (1 h). After cooling in an ice-water bath, 0.5 M aq. HCl (10 mL) was added dropwise and slowly. [**Caution**: methane gas was generated, with potential excessive foaming]. Next, EA (50 mL) was added. The layers were separated and the water layer extracted twice more with EA. Then, the organic layers were combined, dried over Na$_2$SO$_4$, filtered, and evaporated. The residue was purified by column chromatography (10→50% EA/PET) to give 65 (7.7 g, 13.3 mmol) as a yellow foam in 86% yield. ^{1}H NMR (400 MHz, CDCl$_3$) δ: 2.71 (s, 3 H, CH$_3$), 4.65–4.71 (m, 1 H, H-5″), 4.76–4.80 (m, 1 H, H-4′), 4.84–4.89 (m, 1 H, H-5′), 6.16 (dd, J=5.9, 4.4 Hz, 1 H, H-3′), 6.22–6.26 (m, 1 H, H-2′), 6.57 (d, J=3.8 Hz, 1 H, H-1′), 6.73 (d, J=5.9 Hz, 1 H, H-5), 7.31–7.63 (m, 10 H, H-6 and H-OBz), 7.91–7.94 (m, 2 H, H-OBz), 7.98–8.02 (m, 2 H, H-OBz), 8.11–8.14 (m, 2 H, H-OBz), 8.76 (s, 1 H, H-2). HRMS (ESI): calculated for $C_{33}H_{28}N_3O_7$ ([M+H]$^+$): 578.1922, found: 578.1924.

4-Methyl-5-iodo-N7-(β-D–ribofuranosyl)-7H-pyrrolo[2,3-d]-pyrimidine (67).[23] 65 (10 g, 17.3 mmol) was dissolved in anhydrous DMF (120 mL), and NIS (4.67 g, 20.8 mmol, 1.2 eq.) was added. Then, the reaction mixture was stirred at ambient temperature overnight. EA (200 mL) and water (200 mL) were added. The layers were separated and the water layer extracted once more with EA. The organic layers were combined and washed with brine (200 mL), dried over Na$_2$SO$_4$, filtered, and evaporated. The residue was purified by column chromatography (5→30% EA/PET) to give a yellow oil (10.0 g, 14.2 mmol) in 82% yield. This obtained product (4 g, 5.68 mmol) was charged in a 250 mL round bottom flask, and NH$_3$ in MeOH (7 N, 20 mL) was added. The mixture was stirred at ambient temperature overnight. Then, the reaction solution was evaporated till dryness, purified by column chromatography (0→10% MeOH/DCM) to afford 67 (1.95 g, 4.98 mmol) as a slight yellow solid in 88% yield. ^{1}H NMR (400 MHz, DMSO-d_6) δ: 2.89 (s, 3 H, CH$_3$), 3.52–3.58 (m, 1 H, H-5″), 3.61–3.66 (m, 1 H, H-5′), 3.91 (q, J=3.5 Hz, 1 H, H-4′), 4.09 (q, J=4.1 Hz, 1 H, H-3′), 4.38 (q, J=6.0 Hz, 1 H, H-2′), 5.08 (t, J=5.38 Hz, 1 H, OH-5′), 5.16 (d, J=4.75 Hz, 1 H, OH-3′), 5.36 (d, J=6.38 Hz, 1 H, OH-2′), 6.18 (d, J=6.25 Hz, 1 H, H-1′), 8.06 (s, 1 H, H-6), 8.67 (s, 1 H, H-2). ^{13}C NMR (100 MHz, DMSO-d_6) δ: 20.5 (CH$_3$), 53.8 (C-5), 61.4 (C-5′), 70.4 (C-3′), 74.1 (C-2′), 85.3 (C-4′), 86.5 (C-1′), 117.8 (C-4a), 131.4 (C-6), 150.0 (C-7a), 150.9 (C-2), 159.5 (C-4). HRMS (ESI): calculated for $C_{12}H_{15}IN_3O_4$ ([M+H]$^+$): 392.0102, found: 392.0105.

4-Methyl-5-(4-chloro-phenyl)-N7-(β-D–ribofuranosyl)-7H-pyrrolo[2,3-d]-pyrimidine (14). 14 was prepared according to General procedure A. 67 (150 mg, 0.38 mmol) gave rise to 14 (90 mg, 0.24 mmol) as a white solid in 63% yield. Melting point: 166 °C. ^{1}H

NMR (400 MHz, DMSO-d_6) δ: 2.46 (s, 3 H, CH$_3$), 3.49–3.59 (m, 1 H, H-5''), 3.59–3.73 (m, 1 H, H-5'), 3.93 (q, J=3.8 Hz, 1 H, H-4'), 4.13 (d, J=3.8 Hz, 1 H, H-3'), 4.46 (dd, J=11.2, 6.0 Hz, 1 H, H-2'), 5.04 (t, J=5.0 Hz, 1 H, OH-5'), 5.17 (d, J=4.4 Hz, 1 H, OH-3'), 5.37 (d, J=6.4 Hz, 1 H, OH-2'), 6.27 (d, J=6.2 Hz, 1 H, H-1'), 7.45–7.58 (m, 4 H, H–Ph), 7.88 (s, 1 H, H-6), 8.70 (s, 1 H, H-2). ^{13}C NMR (100 MHz, DMSO-d_6) δ: 22.9 (CH$_3$), 61.5 (C-5'), 70.5 (C-3'), 74.0 (C-2'), 85.2 (C-4'), 86.6 (C-1'), 115.7 (C-4a), 115.7 (C-5), 125.0 (C-6), 128.2 (2 C, C–Ph), 131.5 (2 C, C–Ph), 132.0 (C-4$_{Ph}$), 133.2 (C-1$_{Ph}$), 150.7 (C-7a), 150.9 (C-2), 159.2 (C-4). HRMS (ESI): calculated for C$_{18}$H$_{19}$ClN$_3$O$_4$ ([M+H]$^+$): 376.1059, found: 376.1068.

4-Ethyl-N7-(2′,3′,5′-tri-O-benzoyl-β-D–ribofuranosyl)-7H-pyrrolo[2,3-d]-pyrimidine (66).[50] **62**[23,49] (700 mg, 1.17 mmol) and Pd-(PPh$_3$)$_4$ (135 mg, 0.12 mmol, 0.1 eq.) was placed into a 50 mL round bottom flask. The flask was purged with argon thrice after removal of the air *in vacuo*. Next, anhydrous THF (5 mL, 4 mL/mmol) was added via syringe, and AlEt$_3$ solution (1 M in hexanes, 1.4 mL, 1.4 mmol, 1.2 eq.) was added dropwise. After the mixture was stirred for 15 min at ambient temperature, the reaction was refluxed at 100 °C until TLC analysis showed the SM was consumed completely (1 h). After cooling in an ice-water bath, 0.5 M aq. HCl (5 mL) was added dropwise and slowly. [**Caution:** methane gas was generated, with potential excessive foaming]. Next, EA (10 mL) was added. The layers were separated and the water layer extracted twice more with EA. Then, the organic layers were combined, dried over Na$_2$SO$_4$, filtered, and evaporated. The residue was purified by column chromatography (10→50% EA/PET) to give **66** (450 mg, 0.76 mmol) as a colorless foam in 65% yield. ^{1}H NMR (400 MHz, CDCl$_3$) δ: 1.38 (t, J=7.6 Hz, 3 H, CH$_3$), 3.02 (q, J=7.6 Hz, 2 H, CH$_2$), 4.68 (dd, J=12.1, 3.9 Hz, 1 H, H-5''), 4.78 (q, J=3.8 Hz, 1 H, H-4'), 4.87 (dd, J=12.1, 3.2 Hz, 1 H, H-5'), 6.14–6.17 (m, 1 H, H-3'), 6.25 (t, J=5.8 Hz, 1 H, H-2'), 6.59 (d, J=3.8 Hz, 1 H, H-1'), 6.75 (d, J=5.9 Hz, 1 H, H-5), 7.26–7.42 (m, 5 H, H-6 and H-OBz), 7.46–7.62 (m, 5 H, H-OBz), 7.93 (d, J=7.4 Hz, 2 H, H-OBz), 8.00 (d, J=7.3 Hz, 2 H, H-OBz), 8.13 (d, J=7.4 Hz, 2 H, H-OBz), 8.79 (s, 1 H, H-2). HRMS (ESI): calculated for C$_{34}$H$_{30}$N$_3$O$_7$ ([M+H]$^+$): 592.2078, found: 592.2067.

4-Ethyl-5-bromo-N7-(β-D–ribofuranosyl)-7H-pyrrolo[2,3-d]-pyrimidine (68). **66** (430 mg, 0.73 mmol) was dissolved in anhydrous DMF (5 mL), and NBS (168 mg, 0.94 mmol, 1.3 eq.) was added. Then, the reaction mixture was stirred at ambient temperature overnight. EA (10 mL) and water (10 mL) were added. The layers were separated and the water layer extracted once more with EA. The organic layers were combined and washed with brine (10 mL), dried over Na$_2$SO$_4$, filtered, and evaporated. The residue was purified by column chromatography (5→30% EA/PET) to give a colorless foam (356 mg, 0.53 mmol) in 73% yield. This obtained product (350 mg, 0.52 mmol) was charged in a 50 mL round bottom flask, and NH$_3$ in MeOH (7 N, 5 mL) was added. The mixture was stirred at ambient temperature overnight. Then, the reaction solution was evaporated till dryness, purified by column chromatography (0→10% MeOH/DCM) to afford **68** (165 mg, 0.46 mmol) as a white solid in 88% yield. ^{1}H NMR (400 MHz, DMSO-d_6) δ: 1.31 (t, J=7.6 Hz, 3 H, CH$_3$), 3.23 (qd, J=7.5, 1.1 Hz, 2 H, CH$_2$), 3.55 (ddd, J=11.8, 5.6, 4.0 Hz, 1 H, H-5''), 3.64 (ddd, J=12.0, 5.2, 4.2 Hz, 1 H, H-5'), 3.92 (q, J=3.8 Hz, 1 H, H-4'), 4.10 (td, J=4.8, 3.3 Hz, 1 H, H-3'), 4.39 (q, J=5.8 Hz, 1 H, H-2'), 5.08 (t, J=5.4 Hz, 1 H, OH-5'), 5.17 (d, J=4.8 Hz, 1 H, OH-3'), 5.39 (d, J=6.4 Hz, 1 H, OH-2'), 6.22 (d, J=6.1 Hz, 1 H, H-1'), 8.06 (s, 1 H, H-6), 8.75 (s, 1 H, H-2). ^{13}C NMR (100 MHz, DMSO-d_6) δ: 13.4 (CH$_3$), 26.7 (CH$_2$), 61.4 (C-5'), 70.5 (C-3'), 74.1 (C-2'), 85.4 (C-4'), 86.4 (C-1'), 87.6 (C-5), 114.6 (C-4a), 126.4 (C-6), 149.8 (C-7a), 151.6 (C-2), 164.0 (C-4). HRMS (ESI): calculated for C$_{13}$H$_{17}$BrN$_3$O$_4$ ([M+H]$^+$): 358.0397, found: 358.0390.

4-Ethyl-5-(4-chloro-phenyl)-N7-(β-D–ribofuranosyl)-7H-pyrrolo[2,3-d]-pyrimidine (15). **15** was prepared according to General procedure A. **68** (100 mg, 0.28 mmol) gave rise to **15** (53 mg,

0.14 mmol) as a white solid in 49% yield. Melting point: 100 °C. ^{1}H NMR (400 MHz, DMSO-d_6) δ: 1.07 (t, J=7.5 Hz, 3 H, CH$_3$), 2.77 (q, J=7.5 Hz, 2 H, CH$_2$), 3.48–3.58 (m, 1 H, H-5''), 3.59–3.70 (m, 1 H, H-5'), 3.93 (q, J=3.8 Hz, 1 H, H-4'), 4.07–4.20 (m, 1 H, H-3'), 4.47 (q, J=6.1 Hz, 1 H, H-2'), 5.04 (t, J=5.4 Hz, 1 H, OH-5'), 5.17 (d, J=4.8 Hz, 1 H, OH-3'), 5.37 (d, J=6.4 Hz, 1 H, OH-2'), 6.27 (d, J=6.3 Hz, 1 H, H-1'), 7.41–7.60 (m, 4 H, H–Ph), 7.86 (s, 1 H, H-6), 8.75 (s, 1 H, H-2).). ^{13}C NMR (100 MHz, DMSO-d_6) δ: 12.3 (CH$_3$), 28.0 (CH$_2$), 61.5 (C-5'), 70.5 (C-3'), 74.0 (C-2'), 85.2 (C-4'), 86.6 (C-1'), 115.0 (C-4a), 115.5 (C-5), 125.2 (C-6), 128.3 (2 C, C–Ph), 131.4 (2 C, C–Ph), 132.1 (C-4$_{Ph}$), 133.5 (C-1$_{Ph}$), 150.8 (C-7a), 151.0 (C-2), 163.8 (C-4). HRMS (ESI): calculated for C$_{19}$H$_{21}$ClN$_3$O$_4$ ([M+H]$^+$): 390.1215, found: 390.1217.

4-Phenyl-7H-pyrrolo[2,3-d]-pyrimidine (69).[50] 4-Chloro-7H-pyrrolo[2,3-d]pyrimidine (300 mg, 1.95 mmol), phenylboronic acid (480 mg, 3.91 mmol, 2 eq.), K$_2$CO$_3$ (808 mg, 5.85 mmol, 3 eq.) and Pd(PPh$_3$)$_4$ (225 mg, 0.20 mmol, 0.1 eq.) were charged to a 25 mL round-bottom flask, equipped with a stir bar. Next, the flask was purged with argon thrice after removal of the air *in vacuo*. Then, toluene (8 ml, 4 mL/mmol SM) was added into the mixture via syringe. The mixture was stirred at ambient temperature for 5 min, and then heated at 100 °C. After the consumption of SM was observed by analytical LC/MS (1 h), the reaction was cooled to ambient temperature. Then, 0.5 M aq. HCl was added to neutralize the mixture. Next, the solution was evaporated *in vacuo*, and the residue was evaporated till dryness and purified by column chromatography (10→50% EA/PET) to give **69** (360 mg, 1.84 mmol) as an orange solid in 95% yield. ^{1}H NMR (300 MHz, DMSO-d_6) δ: 6.89 (dd, J=3.5, 1.8 Hz, 1 H, H-5), 7.54–7.61 (m, 3 H, H–Ph), 7.66 (dd, J=3.5, 2.5 Hz, 1 H, H-6), 8.16–8.19 (m, 2 H, H–Ph), 8.84 (s, 1 H, H-2), 12.26 (br. s., 1 H, NH). HRMS (ESI): calculated for C$_{12}$H$_{10}$N$_3$ ([M+H]$^+$): 196.0869, found: 196.0874.

4-Phenyl-5-iodo-7H-pyrrolo[2,3-d]-pyrimidine (70). **69** (380 mg, 1.95 mmol) was dissolved in anhydrous DMF (5 mL), and NIS (461 mg, 2.05 mmol, 1.05 eq.) was added. Then, the reaction mixture was stirred at ambient temperature overnight. Then, water (cooled in the ice-water bath, 15 mL) was added and the precipitate generated and was filtered. The solids were washed with ice-cold water. The solid was collected and dried under high vacuum to give **70** (530 mg, 1.65 mmol) as a brown solid in 85% yield. ^{1}H NMR (300 MHz, DMSO-d_6) δ: 7.51–7.55 (m, 3 H, H–Ph), 7.65–7.69 (m, 2 H, H–Ph), 7.86 (s, 1 H, H-6), 8.82 (s, 1 H, H-2), 12.69 (br. s., 1 H, NH). HRMS (ESI): calculated for C$_{12}$H$_9$IN$_3$ ([M+H]$^+$): 321.9836, found: 321.9841.

4-Phenyl-5-iodo-N7-(β-D–ribofuranosyl)-7H-pyrrolo[2,3-d]-pyrimidine (71). **70** (200 mg, 0.62 mmol) was placed in a 25 mL two-neck round bottom flask, after which the flask was purged with N$_2$ gas. Anhydrous MeCN (5 mL, 7.5 mL/mmol of SM) was added. BSA (183 μL, 0.75 mmol, 1.2 eq.) was added to the suspension via syringe. The resulting mixture was stirred until the solid was completely dissolved. Next, 1-O-acetyl-2,3,5-tri-O-benzoyl-β-D-ribofuranose (378 mg, 0.75 mmol, 1.2 eq.) was added, and immediately followed by TMSOTf (147 μL, 0.81 mmol, 1.3 eq.). The reaction mixture was stirred at ambient temperature for 15 min, and was heated at 80 °C. When full conversion of **70** was observed via HRMS, the mixture was cooled to room temperature. Then, EA (10 mL) and aq. sat. NaHCO$_3$ (10 mL) were added. The layers were separated and the water layer extracted twice more with EA. Then, the organic layers were combined, washed with brine, dried over Na$_2$SO$_4$, filtered, and evaporated. The residue was purified by column chromatography (5→30% EA/PET) to give a yellow foam (140 mg, 0.18 mmol) in 29% yield. This obtained product (330 mg, 0.43 mmol) was charged in a 50 mL round bottom flask, and NH$_3$ in MeOH (7 N, 5 mL) was added. The mixture was stirred at ambient temperature overnight. Then, the reaction solution was evaporated until dryness, purified by column chromatography (0→10% MeOH/DCM) to afford **71**

ChemMedChem

Full Papers
doi.org/10.1002/cmdc.202100144

**Chemistry
Europe**
European Chemical
Societies Publishing

(150 mg, 0.33 mmol) as a white solid in 77% yield. ^{1}H NMR (400 MHz, DMSO-d_6) δ: 3.54–3.60 (m, 1 H, H-5''), 3.63–3.68 (m, 1 H, H-5'), 3.95 (q, $J=3.5$ Hz, 1 H, H-4'), 4.12 (q, $J=4.2$ Hz, 1 H, H-3'), 4.45 (q, $J=6.0$ Hz, 1 H, H-2'), 5.11 (t, $J=5.3$ Hz, 1 H, OH-5'), 5.20 (d, $J=4.6$ Hz, 1 H, OH-3'), 5.42 (d, $J=6.4$ Hz, 1 H, OH-2'), 6.28 (d, $J=6.3$ Hz, 1 H, H-1'), 7.52–7.56 (m, 3 H, H–Ph), 7.66–7.68 (m, 2 H, H–Ph), 8.17 (s, 1 H, H-6), 8.89 (s, 1 H, H-2). ^{13}C NMR (100 MHz, DMSO-d_6) δ: 54.5 (C-5), 61.4 (C-5'), 70.5 (C-3'), 74.1 (C-2'), 85.4 (C-4'), 86.6 (C-1'), 116.5 (C-4a), 127.6 (2 C, C–Ph), 129.6 (C–Ph), 130.8 (2 C, C–Ph), 133.5 (C-6), 135.6 (C–Ph), 150.9 (C-2), 151.3 (C-7a), 159.7 (C-4). HRMS (ESI): calculated for $C_{17}H_{17}IN_3O_4$ ([M + H]$^+$): 454.0258, found: 454.0255.

4-Phenyl-5-(4-chloro-phenyl)-N7-(β-D–ribofuranosyl)-7H-pyrrolo[2,3-d]-pyrimidine (16). 16 was prepared according to General procedure A. 71 (140 mg, 0.31 mmol) gave rise to a slightly impure 16 (65 mg, 0.15 mmol) as a white solid. 16 was purified by preparative RP-HPLC gradient: 0.2% formic acid in water:MeCN at a flow rate of 20 mL/min; The initial gradient composition (95% A/05% B) was held for 2.0 min, increased to 80% B in 12 min, then increased to 98% B in 3 min. After RP-HPLC purification, 16 was obtained as a white solid (31 mg, 0.071 mmol) in 23% yield. Melting point: 234°C. ^{1}H NMR (300 MHz, DMSO-d_6) δ: 3.51–3.62 (m, 1 H, H-5''), 3.63–3.74 (m, 1 H, H-5'), 3.97 (q, $J=3.5$ Hz, 1 H, H-4'), 4.09–4.24 (m, 1 H, H-3'), 4.54 (q, $J=6.1$ Hz, 1 H, H-2'), 5.07 (t, $J=5.6$ Hz, 1 H, OH-5'), 5.21 (d, $J=5.0$ Hz, 1 H, OH-3'), 5.43 (d, $J=6.4$ Hz, 1 H, OH-2'), 6.38 (d, $J=6.2$ Hz, 1 H, H-1'), 6.98 (d, $J=8.5$ Hz, 2 H, H–Ph), 7.08–7.27 (m, 4 H, H–Ph), 7.28–7.46 (m, 3 H, H–Ph), 8.09 (s, 1 H, H-6), 8.95 (s, 1 H, H-2). ^{13}C NMR (75 MHz, DMSO-d_6) δ: 61.5 (C-5'), 70.5 (C-3'), 74.0 (C-2'), 85.3 (C-4'), 86.6 (C-1'), 113.3 (C-4a), 115.5 (C-5), 126.4 (C-6), 127.5 (4 C, C-3$_{Ph}$ and C-5$_{Ph}$ and C-3'$_{Ph}$ and C-5'$_{Ph}$), 129.2 (C-4'$_{Ph}$), 129.5 (2 C, C-2'$_{Ph}$ and C-6'$_{Ph}$), 130.5 (2 C, C-2$_{Ph}$ and C-6$_{Ph}$), 131.0 (C-4$_{Ph}$), 132.6 (C-1$_{Ph}$), 137.3 (C-1'$_{Ph}$), 151.0 (C-2), 152.2 (C-7a), 158.7 (C-4). HRMS (ESI): calculated for $C_{23}H_{21}ClN_3O_4$ ([M + H]$^+$): 438.1215, found: 438.1213.

3-(4-Chloro-phenyl)-4-methyl-N1-(β-D–ribofuranosyl)-pyrrolo[2,3-b]pyridine (20). 20 was prepared according to General procedure A. 72[27] (85 mg, 0.22 mmol) gave rise to 20 (50 mg, 0.13 mmol) as a white solid in 61% yield. Melting point: 96°C. ^{1}H NMR (400 MHz, DMSO-d_6) δ: 2.29 (s, 3 H, CH$_3$), 3.51–3.56 (m, 1 H, H-5''), 3.61–3.66 (m, 1 H, H-5'), 3.91 (q, $J=3.4$ Hz, 1 H, H-4'), 4.10–4.14 (m, 1 H, H-3'), 4.48 (q, $J=6.0$ Hz, 1 H, H-2'), 5.11 (d, $J=4.8$ Hz, 1 H, OH-5'), 5.14 (t, $J=5.6$ Hz, 1 H, OH-3'), 5.30 (d, $J=6.4$ Hz, 1 H, OH-2'), 6.29 (d, $J=6.1$ Hz, 1 H, H-1'), 6.97 (d, $J=4.9$ Hz, 1 H, H-5), 7.48 (s, 4 H, H–Ph), 7.76 (s, 1 H, H-2), 8.16 (d, $J=4.8$ Hz, 1 H, H-6). ^{13}C NMR (100 MHz, DMSO-d_6) δ: 19.8 (CH$_3$), 61.7 (C-5'), 70.6 (C-3'), 73.7 (C-2'), 84.9 (C-4'), 87.0 (C-1'), 115.5 (C-3), 118.3 (C-3a), 118.6 (C-5), 124.9 (C-2), 128.0 (2 C, C–Ph), 131.5 (C-4$_{Ph}$), 131.7 (2 C, C–Ph), 134.5 (C-1$_{Ph}$), 140.1 (C-4), 142.7 (C-6), 147.6 (C-7a). HRMS (ESI): calculated for $C_{19}H_{20}ClN_2O_4$ ([M + H]$^+$): 375.1106, found: 375.1110.

3-Bromo-5-fluoro-1H-pyrrolo[2,3-b]pyridine (73).[41–42] 5-Fluoro-1H-pyrrolo[2,3-b]pyridine (500 mg, 3.67 mmol) was dissolved in anhydrous DMF (11 mL, 3 mL/mmol of SM), and NBS (686 mg, 3.86 mmol, 1.05 eq.) was added. Then, the reaction mixture was stirred at ambient temperature overnight. Then, water (cooled in an ice-water bath, 30 mL) was added and the precipitate generated and was filtered. The solids were washed with ice-cold water. The solid was collected and dried under high vacuum to give 73 (753 mg, 3.50 mmol) as a white solid in 95% yield. ^{1}H NMR (300 MHz, DMSO-d_6) δ: 7.71 (dd, $J=8.9$, 2.6 Hz, 1 H, H-2), 7.82 (d, $J=2.8$ Hz, 1 H, H-6), 8.28 (t, $J=2.2$ Hz, 1 H, H-4), 12.24 (br. s., 1 H, NH). ^{19}F NMR (376 MHz, DMSO-d_6) δ: −138.03. HRMS (ESI): calculated for $C_7H_5BrFN_2$ ([M + H]$^+$): 214.9615, found: 214.9623.

3-Bromo-5-fluoro-N1-(β-D–ribofuranosyl)-pyrrolo[2,3-b]pyridine (77). 73 (640 mg, 2.98 mmol) was placed in a 100 mL two-neck round bottom flask, after which the flask was purged with N$_2$ gas.

Anhydrous MeCN (22 mL, 7.5 mL/mmol of SM) was added. BSA (801 μL, 3.28 mmol, 1.1 eq.) was added into the suspension via syringe. The resulting mixture was stirred until the solid was completely dissolved. Next, 1-O-acetyl-2,3,5-tri-O-benzoyl-β-D-ribofuranose (1.80 g, 3.57 mmol, 1.2 eq.) was added, and immediately followed by TMSOTf (646 μL, 3.57 mmol, 1.2 eq.). The reaction mixture was stirred at ambient temperature for 15 min, and was heated at 80°C. When the full conversion of 73 was observed via HRMS, the mixture was cooled to ambient temperature. Then, EA (10 mL) and aq. sat. NaHCO$_3$ (10 mL) were added. The layers were separated and the water layer extracted twice more with EA. Then, the organic layers were combined, washed with brine, dried over Na$_2$SO$_4$, filtered, and evaporated. The residue was purified by column chromatography (5→30% EA/PET) to give a colorless foam (1.17 g, 1.78 mmol). This obtained product (1.15 g, 1.74 mmol) was charged in a 50 mL round bottom flask, and NH$_3$ in MeOH (7 N, 10 mL) was added. The mixture was stirred at ambient temperature overnight. Then, the reaction solution was evaporated till dryness, purified by column chromatography (0→10% MeOH/DCM) to afford 77 (285 mg, 0.82 mmol) as a white solid in 24% yield for two steps. ^{1}H NMR (400 MHz, DMSO-d_6) δ: 3.45–3.58 (m, 1 H, H-5''), 3.59–3.70 (m, 1 H, H-5'), 3.90 (q, $J=3.8$ Hz, 1 H, H-4'), 4.04–4.16 (m, 1 H, H-3'), 4.40 (q, $J=6.1$ Hz, 1 H, H-2'), 5.04 (t, $J=5.4$ Hz, 1 H, OH-5'), 5.15 (d, $J=4.9$ Hz, 1 H, OH-3'), 5.36 (d, $J=6.3$ Hz, 1 H, OH-2'), 6.22 (d, $J=6.1$ Hz, 1 H, H-1'), 7.82 (dd, $J=8.8$, 2.7 Hz, 1 H, H-4), 8.14 (s, 1 H, H-2), 8.32–8.41 (m, 1 H, H-6). ^{13}C NMR (100 MHz, DMSO-d_6) δ: 61.4 (C-5'), 70.4 (C-3'), 74.0 (C-2'), 85.1 (C-4'), 86.8 (C-1'), 88.2 (C-3), 113.1 (d, $J=22.5$ Hz, 1 C, C-4), 119.8 (d, $J=7.3$ Hz, 1 C, C-3a), 128.0 (C-2), 132.6 (d, $J=29.1$ Hz, 1 C, C-6), 143.3 (C-7a), 155.8 (d, $J=242.0$ Hz, 1 C, C-5). ^{19}F NMR (376 MHz, DMSO-d_6)δ: −136.76. HRMS (ESI): calculated for $C_{12}H_{13}BrFN_2O_4$ ([M + H]$^+$): 347.0037, found: 347.0035.

3-(4-Chloro-phenyl)-5-fluoro-N1-(β-D–ribofuranosyl)-pyrrolo[2,3-b]pyridine (21). 21 was prepared according to General procedure A. 77 (100 mg, 0.29 mmol) gave rise to 21 (14 mg, 0.037 mmol) as a white solid in 13% yield. Melting point: 131°C. ^{1}H NMR (400 MHz, DMSO-d_6) δ: 3.44–3.62 (m, 1 H, H-5''), 3.62–3.75 (m, 1 H, H-5'), 3.92 (q, $J=3.9$ Hz, 1 H, H-4'), 4.12–4.19 (m, 1 H, H-3'), 4.49 (q, $J=6.0$ Hz, 1 H, H-2'), 5.05 (t, $J=5.6$ Hz, 1 H, OH-5'), 5.15 (d, $J=4.9$ Hz, 1 H, OH-3'), 5.37 (d, $J=6.3$ Hz, 1 H, OH-2'), 6.27 (d, $J=6.0$ Hz, 1 H, H-1'), 7.44–7.57 (m, 2 H, H–Ph), 7.70–7.83 (m, 2 H, H–Ph), 8.22 (dd, $J=9.7$, 2.7 Hz, 1 H, H-4), 8.32 (s, 1 H, H-2), 8.35 (dd, $J=2.4$, 1.2 Hz, 1 H, H-6). ^{13}C NMR (100 MHz, DMSO-d_6) δ: 61.5 (C-5'), 70.4 (C-3'), 73.8 (C-2'), 84.9 (C-4'), 86.9 (C-1'), 113.7 (d, $J=4.4$ Hz, 1 C, C-3), 114.1 (d, $J=21.1$ Hz, 1 C, C-4), 118.1 (d, $J=6.5$ Hz, 1 C, C-3a), 126.5 (C-2), 128.0 (2 C, C-2$_{Ph}$ and C-6$_{Ph}$), 128.9 (2 C, C-3$_{Ph}$ and C-5$_{Ph}$), 130.7 (C-4$_{Ph}$), 131.3 (d, $J=29.1$ Hz, 1 C, C-6), 132.7 (C-1$_{Ph}$), 144.9 (C-7a), 155.9 (d, $J=241.2$ Hz, 1 C, C-5). ^{19}F NMR (376 MHz, DMSO-d_6) δ: −137.45. HRMS (ESI): calculated for $C_{18}H_{17}BrFN_2O_4$ ([M + H]$^+$): 379.0855, found: 379.0848.

3-Bromo-5-chloro-1H-pyrrolo[2,3-b]pyridine (74).[41–42] 5-Chloro-1H-pyrrolo[2,3-b]pyridine (500 mg, 3.28 mmol) was dissolved in anhydrous DMF (10 mL, 3 mL/mmol of SM), and NBS (642 mg, 3.61 mmol, 1.1 eq.) was added. Then, the reaction mixture was stirred at ambient temperature overnight. The water (cooled in an ice-water bath, 30 mL) was added and the precipitate generated and was filtered. The solids were washed with ice-cold water. The solid was collected and dried under high vacuum to give 74 (700 mg, 3.02 mmol) as a white solid in 92% yield. ^{1}H NMR (300 MHz, DMSO-d_6) δ 7.83 (d, $J=2.3$ Hz, 1 H, H-2), 7.92 (d, $J=2.1$ Hz, 1 H, H-6), 8.29 (dd, $J=1.9$, 1.1 Hz, 1 H, H-4), 12.33 (br. s., 1 H, NH). HRMS (ESI): calculated for $C_7H_5BrClN_2$ ([M + H]$^+$): 230.9319, found: 230.9313.

3-Bromo-5-chloro-N1-(β-D–ribofuranosyl)-pyrrolo[2,3-b]pyridine (78). 74 (640 mg, 2.98 mmol) was placed in a 100 mL two-neck round bottom flask, after which the flask was purged with N$_2$ gas.

269

ChemMedChem

Full Papers
doi.org/10.1002/cmdc.202100144

**Chemistry
Europe**
European Chemical
Societies Publishing

Anhydrous MeCN (22 mL, 7.5 mL/mmol of SM) was added. BSA (801 µL, 3.28 mmol, 1.1 eq.) was added into the suspension via syringe. The resulting mixture was stirred until the solid was completely dissolved. Next, 1-O-acetyl-2,3,5-tri-O-benzoyl-β-D-ribofuranose (1.80 g, 3.57 mmol, 1.2 eq.) was added, and immediately followed by TMSOTf (646 µL, 3.57 mmol, 1.2 eq.). The reaction mixture was stirred at ambient temperature for 15 min, and was heated at 80 °C. When full conversion of **74** was observed via HRMS, the mixture was cooled to room temperature. Then, EA (10 mL) and aq. sat. NaHCO$_3$ (10 mL) were added. The layers were separated and the water layer extracted twice more with EA. Then, the organic layers were combined, washed with brine, dried over Na$_2$SO$_4$, filtered, and evaporated. The residue was purified by column chromatography (5→30 % EA/PET) to give a colorless foam (850 mg, 1.26 mmol). This obtained product (850 mg, 1.26 mmol) was charged in a 50 mL round bottom flask, and NH$_3$ in MeOH (7 N, 10 mL) was added. The mixture was stirred at ambient temperature overnight. Then, the reaction solution was evaporated till dryness, purified by column chromatography (0→10 % MeOH/DCM) to afford **78** (410 mg, 1.13 mmol) as a white solid in 32 % yield for two steps. ^{1}H NMR (400 MHz, DMSO-d_6) δ: 3.47–3.58 (m, 1 H, H-5''), 3.59–3.71 (m, 1 H, H-5'), 3.91 (q, J=3.5 Hz, 1 H, H-4'), 4.04–4.18 (m, 1 H, H-3'), 4.39 (q, J=5.9 Hz, 1 H, H-2'), 5.06 (t, J=5.4 Hz, 1 H, OH-5'), 5.17 (d, J=4.9 Hz, 1 H, OH-3'), 5.39 (d, J=6.3 Hz, 1 H, OH-2'), 6.23 (d, J=6.1 Hz, 1 H, H-1'), 8.01 (d, J=2.3 Hz, 1 H, H-4), 8.15 (s, 1 H, H-2), 8.37 (d, J=2.3 Hz, 1 H, H-6). ^{13}C NMR (100 MHz, DMSO-d_6) δ: 61.4 (C-5'), 70.4 (C-3'), 74.1 (C-2'), 85.1 (C-4'), 86.6 (C-1'), 88.1 (C-3a), 120.5 (C-3), 124.2 (C-5), 126.4 (C-4), 127.6 (C-2), 142.3 (C-6), 145.0 (C-7a). HRMS (ESI): calculated for C$_{12}$H$_{13}$BrClN$_2$O$_4$ ([M+H]$^+$): 362.9742, found: 362.9738.

3-(4-Chloro-phenyl)-5-chloro-N1-(β-D–ribofuranosyl)-pyrrolo[2,3-b]pyridine (22). **78** (100 mg, 0.28 mmol), phenylboronic acid (52 mg, 0.33 mmol, 1.2 eq.), K$_2$CO$_3$ (116 mg, 0.84 mmol, 3 eq.) and Pd(PPh$_3$)$_4$ (16 mg, 0.014 mmol, 0.05 eq.) were charged to a 25 mL round-bottom flask, equipped with a stir bar. Next, the air was removed and backfilled with argon. This was repeated thrice. Then, a mixture solution of 1,4-dioxane and H$_2$O (1:1 ratio, 2 mL) was added into the reaction mixture via syringes. The mixture was then stirred at ambient temperature (5 min), and then was refluxed at 100 °C. The reaction was monitored by HRMS for consumption of SM (1 h), after which it was allowed to cool to ambient temperature. Then, 0.5 M aq. HCl was added to neutralize the mixture. Then, the volatiles were removed *in vacuo*, and the residue purified by column chromatography (0→10 % MeOH/DCM) to give **22** (27 mg, 0.068 mmol) as a light yellow solid in 24 % yield. Melting point: 102 °C. ^{1}H NMR (400 MHz, DMSO-d_6) δ: 3.48–3.61 (m, 1 H, H-5''), 3.64–3.70 (m, 1 H, H-5'), 3.93 (q, J=3.9 Hz, 1 H, H-4'), 4.09–4.22 (m, 1 H, H-3'), 4.48 (q, J=6.0 Hz, 1 H, H-2'), 5.05 (t, J=5.6 Hz, 1 H, OH-5'), 5.16 (d, J=4.9 Hz, 1 H, OH-3'), 5.38 (d, J=6.4 Hz, 1 H, OH-2'), 6.28 (d, J=6.0 Hz, 1 H, H-1'), 7.45–7.58 (m, 2 H, H–Ph), 7.71–7.82 (m, 2 H, H–Ph), 8.31 (s, 1 H, H-2), 8.35 (d, J=2.3 Hz, 1 H, H-6), 8.40 (d, J=2.3 Hz, 1 H, H-4). ^{13}C NMR (100 MHz, DMSO-d_6) δ: 61.5 (C-5'), 70.4 (C-3'), 73.9 (C-2'), 85.0 (C-4'), 86.7 (C-1'), 113.5 (C-3), 118.8 (C-3a), 124.0 (C-5), 126.1 (C-2), 127.3 (C-4), 128.1 (2 C, C-2$_{Ph}$ and C-6$_{Ph}$), 128.9 (2 C, C-3$_{Ph}$ and C-5$_{Ph}$), 130.8 (C-4$_{Ph}$), 132.5 (C-1$_{Ph}$), 141.3 (C-6), 146.5 (C-7a). HRMS (ESI): calculated for C$_{18}$H$_{17}$Cl$_2$N$_2$O$_4$ ([M+H]$^+$): 395.0560, found: 395.0572.

3-Bromo-5-nitro-1H-pyrrolo[2,3-b]pyridine (75). 5-Nitro-1H-pyrrolo[2,3-b]pyridine (500 mg, 3.06 mmol) was dissolved in dry DMF (15 mL, 5 mL/mmol of SM), and NBS (600 mg, 3.37 mmol, 1.1 eq.) was added. Then, the reaction mixture was stirred at ambient temperature overnight. Then, water (cooled in an ice-water bath, 30 mL) was added and the precipitate generated and was filtered. The solids were washed with ice-cold water. The solid was collected and dried under high vacuum to give **75** (625 mg, 3.02 mmol) as a yellow solid in 84 %. ^{1}H NMR (300 MHz, DMSO-d_6) δ: 8.06 (s, 1 H, H-

2), 8.59 (s, 1 H, H-6), 9.13–9.14 (m, 1 H, H-4), 12.92 (br. s., 1 H, NH). HRMS (ESI): calculated for C$_7$H$_5$BrN$_3$O$_2$ ([M+H]$^+$): 241.9560, found: 241.9564.

3-Bromo-5-nitro-N1-(β–D–ribofuranosyl)-pyrrolo[2,3-b]pyridine (79). **75** (620 mg, 2.56 mmol) was placed in a 100 mL two-neck round bottom flask, after which the flask was purged with N$_2$ gas. Anhydrous MeCN (19 mL, 7.5 mL/mmol of SM) was added. BSA (0.7 mL, 2.82 mmol, 1.1 eq.) was added into the suspension via syringe. The resulting mixture was stirred until the solid was completely dissolved. Next, 1-O-acetyl-2,3,5-tri-O-benzoyl-β-D-ribo-furanose (1.55 g, 3.07 mmol, 1.2 eq.) was added, and immediately followed by TMSOTf (0.6 mL, 3.07 mmol, 1.2 eq.). The reaction mixture was stirred at ambient temperature for 15 min, and was heated at 80 °C. When the full conversion of **75** was observed via HRMS, the mixture was cooled to ambient temperature. Then, EA (10 mL) and aq. sat. NaHCO$_3$ (10 mL) were added. The layers were separated and the water layer extracted twice more with EA. Then, the organic layers were combined, washed with brine, dried over Na$_2$SO$_4$, filtered, and evaporated. The residue was purified by column chromatography (5→30 % EA/PET) to give a colorless foam (1.70 g, 2.48 mmol). This obtained product (200 mg, 0.29 mmol) was charged in a 25 mL round bottom flask, and NH$_3$ in MeOH (7 N, 5 mL) was added. The mixture was stirred at ambient temperature overnight. Then, the reaction solution was evaporated until dryness, purified by column chromatography (0→10 % MeOH/DCM) to afford **79** (88 mg, 0.24 mmol) as a light yellow solid in 79 % yield for two steps. ^{1}H NMR (400 MHz, DMSO-d_6) δ: 3.58 (ddd, J=12.0, 5.4, 4.0 Hz, 1 H, H-5''), 3.66 (ddd, J=12.0, 5.2, 4.2 Hz, 1 H, H-5'), 3.95 (q, J=3.7 Hz, 1 H, H-4'), 4.08–4.19 (m, 1 H, H-3'), 4.40 (q, J=5.8 Hz, 1 H, H-2'), 5.10 (t, J=5.4 Hz, 1 H, OH-5'), 5.22 (d, J=5.0 Hz, 1 H, OH-3'), 5.46 (d, J=6.3 Hz, 1 H, OH-2'), 6.33 (d, J=6.0 Hz, 1 H, H-1'), 8.36 (s, 1 H, H-2), 8.65 (d, J=2.4 Hz, 1 H, H-4), 9.21 (d, J=2.4 Hz, 1 H, H-6). ^{13}C NMR (100 MHz, DMSO-d_6) δ: 61.3 (C-5'), 70.4 (C-3'), 74.4 (C-2'), 85.5 (C-4'), 86.9 (C-1'), 90.9 (C-3a), 118.8 (C-3), 123.6 (C-4), 129.4 (C-2), 139.8 (C-5), 140.1 (C-6), 148.3 (C-7a). HRMS (ESI): calculated for C$_{12}$H$_{13}$BrN$_3$O$_6$ ([M+H]$^+$): 373.9982, found: 373.9974.

3-(4-Chloro-phenyl)-5-nitro-N1-(β-D–ribofuranosyl)-pyrrolo[2,3-b]pyridine (22). **22** was prepared according to General procedure A. **79** (150 mg, 0.40 mmol) gave rise to **22** (24 mg, 0.059 mmol) as a white solid in 15 % yield. Melting point: 112 °C. ^{1}H NMR (400 MHz, DMSO-d_6) δ: 3.52–3.64 (m, 1 H, H-5''), 3.65–3.77 (m, 1 H, H-5'), 3.97 (q, J=3.8 Hz, 1 H, H-4'), 4.11–4.27 (m, 1 H, H-3'), 4.49 (q, J=6.0 Hz, 1 H, H-2'), 5.09 (t, J=5.5 Hz, 1 H, OH-5'), 5.22 (d, J=5.0 Hz, 1 H, OH-3'), 5.46 (d, J=6.4 Hz, 1 H, OH-2'), 6.39 (d, J=6.0 Hz, 1 H, H-1'), 7.51–7.65 (m, 2 H, H–Ph), 7.75–7.91 (m, 2 H, H–Ph), 8.48 (s, 1 H, H-2), 9.01 (d, J=2.4 Hz, 1 H, H-4), 9.22 (d, J=2.4 Hz, 1 H, H-6). ^{13}C NMR (100 MHz, DMSO-d_6) δ: 61.3 (C-5'), 70.4 (C-3'), 74.2 (C-2'), 85.4 (C-4'), 86.9 (C-1'), 116.1 (C-3), 117.1 (C-3a), 124.5 (C-4), 127.6 (C-2), 128.5 (2 C, C-2$_{Ph}$ and C-6$_{Ph}$), 129.2 (2 C, C-3$_{Ph}$ and C-5$_{Ph}$), 131.6 (C–Ph), 131.7 (C–Ph), 139.4 (C-5), 139.7 (C-6), 149.7 (C-7a). HRMS (ESI): calculated for C$_{18}$H$_{17}$ClN$_3$O$_6$ ([M+H]$^+$): 406.0800, found: 406.0795.

3-(4-Chloro-phenyl)-5-amino-N1-(β-D–ribofuranosyl)-pyrrolo[2,3-b]pyridine (24). **22** (30 mg, 0.074 mmol) was dissolved in MeOH (5 mL). The flask was purged with N$_2$, and a catalytic amount of Pt/C was added. Then, the N$_2$ gas was exchanged with H$_2$ (balloon; bubbling). The reaction mixture was stirred until the HRMS showed full consumption of the SM (2 h). The solution was filtered over Celite® and washed with MeOH. The filtrate was evaporated to dryness and purified by column chromatography (0→10 % MeOH/DCM) to afford **24** (19 mg, 0.051 mmol) as a white solid in 68 % yield. Melting point: 104 °C. ^{1}H NMR (400 MHz, DMSO-d_6) δ: 3.47–3.58 (m, 1 H, H-5''), 3.62 –3.67 (m, 1 H, H-5'), 3.89 (q, J=3.6 Hz, 1 H, H-4'), 4.09–4.16 (m, 1 H, H-3'), 4.51 (q, J=6.2 Hz, 1 H, H-2'), 4.95 (br. s., 2 H, NH$_2$), 5.08 (d, J=4.8 Hz, 1 H, OH-5'), 5.21 (t, J=5.8 Hz, 1 H, OH-3'), 5.28 (d, J=6.4 Hz, 1 H, OH-2'), 6.10 (d, J=6.3 Hz, 1 H, H-1'),

270

ChemMedChem

Full Papers
doi.org/10.1002/cmdc.202100144

**Chemistry
Europe**

European Chemical
Societies Publishing

7.43–7.53 (m, 3 H, H–Ph and H-4), 7.61–7.70 (m, 2 H, H–Ph), 7.80 (d, $J=2.4$ Hz, 1 H, H-6), 7.97 (s, 1 H, H-2). ^{13}C NMR (100 MHz, DMSO-d_6) δ: 61.8 (C-5′), 70.6 (C-3′), 73.3 (C-2′), 84.8 (C-4′), 87.3 (C-1′), 110.9 (C-4), 111.9 (C-3), 118.6 (C-3a), 124.5 (C-2), 127.5 (2 C, C-2$_{Ph}$ and C-6$_{Ph}$), 128.8 (2 C, C-3$_{Ph}$ and C-5$_{Ph}$), 129.9 (C-4$_{Ph}$), 132.4 (C-6), 134.1 (C-1$_{Ph}$), 140.3 (C-5), 141.9 (C-7a). HRMS (ESI): calculated for C$_{18}$H$_{19}$ClN$_3$O$_4$([M+H]$^+$): 376.1059, found: 376.1065.

3-Bromo-5-methyl-1H-pyrrolo[2,3-b]pyridine (76). 5-Methyl-1H-pyrrolo[2,3-b]pyridine (500 mg, 3.06 mmol) was dissolved in dry DMF (11 mL, 3 mL/mmol of SM), and NBS (741 mg, 4.16 mmol, 1.1 eq.) was added. Next, the reaction mixture was stirred at ambient temperature overnight. Then, water (cooled in an ice-water bath, 30 mL) was added and the precipitate generated and was filtered. The solids were washed with ice-cold water. The solid was collected and dried under high vacuum to give **76** (560 mg) as a yellow solid. Since part of **76** was dissolved in the filtrate, the water was collected and extracted twice with EA (2×20 mL). Then, the organic layers were combined, washed with brine, dried over Na$_2$SO$_4$, filtered, and evaporated. The residue was purified by column chromatography (5→30% EA/PET) to give a yellow solid (90 mg). Total amount of **76** was 650 mg (3.07 mmol) in 81% yield. ^{1}H NMR (300 MHz, DMSO-d_6) δ: 2.40 (s, 3 H, CH$_3$), 7.63–7.64 (m, 2 H, H-6 and H-2), 8.13 (d, $J=1.9$ Hz, 1 H, H-4), 11.91 (br. s., 1 H, NH). HRMS (ESI): calculated for C$_8$H$_8$BrN$_2$ ([M+H]$^+$): 210.9865, found: 210.9870.

3-Bromo-5-methyl-N1-(β-D–ribofuranosyl)-pyrrolo[2,3-b]pyridine (80). **76** (650 mg, 3.08 mmol) was placed in a 100 mL two-neck round bottom flask, after which the flask was purged with N$_2$ gas. Anhydrous MeCN (23 mL, 7.5 mL/mmol of SM) was added. BSA (828 μL, 3.39 mmol, 1.1 eq.) was added into the suspension via syringe. The resulting mixture was stirred until the solid was completely dissolved. Next, 1-O-acetyl-2,3,5-tri-O-benzoyl-β-D-ribofuranose (1.86 g, 3.70 mmol, 1.2 eq.) was added, and immediately followed by TMSOTf (670 μL, 3.70 mmol, 1.2 eq.). The reaction mixture was stirred at ambient temperature for 15 min, and was heated at 80 °C. When the full conversion of **76** was observed via HRMS, the mixture was cooled to ambient temperature. Then, EA (20 mL) and aq. sat. NaHCO$_3$ (10 mL) were added. The layers were separated and the water layer extracted twice more with EA. Then, the organic layers were combined, washed with brine, dried over Na$_2$SO$_4$, filtered, and evaporated. The residue was purified by column chromatography (5→30% EA/PET) to give a yellow foam (1.70 g, 2.59 mmol). This obtained product (1.70 g, 2.59 mmol) was charged in a 25 mL round bottom flask, and NH$_3$ in MeOH (7 N, 10 mL) was added. The mixture was stirred at ambient temperature overnight. Then, the reaction solution was evaporated till dryness, purified by column chromatography (0→10% MeOH/DCM) to afford **80** (650 mg, 1.89 mmol) as a white solid in 61% yield for two steps. ^{1}H NMR (400 MHz, DMSO-d_6) δ: 2.42 (s, 3 H, CH$_3$), 3.52–3.56 (m, 1 H, H-5′′), 3.60–3.65 (m, 1 H, H-5′), 3.89 (q, $J=3.8$ Hz, 1 H, H-4′), 4.10 (q, $J=4.2$ Hz, 1 H, H-3′), 4.42 (q, $J=6.1$ Hz, 1 H, H-2′), 5.09–5.12 (m, 2 H, OH-5′ and OH-3′), 5.31 (d, $J=6.4$ Hz, 1 H, OH-2′), 6.20 (d, $J=6.3$ Hz, 1 H, H-1′), 7.69 (d, $J=1.2$ Hz,1 H, H-4), 7.96 (s, 1 H, H-2), 8.19 (d, $J=1.8$ Hz, 1 H, H-6). ^{13}C NMR (100 MHz, DMSO-d_6) δ: 17.9 (CH$_3$), 61.6 (C-5′), 70.5 (C-3′), 73.8 (C-2′), 85.0 (C-4′), 86.7 (C-1′), 88.0 (C-3a), 119.5 (C-3), 125.8 (C-2), 126.3 (C-5), 126.8 (C-4), 144.7 (C-6), 145.2 (C-7a). HRMS (ESI): calculated for C$_{13}$H$_{16}$BrN$_2$O$_4$([M+H]$^+$): 343.0288, found: 343.0292.

3-(4-Chloro-phenyl)-5-methyl-N1-(β-D–ribofuranosyl)-pyrrolo[2,3-b]pyridine (25). 25 was prepared according to General procedure A. **79** (150 mg, 0.44 mmol) gave rise to **25** (23 mg, 0.061 mmol) as a white solid in 14% yield. Melting point: 112 °C. ^{1}H NMR (400 MHz, DMSO-d_6) δ: 2.44 (s, 3 H, CH$_3$), 3.53–3.58 (m, 1 H, H-5′′), 3.64–3.69 (m, 1 H, H-5′), 3.92 (d, $J=3.4$ Hz, 1 H, H-4′), 4.15 (q, $J=4.0$ Hz, 1 H, H-3′), 4.52 (q, $J=5.8$ Hz, 1 H, H-2′), 5.12–5.17 (m, 2 H, OH-5′ and OH-

3′), 5.32 (d, $J=6.3$ Hz, 1 H, OH-2′), 6.25 (d, $J=6.0$ Hz, 1 H, H-1′), 7.50 (d, $J=8.5$ Hz, 2 H, H–Ph), 7.75 (d, $J=8.5$ Hz, 2 H, H–Ph), 8.14 (s, 2 H, H-4 and H-2), 8.17 (s, 1 H, H-6). ^{13}C NMR (100 MHz, DMSO-d_6) δ: 18.1 (CH$_3$), 61.7 (C-5′), 70.6 (C-3′), 73.6 (C-2′), 84.9 (C-4′), 87.0 (C-1′), 113.0 (C-3), 118.1 (C-3a), 124.7 (C-2), 125.9 (C-5), 127.9 (3 C, C-2$_{Ph}$ and C-6$_{Ph}$ and C-4), 128.8 (2 C, C-3$_{Ph}$ and C-5$_{Ph}$), 130.3 (C-4$_{Ph}$), 133.4 (C-1$_{Ph}$), 143.7 (C-6), 146.8 (C-7a). HRMS (ESI): calculated for C$_{19}$H$_{20}$ClN$_2$O$_4$ ([M+H]$^+$): 375.1106, found: 375.1092.

4-Methyl-5-phenyl-N7-(β-D–ribofuranosyl)-7H-pyrrolo[2,3-d]-pyrimidine (26).[23] **26** was prepared according to General procedure A. **67** (156 mg, 0.40 mmol) gave rise to **26** (105 mg, 0.31 mmol) as a white solid in 77% yield. ^{1}H NMR (300 MHz, DMSO-d_6) δ: 2.46 (s, 3H, CH$_3$), 3.48–3.59 (m, 1 H, H-5′′), 3.60–3.72 (m, 1 H, H-5′), 3.93 (q, $J=3.5$ Hz, 1 H, H-4′), 4.13 (dd, $J=8.2$, 4.7 Hz, 1 H, H-3′), 4.47 (q, $J=6.0$ Hz, 1 H, H-2′), 5.05 (t, $J=5.4$ Hz, 1 H, OH-5′), 5.16 (d, $J=4.7$ Hz, 1 H, OH-3′), 5.37 (d, $J=6.4$ Hz, 1 H, OH-2′), 6.28 (d, $J=5.9$ Hz, 1 H, H-1′), 7.34–7.62 (m, 5 H, H–Ph), 7.85 (s, 1 H, H-6), 8.69 (s, 1 H, H-2). ^{13}C NMR (75 MHz, DMSO-d_6) δ: 22.9 (CH$_3$), 61.4 (C-5′), 70.5 (C-3′), 74.0 (C-2′), 85.2 (C-4′), 86.5 (C-1′), 115.8 (C-4a), 117.0 (C-5), 124.7 (C-6), 127.1 (C–Ph), 128.2 (2 C, C–Ph), 129.8 (2 C, C–Ph), 134.2 (C–Ph), 150.6 (C-7a), 150.8 (C-2), 159.2 (C-4). HRMS (ESI): calculated for C$_{18}$H$_{20}$N$_3$O$_4$ ([M+H]$^+$): 342.1448, found: 342.1443.

4-Methyl-5-(4-fluoro-phenyl)-N7-(β-D–ribofuranosyl)-7H-pyrrolo[2,3-d]-pyrimidine (27). **27** was prepared according to General procedure A. **67** (100 mg, 0.26 mmol) gave rise to **27** (32 mg, 0.089 mmol) as a white solid in 34% yield. Melting point: 203 °C. ^{1}H NMR (300 MHz, DMSO-d_6) δ: 2.44 (s, 3 H, CH$_3$), 3.55 (ddd, $J=12.0$, 5.7, 4.0 Hz, 1 H, H-5′′), 3.64 (ddd, $J=12.0$, 5.3, 4.1 Hz, 1 H, H-5′), 3.93 (q, $J=3.8$ Hz, 1 H, H-4′), 4.06–4.19 (m, 1 H, H-3′), 4.47 (dd, $J=11.4$, 6.4 Hz, 1 H, H-2′), 5.04 (t, $J=5.4$ Hz, 1 H, OH-5′), 5.17 (d, $J=5.0$ Hz, 1 H, OH-3′), 5.37 (d, $J=6.4$ Hz, 1 H, OH-2′), 6.27 (d, $J=6.2$ Hz, 1 H, H-1′), 7.22–7.37 (m, 2 H, H–Ph), 7.47–7.61 (m, 2 H, H–Ph), 7.85 (s, 1 H, H-6), 8.69 (s, 1 H, H-2). ^{13}C NMR (75 MHz, DMSO-d_6) δ: 22.8 (CH$_3$), 61.5 (C-5′), 70.5 (C-3′), 74.0 (C-2′), 85.2 (C-4′), 86.5 (C-1′), 115.0 (C-5), 115.2 (2 C, C-3$_{Ph}$ and C-5$_{Ph}$), 115.9 (C-4a), 124.8 (C-6), 130.6 (C-1$_{Ph}$), 131.8 (d, $J=8.1$ Hz, 2 C, C-2$_{Ph}$ and C-6$_{Ph}$), 150.6 (C-7a), 150.8 (C-2), 159.2 (C-4), 161.6 (d, $J=244.2$ Hz, 1 C, C-4$_{Ph}$). ^{19}F NMR (282 MHz, DMSO-d_6) δ: −115.56−−115.45 (m, 1 F). HRMS (ESI): calculated for C$_{18}$H$_{19}$FN$_3$O$_4$ ([M+H]$^+$): 360.1354, found: 360.1364.

4-Methyl-5-(4-trifluoromethyl-phenyl)-N7-(β-D–ribofuranosyl)-7H-pyrrolo[2,3-d]-pyrimidine (28). **28** was prepared according to General procedure A. **67** (100 mg, 0.26 mmol) gave rise to **28** (33 mg, 0.081 mmol) as a white solid in 31% yield. Melting point: 196 °C. ^{1}H NMR (300 MHz, DMSO-d_6) δ: 2.48 (s, 3 H, CH$_3$), 3.48–3.59 (m, 1 H, H-5′′), 3.60–3.73 (m, 1 H, H-5′), 3.94 (q, $J=3.6$ Hz, 1 H, H-4′), 4.14 (dd, $J=8.4$, 5.0 Hz, 1 H, H-3′), 4.48 (q, $J=6.1$ Hz, 1 H, H-2′), 5.05 (t, $J=5.4$ Hz, 1 H, OH-5′), 5.18 (d, $J=4.7$ Hz, 1 H, OH-3′), 5.40 (d, $J=6.2$ Hz, 1 H, OH-2′), 6.29 (d, $J=6.2$ Hz, 1 H, H-1′), 7.67–7.79 (m, 2 H, H–Ph), 7.79–7.90 (m, 2 H, H–Ph), 7.99 (s, 1 H, H-6), 8.73 (s, 1 H, H-2). ^{13}C NMR (75 MHz, DMSO-d_6) δ: 23.2 (CH$_3$), 61.4 (C-5′), 70.5 (C-3′), 74.1 (C-2′), 85.2 (C-4′), 86.6 (C-1′), 115.6 (C-5 and C-4a), 124.4 (q, $J=271.8$ Hz, 1 H, CF$_3$), 125.1 (q, $J=4.6$ Hz, 2 C, C-3$_{Ph}$ and C-5$_{Ph}$), 125.7 (C-6), 127.5 (q, $J=31.1$ Hz, 1 C, C-4$_{Ph}$), 130.4 (2 C, C-2$_{Ph}$ and C-6$_{Ph}$), 138.6 (C-1$_{Ph}$), 150.8 (C-2), 151.0 (C-7a), 159.3 (C-4). ^{19}F NMR (282 MHz, DMSO-d_6) δ: −60.83. HRMS (ESI): calculated for C$_{19}$H$_{19}$F$_3$N$_3$O$_4$ ([M+H]$^+$): 410.1322, found: 410.1323.

4-Methyl-5-(4-trifluoromethoxy-phenyl)-N7-(β-D–ribofuranosyl)-7H-pyrrolo[2,3-d]-pyrimidine (29). **29** was prepared according to General procedure A. **67** (100 mg, 0.26 mmol) gave rise to **29** (40 mg, 0.094 mmol) as a white solid in 36% yield. Melting point: 188 °C. ^{1}H NMR (300 MHz, DMSO-d_6) δ: 2.47 (s, 3 H, CH$_3$), 3.49–3.59 (m, 1 H, H-5′′), 3.60–3.74 (m, 1 H, H-5′), 3.93 (q, $J=3.4$ Hz, 1 H, H-4′), 4.13 (dd, $J=8.3$, 4.8 Hz, 1 H, H-3′), 4.47 (q, $J=6.1$ Hz, 1 H, H-2′), 5.04 (t, $J=5.4$ Hz, 1 H, OH-5′), 5.17 (d, $J=4.7$ Hz, 1 H, OH-3′), 5.38 (d, $J=$

ChemMedChem

Full Papers
doi.org/10.1002/cmdc.202100144

Chemistry
Europe
European Chemical
Societies Publishing

6.4 Hz, 1 H, OH-2′), 6.28 (d, $J = 6.2$ Hz, 1 H, H-1′), 7.46 (d, $J = 8.5$ Hz, 2 H, H–Ph), 7.65 (d, $J = 8.5$ Hz, 2 H, H–Ph), 7.91 (s, 1 H, H-6), 8.71 (s, 1 H, H-2). ^{13}C NMR (75 MHz, DMSO-d_6) δ: 22.9 (CH$_3$), 61.5 (C-5′), 70.5 (C-3′), 74.0 (C-2′), 85.2 (C-4′), 86.6 (C-1′), 115.5 (C-5), 115.7 (C-4a), 120.1 (q, $J = 255.7$ Hz, 1 C, OCF$_3$), 120.9 (2 C, C-3$_{Ph}$ and C-5$_{Ph}$), 125.2 (C-6), 131.6 (2 C, C-2$_{Ph}$ and C-6$_{Ph}$), 133.7 (C-1$_{Ph}$), 147.6 (d, $J = 2.3$ Hz, 1 C, C-4$_{Ph}$), 150.7 (C-2), 150.9 (C-7a), 159.2 (C-4). ^{19}F NMR (282 MHz, DMSO-d_6) δ: −56.77. HRMS (ESI): calculated for C$_{19}$H$_{19}$F$_3$N$_3$O$_5$ ([M + H]$^+$): 426.1271, found: 426.1244.

4-Methyl-5-(4-cyano-phenyl)-N7-(β-D–ribofuranosyl)-7H-pyrrolo[2,3-d]-pyrimidine (30). 30 was prepared according to General procedure A. 67 (100 mg, 0.26 mmol) gave rise to 30 (30 mg, 0.082 mmol) as a white solid in 31% yield. Melting point: 119–120 °C. ^1H NMR (300 MHz, DMSO-d_6) δ: 2.49 (s, 3 H, CH$_3$), 3.47–3.61 (m, 1 H, H-5′′), 3.61–3.73 (m, 1 H, H-5′), 3.94 (q, $J = 3.7$ Hz, 1 H, H-4′), 4.08–4.19 (m, 1 H, H-3′), 4.47 (dd, $J = 11.5, 6.2$ Hz, 1 H, H-2′), 5.05 (t, $J = 5.6$ Hz, 1 H, OH-5′), 5.18 (d, $J = 5.0$ Hz, 1 H, OH-3′), 5.39 (d, $J = 6.4$ Hz, 1 H, OH-2′), 6.28 (d, $J = 6.2$ Hz, 1 H, H-1′), 7.74 (d, $J = 8.2$ Hz, 2 H, H–Ph), 7.93 (d, $J = 8.2$ Hz, 2 H, H–Ph), 8.01 (s, 1 H, H-6), 8.73 (s, 1 H, H-2). ^{13}C NMR (100 MHz, DMSO-d_6) δ: 23.3 (CH$_3$), 61.4 (C-5′), 70.5 (C-3′), 74.1 (C-2′), 85.5 (C-4′), 86.7 (C-1′), 109.6 (C-4$_{Ph}$), 115.4 (C-4a), 115.6 (C-5), 118.9 (CN), 126.0 (C-6), 130.5 (2 C, C-2$_{Ph}$ and C-6$_{Ph}$), 132.2 (2 C, C-3$_{Ph}$ and C-5$_{Ph}$), 139.4 (C-1$_{Ph}$), 150.9 (C-7a), 151.1 (C-2), 159.4 (C-4). HRMS (ESI): calculated for C$_{19}$H$_{19}$N$_4$O$_4$ ([M + H]$^+$): 367.1401, found: 367.1394.

4-Methyl-5-(4-nitro-phenyl)-N7-(β-D–ribofuranosyl)-7H-pyrrolo[2,3-d]-pyrimidine (31). 31 was prepared according to General procedure A. 67 (100 mg, 0.26 mmol) gave rise to 31 (31 mg, 0.080 mmol) as a yellow solid in 31% yield. Melting point: 172 °C. ^1H NMR (300 MHz, DMSO-d_6) δ: 2.52 (s, 3 H, CH$_3$), 3.50–3.60 (m, 1 H, H-5′′), 3.61–3.75 (m, 1 H, H-5′), 3.95 (q, $J = 3.8$ Hz, 1 H, H-4′), 4.08–4.22 (m, 1 H, H-3′), 4.48 (dd, $J = 11.8, 6.2$ Hz, 1 H, H-2′), 5.06 (t, $J = 5.4$ Hz, 1 H, OH-5′), 5.19 (d, $J = 5.0$ Hz, 1 H, OH-3′), 5.41 (d, $J = 6.2$ Hz, 1 H, OH-2′), 6.29 (d, $J = 5.9$ Hz, 1 H, H-1′), 7.75–7.89 (m, 2 H, H–Ph), 8.08 (s, 1 H, H-6), 8.25–8.39 (m, 2 H, H–Ph), 8.75 (s, 1 H, H-2). ^{13}C NMR (100 MHz, DMSO-d_6) δ: 23.4 (CH$_3$), 61.4 (C-5′), 70.5 (C-3′), 74.1 (C-2′), 85.3 (C-4′), 86.7 (C-1′), 115.2 (C-5), 115.4 (C-4a), 123.5 (2 C, C-3$_{Ph}$ and C-5$_{Ph}$), 126.3 (C-6), 130.6 (2 C, C-2$_{Ph}$ and C-6$_{Ph}$), 141.4 (C-1$_{Ph}$), 146.3 (C-4$_{Ph}$), 151.0 (C-2), 151.2 (C-7a), 159.4 (C-4). HRMS (ESI): calculated for C$_{18}$H$_{19}$N$_4$O$_6$ ([M + H]$^+$): 387.1299, found: 387.1315.

4-Methyl-5-(4-methyl-phenyl)-N7-(β-D–ribofuranosyl)-7H-pyrrolo[2,3-d]-pyrimidine (32). 32 was prepared according to General procedure A. 67 (100 mg, 0.26 mmol) gave rise to 32 (58 mg, 0.16 mmol) as a white solid in 63% yield. Melting point: 114 °C. ^1H NMR (300 MHz, DMSO-d_6) δ: 2.37 (s, 3 H, CH$_3$), 2.45 (s, 3 H, CH$_3$), 3.54 (ddd, $J = 11.8, 5.7, 3.9$ Hz, 1 H, H-5′′), 3.64 (ddd, $J = 11.8, 5.3, 4.1$ Hz, 1 H, H-5′), 3.93 (q, $J = 3.8$ Hz, 1 H, H-4′), 4.13 (td, $J = 4.9, 3.4$ Hz, 1 H, H-3′), 4.46 (dd, $J = 11.8, 6.4$ Hz, 1 H, H-2′), 5.05 (t, $J = 5.6$ Hz, 1 H, OH-5′), 5.16 (d, $J = 5.0$ Hz, 1 H, OH-3′), 5.36 (d, $J = 6.4$ Hz, 1 H, OH-2′), 6.27 (d, $J = 6.2$ Hz, 1 H, H-1′), 7.26–7.28 (m, 2 H, H–Ph), 7.33–7.45 (m, 2 H, H–Ph), 7.79 (s, 1 H, H-6), 8.68 (s, 1 H, H-2). ^{13}C NMR (75 MHz, DMSO-d_6) δ: 20.8 (CH$_3$), 22.8 (CH$_3$), 61.5 (C-5′), 70.6 (C-3′), 74.0 (C-2′), 85.2 (C-4′), 86.5 (C-1′), 115.9 (C-4a), 116.9 (C-5), 124.5 (C-6), 128.8 (2 C, C-3$_{Ph}$ and C-5$_{Ph}$), 129.7 (2 C, C-2$_{Ph}$ and C-6$_{Ph}$), 131.3 (C-1$_{Ph}$), 136.4 (C-4$_{Ph}$), 150.6 (C-2), 150.7 (C-7a), 159.2 (C-4). HRMS (ESI): calculated for C$_{19}$H$_{22}$N$_3$O$_4$ ([M + H]$^+$): 356.1605, found: 356.1581.

4-Methyl-5-(4-ethyl-phenyl)-N7-(β-D–ribofuranosyl)-7H-pyrrolo[2,3-d]-pyrimidine (33). 33 was prepared according to General procedure A. 67 (100 mg, 0.26 mmol) gave rise to 33 (39 mg, 0.11 mmol) as a white solid in 41% yield. Melting point: 105 °C. ^1H NMR (300 MHz, DMSO-d_6) δ: 1.23 (t, $J = 7.5$ Hz, 3 H, CH$_3$), 2.46 (s, 3 H, CH$_3$), 2.67 (q, $J = 7.6$ Hz, 2 H, CH$_2$), 3.46–3.59 (m, 1 H, H-5′′), 3.59–3.70 (m, 1 H, H-5′), 3.93 (q, $J = 3.5$ Hz, 1 H, H-4′), 4.07–4.19 (m, 1 H, H-3′), 4.46 (dd, $J = 11.4, 6.4$ Hz, 1 H, H-2′), 5.05 (t, $J = 5.4$ Hz, 1 H, OH-

5′), 5.16 (d, $J = 5.0$ Hz, 1 H, OH-3′), 5.36 (d, $J = 6.2$ Hz, 1 H, OH-2′), 6.27 (d, $J = 6.2$ Hz, 1 H, H-1′), 7.21–7.35 (m, 2 H, H–Ph), 7.36–7.49 (m, 2 H, H–Ph), 7.80 (s, 1 H, H-6), 8.68 (s, 1 H, H-2). ^{13}C NMR (75 MHz, DMSO-d_6) δ: 15.6 (CH$_3$), 22.8 (CH$_3$), 27.9 (CH$_2$), 61.5 (C-5′), 70.6 (C-3′), 74.0 (C-2′), 85.2 (C-4′), 86.5 (C-1′), 115.9 (C-4a), 116.9 (C-5), 124.5 (C-6), 127.6 (2 C, C-3$_{Ph}$ and C-5$_{Ph}$), 129.7 (2 C, C-2$_{Ph}$ and C-6$_{Ph}$), 131.5 (C-1$_{Ph}$), 142.7 (C-4$_{Ph}$), 150.6 (C-2), 150.7 (C-7a), 159.2 (C-4). HRMS (ESI): calculated for C$_{20}$H$_{24}$N$_3$O$_4$ ([M + H]$^+$): 370.1761, found: 370.1771.

4-Methyl-5-(4-methoxy-phenyl)-N7-(β-D–ribofuranosyl)-7H-pyrrolo[2,3-d]-pyrimidine (34). 34 was prepared according to General procedure A. 67 (100 mg, 0.26 mmol) gave rise to 34 (68 mg, 0.18 mmol) as a white solid in 70% yield. Melting point: 112 °C. ^1H NMR (300 MHz, DMSO-d_6) δ: 2.45 (s, 3 H, CH$_3$), 3.45–3.59 (m, 1 H, H-5′′), 3.59–3.72 (m, 1 H, H-5′), 3.81 (s, 3 H, OMe), 3.93 (q, $J = 3.6$ Hz, 1 H, H-4′), 4.08–4.19 (m, 1 H, H-3′), 4.46 (dd, $J = 11.5, 6.3$ Hz, 1 H, H-2′), 5.05 (t, $J = 5.6$ Hz, 1 H, OH-5′), 5.16 (d, $J = 4.7$ Hz, 1 H, OH-3′), 5.36 (d, $J = 6.2$ Hz, 1 H, H-1′), 6.94–7.10 (m, 2 H, H–Ph), 7.34–7.49 (m, 2 H, H–Ph), 7.76 (s, 1 H, H-6), 8.67 (s, 1 H, H-2). ^{13}C NMR (75 MHz, DMSO-d_6) δ: 22.7 (CH$_3$), 55.1 (OMe), 61.5 (C-5′), 70.6 (C-3′), 74.0 (C-2′), 85.2 (C-4′), 86.5 (C-1′), 113.7 (2 C, C-3$_{Ph}$ and C-5$_{Ph}$), 116.0 (C-4a), 116.6 (C-5), 124.3 (C-6), 126.4 (C-1$_{Ph}$), 131.0 (2 C, C-2$_{Ph}$ and C-6$_{Ph}$), 150.6 (C-2), 150.7 (C-7a), 158.6 (C-4$_{Ph}$), 159.2 (C-4). HRMS (ESI): calculated for C$_{19}$H$_{22}$N$_3$O$_5$ ([M + H]$^+$): 372.1554, found: 372.1550.

4-Methyl-5-(4-hydroxy-phenyl)-N7-(β-D–ribofuranosyl)-7H-pyrrolo[2,3-d]-pyrimidine (35). 35 was prepared according to General procedure A. 67 (100 mg, 0.26 mmol) gave rise to 35 (70 mg, 0.20 mmol) as a white solid in 75% yield. Melting point: 75 °C. ^1H NMR (300 MHz, DMSO-d_6) δ: 2.45 (s, 3 H, CH$_3$), 3.48–3.58 (m, 1 H, H-5′′), 3.59–3.73 (m, 1 H, H-5′), 3.92 (q, $J = 3.5$ Hz, 1 H, H-4′), 4.04–4.18 (m, 1 H, H-3′), 4.45 (t, $J = 5.1$ Hz, 1 H, H-2′), 5.04 (br. s., 1 H, OH-5′), 5.15 (br. s., 1 H, OH-3′), 5.34 (br. s., 1 H, OH-2′), 6.25 (d, $J = 6.2$ Hz, 1 H, H-1′), 6.77–6.90 (m, 2 H, H–Ph), 7.20–7.35 (m, 2 H, H–Ph), 7.72 (s, 1 H, H-6), 8.67 (s, 1 H, H-2), 9.52 (s, 1 H, OH). ^{13}C NMR (100 MHz, DMSO-d_6) δ: 22.5 (CH$_3$), 61.5 (C-5′), 70.6 (C-3′), 73.9 (C-2′), 85.2 (C-4′), 86.5 (C-1′), 115.1 (2 C, C-3$_{Ph}$ and C-5$_{Ph}$), 116.1 (C-4a), 117.1 (C-5), 124.1 (C-6), 124.6 (C-1$_{Ph}$), 131.0 (2 C, C-2$_{Ph}$ and C-6$_{Ph}$), 150.5, 150.5, 156.8 (C-4$_{Ph}$), 159.1 (C-4). HRMS (ESI): calculated for C$_{18}$H$_{20}$N$_3$O$_5$ ([M + H]$^+$): 358.1397, found: 358.1412.

4-Methyl-5-(3-chloro-phenyl)-N7-(β-D–ribofuranosyl)-7H-pyrrolo[2,3-d]-pyrimidine (36). 36 was prepared according to General procedure A. 67 (100 mg, 0.26 mmol) gave rise to 36 (23 mg, 0.061 mmol) as a white solid in 24% yield. Melting point: 158 °C. ^1H NMR (300 MHz, DMSO-d_6) δ: 2.48 (s, 3H, CH$_3$), 3.55 (ddd, $J = 12.0, 5.6, 4.2$ Hz, 1 H, H-5′′), 3.65 (ddd, $J = 12.0, 5.4, 4.2$ Hz, 1 H, H-5′), 3.93 (q, $J = 3.8$ Hz, 1 H, H-4′), 4.13 (dd, $J = 8.2, 5.0$ Hz, 1 H, H-3′), 4.47 (dd, $J = 11.5, 6.0$ Hz, 1 H, H-2′), 5.04 (t, $J = 5.6$ Hz, 1 H, OH-5′), 5.17 (d, $J = 5.0$ Hz, 1 H, OH-3′), 5.38 (d, $J = 6.4$ Hz, 1 H, OH-2′), 6.27 (d, $J = 6.2$ Hz, 1 H, H-1′), 7.38–7.54 (m, 3 H, H–Ph), 7.56–7.65 (m, 1 H, H–Ph), 7.93 (s, 1 H, H-6), 8.71 (s, 1 H, H-2). ^{13}C NMR (75 MHz, DMSO-d_6) δ: 23.0 (CH$_3$), 61.5 (C-5′), 70.5 (C-3′), 74.0 (C-2′), 85.2 (C-4′), 86.6 (C-1′), 115.5 (C-5), 115.6 (C-4a), 125.3 (C-6), 127.0 (C–Ph), 128.8 (C–Ph), 129.2 (C-2$_{Ph}$), 130.0 (C-5$_{Ph}$), 132.9 (C-3$_{Ph}$), 136.5 (C-1$_{Ph}$), 150.7 (C-7a), 150.9 (C-2), 159.2 (C-4). HRMS (ESI): calculated for C$_{18}$H$_{19}$ClN$_3$O$_4$ ([M + H]$^+$): 376.1059, found: 376.1080.

4-Methyl-5-(3-fluoro-phenyl)-N7-(β-D–ribofuranosyl)-7H-pyrrolo[2,3-d]-pyrimidine (37). 37 was prepared according to General procedure A. 67 (100 mg, 0.26 mmol) gave rise to 37 (62 mg, 0.17 mmol) as a white solid in 66% yield. Melting point: 201 °C. ^1H NMR (300 MHz, DMSO-d_6) δ: 2.49 (s, 3 H, CH$_3$), 3.49–3.60 (m, 1 H, H-5′′), 3.61–3.73 (m, 1 H, H-5′), 3.93 (q, $J = 3.8$ Hz, 1 H, H-4′), 4.13–4.14 (d, $J = 3.5$ Hz, 1 H, H-3′), 4.47 (q, $J = 5.8$ Hz, 1 H, H-2′), 5.05 (t, $J = 4.8$ Hz, 1 H, OH-5′), 5.17 (d, $J = 4.7$ Hz, 1 H, OH-4′), 5.38 (d, $J = 6.2$ Hz, 1 H, OH-3′), 6.27 (d, $J = 6.2$ Hz, 1 H, H-1′), 7.13–7.30 (m, 1 H, H–Ph),

These are not the final page numbers! ↗↗

272

ChemMedChem

Full Papers
doi.org/10.1002/cmdc.202100144

Chemistry Europe
European Chemical
Societies Publishing

7.31–7.43 (m, 2 H, H–Ph), 7.51 (td, $J=8.0$, 6.3 Hz, 1 H, H–Ph), 7.92 (s, 1 H, H-6), 8.71 (s, 1 H, H-2). ^{13}C NMR (75 MHz, DMSO-d_6) δ: 23.0 (CH$_3$), 61.5 (C-5′), 70.5 (C-3′), 74.0 (C-2′), 85.2 (C-4′), 86.6 (C-1′), 113.9 (d, $J=21.9$ Hz, 1 C, C–Ph), 115.6 (C-4a), 116.1 (d, $J=59.9$ Hz, 1 C, C–Ph), 116.2 (C-5), 125.3 (C-6), 126.1 (d, $J=2.3$ Hz, 1 C, C–Ph), 130.2 (d, $J=8.1$ Hz, 1 C, C–Ph), 136.7 (d, $J=9.2$ Hz, 1 C, C–Ph), 150.6 (C-7a), 150.9 (C-2), 159.2 (C-4), 161.9 (d, $J=243.0$ Hz, 1 C, C–Ph). ^{19}F NMR (282 MHz, DMSO-d_6) δ: −113.42−−113.33 (m, 1F). HRMS (ESI): calculated for C$_{18}$H$_{19}$FN$_3$O$_4$ ([M+H]$^+$): 360.1354, found: 360.1354.

4-Methyl-5-(2-chloro-phenyl)-N7-(β-D–ribofuranosyl)-7H-pyrrolo[2,3-d]-pyrimidine (38). 38 was prepared according to General procedure A. **67** (100 mg, 0.26 mmol) gave rise to **38** (30 mg, 0.080 mmol) as a white solid in 31% yield. Melting point: 119 °C. ^{1}H NMR (300 MHz, DMSO-d_6) δ: 2.28 (s, 3 H, CH$_3$), 3.55 (ddd, $J=11.8$, 5.6, 4.2 Hz, 1 H, H-5″), 3.65 (ddd, $J=11.8$, 5.3, 4.0 Hz, 1 H, H-5′), 3.94 (q, $J=3.8$ Hz, 1 H, H-4′), 4.07–4.18 (m, 1 H, H-3′), 4.47 (dd, $J=11.5$, 6.1 Hz, 1 H, H-2′), 5.04 (t, $J=5.4$ Hz, 1 H, OH-5′), 5.18 (d, $J=5.0$ Hz, 1 H, OH-3′), 5.38 (d, $J=6.4$ Hz, 1 H, OH-2′), 6.26 (d, $J=6.2$ Hz, 1 H, H-1′), 7.39–7.55 (m, 3 H, H–Ph), 7.56–7.70 (m, 1 H, H–Ph), 7.86 (s, 1 H, H-6), 8.70 (s, 1 H, H-2). ^{13}C NMR (75 MHz, DMSO-d_6) δ: 21.1 (CH$_3$), 61.5 (C-5′), 70.5 (C-3′), 74.1 (C-2′), 85.2 (C-4′), 86.8 (C-1′), 113.4 (C-5), 116.7 (C-4a), 125.4 (C-6), 127.2 (C–Ph), 129.3 (C–Ph), 129.8 (C–Ph), 132.9 (C–Ph), 133.3 (C-1$_{Ph}$), 134.0 (C–Ph), 150.2 (C-7a), 150.9 (C-2), 159.0 (C-4). HRMS (ESI): calculated for C$_{18}$H$_{19}$ClN$_3$O$_4$ ([M+H]$^+$): 376.1059, found: 367.1057.

4-Methyl-5-(3,4-dichloro-phenyl)-N7-(β-D–ribofuranosyl)-7H-pyrrolo[2,3-d]-pyrimidine (39). 39 was prepared according to General procedure A. **67** (100 mg, 0.26 mmol) gave rise to **39** (27 mg, 0.066 mmol) as a white solid in 25% yield. Melting point: 228 °C. ^{1}H NMR (300 MHz, DMSO-d_6) δ: 2.49 (s, 3H, CH$_3$), 3.55 (ddd, $J=12.0$, 5.8, 4.1 Hz, 1 H, H-5″), 3.65 (ddd, $J=11.8$, 5.3, 4.3 Hz, 1 H, H-5′), 3.93 (q, $J=3.8$ Hz, 1 H, H-4′), 4.14 (dd, $J=8.8$, 4.8 Hz, 1 H, H-3′), 4.46 (dd, $J=11.4$, 6.0 Hz, 1 H, H-2′), 5.04 (t, $J=5.6$ Hz, 1 H, OH-5′), 5.18 (d, $J=5.0$ Hz, 1 H, OH-3′), 5.38 (d, $J=6.2$ Hz, 1 H, OH-2′), 6.27 (d, $J=5.9$ Hz, 1 H, H-1′), 7.53 (dd, $J=8.3$, 2.2 Hz, 1 H, H–Ph), 7.72 (d, $J=8.5$ Hz, 1 H, H–Ph), 7.81 (d, $J=2.1$ Hz, 1 H, H–Ph), 7.97 (s, 1 H, H-6), 8.72 (s, 1 H, H-2). ^{13}C NMR (75 MHz, DMSO-d_6) δ: 23.1 (CH$_3$), 61.5 (C-5′), 70.5 (C-3′), 74.0 (C-2′), 85.2 (C-4′), 86.6 (C-1′), 114.5 (C-5), 115.6 (C-4a), 125.6 (C-6), 129.9 (C-4$_{Ph}$), 130.1 (C-6$_{Ph}$), 130.3 (C-5$_{Ph}$), 131.0 (C-3$_{Ph}$), 131.3 (C-2$_{Ph}$), 135.1 (C-1$_{Ph}$), 150.7 (C-7a), 151.0 (C-2), 159.3 (C-4). HRMS (ESI): calculated for C$_{18}$H$_{18}$ClN$_3$O$_4$ ([M+H]$^+$): 410.0669, found: 410.0682.

4-Methyl-5-(3-fluoro-4-chloro-phenyl)-N7-(β-D–ribofuranosyl)-7H-pyrrolo[2,3-d]-pyrimidine (40). 40 was prepared according to General procedure A. **67** (100 mg, 0.26 mmol) gave rise to **40** (40 mg, 0.10 mmol) as a white solid in 39% yield. Melting point: 205 °C. ^{1}H NMR (300 MHz, DMSO-d_6) δ: 2.49 (s, 3H, CH$_3$), 3.49–3.60 (m, 1 H, H-5″), 3.60–3.71 (m, 1 H, H-5′), 3.93 (q, $J=3.8$ Hz, 1 H, H-4′), 4.13 (dd, $J=8.4$, 4.8 Hz, 1 H, H-3′), 4.46 (q, $J=5.9$ Hz, 1 H, H-2′), 5.04 (t, $J=5.6$ Hz, 1 H, OH-5′), 5.18 (d, $J=5.0$ Hz, 1 H, OH-3′), 5.38 (d, $J=6.4$ Hz, 1 H, OH-2′), 6.27 (d, $J=6.2$ Hz, 1 H, H-1′), 7.39 (dd, $J=8.2$, 1.5 Hz, 1 H, H–Ph), 7.61 (dd, $J=10.5$, 2.1 Hz, 1 H, H–Ph), 7.64–7.72 (m, 1 H, H–Ph), 7.95 (s, 1 H, H-6), 8.71 (s, 1 H, H-2). ^{13}C NMR (75 MHz, DMSO-d_6) δ: 23.1 (CH$_3$), 61.5 (C-5′), 70.5 (C-3′), 74.0 (C-2′), 85.2 (C-4′), 86.6 (C-1′), 114.8 (C-5), 115.5 (C-4a), 117.9 (d, $J=20.7$ Hz, 1 C, C–Ph), 118.3 (d, $J=17.3$ Hz, 1 C, C–Ph), 125.6 (C-6), 127.1 (d, $J=3.5$ Hz, 1 C, C–Ph), 130.4 (C–Ph), 135.6 (d, $J=8.1$ Hz, 1 C, C–Ph), 150.7 (C-7a), 151.0 (C-2), 156.9 (d, $J=246.5$ Hz, 1 C, C–Ph), 159.3 (C-4). ^{19}F NMR (282 MHz, DMSO-d_6) δ: −116.42−−116.36 (m, 1F). HRMS (ESI): calculated for C$_{18}$H$_{18}$ClFN$_3$O$_4$ ([M+H]$^+$): 394.0964, found: 394.0960.

4-Methyl-5-(3-trifluoromethyl-4-chloro-phenyl)-N7-(β-D–ribofuranosyl)-7H-pyrrolo[2,3-d]-pyrimidine (41). 41 was prepared according to General procedure A. **67** (100 mg, 0.26 mmol) gave rise to **41** (51 mg, 0.12 mmol) as a white solid in 45% yield. Melting point:

242 °C. ^{1}H NMR (300 MHz, DMSO-d_6) δ: 2.47 (m, 3 H, CH$_3$), 3.48–3.60 (m, 1 H, H-5″), 3.60–3.73 (m, 1 H, H-5′), 3.93 (q, $J=3.8$ Hz, 1 H, H-4′), 4.10–4.20 (m, 1 H, H-3′), 4.47 (q, $J=6.0$ Hz, 1 H, H-2′), 5.03 (t, $J=5.6$ Hz, 1 H, OH-5′), 5.19 (d, $J=5.0$ Hz, 1 H, OH-3′), 5.39 (d, $J=6.2$ Hz, 1 H, OH-2′), 6.28 (d, $J=5.9$ Hz, 1 H, H-1′), 7.76–7.92 (m, 2 H, H–Ph), 7.97 (d, $J=1.8$ Hz, 1 H, H–Ph), 8.03 (s, 1 H, H-6), 8.73 (s, 1 H, H-2). ^{13}C NMR (75 MHz, DMSO-d_6) δ: 23.1 (CH$_3$), 61.4 (C-5′), 70.4 (C-3′), 73.9 (C-2′), 85.2 (C-4′), 86.6 (C-1′), 114.3 (C-5), 115.5 (C-4a), 122.8 (q, $J=274.91$ Hz, 1 C, CF$_3$), 125.9 (C-6), 126.5 (q, $J=31.1$ Hz, 1 C, C-3$_{Ph}$), 128.5 (q, $J=5.8$ Hz, 1 C, C-2$_{Ph}$), 129.4 (d, $J=2.3$ Hz, 1 C, C-4$_{Ph}$), 131.5 (C-5$_{Ph}$), 134.0 (C-1$_{Ph}$), 135.3 (C-6$_{Ph}$), 150.8 (C-2), 151.0 (C-7a), 159.2 (C-4). ^{19}F NMR (282 MHz, DMSO-d_6) δ: −61.154394. HRMS (ESI): calculated for C$_{19}$H$_{18}$ClF$_3$N$_3$O$_4$ ([M+H]$^+$): 444.0932, found: 444.0912.

4-Methyl-5-(3-methyl-4-chloro-phenyl)-N7-(β-D–ribofuranosyl)-7H-pyrrolo[2,3-d]-pyrimidine (42). 42 was prepared according to General procedure A. **67** (100 mg, 0.26 mmol) gave rise to **42** (56 mg, 0.14 mmol) as a white solid in 55% yield. Melting point: 208 °C. ^{1}H NMR (300 MHz, DMSO-d_6) δ: 2.40 (s, 3 H, CH$_3$), 2.47 (s, 3 H, CH$_3$), 3.55 (ddd, $J=11.8$, 5.6, 4.0 Hz, 1 H, H-5″), 3.64 (ddd, $J=12.0$, 5.2, 4.0 Hz, 1 H, H-5′), 3.93 (q, $J=3.7$ Hz, 1 H, H-4′), 4.07–4.19 (m, 1 H, H-3′), 4.46 (dd, $J=11.8$, 6.2 Hz, 1 H, H-2′), 5.04 (t, $J=5.6$ Hz, 1 H, OH-5′), 5.17 (d, $J=4.7$ Hz, 1 H, OH-3′), 5.37 (d, $J=6.2$ Hz, 1 H, OH-2′), 6.27 (d, $J=5.9$ Hz, 1 H, H-1′), 7.35 (dd, $J=8.2$, 1.8 Hz, 1 H, H–Ph), 7.45–7.55 (m, 2 H, H–Ph), 7.86 (s, 1 H, H-6), 8.70 (s, 1 H, H-2). ^{13}C NMR (100 MHz, DMSO-d_6) δ: 19.6 (CH$_3$), 23.0 (CH$_3$), 61.5 (C-5′), 70.5 (C-3′), 74.0 (C-2′), 85.2 (C-4′), 86.5 (C-1′), 115.7 (C-5), 115.8 (C-4a), 124.9 (C-6), 128.6 (C-5$_{Ph}$), 129.0 (C-6$_{Ph}$), 132.2 (C-3$_{Ph}$), 132.4 (C-2$_{Ph}$), 133.2 (C-1$_{Ph}$), 135.3 (C-4$_{Ph}$), 150.7 (C-7a), 150.9 (C-2), 159.3 (C-4). HRMS (ESI): calculated for C$_{19}$H$_{21}$ClN$_3$O$_4$ ([M+H]$^+$): 390.1215, found: 390.1198.

4-Methyl-5-(3-methoxy-4-chloro-phenyl)-N7-(β-D–ribofuranosyl)-7H-pyrrolo[2,3-d]-pyrimidine (43). 43 was prepared according to General procedure A. **67** (100 mg, 0.26 mmol) gave rise to **43** (36 mg, 0.089 mmol) as a light yellow solid in 34% yield. Melting point: 50 °C. ^{1}H NMR (400 MHz, DMSO-d_6) δ: 3.52–3.58 (m, 1 H, H-5″), 3.62–3.67 (m, 1 H, H-5′), 3.91–3.95 (m, 4 H, H-4′ and CH$_3$), 4.13 (q, $J=4.2$ Hz, 1 H, H-3′), 4.47 (q, $J=6.1$ Hz, 1 H, H-2′), 5.05 (t, $J=5.4$ Hz, 1 H, OH-5′), 5.18 (d, $J=4.9$ Hz, 1 H, OH-3′), 5.37 (d, $J=6.5$ Hz, 1 H, OH-2′), 6.27 (d, $J=6.1$ Hz, 1 H, H-1′), 7.08 (dd, $J=8.0$, 1.9 Hz, 1 H, H–Ph), 7.25 (d, $J=1.9$ Hz, 1 H, H–Ph), 7.50 (d, $J=8.0$ Hz, 1 H, H–Ph), 7.90 (s, 1 H, H-6), 8.70 (s, 1 H, H-2). ^{13}C NMR (100 MHz, DMSO-d_6) δ: 23.1 (CH$_3$), 56.2 (OCH$_3$), 61.4 (C-5′), 70.5 (C-3′), 74.0 (C-2′), 85.2 (C-4′), 86.6 (C-1′), 114.3 (C-2$_{Ph}$), 115.8 (C-4a), 116.1 (C-5), 120.0 (C-4$_{Ph}$), 122.7 (C-6$_{Ph}$), 125.1 (C-6), 129.6 (C-5$_{Ph}$), 134.6 (C-$_{Ph}$), 150.6 (C-7a), 150.9 (C-2), 154.1 (C-3$_{Ph}$), 159.3 (C-4). HRMS (ESI): calculated for C$_{19}$H$_{21}$ClN$_3$O$_5$ ([M+H]$^+$): 406.1164, found: 406.1187.

4-Methyl-5-(2-chloro-4-chloro-phenyl)-N7-(β-D–ribofuranosyl)-7H-pyrrolo[2,3-d]-pyrimidine (44). 44 was prepared according to General procedure A. **67** (100 mg, 0.26 mmol) gave rise to **44** (35 mg, 0.085 mmol) as a white solid in 33% yield. Melting point: 120–122 °C. ^{1}H NMR (300 MHz, DMSO-d_6) δ: 2.30 (s, 3 H, CH$_3$), 3.55 (ddd, $J=12.0$, 5.5, 4.0 Hz, 1 H, H-5″), 3.64 (ddd, $J=11.8$, 5.2, 4.2 Hz, 1 H, H-5′), 3.94 (q, $J=3.8$ Hz, 1 H, H-4′), 4.07–4.17 (m, 1 H, H-3′), 4.45 (dd, $J=11.5$, 6.2 Hz, 1 H, H-2′), 5.04 (t, $J=5.4$ Hz, 1 H, OH-5′), 5.18 (d, $J=5.0$ Hz, 1 H, OH-3′), 5.39 (d, $J=6.2$ Hz, 1 H, OH-2′), 6.25 (d, $J=5.9$ Hz, 1 H, H-1′), 7.47–7.59 (m, 2 H, H–Ph), 7.80 (dd, $J=1.5$, 0.9 Hz, 1 H, H–Ph), 7.89 (s, 1 H, H-6), 8.71 (s, 1 H, H-2). ^{13}C NMR (75 MHz, DMSO-d_6) δ: 21.2 (CH$_3$), 61.5 (C-5′), 70.5 (C-3′), 74.1 (C-2′), 85.2 (C-4′), 86.8 (C-1′), 112.2 (C-5), 116.6 (C-4a), 125.7 (C-6), 127.4 (C-3$_{Ph}$), 128.8 (C-5$_{Ph}$), 132.4 (C-1$_{Ph}$), 133.5 (C–Ph), 134.1 (C-2$_{Ph}$), 135.0 (C–Ph), 150.3 (C-2), 151.0 (C-7a), 159.0 (C-4). HRMS (ESI): calculated for C$_{18}$H$_{18}$Cl$_2$N$_3$O$_4$ ([M+H]$^+$): 410.0669, found: 410.0664.

4-Methyl-5-(2-fluorol-4-chloro-phenyl)-N7-(β-D–ribofuranosyl)-7H-pyrrolo[2,3-d]-pyrimidine (45). 45 was prepared according to

273

ChemMedChem

Full Papers
doi.org/10.1002/cmdc.202100144

**Chemistry
Europe**
European Chemical
Societies Publishing

General procedure A. **67** (100 mg, 0.26 mmol) gave rise to **45** (33 mg, 0.084 mmol) as a white solid in 32% yield. Melting point: 223 °C. ^{1}H NMR (300 MHz, DMSO-d_6) δ: 2.39 (s, 3 H, CH$_3$), 3.48–3.60 (m, 1 H, H-5''), 3.60–3.76 (m, 1 H, H-5'), 3.94 (q, J=3.7 Hz, 1 H, H-4'), 4.09–4.18 (m, 1 H, H-3'), 4.47 (q, J=6.2 Hz, 1 H, H-2'), 5.04 (t, J= 5.4 Hz, 1 H, OH-5'), 5.18 (d, J=5.0 Hz, 1 H, OH-3'), 5.40 (d, J=6.4 Hz, 1 H, OH-2'), 6.27 (d, J=6.2 Hz, 1 H, H-1'), 7.42 (dd, J=8.2, 2.1 Hz, 1 H, H–Ph), 7.55 (t, J=6.2 Hz, 1 H, H–Ph), 7.60 (dd, J=9.7, 2.1 Hz, 1 H, H–Ph), 7.94 (s, 1 H, H-6), 8.72 (s, 1 H, H-2). ^{13}C NMR (75 MHz, DMSO-d_6) δ: 21.4 (CH$_3$), 61.5 (C-5'), 70.5 (C-3'), 74.0 (C-2'), 85.3 (C-4'), 86.7 (C-1'), 108.3 (C-5), 116.4 (d, J=21.9 Hz, 1 C, C–Ph), 116.4 (C-4a), 121.2 (d, J=16.1 Hz, 1 C, C–Ph), 124.8 (d, J=3.5 Hz, 1 C, C–Ph), 126.1 (C-6), 133.3 (d, J=10.4 Hz, 1 C, C–Ph), 133.7 (d, J=3.5 Hz, 1 C, C–Ph), 150.5 (C-7a), 151.0 (C-2), 159.2 (C-4), 159.7 (d, J=247.6 Hz, 1 C, C–Ph). ^{19}F NMR (282 MHz, DMSO-d_6) δ: −111.36−−111.30 (m, 1 F). HRMS (ESI): calculated for C$_{18}$H$_{18}$ClFN$_3$O$_4$ ([M+H]$^+$): 394.0964, found: 394.0972.

4-Methyl-5-(3,5-dichloro-phenyl)-N7-(β-D–ribofuranosyl)-7H-pyrrolo[2,3-d]-pyrimidine (46). **46** was prepared according to General procedure A. **67** (100 mg, 0.26 mmol) gave rise to **46** (35 mg, 0.085 mmol) as a white solid in 33% yield. Melting point: 230 °C. ^{1}H NMR (300 MHz, DMSO-d_6) δ: 2.51 (s, 3 H, CH$_3$), 3.55 (ddd, J=12.0, 5.7, 4.3 Hz, 1 H, H-5''), 3.65 (ddd, J=12.0, 5.3, 4.1 Hz, 1 H, H-5'), 3.93 (q, J=4.1 Hz, 1 H, H-4'), 4.09–4.18 (m, 1 H, H-3'), 4.46 (dd, J=11.5, 6.0 Hz, 1 H, H-2'), 5.03 (t, J=5.6 Hz, 1 H, OH-5'), 5.18 (d, J=5.0 Hz, 1 H, OH-3'), 5.38 (d, J=6.4 Hz, 1 H, OH-2'), 6.27 (d, J=5.9 Hz, 1 H, H-1'), 7.56–7.69 (m, 3 H, H–Ph), 8.01 (s, 1 H, H-6), 8.72 (s, 1 H, H-2). ^{13}C NMR (75 MHz, DMSO-d_6) δ: 23.1 (CH$_3$), 61.5 (C-5'), 70.4 (C-3'), 74.0 (C-2'), 85.2 (C-4'), 86.6 (C-1'), 114.3 (C-5), 115.5 (C-4a), 126.0 (C-6), 126.6 (C–Ph), 128.3 (C–Ph), 133.9 (C–Ph), 137.9 (C-1$_{Ph}$), 150.7 (C-2), 151.0 (C-7a), 159.3 (C-4). HRMS (ESI): calculated for C$_{18}$H$_{18}$Cl$_2$N$_3$O$_4$ ([M+H]$^+$): 410.0669, found: 410.0669.

4-Methyl-5-(4–chloro-3,5-difluoro-4-chloro-phenyl)-N7-(β-D–ribofuranosyl)-7H-pyrrolo[2,3-d]-pyrimidine (47). **47** was prepared according to General procedure A. **67** (100 mg, 0.26 mmol) gave rise to **47** (37 mg, 0.090 mmol) as a white solid in 35% yield. Melting point: 212 °C. ^{1}H NMR (300 MHz, DMSO-d_6) δ: 2.54 (s, 3 H, CH$_3$), 3.55 (ddd, J=12.0, 5.6, 4.2 Hz, 1 H, H-5''), 3.65 (ddd, J=12.0, 5.4, 4.2 Hz, 1 H, H-5'), 3.93 (q, J=3.8 Hz, 1 H, H-4'), 4.08–4.20 (m, 1 H, H-3'), 4.45 (q, J=5.8 Hz, 1 H, H-2'), 5.04 (t, J=5.6 Hz, 1 H, OH-5'), 5.19 (d, J=5.0 Hz, 1 H, OH-3'), 5.39 (d, J=6.4 Hz, 1 H, OH-2'), 6.27 (d, J=6.2 Hz, 1 H, H-1'), 7.45–7.61 (m, 2 H, H–Ph), 8.01 (s, 1 H, H-6), 8.73 (s, 1 H, H-2). ^{13}C NMR (75 MHz, DMSO-d_6) δ: 23.3 (CH$_3$), 61.4 (C-5'), 70.4 (C-3'), 74.1 (C-2'), 85.2 (C-4'), 86.6 (C-1'), 106.8 (C–Ph), 113.9 (d, J=45.8 Hz, 1 C, C–Ph), 114.0 (C-5), 116.4 (d, J=21.9 Hz, 1 C, C–Ph), 115.4 (C-4a), 126.1 (C-6), 135.6 (t, J=10.2 Hz, 1 C, C–Ph), 150.7 (C-7a), 151.1 (C-2), 156.5 (d, J=3.6 Hz, 1 C, C-1$_{Ph}$), 158.9 (d, J= 4.4 Hz, 1 C, C–Ph), 159.5 (C-4). ^{19}F NMR (282 MHz, DMSO-d_6) δ: −114.34−−114.31. HRMS (ESI): calculated for C$_{18}$H$_{17}$ClF$_2$N$_3$O$_4$ ([M+H]$^+$): 412.0870, found: 412.0860.

4-Methyl-5-([1,1′-biphenyl]-4-yl)-N7-(β-D–ribofuranosyl)-7H-pyrrolo[2,3-d]-pyrimidine (48). **48** was prepared according to General procedure A. **67** (100 mg, 0.26 mmol) gave rise to **48** (60 mg, 0.14 mmol) as a white solid in 55% yield. Melting point: 134 °C. ^{1}H NMR (300 MHz, DMSO-d_6) δ: 2.53 (s, 3 H, CH$_3$), 3.56 (ddd, J=12.0, 5.6, 4.2 Hz, 1 H, H-5''), 3.66 (ddd, J=12.0, 5.2, 4.2 Hz, 1 H, H-5'), 3.94 (q, J=3.7 Hz, 1 H, H-4'), 4.10–4.22 (m, 1 H, H-3'), 4.49 (dd, J=11.6, 6.2 Hz, 1 H, H-2'), 5.07 (t, J=5.6 Hz, 1 H, OH-5'), 5.17 (d, J=4.7 Hz, 1 H, OH-3'), 5.39 (d, J=6.4 Hz, 1 H, OH-2'), 6.30 (d, J=6.2 Hz, 1 H, H-1'), 7.33–7.43 (m, 1 H, H–Ph), 7.44–7.54 (m, 2 H, H–Ph), 7.57–7.67 (m, 2 H, H–Ph), 7.70–7.83 (m, 4 H, H–Ph), 7.91 (s, 1 H, H-6), 8.71 (s, 1 H, H-2). ^{13}C NMR (100 MHz, DMSO-d_6) δ: 23.0 (CH$_3$), 61.5 (C-5'), 70.6 (C-3'), 74.0 (C-2'), 85.2 (C-4'), 86.6 (C-1'), 115.8 (C-4a), 116.6 (C-5), 124.9 (C-6), 126.5 (C–Ph), 126.6 (C–Ph), 127.5 (C–Ph), 127.8 (C–Ph), 129.0 (C–Ph), 130.3 (C–Ph), 133.4 (C–Ph), 138.8 (C–Ph), 139.7

(C–Ph), 150.8 (C-2 and C-7a), 159.3 (C-4). HRMS (ESI): calculated for C$_{24}$H$_{24}$N$_3$O$_4$ ([M+H]$^+$): 418.1761, found: 418.1749.

4-Methyl-5-(naphthalen-2-yl)-N7-(β-D–ribofuranosyl)-7H-pyrrolo[2,3-d]-pyrimidine (49). **49** was prepared according to General procedure A. **67** (100 mg, 0.26 mmol) gave rise to **49** (25 mg, 0.064 mmol) as a white solid in 25% yield. Melting point: 135 °C. ^{1}H NMR (300 MHz, DMSO-d_6) δ: 2.49 (s, 3 H, CH$_3$), 3.56 (ddd, J=11.8, 5.6, 4.1 Hz, 1 H, H-5''), 3.66 (ddd, J=11.8, 5.2, 4.2 Hz, 1 H, H-5'), 3.95 (q, J=3.6 Hz, 1 H, H-4'), 4.10–4.22 (m, 1 H, H-3'), 4.51 (dd, J=11.5, 6.0 Hz, 1 H, H-2'), 5.06 (t, J=5.4 Hz, 1 H, OH-5'), 5.18 (d, J=4.7 Hz, 1 H, OH-3'), 5.40 (d, J=6.4 Hz, 1 H, OH-2'), 6.31 (d, J=6.2 Hz, 1 H, H-1'), 7.48–7.62 (m, 2 H, H-Nap), 7.68 (dd, J=8.5, 1.8 Hz, 1 H, H-Nap), 7.90–8.13 (m, 5 H, H-Nap and H-6), 8.72 (s, 1 H, H-2). ^{13}C NMR (75 MHz, DMSO-d_6) δ: 23.0 (CH$_3$), 61.5 (C-5'), 70.5 (C-3'), 74.0 (C-2'), 85.2 (C-4'), 86.5 (C-1'), 116.0 (C-4a), 116.9 (C-5), 125.0 (C-6), 126.0 (C-Nap), 126.4 (C-Nap), 127.6 (C-Nap), 127.8 (C-Nap), 128.0 (C-Nap), 128.3 (C-Nap), 131.7 (C-Nap), 132.9 (C-Nap), 150.8 (C-2), 150.9 (C-7a), 159.3 (C-4). HRMS (ESI): calculated for C$_{22}$H$_{22}$N$_3$O$_4$([M+H]$^+$): 392.1605, found: 392.1600.

4-Methyl-5-(benzo[d][1,3]dioxol-5-yl)-N7-(β-D–ribofuranosyl)-7H-pyrrolo[2,3-d]-pyrimidine (50). **50** was prepared according to General procedure A. **67** (150 mg, 0.38 mmol) gave rise to **50** (95 mg, 0.25 mmol) as a white solid in 65% yield. Melting point: 232 °C. ^{1}H NMR (400 MHz, DMSO-d_6) δ: 2.48 (s, 3 H, CH$_3$), 3.52–3.57 (m, 1 H, H-5''), 3.61–3.67 (m, 1 H, H-5'), 3.92 (q, J=3.4 Hz, 1 H, H-4'), 4.13 (q, J=4.5 Hz, 1 H, H-3'), 4.45 (q, J=6.0 Hz, 1 H, H-2'), 5.05 (t, J= 5.4 Hz, 1 H, OH-5'), 5.16 (d, J=4.9 Hz, 1 H, OH-3'), 5.36 (d, J=6.4 Hz, 1 H, OH-2'), 6.08 (s, 2 H, CH$_2$), 6.26 (d, J=6.0 Hz, 1 H, H-1'), 6.94 (d, J=7.9 Hz, 1 H, H–Ph), 7.00 (d, J=7.9 Hz, 1 H, H–Ph), 7.07 (s, 1 H, H–Ph), 7.78 (s, 1 H, H-6), 8.67 (s, 1 H, H-2). ^{13}C NMR (100 MHz, DMSO-d_6) δ: 22.8 (CH$_3$), 61.5 (C-5'), 70.5 (C-3'), 74.0 (C-2'), 85.1 (C-4'), 86.5 (C-1'), 101.1 (CH$_2$), 108.1 (C–Ph), 110.3 (C–Ph), 115.9 (C-4a), 116.7 (C-5), 123.3 (C–Ph), 124.6 (C-6), 127.9 (C–Ph), 146.5 (C–Ph), 147.1 (C–Ph), 150.5 (C-7a), 150.7 (C-2), 159.2 (C-4). HRMS (ESI): calculated for C$_{19}$H$_{20}$N$_3$O$_6$ ([M+H]$^+$): 386.1347, found: 386.1350.

4-Methyl-5-(2,3-dihydrobenzo[b][1,4]dioxin-6-yl)-N7-(β-D–ribofuranosyl)-7H-pyrrolo[2,3-d]-pyrimidine (51). **51** was prepared according to General procedure A. **67** (120 mg, 0.31 mmol) gave rise to **51** (55 mg, 0.14 mmol) as a white solid in 44% yield. Melting point: 127 °C. ^{1}H NMR (400 MHz, DMSO-d_6) δ: 2.48 (s, 3 H, CH$_3$), 3.52–3.57 (m, 1 H, H-5''), 3.61–3.66 (m, 1 H, H-5'), 3.92 (q, J=3.5 Hz, 1 H, H-4'), 4.12 (q, J=4.3 Hz, 1 H, H-3'), 4.29 (s, 4 H, 2CH$_2$), 4.45 (q, J=6.0 Hz, 1 H, H-2'), 5.05 (t, J=5.4 Hz, 1 H, OH-5'), 5.15 (d, J=4.8 Hz, 1 H, OH-3'), 5.35 (d, J=6.4 Hz, 1 H, OH-2'), 6.25 (d, J=6.1 Hz, 1 H, H-1'), 6.93 (s, 2 H, H–Ph), 6.98 (s, 1 H, H–Ph), 7.76 (s, 1 H, H-6), 8.67 (s, 1 H, H-2) . ^{13}C NMR (100 MHz, DMSO-d_6) δ: 22.8 (CH$_3$), 61.5 (C-5'), 64.1 (2CH$_2$), 70.5 (C-3'), 74.0 (C-2'), 85.1 (C-4'), 86.5 (C-1'), 115.9 (C-4a), 116.5 (C-5), 116.8 (C–Ph), 118.3 (C–Ph), 122.9 (C–Ph), 124.5 (C-6), 127.3 (C–Ph), 142.8 (C–Ph), 143.0 (C–Ph),150.5 (C-7a), 150.7 (C-2), 159.2 (C-4). HRMS (ESI): calculated for C$_{20}$H$_{22}$N$_3$O$_6$ ([M+H]$^+$): 400.1503, found: 400.1509.

4-Methyl-5-(1H-indol-6-yl)-N7-(β-D–ribofuranosyl)-7H-pyrrolo[2,3-d]-pyrimidine (52). **52** was prepared according to General procedure A. **67** (120 mg, 0.31 mmol) gave rise to slightly impure **52** (35 mg, 0.092 mmol). **52** was purified by preparative RP-HPLC gradient: 0.2% formic acid in water:MeCN at a flow rate of 20 mL/min; The initial gradient composition (95% A/05% B) was held for 2.0 min, increased to 60% B in 13 min, then increased to 100% B in 1 min. After preparative RP-HPLC, **52** was isolated as a white solid (25 mg, 0.066 mmol) in 21% yield. Melting point: 153 °C. ^{1}H NMR (400 MHz, DMSO-d_6) δ: 2.45 (s, 3 H, CH$_3$), 3.53–3.57 (m, 1 H, H-5''), 3.62–3.66 (m, 1 H, H-5'), 3.94 (q, J=3.7 Hz, 1 H, H-4'), 4.13 (dd, J= 4.9, 3.3 Hz, 1 H, H-3'), 4.50 (t, J=5.7 Hz, 1 H, H-2'), 5.22 (br.s. 3 H, OH-2', OH-3'and OH-5') 6.29 (d, J=6.3 Hz, 1 H, H-1'), 6.47 (br.s., 1 H,

These are not the final page numbers! ↗↗

274

ChemMedChem

Full Papers
doi.org/10.1002/cmdc.202100144

**Chemistry
Europe**
European Chemical
Societies Publishing

H-indole), 7.12 (d, $J=8.1$ Hz, 1 H, H-indole), 7.39 (t, $J=2.7$ Hz, 1 H, H-indole), 7.47 (s, 1 H, H-indole), 7.61 (d, $J=8.1$ Hz, 1 H, H-indole), 7.79 (s, 1 H, H-6), 8.68 (s, 1 H, H-2), 11.16 (br. s., 1 H, NH). ^{13}C NMR (100 MHz, DMSO-d_6) δ: 22.8 (CH$_3$), 61.6 (C-5'), 70.6 (C-3'), 73.9 (C-2'), 85.2 (C-4'), 86.5 (C-1'), 101.0 (C-indole), 112.5 (C-indole), 116.2 (C-4a), 118.3 (C-5), 119.6 (C-indole), 121.5 (C-indole), 124.2 (C-6), 125.8 (C-indole), 126.8 (C-indole), 126.8 (C-indole), 135.8 (C-indole), 150.6 (C-7a and C-2), 159.2 (C-4). HRMS (ESI): calculated for C$_{20}$H$_{21}$N$_4$O$_4$ ([M+H]$^+$): 381.1557, found: 381.1565.

4-Methyl-5-(1-methyl-1H-indol-6-yl)-N7-(β-D-ribofuranosyl)-7H-pyrrolo[2,3-d]-pyrimidine (53). 53 was prepared according to General procedure A. **67** (150 mg, 0.38 mmol) gave rise to **53** (85 mg, 0.22 mmol) as a white solid in 57% yield. Melting point: 135 °C. ^{1}H NMR (400 MHz, DMSO-d_6) δ: 2.45 (s, 3 H, CH$_3$), 3.53–3.58 (m, 1 H, H-5''), 3.62–3.67 (m, 1 H, H-5'), 3.82 (s, 3 H, CH$_3$), 3.94 (q, $J=$ 3.2 Hz, 1 H, H-4'), 4.14 (q, $J=4.2$ Hz, 1 H, H-3'), 4.49 (q, $J=5.7$ Hz, 1 H, H-2'), 5.06 (t, $J=5.4$ Hz, 1 H, OH-5'), 5.17 (dd, $J=4.8$, 1.2 Hz, 1 H, OH-3'), 5.37 (dd, $J=6.4$, 1.4 Hz, 1 H, OH-2'), 6.30 (d, $J=6.1$ Hz, 1 H, H-1'), 6.47 (dd, $J=3.1$, 0.6 Hz, 1 H, H-indole), 7.16 (dd, $J=8.1$, 1.2 Hz, 1 H, H-indole), 7.37 (d, $J=3.1$ Hz, 1 H, H-indole), 7.53 (s, 1 H, H-indole), 7.61 (d, $J=8.0$ Hz, 1 H, H-indole), 7.81 (s, 1 H, H-6), 8.69 (s, 1 H, H-2). ^{13}C NMR (100 MHz, DMSO-d_6) δ: 22.9 (CH$_3$), 32.5 (CH$_3$), 61.6 (C-5'), 70.6 (C-3'), 74.0 (C-2'), 85.1 (C-4'), 86.5 (C-1'), 100.3 (C-indole), 110.9 (C-indole), 116.2 (C-4a), 118.3 (C-5), 119.9 (C-indole), 121.5 (C-indole), 124.3 (C-6), 127.0 (C-indole), 127.1 (C-indole), 130.1 (C-indole), 136.3 (C-indole), 150.6 (C-7a), 150.7 (C-2), 159.3 (C-4). HRMS (ESI): calculated for C$_{21}$H$_{23}$N$_4$O$_4$ ([M+H]$^+$): 395.1714, found: 395.1711.

4-Chloro-5-iodo-N7-(2',5'-di-O-benzoyl-3'-deoxy-β-D–ribofuranosyl)-pyrrolo[2,3-d]pyrimidine (81).[33] 4-chloro-5-iodo-7H-pyrrolo[2,3-d]pyrimidine (500 mg, 1.79 mmol) was placed in a 100 mL two-neck round bottom flask, after which the flask was purged with N$_2$ gas. Anhydrous MeCN (15 mL, 7.5 mL/mmol of SM) was added. BSA (482 μL, 1.97 mmol, 1.1 eq.) was added into the suspension via syringe. The resulting mixture was stirred until the solid was completely dissolved. Next, 1-O-acetyl-2,5-di-O-benzoyl-3-deoxy-α/β-D-ribofuranose (760 mg, 1.97 mmol, 1.1 eq.) was added, and immediately followed by TMSOTf (357 μL, 1.97 mmol, 1.1 eq.). The reaction mixture was stirred at ambient temperature for 15 min, and was heated at 80 °C. When full conversion of 4-chloro-5-iodo-7H-pyrrolo[2,3-d]pyrimidine was observed via HRMS, the mixture was cooled to room temperature. Then, EA (15 mL) and aq. sat. NaHCO$_3$ (15 mL) were added. The layers were separated and the water layer extracted twice more with EA. Then, the organic layers were combined, washed with brine, dried over Na$_2$SO$_4$, filtered, and evaporated. The residue was purified by column chromatography (5→30% EA/PET) to give a colorless foam (800 mg, 1.32 mmol) in 74% yield. ^{1}H NMR (300 MHz, CDCl$_3$) δ: 2.44 (ddd, $J=14.1$, 5.6, 1.8 Hz, 1 H, CH$_2$), 2.76 (ddd, $J=14.1$, 10.4, 6.0 Hz, 1 H, CH$_2$), 4.56–4.61 (m, 1 H, H-5''), 4.73–4.78 (m, 1 H, H-5'), 4.80–4.88 (m, 1 H, H-4'), 5.90–5.92 (m, 1 H, H-2'), 6.45 (d, $J=1.8$ Hz, 1 H, H-1'), 7.45–7.51 (m, 4 H, H-OBz), 7.57–7.65 (m, 3 H, H-6 and H-OBz), 8.01–8.09 (m, 4 H, H-OBz), 8.59 (s, 1 H, H-2). HRMS (ESI): calculated for C$_{20}$H$_{25}$ClIN$_3$O$_5$ ([M+H]$^+$): 604.0131, found: 604.0126.

4-Methyl-N7-(2',5'-di-O-benzoyl-3'-deoxy-β-D–ribofuranosyl)-pyrrolo[2,3-d]pyrimidine (82). 81 (800 mg, 1.32 mmol) was placed in a 25 mL round bottom flask. Then, the flask was purged with argon. Next, anhydrous THF (5 mL) was added, and the reaction solution was stirred at −10 °C for 15 min. i-PrMgCl·LiCl (1.3 M in THF, 1.52 mL, 1.98 mmol, 1.1 eq.) was added dropwise slowly. When full conversion of the SM was observed by TLC (1 h), 0.5 M aq. HCl solution (5 mL) and EA (10 mL) were added. The layers were separated, and the water layer was extracted twice more with EA (2×10 mL). Then, organic layers were combined, dried over Na$_2$SO$_4$, filtered, and evaporated. The residue was used directly for the next

step. This crude product, Pd(PPh$_3$)$_4$ (116 mg, 0.10 mmol, 0.1 eq.) were added in a 25 mL two-neck round bottom flask. The flask was purged with argon three times. Next, anhydrous THF (4 mL, 4 mL/mmol) was added via syringe, and AlMe$_3$ solution (2 M in toluene, 0.6 mL, 1.2 mmol, 1.2 eq.) was added dropwise. After the mixture was stirred for 15 min at ambient temperature, the reaction was refluxed at 100 °C until the TLC showed the SM was consumed completely (1 h). After cooling at ice-water bath, 0.5 M aq. HCl (10 mL) was added dropwise. [**Caution**: methane gas was generated, with potential excessive foaming]. Next, EA (50 mL) was added. The layers were separated and the water layer extracted twice more with EA. Then, the organic layers were combined, dried over Na$_2$SO$_4$, filtered, and evaporated. The residue was purified by column chromatography (10→50% EA/PET) to give **82** (400 mg, 0.87 mmol) as a yellow foam in 66% yield for two steps. ^{1}H NMR (300 MHz, CDCl$_3$) δ: 2.45 (ddd, $J=14.1$, 5.6, 1.8 Hz, 1 H, CH$_2$), 2.71 (s, 3 H, CH$_3$), 2.80–2.90 (m, 1 H, CH$_2$), 4.53–4.59 (m, 1 H, H-5''), 4.68–4.73 (m, 1 H, H-5'), 4.79–4.87 (m, 1 H, H-4'), 5.99 (dt, $J=6.2$, 1.8 Hz, 1 H, H-2'), 6.49 (d, $J=2.1$ Hz, 1 H, H-1'), 6.55 (d, $J=3.8$ Hz, 1 H, H-5), 7.33 (d, $J=3.8$ Hz, 1 H, H-6), 7.41–7.50 (m, 4 H, H-OBz), 7.52–7.71 (m, 2 H, H-OBz), 8.01–8.10 (m, 4 H, H-OBz), 8.74 (s, 1 H, H-2). HRMS (ESI): calculated for C$_{26}$H$_{24}$N$_3$O$_5$ ([M+H]$^+$): 458.1710, found: 458.1718.

4-Methyl-N7-(3'-deoxy-β-D–ribofuranosyl)-pyrrolo[2,3-d]pyrimidine (83). 82 (350 mg, 0.77 mmol) was placed in a 25 mL round bottom flask. Next, 0.5 M NaOMe in MeOH (5 mL) was added, and the reaction mixture was stirred for 2 h. Then, 0.5 M aq. HCl was added to neutralize the reaction solution. The resulting mixture was evaporated till dryness, and purified by flash column chromatography (0→10% MeOH/DCM) to afford **83** (160 mg, 0.64 mmol) as a white solid in 83% yield. ^{1}H NMR (300 MHz, DMSO-d_6) δ: 1.93 (ddd, $J=13.0$, 6.3, 3.2 Hz, 1 H, CH$_2$), 2.22 (ddd, $J=13.1$, 8.7, 6.0 Hz, 1 H, CH$_2$), 2.65 (s, 3 H, CH$_3$), 3.50–3.56 (m, 1 H, H-5''), 3.62–3.67 (m, 1 H, H-5'), 4.28–4.36 (m, 1 H, H-4'), 4.42–4.45 (m, 1 H, H-2'), 4.98 (t, $J=5.6$ Hz, 1 H, OH-5'), 5.60 (d, $J=4.4$ Hz, 1 H, OH-2'), 6.16 (d, $J=2.6$ Hz, 1 H, H-1'), 6.72 (d, $J=3.8$ Hz, 1 H, H-5), 7.78 (d, $J=3.5$ Hz, 1 H, H-6), 8.65 (s, 1 H, H-2). HRMS (ESI): calculated for C$_{12}$H$_{16}$N$_3$O$_3$ ([M+H]$^+$): 259.1186, found: 259.1180.

4-Methyl-5-bromo-N7-(3'-deoxy-β-D–ribofuranosyl)-pyrrolo[2,3-d]pyrimidine (84). 83 (100 mg, 0.40 mmol) was dissolved in DMF (2 mL), and NBS (107 mg, 0.60 mmol, 1.5 eq.) was added. The resulting mixture was stirred at 50 °C for 2 h. Then, the mixture was evaporated till dryness and purified by column chromatography (0→10% MeOH/DCM) to afford **84** (96 mg, 0.29 mmol) as a white solid in 73% yield. ^{1}H NMR (300 MHz, DMSO-d_6) δ: 1.89 (ddd, $J=13.2$, 6.3, 3.1 Hz, 1 H, CH$_2$), 2.22 (ddd, $J=13.2$, 8.8, 5.9 Hz, 1 H, CH$_2$), 2.84 (s, 3 H, CH$_3$), 3.53 (ddd, $J=12.0$, 5.3, 4.1 Hz, 1 H), H-5'', 3.70 (ddd, $J=12.0$, 5.4, 3.4 Hz, 1 H, H-5'), 4.29–4.37 (m, 1 H, H-4'), 4.39–4.44 (m, 1 H, H-4'), 5.05 (t, $J=5.4$ Hz, 1 H, OH-5'), 5.63 (d, $J=4.1$ Hz, 1 H, OH-2'), 6.18 (d, $J=2.3$ Hz, 1 H, H-1'), 8.07 (s, 1 H, H-6), 8.70 (s, 1 H, H-2). HRMS (ESI): calculated for C$_{12}$H$_{15}$BrN$_3$O$_3$ ([M+H]$^+$): 328.0291, found 328.0295.

4-Methyl-5-(4-chloro-phenyl)-N7-(3'-deoxy-β-D–ribofuranosyl)-pyrrolo[2,3-d]pyrimidine (54). 54 was prepared according to General procedure A. **84** (90 mg, 0.27 mmol) gave rise to **54** (35 mg, 0.10 mmol) as a white solid in 36% yield. Melting point: 181 °C. ^{1}H NMR (300 MHz, DMSO-d_6) δ: 1.92 (ddd, $J=13.0$, 6.3, 2.9 Hz, 1 H, CH$_2$), 2.27 (ddd, $J=13.0$, 8.8, 6.0 Hz, 1 H, CH$_2$), 2.46 (s, 3 H, CH$_3$), 3.52 (ddd, $J=11.9$, 5.4, 4.1 Hz, 1 H, H-5''), 3.67 (ddd, $J=11.9$, 5.6, 3.4 Hz, 1 H, H-5'), 4.27–4.40 (m, 1 H, H-4'), 4.42–4.55 (m, 1 H, H-2'), 4.98 (t, $J=5.4$ Hz, 1 H, OH-5'), 5.63 (d, $J=4.4$ Hz, 1 H, OH-2'), 6.25 (d, $J=2.3$ Hz, 1 H, H-1'), 7.44–7.58 (m, 4 H, H–Ph), 7.89 (s, 1 H, H-6), 8.70 (s, 1 H, H-2). ^{13}C NMR (75 MHz, DMSO-d_6) δ: 23.0 (CH$_3$), 34.5 (CH$_2$), 62.5 (C-5'), 75.0 (C-2'), 80.2 (C-4'), 90.0 (C-1'), 115.3 (C-4a), 115.5 (C-5), 124.8 (C-6), 128.2 (2 C, C–Ph), 131.5 (2 C, C–Ph), 131.9 (C-4$_{Ph}$), 133.3

ChemMedChem

Full Papers
doi.org/10.1002/cmdc.202100144

Chemistry Europe
European Chemical
Societies Publishing

(C-1$_{Ph}$), 150.0 (C-7a), 150.8 (C-2), 159.1 (C-4). HRMS (ESI): calculated for $C_{18}H_{19}ClN_3O_3$ ([M+H]$^+$): 360.1109, found: 360.1112.

Biology

In vitro *evaluation*

All *in vitro* compound evaluations were performed as described previously, including drug sensitivity assays on intracellular amastigotes of the Tulahuen (β-galactosidase expressing) *T. cruzi* strain in MRC-5 fibroblasts, Y-strain *T. cruzi* in primary mouse cardiac cells and Y-strain bloodstream trypomastigote forms (BF).[25] Cytotoxicity, as evaluated on MRC-5 fibroblasts and 2D primary mouse cardiac cells, was performed as described.[25]

Three-dimensional cardiac cell cultures: cardiac spheroids were obtained as reported.[45] For cardiotoxicity analyses, non-infected 3-D cultures were incubated for 48 h at 37 °C with increasing concentrations of BZ and compound **14** (up to 200 μM) and cellular viability determined using PrestoBlue® (CC) tests.[45] For determination of anti-*T. cruzi* activity, 3-D cultures were infected with BF (strain Y), using 20:1 parasite:host cell ratios. After 48 h, the cultures were rinsed and either or not incubated with 10 μM compound **14** or BZ (corresponding to the EC$_{90}$ value of the reference drug upon intracellular forms) for 96 h at 37 °C.[51] To determine the parasite load, infected spheroids were transferred to a tube for extraction of total DNA using High Pure PCR Template Preparation Kit, according to manufacturer's instructions (Roche, USA). At the final step of the protocol, DNA was eluted in 100 μL of elution buffer. The absolute quantification of the parasite's DNA was performed in a ABI 7500 Fast Real Time PCR instrument (Applied Biosystems), using the Cruzi 1 (5′-ASTCGGCTGATCGTTTTCGA-3′) and Cruzi 2 (5′-AATTCCTCCAAG-CAGCGGATA-3′) primers and Cruzi 3 probe (5′-FAM-CACACACTG GACACCAANFQ-MGB-3′) targeting *T. cruzi* nuclear satellite DNA, as reported[52] with minor modifications. qPCR were carried out with 5 μL DNA, using 10 μL FastStart Universal Probe Master Mix [2×] (Roche), 750 nM primer Cruzi 1, 750 nM primer Cruzi 2 and 50 nM probe Cruzi 3 (FAM/NFQ-MGB), in a final volume of 20 μL. In parallel, quantification of cardiac cell DNA was performed using a TaqMan assay targeting mouse glyceraldehyde 3-phosphate dehydrogenase (GAPDH) (Cat. No. Mm99999915–g1, Applied Biosystems). Cycling conditions were a first step of 10 minutes at 95 °C followed by 40 cycles at 95 °C for 15 sec. and 58 °C for 1 min. Standard curves were constructed with 1:10 serial dilutions of total DNA obtained from a pool of 7.5×10^4 spheroids spiked with 10^5 epimastigotes. Thus, *T. cruzi* and cardiac cell quantities were quantified and expressed as parasite equivalents/cardiac cell.[45]

Microsomal stability assays

The *in vitro* metabolic stability assays were performed exactly as described elsewhere.[51]

In vivo evaluation

For the *in vivo* evaluation, male Swiss Webster mice were obtained from the Fundação Oswaldo Cruz (FIOCRUZ) animal facilities (ICTB /FIOCRUZ, Rio de Janeiro, Brazil). Mice were housed at a maximum of 6 per cage and kept in a standard room at 20 to 24 °C under a 12 h/12 h light/dark cycle. The animals were provided with sterilized water and chow *ad libitum*. Mice (18 to 23 g) were infected by intraperitoneal (i.p.) route with 10^4 bloodstream trypomastigotes of the Y strain of *T. cruzi*. Age-matched non-infected mice were maintained under identical conditions.[25] These mice were divided into eight experimental groups: non-infected (mice were neither infected nor treated), non-treated (mice were infected but treated with vehicle −10 % (v/v) Tween 80 in sterile deionized water), and treatment (mice were infected and treated with **14** and/or the reference BZ). When a detectable parasitemia was observed at the onset of parasitemia (*i.e.*, 5 dpi), the corresponding treatments were initiated through oral administration. Compound **14** was administrated twice per day in 3 mice groups, using 10-fold dose titration schedules with 3 concentrations, namely 25, 2.5, 0.25 mg/kg, respectively. The reference drug BZ was administered orally at 10 (suboptimal) and 100 mg/kg (optimal dose) once per day, respectively. **14** was co-administered at 2.5 mg/kg (b.i.d) with BZ (once a day) at 10 mg/kg for consecutive 5 days, starting at parasitemia onset (5 dpi). All compounds were formulated freshly before every administration. 5 μL of blood of each individual experimental mouse was obtained via tail vein puncture and the number of parasites was counted under a light microscope to determine the blood parasitemia until 15 dpi. The mortality was monitored daily up to 24 days after the consecutive 5 days treatment (34 dpi) and presented as a percentage of cumulative mortality (CM). For qPCR analysis, at 136 dpi, after euthanasia, 500 μL of animal blood was diluted in 1:2 volume of guanidine solution (guanidine-HCl 6 M/EDTA 0.2 M), and heated for 90 sec. in boiling water. Guanidine-EDTA blood (GEB) samples were processed using the High Pure PCR Template Preparation kit, according to manufacturer's instructions (Roche, USA). At the final step of the protocol, DNA was eluted in 100 μL of elution buffer. Quantitative Real-Time PCR Multiplex assays were performed (40 cycles, threshold set at 0.01) for parasite detection of the *T. cruzi* satellite nuclear DNA and the internal amplification control-IAC (pZErO-2 plasmid containing an insert from the *Arabidopsis thaliana* aquaporin gene), as described.[53] The standard curves for absolute quantification were constructed with 1:10 serial dilutions of total DNA obtained from a negative GEB sample spiked with 10^5 parasite equivalents per milliliter of blood (par. eq./mL).

Ethics statement

All animal studies were carried out in strict accordance with the guidelines established by the FIOCRUZ Committee of Ethics for the Use of Animals (CEUA L038-2017).

Supporting Information

Copies of ^{1}H, ^{13}C and ^{19}F NMR spectra of compounds **77**, **21**, **27**, **28**, **29**, **37**, **40**, **41**, **45**, **47** and ^{1}H-^{13}C gHMBC and 2D NOESY spectra of compounds **67**, **14**, **16**, **20**, **77**, **78**, **79**, **25** and **54** can be found in the Supporting Information.

Abbreviations

BSA	*N,O*-bis(trimethylsilyl)acetamide
CD	Chagas disease
NTD	neglected tropical disease
T. cruzi	*Trypanosoma cruzi*
TMSOTf	trimethylsilyl trifluoromethanesulfonate
TPPTS	trisodium 3-bis(3-sulfonatophenyl) phosphanylbenzenesulfonate

ChemMedChem

Full Papers
doi.org/10.1002/cmdc.202100144

Chemistry Europe
European Chemical
Societies Publishing

Acknowledgements

Conflict of Interest

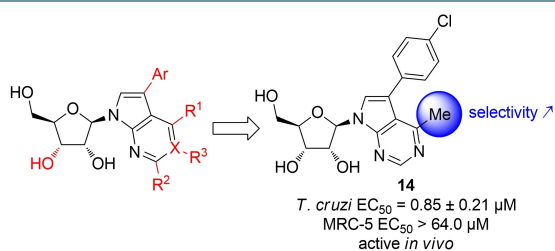The authors declare no conflict of interest.

Keywords: 7-deazapurine nucleosides · structure-activity relationships · *Trypanosoma cruzi* · in vivo efficacy

[1] B. Y. Lee, K. M. Bacon, M. E. Bottazzi, P. J. Hotez, *Lancet Infect. Dis.* **2013**, *13*, 342–348.
[2] J. M. Kratz, *Acta Trop.* **2019**, *198*, 105107.
[3] C. Bern, *N. Engl. J. Med.* **2015**, *373*, 456–466.
[4] C. Franco-Paredes, W. E. Villamil-Gomez, J. Schultz, A. F. Henao-Martinez, G. Parra-Henao, A. Rassi, A. J. Rodriguez-Morales, J. A. Suarez, *Travel. Med. Infect. Dis.* **2020**, *36*, 101565.
[5] S. Antinori, M. Corbellino, *Eur. J. Intern. Med.* **2018**, *48*, E29–E30.
[6] B. Monge-Maillo, R. Lopez-Velez, *Clin. Microbiol. Infect.* **2017**, *23*, 290–295.
[7] Drugs for Neglected Diseases initiative, *https://dndi.org/diseases/chagas/facts/* **2020**.
[8] US Centers for Disease Control and Prevention, *https://www.cdc.gov/parasites/chagas/biology.html* **2019**.
[9] World Health Organization, *https://www.who.int/news-room/fact-sheets/detail/chagas-disease-(american-trypanosomiasis)* **2020**.
[10] E. Bocchi, *Lancet* **2018**, *391*, 2209–2209.
[11] I. L. Galvan, J. Alonso-Padilla, N. Cortes-Serra, C. Alonso-Vega, J. Gascon, M. J. Pinazo, *Expert Rev. Anti-Infect. Ther.* **2020**, 1–10.
[12] I. Beltran-Hortelano, V. Alcolea, M. Font, S. Perez-Silanes, *Eur. J. Med. Chem.* **2020**, *206*, 112692.
[13] J. A. Urbina, *Lancet Infect. Dis.* **2018**, *18*, 419–430.
[14] M. De Rycker, B. Baragana, S. L. Duce, I. H. Gilbert, *Nature* **2018**, *559*, 498–506.
[15] M. C. Field, D. Horn, A. H. Fairlamb, M. A. Ferguson, D. W. Gray, K. D. Read, M. De Rycker, L. S. Torrie, P. G. Wyatt, S. Wyllie, I. H. Gilbert, *Nat. Rev. Microbiol.* **2017**, *15*, 217–231.
[16] M. Berg, P. Van der Veken, A. Goeminne, A. Haemers, K. Augustyns, *Curr. Med. Chem.* **2010**, *17*, 2456–2481.
[17] G. D. Campagnaro, H. P. de Koning, *Med. Res. Rev.* **2020**, *40*, 1679–1714.
[18] H. P. de Koning, D. J. Bridges, R. J. Burchmore, *FEMS Microbiol. Rev.* **2005**, *29*, 987–1020.
[19] A. K. Datta, R. Datta, B. Sen, *Adv. Exp. Med. Biol.* **2008**, *625*, 116–132.
[20] M. Berg, P. Van der Veken, A. Goeminne, A. Haemers, K. Augustyns, *Curr. Med. Chem.* **2010**, *17*, 2456–2481.
[21] P. Perlikova, M. Hocek, *Med. Res. Rev.* **2017**, *37*, 1429–1460.

[22] F. Hulpia, G. D. Campagnaro, M. Scortichini, K. Van Hecke, L. Maes, H. P. de Koning, G. Caljon, S. Van Calenbergh, *Eur. J. Med. Chem.* **2019**, *164*, 689–705.
[23] P. Naus, O. Caletkova, P. Konecny, P. Dzubak, K. Bogdanova, M. Kolar, J. Vrbkova, L. Slavetinska, E. Tloust'ova, P. Perlikova, M. Hajduch, M. Hocek, *J. Med. Chem.* **2014**, *57*, 1097–1110.
[24] A. Bourderioux, P. Naus, P. Perlikova, R. Pohl, I. Pichova, I. Votruba, P. Dzubak, P. Konecny, M. Hajduch, K. M. Stray, T. Wang, A. S. Ray, J. Y. Feng, G. Birkus, T. Cihlar, M. Hocek, *J. Med. Chem.* **2011**, *54*, 5498–5507.
[25] F. Hulpia, K. Van Hecke, C. Franca da Silva, D. da Gama Jaen Batista, L. Maes, G. Caljon, C. S. M. de Nazare, S. Van Calenbergh, *J. Med. Chem.* **2018**, *61*, 9287–9300.
[26] W. E. Gutteridge, J. Knowler, J. D. Coombes, *J. Protozool.* **1969**, *16*, 521–525.
[27] C. Lin, F. Hulpia, C. F. da Silva, D. Batista, K. Van Hecke, L. Maes, G. Caljon, M. N. C. Soeiro, S. Van Calenbergh, *J. Med. Chem.* **2019**, *62*, 8847–8865.
[28] J. L. Avila, T. Rojas, A. Avila, M. A. Polegre, R. K. Robins, *Antimicrob. Agents Chemother.* **1987**, *31*, 447–451.
[29] H. A. Tran, Z. Y. Zheng, X. H. Wen, S. Manivannan, A. Pastor, M. Kaiser, R. Brun, F. F. Snyder, T. G. Back, *Bioorg. Med. Chem.* **2017**, *25*, 2091–2104.
[30] F. Hulpia, J. Bouton, G. D. Campagnaro, I. A. Alfayez, D. Mabille, L. Maes, H. P. de Koning, G. Caljon, S. Van Calenbergh, *Eur. J. Med. Chem.* **2020**, *188*, 112018.
[31] C. Lin, C. Sun, X. Liu, Y. Zhou, M. Hussain, J. Wan, M. Li, X. Li, R. Jin, Z. Tu, J. Zhang, *Antiviral Res.* **2016**, *129*, 13–20.
[32] F. Hulpia, D. Mabille, G. D. Campagnaro, G. Schumann, L. Maes, I. Roditi, A. Hofer, H. P. de Koning, G. Caljon, S. Van Calenbergh, *Nat. Commun.* **2019**, *10*, 5564.
[33] F. Hulpia, G. D. Campagnaro, K. J. Alzahrani, I. A. Alfayez, M. A. Ungogo, D. Mabille, L. Maes, H. P. de Koning, G. Caljon, S. Van Calenbergh, *ACS Infect. Dis.* **2020**, *6*, 2045–2056.
[34] R. Wu, E. D. Smidansky, H. S. Oh, R. Takhampunya, R. Padmanabhan, C. E. Cameron, B. R. Peterson, *J. Med. Chem.* **2010**, *53*, 7958–7966.
[35] C. Lin, J. Yu, M. Hussain, Y. Zhou, A. Duan, W. Pan, J. Yuan, J. Zhang, *Antiviral Res.* **2018**, *149*, 95–105.
[36] E. M. de Souza, M. T. Rivera, T. C. Araujo-Jorge, S. L. de Castro, *Parasitol. Res.* **2001**, *87*, 513–520.
[37] F. Seela, X. Ming, *Tetrahedron* **2007**, *63*, 9850–9861.
[38] P. Naus, O. Caletkova, P. Konecny, P. Dzubak, K. Bogdanova, M. Kolar, J. Vrbkova, L. Slavetinska, E. Tloust'ova, P. Perlikova, M. Hajduch, M. Hocek, *J. Med. Chem.* **2014**, *57*, 1097–1110.
[39] F. Seela, X. Peng, *J. Org. Chem.* **2006**, *71*, 81–90.
[40] P. Perlikova, P. Konecny, P. Naus, J. Snasel, I. Votruba, P. Dzubak, I. Pichova, M. Hajduch, M. Hocek, *MedChemComm* **2013**, *4*, 1497–1500.
[41] M. P. Clark, M. W. Ledeboer, I. Davies, R. A. Byrn, S. M. Jones, E. Perola, A. Tsai, M. Jacobs, K. Nti-Addae, U. K. Bandarage, M. J. Boyd, R. S. Bethiel, J. J. Court, H. Deng, J. P. Duffy, W. A. Dorsch, L. J. Farmer, H. Gao, W. Gu, K. Jackson, D. H. Jacobs, J. M. Kennedy, B. Ledford, J. Liang, F. Maltais, M. Murcko, T. Wang, M. W. Wannamaker, H. B. Bennett, J. R. Leeman, C. McNeil, W. P. Taylor, C. Memmott, M. Jiang, R. Rijnbrand, C. Bral, U. Germann, A. Nezami, Y. Zhang, F. G. Salituro, Y. L. Bennani, P. S. Charifson, *J. Med. Chem.* **2014**, *57*, 6668–6678.
[42] L. J. Farmer, M. P. Clark, M. J. Boyd, E. Perola, S. M. Jones, A. Tsai, M. D. Jacobs, U. K. Bandarage, M. W. Ledeboer, T. Wang, H. Deng, B. Ledford, W. Gu, J. P. Duffy, R. S. Bethiel, D. Shannon, R. A. Byrn, J. R. Leeman, R. Rijnbrand, H. B. Bennett, C. O'Brien, C. Memmott, K. Nti-Addae, Y. L. Bennani, P. S. Charifson, *ACS Med. Chem. Lett.* **2017**, *8*, 256–260.
[43] C. Han, K. Green, E. Pfeifer, F. Gosselin, *Org. Process Res. Dev.* **2017**, *21*, 664–668.
[44] C. H. Franco, L. M. Alcantara, E. Chatelain, L. Freitas-Junior, C. B. Moraes, *Trop. Med. Infect. Dis.* **2019**, *4*, 82.
[45] L. F. de Almeida Fiuza, D. Batista, D. F. Nunes, O. C. Moreira, C. Cascabulho, M. N. C. Soeiro, *Exp. Parasitol.* **2021**, *221*, 108061.
[46] R. Edmondson, J. J. Broglie, A. F. Adcock, L. J. Yang, *Assay Drug Dev. Technol.* **2014**, *12*, 207–218.
[47] F. Hulpia, J. Bouton, G. D. Campagnaro, I. A. Alfayez, D. Mabille, L. Maes, H. P. de Koning, G. Caljon, S. Van Calenbergh, *Eur. J. Med. Chem.* **2020**, *188*, 112018.
[48] F. Hulpia, G. D. Campagnaro, M. Scortichini, K. Van Hecke, L. Maes, H. P. de Koning, G. Caljon, S. Van Calenbergh, *Eur. J. Med. Chem.* **2019**, *164*, 689–705.
[49] S. A. Ingale, P. Leonard, F. Seela, *J. Org. Chem.* **2018**, *83*, 8589–8595.
[50] Q. Li, L. Persoons, D. Daelemans, P. Herdewijn, *J. Org. Chem.* **2020**, *85*, 403–418.

[51] A. J. Romanha, S. L. Castro, N. Soeiro Mde, J. Lannes-Vieira, I. Ribeiro, A. Talvani, B. Bourdin, B. Blum, B. Olivieri, C. Zani, C. Spadafora, E. Chiari, E. Chatelain, G. Chaves, J. E. Calzada, J. M. Bustamante, L. H. Freitas-Junior, L. I. Romero, M. T. Bahia, M. Lotrowska, M. Soares, S. G. Andrade, T. Armstrong, W. Degrave, A. Andrade Zde, *Mem. Inst. Oswaldo Cruz* **2010**, *105*, 233–238.

[52] L. M. Nisimura, P. M. Ferrao, A. D. R. Nogueira, M. C. Waghabi, M. Meuser-Batista, O. C. Moreira, J. A. Urbina, L. R. Garzoni, *Mol. Biochem. Parasitol.* **2020**, *238*, 111283.

[53] T. Duffy, C. I. Cura, J. C. Ramirez, T. Abate, N. M. Cayo, R. Parrado, Z. D. Bello, E. Velazquez, A. Munoz-Calderon, N. A. Juiz, J. Basile, L. Garcia, A. Riarte, J. R. Nasser, S. B. Ocampo, Z. E. Yadon, F. Torrico, B. A. de Noya, I. Ribeiro, A. G. Schijman, *PLoS Neglected Trop. Dis.* **2013**, *7*, e2000.

278

14
T. cruzi EC$_{50}$ = 0.85 ± 0.21 μM
MRC-5 EC$_{50}$ > 64.0 μM
active *in vivo*

C. Lin, L. Ferreira de Almeida Fiuza, C. Cardoso Santos, Dr. D. Ferreira Nunes, Dr. O. Cruz Moreira, J. Bouton, I. Karalic, Prof. L. Maes, Prof. G. Caljon, Dr. F. Hulpia*, Prof. M. de Nazaré C. Soeiro*, Prof. S. Van Calenbergh*

1 – 24

6-Methyl-7-Aryl-7-Deazapurine Nucleosides as Anti-*Trypanosoma cruzi* Agents: Structure-Activity Relationship and *in vivo* Efficacy

A SAR investigation on the pyrimidine part of a previously identified 7-aryl-7-deazapurine nucleoside provided the most promising 6-methyl analogue against *T. cruzi*. A series of 7-aryl-6-methyl derivatives was prepared and evaluated, giving rise to several analogues with sub-micromolar antitrypanosomal activity. Compound **14** was found to be metabolically stable and active against *T. cruzi* after oral dose of 25 mg/kg b.i.d in an acute mouse model.

4E Interacting Protein as a Potential Novel Drug Target for Nucleoside Analogues in *Trypanosoma brucei*

Dorien Mabille [1], Camila Cardoso Santos [1,2], Rik Hendrickx [1], Mathieu Claes [1], Peter Takac [3,4], Christine Clayton [5], Sarah Hendrickx [1], Fabian Hulpia [6], Louis Maes [1], Serge Van Calenbergh [6,†] and Guy Caljon [1,*,†]

1   Laboratory of Microbiology, Parasitology and Hygiene (LMPH), University of Antwerp, 2610 Wilrijk, Belgium; Dorien.Mabille@uantwerpen.be (D.M.); perutha@gmail.com (C.C.S.); Rik.Hendrickx@uantwerpen.be (R.H.); Mathieu.Claes@uantwerpen.be (M.C.); Sarah.Hendrickx@uantwerpen.be (S.H.); Louis.Maes@uantwerpen.be (L.M.)
2   Laboratório de Biologia Celular (LBC), Instituto Oswaldo Cruz (IOC/Fiocruz), Rio de Janeiro 21040-900, Brazil
3   Institute of Zoology, Slovak Academy of Sciences, 84506 Bratislava, Slovakia; peter.takac@savba.sk
4   Scientica, Ltd., 83106 Bratislava, Slovakia
5   DKFZ-ZMBH Alliance, Zentrum für Molekulare Biologie der Universität Heidelberg, 69120 Heidelberg, Germany; cclayton@zmbh.uni-heidelberg.de
6   Laboratory for Medicinal Chemistry, Campus Heymans, Ghent University, 9000 Gent, Belgium; fabian.hulpia@gmail.com (F.H.); serge.vancalenbergh@ugent.be (S.V.C.)
*   Correspondence: guy.caljon@uantwerpen.be
†   These authors contributed equally.

Abstract: Human African trypanosomiasis is a neglected parasitic disease for which the current treatment options are quite limited. Trypanosomes are not able to synthesize purines de novo and thus solely depend on purine salvage from the host environment. This characteristic makes players of the purine salvage pathway putative drug targets. The activity of known nucleoside analogues such as tubercidin and cordycepin led to the development of a series of C7-substituted nucleoside analogues. Here, we use RNA interference (RNAi) libraries to gain insight into the mode-of-action of these novel nucleoside analogues. Whole-genome RNAi screening revealed the involvement of adenosine kinase and 4E interacting protein into the mode-of-action of certain antitrypanosomal nucleoside analogues. Using RNAi lines and gene-deficient parasites, 4E interacting protein was found to be essential for parasite growth and infectivity in the vertebrate host. The essential nature of this gene product and involvement in the activity of certain nucleoside analogues indicates that it represents a potential novel drug target.

Keywords: trypanosomiasis; nucleoside analogues; RNAi; drug target; 4E-interacting protein

1. Introduction

Human African Trypanosomiasis (HAT), often referred to as sleeping sickness, is a neglected tropical disease prevalent in the African continent in an area delineated by the Sahara, Kalahari, and Namibian deserts [1]. The disease is caused by the human-infective *Trypanosoma brucei gambiense* and *T. b. rhodesiense*, which are transmitted by tsetse flies [2]. The disease is characterized first by a haemolymphatic stage in which patients present general flu-like symptoms such as fever, weight loss, and muscles aches. A meningo-encephalitic stage subsequently develops when parasites have entered the central nervous system and cause severe neurological symptoms and an altered sleep/wake cycle that is characteristic of sleeping sickness [3].

Currently, available therapies are rather limited and have multiple shortcomings. For example, pentamidine, suramin, melarsoprol, and nifurtimox/eflornithine combination therapy (NECT) require intravenous or intramuscular injections requiring patient

hospitalization [4]. Additionally, these drugs exhibit problems of toxicity, with melarsoprol being the most toxic, causing reactive encephalopathy in up to 5 per cent of stage-II HAT patients [5]. Recent encouraging developments in HAT treatment were the clinical trial results for fexinidazole as the first oral monotherapy for g-HAT [6]. Fexinidazole has since then been approved by the European Medicines Agency (EMA) and endorsed in the Democratic Republic of Congo (DRC) for the treatment of both stages of HAT, although NECT remains the treatment of choice for severely ill patients [7]. Nonetheless, for all antitrypanosomal drugs, cases of drug resistance have already emerged in the field or were selected experimentally, highlighting a continuous need for novel treatment strategies [8–10].

Given that the parasite lacks de novo purine synthesis and thus solely depends on purine salvage [11], interaction with the involved pathways represents a valid strategy to explore novel antitrypanosomal drugs. Nucleoside analogues such as tubercidin and cordycepin were already proven active against *T. brucei* [12–15]. Tubercidin (7-deazaadenosine), a nucleoside analogue produced by *Streptomyces tubercidicus*, exhibits potent activity against a range of parasites [16–18], but is unfortunately extremely toxic to mammalian cells and therefore of limited therapeutic value [14]. The potent activity of tubercidin (**1**) against *T. brucei* inspired Hulpia et al. to explore a range of C7-substituted tubercidin analogues (Figure 1). Substitution of 7-deazaadenosine with electron-poor phenyl groups gave rise to a series of compounds showing micromolar activity. Replacement of the phenyl group by a pyridine ring resulted in **5** exhibiting sub-micromolar antitrypanosomal activity and largely reduced cytotoxicity compared to tubercidin [19]. A combination of structural elements of tubercidin and cordycepin resulted in the development of 3′-deoxy-7-deazaadenosine nucleosides, with 3′-deoxytubercidin (**2**) as the most promising candidate for late-stage sleeping sickness [20]. Likewise, the screening of a series of 7-substituted 7-deazainosine derivatives provided several 6-O-alkylated analogues (**6–9**) with nanomolar in vitro potency and is thus interesting for further in vivo evaluation [21]. Another advantage of nucleoside analogues is their high likelihood to cross the blood-brain barrier due to the various purine transporters lining this barrier [22]. Sufficient compound exposure in the central nervous system is essential for efficacy against stage-II of the disease and is a requirement in the current target product profile [23].
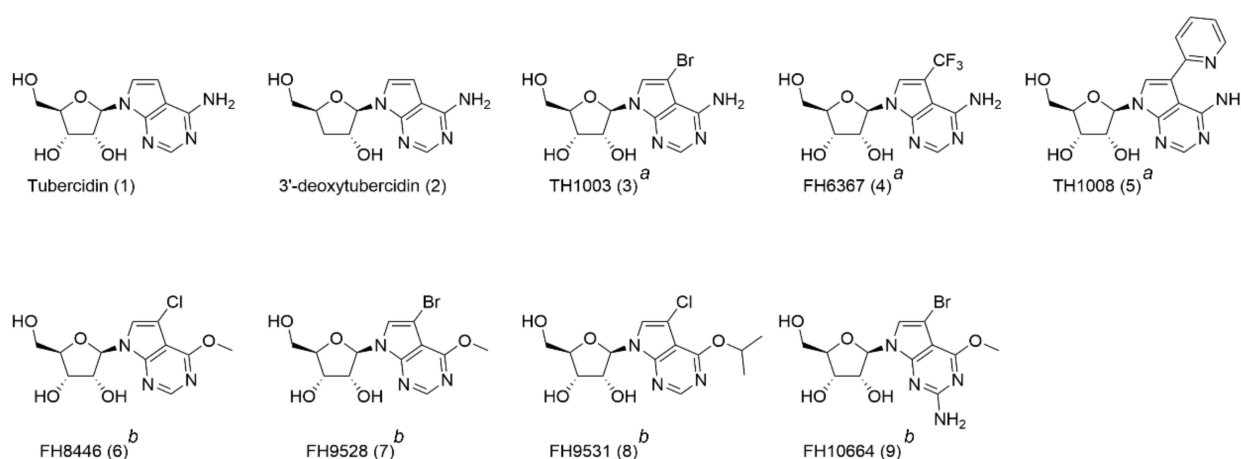

Figure 1. An overview of the nucleoside analogues used in this study. Compound name (compound code). [a] 7-deaza adenosine analogues. [b] inosine analogues. Compound codes in original publication: (Tubercidin (1), 3′-deoxytubercidin (9)) [20], (TH1003 (31), FH6367, TH1008 (13)) [19], (FH8446 (23), FH9531 (36), FH9528 (24), FH10664 (28)) [21].

For most antitrypanosomal drugs, the mode-of-action (MoA) is not yet fully understood setting hurdles for rational use in the field in view of the possible development of drug resistance. Genome-wide RNA interference (RNAi) screening is a powerful tool for the unbiased identification of genes involved in the MoA of novel compounds [24]. This technique has been applied to the current antitrypanosomal drugs confirming the involvement of known drug targets, such as the amino acid transporter 6 (AAT6) for

eflornithine and nitroreductase (NTR) for benznidazole and nifurtimox [25–28]. RNAi libraries of *Trypanosoma* were already extensively applied in procyclics [29–31]; however, bloodstream forms (BSF) are the clinically relevant stage to study the MoA of drugs. Due to their poor transformation efficiency, RNAi libraries in BSF have only emerged later [32–34].

In this study, we successfully applied whole-genome RNAi screening in combination with confirmatory in vitro and in vivo approaches to identify genes participating in the MoA of tubercidin analogues that may represent potential novel drug targets given their essentiality for *T. brucei* infectivity.

2. Materials and Methods

2.1. Ethics Statement

The use of laboratory rodents was carried out in strict accordance with all mandatory guidelines (EU directives, including the Revised Directive 2010/63/EU on the Protection of Animals used for Scientific Purposes that came into force on 1 January 2013, and the declaration of Helsinki in its latest version) and was approved by the Ethical Committee of the University of Antwerp, Belgium (UA-ECD 2017-04).

2.2. Animals and Parasites

Female C57BL/6JRj were purchased from Janvier (Le Genest Saint Isle, France). Food for laboratory rodents (Carfil, Arendonk, Belgium) and drinking water were available ad libitum. The animals were kept in quarantine for at least 5 days before infection and randomly allocated to the experimental units.

The RNAi library (kindly gifted by Professor Isabel Roditi, University of Bern) was constructed in the New York "single marker" line, a derivative of MITat 1.2 BSF trypanosomes [27]. Transfected EATRO1125 cells (wild-type (WT), 4E interacting protein double knock-out (4EIP-KO), EIF4E1 double knock-out (4E1-KO), 4EIP add-back (4EIP-AB), and EIF4E1 add-back (4E1-AB) containing a tetracycline-inducible 4EIP- or 4E1-myc gene) [35] were available from the Clayton lab (University of Heidelberg).

2.3. Compounds

A range of tubercidin analogues (Figure 1) was synthetized as part of a campaign to find novel hits with enhanced selective potency against *T. brucei* compared to tubercidin [19–21]. Experimental details regarding their synthesis are described [19–21]. The synthesis of analogue **4** is described in Supplementary method S1. High activity to treat late-stage sleeping sickness was demonstrated for 3'-deoxytubercidin (**2**) [20]. Substitution of C-7 with a bromide, trifluoromethyl, or pyridin-2-yl group led to compounds **3–5**, with the latter showing sub-micromolar activity in vitro [19]. Compounds **6–9** are 7-substituted 7-deazainosine analogues [21].

2.4. In Vitro Cytotoxicity Assay

Human lung fibroblasts (MRC-5$_{SV2}$ cells) were cultured in Minimum Essential Medium (MEM) (Life Technologies, Carlsbad, CA, United States) supplemented with L-glutamine, NaHCO$_3$, and 5% heat-inactivated fetal bovine serum (iFBS). Cells were seeded at a concentration of 15,000 cells/well, to which 4-fold dilutions of the test compounds were added with 64 µM as the highest in-test concentration. After 72 h of drug exposure at 37 °C and 5% CO$_2$, cell viability was determined by fluorescence reading (Tecan®, GENios, Männedorf, Switzerland) after a 4-h incubation with resazurin (Sigma Aldrich, St. Louis, MO, USA). The 50% cytotoxic concentration (CC$_{50}$) was calculated for each of the compounds.

2.5. Resazurin-Based Susceptibility Assay

T. brucei brucei MITat 1.2 New York "single marker" cells (NY-SM) were cultured in Hirumi's modified Iscove's medium 9 (HMI-9) with 10% iFBS. To determine the in vitro susceptibility, NY-SM were seeded at a concentration of 4000 parasites/well. Four-fold dilutions of the test compounds were added with a highest in-test concentration of 64 µM.

After 72 h of drug exposure at 37 °C and 5% CO_2, the viability was determined by fluorescence reading (Tecan®, GENios, Männedorf, Switzerland) after a 6-h incubation with resazurin (Sigma Aldrich, St. Louis, MO, USA). The 50% inhibitory concentration (IC_{50}) was calculated by comparing cell viability to untreated control wells [36].

2.6. RNAi Library Screening

The RNAi library was cultured in 30 mL HMI-9 culture medium supplemented with 10% iFCS and 1 µg/mL tetracycline to induce the RNAi phenotype. Ten mL of culture without tetracycline induction served as a negative control. After 62 h of induction, different concentrations of **5** (400, 600, and 800 nM) were added to 10 mL of individual cultures containing 1×10^5 cells/mL. The compound concentrations were based on their $IC_{98/99}$ values as determined in the resazurin-based susceptibility assay. The cells were monitored daily. As soon as the non-induced RNAi cultures collapsed and the induced cultures grew normally under drug pressure, they were diluted 1:10 in a fresh medium containing tetracycline and drug compound. After 2–3 passages, the cultures were harvested for further analysis (Figure S1A).

2.7. RNAi Insert Identification

The genomic DNA (gDNA) of the drug-exposed parasites was isolated from 20 mL of a stationary-phase culture using the QIAamp DNA mini kit (QIAGEN, Hilden, Germany). The DNA concentration was determined using nanodrop and diluted to 20 ng/µL gDNA in PCR water. The RNAi inserts were amplified using p2T7_seq (5′-CCGCTCTAGAACTAGTGGA-3′) as forward and p2T7hygPJ4 (5′-GGAAAGCTAGCTTGCATGCCTG-3′) as reverse primer (PCR program: 1 cycle for 1 min at 98 °C, 25 cycles for 1 min at 98 °C, 30 s at 58 °C, 1 min at 72 °C and 1 cycle for 10 min at 72 °C).

PCR products were analyzed on a 1% agarose gel (100 V for 120′) to identify the number and size of amplified inserts. PCR products were purified using the ExoSAP-ITTM PCR Product Cleanup kit (ThermoFisher Scientific, Carlsbad, CA, USA). A nested PCR was performed (PCR program: 1 cycle for 3 min at 94 °C, 30 cycles for 1 min at 94 °C, 1 min at 50 °C, 2 min and 30 s at 72 °C and 1 cycle for 10 min at 72 °C) and PCR products were analyzed on a 1% agarose gel (100 V for 120′). Interesting inserts, only present in the tetracycline clones, were extracted from the gel using the GenEluteTM Gel Extraction Kit (Sigma-Aldrich, St. Louis, MO, USA).

Finally, the PCR products were ligated in the pCR 2.1 vector system (ThermoFisher Scientific, Carlsbad, CA, USA) and transformed into high-efficiency competent *E. coli* (NEB10) and plated onto LB agar with ampicillin. Five colonies per target were selected to perform a colony PCR (PCR program: 1 cycle for 3 min at 94 °C, 30 cycles for 1 min at 94 °C, 1 min at 50 °C, 2 min and 3s at 72 °C and 1 cycle for 10 min at 72 °C) and were subsequently analyzed on a 1% agarose gel (100 V for 120′). Positive clones were selected and sequenced (VIB Genomics Core, Antwerp). The RNAi insert was sequenced bidirectionally with primers p2T7_seq and p2T7linker_rev (5′-AGGGCCAGTGAGGCCTCTAGAG-3′). Sequences were blasted against *T. brucei* transcripts on the TriTrypDB [37]. Retrieved translated sequences were subjected to characteristics determination using the ProtParam [38] and SignalP tool [39] and homology detection using a comparison of hidden Markov Models [40]).

2.8. Independent Confirmation of the RNAi Phenotype

To validate the RNAi effect of the different RNAi inserts, the insert was back-cloned into a p2T7Bern vector for transformation into NY-SM cells (Figure S1B). The RNAi inserts were introduced together with Ndel and Xhol restriction sites in the PCR 2.1 vector using P2T7_seq forward primer containing the NdeI site (GGAATTCCATATGCCGCTC-TAGAACTAGTGGA) and the P2T7linker_rev reverse primer containing the XhoI site (CCGCTCGAGAGGGCCAGTGAGGCCTCTAGAG). PCR products were analyzed on a 1.2% agarose gel and correct lanes were extracted from the gel using the GenEluteTM Gel

Extraction Kit (Sigma-Aldrich). The purified PCR product and the p2T7Bern vector were digested overnight at 37 °C with NdeI and XhoI restriction enzymes. The digested DNA was ligated using a T4 ligase for 2 h at room temperature. Finally, the ligated products were transformed into high-efficiency competent *E. coli* (NEB10) by electroporation and plated onto LB agar with ampicillin. A colony PCR was performed to identify the colonies containing the vector followed by confirmation by sequencing.

Next, 10 μg of the P2T7Bern DNA containing the RNAi inserts was linearized with NotI and purified using the QIAquick PCR purification kit (QIAGEN, Hilden, Germany); 4×10^7 NY-SM cells were transferred to a 2 mm gap cuvette together with 10 μg linear plasmid DNA. The cells were subjected to two consecutive pulses of 1.2 kV with 186 Ω resistance and 50 μF capacitance. After transformation, the cells were transferred to HMI-9 medium containing 10% iFCS. After 18–22 h, 2.5 μg/mL of hygromycin B was added to the cells. After 6 days, the hygromycin B pressure was increased to 5 μg/mL. After sufficient cell growth, the culture was used to generate monoclonal cell lines. Monoclonal lines were subjected to resazurin-based susceptibility assays to determine the 50% inhibitory concentration, as described above.

2.9. Efficiency of the RNAi Silencing

To determine the degree of knock-down of the different RNAi inserts after tetracycline induction, an RT-qPCR was performed. The different RNAi clones were cultured in HMI-9 culture medium in the presence or absence of 1 μg/mL of tetracycline. Cultures were diluted 1 in 10 every 24 h in fresh HMI-9 with or without tetracycline. After 68 h, RNA was extracted using the RNA blood mini kit (QIAGEN, Hilden, Germany). cDNA was prepared using the Tetro™ cDNA Synthesis Kit (Bioline). RT-qPCR was performed using the Sensi-FAST™ SYBR® Hi-ROX Kit (Bioline) (PCR program: 1 cycle for 2 min at 95 °C, 40 cycles for 5 s at 95 °C, 20 s at 60 °C, 15 s at 95 °C, 1 min at 60 °C and 15 s at 95 °C). *TERT*, *Actin A*, and *H2B* were used as reference genes [41,42].

2.10. In Vitro Growth

The in vitro growth of RNAi clones was compared to the NY-SM background strain. Parasites were seeded at a concentration of 4×10^5 cells/mL in 2 mL of HMI-9 with 10% iFBS with or without the addition of 1 μg/mL tetracycline. Cell growth was monitored by microscopic counting using a Neubauer improved haemocytometer for a period of 9 days. Cells were diluted 1:5 daily.

2.11. Cell Cycle Analysis and RNA Quantification

NY-SM cells were exposed to different concentrations of 5 (corresponding to the IC_{50}, $IC_{50}/2$, and $IC_{50}/5$) for 24 h. For cell cycle analysis, the cells were harvested and washed with PBS before staining with 5 μg/mL Hoechst 33,342 for 25 min at 37 °C. Cells were analyzed on a MACSQuant flow cytometer (Miltenyi Biotec, Gladbach, Germany) using the FlowJo X software package. For RNA quantification, extracts were made from a normalized number of cells to correct for the impact of 5 on the number of recovered trypanosomes. RNA was extracted using the QIAamp RNA blood mini kit (QIAGEN, Hilden, Germany). Total RNA yields were determined using both Nanodrop 2000 spectrometry and Qubit fluorimetric RNA content analysis. Additionally, specific transcripts in the RNA pool were quantified using quantitative reverse transcription PCR (RT-qPCR) targeting the spliced-leader RNA (SL-RNA), 18S rRNA, and transcripts encoding the telomerase reverse transcriptase (*TERT*) (Table S1) [41,43].

2.12. Western Blot Analysis of PAD1

Tetracycline-induced 4EIP-AB parasites were seeded at a concentration of 5×10^5 cells/mL and exposed to various concentrations of **5** and 3'-deoxytubercidin [20] (corresponding to the IC_{50}, $IC_{50}/2$ and $IC_{50}/5$) for 48 h. Cells were resuspended in Laemmli sample buffer (Bio-Rad, Hercules, CA, USA) containing β-mercaptoethanol. Genomic DNA

was sheared by sonication and samples were stored at −80 °C until further analysis; 10 μL of protein sample was loaded on 10% Mini-PROTEAN® TGX Stain-Free™ Protein Gel (Bio-Rad) at 100 V. Proteins were transferred to a polyvinylidene difluoride (PVDF) membrane at 100 V. Primary antibodies for PAD1 and EF1α (kindly gifted by Prof. Keith Matthews, University of Oxford) were used at 1:1000 and 1:7000, respectively [44]. For protein detection, anti-rabbit (1:7000) or anti-mouse (1:1000) HRP-conjugated antibodies were used with the Clarity Western ECL Substrate (Bio-Rad) detection system.

2.13. In Vivo Infectivity

Twelve female C57BL/6JRj were randomly divided into four groups. Two groups (tetracycline-positive groups) were pre-treated for 48 h with 1 mg/mL of doxycycline and 5% sucrose in the drinking water. Doxycycline exposure was maintained throughout the entire experiment and fresh doxycycline solutions were prepared every 2–3 days. The tetracycline-negative groups received water with 5% sucrose. On day 0, mice were infected intraperitoneally with 5000 parasites. Each group was infected with a different strain: NY-SM + (pre-induced with tetracycline in vitro), NY-SM—(not induced with tetracycline), ADKIN A + (NY-SM cells transfected with RNAi insert Tb927.6.2300 and pre-induced with tetracycline in vitro), and ADKIN A—(NY-SM cells transfected with RNAi insert Tb927.6.2300 and not induced with tetracycline). Parasitaemia and anaemia were determined using a Neubauer improved haemocytometer. To confirm adequate knock-down of the genes of interest, 100 μL of blood was collected at day 4 post-infection (dpi). RNA was extracted using the RNA blood mini kit (QIAGEN) and subjected to RT-qPCR to determine the percentage of gene knock-down.

The role of 4EIP RNAi-mediated knockdown (NY-SM cells transfected with RNAi insert Tb927.9.11050) and knockout (4EIP-KO and 4EIP-AB strains) in in vivo infectivity was evaluated in a similar manner as described above.

2.14. Tsetse Fly Infections

T.b.b. AnTat1.1EPpyRE9 parasites were used to infect teneral tsetse flies (*Glossina morsitans morsitans*) through a parasitized blood meal supplemented with 10 mM reduced L-glutathione. The infected blood meal consisted of a mixture of infected mouse blood (5–7 dpi) and defibrinated horse blood to obtain a final concentration of >10^6 BSF parasites/mL. Newly emerged tsetse flies were divided into three groups and offered an infected blood meal with or without **5** or 3′-deoxytubercidin at a concentration corresponding to the IC_{50}. After the infected blood meal, tsetse flies were fed every 2–3 days with uninfected defibrinated horse blood. At 7 dpi, tsetse flies were dissected to evaluate midgut infection ratios.

2.15. Graphs and Statistical Analyses

All graphs and statistical analyses were prepared using GraphPad Prism 7 software.

3. Results

3.1. 7-Deaza Adenosine Analogues Act Independently of DNA and RNA Synthesis Inhibition

All 7-deaza adenosine analogues **2**–**9** showed sub-micromolar activity against *T. brucei* parasites in vitro. Tubercidin was cytotoxic at low concentrations, as described in literature [45]. Analogues **4** and **9** showed a modest increase in selectivity, whereas the remaining analogues showed a significantly improved selectivity (Table 1). Cell cycle analysis by flow cytometry indicated no major impact on DNA synthesis (Figure 2A–D), suggesting that 5 does not inhibit the parasite's DNA polymerase. The impact of various concentrations of 5 on RNA synthesis was analyzed next using standard quantification methods on the total RNA extracts and specific RT-qPCR for quantitative detection of *T. brucei* SL-RNA, rRNA, and *TERT* transcripts (Figure 2E–H). The results indicate that **5** does not act as a substrate nor chain terminator for RNA synthesis given the absence of a major impact on the total RNA pool and the levels of specific transcripts produced by RNA polymerase I and II.

Table 1. Overview of the in vitro activity and cytotoxicity of the 7-deaza adenosine analogues on NY-SM cells (IC$_{50}$) and MRC-5 cells (CC$_{50}$) [19–21].

Compound	IC$_{50}$ $\pm$ SEM (µM)	CC$_{50}$ $\pm$ SEM (µM)	SI [1]
Tubercidin (1)	0.12 $\pm$ 0.003	2.23 $\pm$ 0.68	18
3	0.38 $\pm$ 0.064	33.3 $\pm$ 12.6	88
4	0.38 $\pm$ 0.017	19.2 $\pm$ 15.2	50
5	0.15 $\pm$ 0.005	15.1 $\pm$ 4.1	103
6	0.05 $\pm$ 0.003	48 $\pm$ 16	960
7	0.08 $\pm$ 0.001	>64	800
8	0.10 $\pm$ 0.008	>64	640
9	0.10 $\pm$ 0.001	3.24 $\pm$ 0.01	32

[1] The selectivity index (SI) represents the CC$_{50}$/IC$_{50}$. SEM: Standard Error of the Mean.

3.2. Involvement of Adenosine Kinase and 4E-Interacting Protein in the Antitrypanosomal Activity

To determine the MoA of **5**, selection of a genome-wide *T. b. brucei* RNAi library identified four RNAi inserts (Table S2), most notably FLA1-binding protein (FLA1BP; Tb927.8.4050), endonuclease G (EndoG; Tb928.8.4040), adenosine kinase (ADKIN; Tb927.6.2300), and 4E-interacting protein (4EIP; Tb927.9.11050). To confirm the involvement of the different inserts in the MoA of 5, the RNAi inserts were back-cloned into NY-SM cells. Two independent clones of each RNAi insert were tested for their susceptibility to **5**.

Out of the four knock-down constructs tested, only those silencing ADKIN and 4EIP exhibited an approximately 3-fold decrease in susceptibility to **5** (Figure 3). RT-qPCR indicated variable gene silencing levels in the various RNAi clones, suggesting that residual target activity may be responsible for the partial activity of the compound (Table 2).

For the RNAi clones FLA1BP and EndoG, no significant differences in susceptibility could be observed between tetracycline-induced and non-induced clones. To confirm these findings, the in vitro susceptibility assays were also conducted under continuous tetracycline pressure, yielding similar results.
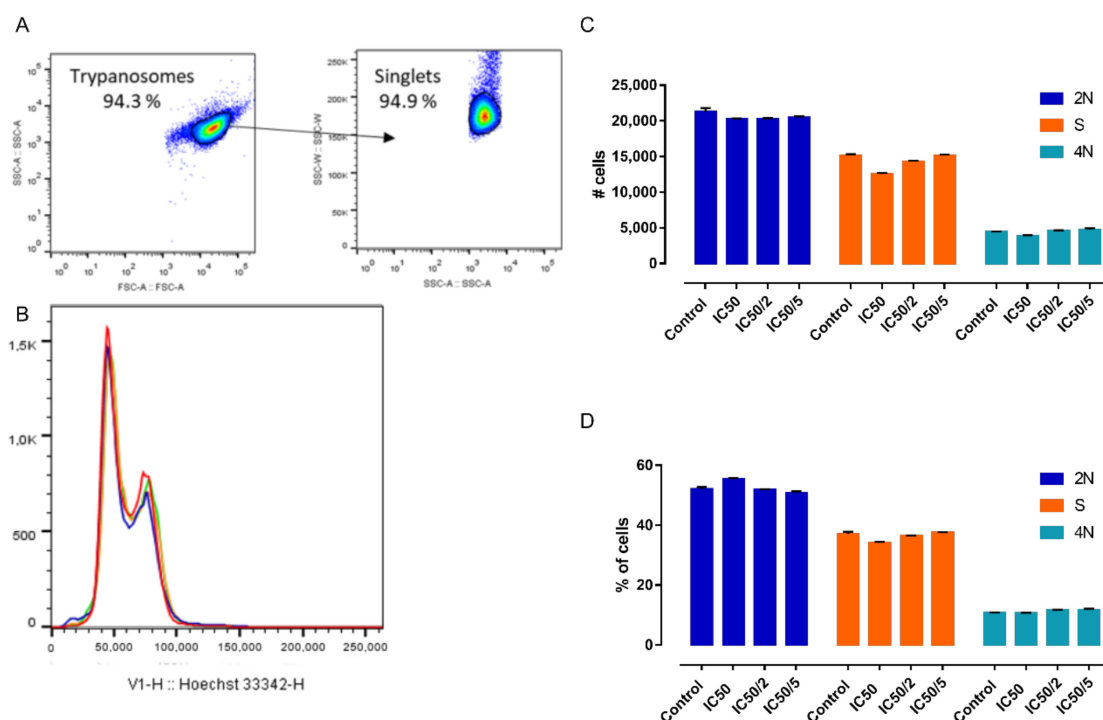

Figure 2. *Cont.*
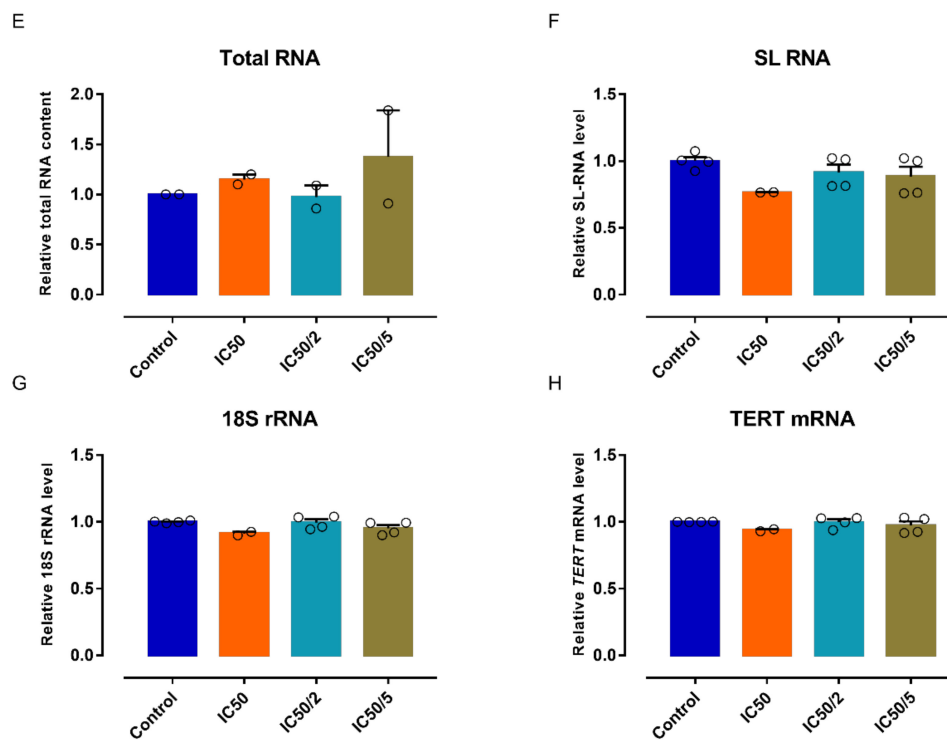
Figure 2. Effect of **5** on cell cycle regulation and RNA synthesis. (**A**) Gating strategy. (**B**) Results of the cell cycle analysis after 24 h exposure to different concentrations of 5. Results of the cell cycle analysis (2N, S phase, 4N) expressed in total cell numbers. (**C**) $n = 2$ and relative cell numbers. (**D**) $n = 2$. (**E**) Total RNA yield from trypanosomes exposed for 24 h to different concentrations of 5 ($n = 2$). RNA content quantified using quantitative reverse transcription PCR (RT-qPCR) specifically targeting SL-RNA. (**F**) $n = 2$ with two replicates, 18S rRNA. (**G**) $n = 2$ with two replicates and *TERT* mRNA. (**H**) $n = 2$ with two replicates. RNA content and transcript levels are expressed as relative to the non-treated trypanosomes (control). Error bars are SEM.
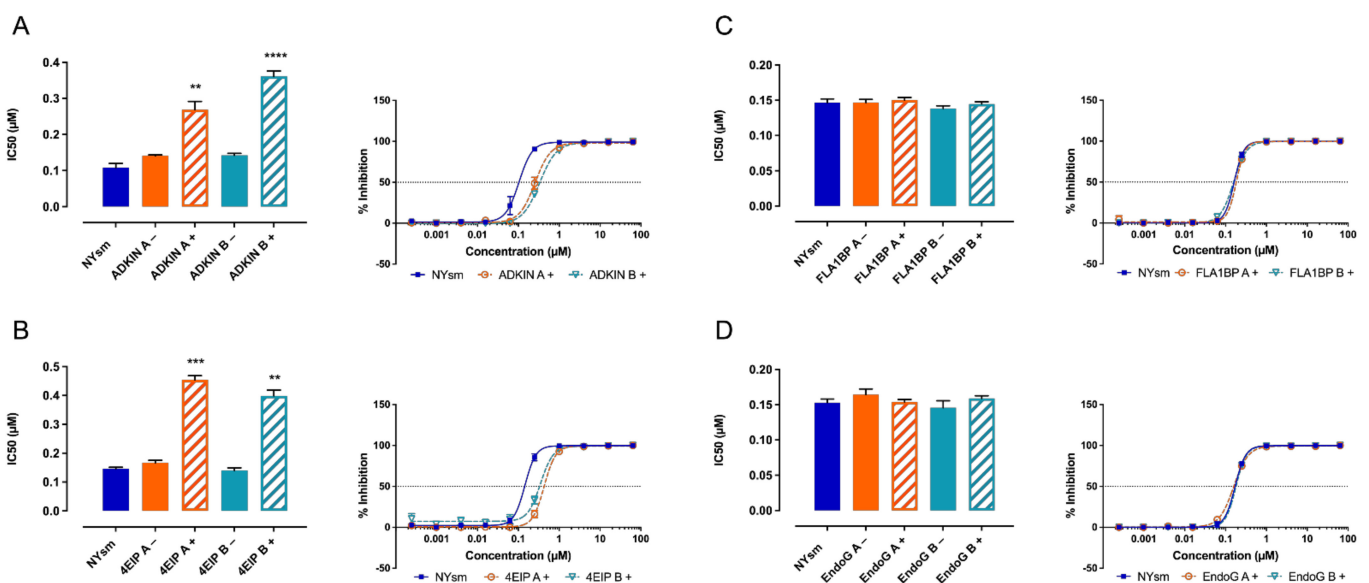
Figure 3. Drug susceptibility of RNAi clones targeting (**A**) ADKIN, (**B**) 4EIP, (**C**) FLA1BP, and (**D**) EndoG to **5**. Results are expressed as the mean IC_{50} (μM), and error bars represent SEM, and are based on at least two independent experiments ($n = 2$), each with two biological replicates. + = tetracycline-induced clones; − = non-induced clones. All experiments were performed with two independently generated RNAi clones. ** $p < 0.01$, *** $p < 0.001$, **** $p < 0.0001$ Kruskal–Wallis test with Dunn's multiple comparison test.

Table 2. Overview of the RNA knock-down levels following in vitro induction with tetracycline.

	% Knock-Down	
Target	Clone A [1]	Clone B [1]
FLABP1	44.1 ± 1.7	42.8 ± 0.6
EndoG	33.2 ± 0.9	31.0 ± 0.9
ADKIN	81.2 ± 0.2	83.4 ± 0.5
4EIP	85.0 ± 0.7	85.1 ± 0.3

[1] Mean percentage knock-down compared to NY-SM cells $\pm$ standard error of mean.

3.3. 7-Deaza Adenosine Analogues Show a Variable Dependence on ADKIN and 4EIP

The susceptibility of ADKIN RNAi-mediated knockdown to other 7-deaza purine analogues was evaluated in vitro. Four of the compounds showed a large decrease in susceptibility (Figure 4) of which two (6 and 7) even completely lost their activity (up to the highest concentration tested (64 µM)) against the ADKIN-knockdown strains. The large dependency on ADKIN for antitrypanosomal activity proved particularly relevant for the 6-O-alkylated analogues **6–9** (Figure 4, red circles). For 4EIP, the susceptibility to other 7-deaza adenosine analogues was tested using both the RNAi-mediated knockdown and knockout cell lines. Only 5 showed a partial dependence on 4EIP for its antitrypanosomal activity (Figure 5). The effect seemed to be specific for 4EIP and not for the cap-binding protein 4E1. The variable dependence of the different compounds on ADKIN and 4EIP suggests a diverse MoA of the nucleoside analogues.
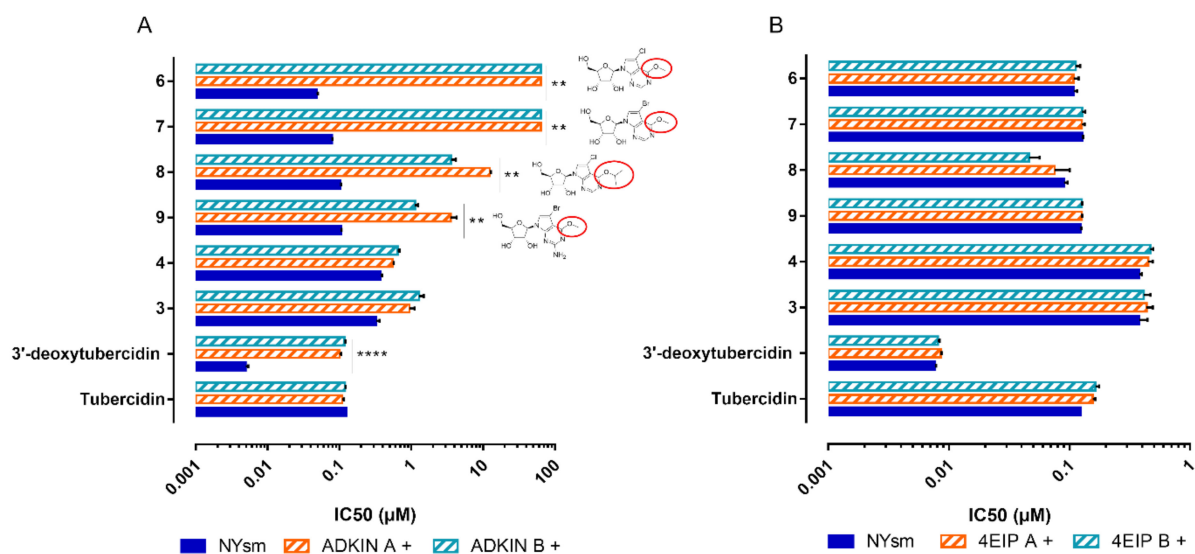

Figure 4. Susceptibility of ADKIN (**A**) and 4EIP (**B**). RNAi-mediated knockdown to compounds **1–4**, and **6–9**. Results are expressed as the mean IC$_{50}$ (µM), and error bars represent SEM and are based on at least two independent experiments ($n = 2$), each with two biological replicates. + = tetracycline-induced clones. All experiments were performed with two independently generated RNAi clones. ** $p < 0.01$,**** $p < 0.0001$, Mann–Withney test comparing NY-SM with RNAi knock-down strains. ADKIN 3'-deoxytubercidin data was previously published [20].
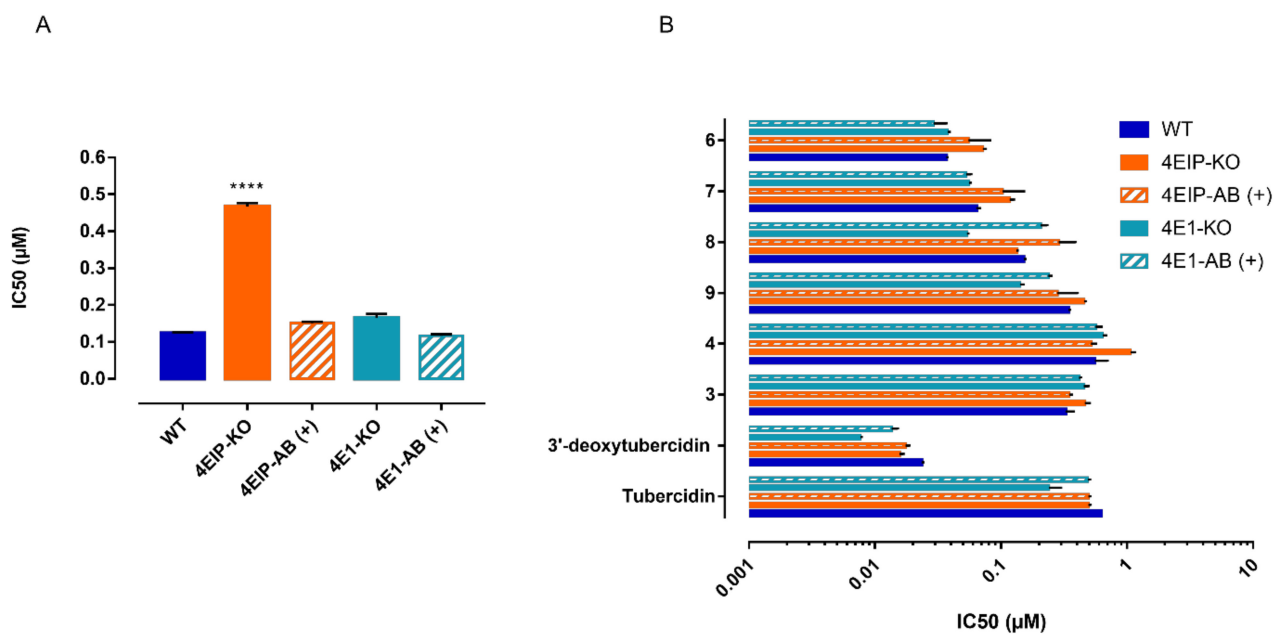
Figure 5. Susceptibility of 4EIP and 4E1 knockout cell lines to **5** (**A**) and compounds **1**–**4**, and **6**–**9** (**B**). Results are expressed as the mean IC$_{50}$ (μM), and error bars represent SEM and are based on at least two independent experiments ($n = 2$), each with two biological replicates. + = tetracycline-induced clones. **** $p < 0.0001$, Kruskal–Wallis test with Dunn's multiple comparison test.

3.4. 4 EIP but Not ADKIN Is Essential for In Vivo Infectivity in Mice

To evaluate the role of ADKIN and 4EIP, the impact of gene silencing on in vitro growth and in vivo infectivity were determined. Knockdown of ADKIN did not alter parasite growth in vitro and parasites retained a normal infectivity profile in mice (Figure 6A,B). In contrast, 4EIP RNAi parasites showed a significant growth deficit already evident after 24 h of tetracycline induction (Figure 6C). In mice, knockdown of 4EIP was responsible for a strikingly reduced infectivity (Figure 6D); however, the mice still succumbed to infection within 2 weeks, most likely due to a loss of the RNAi phenotype in vivo. This hypothesis was confirmed using 4EIP-KO parasites which could be detected during the first week of infection but were undetectable from day 7 onwards until the pre-set endpoint of 70 dpi (Figure 6E). Even after immunosuppressive treatment with 150 mg/kg cyclophosphamide, parasitaemia did not reappear confirming the essential nature of 4EIP for in vivo infectivity.
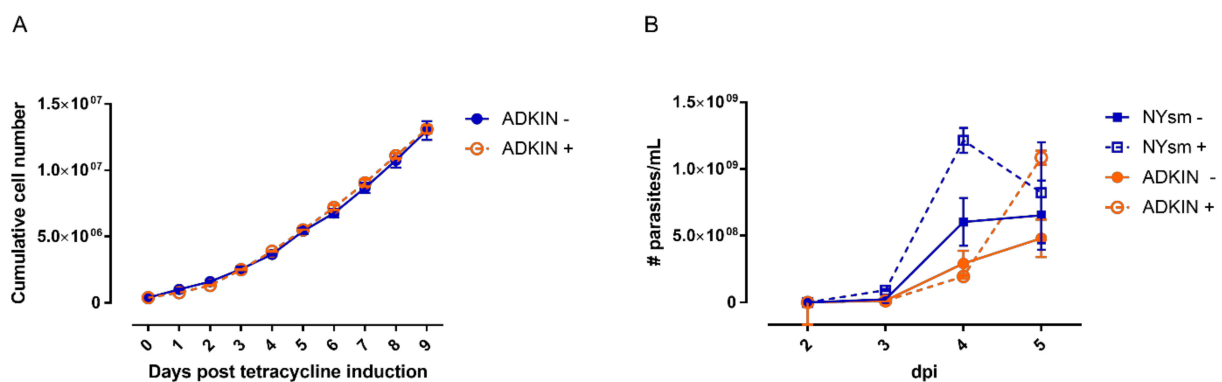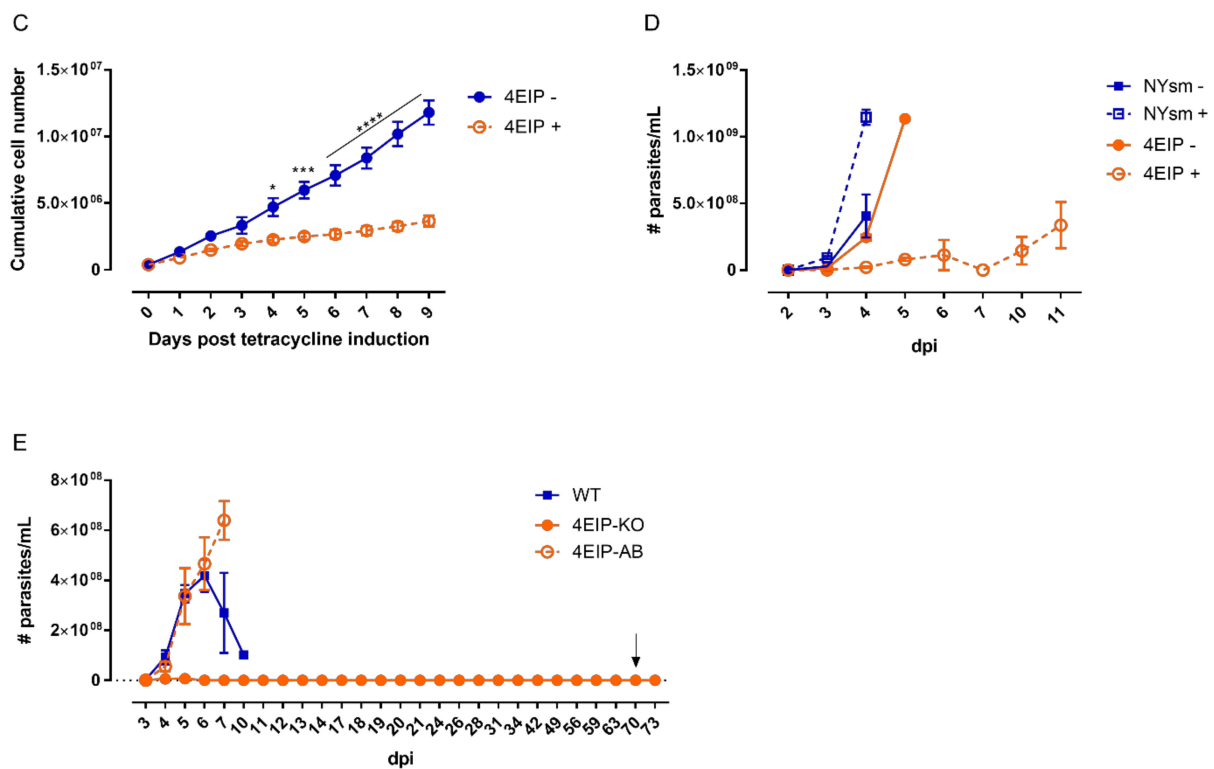

Figure 6. *Cont.*

Figure 6. The role of ADKIN and 4EIP in parasite growth and infectivity. Impact of ADKIN RNAi-mediated knockdown on (**A**) in vitro growth and (**B**) and in vivo infectivity. Impact of 4EIP RNAi-mediated knockdown on (**C**) in vitro growth and (**D**) and in vivo infectivity. (**E**) Impact of 4EIP knockout (4EIP-KO) and add-back (4EIP-AB) on in vivo infectivity. The arrow indicates the moment of immunosuppressive treatment. Results are expressed as the average cell numbers, and error bars represent the SEM. The in vitro experiments are based on two independent experiments (*n* = 2), each with two biological replicates. + = tetracycline-induced clones; − = non-induced clones. The in vitro cumulative growth curves were performed with two independently generated RNAi clones. * $p < 0.01$, *** $p < 0.001$, **** $p < 0.0001$.

3.5. 5 Does Not Specifically Impact Parasite Differentiation

Given the known involvement of 4EIP in parasite differentiation, the impact of **5** on short stumpy differentiation was assessed. PAD1 protein expression was used as a stumpy-specific marker using Western blot. To discern between the effects of changes in parasite density as a result of the antiparasitic activity and 4EIP-specific compound effects on PAD1 expression, the impact of **5** was compared to that of 3′-deoxytubercidin, which is 4EIP-independent. A concentration-dependent variation in PAD1 expression could be observed, most likely dependent on parasite density instead of target-dependent effects, since the same observations were made for 3′-deoxytubercidin (Figure 7). Additionally, no impact was observed of compound addition to infectious blood meals on midgut infection ratios in the tsetse fly vector (Figure 8).
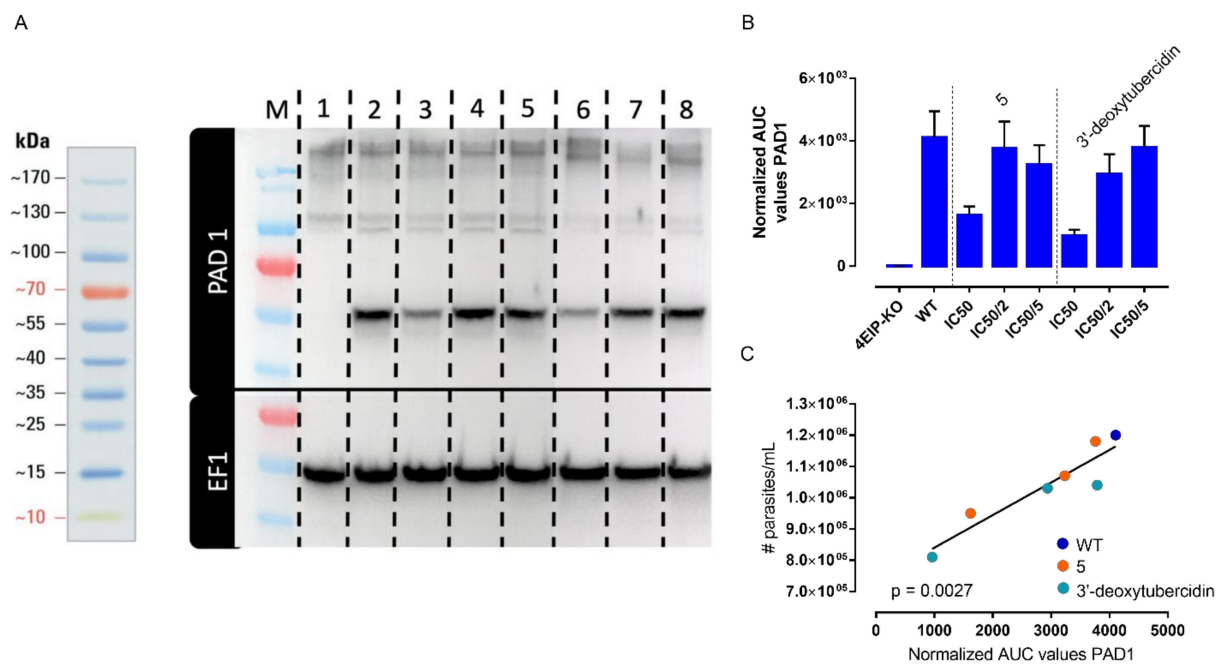
Figure 7. Western blot analysis for PAD1 expression. (**A**) PAD1 and EF1 protein expression (1: 4EIP-knockout, 2: untreated controls, 3–5: **5**-treated with IC_{50}, $IC_{50}/2$ and $IC_{50}/5$ and 6–8: 3′-deoxytubercidin-treated with the IC_{50}, $IC_{50}/2$ and $IC_{50}/5$). (**B**) EF1-normalized area under the curve (AUC) values for PAD1. (**C**) Correlation between the normalized AUC values for PAD1 and culture density at time of collection.
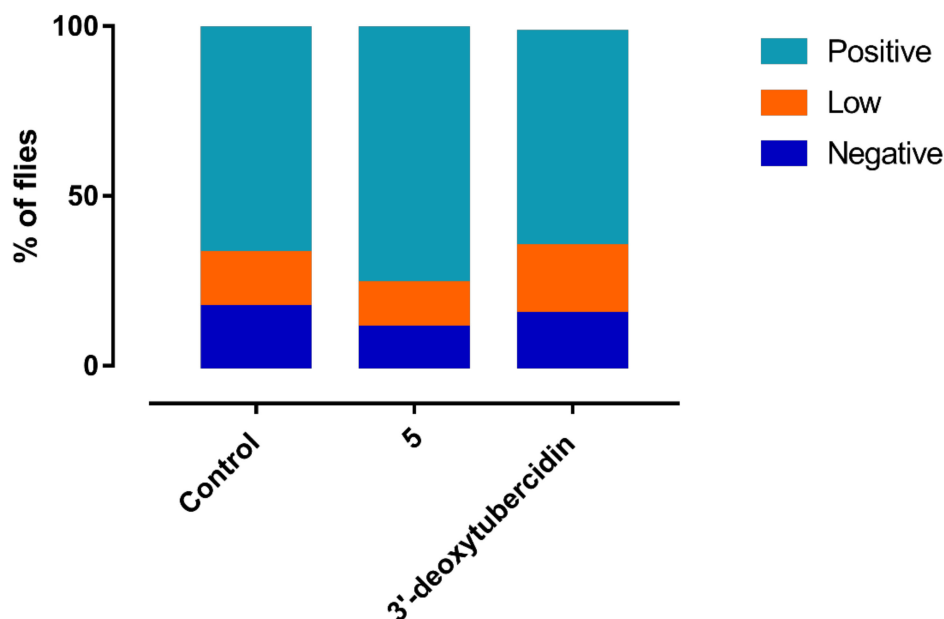

Figure 8. Impact of **5** supplementation on establishment of *T. brucei* in the tsetse fly midgut. Infectious blood meals were supplemented with **5** or 3′-deoxytubercidin at the IC_{50}. Results represent the percentage of *G. m. morsitans* flies with a negative, low, or positive infection in the midgut and are a representation of two independent experiments with a minimum of 25 flies per group.

4. Discussion

While limitations of currently used treatments for HAT should stimulate additional drug discovery initiatives, it remains a challenge to identify non-toxic lead compounds capable of crossing the BBB to treat stage-II infection. Since *T. brucei* parasites solely depend on purine salvage, nucleoside analogues may offer opportunities as novel tools

against HAT with CNS involvement [11]. Based on the previously identified nucleoside analogues tubercidin and cordycepin with known antitrypanosomal potential, a range of novel analogues were explored. The combination of structural elements of tubercidin and cordycepin resulted in the discovery of 3′-deoxytubercidin as a highly interesting lead compound to treat second-stage sleeping sickness [20]. 7-Deazaadenosines substituted with phenyl groups or a pyridine ring resulted in excellent in vitro potency and selectivity profile against African trypanosomes [19]. Finally, a series of 6-O-alkylated analogues was highly promising with nanomolar in vitro activity against *T. brucei* parasites [21].

The occurrence of drug resistance in the field emphasizes the need for identification of the potential mechanisms of resistance early on in the drug development process. RNAi screening provides a whole-genome unbiased approach for the identification of drug targets [28,46] and has been successfully used in identifying the MoA of the existing antitrypanosomal drugs eflornithine and nifurtimox [26]. In the present study, we used whole-genome RNAi screening to gain insight into the MoA of **5**, whereby the involvement of four targets, namely FLA1BP, EndoG, ADKIN and 4EIP, was demonstrated.

FLA1BP is responsible for joining the flagellar membrane to the cell membrane of the parasite. RNAi knockdown of FLA1BP has been described to cause detachment of the flagellum from the cell body, however, without any impact on parasite proliferation rates [47]. The fact that FLA1BP is more abundantly found in procyclic cells than in BSF may explain the inability to confirm this target and the lack of morphological changes in our FLA1BP knockdown parasites.

EndoG plays a role in trypanolysis induced by the human serum apolipoprotein 1 (APOL1). Uptake of APOL1 by the parasite causes lysosomal and mitochondrial membrane permeabilization and the subsequent translocation of mitochondrial EndoG to the parasite nucleus causing DNA damage and cell death [42]. This target, however, could not be confirmed, possibly due to experimental limitations.

ADKIN is a known enzyme in the purine salvage pathway of the parasite and is responsible for the direct phosphorylation of adenosine to AMP following uptake of the former [48,49]. The reduced sensitivity of ADKIN RNAi strains to **5** suggests the occurrence of compound phosphorylation upon uptake by the parasite. This phenomenon has already been described for other nucleoside analogues [20]. However, the fact that **5** remained active against the ADKIN knockdown strains at sub-micromolar levels indicates that this phosphorylation may not be essential or only partially contributes to the overall activity. It is clear from a broader compound evaluation on the developed ADKIN RNAi strains that various analogues exhibit different degrees of dependency on ADKIN or may be subject to different rates of enzymatic conversion by ADKIN. ADKIN plays an important role in trypanosomal purine salvage [48,49], but the in vitro and in vivo growth curves [50,51] reveal that it is not essential for growth and infectivity. This can be attributed to the fact that loss of ADKIN activity redirects adenosine salvage through the alternative cleavage-dependent pathway. Additionally, the parasite can salvage hypoxanthine, inosine, and adenine to form all of its required purines [48].

The second identified target, 4EIP, has been extensively studied in *Leishmania major*. 4EIP binds with its N-terminal domain to the mRNA cap-binding protein LeishIF4E, leading to dissociation from the cap and a suppression of active translation [52]. Similar binding properties and functions were later described for African trypanosomes [35]. The MoA of **5** can be partially attributed to 4EIP as confirmed by the use of knock-out and add-back control parasites. However, the cap-binding protein 4E1 was not influenced by **5**, indicating that the inhibition of 4EIP works independently of 4E1. The suppression of translation in *T. brucei*, as regulated by 4EIP, is required for successful differentiation into short stumpy parasites in the bloodstream. This is an essential adaptation of the parasite for successful transmission to the tsetse fly vector [35] and subsequent transformation to procyclic parasites in the tsetse fly midgut. In this study, we showed a large growth deficit of 4EIP knockdown parasites in culture conditions, while in mice, 4EIP knockout led to a rapid clearance of parasite burdens. The underlying basis for the essential role of

4EIP in vivo remains to be elucidated and this study could not demonstrate a link between compound activity and inhibition of parasite differentiation in vitro and in the tsetse fly.

In summary, we here describe the acquired insights in the MoA of novel 7-deazaadenosine nucleoside analogues for the treatment of HAT. RNAi screening in combination with confirmatory in vitro and in vivo experiments using knockout strains identified the involvement of 4EIP in the activity of some antitrypanosomal nucleoside analogues. The reliance of some compounds on this gene product and the essential nature for in vivo infectivity indicate that 4EIP represents a potential drug target. The available RNAi and knockout clones will allow a more in depth analysis of the structural requirements for metabolic activation and 4EIP interaction of newly synthetized nucleoside analogues.

Supplementary Materials: The following are available online at https://www.mdpi.com/article/10.3390/microorganisms9040826/s1, Supplementary method S1: Synthesis of compound **4**, Figure S1: Overview of the RNAi screening protocol. (A) Experimental overview of the screening protocol of RNAi libraries for compound **5**. (B) Graphic representation of the P2T7Bern vector [25], Table S1: Overview of the used primers, Table S2: Sequencing results of the RNAi inserts.

Institutional Review Board Statement: The use of laboratory rodents was carried out in strict accordance with all mandatory guidelines (EU directives, including the Revised Directive 2010/63/EU on the Protection of Animals used for Scientific Purposes that came into force on 1 January 2013, and the declaration of Helsinki in its latest version) and was approved by the Ethical Committee of the University of Antwerp, Belgium (UA-ECD 2017-04).

Informed Consent Statement: Not applicable.

Data Availability Statement: Data is contained within the article or Supplementary Materials.

Conflicts of Interest: The authors declare no conflict of interest. The funders had no role in the design of the study; in the collection, analyses, or interpretation of data; in the writing of the manuscript, or in the decision to publish the results.

References

1. Kennedy, P.G. Clinical features, diagnosis, and treatment of human African trypanosomiasis (sleeping sickness). *Lancet Neurol.* **2013**, *12*, 186–194. [CrossRef]
2. Tirados, I.; Esterhuizen, J.; Kovacic, V.; Mangwiro, T.N.; Vale, G.A.; Hastings, I.; Solano, P.; Lehane, M.J.; Torr, S.J. Tsetse Control and Gambian Sleeping Sickness; Implications for Control Strategy. *PLoS Negl. Trop Dis.* **2015**, *9*, e0003822. [CrossRef] [PubMed]
3. Malvy, D.; Chappuis, F. Sleeping sickness. *Clin. Microbiol. Infect. Off. Publ. Eur. Soc. Clin. Microbiol. Infect. Dis.* **2011**, *17*, 986–995. [CrossRef]
4. Babokhov, P.; Sanyaolu, A.O.; Oyibo, W.A.; Fagbenro-Beyioku, A.F.; Iriemenam, N.C. A current analysis of chemotherapy strategies for the treatment of human African trypanosomiasis. *Pathog. Glob. Health* **2013**, *107*, 242–252. [CrossRef] [PubMed]
5. Eperon, G.; Balasegaram, M.; Potet, J.; Mowbray, C.; Valverde, O.; Chappuis, F. Treatment options for second-stage gambiense human African trypanosomiasis. *Expert Rev. Anti Infect. Ther.* **2014**, *12*, 1407–1417. [CrossRef]

6. Mesu, V.; Kalonji, W.M.; Bardonneau, C.; Mordt, O.V.; Blesson, S.; Simon, F.; Delhomme, S.; Bernhard, S.; Kuziena, W.; Lubaki, J.F.; et al. Oral fexinidazole for late-stage African *Trypanosoma brucei* gambiense trypanosomiasis: A pivotal multicentre, randomised, non-inferiority trial. *Lancet* **2018**, *391*, 144–154. [CrossRef]

7. Dickie, E.A.; Giordani, F.; Gould, M.K.; Maser, P.; Burri, C.; Mottram, J.C.; Rao, S.P.S.; Barrett, M.P. New Drugs for Human African Trypanosomiasis: A Twenty First Century Success Story. *Trop. Med. Infect. Dis.* **2020**, *5*, 29. [CrossRef]

8. Baker, N.; de Koning, H.P.; Maser, P.; Horn, D. Drug resistance in African trypanosomiasis: The melarsoprol and pentamidine story. *Trends Parasitol.* **2013**, *29*, 110–118. [CrossRef]

9. Sokolova, A.Y.; Wyllie, S.; Patterson, S.; Oza, S.L.; Read, K.D.; Fairlamb, A.H. Cross-resistance to nitro drugs and implications for treatment of human African trypanosomiasis. *Antimicrob. Agents Chemother.* **2010**, *54*, 2893–2900. [CrossRef]

10. Wyllie, S.; Foth, B.J.; Kelner, A.; Sokolova, A.Y.; Berriman, M.; Fairlamb, A.H. Nitroheterocyclic drug resistance mechanisms in *Trypanosoma brucei*. *J. Antimicrob. Chemother.* **2016**, *71*, 625–634. [CrossRef]

11. Berg, M.; Van der Veken, P.; Goeminne, A.; Haemers, A.; Augustyns, K. Inhibitors of the Purine Salvage Pathway: A Valuable Approach for Antiprotozoal Chemotherapy? *Curr. Med. Chem.* **2010**, *17*, 2456–2481. [CrossRef]

12. Vodnala, S.K.; Ferella, M.; Lundén-Miguel, H.; Betha, E.; van Reet, N.; Amin, D.N.; Öberg, B.; Andersson, B.; Kristensson, K.; Wigzell, H.; et al. Preclinical Assessment of the Treatment of Second-Stage African Trypanosomiasis with Cordycepin and Deoxycoformycin. *PLoS Negl. Trop Dis.* **2009**, *3*, e495. [CrossRef]

13. Vodnala, S.K.; Lundbäck, T.; Yeheskieli, E.; Sjöberg, B.; Gustavsson, A.-L.; Svensson, R.; Olivera, G.C.; Eze, A.A.; de Koning, H.P.; Hammarström, L.G.J.; et al. Structure–Activity Relationships of Synthetic Cordycepin Analogues as Experimental Therapeutics for African Trypanosomiasis. *J. Med. Chem.* **2013**, *56*, 9861–9873. [CrossRef] [PubMed]

14. Drew, M.E.; Morris, J.C.; Wang, Z.; Wells, L.; Sanchez, M.; Landfear, S.M.; Englund, P.T. The Adenosine Analog Tubercidin Inhibits Glycolysis in *Trypanosoma brucei* as Revealed by an RNA Interference Library. *J. Biol. Chem.* **2003**, *278*, 46596–46600. [CrossRef] [PubMed]

15. Rottenberg, M.E.; Masocha, W.; Ferella, M.; Petitto-Assis, F.; Goto, H.; Kristensson, K.; McCaffrey, R.; Wigzell, H. Treatment of African trypanosomiasis with cordycepin and adenosine deaminase inhibitors in a mouse model. *J. Infect Dis.* **2005**, *192*, 1658–1665. [CrossRef]

16. Smulson, M.E.; Suhadolnik, R.J. The biosynthesis of the 7-deazaadenine ribonucleoside, tubercidin, by Streptomyces tubercidicus. *J. Biol. Chem.* **1967**, *242*, 2872–2876. [CrossRef]

17. El Kouni, M.H.; Diop, D.; O'Shea, P.; Carlisle, R.; Sommadossi, J.P. Prevention of tubercidin host toxicity by nitrobenzylthioinosine 5′-monophosphate for the treatment of schistosomiasis. *Antimicrob. Agents Chemother.* **1989**, *33*, 824–827. [CrossRef] [PubMed]

18. Aoki, J.I.; Coelho, A.C.; Muxel, S.M.; Zampieri, R.A.; Sanchez, E.M.; Nerland, A.H.; Floeter-Winter, L.M.; Cotrim, P.C. Characterization of a Novel Endoplasmic Reticulum Protein Involved in Tubercidin Resistance in Leishmania major. *PLoS Negl. Trop Dis.* **2016**, *10*, e0004972. [CrossRef]

19. Hulpia, F.; Campagnaro, G.D.; Scortichini, M.; Van Hecke, K.; Maes, L.; de Koning, H.P.; Caljon, G.; Van Calenbergh, S. Revisiting tubercidin against kinetoplastid parasites: Aromatic substitutions at position 7 improve activity and reduce toxicity. *Eur. J. Med. Chem.* **2019**, *164*, 689–705. [CrossRef] [PubMed]

20. Hulpia, F.; Mabille, D.; Campagnaro, G.D.; Schumann, G.; Maes, L.; Roditi, I.; Hofer, A.; de Koning, H.P.; Caljon, G.; Van Calenbergh, S. Combining tubercidin and cordycepin scaffolds results in highly active candidates to treat late-stage sleeping sickness. *Nat. Commun.* **2019**, *10*, 5564. [CrossRef]

21. Hulpia, F.; Bouton, J.; Campagnaro, G.D.; Alfayez, I.A.; Mabille, D.; Maes, L.; de Koning, H.P.; Caljon, G.; Van Calenbergh, S. C6-O-alkylated 7-deazainosine nucleoside analogues: Discovery of potent and selective anti-sleeping sickness agents. *Eur. J. Med. Chem.* **2020**, *188*, 112018. [CrossRef]

22. Ho, H.T.B.; Wang, J. The Nucleoside Transporters CNTs and ENTs. In *Drug Transporters: Molecular Characterization and Role in Drug Disposition*, 2nd ed.; Guofeng You, M.E.M., Ed.; Wiley: Hoboken, NJ, USA, 2014; pp. 107–126.

23. Target Product Profile Sleeping Sickness, DNDi. Available online: https://dndi.org/diseases/sleeping-sickness/target-product-profile (accessed on 29 January 2021).

24. Van den Kerkhof, M.; Sterckx, Y.G.; Leprohon, P.; Maes, L.; Caljon, G. Experimental Strategies to Explore Drug Action and Resistance in Kinetoplastid Parasites. *Microorganisms* **2020**, *8*, 950. [CrossRef]

25. Alsford, S.; Eckert, S.; Baker, N.; Glover, L.; Sanchez-Flores, A.; Leung, K.F.; Turner, D.J.; Field, M.C.; Berriman, M.; Horn, D. High-throughput decoding of antitrypanosomal drug efficacy and resistance. *Nature* **2012**, *482*, 232–236. [CrossRef] [PubMed]

26. Baker, N.; Alsford, S.; Horn, D. Genome-wide RNAi screens in African trypanosomes identify the nifurtimox activator NTR and the eflornithine transporter AAT6. *Mol. Biochem. Parasitol.* **2011**, *176*, 55–57. [CrossRef] [PubMed]

27. Burkard, G.S.; Jutzi, P.; Roditi, I. Genome-wide RNAi screens in bloodstream form trypanosomes identify drug transporters. *Mol. Biochem. Parasitol.* **2011**, *175*, 91–94. [CrossRef]

28. Moss, C.X.; Brown, E.; Hamilton, A.; Van der Veken, P.; Augustyns, K.; Mottram, J.C. An essential signal peptide peptidase identified in an RNAi screen of serine peptidases of *Trypanosoma brucei*. *PLoS ONE* **2015**, *10*, e0123241. [CrossRef]

29. Povelones, M.L.; Tiengwe, C.; Gluenz, E.; Gull, K.; Englund, P.T.; Jensen, R.E. Mitochondrial shape and function in trypanosomes requires the outer membrane protein, TbLOK1. *Mol. Microbiol.* **2013**, *87*, 713–729. [CrossRef] [PubMed]

30. Monnerat, S.; Clucas, C.; Brown, E.; Mottram, J.C.; Hammarton, T.C. Searching for novel cell cycle regulators in *Trypanosoma brucei* with an RNA interference screen. *BMC Res. Notes* **2009**, *2*, 46. [CrossRef]

31. Morris, J.C.; Wang, Z.; Drew, M.E.; Englund, P.T. Glycolysis modulates trypanosome glycoprotein expression as revealed by an RNAi library. *EMBO J.* **2002**, *21*, 4429–4438. [CrossRef]

32. Glover, L.; Alsford, S.; Baker, N.; Turner, D.J.; Sanchez-Flores, A.; Hutchinson, S.; Hertz-Fowler, C.; Berriman, M.; Horn, D. Genome-scale RNAi screens for high-throughput phenotyping in bloodstream-form African trypanosomes. *Nat. Protoc.* **2015**, *10*, 106–133. [CrossRef]

33. Glover, L.; Horn, D. Site-specific DNA double-strand breaks greatly increase stable transformation efficiency in *Trypanosoma brucei*. *Mol. Biochem. Parasitol.* **2009**, *166*, 194–197. [CrossRef]

34. Burkard, G.; Fragoso, C.M.; Roditi, I. Highly efficient stable transformation of bloodstream forms of *Trypanosoma brucei*. *Mol. Biochem. Parasitol.* **2007**, *153*, 220–223. [CrossRef]

35. Terrao, M.; Marucha, K.K.; Mugo, E.; Droll, D.; Minia, I.; Egler, F.; Braun, J.; Clayton, C. The supressive cap-binding-complex factor 4EIP is required for normal differentiation. *Nucleic Acids Res.* **2018**, *46*, 8993–9010. [CrossRef]

36. Maes, L.; Cos, P.; Croft, S.L. The Relevance of Susceptibility Tests, Breakpoints, and Markers. In *Drug Resistance in Leishmania Parasites: Consequences, Molecular Mechanisms and PossibleTreatments*; Ponte-Sucre, A., Diaz, E., Padrón-Nieves, M., Eds.; Springer: Vienna, Austria, 2013; pp. 407–429.

37. Tritryp Database. Available online: http://tritrypdb.org/tritrypdb (accessed on 11 April 2017).

38. ProtParam. Available online: http://web.expasy.org/protparam (accessed on 11 April 2017).

39. SignalIP Tool. Available online: www.bds.dtu.dk/services/SignalIP (accessed on 11 April 2017).

40. Toolkit. Available online: https://toolkit/tuebingen.mpg.de/hhpred (accessed on 11 April 2017).

41. Brenndorfer, M.; Boshart, M. Selection of reference genes for mRNA quantification in *Trypanosoma brucei*. *Mol. Biochem. Parasitol.* **2010**, *172*, 52–55. [CrossRef] [PubMed]

42. Vanwalleghem, G.; Fontaine, F.; Lecordier, L.; Tebabi, P.; Klewe, K.; Nolan, D.P.; Yamaryo-Botte, Y.; Botte, C.; Kremer, A.; Burkard, G.S.; et al. Coupling of lysosomal and mitochondrial membrane permeabilization in trypanolysis by APOL1. *Nat. Commun.* **2015**, *6*, 8078. [CrossRef]

43. Gonzalez-Andrade, P.; Camara, M.; Ilboudo, H.; Bucheton, B.; Jamonneau, V.; Deborggraeve, S. Diagnosis of trypanosomatid infections: Targeting the spliced leader RNA. *J. Mol. Diagn.* **2014**, *16*, 400–404. [CrossRef]

44. Dean, S.; Marchetti, R.; Kirk, K.; Matthews, K.R. A surface transporter family conveys the trypanosome differentiation signal. *Nature* **2009**, *459*, 213–217. [CrossRef] [PubMed]

45. Acs, G.; Reich, E.; Mori, M. Biological and Biochemical Properties of the Analogue Antibiotic Tubercidin. *Proc. Natl. Acad. Sci. USA* **1964**, *52*, 493–501. [CrossRef]

46. Berriman, M.; Ghedin, E.; Hertz-Fowler, C.; Blandin, G.; Renauld, H.; Bartholomeu, D.C.; Lennard, N.J.; Caler, E.; Hamlin, N.E.; Haas, B.; et al. The genome of the African trypanosome *Trypanosoma brucei*. *Science* **2005**, *309*, 416–422. [CrossRef]

47. Sun, S.Y.; Wang, C.; Yuan, Y.A.; He, C.Y. An intracellular membrane junction consisting of flagellum adhesion glycoproteins links flagellum biogenesis to cell morphogenesis in *Trypanosoma brucei*. *J. Cell Sci.* **2013**, *126*, 520–531. [CrossRef] [PubMed]

48. Vodnala, M.; Fijolek, A.; Rofougaran, R.; Mosimann, M.; Maser, P.; Hofer, A. Adenosine kinase mediates high affinity adenosine salvage in *Trypanosoma brucei*. *J. Biol. Chem.* **2008**, *283*, 5380–5388. [CrossRef] [PubMed]

49. Luscher, A.; Onal, P.; Schweingruber, A.M.; Maser, P. Adenosine kinase of *Trypanosoma brucei* and its role in susceptibility to adenosine antimetabolites. *Antimicrob. Agents Chemother.* **2007**, *51*, 3895–3901. [CrossRef] [PubMed]

50. Vigueira, P.A.; Paul, K.S. Requirement for acetyl-CoA carboxylase in *Trypanosoma brucei* is dependent upon the growth environment. *Mol. Microbiol.* **2011**, *80*, 117–132. [CrossRef] [PubMed]

51. Ong, H.B.; Sienkiewicz, N.; Wyllie, S.; Patterson, S.; Fairlamb, A.H. *Trypanosoma brucei* (UMP synthase null mutants) are avirulent in mice, but recover virulence upon prolonged culture in vitro while retaining pyrimidine auxotrophy. *Mol. Microbiol.* **2013**, *90*, 443–455. [CrossRef]

52. Meleppattu, S.; Arthanari, H.; Zinoviev, A.; Boeszoermenyi, A.; Wagner, G.; Shapira, M.; Leger-Abraham, M. Structural basis for LeishIF4E-1 modulation by an interacting protein in the human parasite Leishmania major. *Nucleic Acids Res.* **2018**, *46*, 3791–3801. [CrossRef] [PubMed]